# IV. Applied Battery Research for Transportation

## IV.A Introduction

The widespread adoption of electric vehicles is crucial to reaching both the environmental and energy security goals of the United States of America. Reaching the necessary fleet electrification levels could also enable a strong U.S.-based battery manufacturing sector. Critical to the invention-to-product process that has to take place is the translation of materials discovery and device innovation in the R&D community into commercially viable products and processes. Such applied research activities are inherently high risk; coupling the frontier, cutting edge nature of materials discovery with the performance and cost needs of a market-changing new product.

A significant portfolio of VTO energy storage projects that meet these criteria are grouped together in the Applied Battery Research (ABR) for transportation program. The ABR program is comprised of high risk projects investigating issues and advances at the cell level. Success in ABR projects means electric drive vehicle energy storage products that can be realized (manufactured) and that lead to cost reduction; thus fulfilling the energy storage component of EERE's *EV Everywhere* Initiative. Such improvements will be accomplished through novel materials, particularly the active components of the cell, but also through innovative cell design and electrode composition. Also, materials production, electrode processing, and cell manufacture are important R&D areas within ABR. Completing the suite of project modalities is the Critical Barrier Focus (CBF). Applied research programs always contain and are often defined by a major barrier, a set of structurally and functionally interrelated problems that simultaneously appear intractable and absolutely require mitigation or adaptation in order to achieve a particular technical target. Solutions, if possible, require understanding across the dimensions of the problem, and such understanding requires in-depth science practiced by a multi-disciplinary team—and a lot of data. In FY 2015, the first CBF project, Mitigating Voltage Fade, was completed and the second CBF, Enabling High Energy, High Voltage Li-ion Batteries, was initiated.

The R&D projects in the 2015 ABR portfolio are divided into five distinct but complementary groups:

- Core and Enabling Support Facilities;
- Critical Barrier Focus —Enabling High Energy, High Voltage Li-ion Batteries;
- Next-Generation Li-ion Chemistries "Improvements in Cell Chemistry, Composition, and Processing";
- Process Development and Manufacturing R&D at National Laboratories;
- Process Development and Manufacturing R&D with U.S. Industry.

**Core and Enabling Support Facilities:** Across several of the national laboratories, infrastructure has been created and resources grouped into facilities that support complex activities critical to applied battery research. This provides the U.S. energy storage research community a powerful tool to carry out scientific investigations by using, for example, state-of-the-art fabricated Li-ion battery electrodes, commercially viable and high purity electrolyte additives, chemical and electrochemical analysis of cycled battery components, and component-level abuse response analysis. The services and products of these facilities are fully funded through the ABR program and are available hierarchically, with VTO funded projects first, followed by other DOE funded projects (BES, ARPA-E), then other government agencies down the line through to U.S. commercial entities. The anchor facility among ABR's support facilities is the Cell Analysis, Modeling, and Prototyping Facility (CAMP) based at the Argonne National Laboratory. More than an arrangement of equipment, the CAMP Facility is an integrated team effort designed to support the production of prototype electrodes and cells, including materials validation (benchmarking), modeling, and diagnostics. A majority of the individual projects undertaken within CAMP this year centered on fabricating, testing, and characterizing silicon-based anodes.

**Enabling High Energy, High Voltage Li-ion Batteries:** The overall objective of this three year Critical Barrier Focus project is to understand the failure mechanisms that prevent state-of-the-art Li-ion battery systems from achieving higher practical energy densities than are currently obtainable. The inability to delithiate commercially available cathode materials beyond ~4.3 V (vs. Li/Li+) without incurring excessive surface

damage, electrolyte decomposition, and bulk structural instabilities is a significant challenge. As such, four areas of research, or thrusts, exist within the High Energy / High Voltage CBF: Cathodes, Electrolytes and Additives, Surfaces and Interfaces, and Testing and Analysis. More than fifteen staff scientists and post-doctoral fellows resident at Argonne and Oak Ridge National Laboratories work across these research thrusts.

**Next-Generation Li-ion Chemistries "Improvements in Cell Chemistry, Composition, and Processing":** In September 2013, DOE VTO awarded six contracts to develop cells that met or exceeded performance targets for EV or PHEV batteries. Contracts were awarded to teams led by 3M Company, Envia Systems, Farasis, Penn State University, TIAX (now CAMX Power), and Argonne National Laboratory. Each development team has used next-generation anodes and cathodes. The active material in all cases for the anode was a carbon-Si (or silicon-based nanocomposite) blend. For the cathode, each development team investigated either high voltage NMC-based cathodes with high Ni content or lithium rich, manganese rich oxide-based cathodes or both.

In this second full year of a nominally three year project, advances include:

- demonstrating that using SiO blended anodes increases cell energy density (Wh/kg) by approximately 45%;
- identifying a high voltage electrolyte that improved the cycle life of full cells (cycled to 4.4V) from 50 to over 700 cycles;
- improving full cell cycle life for cells with SiOx-containing anodes from approximately 60 to over 600 cycles while achieving PHEV cell energy densities greater than 200Wh/kg;
- reducing capacity fade from 20% to under 5% over 100 cycles by pre-lithiating the Si-graphite

Good progress has been made across the board in stabilizing high voltage cathode materials and in extending the life of Si-containing anodes. These results lead VTO to conclude that Si/high V cathode cells continue to be the most likely path toward achieving the full EV and PHEV battery performance goals. Currently, achieving good cycle life results with cells using a significant amount of silicon continues to be an issue. This realization is the one of the major drivers in establishing a third Critical Barrier Focus beginning in FY2016: Next Generation Anodes for Li-ion Batteries, which is a multilab consortium dedicated to an increased understanding of current failure modes and to achieving a full utilization of this high energy material in automotive cells.

**Process Development and Manufacturing R&D at National Laboratories:** Critical to establishing a U.S.-based battery manufacturing industry is the development of process-oriented intellectual property. However, many of the opportunities to develop such IP have long lead times associated with process development, novel equipment design, and the time associated with technology learning. This often means there is a strategic financial barrier for for-profit entities. Too much business risk exists associated with process technology development. Considering the potential reward to the US economy and to society in general, where possible – and relevant – this risk should be assumed by the government. The reports contained in this section detail work across three national labs that not only has led to IP creation on its own, but the research teams have also leveraged EERE-funded work to partner with American companies developing proprietary processing technologies. A variety of U.S. companies have collaborated on those projects, ranging from multinational corporations to start-up small businesses. As new processing resources are developed, they are also made available to the U.S. energy storage research community via the support facilities described above.

**Process Development and Manufacturing R&D with Industry:** The EERE-VTO Energy Storage program, in addition to process R&D at the national labs, supports the development of advanced battery manufacturing processes through funded agreements with for-profit entities, leveraging entrepreneurial investment and allowing private sector innovators to stretch their precious resources through DOE funding. Over the past two fiscal years several high risk / high reward projects at commercially entities have been funded. Four of the six projects reported on deal with various approaches to or aspects of battery electrode or separator fabrication. Miltec International, for example, is developing a novel approach to introduce ceramic subcomponents into battery separators to dramatically improve thermal abuse prevention. An important aspect of battery electrode fabrication is solvent removal after electrode coating; Lambda Technologies is showing some success in reducing the drying residence time and energy used via a microwave-assisted drying approach. The other two industrial projects in this section deal with, respectively, an inventive and promising method to produce a potentially game-changing new active cathode material: Sila Nanotechnologies' gas-phase synthesis of

transition metal fluoride conversion cathode materials and with an innovation in cell design and architecture, Parthian Energy's efforts to substantially increase energy density via a non-parallel plate full cell geometry, their S-cell design.

The remainder of this section provides technical highlights and progress reports on the Applied Battery Research program for FY 2015 organized by the project groups discussed above. Each report was prepared to capture the purpose, approach, major gains and setbacks (if any) of the project (or its component). For more technical detail, actual experimental methods, and data analytics, please see each report's referenced scientific publications or contact the appropriate project lead.

# IV.B Core and Enabling Support Facilities

# IV.B.1 Cell Analysis, Modeling, and Prototyping (CAMP) Facility Research Activities (ANL)

## Objectives

- The objective of this core-funded effort is to design, fabricate, and characterize high-quality prototype cells based on the latest discoveries involving high energy anode and cathode battery materials. Using this multi-disciplined facility, analytical diagnostic results can be correlated with the electrochemical performance of advanced lithium-ion battery technologies for plug-in electric vehicle (PEV) applications.
  - Link experimental efforts through electrochemical modeling studies.
  - Identify performance limitations and aging mechanisms.

## Technical Barriers

- The primary technical barrier is the development of a high energy density battery (for PEV applications) that is safe, cost-effective, and has a long cycle life.
  - Interpret complex cell electrochemical phenomena.
  - Identification of cell degradation mechanisms for a variety of novel high energy materials.

## Technical Targets

- Recommend optimal concentration of VC and FEC electrolyte additives in silicon//LMR-NMC cell system.
- Assess electrochemical performance of coatings on LMR-NMC particles deposited under various conditions.
- Report on the optimal PAA binder system for silicon-graphite electrode with a goal of 3 mAh/cm².
- Summarize CAMP Facility's Electrode Library activity.
- Fabricate Deliverable pouch cells for the ABR FOA Award entitled "New high energy electrochemical couple for automotive applications" (PI: Khalil Amine).
- Fabricate pouch cell build with silicon anode and LMR-NMC cathode.
- Advance development of electrochemical models focusing on silicon-graphite negative electrodes and LMR-NMC positive electrode.

### Project Details

**Peter Faguy (EERE-VTO-ABR Program Manager)**

**Andrew N. Jansen (Argonne National Lab - PI)**
9700 South Cass Avenue, CSE-200
Lemont, IL 60439
Phone: 630-252-4956; Fax: 630-972-4461
Email: Jansen@anl.gov

Collaborators:
Daniel P. Abraham, Argonne National Laboratory
Dominick N. Baker, Argonne National Laboratory
Dennis W. Dees, Argonne National Laboratory
Kevin G. Gallagher, Argonne National Laboratory
James A. Gilbert, Argonne National Laboratory
Matilda Klett, Argonne National Laboratory
Jianlin Li, Oak Ridge National Laboratory
Wenquan Lu, Argonne National Laboratory
Bryant J. Polzin, Argonne National Laboratory
Robert C. Tenent, National Renewal Energy Lab
Stephen E. Trask, Argonne National Laboratory
David L. Wood III, Oak Ridge National Laboratory
Qingliu Wu, Argonne National Laboratory

Organizations listed in report (Figure 35)
MERF & PTF, Argonne National Laboratory

Start Date: October 2015

Projected End Date: September 2018

## Accomplishments

- Fabricated double-sided silicon-graphite electrodes with 0, 5, and 15 wt.% silicon that have good flexibility, mechanical robustness, and capacity loading over 3 mAh/cm², and cycled them in multi-stack pouch cells (versus NCM523 cathodes) with >300 mAh capacity.

- Fabricated single-sided electrodes with 0, 5, 10 and 15 wt. % silicon with optimized LiPAA binder system and entered into the electrode library.
- Explored voltage window of silicon-graphite electrodes.
- Measured electrode swelling as a function of SOC and silicon content.
- Initiated study of silicon-graphite cells with Argonne's Post-Test-Facility.
- Explored new applications for conductive binder from LBNL with Argonne's MERF.
- Applied and tested $Al_2O_3$ coating on LMR-NMC cathode particles.
- Supplied numerous baseline electrodes for high-energy high-voltage project and assisted in developing assembly and testing protocols.
- Fabricated interim pouch cell build for the award entitled "New high energy electrochemical couple for automotive applications" (PI: Khalil Amine)
- Fabricated baseline, interim, and final pouch cell builds for award entitled "Fluorinated Electrolyte for 5-V Li-Ion Chemistry" (PI: John Zhang).
- Fabricated and tested NASA-JPL baseline and coated LMR-NMC electrodes in pouch cells.
- Conducted study on impact of electrode thickness on cell performance.
- Worked with PPG Industries in CRADA on novel aqueous cathode binder.
- Expanded electrochemical model for interfacial impedance and bulk transport.
- Determined optimum amount of FEC and VC as electrolyte additives in silicon-graphite electrode cells.
- Supplied numerous electrodes from the CAMP Facility's electrode library; distribution increased to 1,690 sheets to 49 different organizations.

## Introduction

The "valley of death" is a phrase often used to describe the path that a new discovery traverses to become a commercial product. This is especially true for novel battery materials invented in research laboratories around the world. Often researchers are resource-limited and only able to make gram quantities of their new material. A few grams is enough for several coin cells to prove the concept, but not for a battery manufacturer to test in a realistic format. Considering that a typical coin cell has a capacity near 4 mAh, while a cell in a PEV battery would have a capacity near 40 Ah – four orders of magnitude larger – an unwarranted amount of resources could be gambled to make the tens of kilograms needed for a full-sized cell industrial demonstration. Many promising materials may have been abandoned on the benchtop because the associated scale-up risks were deemed too excessive.

This is where the CAMP facility comes in. The facility is appropriately sized to enable the design, fabrication, and characterization of high-quality prototype cells using just a few hundred grams of the latest discoveries involving high energy battery materials. Prototype cells made in the facility generally have a near 400-mAh capacity, which straddles the gap between coin cells and full cells nicely – nearly two orders of magnitude from each end point. Thus, a realistic and consistent evaluation of candidate chemistries can take place in a time-effective manner using practical quantities of novel materials in cell formats commonly used in industry.

The CAMP Facility is more than an arrangement of equipment, it is an integrated team effort designed to support the production of protype electrodes and cells, and includes activities in materials validation (benchmarking), modeling, and diagnostics. It is not the aim of this facility to become a small battery manufacturer, but a laboratory research facility with cell production capabilities adequate to evaluate the merits and limitations of mid- to long-term lithium-ion chemistries in a quasi-realistic industrial format.

As new cell chemistries and systems progress, they reach a point when they are considered for further development in larger prototype cells. When that happens, a limited quantity of them, along with preliminary data, are transferred from the inventor or originator to the CAMP Facility for materials validation to determine if they warrant further consideration. The source of these materials (anodes, cathodes, electrolytes, additives, separators, and binders) may originate from the ABR or the BMR Program, or from other domestic and foreign organizations such as universities, national labs, and industrial vendors. Electrochemical couples with high power and energy density receive priority. Lately, efforts have focused on silicon-based anodes and lithium-manganese-rich nickel-manganese cobalt (LMR-NMC) cathodes.

The CAMP Facility has the capability to make two prototype cell formats in their 45 m² dry room: pouch cells (xx3450 format, with capacity around 0.4 Ah) and 18650 cells. Pouch cells are anticipated to be easier to assemble, but may suffer from bulging if gases are evolved during cell aging and cycling. The 18650 cells, which are rigid containers, may be used if the pouch cell format is deemed unreliable due to gassing, or if higher capacity cells are needed (i.e., capacities greater than 1 Ah). Central to this effort is a pilot-scale coating machine that operates with slurry sizes ranging from 20 grams to a few kilograms. This is a key feature of the CAMP facility that enables a professional evaluation of small quantities of novel materials. If needed, the MERF is available for scaling up materials for these prototype cell builds.

In general, two types of modeling are employed in this project. First, battery design modeling is a spreadsheet-based simulation tool used to determine impedance behavior, available capacity, and thermal effects for general and specific cell, battery module, and battery pack designs. It is also capable of performing simulations on multiple battery designs for comparison and optimization. In addition, it includes a module that calculates battery costs by combining material and component costs with manufacturing expenses based on a plant design. A publically available version of this work, called the battery performance and cost (BatPaC) model, represents the only such public domain model capturing the interplay between design and cost of lithium-ion batteries for transportation applications.

Electrochemical modeling is aimed at associating electrochemical performance measurements with diagnostic studies of lithium-ion cells. The methodology for the electrochemical model is described in detail in literature [1-3]. Essentially, continuum-based transport equations are combined with kinetic and thermodynamic relations to allow the potential, concentration, and current distributions to be calculated throughout the cell. Two versions of the cell electrochemical model with the same basis are utilized to fully examine the broad range of electrochemical studies. One version of the model is used to simulate the cell response from Electrochemical Impedance Spectroscopy (EIS) studies, and the other for examining DC studies, such as controlled current or power cycling and diagnostic HPPC tests.

### Approach

The general approach used in this effort is to start small and grow large in terms of cell size and amount of resources devoted to each novel battery material. At various points in the development process, decisions are made to either advance, modify, or terminate studies to maximize utilization of available resources.

Coin cells (2032 size) are used for materials validation purposes with initial studies performed at room temperature or 30°C. After formation cycles, the coin cells go through hybrid pulse power characterization (HPPC) testing, rate capability testing, and limited cycle life testing. Accelerated aging studies are also performed at 45°C to 55°C for promising materials to obtain a preliminary estimate of life. Where appropriate, thermal abuse response is studied using a differential scanning calorimeter.

Using the recommendations and results obtained by the materials validation of promising materials, single-sided electrodes are fabricated on the larger dry-room coater for a diagnostic study. The new cell chemistries are studied in detail using advanced electrochemical and analytical techniques, including micro-reference electrode cells. Factors are identified that determine cell performance and its degradation (capacity fade, impedance rise) on storage and on extensive deep-discharge cycling. Results of these tests are used to formulate data-driven recommendations to improve the electrochemical performance/life of materials and electrodes to be incorporated in the prototype cells later fabricated in the dry room. This information also lays the foundation for electrochemical modeling focused on correlating the electrochemical and analytical studies to identify performance limitations and aging mechanisms.

The approach for electrochemical modeling activities is to build on earlier successful characterization and modeling studies extending those to new PEV technologies. The earlier studies involved developing a model based on the analytical diagnostic studies, establishing model parameters, and conducting parametric studies with the model. The parametric studies were conducted to gain confidence with the model, examine degradation mechanisms, and analyze cell limitations. Efforts are ongoing to expand and improve the model's capabilities with the focus on LMR-NMC active material cathodes, and eventually silicon-graphite composite electrodes.

In addition, the battery design spreadsheet model (BatPac) is used to determine the impact of advanced materials on the current technology. The performance of the materials within the battery directly affects the

end energy density and cost of the integrated battery pack. Both modeling efforts complement each other and are specifically aimed at supporting the CAMP Facility goals.

If the results from diagnostics and modeling still look promising, full cell builds are conducted using double-sided electrodes. The electrodes are then either punched (in the case of pouch cells) or slit (in the case of 18650 cells) and assembled into full cells in the dry room using the semi-automated cell assembly equipment. Formation procedures are conducted on the cells to encourage electrolyte wetting and solid-electrolyte-interface (SEI) formation. These cells undergo rigorous electrochemical evaluation and aging studies under the combined effort of the CAMP Facility team, and Argonne's Electrochemical Analysis and Diagnostic Laboratory (EADL) and Post-Test Facility. After testing, select cells are destructively examined by the Post-Test Facility to elucidate failure mechanisms. This information is then used to further improve the new chemistry, as well as future electrode and cell builds. The results of these tests are shared with other members of the ABR & BATT Programs and to the materials origin, and to battery developers (when practical).

## Results

The following progress was achieved:

### Silicon-containing Anodes: Electrode Development

Promising results from previous work in electrode development was utilized heavily in the fabrication of silicon-containing anodes for FY 15. The key factors for making robust and high integrity electrodes with >3 mAh/cm$^2$, previously highlighted in FY 14, were the silicon size and source, graphite type, binder type, mixing procedure, coating parameters, and flexibility testing. This experience and approach increased the CAMP Facility's ability and effectiveness to fabricate electrodes for various experiments.

This year's effort in silicon-containing anodes continued to utilize Li-PAA as the binder (partially lithiated poly(acrylic acid) and silicon from Nanostructured and Amorphous Materials Incorporated (NanoAmor) at 50-70 nm particle size. Silicon-containing anodes were fabricated with various amounts of silicon content (0 wt.%, 5 wt.%, 10 wt.%, and 15 wt.%) to evaluate the impact on cycling performance. Electrodes were fabricated for both multilayer and single layer xx3450 pouch cells, as well as coin cell studies. These electrodes were also entered into the CAMP Facility's Electrode Library (see Table IV- 1).

The Si component increased electrode capacity as expected (Figure IV- 1). This, however, resulted in voltage hysteresis and slow electrode kinetics. There is a strong correlation between plateaus in Si-Gr and Gr electrodes. The influence of LiPAA was also investigated by comparing cells made with PVDF and LiPAA for with only graphite as the active material. It was found that the use of LiPAA as binder does not significantly change the graphite's capacity or voltage profile (see Figure IV- 1, Figure IV- 2, and Table IV- 2).

Silicon-based electrodes were also fabricated and evaluated in partnership with the Materials Engineering Research Facility (MERF) by using conductive binders they scaled up for evaluation of silicon performance. These conductive binders were developed based on the work of Gao Liu of LBNL. Electrode development proceeded with these materials and alternative routes of "pre-coating" the conductive binders on the silicon particles were also explored. This work is still ongoing.

**Table IV- 1: Electrodes fabricated for the Electrode Library in order to perform silicon-based electrode studies using varying amount of silicon content**

| | 0% silicon-based anode | 5% silicon-based anode | 10% silicon-based anode | 15% silicon-based anode | 15% silicon-based anode |
|---|---|---|---|---|---|
| Electrode Library ID | A-A007 | A-A009 | A-A008 | A-A006 | A-A006A |
| Silicon powder | - | NanoAmor, 50-70 nm particle size | NanoAmor, 50-70 nm particle size | NanoAmor, 50-70 nm particle size | NanoAmor, 50-70 nm particle size |
| Graphite powder | Hitachi MAGE | Hitachi MAGE | Hitachi MAGE | Hitachi MAGE | Hitachi MAGE |
| Binder | Kureha 9300 PVDF | Sigma Aldrich PAA 450,000 m.w., pre-titrated with $LiOH•H_2O$ | Sigma Aldrich PAA 450,000 m.w., pre-titrated with $LiOH•H_2O$ | Sigma Aldrich PAA 450,000 m.w., pre-titrated with $LiOH•H_2O$ | Sigma Aldrich PAA 450,000 m.w., pre-titrated with $LiOH•H_2O$ |
| Compositions (dry wt.%) | **0** / 91.83 / 2 / 6 / 0.17 Si / Gr / carbon black / PVDF / oxalic acid | **5** / 83 / 2 / 10 Si / Gr / carbon black / LiPAA | **10** / 83 / 2 / 10 Si / Gr / carbon black / LiPAA | **15** / 73 / 2 / 10 Si / Gr / carbon black / LiPAA | **15** / 73 / 2 / 10 Si / Gr / carbon black / LiPAA |
| Mixing method(s) | Retsch, Thinky | Retsch, Thinky | Retsch, Thinky | Polytron, Thinky | Retsch, Thinky |
| Coating Thickness - Single Side (µm) | 41 | 49 | 33 | 25 | 30 |
| Porosity (%) | 29.9 | 46.1 | 46.0 | 42.4 | 46.4 |
| Coating Density ($g/cm^3$) | 1.52 | 1.10 | 1.10 | 1.18 | 1.10 |
| Total Coating Loading ($mg/cm^2$) | 6.23 | 5.36 | 3.63 | 2.94 | 3.28 |

Investigations have been performed in collaboration with the Post Test Facility (PTF) to explore and try to better understand the failure mechanisms and characteristics of binders. Multiple samples of Li-PAA based electrodes made by the CAMP Facility have been delivered to PTF for analysis. Surface analysis is being performed by PTF on cycled silicon-graphite electrodes that they harvested from cells cycled in the CAMP Facility. It is clear from these activities that the MERF/CAMP/PTF partnership can speed the development of silicon-based electrodes and elucidate their failure mechanisms.

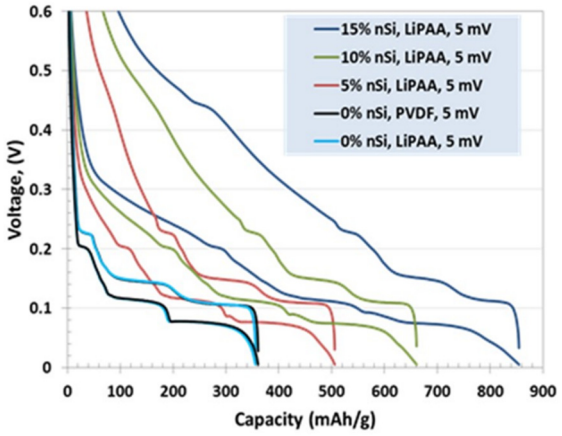


**Figure IV- 1: Representative lithiation and delithiation voltage profiles of Li//various silicon content Si-Gr coin cells at room temperature. The cells were cycled from at ~C/10 from 1.5 to 0.005V (LCV) using the electrolyte 1.2 M $LiPF_6$ in EC:EMC (3:7 wt.%) with 10 wt.% FEC additive**

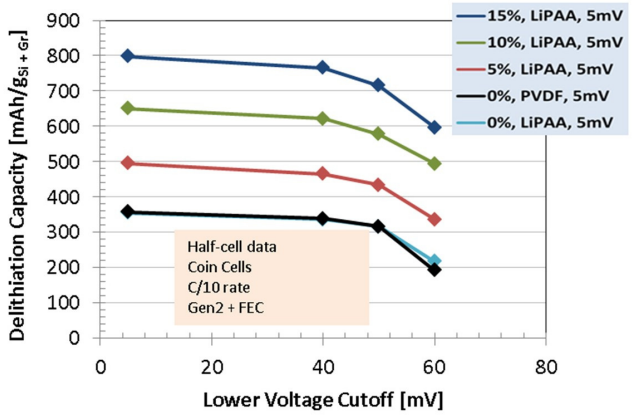


**Figure IV- 2: Representative delithiation capacities of Li//Si-Gr coin cells at room temperature. The cells were cycled from at ~C/10 from 1.5V to various lower voltage cutoffs (LCV)**

**Table IV- 2: Capacity values for varyings amount of silicon content in electrodes at different lower cutoff voltages (LCV). Refer to the prior table for composition and material information**

| Lower Cutoff Voltages (LCV) | 0% silicon-based anode (PVDF) [mAh/g] | 0% silicon-based anode (LiPAA) [mAh/g] | 5% silicon-based anode [mAh/g] | 10% silicon-based anode [mAh/g] | 15% silicon-based anode [mAh/g] |
|---|---|---|---|---|---|
| **60 mV** | 192 | 217 | 337 | 494 | 597 |
| **50 mV** | 316 | 316 | 434 | 578 | 716 |
| **40 mV** | 339 | 337 | 465 | 621 | 766 |
| **5 mV** | 357 | 355 | 495 | 650 | 798 |

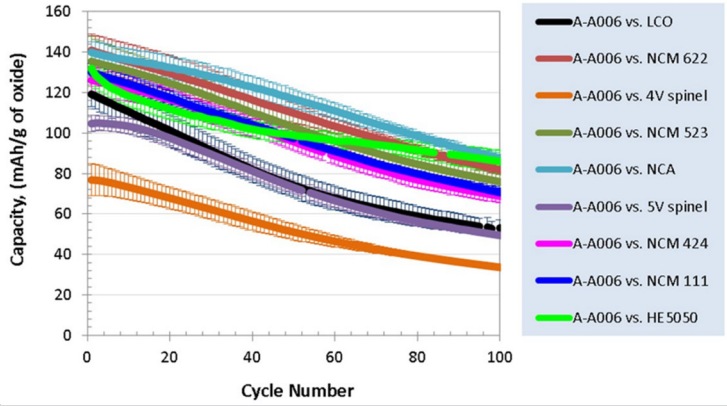


**Figure IV- 3: Average cycling performance of various positive electrodes//Si-Gr coin cells at room temperature, following the initial formation procedure. The cells were cycled from 3.0 to 4.1V at a C/5, with the exceptions of 5V spinel (3.5 to 4.7V) and HE5050 (3.0 to 4.4V). The error bars represent 2σ standard deviation**

### Silicon-containing Anodes: Coin Cell Scoping Experiments

Investigations were performed in full coin cells of various cathodes in the Electrode Library versus the A-A006 silicon-containing anode (see Table IV-1). The testing was performed to evaluate the impact that the cathode material may have on the overall cycling performance. The materials included: NCA, NCM111, NCM424, NCM523, NCM622, HE5050 (LMR-NMC), LCO, 4V spinel, and 5V spinel. The cycling testing revealed that the top performing cathode material when tested against the A-A006 silicon-containing anode was NCA (see Figure IV- 3). However, even this cathode experienced a significant capacity fade. The various NCM electrodes were the second best performing group. It was clear from this study that none of the cathodes studied here will improve the performance of silicon – the problem lies with the silicon.

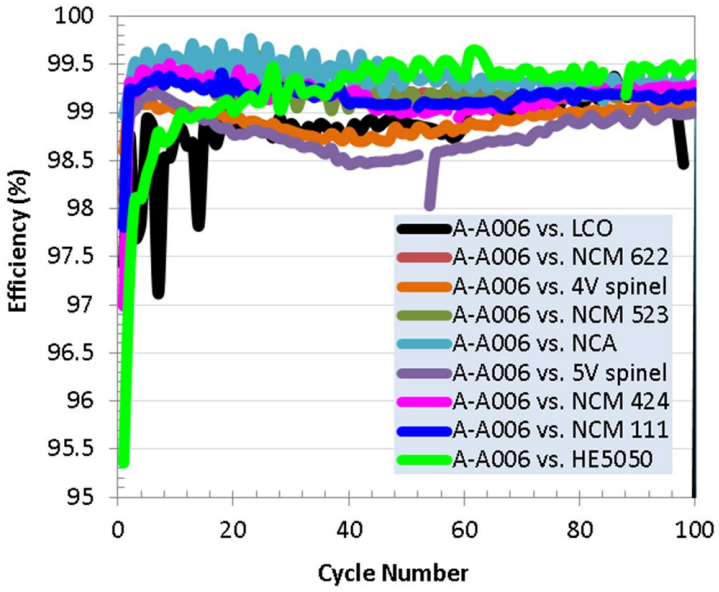


**Figure IV- 4: Average coulombic efficiency during cycling of various positive electrodes//Si-Gr coin cells at room temperature, following the formation procedure (see plot above). The cells were cycled from 3.0 to 4.1V at a C/5, with the exceptions of 5V spinel (3.5 to 4.7V) and HE5050 (3.0 to 4.4V). Error bars not included**

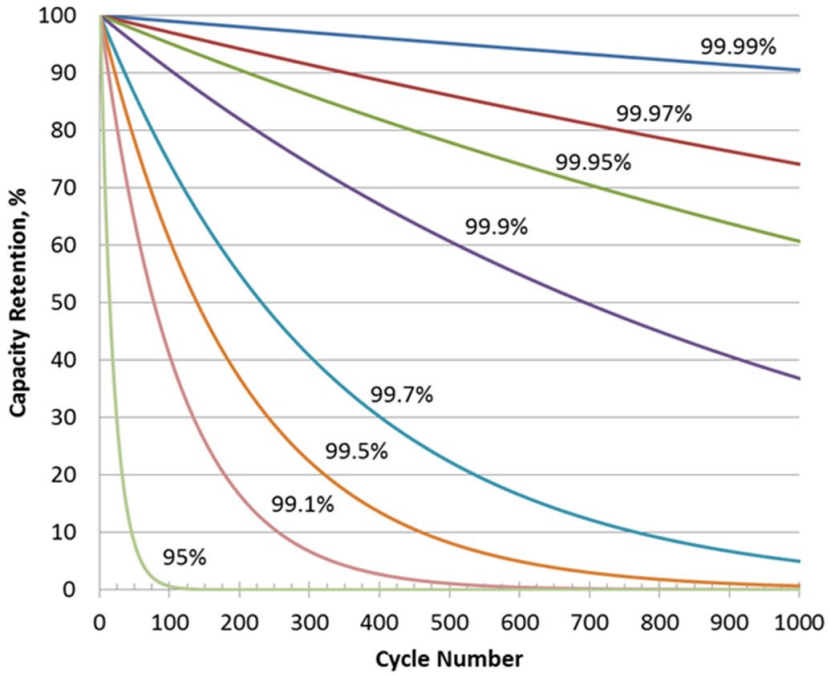


Figure IV- 5: Simple modeling plot showing the capacity rention based on various coulombic efficiencies during cycling of a hypothetical cell

The poor performance of silicon-based cells can be attributed to its poor coulombic efficiency. Graphite-only based electrodes are able to approach 99.99% coulombic efficiency. Silicon-containing electrodes achieve commonly around 99.5% coulombic efficiency (Figure IV- 4). The relative slight difference yields drastically different cycle life performance (Figure IV- 5). This poor coulombic efficiency can be attributed to the large volume expansion of the silicon particle upon lithiation, which tears the SEI layer and causes repeated electrolyte decomposition on every charge. Ideally, the combination of materials used, electrolyte additives, surface treatments, functional binders, and possibly other factors could be discovered or processed in a way to bring the silicon-based system up to 99.99% coulomic effiency.

Tests were also performed to evaluate the shelf life and quality of two fluoroethylene carbonate samples using the A-A006 anode and counter NCM523 cathode. The experiments looked to investigate different vendors ($F_1$EC vs. $F_2$EC), and shelf life of $F_1$EC, against a baseline electrolyte with no FEC additives present. The samples tested were:

- "Gen2 only", 1.2M $LiPF_6$ in EC:EMC (3:7 wt.%)
- "$F_1$EC, A, stored stock, old mix", 90wt.% Gen2 + 10wt.% $F_1$EC VenderA, 2 yr old container, 1 month old mixture
- "$F_1$EC, A, stored stock, fresh mix", 90wt.% Gen2 + 10wt.% $F_1$EC VenderA, 2 yr old container, fresh mixture
- "$F_1$EC, A, fresh stock, fresh mix", 90wt.% Gen2 + 10wt.% $F_1$EC VenderA, fresh container, fresh mixture container, fresh mixture
- "$F_2$EC, A, fresh stock, fresh mix", 90wt.% Gen2 + 10wt.% $F_2$EC VenderA, fresh container, fresh mixture container, fresh mixture
- "$F_1$EC, B, fresh stock, fresh mix", 90wt.% Gen2 + 10wt.% $F_1$EC VenderB, fresh container, fresh mixture

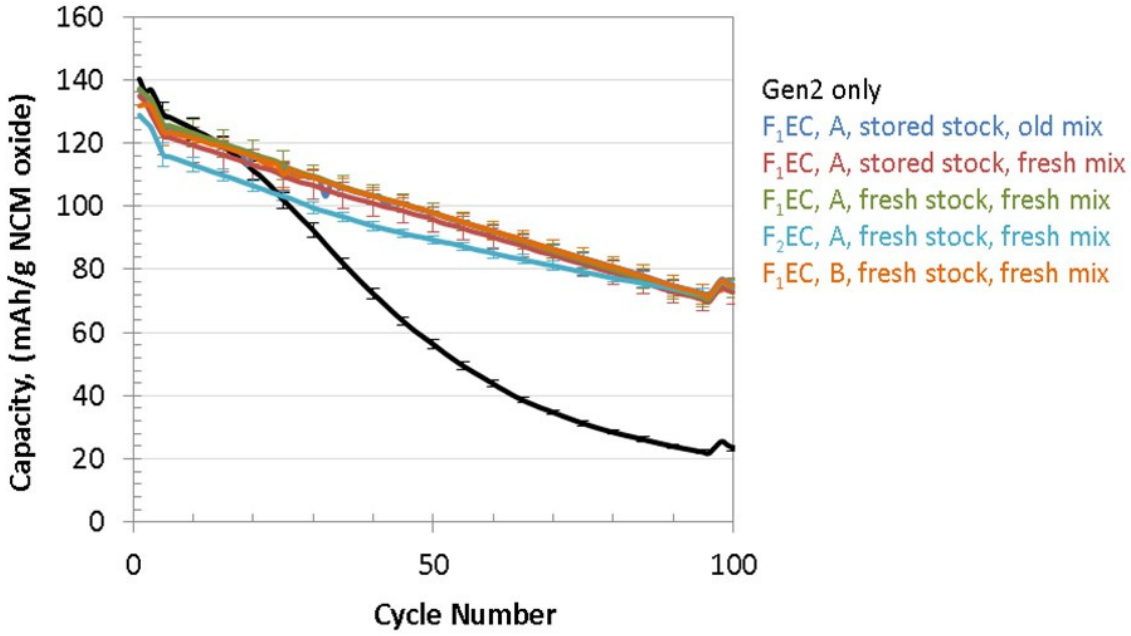


**Figure IV- 6: Average cycling performance of NCM523//Si-Gr coin cells at room temperature. The cells were cycled from 3.0 to 4.1V at a C/3 rate with RPT's (C/24 cycle and HPPC) occurring at the beginning and at cycle 97. The error bars represent 2σ standard deviation**

The results showed that there were no significant differences between the $F_1EC$ samples. It was especially reassuring that the FEC did not degrade in the original container over the two year period and it did not degrade during the month it was mixed with the stock electrolyte. The vendor source and electrolyte preparation/storage experiments yielded similar cycling (see Figure IV- 6 and Figure IV- 7) and impedance performance (Figure IV- 8). The $F_2EC$ electrolyte showed an initial slight decrease in capacity during the cycling test, but similar efficiency and impedance behavior.

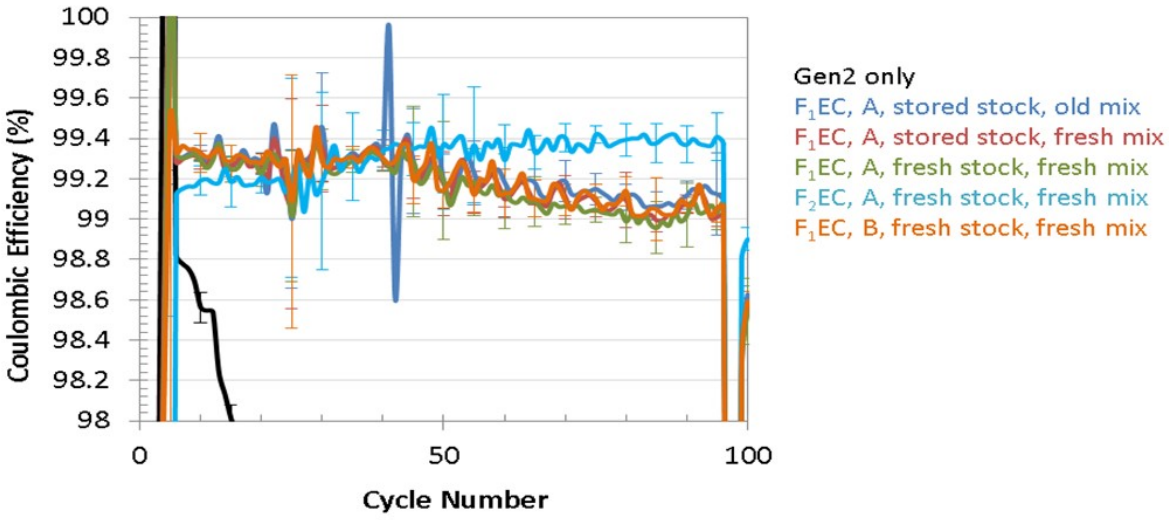


**Figure IV- 7: Average coulombic efficiency during cycling (see the prior figure) of NCM523//Si-Gr coin cells at room temperature. Error bars represent 2σ standard deviation**

From this study, it was concluded that the poor coulombic efficiency of the silicon-based electrodes was due to the quality of the FEC electrolyte additive.

### Silicon-containing Anodes: xx3450 Pouch Cell Builds

Multilayer xx3450 pouch cells have been fabricated and evaluated to test various parameters using 1.2 M $LiPF_6$ in EC:EMC (3:7 wt.%) with 10 wt.% FEC additive. The electrodes used in these pouch cells are

described in Figure IV- 9. The results the cycle life tests is summarized in Figure IV- 10, which includes cell data from the previous year for comparison. The "5wt.%" and "MagE" series were cell builds fabricated and tested in FY15.

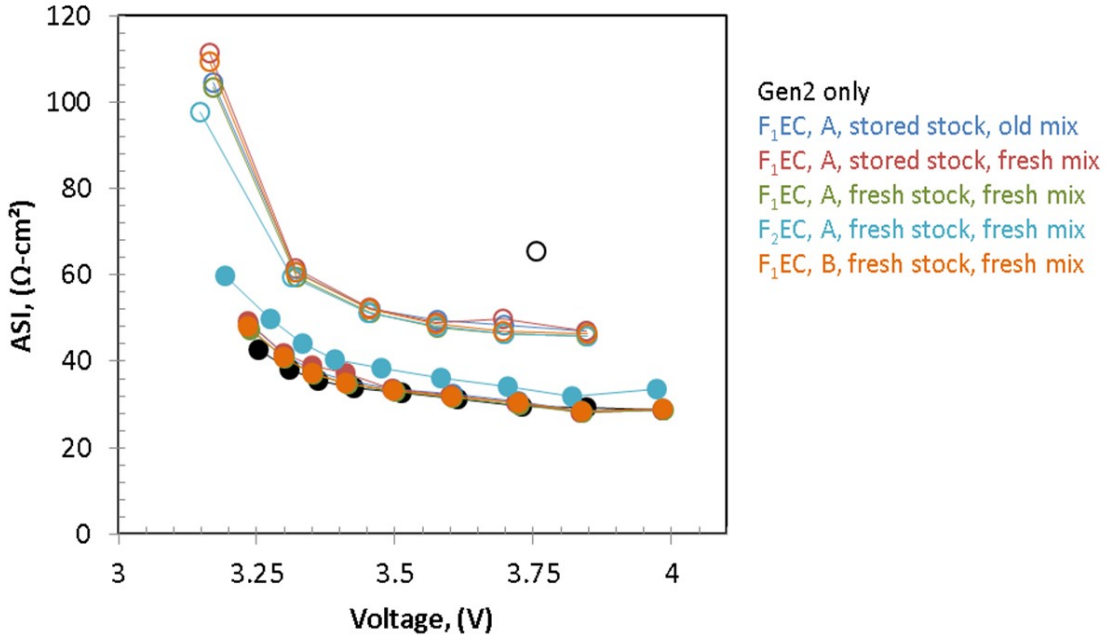


**Figure IV- 8: Representative area specific impedance (ASI) vs. cell voltage for NCM523//Si-Gr coin cells at room temperature, before (filled symbols) and after (open symbols) aging cycles. The ASI data shown were obtained with a 3C discharge pulse**

The "Reform-1, Si-Gr" used 15 wt.% of silicon in the anode and was fabricated using a composition of silicon-graphite blended with a lithiated PAA binder (450,000 m.w.). The capacity loading of this anode was 3.7 mAh/cm$^2$ capacity. Mixing was performed using the Retsch planetary ball mixer to break up agglomerates.

The "Reform-2, Si-Gr" used 5 wt.% of silicon in the anode and was fabricated in a manner very similar to "Reform-1, Si-Gr" so that a direct comparison could be made. The capacity loading of this anode was also 3.7 mAh/cm$^2$. The "Baseline-2" used 0 wt.% silicon and also MagE graphite, but it used PVDF binder instead of LiPAA. This cell build was designed to show the best performance possible for the MagE graphite with a traditional PVDF binder. Future plans are to make a cell build using 0 wt.% silicon and LiPAA as the binder, and another cell build using 10 wt.% silicon and LiPAA binder. This will complete the study based on 50-70 nm silicon, which is no longer available from NanoAmor (they replaced this product with 30-50 nm silicon powder).

From the data summarized in Figure IV- 10 and Figure IV- 11, it is clear that despite the creation of a mechanically robust silicon-graphite electrode and an FEC electrolyte additive, the cycle life is severely limited due to poor coulombic efficiency. However, as expected, using less silicon in the electrode delays the capacity fade.

The coulombic efficiency for silicon-containing electrodes continues to show an approximate maximum values of 99.5%, which again suggests the continued need for advancements in materials and electrode development centered on the silicon-to-electrolyte interface. The coulombic efficiency for all the silicon-containing electrodes show the same limitations, even with smaller amounts of silicon (5 wt.% vs. 15 wt.%).

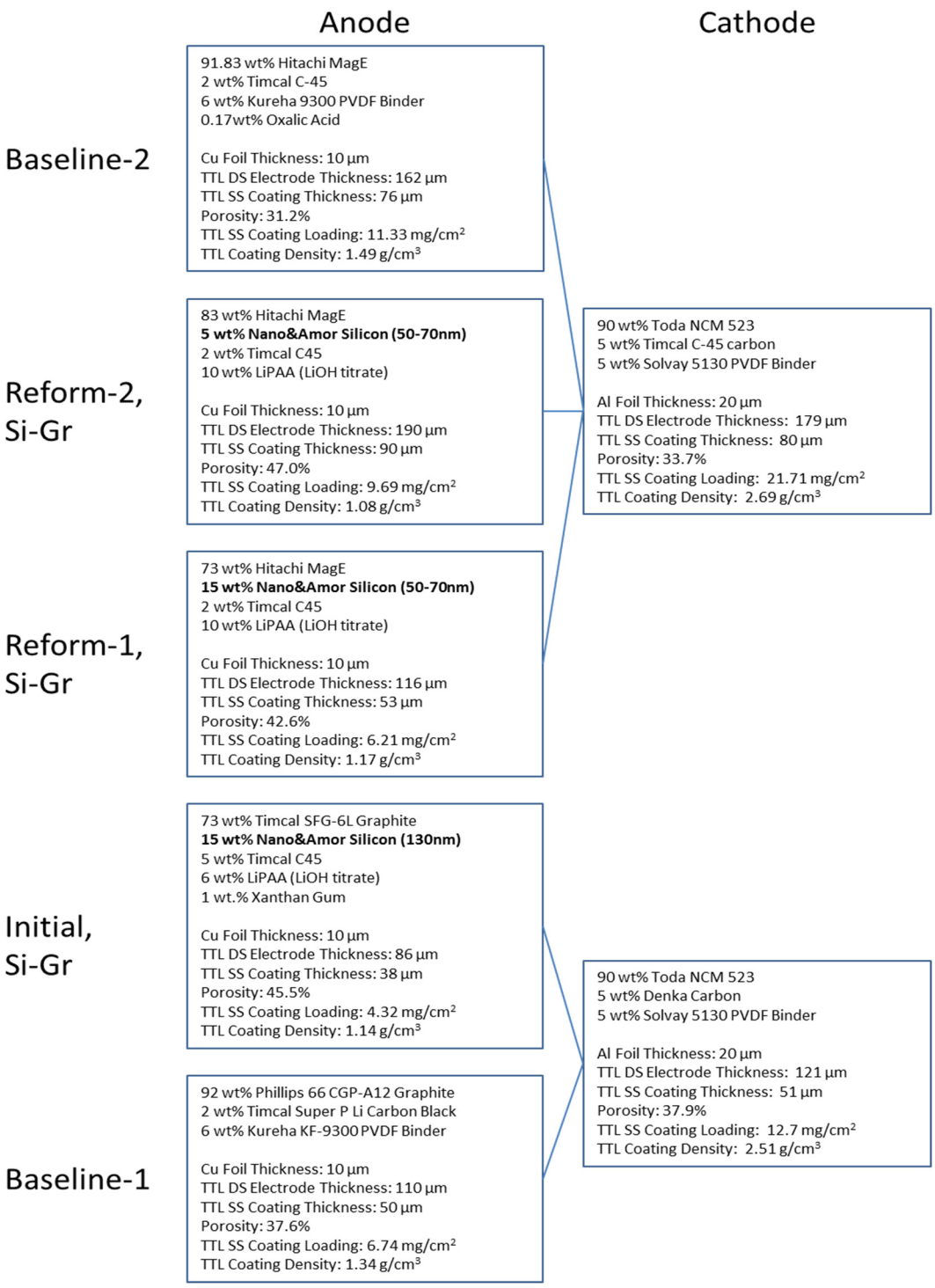


**Figure IV- 9: Anodes fabricated by the CAMP Facility and their matching cathode couple for xx3450 pouch cell evaluation. Refer to the nomenclature on the left for reference to the figures that follow**

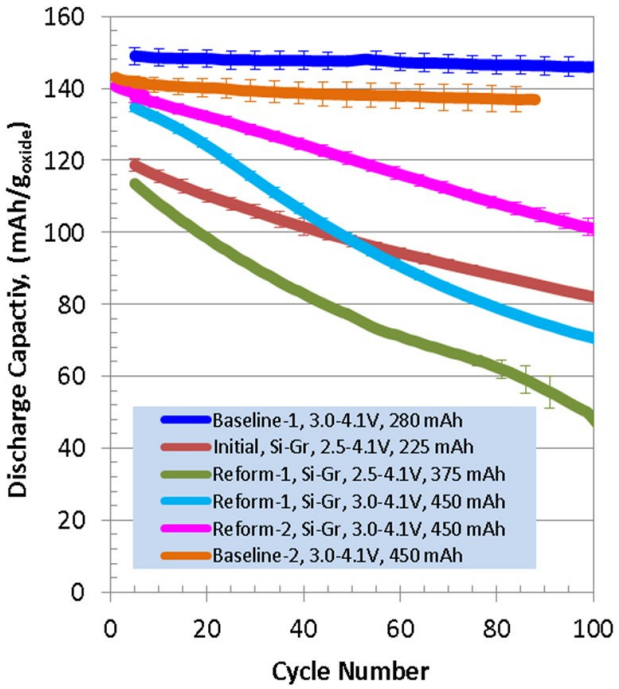


Figure IV- 10: Average cycling performance of various generations of the NCM523//Si-Gr xx3450 pouch cells at 30°C, with complementary NCM523//Gr xx3450 pouch cells representing baseline data, following the initial formation procedure. The cells were cycled at a ~C/3 rate. The error bars represent 2σ standard deviation

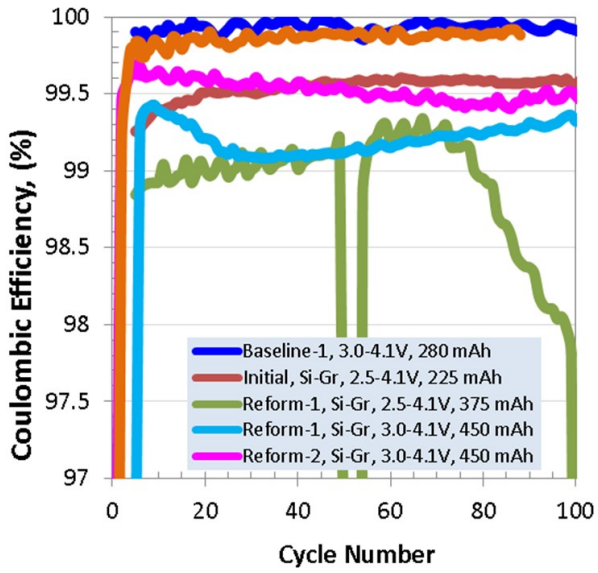


Figure IV- 11: Average coulombic efficiency of various generations of the NCM523//Si-Gr xx3450 pouch cells at 30°C, with complementary NCM523//Gr xx3450 pouch cells representing baseline data, following the initial formation procedure. The cells were cycled at a ~C/3 rate

### Electrode Swelling Study

Concern exists regarding the effect silicon particle has on the negative electrode and on the overall cell thickness. Cell manufacturers often have to design their cells under a 5 to 10% volume expansion constraint. A study was designed to determine the influence of silicon content on electrode swelling using single-sided silicon-graphite electrodes from the electrode library in single-layer pouch cells. Multiple cells of each silicon content were cycled for three cycles and then stopped at various states of charge. The electrodes were then harvested in a dry room, rinsed with DMC, photographed, and thickness measured with a micrometer after air drying. The photos (see Figure IV- 12) of the electrodes reveal the brass color of the lithiated anode, which is expected.

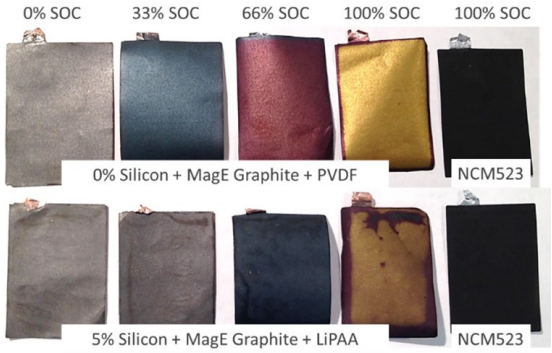


Figure IV- 12: Photo of electrodes from xx3450 pouch cells that have been disassembled in various states of charges (SOC). The top row is from graphite only electrodes with PVDF binder. The bottom is from 5wt.% silicon-based electrode with LiPAA binder. The electrodes to the far right are representative cathodes

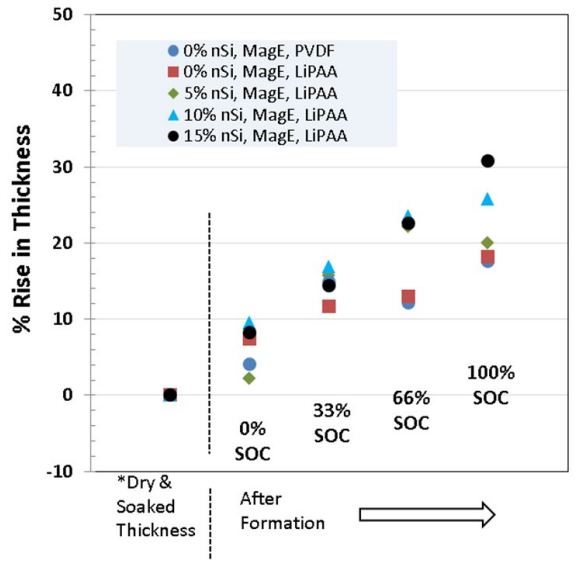


**Figure IV- 13: Summary of electrode thickness changes as a function of state of charge for various electrodes with differing amounts of silicon present in the electrode**

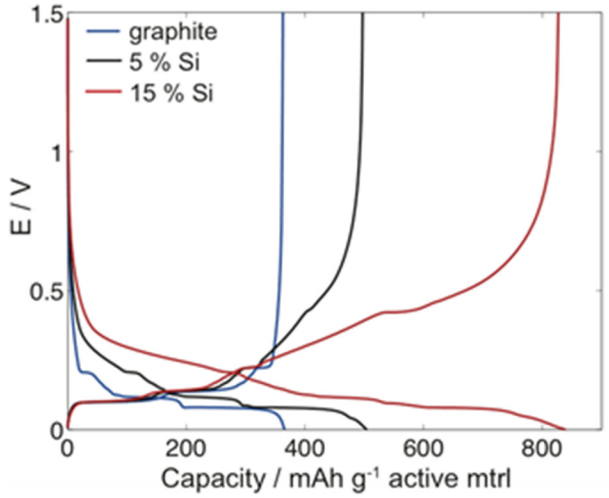


**Figure IV- 14: Third cycle capacity (1.5-0.0 V) per g of active material for graphite-Si (0-15 wt%) electrodes as measured with a 0.085 mA-cm-2 current in coin cells with a Li-metal counter electrode and Gen2 + 10 % FEC electrolyte. Silicon, graphite, and C-45 are included in the active material weight**

The measured values for the various SOC anodes are reported in Figure IV- 13. The NCM523 cathodes did not show noteable changes in thicknesses.

Having even small amounts (5 wt.%) of silicon in the electrode resulted in a significant increase in electrode thickness (except at 100% SOC), when compared to the graphite only electrodes. The largest% rise in thickness was for the 15 wt.% silicon at 100% SOC, and slightly lower for the 10 wt.%. Swelling in the 5 wt.% electrode was similar to the higher content silicon electrodes, except at 100% SOC where it was similar to graphite. This electrode swelling is an important factor to understand for final cell and pack design that has specified tolerances. In addition, it is anticipated that the swelling will continue to increase as the electrode is cycled over hundreds of cycles – the extent to which is still under investigation.

### Silicon-Graphite Anodes – Two Reference Electrode Set-up

In the continuing effort to develop functioning electrochemical couples with Si-containing electrodes as a drop-in replacement for the standard graphite electrode, variables such as electrode composition, electrolyte composition, and voltage windows have been probed and are described in the following sections. Tests have been performed in several set-ups; coin cells with the objective of faster screening of multiple variables, and a reference electrode (RE) setup, which allows for the separate characterization of positive and negative electrodes in a full cell setting. In previous years, a $Li_xSn_y$ micro-RE has been used for impedance measurements; here, the micro-reference electrode is placed in between two separators in the center of the positive/negative electrode stack. Due to its central position, this micro-RE can be favorably used for impedance measurement, but the $Li_xSn_y$ alloy potential is metastable and has the drawback of being unstable with time. This past year, an additional Li-metal RE, placed at the edge of the electrode stack, has been introduced in the cell set-up. This RE provides a stable and constant rest potential. Together, the reference electrodes provide valuable information: the $Li_xSn_y$ RE is used for AC and DC impedance measurements while the Li-metal RE provides accurate electrode rest potentials and good approximations of electrode potentials at low currents.

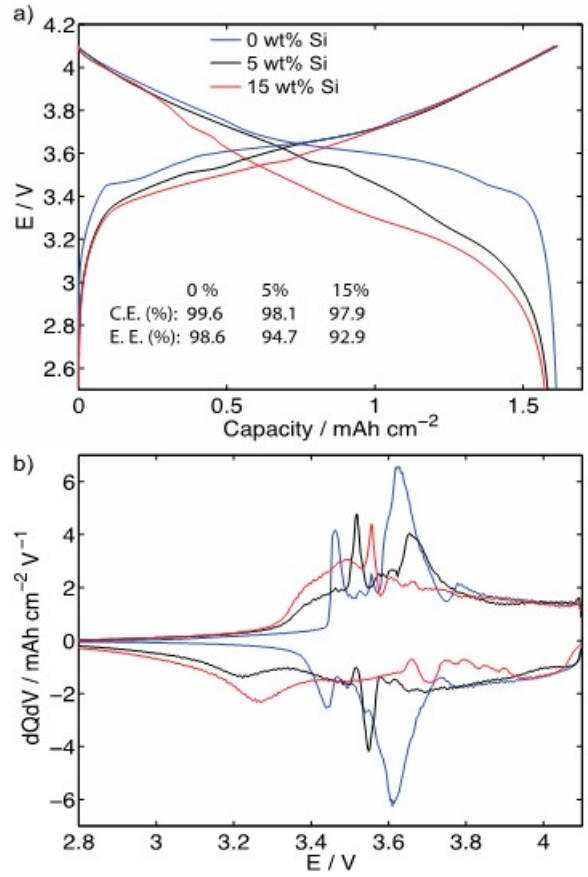


**Figure IV- 15: Plots from graphite-Si//NCM523 full cells with Gen2 + 10% FEC electrolyte cycled between 2.5 and 4.1 V and 0.05 mA cm-2 current (~C/20 rate) for 0-15 wt% Si-content. The (a) charge-discharge profiles, and (b) differential capacity plots as a function of cell voltage shown, are from the second cycle**

lithiation/delithiation. Therefore, both energy efficiency (E.E.) and coulombic efficiency (C.E.) decrease with increasing Si-content.

Cell impedance is also affected by the introduction of Si to the graphite negative electrode. The kinetics of Si has been described as more sluggish than graphite, often with lower reported diffusion coefficients for lithium. However, in these porous electrodes containing nano-sized silicon in a mixture with graphite, the negative electrode impedance is comparable to that of graphite at higher full cell voltages (i.e. low anode voltages) (Figure IV- 16). In this voltage range, the graphite and silicon potentials overlap in the mixed electrode. Figure IV- 16 compares the impedance after formation cycling of cells with 0 and 15 wt.% Si. At lower full cell voltages (<3.7 V) the impedance of the Si-containing electrode diverges from the graphite to higher values. The measurements using the RE setup here provide clear distinctions between the electrodes, and the graphite-Si and graphite electrode behavior can be

### Effect of silicon content in mixed Si-graphite electrodes

When compared to graphite, the large volume expansion of silicon during lithiation causes issues of electrode stability and lithium consumption during SEI formation and continuous side reactions. With the addition of nano-sized silicon to the graphite electrode the initial specific capacity of the electrode increases (Figure IV- 14), but the cyclability could be expected to correlate negatively with silicon content, especially in full cells. Initial performance and capacity retention upon cycling in full cells have been measured to investigate the incremental change in performance as the Si-content is increased from 0 to 15 wt.%.

Several observations of the cell potential characteristics, examined in the 2.5 - 4.1 V voltage window (Figure IV- 15), can be made, as follows: (i) the silicon addition lowers the average cell voltage, due to the higher potential of lithium alloying in silicon compared to graphite lithiation (Figure IV- 14). Still, the specific energy density, based on the weight of the negative electrode active material, increases with both 5 and 15 wt.% Si content.

(ii) Even though, the decrease in average cell voltage is seen both during cell charge and discharge, the voltage drop is particularly significant during cell discharge because of the intrinsic voltage hysteresis associated with Si

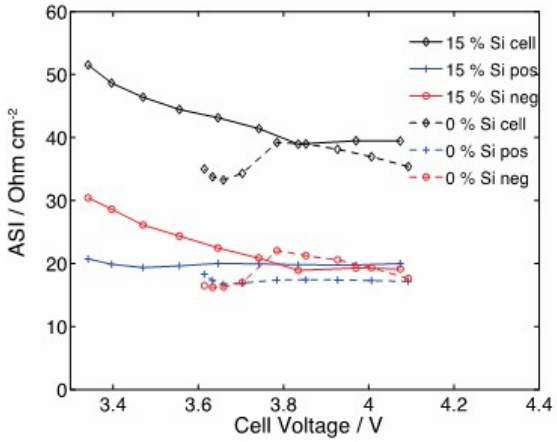


**Figure IV- 16: HPPC test data from full cells with either the mixed graphite-15 wt% Si electrode (15 wt% Si) or graphite-only electrode (0 wt% Si), NCM523 positive electrode, and Gen2 + 10 wt% FEC electrolyte. The data were measured in a three-electrode setup, and deconvolutes contributions from the positive and negative electrodes to the full cell impedance, after formation cycling**

compared directly in a full cell. Such comparisons will be used to characterize the electrochemistry and kinetics of Si-bearing graphite electrodes in future efforts.

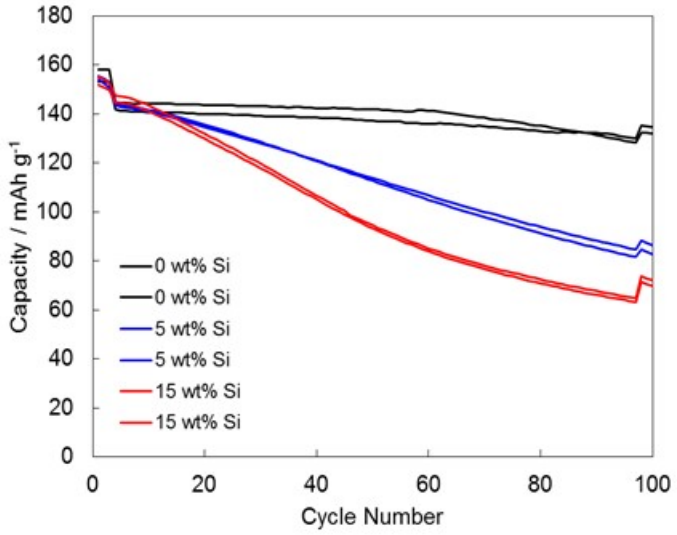


**Figure IV- 17: Capacity as a function of cycle number of Si-graphite // NCM523 full cells (0-15 wt% Si) with Gen2 + 10% FEC electrolyte, cycled in a 2.5-4.1 V voltage window using 0.05 mA cm-2 (~C/20, first 3 and last 3 cycles) and 0.33 mA cm-2 (C/3, intermediate cycles) currents. The specific capacity refers to g of the oxide active material. Data shown are from duplicate cells prepared from each electrode**

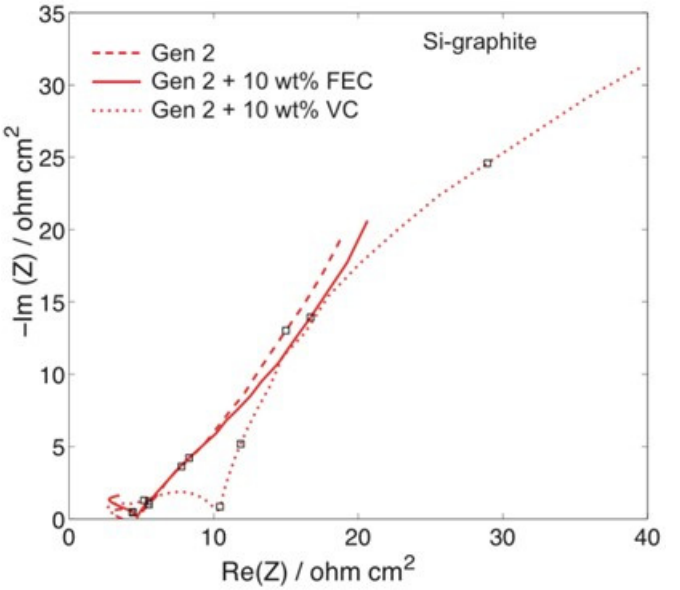


**Figure IV- 18: AC impedance spectra after formation cycling for 15 wt% Si-graphite electrodes, obtained with a LixSny micro-reference electrode, in cells containing different electrolyte compositions**

Cycling performance was evaluated in the 2.5-4.1 V voltage range, at an approximately C/3 rate (Figure IV- 17). As expected, there is a correlation between the amount of silicon and the capacity retention: cells with the 15 wt.% Si electrode show quicker capacity fade than cells with the 0 and 5 wt% Si electrodes. Note that the divergences in capacities between cells containing 0 and 5 wt.% Si are larger than those containing 5 and 15 wt.% Si. That is, the capacity fade is not a linear function of Si content in the electrodes.

### Effect of Electrolyte Composition on Performance in Silicon-containing Cells

FEC (fluoroethylene carbonate) and VC (vinylene carbonate) are common additives in both graphite and silicon-containing lithium-ion cells. However, compared to amounts commonly used in graphite-bearing cells, the amounts are generally higher in Si-containing cells. To determine an optimal content of these additives, and to examine similarities and differences between FEC and VC, we examined electrolytes addition of these compounds in the 2.5 to 20 wt.% range to the Gen2 (EC:EMC, 3:7 w/w + 1.2M $LiPF_6$) electrolyte.

The addition of VC and FEC lowered the initial capacity by a few percentage points in all cases compared to the pure Gen2 electrolyte. The initial impedance for the 10 wt% FEC cell was similar to that for the Gen2 cell, but was higher for the 10 wt.% VC cell. This increase for the VC cell could be attributed to the Si-graphite negative electrode. Measurements using the $Li_xSn_y$ micro-reference electrode showed an increase at mid-to-low frequencies in the AC impedance spectra of the negative electrode (Figure IV- 18), while the impedance of the NCM523-based electrode remained similar with both additives.

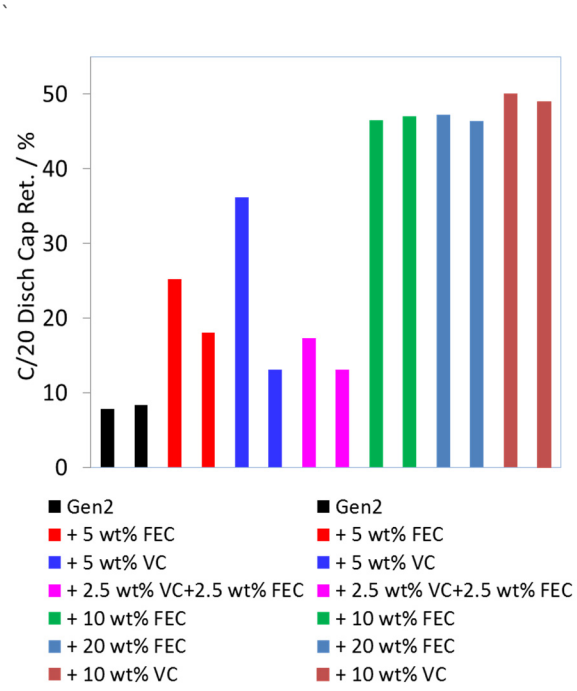


Figure IV- 19: Discharge capacity retention after 100 cycles for graphite-15 wt% Si // NCM523 cells, containing various electrolyte compositions, cycled in a 2.5-4.1 V voltage window. Data shown are from duplicate cells prepared for each electrolyte composition

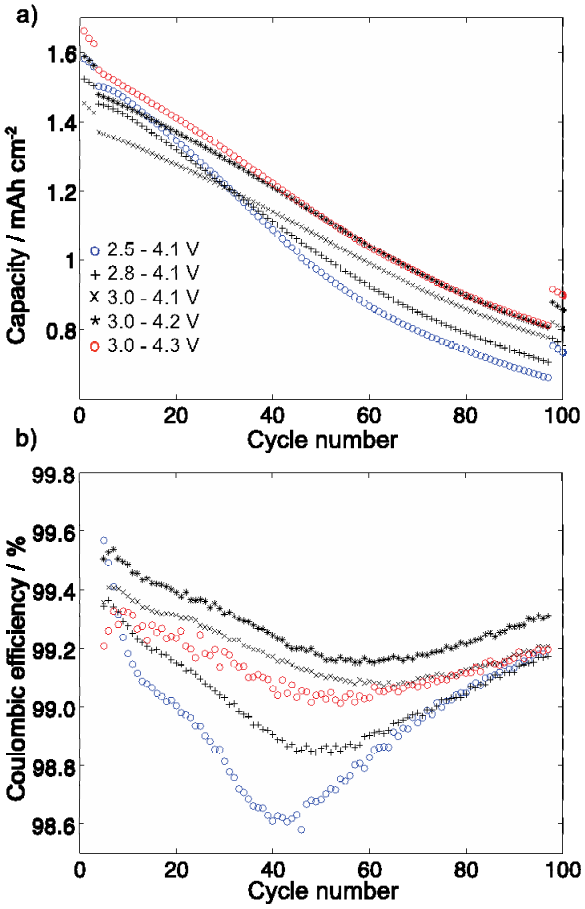


Figure IV- 20: Effect of cycling range on (a) discharge capacity and (b) coulombic efficiency, over 100 cycles for graphite-15 wt% Si // NCM523 cells containing Gen2 +10 wt% FEC electrolyte

Among the different electrolyte compositions, the addition of 10 wt% VC resulted in the best capacity retention after 100, 2.5-4.1 cycles, followed closely by 10 and 20 wt% FEC (Figure IV- 19). After an additional 100 cycles, the capacity retentions of cells with VC and FEC additives diverge further, with the VC cells showing the higher retention (data not shown). The lowest capacity retention was seen for cells with the pure Gen2 electrolyte (Figure IV- 20a), which retains less than 10% of its initial capacity. It is interesting to note that increasing the FEC addition from 10 to 20 wt.% did not result in an increased capacity retention. Furthermore, note that even our best performing cells lost approximately 50% capacity over the 100 cycles. Therefore, work continues to identify other electrolyte systems that could show a better performance (low capacity fade and impedance rise).

### Effect of Voltage-Cycling Windows on Performance in Silicon-Containing Cells

Various voltage windows were explored to optimize the cycle life of Si-containing cells. It is important to point out that the effect of voltage cutoff is strongly correlated to the electrode capacity matching or n-to-p capacity ratio of a given electrochemical couple. The matching will determine how high/low the individual electrodes reach in electrode potential at a specific cell voltage. In our experiments, the graphite-15 wt.% Si (A-A006) and NCM523 (C013) of the CAMP electrode library were screened to determine the cycling window. The initial voltage-cycling window was set between 2.5 and 4.1 V but it was clear that by increasing the lower cut-off potential to 3.0 V the capacity retention improved. The upper potential cut-off was then increased to maintain a cell capacity similar to that of the original voltage window, and the highest coulombic efficiencies were obtained when cycled between 3.0-4.2 V (Figure IV- 20b). Most notable is the increase in cycle life and coulombic efficiency when increasing the lower cutoff voltage from 2.5 V to 2.8 and 3.0 V

(Figure 20b). Measured in our RE-set-up, the electrode potentials of the NCM523 and Si-graphite electrode were monitored separately. In this reference cell data (Figure IV- 21) it can be seen that changing the full cell voltage from 2.5 V to 3.0 V results in a decrease of delithiation cut-off potential from 1.13 V to 0.69 V for the Si-graphite negative electrode. It is likely that high negative electrode potentials are detrimental to SEI stability, given that the SEI typically forms by the reduction potential of carbonate solvents at potentials less than ~0.8 V vs Li/Li$^+$. Increasing the lower cut-off voltage could hence mitigate SEI degradation and potential gas evolution, thereby yielding a better cycle-life.

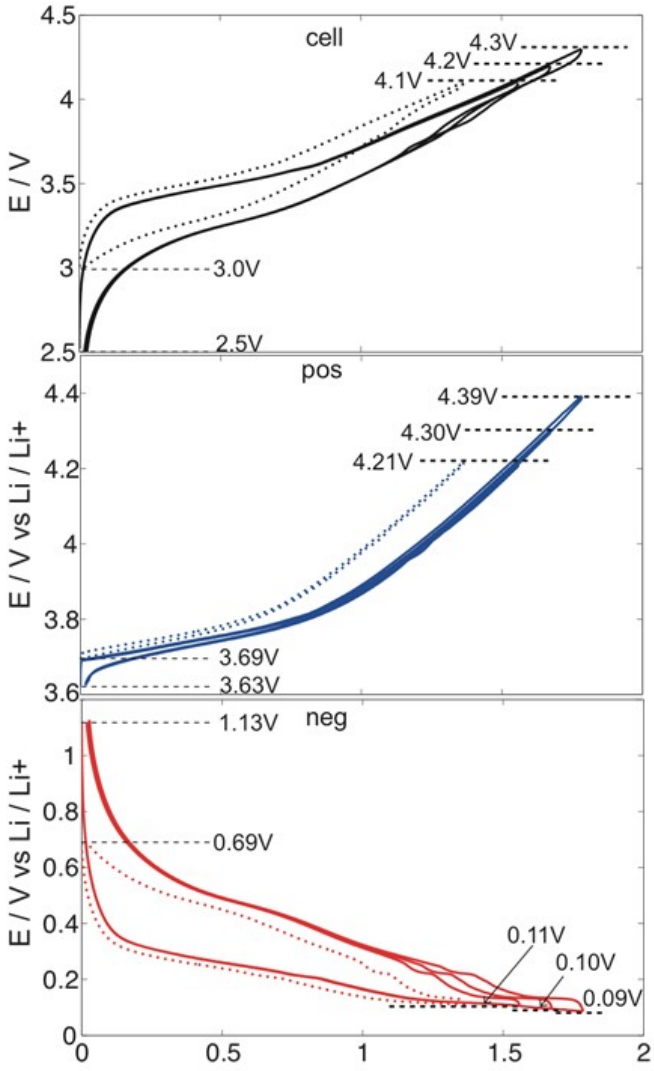


**Figure IV- 21: Full cell (top), positive electrode (middle), and negative electrode (bottom) potentials, obtained with a Li metal reference, from graphite-15 wt% Si // NCM523 cells with Gen2 + 10% FEC electrolyte cycled in various voltage windows (0.06 mAh cm² current)**

At the slow rate used in these measurements (~C/20), the Li-metal RE allows us to follow the electrode potentials, with the electrode potentials for a number of voltage windows as exemplified in Figure IV- 21. This feature has furthermore been used to compare the evolution of electrode potentials as the cell cycles. Such monitoring has allowed us to determine "electrode capacity slippage" and material utilization as the cells age. From cycling experiments on graphite-15 wt.% Si //NCM523 reference electrode cells containing Gen2, Gen2 + 10 wt.% FEC and Gen2 + 10 wt.% VC electrolytes, we have reached the following conclusions:

- Electrode slippage is observed in all the cells and is most severe for the Gen2 cells, which show a significant loss of capacity.
- The direction of electrode slippage relates to net reductive side reactions, which is in agreement with extensive lithium-consuming side reactions at the mixed graphite-15 wt% Si negative electrode.
- After 50 cycles between 3.0-4.2 V, the negative electrode does not see potentials below ~0.13-0.15 V; consequently only a small fraction of the graphite, which constitutes 73 wt.% of the electrode, is used.
- The loss of cyclable Si material loss can be directly gauged from the RE cell data, which show that the presence of either VC or FEC in the Gen2 electrolyte greatly reduces this loss.

Cell impedance is also found to increase as a result of electrochemical cycling. Area specific impedance (ASI) values, obtained with a 10-s discharge pulse on a Gen2 + 10 wt% FEC cell cycled in the 3.0-4.2 V range, are shown in Figure IV- 22. The NCM523-based positive electrode is the main contributor to the full cells impedance rise; the impedance of this electrode increases ~50% during the cycling across the cell voltage span. The increase in the Si-graphite impedance is seen only at low cell potentials and is a consequence of the electrode capacity shift described earlier. The graphite-15 wt% Si negative electrode impedance shows negligible changes with cycling; this result is interesting because it indicates that the SEI formed from the substantial reductive side reactions consuming cyclable lithium, does not significantly hinder the transport of lithium ions. This is an important reminder of how different design parameters of porous electrodes, including surface area and porosity, can determine the sensitivity to performance degradation factors, such as electrode surface films. Ongoing work includes the development of electrochemical models for

the graphite-silicon electrodes that can describe both the initial experimental data and the performance changes on cycling.

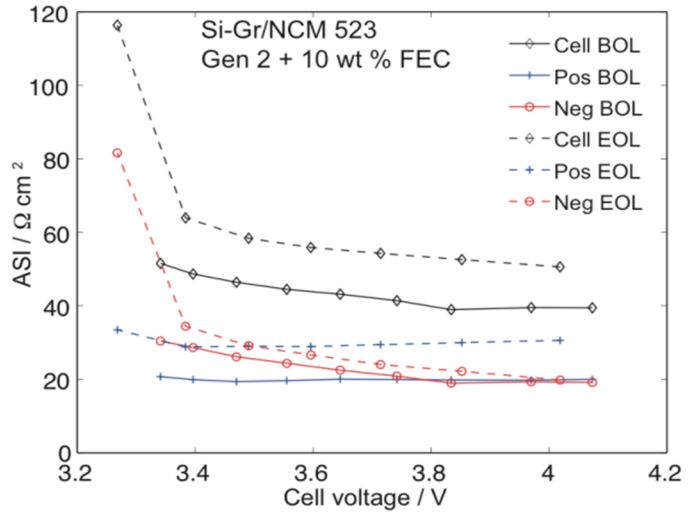


Figure IV- 22: 10-s discharge DC impedance as a function of cell voltage, before (BOL) and after (EOL) 50 cycles, from graphite-15 wt.% Si // NCM523 cells, measured with a $Li_xSn_y$ reference in a three-electrode setup

**Electrochemical Modeling**

This effort focuses on the development of electrochemical models to describe advanced electrodes, such as silicon-graphite negatives and cutting-edge NMC positives (e.g. LMR-NMC and high-nickel -voltage NMC). The electrochemical modeling studies rely heavily on experimental analytical and electrochemical diagnostic and characterization studies conducted by the CAMP Facility and across the Enabling High-Energy/Voltage Lithium-Ion Cells for Transportation Applications (HE-HV) program (see IV.C.1-3). Experimental data presented in this section are part of those efforts.

As the development of silicon-graphite negative electrodes has progressed within the CAMP Facility, likewise the framework for an electrochemical model of this electrode is progressing. A previously developed model for graphite electrodes that includes phase changes in the graphite during cycling forms the basis [1].

Even though silicon is typically a minor component of the electrode, its addition considerably improves capacity and adversely affects its behavior. This includes observed significant voltage hysteresis and volume change during cycling, as well as silicon/electrolyte interfacial instability resulting in an unacceptably low current efficiency. While these phenomena are interrelated, developing an electrochemical model that can track these effects during operation continues to be a challenge. There are a number of useful models already available in the literature, but to-date none have been found that describes all the observed pertinent phenomena. The silicon active material electrochemical model being developed relies on existing models, but also builds on previous modeling studies for active materials that go through a significant structural change during cycling. Key to this development is the concept that the structural change is driven by lithium concentration changes in the material, but is generally slower than the lithium diffusion. While this electrochemical modeling effort is still in the early stages of development, it shows considerable promise.

NMC-532 is one of a series of high-nickel NMCs that are promising cathode active materials capable of delivering more than 200mAh/g capacity as the electrode end-of-charge voltage is raised to greater than 4.5 volts vs lithium. This material is also one of the baseline active materials within the HE-HV program, tasked with pushing the lithium-ion cell technology to higher voltages. As part of an integrated effort with the HE-HV program an electrochemical modeling study of the NMC-532 positive electrode was initiated.

**Transport through Cell Sandwich**

$$\varepsilon\frac{\partial c}{\partial t}=\frac{\varepsilon}{\tau}\nabla\cdot(D\nabla c)+\frac{\nabla\cdot\left[\left(1-c\overline{V}_e\right)\left(1-t_+^o\right)\vec{i}_2\right]}{z_+\nu_+F}$$

$$\vec{i}_2=-\frac{\kappa\varepsilon}{\tau}\nabla\Phi_2-\nu RT\frac{\kappa\varepsilon}{F\tau}\left(\frac{s_+}{n\nu_+}+\frac{t_+^o}{z_+\nu_+}\right)\left(1+\frac{\partial\ln f_\pm}{\partial\ln c}\right)\nabla\ln c$$

$$\nabla\cdot\vec{i}_2=Fz_+aj_n \qquad \vec{i}_1+\vec{i}_2=\vec{I} \qquad \vec{i}_1=-\sigma_{eff}\nabla\Phi_1$$

**Bulk Solid-State Diffusion**

$$\frac{\partial c_S}{\partial t}=\nabla\cdot\left(D_S\nabla c_S\right)$$

Figure IV- 23: Intercalation electrochemical model equations, grouped according to electronic and ionic transport through cell sandwich and solid-state diffusion in active material

Electrochemical modeling studies within this effort have focused on quantifying the lithium transport in the NMC-532 electrode. The methodology for the electrochemical model is described in detail in literature [2-4]. The model combines thermodynamic, kinetic, and interfacial effects with continuum based transport equations. The bulk transport model equations are given in Figure IV- 23. Volume averaged transport equations account for the composite electrode geometry. Continuum-based transport equations using concentrated solution theory describe the movement of salt in the electrolyte. The transport of ionic and electronic current throughout the cell is included, as is the diffusion of lithium in the solid-state active materials.

Critical to quantifying the lithium transport in the NMC-532 is determining the electrochemical model parameter set, which includes establishing the bulk lithium diffusion coefficient ($D_S$) for the NMC-532 active material as a function of lithium content. The diffusion coefficient can be extracted from fitting the model to a wide range of electrochemical studies, including electrochemical impedance spectroscopy (EIS) and DC current pulse/relaxation studies. Ideally, reference electrode cell studies can provide the highest quality results because it is possible to eliminate effects from the counter electrode. Since quality reference electrodes cell studies can be a challenge, Galvanostatic Intermittent Titration Technique (GITT) studies on half-cells have been used to extract the diffusion coefficient of the active material. The issue with these studies is the stability and impact of the lithium counter electrode. In the half-cell studies, measurements on multiple cells were conducted and reproducibility between tests was the primary indicator of the quality of the data.

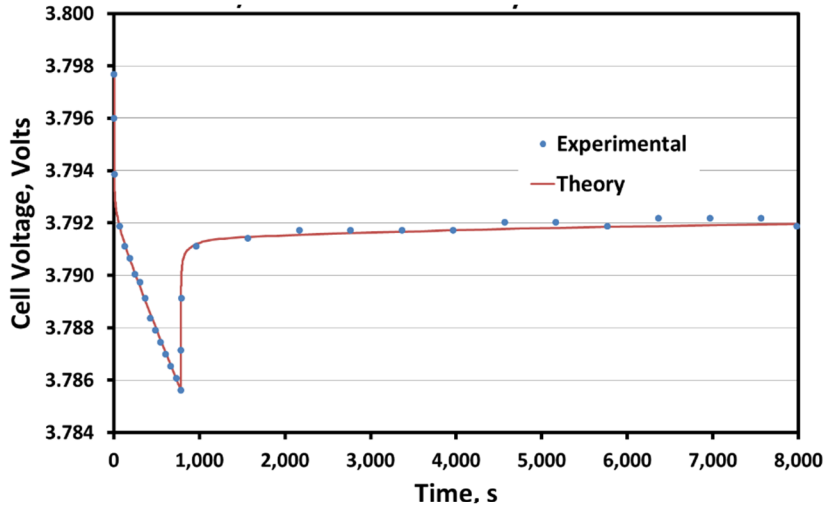


Figure IV- 24: NMC-532 half-cell voltage during a GITT 13m C/21 current pulse and 120m relaxation

In the GITT studies, a relatively long low current pulse is applied to the half-cell and then the cell is allowed to fully relax. The diffusion coefficient is obtained by fitting the electrochemical model to the voltage trace of the cell. Since lithium diffusion in the active material tends to be the slowest phenomenon in the cell, the diffusion coefficient can be effectively extracted. The length and size of the current pulse is not particularly crucial, but it is helpful for the fitting process if the active material diffusion coefficient can be considered constant over the length of the pulse and the thermodynamic relations can be linearized. A GITT current pulse/relaxation for a NMC-532 half-cell is given in Figure IV- 24, along with its corresponding electrochemical model simulation. While the electrochemical model fit is generally good, a few different active material model options were considered before an adequate fit was obtained. In general, the slow voltage relaxation after the current pulse was the challenge to fit.

The electrochemical model presented (earlier) in Figure IV- 23 was applied to the one-dimensional half-cell geometry, along with diffusion in the active material. A linear Butler-Volmer electrochemical reaction expression was used to account for the SEI impedance of the NMC and lithium electrodes. Initial work with this model resulted in both an inadequate fit of the model and a relatively low diffusion coefficient. Earlier work with lithium- and manganese-rich NMC (i.e. LMR-NMC) suggested that the slow relaxation could be associated with the $Li_2MnO_3$ domains in the nanometer scale composite structure of the NMC [see 1 and 2 in FY2015 Publications]. However, modeling the NMC-532 active material with a more complex dual-domain model did not result in a significantly better fit of the data. The slow voltage relaxation was eventually fit by including multiple particle fractions of active material in the electrochemical model. The individual particle fractions of the active material only varied in the characteristic diffusion length and only a small fraction of the active material needed to have a significantly longer diffusion length to account for the slow relaxation. Multiple particle fractions are typically used in modeling the low frequency Warburg impedance in cathode EIS studies, but are generally not needed in DC studies. The distribution of characteristic lengths of the active

material particle fractions are assumed to be related to the extent to which the electrochemical reaction penetrates into the secondary particles.

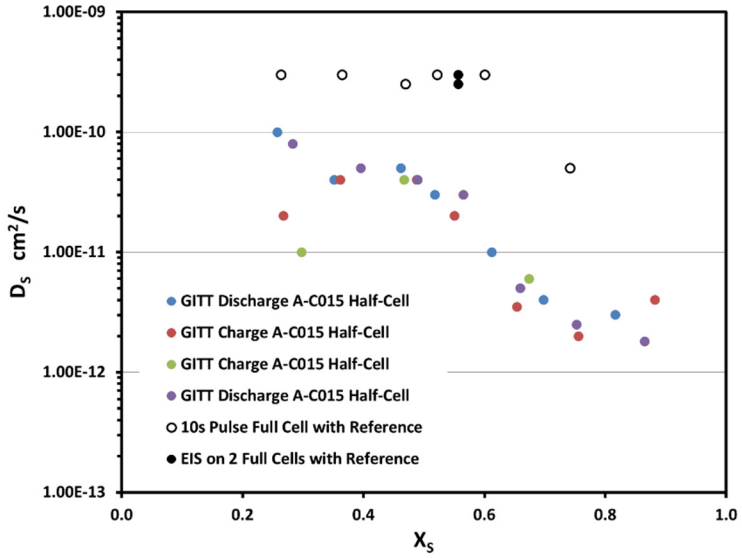


Figure IV- 25: Lithium diffusion coefficients for the bulk NMC-532 as a function of the fraction of lithium in the material (i.e. lithium concentration over maximum lithium concentration)

The lithium diffusion coefficients obtained from electrochemical modeling studies on GITT data taken during charge and discharge half-cycles from two NMC-532 baseline cathodes (A-C015) half-cells is given in Figure IV- 25. In general, there is relatively little spread in the results except at high and low states-of-charge (SOCs). At these extremes, the assumption of constant lithium diffusion coefficient over the length of the pulse and of that the thermodynamics can be linearized may not be totally valid. However, the electrochemical model fits for these SOCs were still good. These bulk lithium diffusion coefficients are comparable to previously obtained results for the NCA active material, although the drop off for the NMC-532 at low SOCs (i.e. $X_S$ approaching 1) is more dramatic. Also, Figure IV- 25 includes several data points obtained from fitting the electrochemical model to positive NMC-532 electrode EIS measurements (black circles) and 10s 3C current pulse data (open circles) taken on full reference electrode cells.

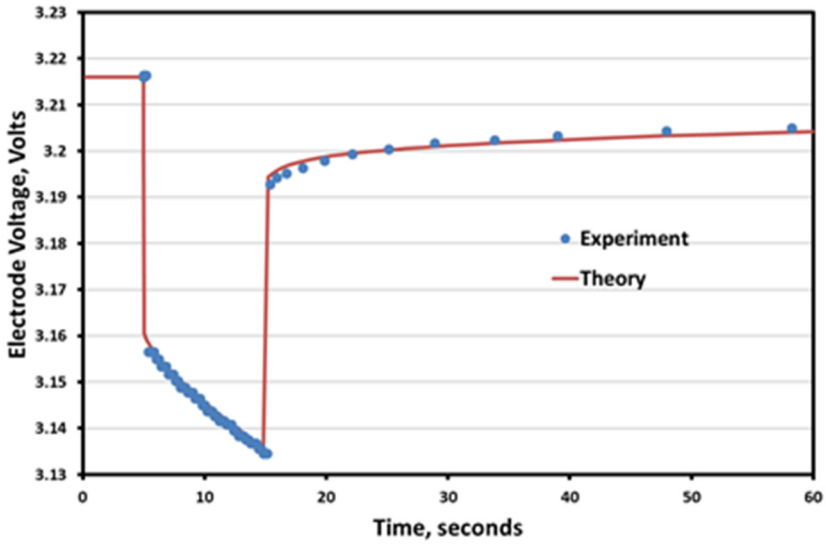


Figure IV- 26: Positive electrode results from 10s 3C discharge current pulse on NMC-532/Graphite cell (full cell at 3.788v) with a LiSn micro-reference electrode

The lithium diffusion coefficients obtained from the NMC-532 electrodes in the reference electrode cells agree, but are consistently higher than the half-cell GITT studies. At this time the exact reason for the difference is unclear and is the source of ongoing studies. It is certainly more than would be expected from cell-to-cell variations between tests. Furthermore, all tests were conducted with NMC-532 electrodes from the same laminate. It was found that the 10s current pulse data was not particularly sensitive to the characteristic length distribution of the particle fractions, but that a distribution of sizes did improve the overall fit. A sample fit using the multiple particle fractions model is shown in Figure IV- 26. Conversely the other studies were quite sensitive to the distribution of characteristic lengths. However, because the EIS studies typically stop at 10 mHz the Warburg impedance is more sensitive to the shorter characteristic lengths, while the GITT results are more sensitive to the longer lengths.

**CAMP Facility Support of HEHV Program: Establish Baseline Cell System(s) and Protocols**

In order to measure progress in the HEHV Program, it was necessary to establish a baseline cell system as early as possible. Graphite was selected as the anode electrode and 1.2 M $LiPF_6$ in EC:EMC (3:7 by wt.) was selected as the electrolyte baseline, with no additives. However, at the start of the program, several cathode materials were viable candidates for exploration. Thus, it was decided to have multiple baseline cathode electrodes to cover the major classes of lithium-ion cathode systems - these were selected to be NCM523, NCA, and HE5050.

All baseline cathode electrodes were balanced against a single graphite baseline electrode with a negative-to-positive ratio near 1.15. It was anticipated that overall system improvements would be achieved by increasing the voltage stability of the cathodes incrementally. Thus, not only would there be three baseline cathodes, there would be several baseline cathode electrodes balanced for different voltage windows for each cathode system. The voltage windows of interest were initially selected to be 4.3, 4.4, 4.5, 4.6, and 4.7 V versus lithium. The CAMP Facility's Electrode Library already fulfilled the 4.3 V baseline (NCM523 (A-C013), NCA (S-C002), and HE5050 (A-C006)), but the capacity of each cathode had to be determined at each upper cutoff voltage beyond 4.3 V. Coin-cell half-cells were made with each cathode system from the Electrode Library. These results are summarized in Table IV- 3.

**Table IV- 3: Effect of Upper Cutoff Voltage for NCM523, NCA, and HE5050**

| Source | Half Cell Voltage Window (V) | First De/Lethiation Capacity @~C/10 (mAh/g) | Irreversible Capacity Loss @~C/10 (mAh/g) | Reversible Capacity Loss @~C/10 (mAh/g) | Reversible Capacity Loss @~C/10 (mAh/g) |
|---|---|---|---|---|---|
| Toda – NCM523 | 3.0 to 4.3 | 193 | 20 | 173 | 157 |
| | 3.0 to 4.4 | 207 | 22 | 185 | 169 |
| | 3.0 to 4.5 | 220 | 22 | 198 | 180 |
| | 3.0 to 4.6 | 231 | 26 | 205 | 184 |
| | 3.0 to 4.7 | 243 | 38 | 205 | 179 |
| Toda – NCM523 | 3.0 to 4.3 | 214 | 24 | 191 | 168 |
| | 3.0 to 4.4 | 221 | 25 | 196 | 173 |
| | 3.0 to 4.5 | 227 | 27 | 200 | 173 |
| | 3.0 to 4.6 | 237 | 38 | 199 | 172 |
| | 3.0 to 4.7 | 251 | 50 | 201 | 180 |
| Toda – NCM523 | 3.0 to 4.3 | 325 | 134 | 190 | 161 |
| | 3.0 to 4.4 | 326 | 116 | 211 | 176 |
| | 3.0 to 4.5 | 328 | 95 | 233 | 191 |
| | 3.0 to 4.6 | 326 | 74 | 252 | 215 |
| | 3.0 to 4.7 | 325 | 63 | 262 | 153 |

During the development of the baseline cell systems, the CAMP Facility participated in numerous discussions regarding the development of standardized electrochemical testing protocols that would be used to evaluate every proposed cell system in an apples-to-apples comparison. The resulting protocol is described elsewhere.

The first set of baseline cathode electrodes (beyond 4.3 V vs. Li) to be developed were the cathode electrodes designed for 4.5 V vs. Li, and balanced to match the baseline anode (A-A002A) to create a full cell couple that charges up to 4.4 V. These electrodes are: NCM 523 (A-C015), NCA (A-C016), and HE5050 (A-C017), and are described in Figure IV- 27 (on the next page). The electrodes were added to the CAMP Facility's electrode library and made available for the entire HEHV Program. Over 200 electrode sheets (> 5 $m^2$) have been distributed.

Half way through FY 15, it was decided to replace the HE5050 cathode baseline, which suffers from voltage fade, with a more commercially relevant cathode such as NCM622. The table below summarizes the current test status of full cells with the baseline cathode materials. For all the cathode materials, except NCM622, the full cells with 4.4 V cut-off voltage have been completed. For NCM523 and NCA, a stable and reasonable cycle life was obtained using the standardized test protocol. For detailed information, please see Section

IV.C.1 “Enabling High-Energy/Voltage Lithium-Ion Cells for Transportation Applications: Part 1 Baseline Protocols and Analysis (ANL)”.

The full cells based on NCM523 and NCA with the 4.5 V cut-off voltage (4.6 V vs. Li) were put on test and are waiting for test completion. The full cells with 4.3 V cut-off voltage for NCM523 and NCA will be tested in the near future. As for NCM622, a viable material source has been identified and the CAMP Facility has used this NCM622 to produce a preliminary electrode to determine the capacity as a function of upper cutoff voltage. Half cells were recently made and put on test. The full cell with various cut-off voltages will be tested once the balanced electrodes are produced.

**Cathode: A-C015**
90 wt% Toda NCM 523
5 wt% Timcal C-45
5 wt% Solvay 5130 PVDF Binder

*Matched for HE/HV Project anode for 4.4V full cell cycling*
Al Foil Thickness: 20 µm
Total Electrode Thickness: 54 µm
Coating Thickness: 34 µm
Porosity: 33.5%
TTL Coating Loading: 9.17 mg/cm$^2$
TTL Coating Density: 2.70 g/cm$^3$

Made by CAMP Facility

**Cathode: A-C016**
90 wt% Toda NCA
5 wt% Timcal C-45
5 wt% Solvay 5130 PVDF Binder

*Matched for HE/HV Project anode for 4.4V full cell cycling*
Al Foil Thickness: 20 µm
Total Electrode Thickness: 53 µm
Coating Thickness: 33 µm
Porosity: 35.3%
TTL Coating Loading:8.79 mg/cm$^2$
TTL Coating Density: 2.67 g/cm$^3$

Made by CAMP Facility

**Cathode: A-C017**
92 wt% Toda HE5050
4 wt% Timcal C-45
4 wt% Solvay 5130 PVDF Binder

*Matched for HE/HV Project anode for 4.4V full cell cycling*
Al Foil Thickness: 20 µm
Total Electrode Thickness: 46 µm
Coating Thickness: 26 µm
Porosity: 39.6%
TTL Coating Loading: 6.06 mg/cm$^2$
TTL Coating Density: 2.33 g/cm$^3$

Made by CAMP Facility

**Anode: A-A002A (ABR High Voltage Project Anode)**
91.8 wt% Phillips 66 CPreme A12
2 wt% Timcal C45 carbon
6 wt% Kureha 9300 PVDF Binder
0.17 wt% Oxalic Acid

Cu Foil Thickness: 10 µm
Total Electrode Thickness: 54 µm
Coating Thickness: 44 µm
Porosity: ~38.4%
TTL Coating Loading: 5.88 mg/cm$^2$
TTL Coating Density: 1.34 g/cm$^3$

Made By CAMP Facility

**Figure IV- 27: Baseline electrodes developed for ABR High Energy-High Voltage Project**

While the graphite electrode is used as the baseline negative electrode for the bulk of the HEHV investigations of cathode materials, more insight can be gained from the use of a negative electrode with a fixed voltage plateau and a minimal SEI layer. $Li_4Ti_5O_{12}$ (LTO) serves this function very well with its 1.55 V voltage plateau, which sits well in the voltage stability window of most solvents (less SEI formation), and its spinel structure exhibits zero lattice strain upon lithiation (results in long stable cycle life). However, LTO’s useable capacity is only 160 mAh/g as compared to graphite’s capacity near 350 mAh/g. If LTO is to serve as an ideal counter/reference electrode in the HEHV Program, its electrode coating loading must be oversized enough to provide a flat voltage profile to accommodate all of the capacity from the cathode electrodes of interest. A coating loading for the LTO electrode near 34 mg/cm² would be ideal, which is quite high as the baseline graphite electrode in this program is near 6 mg/cm².

The two most common cell formats used in the HEHV Program are the 2032-sized coin cell and the single-layer pouch cell. Most initial exploratory work is performed in coin cells, and verified in pouch cells if the initial results look promising. The question exists regarding the relevance of the coin cell data versus the pouch cell data. A comparison was made to establish this relationship using the baseline NCM523 electrode (A-C015, designed for 4.4 V vs. graphite) and the baseline A12 graphite electrode (A-A002A). A total of 12 single-layer pouch cells were fabricated by CAMP in 2 sets of 6 with different electrolyte-to-pore-volume factors (2.99 and 7.47). These pouch cells were placed on the protocol test regime after formation and compared against 30 coin cells that were tested earlier in the program.

The CAMP Facility made several attempts to produce an oversized LTO electrode for this HEHV project. Two electrodes were developed that should perform well for this project. However, their loadings were only 25 and

27 mg/cm², respectively – short of the 34 mg/cm² target. It is unlikely that higher loadings will be achieved as these electrodes are near the mechanical limit of usefulness – there is too much cracking in the electrode after drying. Efforts are now directed to making low-loading positive electrodes with the cathodes of interest that will pair well with the high-loading LTO electrodes. A thin 5V spinel was made, and plans exist to make a thin NCM523 electrode.

### CAMP Facility Support of HEHV Program: Electrodes of NCM523 Coated with $Al_2O_3$

A main focus of the HEHV Program is the stabilization of the cathode particle/electrode at high potentials. A natural approach is to coat the particle and/or the electrode with a protective coating. The initial coating choice was $Al_2O_3$. Several approaches to applying the $Al_2O_3$ were followed by researchers in HEHV and the resulting cathode powder was delivered to the CAMP Facility for processing into electrodes that match the baseline capacities. Once the powders were received by CAMP, a small slurry batch was made for a trial electrode, which was then used in coin-sized half cells to establish the useable capacity in the voltage window of interest. A larger electrode run was then made with the coated powders using the measured capacity value. These electrodes were delivered to various researchers for evaluation and comparison to the baseline electrodes. See Section IV.C.2 “Enabling High-Energy/Voltage Lithium-Ion Cells for Transportation Applications: Part 2 Materials (ANL)” for more discussion. A list of the relevant electrodes and their composition are described in Figure IV- 28 (on the next page).

NREL is also developing an in-line Atomic Layer Deposition system that will be capable of applying an $Al_2O_3$ coating on electrode sheets. The ultimate goal for this system is high speed roll-to-roll coating of $Al_2O_3$ onto negative and/or positive electrodes. The CAMP Facility provided relatively long lengths (~5 m) of baseline A12 graphite electrodes for early stage demonstration of their roll-to-roll ALD coater.

Smaller samples of A12 graphite electrodes and NCM523 electrodes were also coated at NREL with four different coating levels (10, 20, 50, and 100 cycles) and tested using half cells at Argonne. For the A12 graphite electrodes, an optimum ALD coating of 20 cycles was observed. As for NCM523, the specific capacity decreases with ALD coating cycles. These results (see Figure IV- 29, on the next page) are only preliminary since the ALD coated electrodes represented the first attempt by NREL in scaled up coating system. The ALD coating effect on A12 graphite and NCM523 electrodes will be further studied when new ALD coated electrodes are ready.

### Collaboration with ORNL on Pouch Cell Fabrication

Pouch cell fabrication efforts were coordinated between Argonne’s CAMP Facility and ORNL cell fabrication facility. Several CAMP personnel visited ORNL to observe their electrode and cell making operations, which was followed by a visit to Argonne of a few key personnel from ORNL. A single layer pouch cell build was performed in the CAMP Facility with Jianlin Li of ORNL with discussions to highlight common cell making practices.

Further discussions were held with ORNL on the appropriate amount of electrolyte to add into the pouch cells. ORNL followed the approach that the CAMP Facility adopted for basing the amount of electrolyte to be relative to the total pore volume of the electrodes and the whole separator piece within each cell. ORNL built several single-layer pouch cells with varying ratios of electrolyte volume to pore volume and tested their electrochemical performance. Their results agreed with Argonne’s, which indicate the ratio should be near 2.5 to 3.0 for coin cells and pouch cells.

**Cathode: LN3012-91-5**
90 wt% Toda NCM 523 (1nm $Al_2O_3$ coating via ALD)
5 wt% Timcal C-45
5 wt% Solvay 5130 PVDF Binder

NCM-04ST, Lot#: 240202, D. Abraham
Al Foil Thickness: 20 µm
Total Electrode Thickness: 63 µm
Coating Thickness: 43 µm
Porosity: 35.5%
TTL Coating Loading: 11.25 mg/cm$^2$
TTL Coating Density: 2.62 g/cm$^3$

Made by CAMP Facility

**Cathode: LN3012-79-3**
90 wt% Toda NCM 523 (2nm $Al_2O_3$ coating via ALD)
5 wt% Timcal C-45
5 wt% Solvay 5130 PVDF Binder

NCM-04ST, Lot#: 240202, Batch 2, 18C, ALO, D. Abraham
Al Foil Thickness: 20 µm
Total Electrode Thickness: 64 µm
Coating Thickness: 44 µm
Porosity: 36.3%
TTL Coating Loading: 11.37 mg/cm$^2$
TTL Coating Density: 2.59 g/cm$^3$

Made by CAMP Facility

**Cathode: LN3012-80-2**
90 wt% Toda NCM 523(2wt.% $Al_2O_3$ coating via wet coating)
5 wt% Timcal C-45
5 wt% Solvay 5130 PVDF Binder

NCM-04ST, Lot#: 240202, A. Hubaud coating
Al Foil Thickness: 20 µm
Total Electrode Thickness: 65 µm
Coating Thickness: 45 µm
Porosity: 38.2%
TTL Coating Loading: 11.28 mg/cm$^2$
TTL Coating Density: 2.51 g/cm$^3$

Made by CAMP Facility

**Cathode: LN3032-61-4**
90 wt% Toda NCM 523
(2C $Al_2O_3$ coating via ALD)
5 wt% Timcal C-45
5 wt% Solvay 5130 PVDF Binder

NCM-04ST, Lot#: 240202,
2C ALO 369 PCR 5-29-15, D. A.
Al Foil Thickness: 20 µm
Total Electrode Thickness: 54 µm
Coating Thickness: 34 µm
Porosity: 33.2%
TTL Coating Loading: 9.22 mg/cm$^2$
TTL Coating Density: 2.71 g/cm$^3$

Made by CAMP Facility

**Cathode: LN3032-62-2**
90 wt% Toda NCM 523
(4C $Al_2O_3$ coating via ALD)
5 wt% Timcal C-45
5 wt% Solvay 5130 PVDF Binder

NCM-04ST, Lot#: 240202,
4C ALO 369 PCR 6-2-15, D. A.
Al Foil Thickness: 20 µm
Total Electrode Thickness: 54 µm
Coating Thickness: 34 µm
Porosity: 33.2%
TTL Coating Loading: 9.22 mg/cm$^2$
TTL Coating Density: 2.71 g/cm$^3$

Made by CAMP Facility

**Figure IV- 28: Electrodes made with alumina-coated NCM523 developed for ABR High Energy-High Voltage Project**

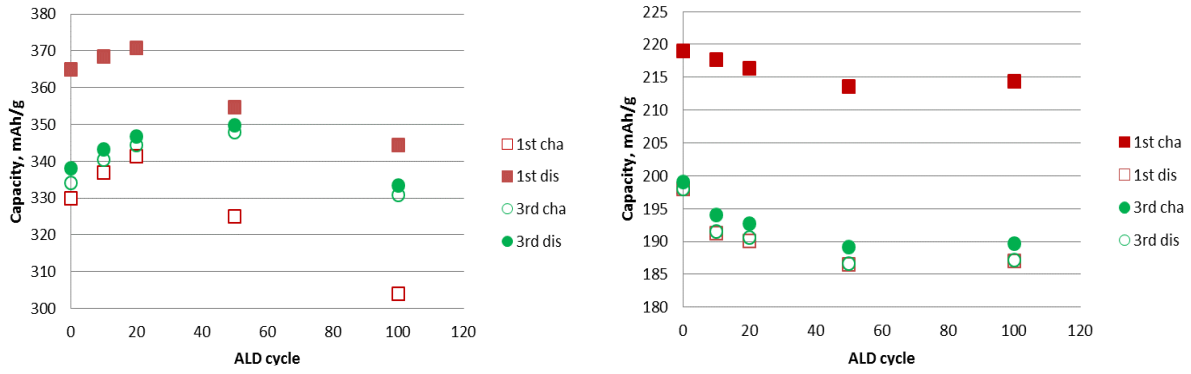


**Figure IV- 29: 1st and 3rd cycle capacity of A12 graphite (left) and NCM523 (right) with various ALD coating cycles**

**Table IV- 4: Electrode parameters used in electrode curling study**

| Name | Electrode ID | Coating Loading (mg/cm$^2$) | Coating Thickness (µm) | Coating Density (g/cm$^3$) | Coating Porosity (%) |
|---|---|---|---|---|---|
| A | LN2012-57-2A | 6.32 | 64 | 0.99 | 54.5 |
| B | LN2012-57-2B | 6.32 | 57 | 1.11 | 48.9 |
| C | LN2012-57-2C | 6.32 | 52 | 1.21 | 44.0 |
| D | LN2012-57-2D | 6.32 | 48 | 1.32 | 39.3 |
| E | LN2012-57-2E | 6.32 | 45 | 1.41 | 35.2 |
| F | LN2012-57-2F | 6.32 | 42 | 1.50 | 30.6 |

### Porosity Influence on Electrode Curling

A common problem with single-sided electrodes with electrode loadings over 1 mAh/cm² is the issue of electrode curling, which can make coin cell assembly difficult and prevent proper alignment of the electrodes over each other. This is thought to be one of the causes of cell-to-cell variability in cycling performance. The electrode curling is generally thought to be influenced by the degree of calendering, *i.e.,* the lower the electrode porosity, the greater the electrode curling. A test was devised to explore the influence of porosity on curling using negative electrodes based on Superior Graphite's graphite (SLC1520P) that have a loading of 6.3 mg/cm² (~2.0 mAh/cm²). A fresh electrode was made and then portions of it were calendered to targeted porosities between 30 and 60%. The resulting electrode parameters are shown in Table IV- 4.

After calendering, the electrodes were vacuum dried overnight at 120°C using two methods. In the first method the electrodes were dried in a flat format (sandwiched between metal platens), and in the second method the electrodes were dried in a reverse curl format (rolled over a 6-cm diameter metal pipe opposite of the natural curl direction). These drying methods were used for electrodes that were a full sheet (before punching) and after punching into electrode disks (15 mm diameter) for each porosity sample. (Electrode disks were then punched from the dried full sheets after vacuum drying). An evaluation of the curling properties of each electrode was made after dripping electrolyte on each dried electrode disk (see Figure IV- 30). This approach was thought to best simulate the coin cell assembly process. The results of this demonstration, as seen here, show an indirect correlation between electrode porosity and the degree of curling. Electrodes with porosity above 45% show the least amount of curling. However, it remains to be seen if electrodes with such a high porosity will be representative of the electrochemical performance of the active material. It was also observed that drying the electrodes in a reverse curl format helped to minimize the curling problem.

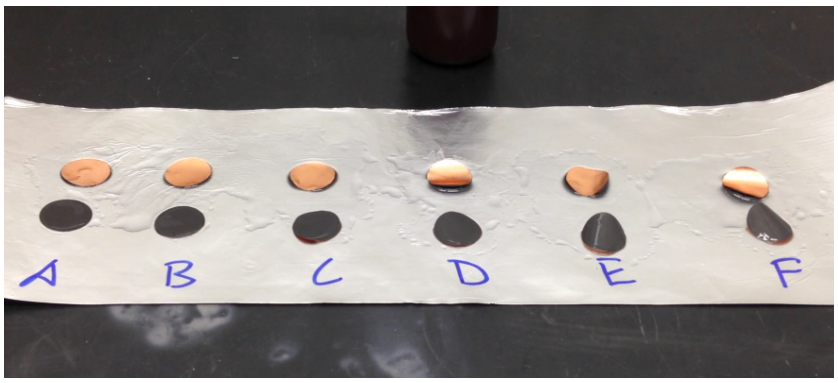


Figure IV- 30: Photo depicting degree of curling of electrodes from Table 4 upon application of electrolyte drops

### Effect of Electrode Thickness Study

Argonne collaborated with BMW in a study to determine the influence of electrode thickness on rate performance and cycle life. This work yielded several significant conclusions regarding the maximum practical electrode loading per discharge rate (application), and the detrimental effects (lithium plating) of charge rates faster than 1C. These results are discussed more in the section on PHEV and EV Battery Performance and Cost Assessment, and in a JES manuscript that has been accepted for publication.

### Electrode Library

The CAMP Facility created the Electrode Library to advance battery research, not only at Argonne National Laboratory, but also in industry, universities and other national laboratories. The Electrode Library utilizes the industrial battery manufacturing coating and rolling equipment in the CAMP Facility to produce standard anode and cathode electrodes. The unique nature of the Electrode Library electrodes is that all the anodes and

cathodes have a matched capacity. By doing this, any company, university or national laboratory working on one side of the cell will have multiple choices of materials to use on the other side of the cell using the electrode library electrodes. Thus the quality and speed of research at these facilities are greatly improved.

In FY15, the CAMP Facility added a number of new materials/electrodes to the Electrode Library. These include Hitachi MagE graphite and several new silicon/graphite electrodes. Anodes are now available with 0 wt.%, 5 wt.%, 10 wt.% and 15 wt.% nano-silicon/ graphite electrodes. These electrodes will enable researchers to understand the effect of silicon content on cell performance. In FY16, the electrode library will look to add several new and different types of graphite/carbon to the library. Additionally, the silicon/graphite composite electrodes will be further refined and updated as data on current electrodes becomes available.

As for the cathode side of the cell, no new cathode materials were added to the electrode library this year. However, cathodes of Lithium Nickel Cobalt Manganese Oxide (NCM 523), Lithium Nickel Cobalt Manganese Oxide (HE5050), and Lithium Nickel Cobalt Aluminum Oxide (NCA) were produced for the High-Energy/ High-Energy project. These electrodes were designed to match the anodes currently in the Electrode Library, where the cathodes are taken to a higher voltage, thus changing the available capacity of the cathode materials. These electrodes have been established as baseline electrodes for the project. In FY16, a new NMC 622 baseline electrode will be made along with a new graphite baseline electrode and distributed to participants in the project.

At the end of FY15, the Electrode Library contained eleven anode electrodes and eighteen cathode electrodes. New material candidates are continuously being studied and may be added to the electrode library in FY16, if needed. Table IV- 5 shows the year over year distributions of electrodes made by the CAMP Facility. These include electrodes from the electrode library along with Special Order Electrodes. The CAMP Facility has approximately doubled the number of electrodes over the past 3 years with the greatest increase in the industry usage. In FY15, a total of 49 different organizations utilized the electrode library. The breakdown of these organizations is as follows: 23 companies, 10 national laboratories (including ANL) and 16 universities. Figure IV- 31 contains a summary of the many organizations that have used the CAMP Facility's services in the last several years. The total amount of electrodes used by all of the organizations was 1690 sheets of electrodes (1 sheet = 220 mm x 110 mm), yielding a total electrode area of 40.9 square meters. This is almost double of what was distributed in FY14. The 1690 sheets breaks down to the following usage: 1745 sheets to industry, 373 sheets to other national laboratories, 206 sheets to Argonne researchers, and 83 sheets to universities. The usage data has shown a trend of doubling the usage annually for the past 3 years, this trend is expected to continue and the number of electrode library users is likely to increase further in FY16.

**Table IV- 5: Distribution of electrode sheets from the CAMP Facility's Electrode Library**

| | CAMP Facility Electrodes Delivered | | | | | |
|---|---|---|---|---|---|---|
| | FY13 | | FY14 | | FY15 | |
| Argonne | 79 | 23.5% | 116 | 13.3% | 206 | 12.2% |
| Other labs | 102 | 30.4% | 213 | 24.4% | 373 | 22.0% |
| Universities | 56 | 16.7% | 119 | 13.6% | 83 | 4.9% |
| Industry | 98 | 29.2% | 423 | 48.5% | 1028 | 60.8% |
| | | | | | | |
| Total | 335 | | 871 | | 1690 | |

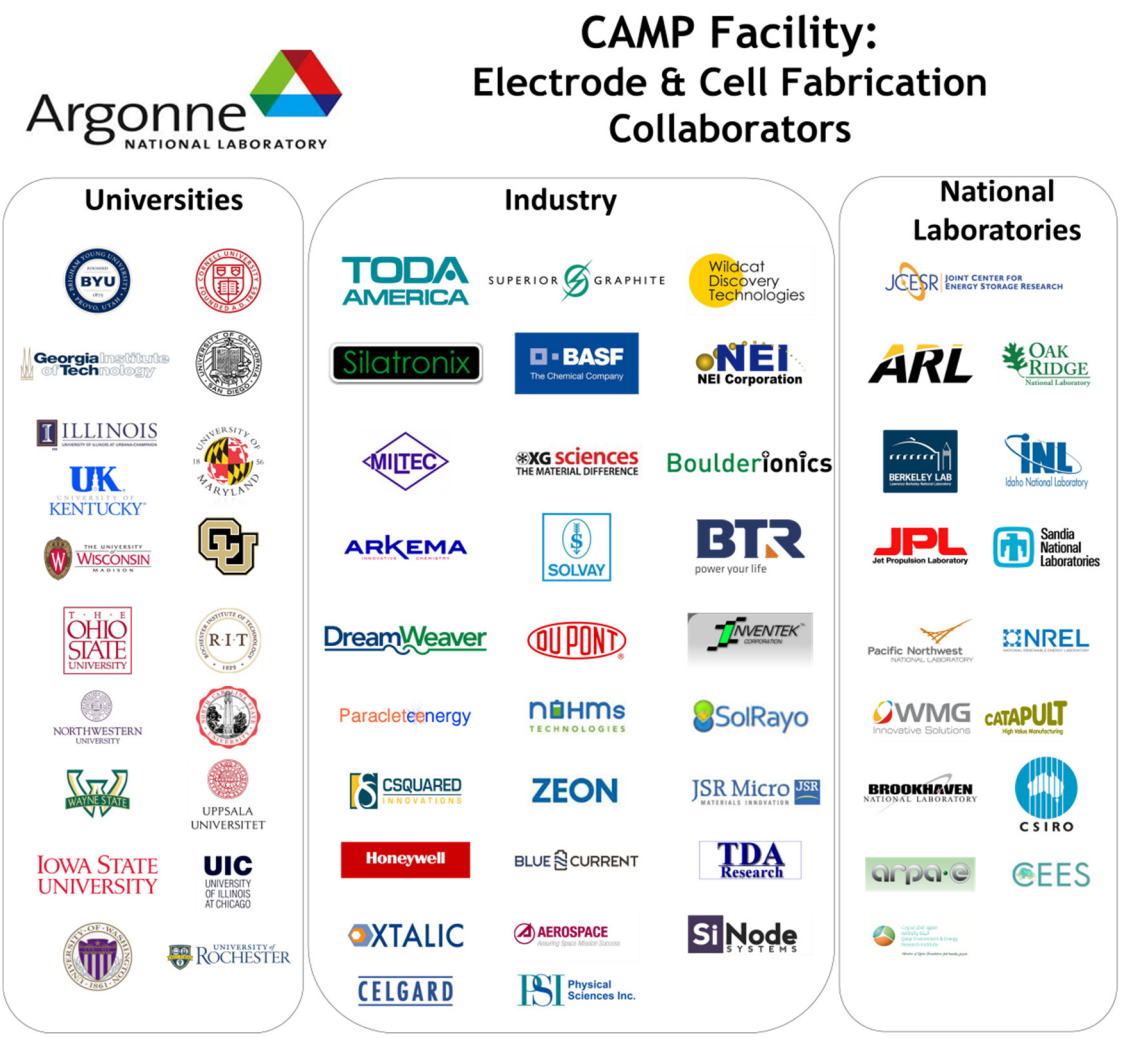


Figure IV- 31: Organizations that have utilized the CAMP Facility's resources

### Interim Deliverable Pouch Cell Builds for ABR-Amine-FOA

The interim deliverable pouch cell build for the ABR FOA Award (Project: New High energy electrochemical couple for automotive applications, PI: Khalil Amine) was completed and delivered to Idaho National Laboratory for independent testing. Initial characterization tests (formation, rate, and HPPC) were completed before delivery. The interim cell build constists of the full concentration gradient (FCG) materials made at ANL paired against graphite (Hitachi MagE) (Figure IV- 32). The electrodes were designed to target a specific capacity of approximately 500 mAh for the 13-layer xx3450 pouch cell.

| | |
|---|---|
| 90 wt% FCG, Khal ABR 2014<br>5 wt% Timcal C-45<br>5 wt% Solvay 5310 PVDF Binder | 91.83 wt% Hitachi MagE<br>2 wt% Timcal C-45<br>6 wt% Kureha 9300 PVDF Binder<br>0.17wt% Oxalic Acid |
| TTL DS Electrode Thickness: 159 µm<br>TTL SS Coating Thickness: 69 µm<br>Porosity: 39.5%<br>TTL SS Coating Loading: 17.20 mg/cm$^2$<br>TTL Coating Density: 2.47 g/cm$^3$ | TTL DS Electrode Thickness: 162 µm<br>TTL SS Coating Thickness: 76 µm<br>Porosity: 31.2%<br>TTL SS Coating Loading: 11.33 mg/cm$^2$<br>TTL Coating Density: 1.49 g/cm$^3$ |
| Made by CAMP Facility | Made by CAMP Facility |

Figure IV- 32: ABR-Amine-FOA cathode (Left) and anode (Right) compositon and specifications fabricated at the CAMP Facility for the interim xx3450 pouch cell build

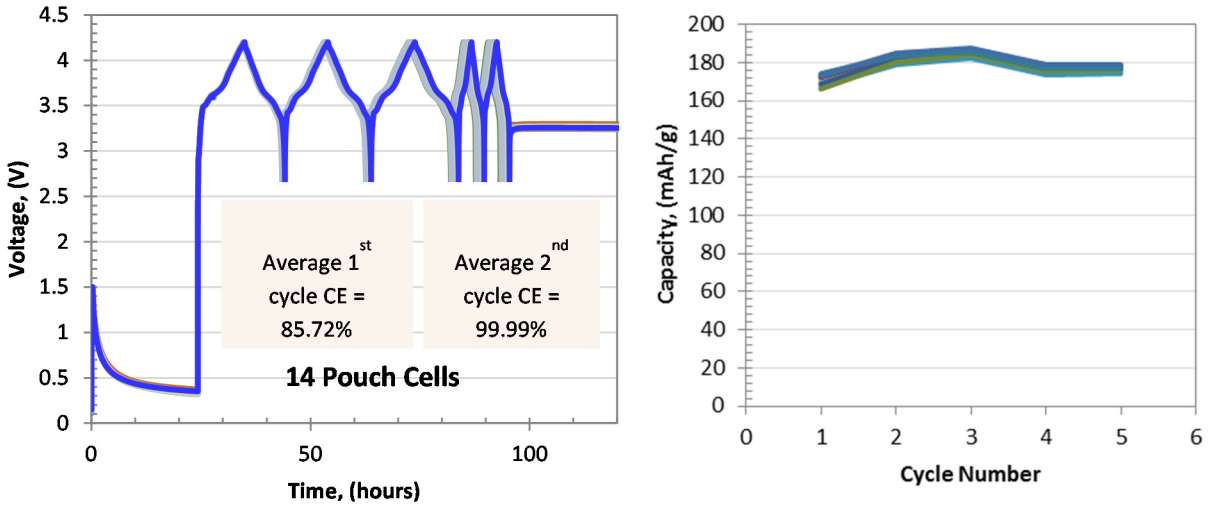


**Figure IV- 33: (Left) Formation voltage profile of the FCG//graphite xx3450 pouch cells tested at 30°C. (Right) Formation capacities of the FCG//graphite xx3450 pouch cells tested at 30°C**

Figure IV- 33 is a plot overlay of the 14 cells delivered to INL for the formation voltage profiles (left) and the formation capacities (right). The cells were initially charged to 1.5V for 15 minutes and then rested for 24 hours to minimize copper corrosion during the electrode wetting process. The cells were then cycled from 2.7 to 4.2V at a C/10 rate for 3 cycles, then C/3 for 2 cycles, and finally an OCV rest for an extended time to monitor the stability of the cells. The 1st cycle efficiency was 85.72% and the 2nd cycle efficiency was 99.99%.

### Baseline, Interim, and Final Deliverable Pouch Cell Builds for ABR-Zhang-FOA Award

The baseline, interim, and final deliverable pouch cell builds for ABR-Zhang FOA award were completed and delivered to the Electrochemical Analytical and Diagnostics Lab (EADL) at ANL for independent testing. Initial characterization tests (formation, rate, and HPPC) were completed before delivery. The baseline, interim, and final cell builds all constisted of identical electrode couples. The full cell testing was perfomed using the Phillips 66 A12 graphite against $LiMn_{1.5}Ni_{0.5}O_4$. The electrodes are part the Electrode Library (see Figure IV- 34) and were used to assemble single layer xx3450 pouch cells with a capacity of approximately 15 mAh. High voltage electrolytes were examined in the formation, rate study, and HPPC testing. 10 cells, for each deliverable, were sent to the EADL during FY15. The voltage profiles of the formation cycles are shown in Figure IV- 35.

| | |
|---|---|
| 84 wt% $LiMn_{1.5}Ni_{0.5}O_4$ "5V spinel"<br>8 wt% Timcal C45<br>8 wt% Solvey 5130 PVDF Binder<br><br>Al Foil Thickness: 20 µm<br>Total Electrode Thickness: 84 µm<br>Coating Thickness: 64 µm<br>Porosity: 36.3%<br><br>TTL Coating Loading: 14.79 mg/cm$^2$<br><br>TTL Coating Density: 2.30 g/cm$^3$<br>Made by CAMP Facility | 91.83 wt% Phillips 66 CPreme A12<br>2 wt% Timcal C45 carbon<br>6 wt% Kureha 9300 PVDF Binder<br>0.17 wt% Oxalic Acid<br><br>Cu Foil Thickness: 10 µm<br>Total Electrode Thickness: 54 µm<br>Coating Thickness: 44 µm<br>Porosity: ~38.4%<br><br>TTL Coating Loading: 5.88 mg/cm$^2$<br><br>TTL Coating Density: 1.34 g/cm$^3$<br>Made By CAMP Facility |

**Figure IV- 34: Cathode (Left) and anode (Right) compositons and specifications fabricated at the CAMP Facility and used for the baseline, interim, and final ABR-Zhang-FOA xx3450 pouch cell builds**

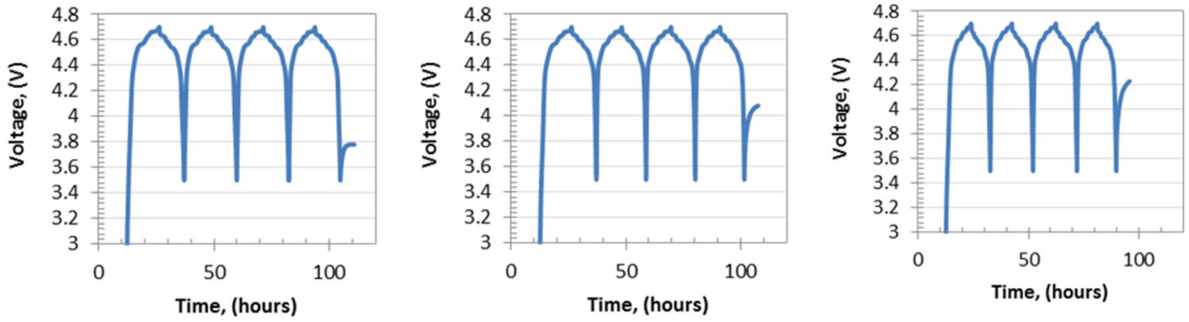


**Figure IV- 35: (Left, Middle, Right) Representative Baseline, Interim, and Final formation voltage profiles (excluding the 15 minute tap charge and 12 hour rest), respectively, of the graphite//5V spinel xx3450 single-layer pouch cells tested at 30°C**

The cells were initially charged to 1.5 V for 15 minutes and then rested for 12 hours to minimize copper corrosion during the electrode wetting process. The cells were then cycled from 3.5 to 4.7 V at a ~C/10 rate for 4 cycles and then sat at OCV for an extended time to monitor the stability of the cells. The cells then went through a rate performance test where the cells were cycled from 3.5 to 4.7 V at a C/24 rate for 2 cycles, C/10 for 3 cycles, C/5 for 3 cycles, C3 for 3 cycles, C/3 charge and C/2 discharge for 3 cycles, C/3 charge and 1C discharge for 3 cycles, C/3 charge and 2C discharge for 3 cycles. Finally, an HPPC test was performed on each cell to obtain ASI data with a 5C discharge pulse and 3.75C charge pulse, where C refers to the initial C/1 capacity of the cells. The cells were then taken to a safe SOC and delivered to EADL for further testing.

## Conclusions and Future Directions

The main focus of the CAMP Facility's effort was devoted to improving the cycle life of the silicon-containing anodes. This effort benefitted greatly from the advances made last fiscal year in developing a viable silicon-graphite anode that is flexible, mechanically robust, and with a loading of ~4 mAh/cm² and ~700 mAh/g (active material). The key to that success was a combination of: the selection of a commercially available silicon nanomaterial; optimization of the LiPAA binder system to around 10 wt.% LiPAA; selection of a graphite material with morphology conducive to mixing with silicon and LiPAA binder; and optimization of mixing processes with additional equipment. Unfortunately, having a physically robust electrode is only part of the story, as cells made with these electrodes are useful for only a few hundred cycles.

The problem lies in the poor coulombic efficiency, which is most likely due to the large volume expansion (~280%) of the silicon particle upon lithiation. On top of the problem of the silicon particle expanding to crack the SEI layer, this particle expansion results in an expansion of the silicon electrodes, which must be accounted for in the electrode and battery design. Methods used to improve the cycle life this year included reducing the amount of silicon in the negative electrode and variations in the electrolyte additives. The use of 10 wt.% FEC improves the capacity retention and coulombic efficiency, but cycling performance is still not sufficent enough for practical applications. Also, silicon has negative impact on voltage profile and electrode kinetics. These results are discussed in detail in this report and in manuscripts recently accepted for publication or in preparation.

The CAMP Facility was also very busy in other activities that support the battery R&D community as a whole. As discussed in this report, these activities included numerous electrode and cell builds (coin and single-layer pouch formats) and testing to establish a baseline (s) and protocols for the ABR's new High-Energy High-Voltage Project. Once this was established, the CAMP Facility provided further support in developing electrodes using alumina coatings on particles and electrodes. Many single-layer and multi-layer pouch cell builds were also conducted to support other projects such as two DOE-EERE FOA Awards and the electrode loading study with BMW. The CAMP Facility's Electrode Library is also proving to be ever-more popular.

In FY16, efforts will continue on improving the electrochemical and mechanical performance of the silicon-graphite anode. Silicon offers high gravimetric and volumetric capacity in lithium-ion negative electrodes, and is certainly worth further study. The ABR Program has created a new project devoted to the understanding and development of high energy anode systems (mostly silicon-based). The CAMP Facility will be very active in supporting this new project. Its experience in silicon-containing electrodes and studies in SEI formation will be

of great value. Efforts will continue to be directed to developing electrolyte additives and binder systems that can form a robust and harmonious SEI layer on the silicon and graphite surfaces. Preliminary data from Argonne's Post-Test Facility is shedding light on the failure mechanisms of the silicon electrodes. The CAMP Facility will supply silicon-based electrodes to SNL for thermal abuse testing in 18650 cells. More development of the silicon-graphite electrode system in the electrode electrochemical model will continue.

The CAMP Facility will continue to work closely with the new High-Energy/High-Voltage Project at Argonne with effort directed toward fabricating electrodes (and pouch cells) that use uncoated and coated NMC or NCA particles/electrodes. Electrodes will be provided to NREL in support of their development of a high-speed roll-to-roll ALD coating system.

Several DOE energy-storage FOA Awards were also given to companies that have partnered with Argonne's CAMP Facility and MERF. They will work closely with each other to help these companies meet their program deliverables and hopefully create a new battery product for the market.

## References


1. *A Volume Averaged Approach to the Numerical Modeling of Phase-Transition Intercalation Electrodes Presented for $Li_xC_6$.* **K.G. Gallagher, D.W. Dees, A.N. Jansen, D.P. Abraham, S.-H. Kang.** 12, 2012, J. Electrochem. Soc., Vol. 159, pp. A2029-A2037.
2. *Alternating Current Impedance Electrochemical Modeling of Lithium-Ion Positive Electrodes.* **D. Dees, E. Gunen, D. Abraham, A. Jansen, and J. Prakash.** 7, 2005, J. Electrochem. Soc., Vol. 152, pp. A1409-A1417.
3. *Electrochemical Modeling of Lithium-Ion Positive Electrodes during Hybrid Pulse Power Characterization Tests.* **D. Dees, E. Gunen, D. Abraham, A. Jansen, J. Prakash.** 8, 2008, Vol. 155, pp. A603-A613.
4. *Analysis of the Galvanostatic Intermittent Titration Technique (GITT) as Applied to a Lithium-Ion Porous Electrode.* **D.W. Dees, S. Kawauchi, D.P. Abraham, J. Prakash.** 2009, J. Power Sources, Vol. 189, pp. 263–268.


## FY 2015 Publications/Presentations

1. *Electrochemical Modeling and Performance of a Lithium and Manganese-Rich Layered Transition-Metal Oxide Positive Electrode.* **Dennis W. Dees, Daniel P. Abraham, Wenquan Lu, Kevin G. Gallagher, Martin Bettge, Andrew N. Jansen.** 4, 2015, J. Electrochem. Soc., Vol. 162, pp. A559-A572.
2. *Examining the Electrochemical Impedance at Low States of Charge in Lithium- and Manganese-Rich Layered Transition-Metal Oxide Electrodes.* **Sanketh R. Gowda, Dennis W. Dees, Andrew N. Jansen, Kevin G. Gallagher.** 7, 2015, J. Electrochem. Soc., Vol. 162, pp. A1374-A1381.
3. *Exploring Electrochemistry and Interface Characteristics of Lithium-Ion Cells with $Li_{1.2}Ni_{0.15}Mn_{0.55}Co_{0.1}O_2$ Positive and $Li_4Ti_5O_{12}$ Negative Electrodes.* **Yan Li, Martin Bettge, Javier Bareño, Stephen E. Trask, Daniel P. Abraham**, Journal of The Electrochemical Society. 10.1149/2.0071513jes (July 2015)
4. *Optimizing areal capacities through understanding the limitations of lithium-ion electrodes*. **Kevin G. Gallagher, Stephen E. Trask, Christoph Bauer, Thomas Woehrle, Simon F. Lux, Matthias Tschech, Bryant J. Polzin, Seungbum Ha, Brandon Long, Qingliu Wu, Wenquan Lu, Dennis W. Dees, Andrew N. Jansen**, Journal of The Electrochemical Society (accepted October 2015)
5. *Cell Fabrication in the Cell Analysis, Modeling, and Prototyping (CAMP) Facility*. **Stephen E. Trask**, oral presentation, PNNL Workshop on the Development of Pouch Cells for Advanced Batteries, Richland, WA, July 24th, 2015.
6. *High-Energy Li-Ion Batteries: Full Cell and Electrode Monitoring for Evaluating Cycling and Impedance Performance of Layered Oxide//Si-Graphite Cells*. **Matilda Klett, James A. Gilbert, Stephen E. Trask, Bryant J. Polzin, Andrew N. Jansen, Dennis W. Dees, Daniel P. Abraham**, 227th Electrochemical Society Meeting, May 2015, Chicago, USA

7. *Silicon-Graphite Development: Robust, Practical, and Scalable High Performance Electrodes*. **Stephen E. Trask, Bryant J. Polzin, Joseph J. Kubal, Wenquan Lu, Nancy Dietz-Rago, Andrew N. Jansen**, oral presentation, 227th ECS Meeting, Chicago, IL, May 25th, 2015.
8. *Silicon-Graphite Electrode Performance in Lithium Ion Batteries: From Coin Cells to 500mAh-Pouch Cells.* **Bryant J. Polzin, Stephen E. Trask, Andrew N. Jansen, Wenquan Lu**, oral presentation, 227th ECS Meeting, Chicago, IL, May 25th, 2015.
9. *Impact of Silicon Expansion upon Lithiation on Electrode and Cell Thickness*. **Andrew N. Jansen, Stephen E. Trask, Bryant J. Polzin**, oral presentation, 227th ECS Meeting, Chicago, IL, May 25th, 2015.
10. *Silicon-Graphite Slurry and High-Loading Electrode Process Development*. **Stephen E. Trask, Bryant J. Polzin, Andrew N. Jansen**, poster presentation, 32nd Battery Seminar & Exhibit in Fort Lauderdale, FL, March 9-12, 2015.

# IV.B.2 Materials Benchmarking Activities for CAMP Facility (ANL)

## Objectives

- The primary objective is to identify and evaluate low-cost materials and cell chemistries that can simultaneously meet the life, performance, and abuse tolerance goals for batteries used in PHEV and EV applications.
- A secondary objective is to enhance the understanding of the impact of advanced cell components and their processing on the electrochemical performance and safety of lithium-ion batteries.

## Technical Barriers

- On one hand, an overwhelming number of materials are being marketed by vendors for lithium-ion batteries. It is a challenge to down select and screen these materials effectively within the allocated scope of this project.
- On the other hand, there are no commercially available high energy materials that can produce a battery capable of meeting the 40-mile all-electric-range (AER) within the weight and volume constraints established for PHEVs by DOE and the USABC. Identification of new high-energy electrode materials is the primary goal for this project.
- During the validation process, we often encounter a broad variation in chemical and physical properties when validating their electrochemical performance and safety related characteristics. This makes it very challenging to fabricate optimized electrodes with little knowledge of the impact of formulation and processing on electrode performance.

## Technical Targets

- To identify higher energy density electrode materials to meet USABC requirements.
- To characterize inert, but critical cell components which can enable better cell performance.
- Technical support to the Cell Assembly Modeling and Prototyping (CAMP) facility and Materials Engineering Research Facility (MERF).
- To summarize the battery material validation activities.

## Project Details

**Peter Faguy (ABR Program Manager)**

**Wenquan Lu (ANL/PI)**
9700 S. Cass Avenue
Argonne, IL 60439
Phone: 630-252-3704;
Fax: 630-972-4414
Email: luw@anl.gov

Collaborators:
Daniel Abraham (ANL)
Dennis Dees (ANL)
Kevin Gallagher (ANL)
Seonbaek Ha (IIT)
Manar Ishwait (ANL)
Andrew Jansen (ANL)
Christopher Johnson (ANL)
Victor Maroni (ANL)
Bryant Polzin (ANL)
Xin Su (ANL)
Steve Trask (ANL)
Qingliu Wu (ANL)
CAMPF (ANL)
MERF (ANL)

Cabot (USA)
Celgard (USA)
Daikin (Japan)
FMC (USA)
JSR Micro (Japan)
PPG (USA)
PSI (USA)
ShuangAo Energy Tech. (China)
Superior Graphite (USA)
Toda Kogyo (Japan)
XG Sciences (USA)

Start Date: October 2015
Projected End Date: March 2018

## Accomplishments

- Robust silicon electrode was developed by combining PAA and SBR binders.
- FEC effect on silicon electrode was investigated in terms of electrochemical and thermal properties.
- Prelithiation study was conducted on silicon electrode and its effect on full cell was completed.
- Raman-Based Investigation of the Fate of $Li_2MnO_3$ in Lithium- and Manganese-Rich Cathode Materials for Lithium-ion Batteries (refer to the publication #2, not discussed in this report).
- Various separators were investigated for both 4V and 5V lithium-ion batteries.

## Introduction

This benchmarking effort is conducted as part of the Cell Analysis Modeling and Prototyping (CAMP) facility (see section IV.B.1 of this report) to identify and support promising new materials and components across the "valley of death", which happens when pushing a new discovery towards a commercial product. The CAMP Facility is appropriately sized to enable the design, fabrication, and characterization of high-quality prototype cells with around 400-mAh capacity, which straddles the gap between coin cells and full cells nicely – two orders of magnitude from each end point. Thus, a realistic and consistent evaluation of candidate chemistries is enabled in a time-effective manner with practical quantities of novel materials.

However, the CAMP facility is more than an arrangement of equipment, it is an integrated team effort designed to support the production of prototype electrodes and cells. In order to utilize the facility more efficiently and economically, cell chemistries are validated internally to determine if they warrant further consideration.

High energy density electrode materials are required in order to achieve the 40-mile AER within the weight and volume constraints established by DOE and the USABC. One would need a combination of anode and cathode materials that provide 420mAh/g and 220mAh/g, respectively, as predicted by Argonne's battery design model, if one uses a 20% margin for energy fade over the life of the battery assuming an average cell voltage of 3.6 volts. Therefore, the search for new high energy density materials is the focus of this project.

In addition to electrode materials, other cell components, such as separators, binders, current collectors, etc., are evaluated to establish their impact on electrochemical performance, thermal abuse, and cost.

## Approach

Once the promising chemistries, from new commercially available materials, as well as new high energy density materials under development, are identified, coin cells (2032 size) will be used as test vehicle for the initial screening studies, which typically includes formation cycles, hybrid pulse power characterization (HPPC) tests, rate capability testing, and limited cycle life testing. Accelerated aging studies are also performed at 45°C to 55°C for promising materials to give a preliminary indication of life. Where appropriate, the thermal abuse response is studied using a differential scanning calorimeter.

After validation, a decision will be made to either advance, modify, or terminate studies to maximize utilization of available resources. If promising results are obtained with coin cells, the promising chemistries will be recommended for more extensive evaluation under the CAMP Facility, which includes advanced electrochemical analysis, electrochemical modeling, larger format cell design and long term testing.

## Results

### Robust Silicon Electrode Development

It has been reported that PAA is an efficient polymer binder for silicon-based anode. The mechanical and adhesive strength of electrode improved with increasing PAA binder. However, large percentage of PAA binder as an inactive material can lead to lose an absolute capacity and a gravimetric energy density because of less active material in the electrode. Furthermore, the silicon electrode with PAA binder is still brittle compared to that of silicon electrode with PVDF binder. In order to address these two issues, firstly, the optimum contents of PAA binder have been investigated to reduce the loss of the absolute capacity and gravimetric energy density. Secondly, PAA/SBR binder system with different binder compositions has been tested on the integrity of silicon electrode and its electrochemical performance, such as rate capability and cyclic performance.

Figure IV- 36 shows lithiation/delithiation capacity of Li/Si cells as function of cycle number, which includes initial three formation cycles and rate capability cycles. Three silicon electrodes with various PAA compositions (20, 15, and 10wt%) were prepared and their electrochemical performance was compared to that of the silicon electrode with PVDF binder. Apparently, the silicon electrode with PAA binder showed better electrochemical performance compared to the silicon electrode with PVDF binder. It is also observed that at least 15wt % PAA is needed to achieve the reasonable electrochemical performance.

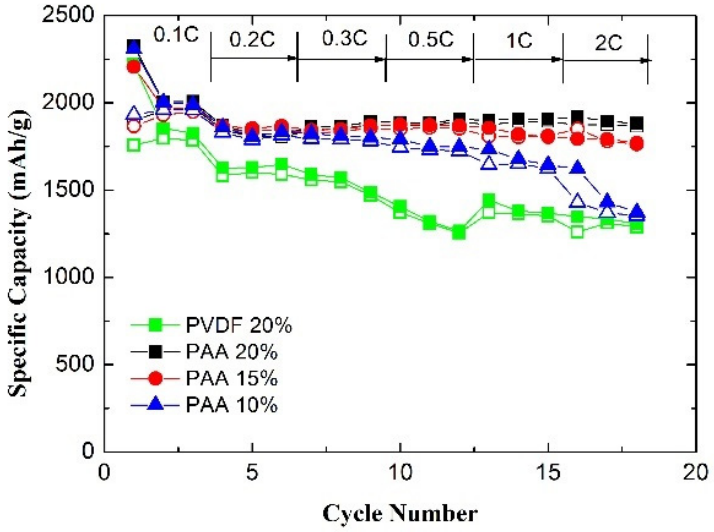


Figure IV- 36: Rate performance of Li/Si half cell with various PAA binders

As mentioned above, the silicon electrode with PAA binder is still brittle (Figure IV- 37) even though good electrochemical performance was obtained. To improve the flexibility, the effect of additional SBR to PAA binder on electrode integrity was investigated. Since both PAA and SBR are used as aqueous binders, they can be easily mixed together during slurry fabrication. Figure IV- 37 shows the SBR effect on the mechanical integrity of silicon electrode using PAA as binder. The punched electrode discs were put into small plastic bags and manually flexed and bent over 20 times inside the bag. The magnitude of the electrode mechanical stability can be easily validated by checking the delamination of the silicon electrode. As shown in Figure IV- 37, the higher the content of SBR in the electrode, the less delamination was observed, which indicated the improvement of SBR on both adherence between the coating and current collector and coherence between electrode materials. The electrochemical performance of the silicon electrodes with PAA/SBR binder were tested using Li/Si half cells and the test results are shown in Figure IV- 38. No detrimental effect on electrochemical performance was observed when SBR was introduced into the electrode.

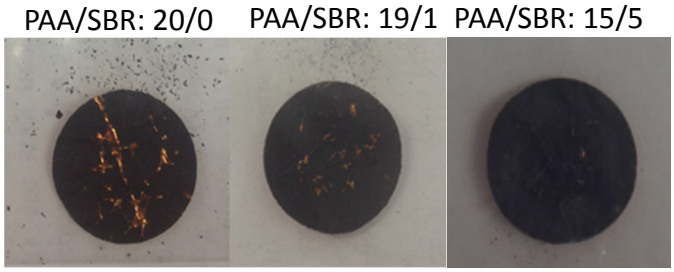


Figure IV- 37: SBR effect on the integrity of silicon electrode

**Fluoro Ethylene Carbonate (FEC) Effect on Silicon Electrode**

FEC has been well accepted as an efficient additive for Si-based anodes by forming a better solid electrolyte interface (SEI). However, it is still not clear how much FEC is needed as additive. Also, its effect on thermal properties needs to be better understood. In this work, we first looked at the FEC concentration effect on electrochemical performance of silicon/graphene (Si-Gn) composite electrode. In addition, the electrode morphology and SEI composition have been investigated via SEM and EDX. The thermal stability of fully lithiated Si/Gn electrode was also investigated using differential scanning calorimeter (DSC). Figure IV- 39 shows cycle performance of Li/Si-Gn half cells with various FEC contents. The cells without FEC additive showed continuous capacity degradation over cycling. The cycle performance increased dramatically for all the cells with any amount of FEC additives. However, the cells containing 3wt% FEC had initially higher capacity until the 20th cycle, then the capacity gradually decreased and drastically dropped after 56th cycle.

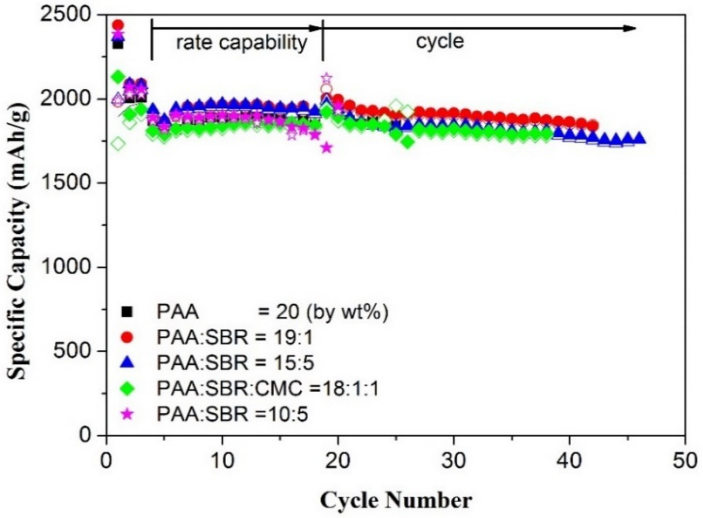


Figure IV- 38: Electrochemical performance of silicon electrode with PAA/SBR binder

By increasing the FEC content from 5wt.% to 25wt.% in the electrolyte, all the cells showed good capacity retention in 70 cycles and no discernable improvement was observed by adding more FEC into the electrolyte. Therefore, 5wt.% FEC additive in electrolyte seems to be the minimum amount of FEC for good electrochemical performance.

Figure IV- 40 shows SEM images of Si/Gn electrodes after the initial cycles with 0.1C rate charge and discharge with no FEC (left) and with 10wt% FEC (right). The electrode containing with no-FEC was clearly covered by thick and nonuniform SEI layer, which is probably the reaction products of

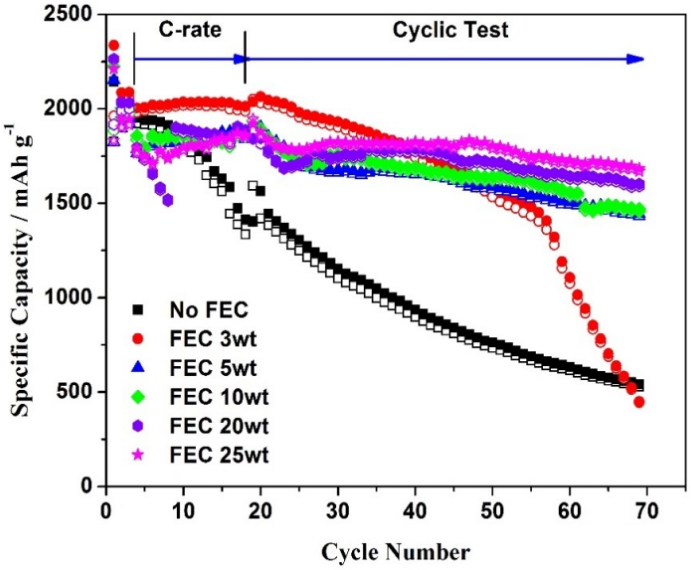


Figure IV- 39: FEC effect on the silicon electrode in Li/Si half cells

electrolyte. This is never observed for graphite electrode. Then, the side reaction could be contributed to silicon material. Conversely, no surface film was observed for the electrode containing 10wt% FEC, which suggest the possible thin and/or uniform SEI formation on the Si/Gn electrode. The electrode morphology difference agrees well with the previous report.

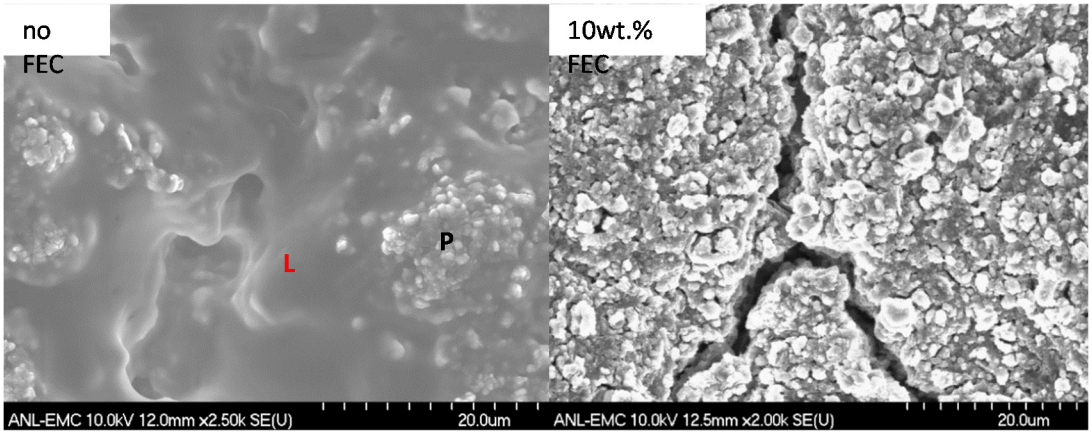


Figure IV- 40: SEM images of Si/Gn electrodes after the initial cycles at 0.1C with no FEC (left) and 10wt% FEC (right)

The elemental analysis of SEI was conducted using EDX and the atomic concentration results are shown in Figure IV- 41. The element concentration difference for FEC-free electrode was observed on the top of particles (P) and on the surface film layers (L). Relatively more silicon element was observed on the particle since it was not covered by the surface film. Similarly, more carbon element was observed on the particle compared to that on the surface layer, which can be attributed to the carbon content in the composite electrode. On the layer, relatively more O, F and P were obtained, which could be easily attributed to the product of electrolyte reduction. Compared the electrodes with FEC to that without FEC (but particle site), the element concentrations are very similar. This confirmed that the FEC did prevent the side reactions between silicon and electrolyte.

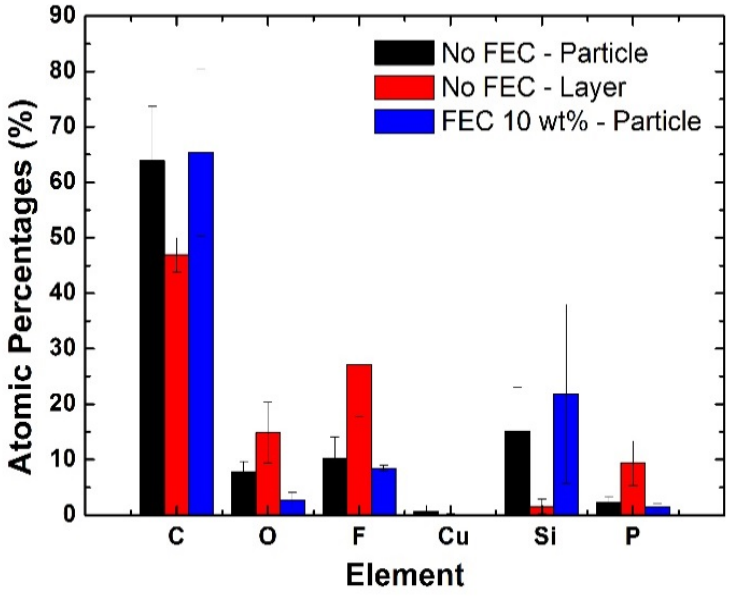


Figure IV- 41: Elemental concentrations measured by EDX at least four different positions for Si-Gn electrode after initial cycles with and without FEC

Even though the FEC can prevent the side reaction, the cracks were still observed on the surface of electrode with FEC additive, which can be attributed to the volume expansion and contraction of silicon electrode during lithiation and delithiation process. No such cracks were observed on the surface of silicon electrode without FEC additive. We believe that the volume expansion and contraction still occurred of the FEC-free electrode. The reason why we could see the cracks from the FEC-free electrode is that they were covered by the surface film.

The thermal stability of FEC effect on silicon electrode materials was also investigated using DSC and the results are shown Figure IV- 42. The DSC traces of Si-Gn electrode without FEC are very similar to the DSC results from graphite electrode. The exothermic heat flow was significantly reduced between 200°C once the FEC was added to the electrolyte. The less heat generation of Si-Gn electrode with FEC additive is due to the less SEI formation, which can improve the thermal stability of the silicon electrode.

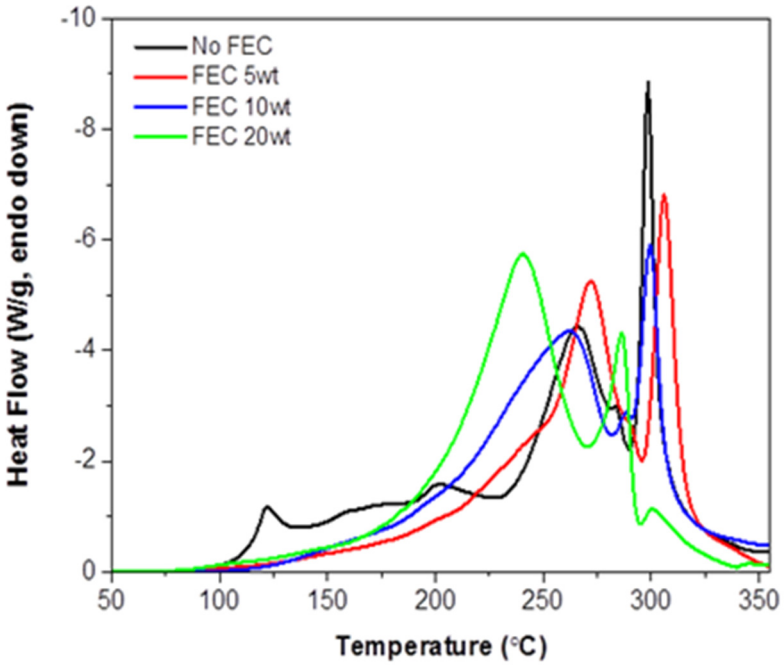


Figure IV- 42: FEC effect on thermal stability of fully lithiated Si-Gn electrode

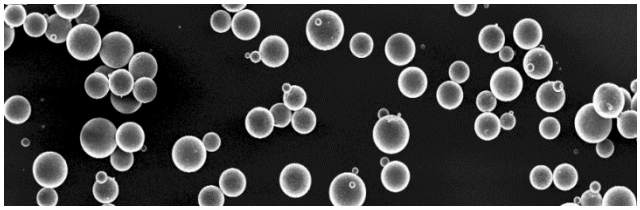

Figure IV- 43: SEM image of Lithium Powder (SMLP)

**Prelithiation on Silicon Electrode**

Even though the silicon electrode can provide high capacity, a high irreversible capacity loss will limit the reversible capacity of the full cell. One approach to address this issue is to prelithiate the anode with lithium. We have been working closely with FMC to prelithiate the silicon electrode using stabilized lithium metal powder (SLMP), which is shown in Figure IV- 43. A controlled amount of lithium powder was applied to the surface of the silicon anode when the full cells were assembled using a $LiNi_{0.8}Co_{0.15}Al_{0.05}O_2$ (NCA) cathode. The capacity retention as a function of cycling of full cells with and without prelithiation is shown Figure IV- 44. Clearly, more reversible capacity was obtained for the same silicon electrode with prelithiation. Correspondingly, more reversible capacity usage of cathode material was obtained, which is not shown here. This can dramatically increase the energy density of the full cell. In terms of cycle life, the similar capacity retention was observed for the full cell with and without prelithiation. However, the better coulombic efficiency was obtained for the full cells with prelithiation, as shown in Figure IV- 45. It can be seen from this figure that the coulombic efficiency is close to 100% right from the cell formation. However, the coulombic efficiency of the full cells without prelithiation was low at beginning due to high irreversible capacity loss and rose continuously to close to 100% with cycles. This phenomena will also affect the cycle life eventually.

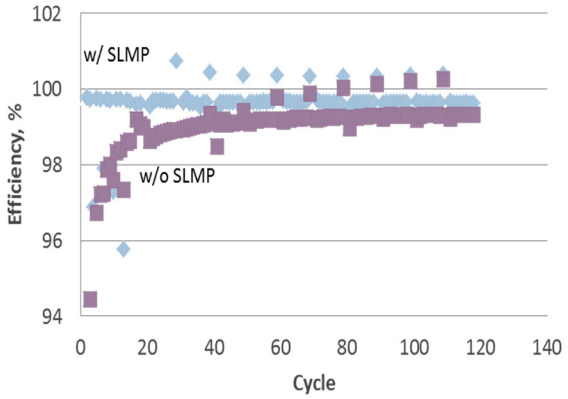


Figure IV- 44: Capacity retention of Si/NCA cell w/ and w/o prelithiation

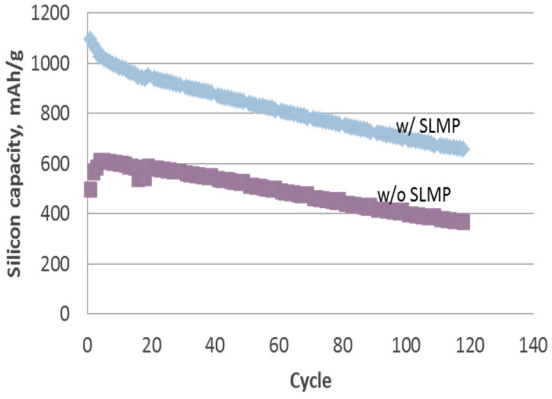


Figure IV- 45: Coulombic efficiency of Si/NCA cell w/ and w/o prelithiation

**Ceramic Coated Separator Effect on Cell Performance**

Separator, as one of the key components for lithium-ion batteries (LIB), simultaneously separates the anode from cathode electrode electronically and allows lithium ions diffuse through it to provide the current. Its properties, including electrochemical stability, mechanical strength, porosity, thickness, pin holes, heat shrinkage, etc. significantly affect the battery's performance, such as rate, power, safety, and cycles.

For this report, the ceramic coated PE based separator (SA-1, shown in Figure IV- 46) was received from ShuangAo Energy Tech. (Shanghai, China). The electrochemical properties of the separators were characterized, together with the physical and thermal properties. The tensile strength test results indicated that the SA-1 has the same tensile strength in both machine and transverse directions, which are important for cell safety.

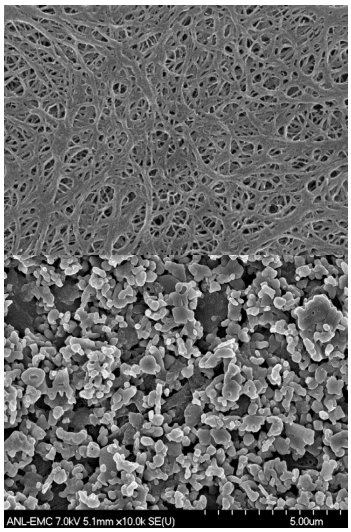


Figure IV- 46: SEM Images Polyethylene Separator with and without Ceramic Coating

The thermal shrinkage test was conducted by punching the separators into ¾ inch discs. The discs were heated at 110°C in the oven for 1 hour before visual check. The size change of the heat-treated samples is shown in Figure IV- 47. In order to make comparison, same size paper disc was put just behind separator. There was almost no shrinkage observed for ceramic coated PE separator, indicating that the ceramic coated separators has a better thermal stability.

Hybrid Pulse Power Characterization was carried out to the graphite/NCA cell using the SA-1 separator and internal control separator. Total 9 groups of pulses with current of 2C rate were applied at various Depth of Discharge (DOD) after the cell was fully charged. Area Specific Impedance (ASI) from discharge pulses were calculated by dividing the voltage difference (between the voltage before the pulse and the voltage at the end of the pulse) by the pulse discharge current. Relative low ASI was obtained, shown in Figure IV- 48, compared to our internal baseline, which can be attributed to the high porosity of the separator. Figure IV- 49 shows the cycle performance of graphite/NCA full cell. After three formation cycles, the cell was charged and discharged between 4.1V and 3.0V at C/2 rate. No capacity fading was observed in 100 cycles.

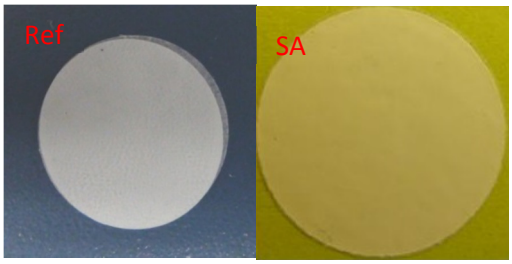


Figure IV- 47: Heat shrinkage of ceramic coated PE separator

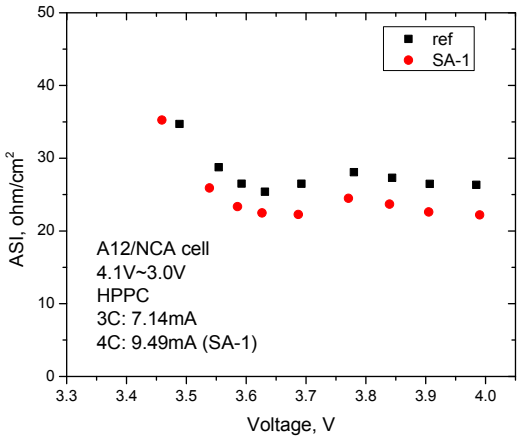


Figure IV- 48: ASI of A12/NCA cell

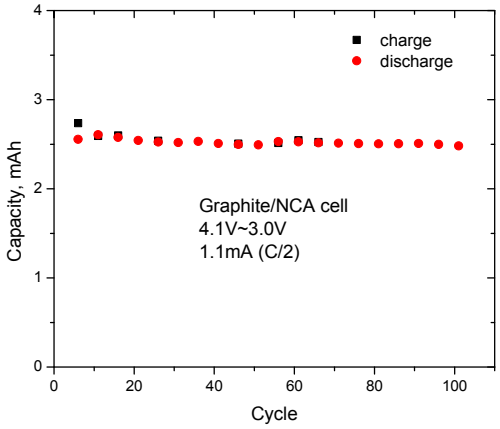


Figure IV- 49: Cycle performance of A12/NCA cell

### Support to HE-HV Program

Even with standardized cell fabrication and testing protocols, electrochemical performance variations are still expected from numerous factors, such as: operator; box condition; electrolyte condition; electrode condition; and more. Also, researchers are often limited by the number of channels in temperature controlled ovens, which negatively affects the statistical analysis of the results.

With dedicated personnel and an adequate number of channels, electrochemical performance validation will provide reasonably consistent results, which would allow us to make sound decisions for further investigation of promising technologies for HE-HV. In addition, the lessons learned during electrochemical performance validation will allow us to better understand new materials and to aid the large format cell design and testing.

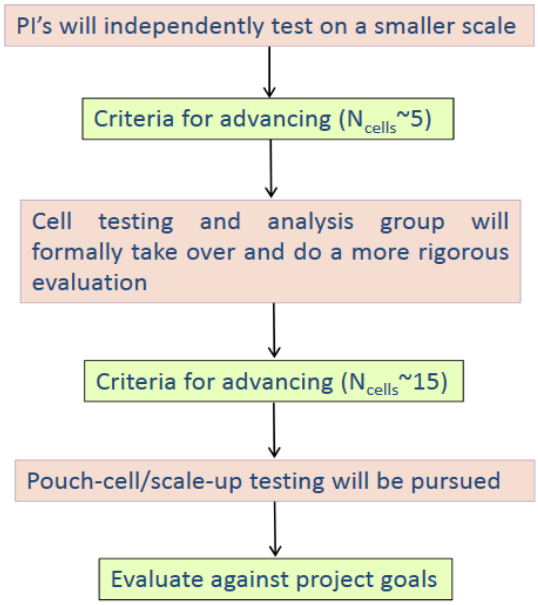


Figure IV- 50: Flow chart of the operating procedure

Under this task, promising materials are reviewed and decisions to proceed with validation are made in group meetings. Once the validation decision is made, 15 cells based on each material sample can be tested using the standardized test protocol. The electrochemical performance validation results are then summarized and reported. The flow chart for this process is shown in Figure IV- 50.

### Separator for High Voltage Application

There is concern that separators based on polyethylene (PE) will be oxidized at the high potentials targeted in the HEHV Program, whereas separators based on polypropylene (PP) should be better able to withstand high potentials. A small sampling of four commercial separators was obtained for a preliminary scoping study. These separators included: a trilayer (PP/PE/PP); polypropylene only; a coated polypropylene with a functionalized coating; and an alumina coated polyethylene separator. Three coin cells were made with each of these separators using the A12 graphite and NCM523 baseline electrodes, and cycled between 3.0 and 4.5 V. Figure IV- 51(left) shows the 1st cycle formation and rate test of A12 graphite/NCM523 full cell using the selected separators. All the separators showed similar electrochemical performance except coated PP separator, which exhibited low coulombic efficiency and poor rate performance. A closer look at the rate test results (Figure IV- 51(right)) suggests slightly better rate performance for the cells using the alumina-coated PE separator, but this needs to be confirmed in a larger study.

In order to determine the potential root cause of the poor performance of the coated PP separator, one cell from each group after cycle life testing was dissembled. As can be seen from Figure IV- 52, the greatest color change was observed for the coated PP separator, which may be due to decomposition of the functional coating on the PP at high potentials. Interestingly, the alumina coated PE separator showed the least color change.

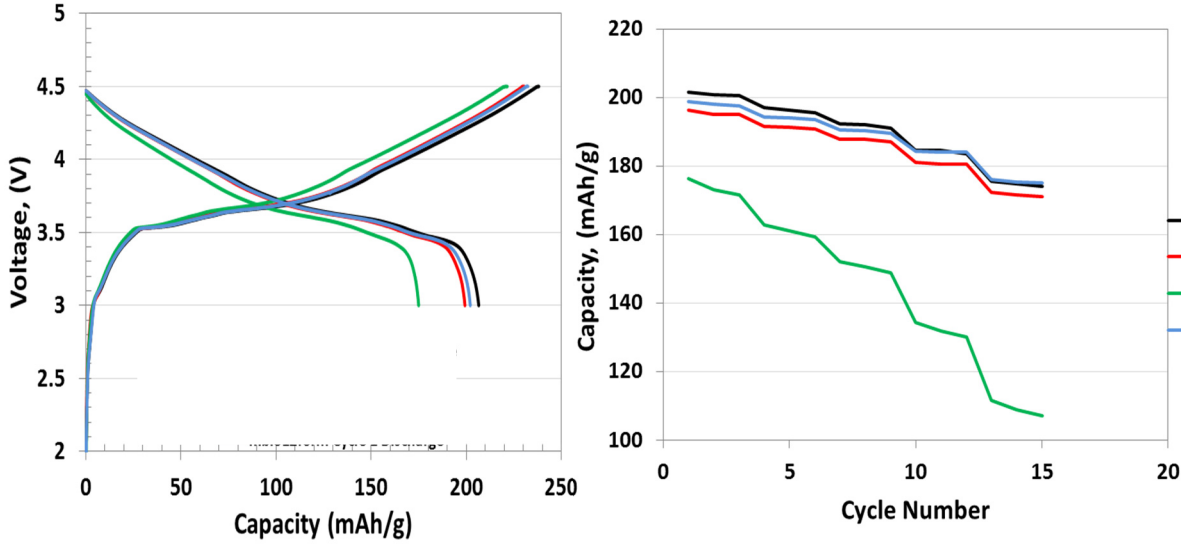


Figure IV- 51: 1st formation (left) and rate test (right) of A12 graphite/NCM523 full cell with various separators. Color code: black/PP:PE:PP; red/PP only; green/coated PP; and blue/alumina-coated PE

In order to confirm these preliminary findings of separator effect on the cell electrochemical performance, plans were made to conduct a larger study using fifteen A12 graphite/NCM523 full cells using the separators based on PP and PE (except for the coated PP, which failed the preliminary screening) and test them using the standardized protocol.

## Conclusions and Future Directions

Silicon and its composite were investigated as anode materials for lithium-ion batteries.

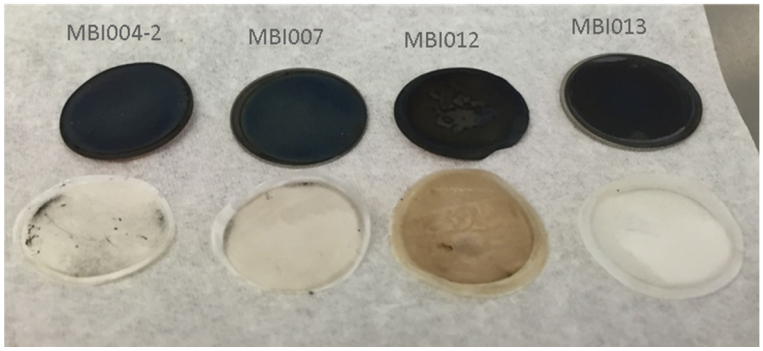


Figure IV- 52: Photo of separators after cycling

- Good electrochemical performance and mechanical properties were obtained using blend binder – PAA + SBR.
- FEC content study suggested that at least 10wt.% FEC is needed for Si electrode.
- DSC results indicate that the better thermal stability of Si electrode with FEC containing electrolyte.

The separator study suggested that the both PE and PP based separators have similar electrochemical stability. Preliminary results indicate that the ceramic coating can improve the cell performance.

Other cell components, such as redox shuttle, binder, separator, carbon additive have been studied and information was delivered to the material supplier and internal facilities. Under the CAMP Facility, several electrode library materials were collected and validated. Electrolyte and electrode materials from MERF were also validated.

In the coming fiscal year, we will continue to search and evaluate high energy density cathode and anode materials, such as silicon/silicon composite, nickel rich lithium metal oxides, et al. as they become available. Surface modification and electrolyte effects on electrochemical and thermal stability of high energy electrode materials will be investigated. Various electrode materials and cell chemistries will be evaluated under cell fabrication facility to help to build the electrode library. Materials scaled-up by Material Engineering and

Research Facility (MERF) will be validated. We will continue to work closely with research institutes and industrial suppliers to enable the LIB technology for PHEV and/or EV applications.

### FY 2015 Publications/Presentations

1. Materials Benchmarking Activities for CAMP Facility, ES028_luw_2015_p, US DOE Vehicle Technologies AMR, 2015.
2. A Raman-Based Investigation of the Fate of Li2MnO3 in Lithium- and Manganese-Rich Cathode Materials for Lithium Ion Batteries, Qingliu Wu, Victor A. Maroni, David J. Gostola, Dean J. Miller, Dennis W. Dees, and Wenquan Lu, J. of The Electrochem. Soc., 162 (7) A1255-A1264 (2015)
3. Synthesis of high performance LiNi1/3Mn1/3Co1/3O2 from lithium ion battery recovery stream, Qina Sa, Eric Gratz, Meinan He, Wenquan Lu, Diran Apelian, Yan Wang, J. of Power Sources 282 (2015) 140-145.
4. Electrochemical Modeling and Performance of a Lithium- and Manganese-Rich Layered Transition-Metal Oxide Positive Electrode, Dennis Dees, Daniel P. Abraham, Wenquan Lu, Kevin G. Gallagher, Martin Bettge, and Andrew N. Jansen, J. Electrochem. Soc. 162 (4) A559-A572 (2015).
5. A New Process for Atomic Layer Deposition of Al2O3 and Applications in Lithium-ion Batteries, Xiangbo Meng, Yanqiang Cao, Joseph A Libera, Wenquan Lu, Shaista Babar, and Jeffrey W. Elam, AVS 62nd Inter. Symp. & Exhibit. San Jose, Oct. 2015.
6. Silicon-Graphite Development: Robust, Practical, and Scalable High Performance Electrodes, Stephen Trask, Bryant Polzin, Joseph Kubal, Wenquan Lu, Nancy Dietz Rago, Andrew Jansen, 227th electrochemical Society Meeting, Chicago, IL, USA, 05/2015.
7. Silicon-Graphite Electrode Performance in Lithium Ion Batteries: From Coin Cells to 500mAh-Pouch Cells, Bryant Polzin, Stephen Trask, Andrew Jansen, Wenquan Lu, 227th electrochemical Society Meeting, Chicago, IL, USA, 05/2015.
8. Electrochemical Modeling and Performance of a Lithium- and Manganese-Rich Layered Transition-Metal Oxide Positive Electrode, Dennis W. Dees, Daniel P. Abraham, Wenquan Lu, Kevin G. Gallagher, Martin Bettge, and Andrew N. Jansen, 227th electrochemical Society Meeting, Chicago, IL, USA, 05/2015.
9. Enhanced Thermal Stability of Si/Graphene Composite Anode in the Presence of Fluoroethylene Carbonate Additive, Seonbaek Ha, Qingliu Wu, Jai Prakash, and Wenquan Lu, 227th electrochemical Society Meeting, Chicago, IL, USA, 05/2015.
10. Influence of Fluoroethylene Carbonate Additive Concentration on Silicon/Graphene Composite Anode, S. Ha, Q. Wu, A. N. Jansen, J. Prakash, and W. Lu, 227th electrochemical Society Meeting, Chicago, IL, USA, 05/2015.
11. Silicon-Graphite Slurry and High-Loading Electrode Process Development, Stephen Trask, Wenquan Lu, Bryant Polzin, Joseph Kubal, Nancy Dietz Rago, Andrew Jansen, 32nd International Battery Seminar and Exhibit, Fort Lauderdale, FL, US, 03/2015.

# IV.B.3 Abuse Tolerance Improvements (SNL)

## Objectives

- Elucidate degradation mechanisms in lithium-ion cells that lead to poor abuse tolerance (runaway thermodynamics, gas evolution, electrolyte combustion)
- Develop and evaluate advanced materials (or materials combinations) that will lead to more abuse-tolerant lithium-ion cell and battery systems.
- Build 18650 cells in the SNL fabrication facility for cell level evaluation of new materials in support of all ABR thrust areas.


**Project Details**

**Christopher J. Orendorff, Ganesan Nagasubramanian, Kyle R. Fenton, and Eric Allcorn**

Sandia National Laboratories
P. O. Box 5800, Mail Stop 0613
Albuquerque, NM 87185-0613
Phone: 505-844-5879; Fax: 505-844-6972
E-mail: corendo@sandia.gov

Collaborators:
Prof. Steven George, CU-Boulder
Rob Privette, XG Sciences
Andrew Jansen, ANL
Greg Krumkick, ANL
Ira Bloom, ANL



Start Date: October 2014

Projected End Date: September 2015


## Technical Barriers

There are several technical barriers to achieving the goals stated above, including:

- Developing advanced material components designed to improve the intrinsic abuse tolerance of lithium-ion cells which do not lead to high order catastrophic failures.
- Mitigating the gas evolution and decomposition of the electrolyte.
- Passivation of cathode runaway reactions and interfacial reactions with electrolyte.
- Limited quantities of advanced materials (and numbers of cells with new materials) to evaluate abuse response.

## Technical Targets

- Quantify the thermal runaway response of materials at the cell level (18650).
- Determine the effect of high energy materials, electrolyte salts, solvents and additives on the abuse response of lithium-ion cells.
- Determine the effect of advanced material components on the abuse response of lithium-ion cells.
- Optimize electrochemical performance of new electrolyte components to meet DOE goals.

## Accomplishments

- Determined the thermal runaway response of high capacity LMR-NMC cathode materials.
- Evaluated several advanced lithium-ion electrolytes to determine relative performance and abuse tolerance attributes.
- Scaled the synthesis of LiF/ABA to the 1 kg scale (ANL MERF) and confirmed the performance of the scaled material.
- Demonstrated the performance of LiF/ABA cells under overcharge and thermal abuse conditions.

### Introduction

As lithium-ion battery technologies mature, the size and energy of these systems continues to increase (> 50 kWh for EVs); making safety and reliability of these high energy systems increasingly important. While most material advances for lithium-ion chemistries are directed toward improving cell performance (capacity, energy, cycle life, etc.), a variety of materials advancements can be made to improve lithium-ion battery safety. Issues including energetic thermal runaway, electrolyte decomposition and flammability, anode SEI stability, and cell-level abuse tolerance continue to be critical safety concerns. This report highlights work with our

collaborators to develop advanced materials to improve lithium-ion battery safety and abuse tolerance and to perform cell-level characterization of new materials.

## Approach

The effect of cell materials (electrolytes, additives, anodes, and cathodes) on the thermal response of full cells is determined using several techniques. One of the most useful and quantitative techniques is accelerating rate calorimetry (ARC). The ARCs at SNL are fitted with uniquely designed high pressure fixtures to not only measure quantitative energy release but also gas generation under ideal adiabatic conditions during full cell runaway. Cells were fabricated using a variety of active materials, electrolytes, and additives in the SNL cell prototyping facility. The in-house prototyping capability gives us the versatility to target candidate materials, perform full cell evaluation, and correlate cell response to fundamental materials properties.

Abuse testing is performed to determine the cell response to potential abuse conditions and document the outcomes including 1) failure point of energy storage device 2) conditions that cause failure 3) failure modes and 4) quantify cell or module response to the abuse condition.

Our approach to developing advanced materials to improve abuse response focuses on redesigning lithium-ion cell electrolytes. This work starts with developing novel two-part electrolyte salts based on inherently stable lithium salts and anion binding agents (ABAs). The ABA components have two important design features: (1) improve the solubility of lithium salts in carbonate solvents by coordinating the salt negative ion at the electron withdrawing coordination site of the ABA and (2) passivate chemical decomposition reactions at electrode interfaces or in the bulk electrolyte to minimize the consequences and severity of thermal runaway and electrolyte combustion.

## Results

### High Energy Materials

One objective for FY15 was to determine the baseline thermal runaway response of high energy LMR-NMC materials. While there is a great deal of interest in the LMR-NMC class of materials as high capacity alternatives to NMC, little is known about the safety of LMR-NMC relative to conventional NMC. ARC was used to measure the cell-level thermal runaway of LMR-NMC cells and compare that behavior to other materials in cells. Figure IV- 53 shows cell normalized heating rate and exotherm temperature for LMR-NMC/graphite, NMC 523/graphite, NMC 523/Si-C, NMC 111/graphite, and LFP/graphite cells. The LMR-NMC cell runaway shows the highest peak heating rate (~350 °C/min) relative to the other NMC cathode cells (175-225 °C/min). It is important to note that the LMR-NMC cell is measured at 4.4 V at 100% SOC, compared to 4.2 V for the NMC cells, which will contribute to the difference in the observed normalized heating rate. As a point of reference, the peak heating rate of the LFP/graphite cells (measured at 3.8 V at 100% SOC), is on the order of 1.5 °C/min. The total temperature rise during the runaway (related to the total heat release) is comparable for the NMC/graphite and LMR-NMC/graphite cells, but is significantly greater for the NMC/Si-C cell. This is attributed to more heat release at higher temperature during runaway for Si-C compared to graphite (determined by DSC measurements in FY14).

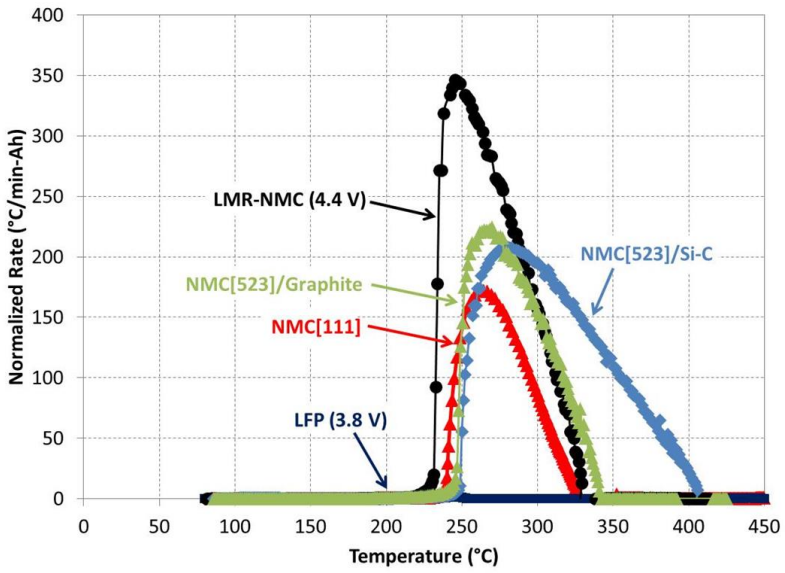


Figure IV- 53: Normalized heating rate (°C/min) as a function of temperature measured by accelerating rate calorimetry (ARC) for LMR-NMC, NMC 523/graphite, NMC523/Si-C, NMC 111, and LFP 18650 cells

### Abuse Tolerance of Advanced Electrolytes

There are several recently developed electrolytes based on LiF, TFSI, ionic liquids, fluorinated ethers, phosphines, phosphazenes, and siloxanes that have one or more advertised abuse tolerant attributes including non-flammable, thermally stable, and high voltage (to 5 V vs. lithium). However, there are no independent, systematic studies of any of these electrolytes to study the safety attributes and any trade-offs with electrochemical performance. This work focuses on studying the electrochemical performance, cell thermal runaway reactivity, abuse tolerance, and flammability of these types of electrolytes in NMC/graphite cells.

The electrolytes studied and their intended attributes related to cell safety are provided in Table IV- 6. The baseline electrolyte is 1.2 M $LiPF_6$ in EC:EMC (3:7). ABA electrolyte includes an alternative lithium salt based on LiF and a binding agent. FM2 contains a phosphazene additive. OS contains an organosilicon co-solvent. HFE is based on hydrofluoroether co-solvents. Compositions of ABA and HFE, developed at Sandia, are provided in Table IV- 6. Compositions of the FM2 and OS electrolytes are not provided in this report. It is important to note that the quantities of each electrolyte component will dramatically impact their overall performance. All of this work presented is for one specific composition of each electrolyte type, with the exception of OS, where there are two formulations in this study (OS1 and OS2). Other compositions may give different performance than what is shown here.

**Table IV- 6: Electrolytes evaluated for performance and abuse tolerance**

| Electrolyte | Formulation | Intended Attributes |
|---|---|---|
| Baseline | 1.2 M $LiPF_6$ in EC:EMC (3:7) | (Baseline) |
| ABA | 1.0 M LIF/ABA + 2% VC | Mitigate thermal runaway severity, enhanced abuse tolerance |
| FM2 | Proprietary | Flame retardant |
| OS | Proprietary | Enhanced thermal stability |
| HFE | 1.0 M LiTFSI in EC:DEC:HFE (5:45:50) | Non-flammable, good electrochemical performance |

Figure IV- 54 shows the discharge capacity of ~1 Ah NMC 523/graphite cells with the 5 electrolytes. The FM2, ABA, and baseline electrolytes have very consistent discharge capacities (measured at a C/5 discharge rate). OS1 and HFE electrolytes give slightly lower discharge capacities (5% less than the baseline), which could be attributed to the poorer ambient temperature conductivity of both OS1 and HFE relative to the baseline (Figure IV- 55). Cycle life of each electrolyte in NMC 523/graphite cells was started in FY15 and some experiments are still in progress. Current results are shown in Figure IV- 56 for the baseline, FM2 and ABA cells. The ABA cell shows 80% capacity retention at 200 cycles, while FM2 and baseline cells show 80% capacity retention at 260 and 300 cycles.

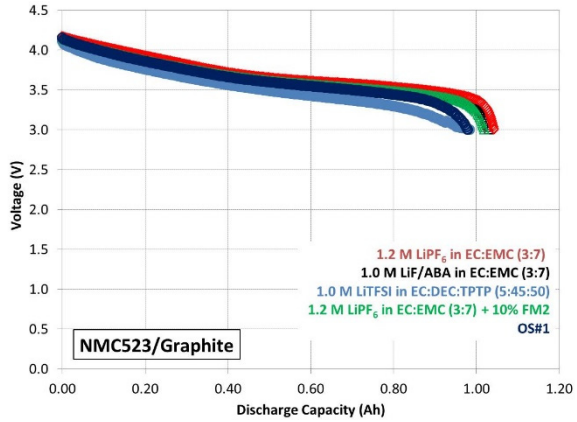


Figure IV- 54: A plot of cell voltage and discharge capacity for NMC523 cells with different electrolytes

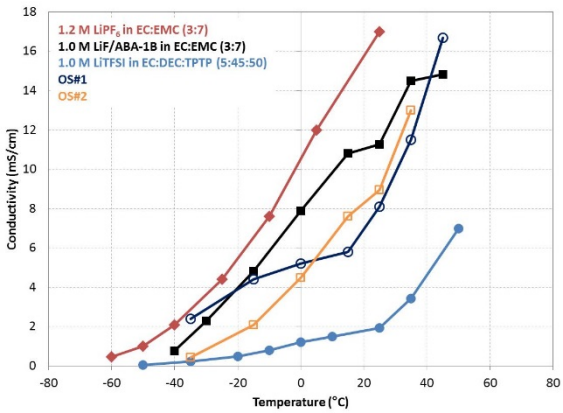


Figure IV- 55: A plot of electrolyte conductivity vs. temperature for various electrolytes

The rate capability of each NMC/graphite cell with different electrolytes from C/10 to 2C is shown in Figure IV- 57. Interestingly, the baseline OS1 electrolyte shows the best capacity retention at 2C, while having an ambient temperature conductivity that is only ~7 mS/cm (compared to >17 mS/cm for the baseline). This suggests that while the bulk liquid conductivity of the OS1 electrolyte is relatively low, the interfacial conductivity must be relatively high in order to give good rate capability. This behavior will be confirmed by complex impedance spectroscopy measurements.

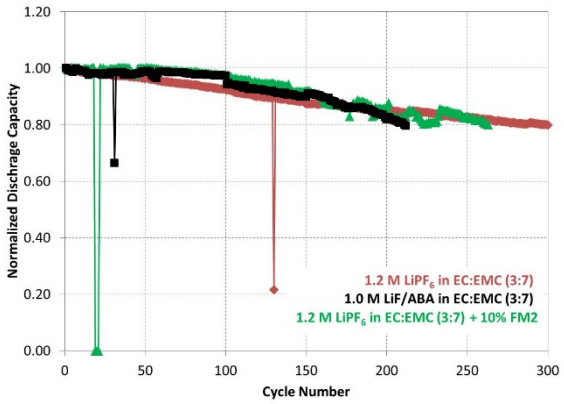


Figure IV- 56: Normalized discharge capacity as a function of cycle number for NMC cells with various electrolytes

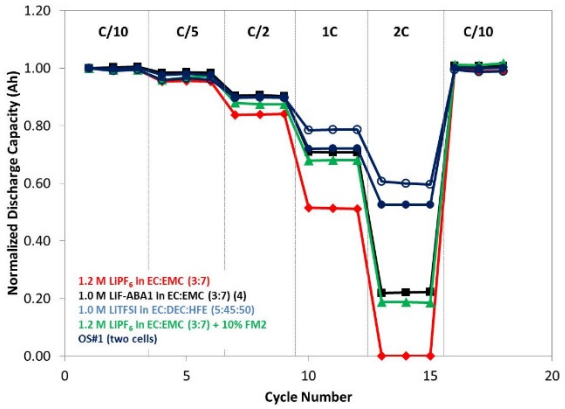


Figure IV- 57: Rate capability plotted as normalized discharge capacity for discharge rates from C/10 to 2C

Thermal runaway behavior of each of these electrolytes in NMC/graphite cells is evaluated by ARC. Figure IV- 58 shows the normalized heating rate (°C/min) as a function of temperature during the exotherm region of the thermal runaway measured by ARC. The baseline cell has a runaway onset temperature of ~225°C, a peak heating rate of ~200°C/min and a total temperature rise of ~330°C. The OS1, OS2, FM2 electrolytes all have similar thermal runaway behavior to the baseline cells. The two notably different performing cells are the HFE and ABA cells. The HFE cell has a significantly lower thermal runaway onset temperature of ~205°C and a higher peak heating rate of ~300°C/min relative to the baseline cell. While this could be attributed to the reactivity of the HFE electrolyte component, the DEC co-solvent may also play a role (note that the baseline cell is 70% EMC and the HFE cell is 45% DEC). The combustion enthalpy for DEC is 2715 kJ/mole and for EMC is 2000 kJ/mole, which could contribute to a lower onset temperature and a more energetic thermal runaway for the DEC containing HFE electrolyte relative to the EMC containing baseline cell.

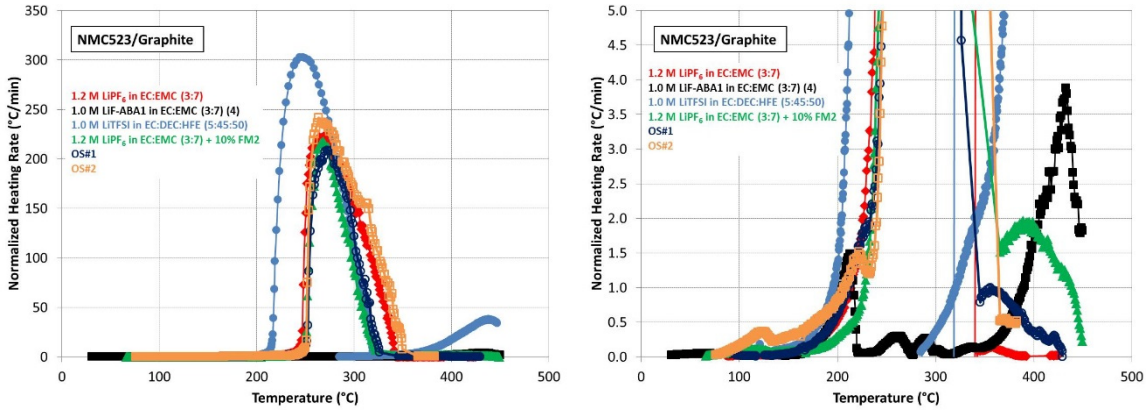


Figure IV- 58: Normalized heating rate as a function of temperature for ARC measurements of NMC cells with different electrolytes (expanded view on the right side)

The thermal runaway reactivity of the ABA cell is significantly less than baseline cell (and all of the other cells in this study). The peak heating rate of the ABA cell is ~1.5°C/min and the entire high rate portion of the runaway is completely eliminated (shown in the expanded view of Figure IV- 58). This is consistent with the behavior of ABA electrolytes in NMC cells reported in FY13 and 14, during the development of these electrolytes. Characterization studies of the mechanism of ABA behavior were initiated in FY15 in

collaboration with the ANL CAMP facility and will continue in FY16. The ABA electrolyte is the only one in this series that exhibits a measureable improvement in NMC/graphite thermal runaway performance relative to the baseline.

In addition to the ARC measurements, the abuse tolerance of each of these electrolytes is also evaluated in NMC cells. Figure IV- 59 shows plots of cell voltage (dashed line) and temperature (solid line) as a function of % SOC for each of these cells during a 1C overcharge abuse test. The ABA cell reaches the compliance voltage at 160% SOC and the test is ended without the cell going into thermal runaway (peak temperature of ~120°C). All of the other cells exhibit an energetic failure at ~170-175%SOC with peak temperatures as high as >400°C.

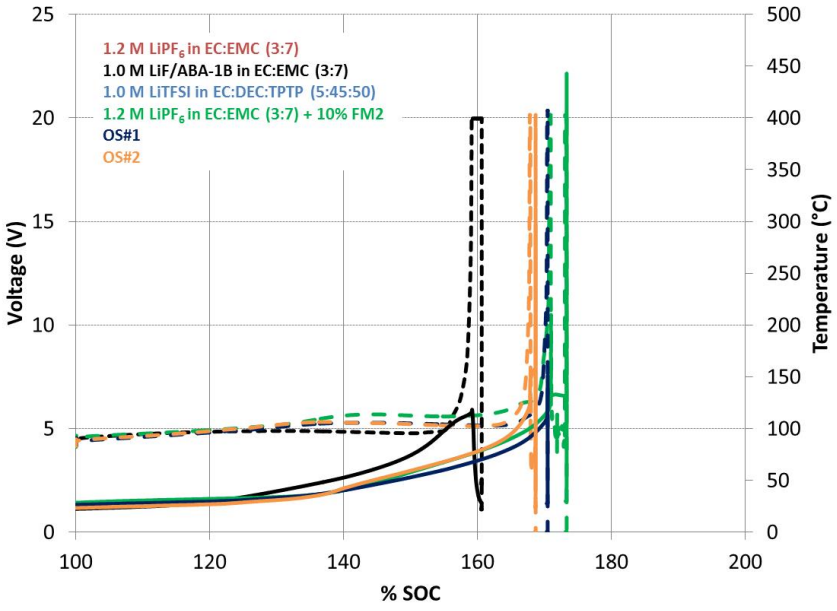


**Figure IV- 59: Cell voltage and temperature as a function of SOC during 1C overcharge testing of NMC cells with various electrolytes. measurements**

Electrolyte flammability was measured by the approach developed at SNL and reported by Nagasubramanian et al.[15] Cells are heated until they vent directly into an ignition source to measure of electrolyte flammability during an actual cell vent failure. Figure IV- 60 shows still images from the video of flammability tests of NMC cells with various electrolytes. All of the electrolytes tested ignite and sustain a fire for at least several seconds, with the exception of the HFE electrolyte which does not ignite or burn under these test conditions. At 50% HFE co-solvent, there is no ignition of this electrolyte during a cell vent. We have determined that the flammability of HFE electrolytes is somewhat variable at 30% HFE co-solvent, but have not done a systematic study through the co-solvent fractions. This suggests that in this co-solvent approach to non-flammable electrolytes, a significant fraction of non-flammable co-solvent needs to be used in order to achieve non-flammable characteristics of the blended electrolyte.

[15] G. Nagasubramanian, C. J. Orendorff, "Hydrofluoroether electrolytes for lithium-ion batteries: Reduced gas decomposition and nonflammable" J. Power Sources, 196 (2011) 8604-8609.

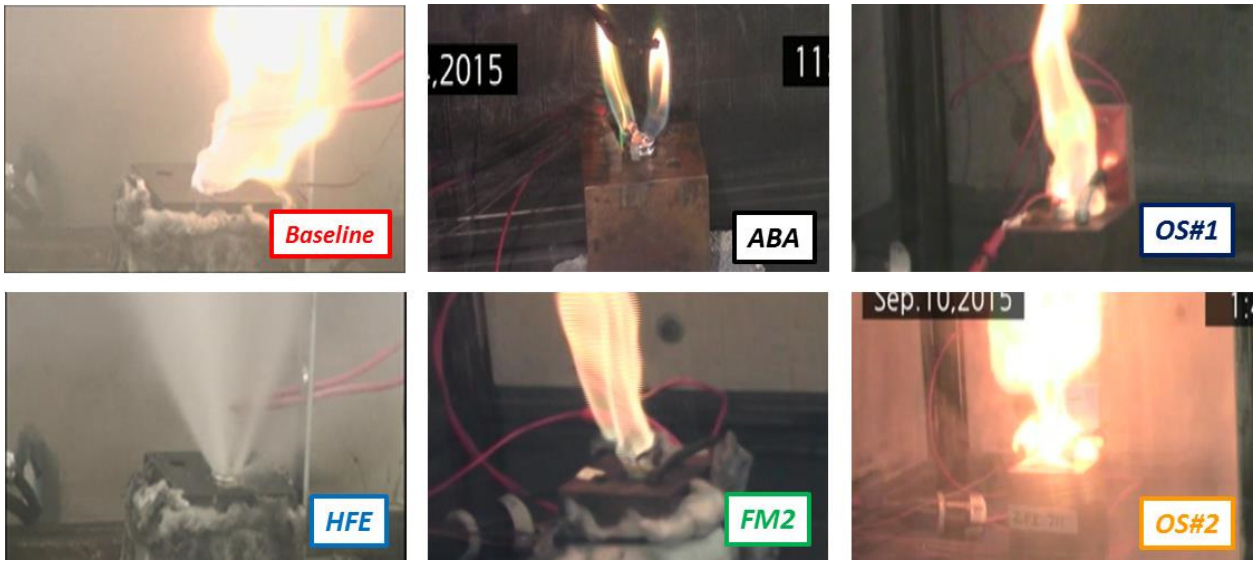


Figure IV- 60: Still images during flammability tests of various electrolytes in NMC cells

## Conclusions and Future Directions

This work demonstrates how specific advances in a variety of materials areas (anode, cathode, and electrolyte) can impact cell-level safety and thermal characteristics. We have reported on the thermal runaway properties of cells containing LMR-NMC cathodes to better understand how this class of high energy cathode materials will impact cell and battery-level safety and abuse tolerance. Results show the LMR-NMC cells to be kinetically more reactive than conventional NMC cells during thermal runaway. The magnitude of this change is expected given the higher cell voltage of LMR-NMC (4.4 V) relative to NMC (4.2 V). We have also evaluated the performance and safety of a series of lithium-ion battery electrolytes. Results show some improvement in the performance metrics with the advanced electrolytes, namely the rate capability of the OS electrolytes at 2C in spite of the fact that is exhibits lower bulk conductivity than conventional $LiPF_6$ in EC:EMC electrolyte. Only the LiF/ABA electrolyte shows a benefit in the thermal runaway behavior and tolerance to overcharge of NMC cells relative to cells with the baseline electrolyte. Only the HFE electrolyte was shown to be non-flammable under cell vent test conditions (for the electrolyte that contains 50% HFE co-solvent). Work will continue in developing a better understanding of the abuse response and thermal runaway behavior of high energy alloy anode and electrolyte materials for these electrolyte materials for lithium-ion and other advanced energy storage technologies.

## FY 2015 Publications/Presentations

1. C. J. Orendorff et al., “Quantifying Thermal Runaway by Battery Calorimetry and Opportunities for Improvement” IAPG Safety Panel, San Diego, CA, February 2015
2. J. Lamb et al. “Failure Propagation in Multi-Cell Lithium Ion Batteries” J. Power Sources 283 (2015), 517-523.
3. C. J. Orendorff et al., “Advancing Battery Safety through Materials Development and Testing” Next Generation Batteries 2015, San Diego, CA, April 2015
4. J. Lamb et al. “Safety Testing Challenges for Grid-Scale Energy Storage Systems” Next Generation Batteries 2015, San Diego, CA, April 2015.
5. J. Lamb et al., “Studies on the thermal breakdown of common li-ion battery electrolyte components” J. Electrochem. Soc., 162 (2015), A2131-A2135.
6. J. Lamb, et al., “Advances Toward Inherently Safe Lithium-Ion Batteries,” Advanced Automotive Batteries Conference (AABC) 2015, Detroit, MI, June 2015.

# IV.B.4 Post-Test Diagnostic Facility Activities

## Objectives

- To accelerate the R&D cycle of DOE and industrial collaborators by developing and conducting standard proceudres for post-test characterization of batteries in order to provide insight into the physicochemical casuses of performance degradation.


**Project Details**

**Peter Faguy (DOE Program Manager)**

**Ira Bloom (PI), Nancy Dietz Rago, Javier Bareño**
Argonne National Laboratory
9700 South Cass Avenue
Argonne, IL 60439
Phone: 630-252-4516; Fax: 630-972-4516


Start Date: April 2010

Projected End Date: Open

## Technical Barriers

This project addresses the following technical barriers as described in the USABC goals [1, 2, 3]:

- Performance at ambient and sub-ambient temperatures
- Calendar and cycle life

## Technical Targets

- EV: 5-year calendar life; 1,000 80% DOD DST cycles
- HEV: 15-year calendar life, 300,000 charge-sustaning cycles; EOL performance (min): 25 kW and 300 Wh
- PHEV: 15-year calendar life, 300,000 charge-sustaning cycles, 5,000 charge-depleting cycles; EOL performance (min): 45 kW and 300 Wh
- LEESS: 15-year calendar life, 300,00 charge-sustaning cycles; EOL performance (min): 20 kW and 56 Wh
- 12 V SS: 15-year calendar life, 450,000/150,000 starts/miles at 30 and 45°C

## Accomplishments

- Established a standard technique for opening 18650-sized cells for the facility.
- Characterized the physical and chemical changes caused by fast-charging lithium-ion cells.
- Completed collaboration with industrial developer: JohnsonControls, Inc.
- Started/continued collaborations with CAMP Facility, Jet Propulsion Laboratory, Army Research Laboratory, University of Hawaii, CIC Energigune (Spain), Oak Ridge National Laboratory, University of Warwick (UK) and Illinois Institute of Technology
    - Started characterization of high energy Li-ion cells comprising Si/Grpahite-based anodes
    - On-going support of Voltage Fade and High Energy / High Voltage deep-dive projects

### Introduction

Batteries are evaluated using standard tests and protocols which are transparent to technology [1, 2, 3]. The evaluation provides information about how battery performance changes with time under a given set of conditions. Post-test characterization of aged batteries provides additional information regarding the underlying physicochemical mechanisms causing of performance degradation, which previously was only inferred. Mechanistic understanding of performance degradation may enable the development of new strategies to sustain performance of next-generation Li-ion technologies with longer service lives.

### Approach

Post-test analysis consists of physical, spectroscopic, metallographic, and electrochemical characterization of battery components that have been harvested from aged cells. The aged cells have undergone standardized testing. The cells can come either from exploratory DOE programs, such as ABR and BATT, or from pre-

competitive R&D programs managed by USABC and USDRIVE. The Post-Test Facility uses the experience and techniques developed in DOE's applied battery program in a standardized fashion.

## Results

### Standard Procedure to Open an 18650-Sized Cylindrical Cell

According to current practice, 18650-sized cylindrical cells are opened with either a Dremel® multi-tool or some type of hand tool [4-6]. This can increase the local temperature; contaminate exposed active material; and short circuit the cell [7]. We created a method that allows the cell to be opened safely (no short circuits), to have the active roll removed completely intact (no contamination) and all without traditional cutting (no temperature rise). The method cuts the top off with a tubing cutter, carefully peels the sides of the 18650-sized cell can apart with pliers and produces the intact cell roll (see Figure IV- 61).

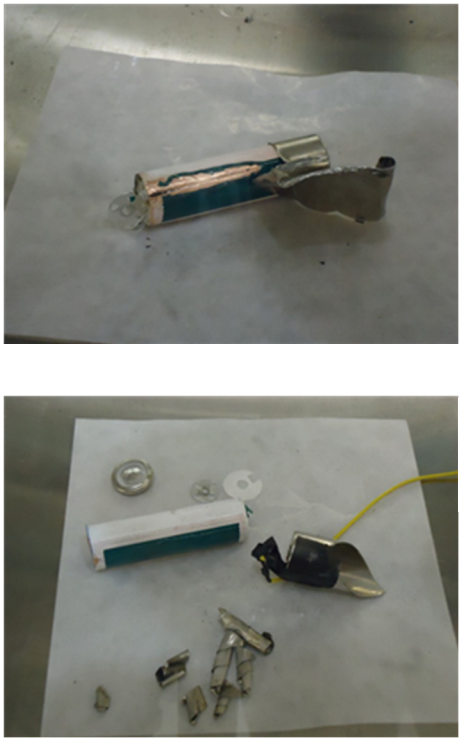


Figure IV- 61: (a) Photograph of an 18650-sized cell being dismantled using traditional methods. The hand saw cut into the electrode material, causing a short circuit. (b) Photograph of cell materials harvested using a tubing cutter, showing that materials were removed intact

### Effect of Fast-Charging Lithium-Ion Cells: Post-Test Results

Typically, fueling an internal-combustion-engine-powered vehicle takes ~5-15 minutes at a service station. On the other hand, fully charging a lithium-ion battery system can take 1-2 hr. Further, if a motorist runs out of gasoline on the highway, 20 L of fuel can be quickly added to the tank, partially refilling the tank and enabling the motorist to get to his next destination.

To meet the expectations set by the internal combustion engine, the battery system would have to be charged at the 4-to-6-C rate. The Fast-Charge Test in USABC EV Manual [1] served as the basis to investigate the effect of the high charge rate and of partial charge on the life using commercially-available, 18650-sized lithium-ion cells based on NMC/graphite chemistry.

The cells were charged at 0.7-, 2-, 4- and 6-C rates from 0 to 100% SOC (full charge) or from 40 to 80% SOC (fast-charge). The cells were discharged at the C/1 or C/3 rates, respectively. The effect of charge time, charging method and charging rate on cell resistance is shown in Figure IV- 62. From the figure, cells that were charged using the fast-charge method displayed a greater rate of resistance rise.

Plotting these data against $i^2R\Delta t$ shows that both the full- and fast-charged cells displayed similar trends. Both were linear with $i^2R\Delta t$, as shown in Figure IV- 63 and Figure IV- 64. As can be seen from these figures, the change in relative resistance was greater per $i^2R\Delta t$ unit in the fast-charge cells than in those full-charged. The $i^2R\Delta t$ term can be interpreted as the energy throughput used to charge the cell (Wh); or, alternatively, as proportional to the total heat generated in the cell during the changing process.

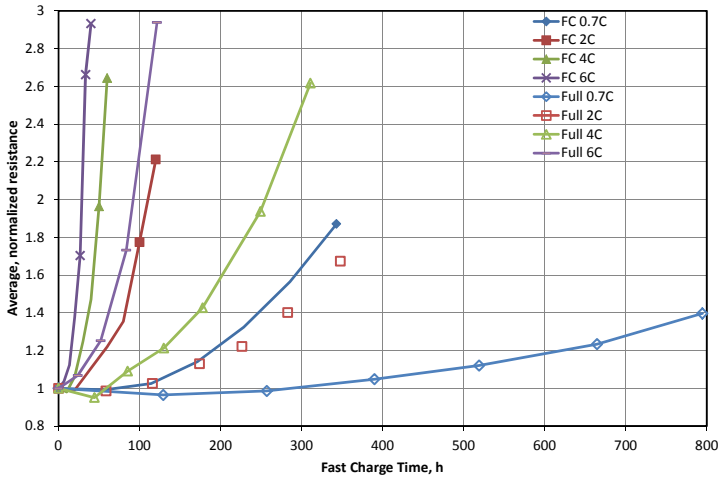


Figure IV- 62: Average, normalize resistance vs. charge time, charging method and charging rate. FC=fast charge

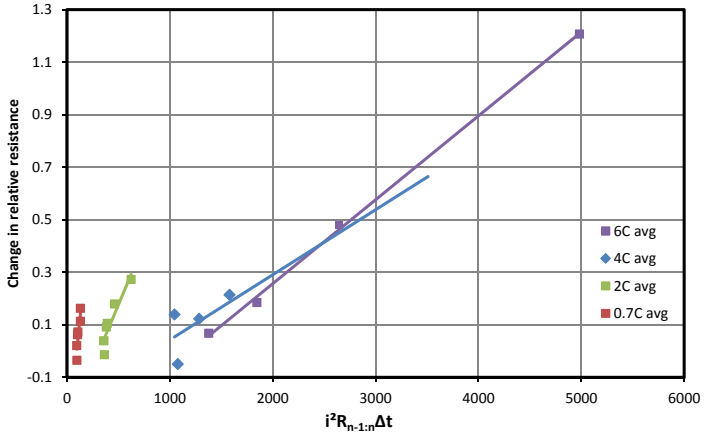


Figure IV- 63: Change in relative resistance vs. i2RΔt and charge rate for the full-charged cells

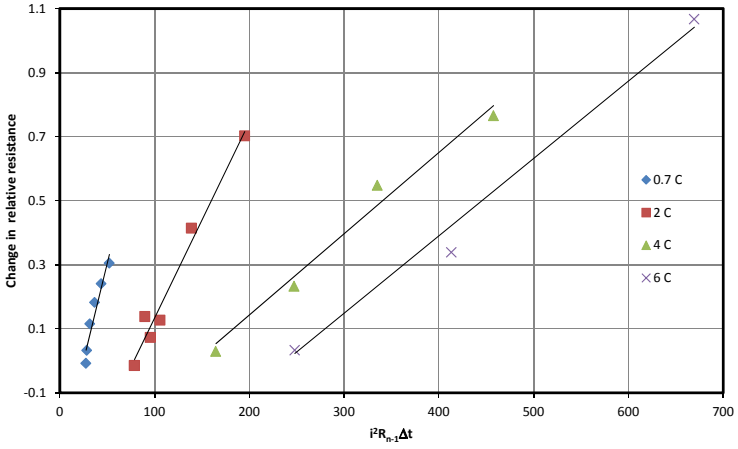


Figure IV- 64: Change in relative resistance vs. i2RΔt and charge rate for the fast-charged cells

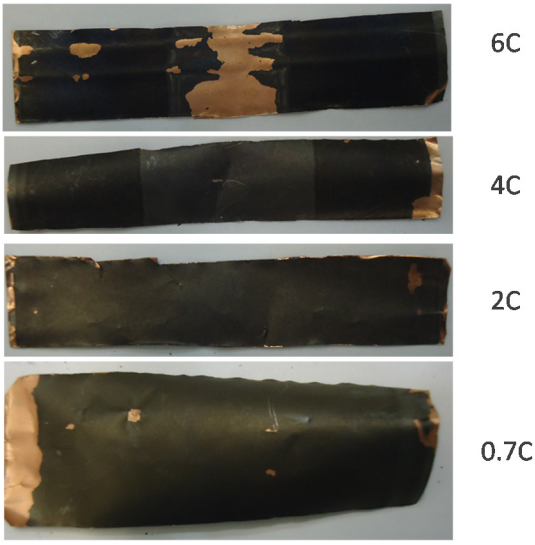


Figure IV- 65: Optical photographs of anodes from full-charged cells

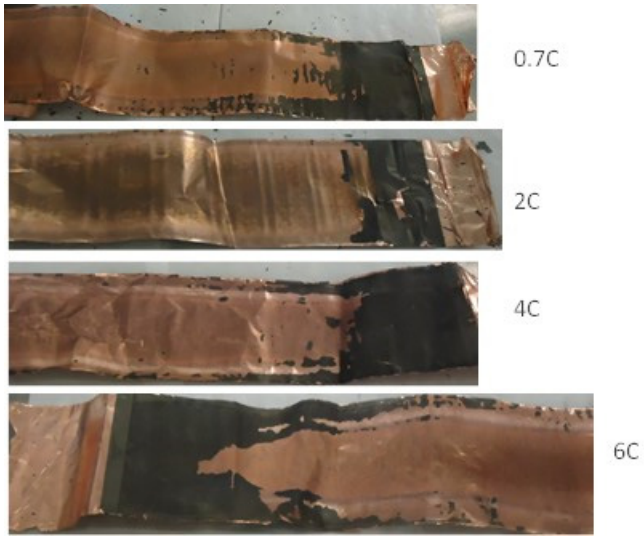


Figure IV- 66: Optical photographs of anodes from fast-charged cells

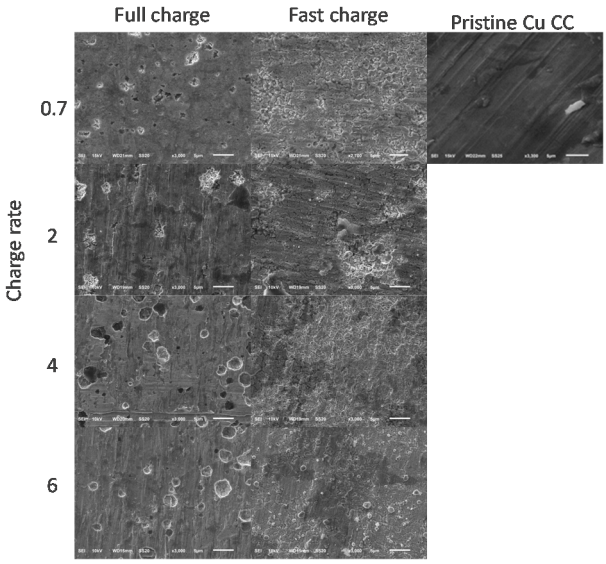


Figure IV- 67: SEM micrographs of anodes from fast-charged cells

## Conclusions and Future Directions

Fast-charging caused performance decline in lithium-ion batteries. The extent of the decline was proportional to charge rate. Post-test examination of the cells indicated that one cause of performance decline was from the degradation of the binder in the anode, causing loss of contact between the current collector and the active anode material. Even though this study exacerbated the effect of fast-charging, infrequent fast charging of electric vehicles may introduce similar degradation modes. It may be possible to lessen these effects through effective thermal management of the vehicle battery pack.

The next steps for the Post-Test Facility are as follows.

- Actively engage USABC and DOE battery contractors to help them understand the sources of performance decline
- Collaborate with ABR, BATT and USABC programs
- Participate / lead in the characterization of Si-binder interactions to enable development of high energy couples employing Si/Graphite-based anodes.

## List of Abbreviations

ABR: Advanced Battery Research
ANL: Argonne National Laboratory
BATT: Batteries for Advanced Transportation Technologies
CAMP Facility: Cell Analysis, Modeling and Prototyping Facility at Argonne.
EV: electric vehicle
HEV: hybrid electric vehicle
LEESS: Low-Energy Energy Storage System
PHEV: plug-in hybrid electric vehicle

SEM: scanning-electron microscope
SOC: state of charge
USABC: United States Advanced Battery Consortium (DOE, GM, Chrysler and Ford)

## FY 2015 Publications/Presentations

1. "Post-test Analysis of Lithium-Ion Battery Materials at Argonne National Laboratory", J. Bareño, N. Dietz-Rago, and I. Bloom, U.S. Department of Energy Vehicle Technologies Office Annual Merit Review and Peer Evaluation Meeting, June 8–12, 2015, Arlington, VA2015 "Effects of Fast Charging Lithium-Ion Cells," IEA Meeting, IA-HEV Annex, September 2014, Nice, France.
2. "Effect of Fast Charging on Lithium-Ion Cells: Performance and Post-test Results," L. Somerville, P. Prezas, J. K. Basco, T. Duong and I. Bloom, International Battery Association-Pacific Power Sources Symposium, January 5-9, 2015, Kona, HI.
3. "Effect of Fast Charging on Lithium-Ion Cells: Performance and Post-test Results," I. Bloom, L. Somerville, P. Prezas, J. K. Basco, and T. Duong, Department seminar, Illinois Institute of Technology, January 14, 2015.
4. "Effects of Fast Charging on Lithium-Ion Cells," I. Bloom, P. Prezas, J. K. Basco, L. Somerville and T. Duong, 249th ACS National Meeting & Exposition, March 22-26, 2015, Denver, CO.
5. "Argonne National Laboratory's Post-Test Facility for Analysis of Lithium-Ion Battery Materials," N. Dietz-Rago, J. Bareño, I. Bloom, and V. Maroni, Tech-to-Market Workshop, Idaho Falls, ID, May 18-20, 2015.
6. "Effects of Fast Charging On Lithium-Ion Cell," L. Somerville, P. Jennings, A. McGordon, C. Lyness, P. Prezas, J. K. Basco, J. Bareno, T. Duong and I. Bloom, 227$^{TH}$ ECS Meeting, Chicago, IL, May 24-28, 2015.
7. "A Case Study: Li/S Battery Characterization in Argonne National Laboratories Post-test Facility and Center for Nanoscale Materials," N. Dietz Rago, L. Chen, Y. Liu, L. Shaw, and I. Bloom, 227$^{TH}$ ECS Meeting, Chicago, IL, May 24-28, 2015.
8. "Understanding the Effect of Fluorinated Ether on the Improved Performance of Lithium-Sulfur Batteries," Nasim Azimi, Zheng Xue, Ira Bloom, Mikhail Gordin, Donghai Wang, Tad Daniel, Christos Takoudis, and Zhengcheng Zhang, ACS Applied Materials & Interfaces, 7 (2015) 9169-9177.
9. "The Synthesis of Ternary Acetylides with Tellurium: $Li_2TeC_2$ and $Na_2TeC_2$," Károly Németh, Aditya K. Unni, Christopher Kalnmals, Carlo U. Segre, James Kaduk, Ira D. Bloom and Victor A. Maroni, RSC Adv., 5 (2015) 55986, DOI:10.1039/c5ra08983b

## References


1. FreedomCAR Battery Test Manual for Power-Assist Hybrid Electric Vehicles, DOE/ID-11069, October 2003.
2. FreedomCAR Battery Test Manual for Plug-In Hybrid Electric Vehicles, June 2010.
3. Electric Vehicle Battery Test Procedures Manual, Revision 2, January 1996.
4. G. Nagasubramanian, "Two-and three-electrode impedance studies on 18650 Li-ion cells," J. *Power Sources*, 87 (2000) 226-229.
5. D. Aurbach, et al., "An analysis of rechargeable lithium-ion batteries after prolonged cycling," *Electrochimica Acta*, 47 (2002) 1899-1911.
6. S. L. Poe, et al., US Patent 20,140,306,162 (2014).
7. N. Williard, B. Sood, M. Osterman, and M. Pecht, "Disassembly methodology for conducting failure analysis on lithium–ion batteries," *J. Mater. Science: Materials in Electronics*, 22 (2011) 1616-1630.

# IV.C Critical Barrier Focus —Enabling High Energy, High Voltage Li-ion Batteries

# IV.C.1 Enabling High-Energy/Voltage Lithium-Ion Cells for Transportation Applications – Part 1: Baseline Protocols and Analysis (ANL)

## Objectives

- High-performing, high-energy, safe and long-life batteries are needed to reduce petroleum consumption in vehicular applications. The performance targets of these batteries can be met by cells containing layered-oxide-based positive electrodes. To achieve the energy and power density targets, these cells need to be cycled to voltages that exceed 4.5 V vs. $Li/Li^+$. On extended cycling at these voltages, however, capacity loss, impedance rise and voltage fade reduces the cell's energy and power output. Our objective is to mitigate this performance degradation, thereby reducing the lifetime cost of these high-energy batteries.

**Project Details**

**Peter Faguy (EERE-VTO-ABR Program Manager)**
HE/HV Team (Argonne National Lab)
9700 South Cass Avenue, CSE-200
Lemont, IL 60439
Phone: 630-252-2629; Fax: 630-972-4461
Email: burrell@anl.gov

Start Date: October 2014

Projected End Date: September 2018

## Technical Barriers

- Calendar/cycle life of lithium-ion cells being developed for PHEV and EV batteries that meet or exceed DOE/USABC goals.

## Accomplishments

- Physical parameters for the full cell, coin-cell format were studied and standardized.
- Standard electrochemical cycling protocols were defined.
- Analysis procedures for arbitrarily-sized data sets were defined and used to gauge relative changes in data trends against large baseline data sets.

### Introduction

The overall objective of this project is to understand the failure mechanisms that prevent state-of-the-art Li-ion battery systems from achieving higher practical energy densities than are currently obtainable. The inability to delithiate commercially available cathode materials beyond ~4.3 V (vs. Li/Li+) without incurring excessive surface damage, electrolyte decomposition, and bulk structural instabilities is a significant challenge. As such, four areas of research, or thrusts, will be focused on during the course of this project; cathodes, electrolytes and additives, surfaces and interfaces, and testing and analysis. So that all thrusts can communicate data in a meaningful way, and to ensure the reliability of reported results and materials improvements, standardization of all cell-related procedures and testing must be realized. It is expected that the protocols developed for this project will serve as a tool for the ABR battery community (and beyond) to allow effective, transferable communication of results between various researchers and institutions.

### Approach

Due to practical considerations and available resources, 2032-type coin-cells were chosen as the standard format for research and development work. The goal of coin-cell work will be to readily produce reliable data

on the performance of cells and cell components (cathodes, anodes, additives, etc.) for which one is capable of predicting, within reason, correlated performance in larger-format pouch-cells. Subsequently, resources can be confidently allocated to the production and evaluation of larger-format cells containing promising materials. Several protocols must first be developed and related to the physical parameters of cells such as electrolyte volume, electrode area, and cell assembly. In addition, electrochemical cycling procedures, data analysis, and data presentation must be standardized in order to verify data from multiple cell sets and/or sources.

Commercially available cathode powders including layered NMC-532 and NCA were chosen as baseline cathode powders for this project. These cathode materials cover a wide range of operating voltages, compositions, and surface chemistries while remaining practically relevant. The baseline anode material for all cells will be graphite. All baseline electrode laminates will be fabricated in-house at Argonne's cell analysis, modeling, and prototyping (CAMP) facility. The standard electrolyte will be GEN2-based ($LiPF_6$ in EC:EMC). Components used in the standardization studies herein are as listed in the text.

## Results

### Assembly: effect of cathode to anode area

Coin-cell assembly must be reproducible. An important factor influencing reproducibility is the physical ability of individual researchers to accurately align electrodes by hand. A test was conducted to determine if oversizing the anode, relative to the cathode, could lead to more reproducibility in coin-cell assembly without artificially affecting the electrochemical data. Table IV- 7 shows the components of the study.

**Table IV- 7: 2032-type coin cell components and sizes/volume**

| Part | Size/Volume | Type |
|---|---|---|
| cathodes | 14.0, 14.3 mm | NMC-532 |
| anodes | 14.0, 14.3, 15 mm | Graphite |
| electrolyte | flooded (~60 µl) | 1.2 M $LiPF_6$ in EC:EMC (3:7) |
| separator | 16.0 mm | 25µm, tri-layer (PP/PE/PP) |
| spacers | 15.8 mm | stainless |
| seal | 16.0 mm (i.d.) | plastic |
| spring | --- | stainless |

It was initially found that the single-sided CAMP laminates of the baseline NMC-532 cathodes and graphite anodes have a tendency to curl due to uneven strain after compression, as shown in Figure IV- 68(a). The anode laminates, cast on the thinner copper foil, showed a higher degree of curling. This was attributed to the low porosity (~35.6% for the anode, 33.5% for the cathode) to which the electrodes are compressed as well as the heat used in the automated calendaring process (at 80°C). The effect of porosity on anode curling has been verified through a separate study where higher porosities were correlated with less electrode curling. Although curling is not an issue during the assembly of electrodes into pouch cells, coin-cell electrodes must be flat to allow for the proper alignment (as described below); an important consideration since both cell formats must be constructed from the same laminates for systematic electrochemical comparisons.

Figure IV- 69 (a)-(c) show results for a series of 14 mm diameter, NMC-532 cathodes paired with 14.0, 14.3, and 15.0 mm diameter graphite anodes. Table IV- 8 shows the area oversize percent for the different anode and cathode pairs used in the study. No matter what the cathode/anode pairing size, the data show that reproducibility was poor. Figure IV- 69 (d) shows examples of 14 mm/14 mm cathode/anode cells with two cells (labelled bad 1&2) having intentionally misaligned electrodes. The result is a larger spread in reproducibility when including the misaligned cells and an apparent decrease in capacity from the purposefully misaligned cells. Therefore, care should be taken not to misinterpret such behavior in full-cell studies.

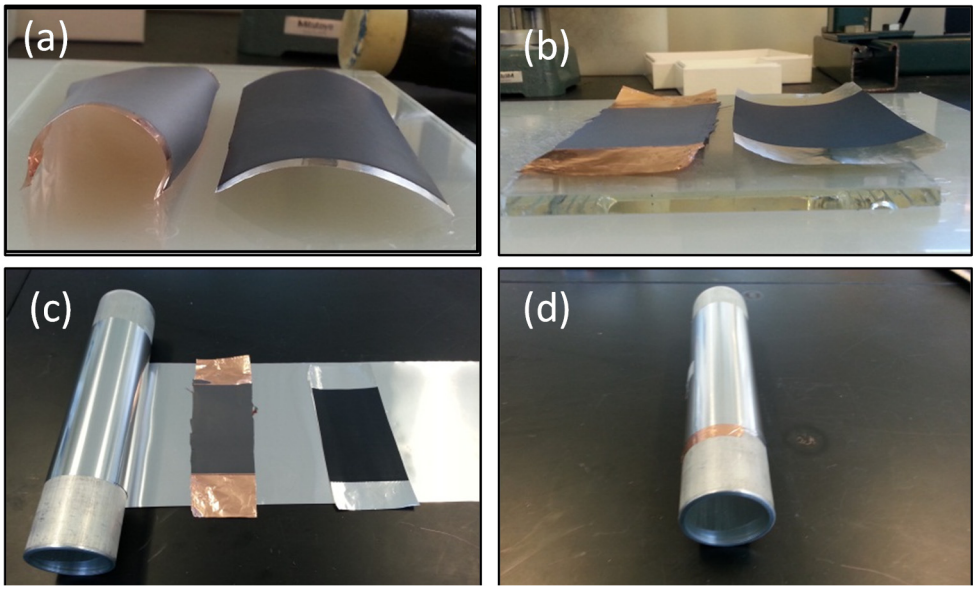


Figure IV- 68: (a) Curling of single-sided anode (left) and cathode (right) laminates due to uneven strain. (b) Flat laminates after vacuum drying wound on metal cylinder. (c) and (d) Laminates being wound on metal cylinder to counter natural curvature

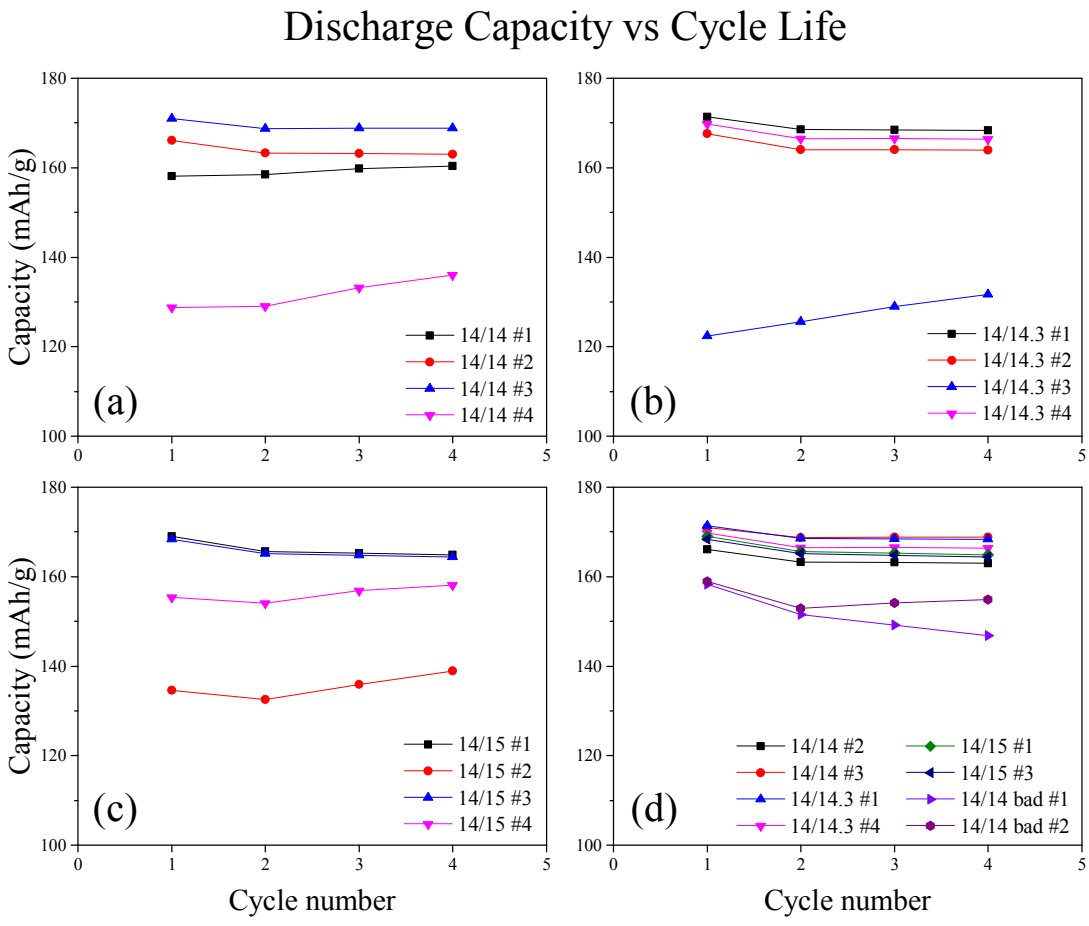


Figure IV- 69: (a)-(c) show the first 4 cycles between 4.25-3.0 V (C/10) for NMC-532/graphite cells having different cathode to anode areas. (d) Shows an example of two cells (14/14 bad 1&2) with purposely misaligned electrodes

**Table IV- 8: Area oversize percent for the anode and cathode pairs used in this study**

| Cathode | Anode | Area Oversize |
|---|---|---|
| 14 mm | 14 mm | 0% |
| 14 mm | 9/16” | 4% |
| 9/16” | 15 mm | 11% |
| 14 mm | 15 mm | 15% |

Vacuum drying of the single-sided electrodes at ~90°C with laminates wound on a metal cylinder, between aluminum foil, was found to counter the natural curvature of the compressed laminates allowing for flatter electrode punches to be obtained [Figure IV- 68(b)-(d)]. The study shown in Figure IV- 69, using increasingly oversized anodes, was repeated using the flat electrodes and the results are shown in Figure IV- 70.

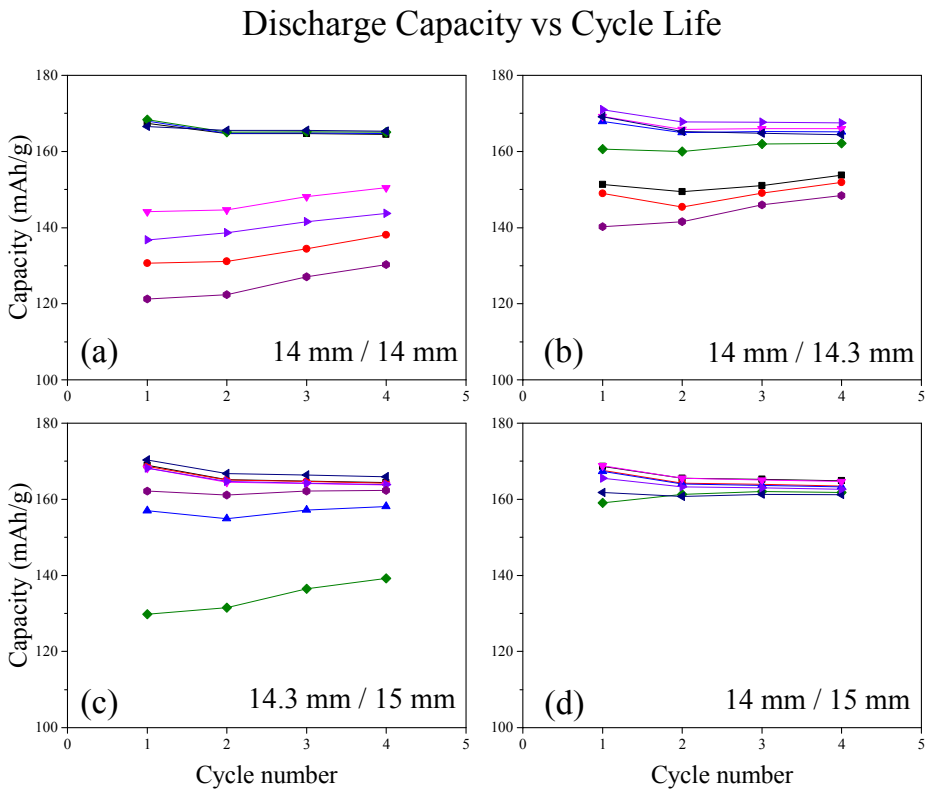


**Figure IV- 70: First 4 cycles between 4.25-3.0 V for NMC-532/graphite cells after flattening curled electrodes**

Figure IV- 70 shows that the easier-to-work-with flat electrodes resulted in a clear trend with increasingly oversized anodes [(a) → (d)] leading to more reproducible assembly of coin cells with the 14 mm/15 mm pair resulting in the best data set in terms of reproducibility [Figure IV- 70 (d)]. This is due to the decreasing probability of misaligning electrodes (overlapping edges) during cell assembly with the larger anodes. The 14 mm/15 mm pair gives an anode:cathode area of ~1.15. In order to determine if this amount of oversizing has an adverse effect on electrochemical performance, the top two performing cells from each group in Figure IV- 70 were compared during 80 cycles.

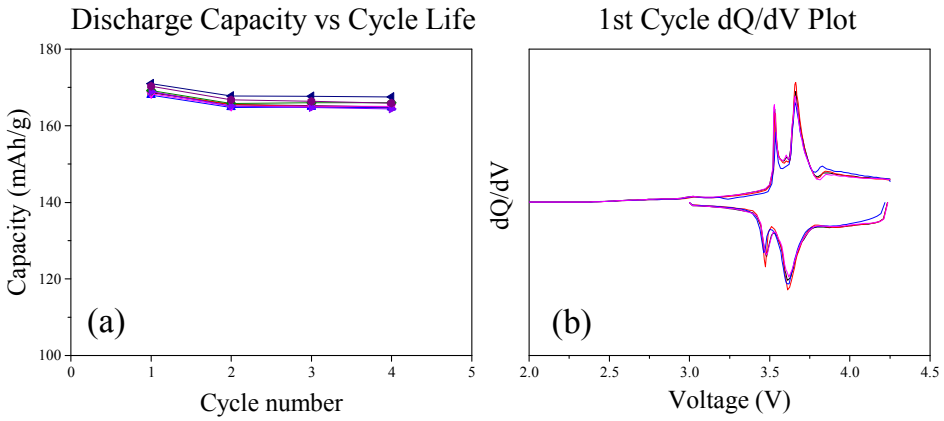


**Figure IV- 71: (a) First 4 cycles and (b) first-cycle dQ/dV of the top performing cells from each group shown in the previous figure**

The best performing cells from each group shown in Figure IV- 70 gave identical performance for the formation cycles as shown in Figure IV- 71. These cells were assumed to be properly aligned and having all other parameters being equal, except the anode size, served as a basis for looking at the effects of oversizing the anode on electrochemical performance during extended cycling. Figure IV- 72(a) and (b) show extended cycling averages for the three best cells with properly aligned electrodes for each anode:cathode area. The discharge capacity plot, Figure IV- 72(a), shows that all anode: cathode ratios fall within a very narrow margin (±~3 mAh/g). The Coulombic efficiency data in (b) show that an area oversize >10% results in differences in efficiency after HPPC cycles, where the HPPC cycles appear as breaks in the data. However, these differences are on the order of 0.05% and show no correlation with long term cycling, impedance, or capacity retention.

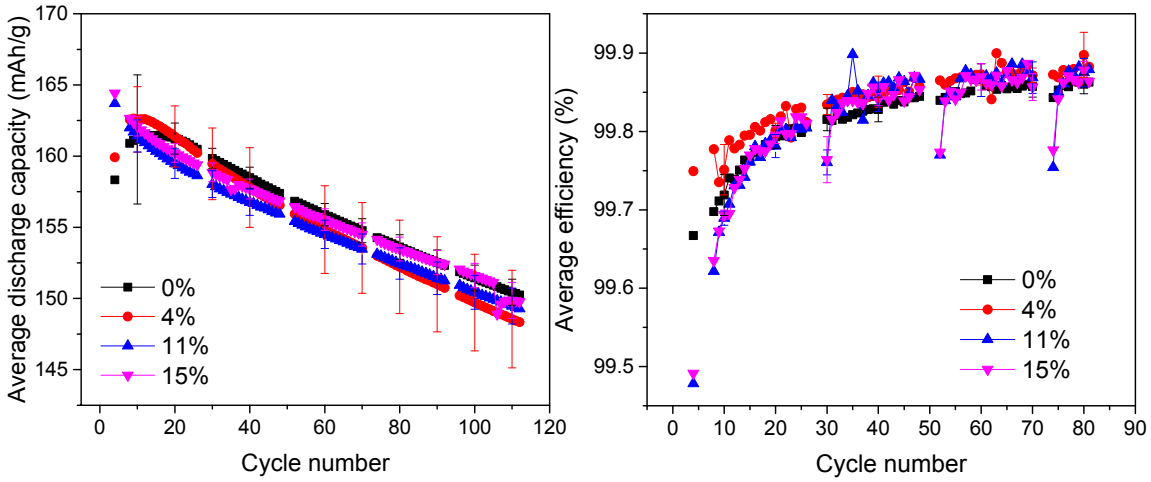


**Figure IV- 72: Extended cycling results (4.25-3.0 V) for cells with increasing anode:cathode areas. (a) Average discharge capacity for three cells of each anode:cathode area. (b) Average Coulombic efficiency for three cells of each anode:cathode area**

The results of the above studies indicate that flat electrodes and oversized anodes are essential for reproducible full cell, coin-cell construction and data. Furthermore, an anode to cathode area of ~1.15 (14 mm cathodes and 15 mm anodes) substantially decreases the probability of misaligned electrodes without adversely affecting the electrochemical performance in the coin-cell format studied here.

### Electrolyte Volume

Another factor influencing the performance of coin-cells is the total volume of electrolyte used in their assembly. For example, studies aimed at determining the effects of electrolyte additives must be systematic

and therefore utilize the same volume of electrolyte from cell to cell. A study has been done to determine a suitable electrolyte volume based on the porosity of cell components (cathode, anode, and separator). The relevant parameters are given below in Table IV- 9.

**Table IV- 9: Values of relevant parameters in estimating the electrolyte volume**

| Parameter(s) | Value(s) |
|---|---|
| **Cell Components** | Laminates: fabricated by the CAMP facility, reverse rolled to limit curling as previously described.<br>Anode: Superior Graphite (15 mm punch)<br>Cathode: NMC-532 (14 mm punch)<br>15% oversized anode:cathode area was chosen based on Figure IV- 70 and Figure IV- 72<br>Separator: 16 mm Celgard 2325<br>Electrolyte: 1.0 M $LiPF_6$ in EC:DMC (3:7) with 2% VC<br>30°C temperature controlled chamber<br>Cycling protocol: fixed window of 4.25-3.0 V, C/10 formation, C/3 ageing, HPPC diagnostics every 20 cycles. |
| **Cell pore volume calculations** | *Pore volume* = Area * Thickness * Porosity<br>**Cathode:**<br>42 µm thick<br>1.54 $cm^2$ area<br>33.5% porosity<br>Pore volume = (0.0042 cm)(1.54 $cm^2$)(0.335) = 0.00225 $cm^3$ = **2.17 µL**<br>**Anode:**<br>45 µm thick<br>1.77 $cm^2$ area<br>35.6% porosity<br>Pore volume = (0.0045 cm)(1.77 $cm^2$)(0.356) = 0.002836 $cm^3$ = **2.84 µL**<br>**Separator**:<br>25 µm thick<br>2.01 $cm^2$ area<br>39% porosity<br>Pore volume = **1.96 µL**<br>Total Pore Volume = 2.17 + 2.84 + 1.96 = **6.97 µL** |

**Table IV- 10: Electrolyte volumes used, in multiples of total pore volume of relevant cell components (cathode, anode, and separator)**

| Factor of pore volume | Volume (µL) |
|---|---|
| 1.7x | 12 |
| 2.7x | 19 |
| 4.7x | 33 |
| 8.7x | 61 |

Figure IV- 73 shows the first 4, formation-cycling voltage profiles of baseline NMC-532/graphite cells with electrolyte volumes from 1.7 to 8.7 times the calculated, total pore volume as given in (Table IV- 10). All cells were assembled using a micropipette (accuracy ~0.2 µL) to measure the amount of electrolyte added to each cell. Each figure shows data from 4 separate cells with the same total electrolyte volume to test for reproducibility. Aside from two sporadic cells in the 1.7x series, all cells appear to give similar performance, for the limited cycling presented, as shown by the comparison in Figure IV- 74. However, HPPC tests (Figure IV- 75) show that the ASI of the 1.7x series is considerably higher than those of the 2.7x, 4.7x, and 8.7x series.

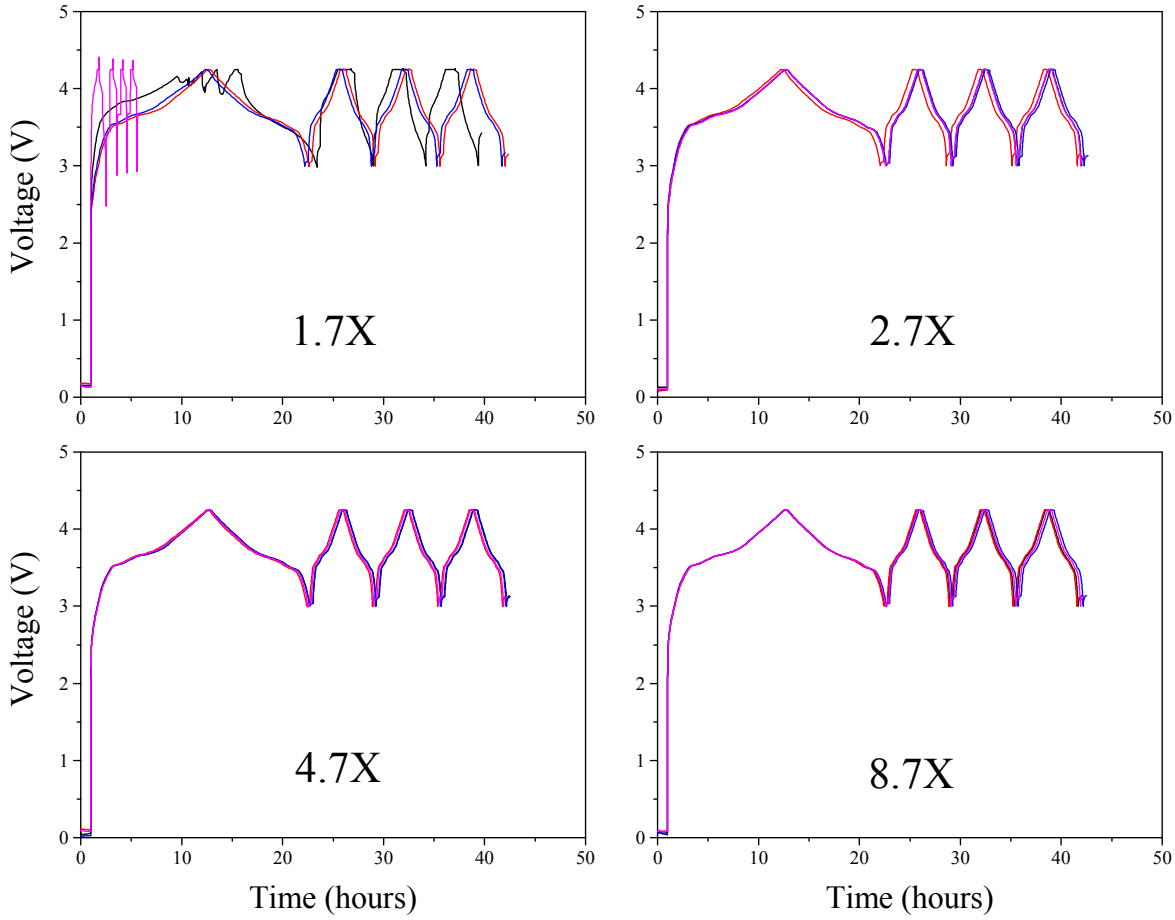


**Figure IV- 73: Formation cycling voltage profiles of baseline NMC-532/graphite cells with electrolyte volumes from 1.7x to 8.7x the calculated, total pore volume as given in the previous table. Shown in each figure are data from 4 separate cells with the same total electrolyte volume as labeled**

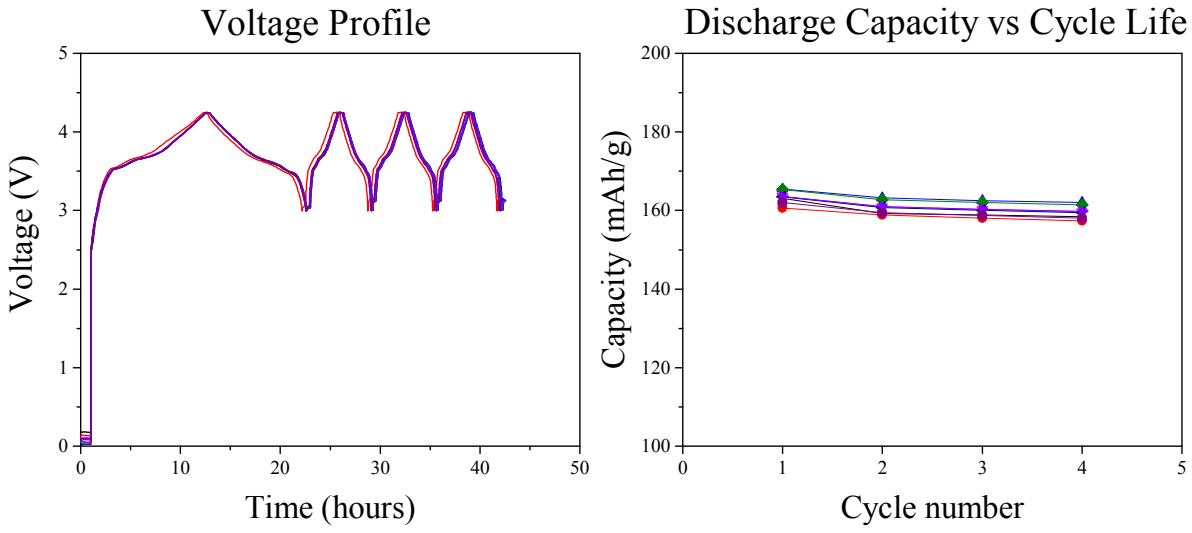


**Figure IV- 74: Comparison of formation-cycling voltage profiles (left) and cycle performance (right) for the best two performing cells of each electrolyte volume group, 1.7-8.7x, shown in the previous figure**

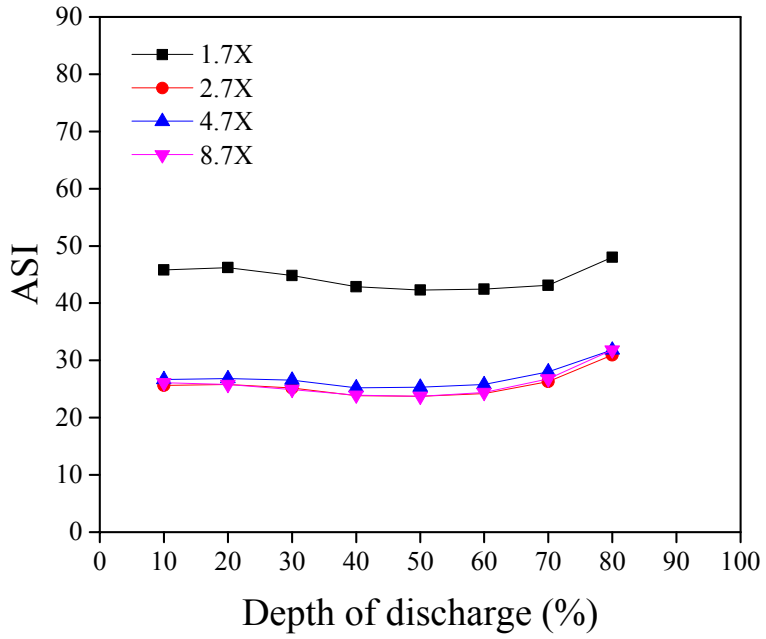


Figure IV- 75: First HPPC discharge ASI vs. depth of discharge (%) for the best performing cells in the electrolyte volume groups listed in a previous table

Figure IV- 76 shows the discharge capacity (a) and discharge capacity retention (b), after 4 formation cycles, of the best 2 performing cells for each volume used in the electrolyte volume study. As shown, the 1.7x series (black) again shows poor performance implying that an electrolyte volume of 1.7x is not ideal.

Figure IV- 77 shows the average discharge capacity and Coulombic efficiency for 4 cells of each series (excluding the 1.7x series due to poor initial performance). The 2.7x and 4.7x cells show the best performance based on capacity, whereas the 8.7x cells showed decreased, relative performance. The data presented in Figure IV- 76 and Figure IV- 77 suggest that a volume of electrolyte ~3 times the total pore volume is a reasonable minimum volume for the coin-cell format.

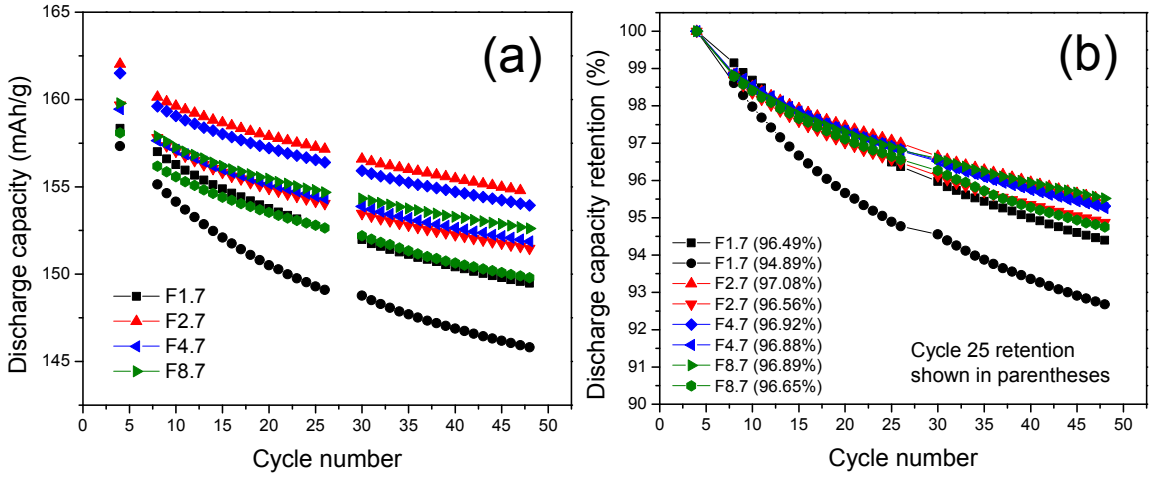


Figure IV- 76: (a) Discharge capacity and (b) discharge capacity retention for the best 2 performing cells of each group, 1.7-8.7x, as a function of cycle number. 100% is taken as the discharge capacity of the last formation cycle (i.e. cycle 4)

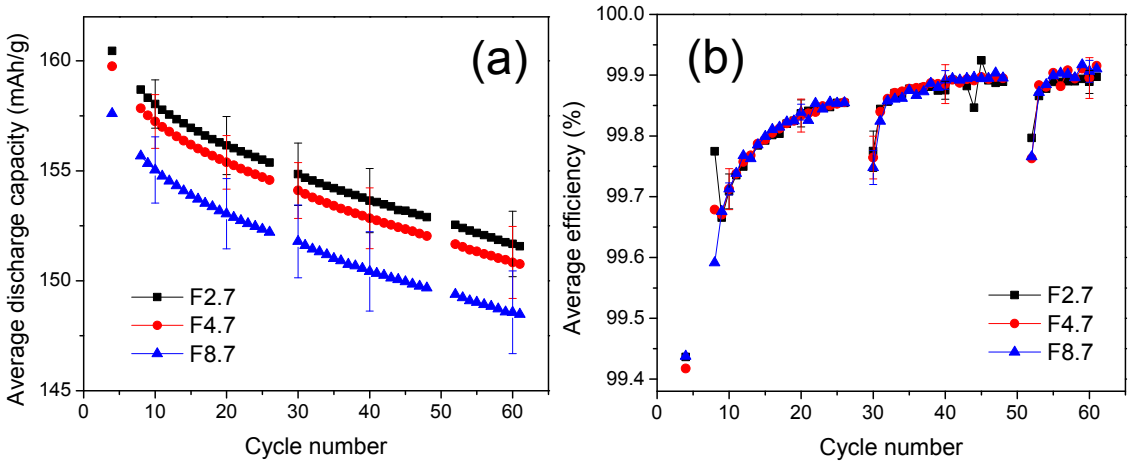


**Figure IV- 77: (a) Average discharge capacity vs. cycle number and (b) Coulombic efficiency for 4 cells from the 2.7, 4.7, and 8.7x electrolyte volume study. Error bars are 2 standard deviations**

### Data Presentation and Analysis

An important consideration when standardizing data collection and distribution is data analysis and presentation format. Figure IV- 78 shows cycling data for 30, identically-prepared NMC-532/graphite coin-cells. The inset shows Coulombic efficiencies for the same cells.

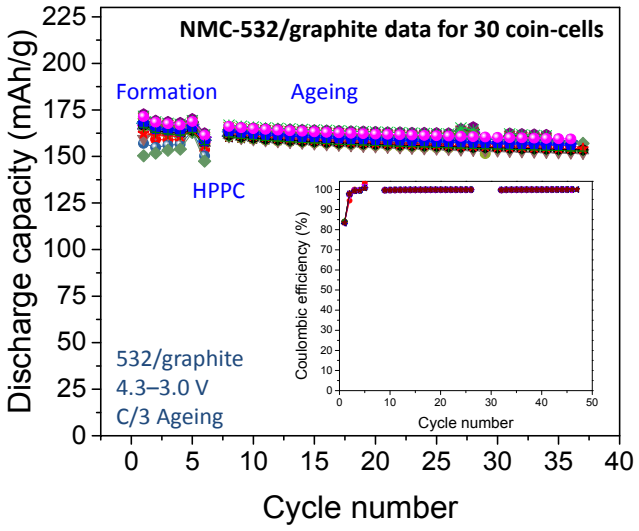


**Figure IV- 78: Cycling performance and Coulombic efficiencies (inset) for 30, identically-prepared NMC-532/graphite, baseline cells**

As shown in the figure, the reproducibility in cell performance appears quite good from cell to cell. Furthermore, Coulombic efficiencies appear to be 100% with no cell-to-cell variation. However, plotting data in this way is misleading and can mask important information.

Figure IV- 79 shows an expanded view of the data in Figure IV- 78. As shown in (a), the expanded scale reveals that, in actuality, cell-to-cell variability exists in the data. Figure IV- 79 (b) gives a more detailed look at how Coulombic efficiencies behave; especially important information for early cycling. As each of the cells in Figure IV- 78 and Figure IV- 79 were "identical", and prepared by the same researcher, the cell-to-cell differences reflect the degree of process control that exists when dealing with hand-made, small format, full cell, coin-cells. It has been our experience that the data in Figure IV- 78 (a) is typical among similar sets prepared by different researchers. The natural question that arises is how to best ascertain a true representation of the electrochemical performance of any particular cell configuration (cathode, anode, electrolyte, additive, etc.) Specifically, it is not desirable to artificially underestimate or overestimate performance parameters of interest. This situation can lead to false results when testing whether or not actual improvements have occurred when comparing new data to baseline results. How to address the variability of the process that shows up in the data is important for consistent interpretations.

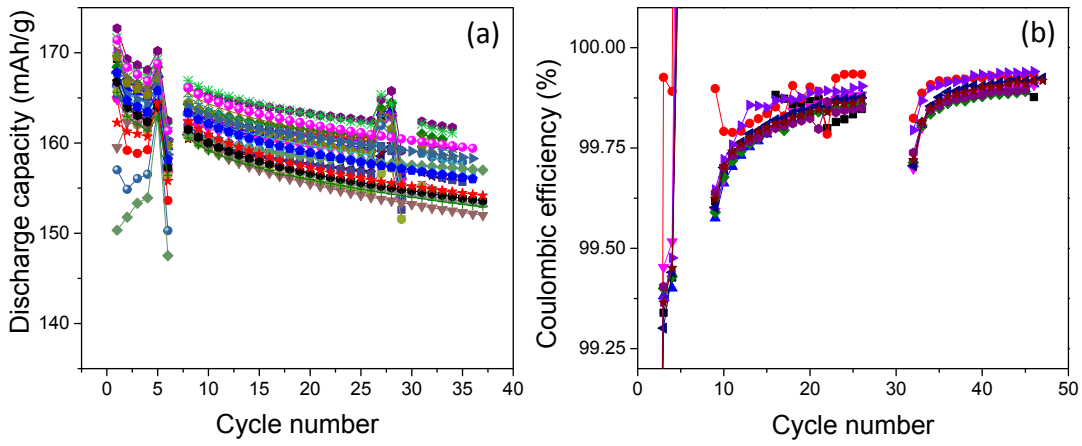


**Figure IV- 79: Expanded view of cycling data shown in the previous figure for 30, identically-prepared NMC-532/graphite baseline cells. HPPC diagnostic cycles appear as breaks in the data**

Figure IV- 80 shows an expanded view of the first 4 formation cycles of the 30 cells presented in Figure IV-78 and Figure IV- 79. The red and blue dashed lines represent the lower limit in capacities for 2 and 3 standard deviations, respectively, of the 30-cell set on cycles 1 and 4. As can be seen, most of the cells behave in a similar fashion with roughly ~3 or 4 cells that might be considered faulty. Although process knowledge and subject matter expertise can be useful in determining outliers, a more objective approach is of interest for consistency. Furthermore, even within 2 standard deviations (largely controlled by process control), at the 95% expectation level, several questionable cells remain that may adversely affect averages.

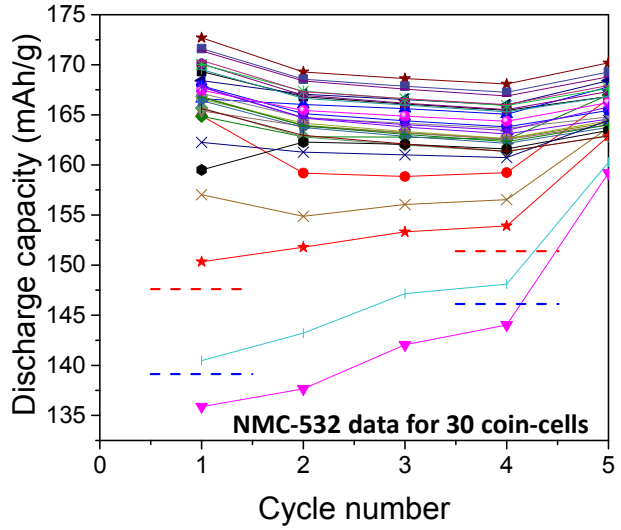


**Figure IV- 80: Expanded view of the first 4, formation cycles of the cells shown in the previous two figures. The red and blue dashed lines represent 2 and 3 standard deviations of the 30 cell set, respectively, on cycles 1 and 4**

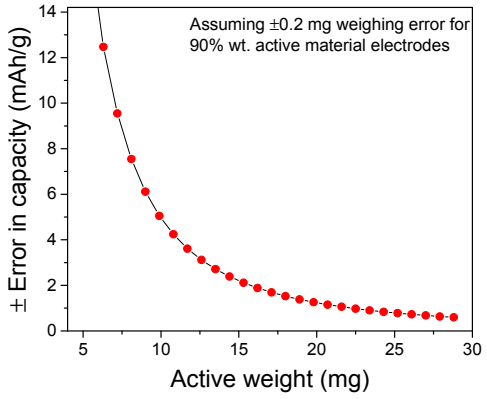


**Figure IV- 81: Propagated error in capacity from a ±0.2 mg error in materials weighing**

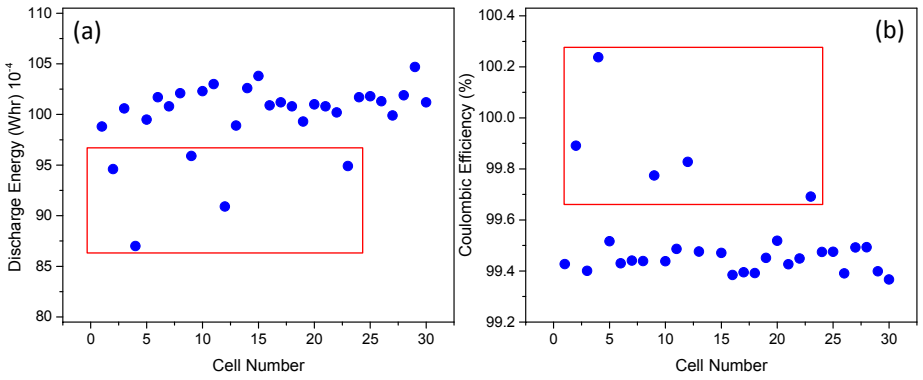


**Figure IV- 82: (a) Discharge energies and (b) Coulombic efficiencies on the last formation cycle (cycle 4) for individual cells of the 30-cell NMC-532/graphite set. Red boxes show the cells identified as outliers**

Under-performing cells might be more likely expected as a result of poor process as we have shown that issues of electrode overlap and electrolyte volume can problematic. In addition, wetting issues in the early cycles, which can be hard to quantify, may also hinder cell performance. However, slightly over-performing cells can also be present and contribute to the initial spread in the data. For example, Figure IV-81(a) shows the propagated error in capacity that can result from a total active-weight, weighing error of ±0.2 mg in the electrode/cell making process.

The graph shows that as the cathode-electrode active mass decreases the inherent error in capacity increases. For the 14 mm diameter, NMC-532 cathodes herein, the active mass is ~15 mg giving an error of ± ~2-3 mAh/g. This implies that two cells in any given test set can differ by ~5 mAh/g and still be considered identical. This is approximately the spread in the data for the majority of cells shown in Figure IV- 80. Assuming all cells are, within practical reason, truly identical then we might expect that a narrow, Gaussian distribution would be obtained from a large enough number of cells. Following this reasoning, we adopt two standard statistical outlier tests, applied early in the cycling, to quickly identify and track outlying cells; specifically, cells which move the distribution away from Gaussian. The outliers identified can be tracked throughout their cycle life and used to understand process control.

Figure IV- 82(a) and (b) show discharge energies and Coulombic efficiencies, respectively, on the last formation cycle (cycle 4) for individual cells of the 30-cell, NMC-532/graphite set. Two statistical outlier tests, known as Grubb's and Mod-Z, were applied to each data set. Details of these tests are readily available elsewhere. In short, both tests are based on the assumption that the data points are randomly selected from a data set having a Gaussian distribution, as was argued above for data from identically-prepared coin-cells. The red boxes in Figure IV- 82 (a) and (b) show the outliers calculated from the Grubb's and Mod-Z tests. Both tests identified the same cells in each set of data. Postmortem information on these cells, in combination with initial statistical details of any given set, may provide important information leading to better reproducibility and process control.

### Small Scale Testing

As shown above, statistical information on a given system is important to properly define electrochemical parameters of interest; especially with coin-cells assembled by hand. However, it cannot be expected that bench-scale research and development will be carried out using 30-cell sets to identify changes in performance each time a material's parameters are modified. Therefore, a "gate" is developed whereby the data from a smaller number of cells can be mapped against the larger baseline set of cells to identify potential differences in performance. Figure IV- 83 shows a probability map that can be used as such a gate. It was constructed via bootstrap analysis of the 30-cell baseline data. The shaded probability regions give an estimate of the likelihood that the mean, cycle-3 Coulombic efficiency, measured for a non-baseline sample of size N, differs from the baseline data. For example, if a new cell couple (non-baseline) has a five-sample, mean cycle-3 Coulombic efficiency of 98.8%, qualitative comparison with Figure IV- 83 would suggest a probability (P) in the range of 95% ≥ P ≥ 10% that this value differs from the baseline value. In this case, justification for actual improvements over the baseline cannot be given and the gate is not passed. A sample size of N=10 with an efficiency of 99.0%, however, has a ≥ 95% probability of differing from the baseline and would be of interest for further research and evaluation. These gates can, of course, be applied to any performance parameters or combinations of interest.

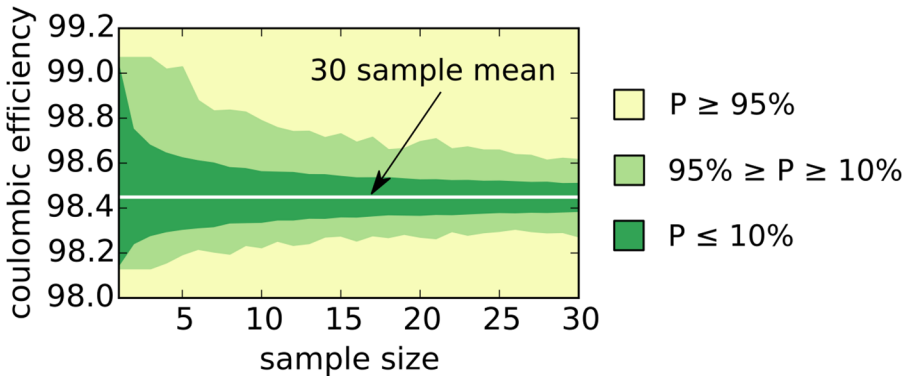


Figure IV- 83: Probability map used as a gate for small data sets. Shaded areas correspond to probability regions that give an estimate of the likelihood that the mean cycle-3 Coulombic efficiency for a sample of size N is different than the mean for the baseline data

**Testing Protocols**

Coin-cell testing protocols are constructed not only to extract essential system parameters such as capacity, efficiency, impedance, and cycle-life but also to ascertain the relative changes in these parameters as the system is pushed to higher, upper cutoff voltages. As shown above, cell-to-cell variations make it necessary to compare averaged performance metrics. Therefore, distinguishing changes in the trends of data sets becomes essential. The general procedures adopted for full cell, coin-cell testing are shown in Table IV- 11.

Figure IV- 84 shows the average Coulombic efficiencies for two 10-cell sets of NMC-532/graphite using either a current cutoff (black) or a time cutoff (red) at the top of each charge (4.25-3.0V, C/3, 30°C). Error bars represent 2 standard deviations. These data give insights into two important questions regarding the testing of coin-cells; 1) is the process sufficient to allow for small but important changes to be detected in the data? 2) How do we efficiently probe these changes? The ageing cycles in Figure IV- 79 were conducted with two different top of charge cutoff criteria; either current (i≤0.05C) or time (3 hours). As revealed in the data, a ~0.25% difference in Coulombic efficiencies is seen with the 3-hour criteria yielding lower efficiencies. The observation that longer exposure to high voltage results in lower Coulombic efficiency is not surprising. The important observation is that the small differences in the data sets (~0.3%) can be statistically verified and, therefore, taken with a higher level of confidence. As Coulombic efficiency is an important indicator of the stability of electrolytes, additives, coatings, and long-term cell performance, the ability to detect small differences in early cycles is of interest. Similar analysis on other metrics such as capacity and energy fade can also be carried out on these and other sample sets.

**Table IV- 11: The general procedures adopted for full cell, coin-cell testing**

| Procedure | Details |
|---|---|
| **Formation** | • 1.5 V tap charge for 15 min<br>• 6 hour rest<br>• 4, C/10 cycles with a current cutoff (i≤0.05C) at the top of charge. |
| **HPPC characterization** | Preparation cycles<br>• 1, C/10 cycle<br>• C/3 charge followed by C/1 discharge<br>• C/3 charge with a 1 hour rest<br>HPPC<br>• C/3 discharge to 0.1C followed by a 1 hour rest<br>• 2C discharge (10 s pulse) followed by a 40 s rest<br>• 1.5C charge (10 s pulse) followed by a 40 s rest<br>Repeat HPPC |
| **Ageing** | • 20, C/3 cycles with a three hour voltage hold at the top of each charge<br>• Voltage hold at the end of cycle-20 discharge (i≤0.05C cutoff)<br>• Repeat HPPC characterization every 20 ageing cycles |

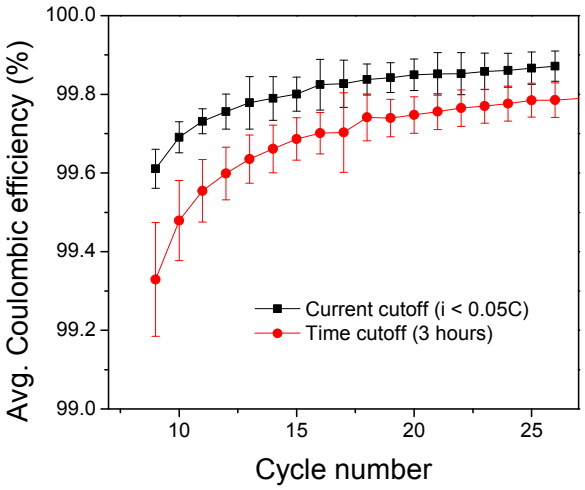


**Figure IV- 84: Average Coulombic efficiencies for two, 10-cell sets of NMC-532/graphite using either a current cutoff (black) or a time cutoff (red) at the top of each charge (4.25-3.0V, C/3, 30°C). Error bars are 2 standard deviations**

As a note on the protocols, separate experiments found that the frequency of HPPC testing (i.e., every 20 cycles) did not greatly effect cell performance compared to less HPPC testing (i.e., every 40 cycles). As such, a frequency of 20 cycles was chosen to better track impedance rise in cycled cells. The three hour voltage cutoff was chosen over a current cutoff in order to accelerate the effects of high voltage exposure. Finally, small format, hand-made coin-cells are less than ideal compared to larger-format pouch-cells and will always be somewhat limiting in scope. The above protocols are meant to identify and verify important *trends* in coin-cell data and when applied in a consistent manner should adequately serve this purpose.

From the above discussions a system of testing will proceed as follows:

1. Electrochemical data will be collected using the above-outlined protocols on several systems of interest and used as baseline data. Baseline statistics will be collected on sample sets of N=30 full cell, coin-cells.
2. Individual PI's conducting research on materials improvements (e.g., additives, coatings, etc.) will verify, statistically, enhanced performance metrics on sample sets of N≥5 cells. This will be done by mapping the N sample mean against baseline data as described in Figure IV- 83.
3. After passing the gate in step 2, cell testing and analysis will be performed on larger (N≥15) sample sets, again mapping against the baseline, to statistically verify results/improvements.
4. If promising materials pass the first two gates then resources can be discussed/allocated to explore their performance in larger-format cells. Therefore, the first two gates serve as a means to justify the effort necessary for the construction and testing of pouch-cells.

## FY 2015 Publications/Presentations

1. "High Energy Lithium-Ion Research and Development at Argonne National Laboratory", Jason R. Croy, K. Gallagher, M. Balasubramanian, J.S. Park, B.R. Long, and M.M. Thackeray, IAOEES-EEST (Vancouver, BC, Canada) 2015.
2. "Current Research on High Energy Li-Ion Batteries at Argonne National Laboratory" Jason R. Croy, K.G. Gallagher, J.S. Park, B.R. Long, S.G. Rinaldo, T. Wood, W.I.F. David, M. Balasubramanian, and M.M. Thackeray, AABC (Detroit, MI) 2015.
3. "Enabling High-Energy/Voltage Lithium-Ion Cells for Transportation Applications Part 1: Baseline Protocols and Analysis", ES252, Jason R. Croy, DOE Vehicle Technologies Annual Merit Review (Arlington, VA) 2015.

# IV.C.2 Enabling High-Energy/Voltage Lithium-Ion Cells for Transportation Applications – Part 2: Materials (ANL)

## Objectives

- Develop an understanding of the cathode surface for the baseline materials in order to propose and evaluate materials that lead to improvements in stability and performance.
- Develop surface sensitive characterization tools to determine the impact that interfacial inorganic and organic compounds have on the electrochemical performance of Ni-rich cathodes.


**Project Details**

**Peter Faguy (OVT, EERE)**

**HE-HV team (Argonne National Laboratory – PD/PI)**
Chemical Sciences and Engineering
9700 S Cass Avenue
Argonne, IL 60439
Phone: 630-252-2629
Email: burrell@anl.gov



Start Date: October 2014

Projected End Date: September 2017


## Technical Barriers

- Calendar/cycle life of lithium-ion cells being developed for PHEV and EV batteries that meet or exceed DOE/USABC goals.

  Barriers addressed:
- Cycling efficiency and cycle life.

## Technical Targets

- Define surface functionality and species present of baseline cathodes and the processing parameters involved in changing/altering the groups as desired.
- Evaluate the role of synthesis, coating method, and sample history of alumina coatings on baseline Ni-rich cathodes.

## Accomplishments

- Utilized spectroscopic characterization of the pristine NCM 523 baseline cathode to evaluate surface proton and lithium bearing species by FTIR, $^{1}H$ and $^{7}Li$ MAS NMR in support of the coating team.
- Synthesized various thicknesses of an $Al_2O_3$ coating on baseline NCM 523 cathodes via wet coating and ALD techniques. Utilized the wet coating procedure to create alumina coated NCA and LCO as comparative cathode to better understand the coating degradation on NCM 523.
- Evaluated the role of calcination temperature and time on the stability of the alumina coatings. Identified several phases that form and their role in the electrochemical performance.
- Studied the effect of calcination temperature on electrochemical performance of wet coated NCM 523 using non-aluminum containing coatings, e.g. $Ga_2O_3$.
- Structurally characterized wet and ALD $Al_2O_3$ coated NCM 523 by $^{1}H$ and $^{7}Li$ MAS NMR to study formation of surface species and presence of lithium loss and correlated results with electrochemical performance.
- Using DFT methods, modeled the structure of our baseline cathode to better understand the role of anti-site mixing, surface reconstruction, and cation segregation.
- With the electrolytes team, developed novel *ex situ* process to coat NCM 523 with lithium-ion conductive thin polymer films.
- Determined the role of annealing atmosphere in the synthesis and performance of stoichiometric nickel-rich cathode phases in the ternary $LiNiO_2$-$LiMnO_2$-$LiCoO_2$ phase diagram.

## Introduction

The ABR HE/HV program seeks to utilize a combination of spectroscopic tools, modeling, synthesis, and electrochemical testing to identify mechanisms in nickel-rich cathodes that preclude their use at higher voltages than normally utilized. The Materials section covers several research fronts including (1) evaluating the stability of the nickel-rich cathode $Li(Ni_{0.5}Mn_{0.3}Co_{0.2})O_2$ (NCM523), one of the three designated baseline materials (w/ NCA, HE5050), its reactivity, and how the surface of the material contributes to various failure mechanisms, (2), a DFT-based modeling effort to define the cation ordering and anti-site mixing at the surface, and (3) the role of synthetic conditions on the electrochemical performance of nickel-rich cathodes.

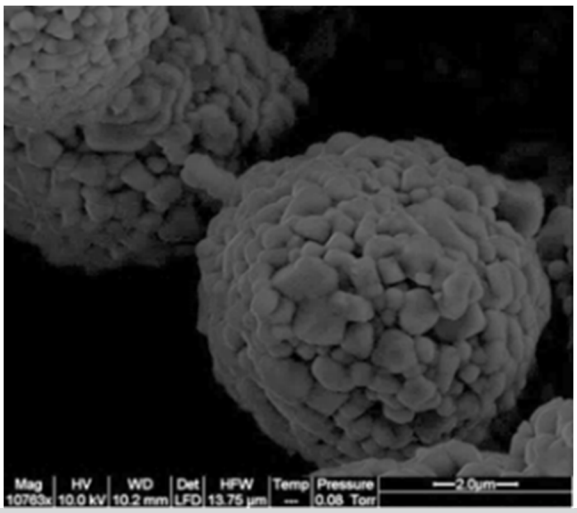


Figure IV- 85: SEM picture of 523 as provided by CAMP (Trask, ANL). The samples appear as approximately 8 µm spheres composed of platy primary particles

## Approach

- Alumina systems, in literature, are considered beneficial and amenable to a variety of synthetic and spectroscopic analyses, and electrochemically inactive. An initial literature search identified two methods (wet coating, ALD) that could be used to scale up a coated cathode sample.
- Utilizing a variety of spectroscopic techniques, notably multinuclear MAS-NMR and FTIR, the active species on the surface of the cathode and their state after reactions with various coatings can be tracked. Specifically $^{27}Al$ NMR is a useful tool to track the state of the Al(III) as it moves and interacts with the available surface species and the bulk of the cathode. Organic species can be tracked in a similar manner and by FTIR to verify retention or reaction of active groups.
- Idealized model surfaces can be created in silico of these types of cathode materials. These flat surfaces are very useful for

## Results

### Baseline Systems: Alumina Coatings

Previous work within the ABR-Voltage Fade program had shown that a thin $Al_2O_3$ coating on HE5050 composition had no effect on the voltage fade phenomenon but some impact on the interfacial stability. Because of the relatively well-studied nature of alumina as a cathode coating and our team's (ANL, NREL) familiarity with it, we chose it as a starting baseline material for initial work with NCM523 in terms of thickness, methodology, and types of coating.

Several methods were evaluated to define a baseline NCM 523 alumina coated electrode. Initial work on wet coating methods (surface precipitation from an aqueous solution, followed by annealing) was used to make samples with 2-6 wt % $Al_2O_3$. These samples had the advantage of even coatings and ease of scale up, however the coatings tended to be 50-100 nm thick which should have a significant impact on lithium diffusion from the electrolyte. Conversely very thin alumina coatings can be created using the ALD technology. Samples were provided by NREL and other collaborators having access to the methodology. SEM analysis of these samples indicated an island growth mechanism and areas of unprotected surface. Based on early results and literature survey, two types of samples were made in quantities required by CAMP for initial baseline samples:

- Wet coated 4 wt% $Al_2O_3$ on NCM523, annealed at 600 C for 8h.
- 1nm $Al_2O_3$ on NCM523

Samples, coated and uncoated NMC523, were characterized with different techniques including XRD, SEM/EDS, NMR, FTIR, XPS, and evaluated electrochemically. An SEM of the starting materials is shown in Figure IV- 85. Samples of commercial NCM523 were provided by the CAMP facility. Wet coated samples

were synthesized using methods in literature using an aqueous solution of aluminum nitrate as the source of aluminum cations. NCM523 was added to a solution of aluminum nitrate, stirred, and heated at 60ºC until nearly dry. The material was then vacuum dried, annealed at several temperatures, and analyzed by solid state NMR and powder XRD. Initial evaluation and literature precedent indicated that samples annealed at 600ºC for 8h were representative. The materials were scaled to 0.5 kg and passed onto CAMP for lamination.

***Structural Characterization***

***I. Diffraction***

For the wet coated samples, materials were annealed at several temperatures up to 800◦ C to assess the reactivity of the coating with the cathode and its effect on cathode surface and bulk structure. For the samples annealed 8 hours, no significant change in unit cell volume was detected below the 400˚C annealing temperature, above that temperature the alumina starts to diffuse into the NCM523. Figure IV- 86 shows the change in unit cell volume versus annealing temperature (2 wt% $Al_2O_3$, 8hr anneal). Table IV- 12 shows the unit cell constants for the 2h and 8h annealing time assessments. While after 8h the $Al_2O_3$ has time to diffuse into the lattice, after 2h, little change is noted.

**Table IV- 12: Lattice constants of NCM523 vs annealing time and temperature**

| Temp (°C) | Time (h) | A | C | Vol |
|---|---|---|---|---|
| 25 | 0 | 2.872 | 14.13 | 302.75 |
| 200 | 2 | 2.872 | 14.13 | 302.75 |
| 400 | 2 | 2.872 | 14.09 | 301.88 |
| 600 | 2 | 2.872 | 14.12 | 302.54 |
| 800 | 2 | 2.871 | 14.12 | 302.39 |
| 200 | 8 | 2.871 | 14.12 | 302.37 |
| 400 | 8 | 2.874 | 14.10 | 302.53 |
| 600 | 8 | 2.875 | 14.18 | 304.57 |
| 800 | 8 | 2.876 | 14.21 | 305.40 |

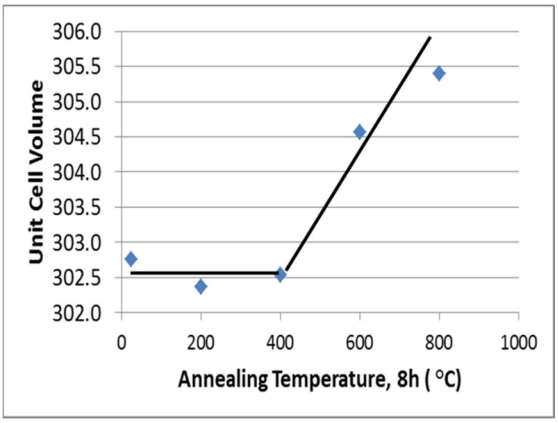


Figure IV- 86: Unit cell volume vs annealing temperature for 2 wt% Al2O3 on NCM523

Because powder XRD typically requires about 5 wt% of a sample component to be detected, we believe the longer time is necessary (> 600 °C, 8h) to see the effect as a bulk phenomenon. ALD-alumina coated samples do not have sufficient alumina content to be detectable using an XRD method.

***II. Spectroscopic Analysis on pristine NCM 523***

Initial studies of the uncoated materials by FTIR and solid state $^1$H NMR showed only weak OH stretching bands and trace proton species. This is important for the ALD studies as the process requires surface hydroxyls to initiate the surface bonding with the aluminum alkyls. XPS studies (ANL-CSE-PTF, Javier Bareno) were in agreement with the FTIR and studies with regards to the low surface concentration of protons.$^7$Li MAS NMR studies on uncoated NCM 523 for surface lithium bearing species has shown little evidence for lithium compounds (e.g. $Li_2CO_3$) on the surface.

### *III. NMR Spectroscopy on coated NCM 523*

For $Al_2O_3$-coated NCM523 a combination of $^{7}Li$ and $^{27}Al$ MAS NMR applications were used to investigate: coordination/composition of Al species at the interface and coating layer, possible Al diffusion into the bulk, surface morphology and possible lithium loss from the bulk. Model compounds in the Li-Al-O system were analyzed for fingerprinting observed peaks with specific aluminum species. Figure IV- 87 shows several of the characteristic $^{27}Al$ peaks for materials expected to be seen for the coated samples.

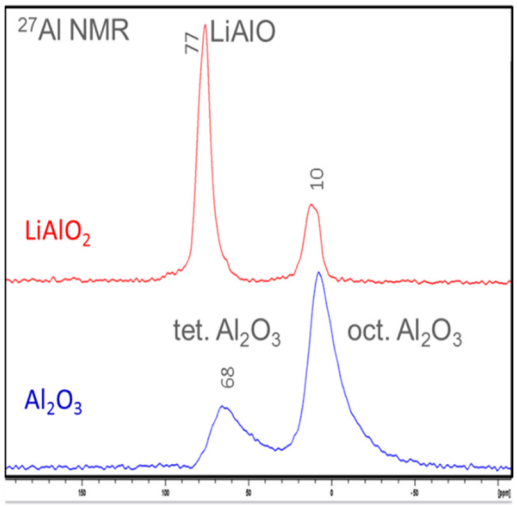


Figure IV- 87: $^{27}Al$ MAS-NMR spectrum for $LiAlO_2$ and alumina

*$^{27}Al$ MAS NMR: Effect of calcination temperature*

Figure IV- 88 highlights the effect of calcination temperature on aluminum local structure change and its interaction with the bulk material. Because the bulk material is paramagnetic, the interaction of NCM 523 surface species with the bulk or any aluminum diffusion within the lattice can be studied with $^{27}AL$ MAS NMR. Up to 400°C, there is no major change in the local Al environment. Increasing the temperature to 600ºC and 800ºC, formation of $LiAlO_2$ is observed as well as a wider sideband envelope and an increase in sideband intensity which is due to interaction of the surface species with the paramagnetic bulk material. This shows that with increasing temperature alumina reacts with surface lithium pulling lithium out of the lattice. The $LiAlO_2$ and $Al_2O_3$ appear to diffuse into the solid, forming an interface and depleting the surface layers of lithium cations and hindering the cycling performance of the material. Increase in the interaction of the surface coating with the bulk with annealing also shows that the coating gets more uniform and well dispersed over the cathode particle (Figure IV- 88).

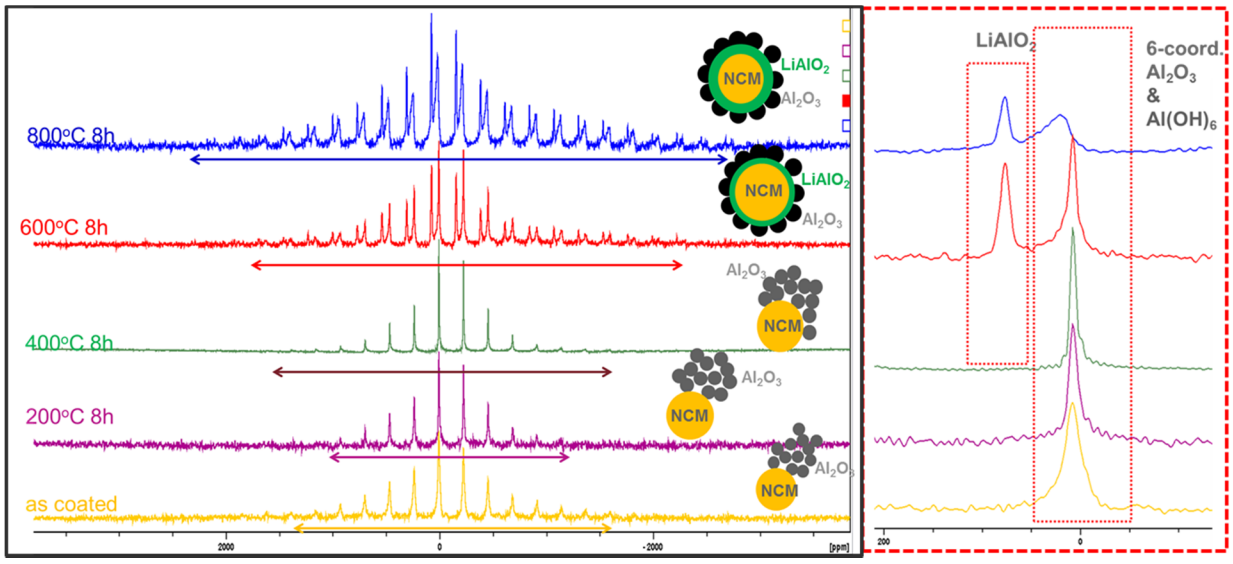


Figure IV- 88: $^{27}Al$ NMR of NCM523 coated with 2 wt% $Al_2O_3$ at various annealing temperatures for 8h

Analysis of $^{27}Al$ MAS NMR of ALD coated NCM 523 samples showed distorted aluminum oxide environments consistent with either due to small amount of alumina present or due to presence of 3-coordinate aluminum on the surface of the cathode material.

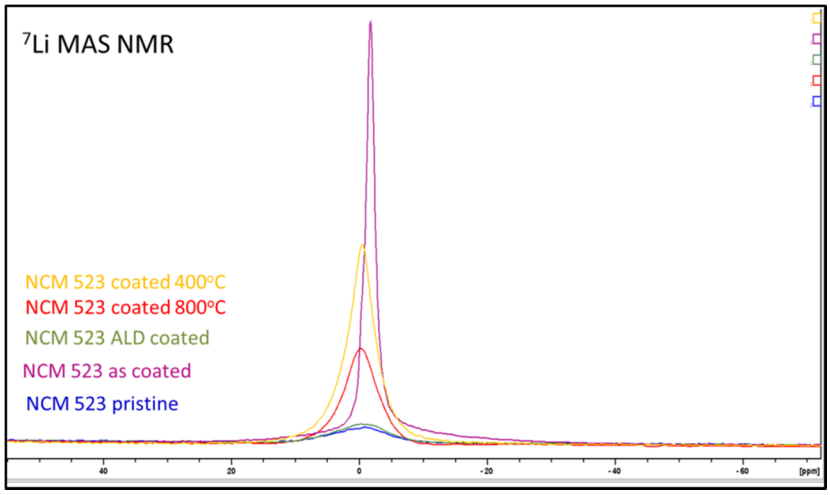


Figure IV- 89: $^{7}$Li MAS NMR of pristine and alumina coated NCM 523

$^{7}$Li MAS NMR is performed on the alumina coated samples to study the effect of coating process and annealing temperature on formation of lithium bearing surface species and possible lithium loss from the lattice. As shown in Figure IV- 89, pristine NCM 523 and ALD alumina coated material have trace surface lithium compounds whereas wet alumina coating process results in formation of surface lithium bearing species such as LiOH, $LiO_2$ and $LiAlO_2$.

Additional effort to increase the surface proton population has been accomplished by exposing the sample to water vapor or wet solvents (e.g. water in ethanol) and drying under vacuum. Preliminary characterization has shown a significant increase in proton concentrations and the effect on coatings or electrochemical performance is under evaluation.

***Electrochemical Studies***

Laminates produced from these powders by CAMP were evaluated electrochemically. Representative data are shown in Figure IV- 90. Consistently, the capacity and rate capability of these coated samples was inferior to the uncoated samples. The materials were cycled in half-cells from 3.0 - 4.5V at 30 °C. This experiment has been repeated with new samples, alternative ALD coating methods, and other sources of aluminum cations all with the same result. Attempts to make better ALD alumina coatings on NCM523 continue.

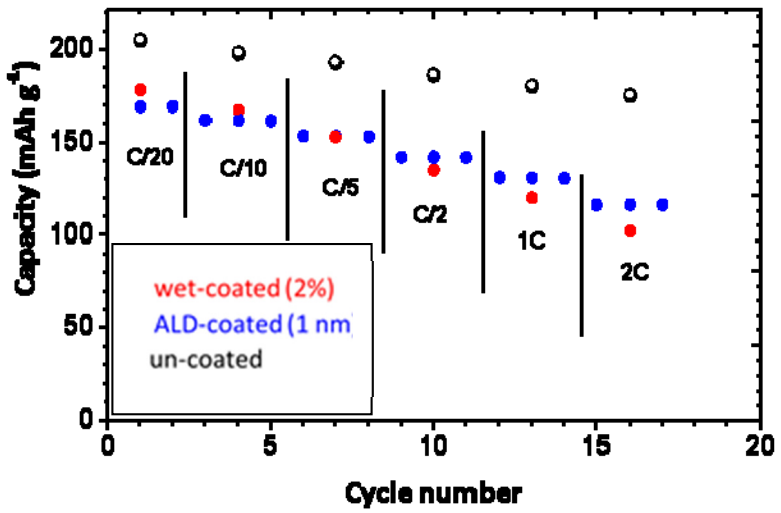


Figure IV- 90: Cycling data for NCM523 coated with alumina by various methods

In addition to these studies, the effect of annealing temperature and formation of $LiAlO_2$ on electrochemical performance was studied with loose powder cells cycled in half-cells from 3.0 - 4.5V at 30°C (Figure IV- 91). As the half-cell data suggests, high temperature annealing of the materials after wet coating stabilizes the coating layer improving cycle-ability over cathodes annealed at low temperatures. However the capacity obtained with the coated samples, even ALD samples, are still lower than the uncoated NCM 523.

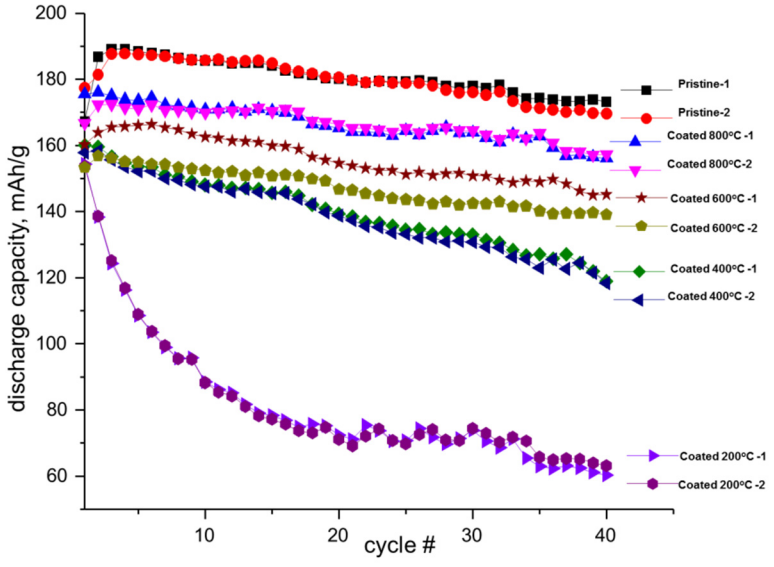


Figure IV- 91: Cycling data for NCM523 coated with alumina annealed at different temperatures

**Atomic Scale Modeling of Cathode Materials for HEHV**

NCM cathode materials are modeled at the atomic scale to characterize the structure of the starting material and their stability with cycling. We also identify and evaluate strategies for the design of high capacity, high energy-density cathode materials.

We perform first-principles density functional theory (DFT) at the GGA+U level. The U-ramping method[1] as well as the more computationally expensive (and accurate) method based on the hybrid functional HSE06[2] as implemented in the VASP code, are employed to check for electronic ground state in few cases, when needed (magnetic ground state not always accurate with DFT+U). The stability is further investigated using *ab initio* Molecular Dynamics (AIMD) to access activated states. Computational cells including up to four hundred atoms in the periodic unit are employed. This work is being coordinated with experimental efforts, particularly with the synthesis and characterization groups such as NMR and XAS.

***I. Atomic Structure of Pristine NMC532, NMC622***

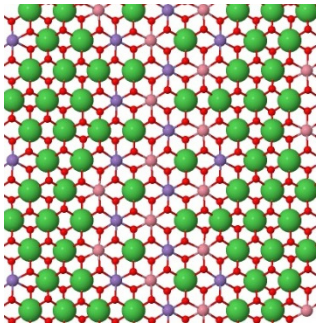

Figure IV- 92: Pristine structure of NMC 622, showing the transition metal only. Ni is in green, Co in pink, Mn in purple, and O in red. Ni-rich domains are visible

We addressed first the issue of whether the NMC532, NMC622 materials show any Ni segregation (clustering) as a result of the increased Ni content with respect to NMC333. Starting from the structure of the well mixed solid solution NMC333, obtained from previous simulations combining Cluster Expansion and DFT (Voltage Fade program), we substitute Mn and Co for Ni to obtain the desired new compositions (NMC532, NMC622). The relative energies of several configurations of Ni distributions were calculated. The simulation results show that the extra Ni (w.r.t NMC333 composition) tends to segregate into domains within the matrix in the transition metal (TM) layer, forming Ni-rich ribbon-like extended domains (Figure IV- 92). The oxidation state of Ni was found to accommodate the oxidation state of the substituted transition metal, such that all Ni that is in the NMC333 domains remained in the 2+ charge state, while Ni in the Mn site takes the 4+ charge state, and 3+ at the Co site, hence maintaining the overall charge compensation mechanism on the TM sites.

***II. Atomic Structure Instabilities during first charge activation***

AIMD simulations (1500K, 3.54ps) were performed at different levels of delithiation (states of charge) to explore possible structural transformations that would result from an extended Li vacancy concentration. The results show that Ni-rich domains are most instable and undergo structural transformations, starting with O migration, then Ni migration to the Li layer, and followed by Mn and Co migration at a lesser extent. NMC333 domains also show some TM migration and O-O formation (Figure IV- 93). This effect is similar to the effect observed in LMRNMC materials (Croy et al. recently-accepted PCCP (2015)). In LMRNMC materials, the major displacements were observed in the $Li_2MnO_3$ domains (i.e. Mn-rich domains). If such structural bulk transformations occur as a result of activation and cycling, surface coatings will only have limited beneficial effect on the electrochemical performance of the battery. The AIMD were performed (for fully delithiated, but

likely unrealistic) at temperatures up to 1500 K to sample the dynamical evolution of the structure at much shorter times than of the real system at room temperature and laboratory time scales. AIMD at lower delithiation levels for NMC333 (75%) did not show any TM migration or O-O formation. Higher capacities might be achievable without destabilizing the bulk structure. Such simulations (NMC333, NCM523 and NCM622) are currently being performed, to investigate the maximum capacity one can get before triggering such transformations.

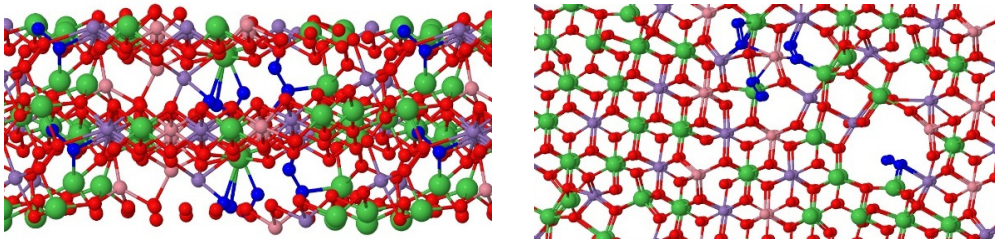

Figure IV- 93: NMC532 All Li removed AIMD+DFT. Left panel: view along the TM planes. O-O bonds are shown in blue. O is in red, Ni in green, Co in pink, and Mn in gray. Right panel: view along the c-axis perpendicular to the TM planes

We removed groups of Li atoms, based on their coordination to Ni, being groups with the highest number of Li-O-Ni coordination paths (near Ni-rich domains) to the lowest ones (far from Ni-rich domains). The voltage did not show any appreciable dependence on the specific location of Li site in the LL, but remained near 4.1 V for NMC532 and NMC622 (Note that DFT is known to systematically underestimate the voltage.)

Li-Ni exchange was not found to be favorable in the pristine state (0.6 eV per Li-Ni pair). However, some exchange might occur during synthesis and get trapped in that state. Also, based on the simulation results mentioned above, following the first activation (charge), Ni and the TM in general migrates to the Li layer. Hence it is likely that during the first discharge some of the TM may stay in the Li layer and Li will hence occupy the available sites in the TM layer. These new Li sites in the TM will be less accessible during the subsequent cycles, and also the TM in the Li layer will hinder Li diffusion within the Li layer: both capacity and rate will be reduced.

### *III. NMC333 low index surfaces*

Low surface energy configurations need to be determined before one can investigate the effect of surface doping or coating. Given the complexity of NMC532 and NMC622 structures, we focus on NMC333 that presents relatively limited and less complicated surface terminations/compositions than Ni-rich compositions. However, it can serve as a model system to investigate the reactivity of the surfaces with the electrolyte. In future, we plan to add complexity by looking at the effect of Ni-rich surfaces as well.

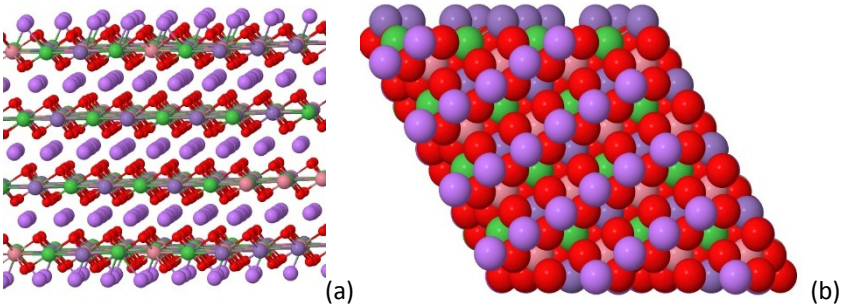


Figure IV- 94: NMC333 (001) stoichiometric Li-O terminated lowest energy surface (1.39 J/m$^2$). (a) View along [100]. (b) View along [001] perpendicular to the surface, the atom sizes have been increased to show the line ordering of Li vacancies (Li shown in purple)

We have calculated the surface energies of several possible surface orientations and terminations of NMC333. We have considered both stoichiometric and non-stoichiometric cell compositions. Non-stoichiometric compositions resulted from symmetric slabs, and satisfy charge compensation. In this case the surface energy is dependent on the chemical potential of the non-stoichiometric component, and hence the experimental conditions, such as O partial pressure, Co, Mn or Ni rich or poor synthesis conditions. To keep the simulations tractable, we focus on the stoichiometric surfaces instead, for which surface energies will be fixed. To satisfy the stoichiometry, the number of top and bottom atoms are adjusted accordingly.

The lowest energy surface is found to be the (001) (parallel to the TM planes), with Li, and O termination (Figure IV- 94a), the amount of Li on top and bottom layers were adjusted (Li vacancies). The lowest energy configuration for Li vacancies ordering is the aligned configuration (Figure IV- 94b).

Note that for fully lithiated pristine NMC333 stoichiometric compositions, surface terminations with O only, Li only, or TM only cannot be created. The only surface termination that can satisfy the constraint of stoichiometry is the (Li,O) termination. The second lowest surface energy is for (120) surface orientation (perpendicular to the TM layers), and also presents (Li,O) terminations.

The lowest surface energies for the stoichiometric compositions are listed in Table IV- 13. Instabilities in the Co magnetization values were observed in some cases, which affect the calculated surface energies. More expensive calculations based on the hybrid HSE06 method were performed to investigate this issue. The new surface energies determined using HSE06 seem to confirm the low energy values of the (001) and (120) surfaces. Contrary to the GGA+U results, (100) Ni-rich surface is found to be more energetically favorable than the Co-rich surface.

**Table IV- 13: NMC333 surface energies**

| Surface Orientation | Surface Termination | Surface Energy ($J/m^2$) PBE | Surface Energy ($J/m^2$) HSE |
|---|---|---|---|
| (100) (010)(110) | Co,O | 1.67 | 2.24 |
| | Mn,O | 1.88 | 2.46 |
| | Ni,O | 1.77 | 1.90 |
| | | | |
| (120) | Li,O | 1.50 | 1.56 |
| (001) | Li,O | 1.39 | 1.31 |
| (210) | O | 1.91 | 2.05* |
| (661) | | 1.76 | |
| | | | (*) value not final. |

***IV. Pristine $LiNi_{1-x}Co_xO_2$: Cluster Expansion (CE)***

Ternary CE formulation of $LiNi_{1-x}Co_xO_2$ at fully lithiated state is being conducted to determine the structure of the pristine $LiNi_{1-x}Co_xO_2$ material, and particularly to understand the Li-Ni exchange as a function of composition and temperature.

- Three degrees of freedom at lattice site: Li, Ni, or Co.
- Occupation variables indicate Li, Ni, and Co by 1, 0, -1.

The initial results (based on DFT+U) show that Co does not cluster at low concentrations ($x<0.33$). However HSE calculations show that in the dilute case 2 Co atoms would rather be next nearest neighbors than apart, while DFT+U do not show any preference. We are currently running HSE calculations for some specific configurations to test these findings.

In agreement with the experiment, the preliminary results show that Co doping increases the temperature at which Li-Ni exchange would start to occur in $LiNi_{0.8}Co_{0.2}O_2$, and Ni antiferromagnetic ordering plays a major role in controlling the energetics of local ordering, even in the presence of Co. Aluminum will be introduced by substituting Co to investigate the structure of NCA materials.

**Understanding the Role of Synthesis on Electrochemical Performance**

While the initial focus has been on determining the properties of the baseline cathode material NCM 523, the insights gained from these studies are to be applied to new and better designed materials. An initial study was undertaken to learn more about the role of synthesis and processing on the electrochemical properties of nickel rich cathodes.

The objectives here are to (1) establish the role of atmosphere and materials handling of nickel rich cathodes. Because high temperature is a reducing environment, oxygen vacancies and defects should form during

synthesis and be concentrated near the surface, and (2) establish the stability and electrochemical activity of various materials in the ternary $LiCoO_2$-$LiNiO_2$-$LiMnO_2$ phase diagram.

The approach here is to synthesize under various conditions and electrochemically evaluate materials in the ternary $LiCoO_2$-$LiMnO_2$-$LiNiO_2$ phase diagram and to determine the significance of surface defects on the electrochemical performance of nickel-rich cathodes.

Utilizing procedures common to the field of cathode synthesis, we have synthesized materials in the ternary $LiCoO_2$-$LiMnO_2$-$LiNiO_2$ phase diagram under a variety of conditions. Figure IV- 95 highlights the relationship of the materials studied.

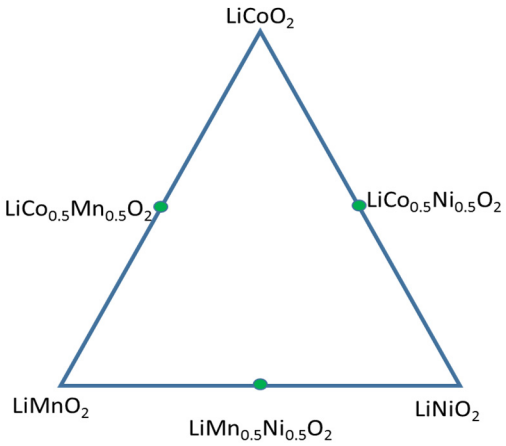


**Figure IV- 95: Ternary phase diagram for the system $LiCoO_2$-$LiMnO_2$-$LiNiO_2$**

### *I. $LiNiO_2$*

Lithium nickel oxide was evaluated in the voltage window 2.0-4.7V (vs Li) in order to evaluate its stability and cycling performance in a voltage range above its normal range of stability. In Figure IV- 96(a), it can be seen that both powder diffraction patterns of the samples calcined under air and oxygen can be indexed to R-3m symmetry, however for the sample calcined under air (at 800 °C) a small amount of $Li_2CO_3$ impurity was observed. Electrochemical evaluation showed that $LiNiO_2$ showed quick capacity fade when cycled to 4.7 V (~$Li_{0.25}NiO_2$), consistent with the literature reports of these phases and the recognized stability of Ni(IV) compounds. Analysis of the first cycle of $LiNiO_2$ for both synthetic processes is shown in Figure IV- 96 (c). The chemistry of $LiNiO_2$ is quite complicated with at least 4 active electrochemical processes during charge being observed. For these two types of samples, the material calcined under oxygen showed better electrochemical performance with much more defined peaks in the CV curve.

### *II. 0.5 $LiCoO_2$ – 0.5 $LiNiO_2$*

Lithium nickel cobalt oxide was evaluated in the voltage window 2.0-4.0V (vs Li) in order to evaluate its stability and cycling performance. In Figure IV- 97, it can be seen that the powder diffraction pattern of the samples calcined under oxygen can be indexed to R-3m symmetry. Electrochemical evaluation showed that $Li(Co_{0.5}Ni_{0.5})O_2$ in the window evaluated, showed a simpler electrochemical performance, consistent with the literature reports. Analysis of the first cycle of $LiNiO_2$ for both synthetic processes is shown in Figure IV- 96(c).

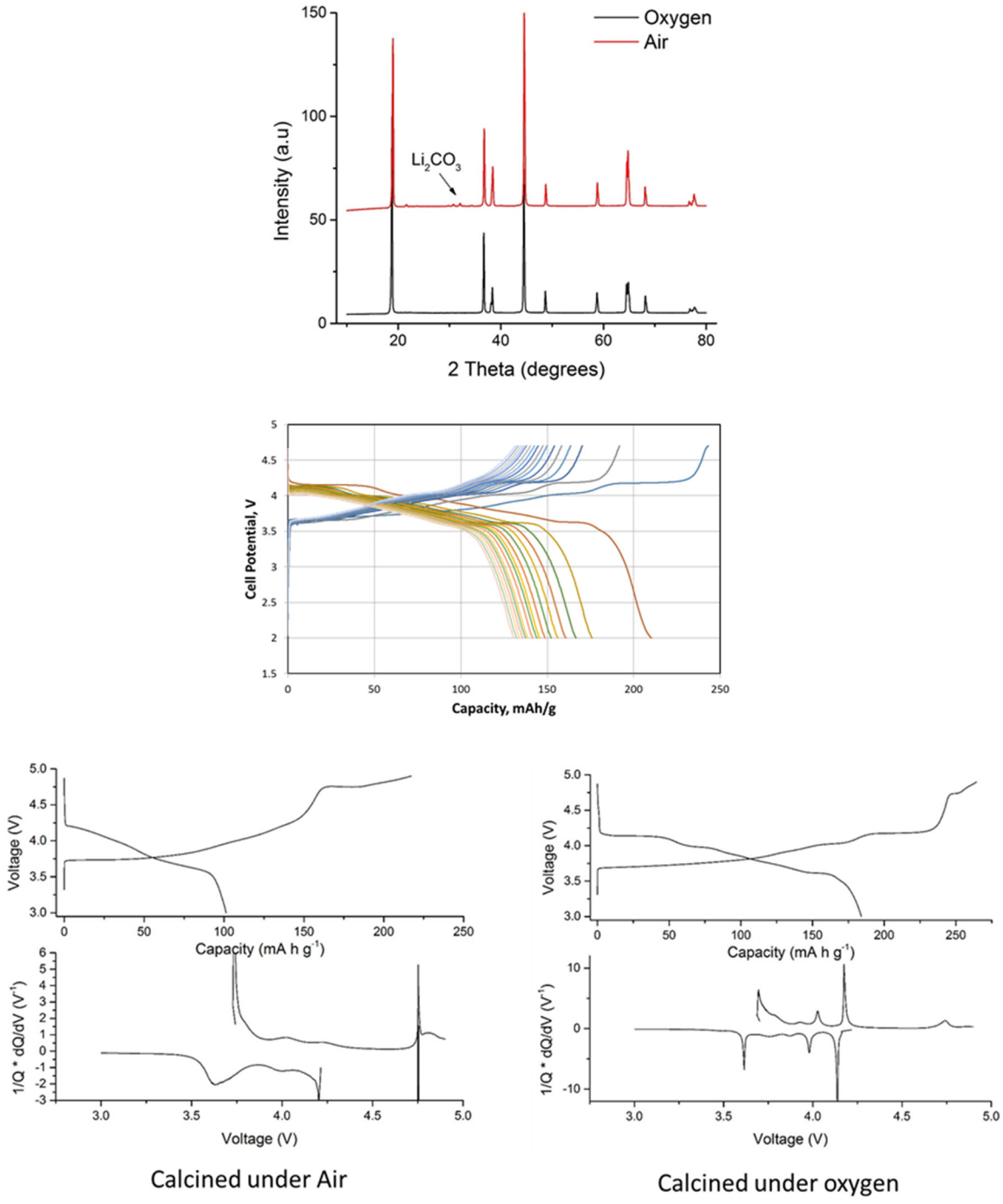


**Figure IV- 96: (a) XRD patterns of $LiNiO_2$ synthesized under two different atmospheres, (b) Cycling performance of the oxygen cycled material cycled to 4.7V, (c) first cycle CV of the two samples**

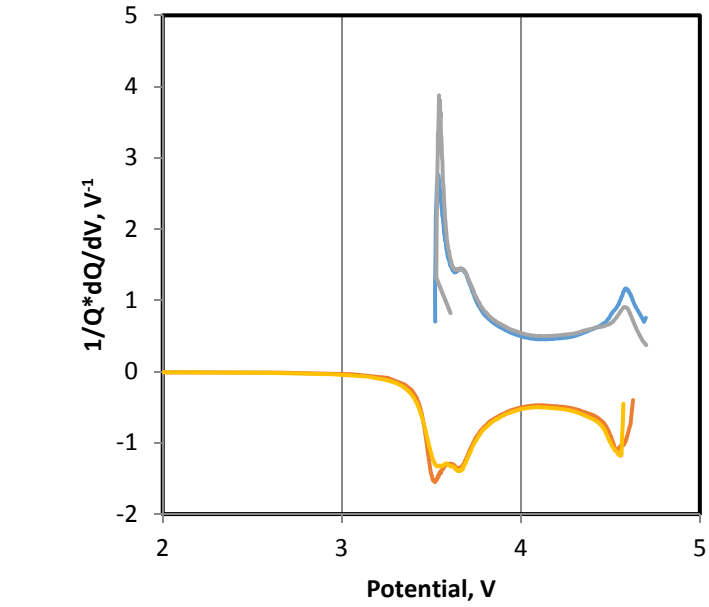


(a)

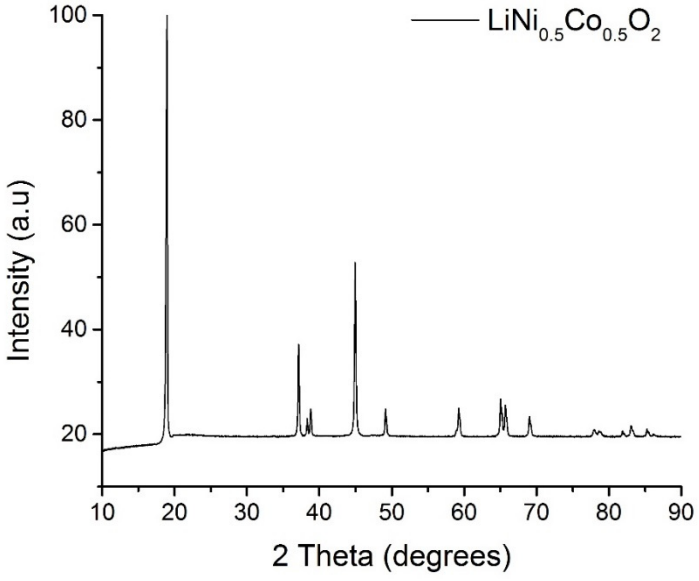


(b)

**Figure IV- 97: (a) CV cycling data for 0.5 $LiCoO_2$-0.5 $LiNiO_2$, (b) XRD patterns of 0.5 $LiCoO_2$-0.5 $LiNiO_2$**

## Conclusions

1. The structural and electrochemical characterization studies have shown that the alumina coatings on NCM523 are not stable or inert. Our intention was to devise a blocking layer and inhibit electrolyte components from reacting with the charged surface and inhibit oxygen loss at top of charge. Alumina coatings appear to be too reactive with the baseline cathode material – even at the level of 1nm thickness the electrochemical performance is severely inhibited. This conclusion appears consistent with data from NREL and LBNL presented at the recent AMR in Washington DC.
2. $LiNiO_2$, $LiCoO_2$ and their 50% mixtures are not stable when cycled to high voltage (4.7 V)
3. These compounds are subjected to both capacity fade and voltage fade most likely via oxygen loss, resulting in surface concentrated structural damage

## References

1. B. Meredig, A. Thompson, H. A. Hansen, C. Wolverton and A. van de Walle, *Physical Review B*, 2010, 82, 195128.
2. J. Heyd, G. E. Scuseria and M. Ernzerhof, *The Journal of Chemical Physics*, 2003, 118, 8207-8215.
3. M. K. Aydinol, A. F. Kohan, G. Ceder, K. Cho and J. Joannopoulos, *Physical Review B*, 1997, 56, 1354-1365.

## FY 2015 Publications/Presentations

1. Anthony K. Burrell, J. Vaughey, A. Hubaud, F. Dogan, H. Ibbir, J. Zhang, C. Liao, A. Tornbein, C. S. Johnson, A. Vu "Materials for High Energy High Voltage Batteries" DOE Hydrogen Program and Vehicle Technologies Program Annual Merit Review, Washington, DC, June, 2015.
2. Fulya Dogan, Jason R. Croy, Mahalingam Balasubramanian, Michael Slater, Hakim Iddir, Christopher Johnson, John T. Vaughey, Baris Key "Solid State NMR Study of $Li_2MnO_3$ and Li-Rich NMC Cathodes: Proton Insertion, Local Structure, and Voltage Fade", *J. Electrochem. Soc.*, **162**, 235 (2015).
3. F. Dogan, B. Long, J. Croy, K. Gallagher, H. Iddir, J. Russell M. Balasubramanian, B. Key "Re-entrant Lithium Local Environments and Defect Driven Electrochemistry of Li- and Mn-Rich Li-Ion Battery Cathodes". *J. Amer. Chem. Soc.,* **137**, 2328 (2015).
4. H. Iddir, B. Key, F. Dogan, J. Russell, B. Long, J. Bareno, J. Croy, R. Benedek "Pristine-state structure of lithium-ion-battery cathode material $Li_{1.2}Mn_{0.4}Co_{0.4}O_2$ derived from NMR bond pathway analysis" *J. Mater Chem A.*, **21**, 11471 (2015).
5. J. Croy, J. S. Park, F. Dogan, C. S. Johnson, B. Key, M. Balasubranmanian "First-Cycle Evolution of Local Structure in Electrochemically Activated $Li_2MnO_3$" *Chem Materials*, **26** 7091 (2014).
6. Jason R. Croy, Hakim Iddir, Kevin Gallagher, Christopher S. Johnson, Roy Benedek, and Mahalingam Balasubramanian, "Instabilities of Layered-Layered Lithium-ion-Battery Materials: Oxygen Vacancy Formation and Mn Migration" Physical Chemistry Chemical Physics, 2015, **17**, 24382 – 24391.
7. Z. Z. Yang, B. J. Ingram, L. Trahey "Interfacial Studies of Li-Ion Battery Cathodes Using In Situ Electrochemical Quartz Microbalance with Dissipation" *J. Electrochem Soc*., **161** A1127 (2014).

# IV.C.3 Enabling High-Energy/Voltage Lithium-Ion Cells for Transportation Applications – Part 3: Electrochemistry (ANL)

## Objectives

- High-performing, high-energy, safe and long-life batteries are needed to reduce petroleum consumption in vehicular applications. The performance targets of these batteries can be met by cells containing layered-oxide-based positive electrodes. To achieve the energy and power density targets, these cells need to be cycled to voltages that exceed 4.5 V vs. $Li/Li^+$. On extended cycling at these voltages, however, capacity loss, impedance rise and voltage fade reduces the cell's energy and power output. Our objective is to mitigate this performance degradation, thereby reducing the lifetime cost of these high-energy batteries.


**Project Details**

**Peter Faguy (EERE-VTO-ABR Program Manager)**

**HE/HV Team (Argonne National Lab)**
9700 South Cass Avenue, CSE-200
Lemont, IL 60439
Phone: 630-252-2629; Fax: 630-972-4461
Email: burrell@anl.gov



Start Date: October 2014

Projected End Date: September 2018


## Technical Barriers

- Calendar/cycle life of lithium-ion cells being developed for PHEV
- and EV batteries that meet or exceed DOE/USABC goals.

## Accomplishments

- Established standard protocol to track performance changes in lithium-ion cells. Protocol has been applied to cells containing the following chemistries (voltage cycling windows, in parenthesis): NCM523//Graphite (3.0-4.4 V); NCA//Graphite (3.0-4.4 V); HE5050//Graphite (2.5-4.4 V).
- Data obtained from the above baseline cells indicate the following trends – capacity loss: HE5050 > NCM523 > NCA; impedance rise: HE5050 > NCM523 > NCA.
- A "bootstrap" methodology has been developed to evaluate performance degradation characteristics resulting from modifications to baseline chemistry. For example, for a sample size of $n = 5$ any modification to the NCM523 baseline chemistry should yield a normalized capacity loss of less than ≈ 0.09 and an impedance rise of less than ≈ 5.2 $\Omega$-$cm^2$ to be considered an improvement.
- Cycling experiments have been initiated in cells containing reference electrodes to identify electrode contributions to cell performance degradation. For example, data from NCM523//Graphite cells show that cell impedance rise, which results from ~100, C/3 cycles in the 3.0-4.4 V range, arises mainly at the positive electrode. Capacity fade, on the other hand, arises from lithium trapping in the graphite negative electrode.
- Electrochemical Modeling Studies on NCM523 Electrodes have been initiated and phenomenological models have been developed to model AC impedance and DC studies using the same constituent equations and parameters. These models are used to interpret the experimental data and have yielded insights that include the following: (i) the bulk lithium diffusion coefficient for NCM523 oxide is on the order of $10^{-10}$ $cm^2/s$; and (ii) electrode misalignment during cell preparation makes the current distribution more non-uniform, causing greater variation in cell-to-cell performance.

### Introduction

New cathode, anode, electrolyte and separator materials, and novel synthesis approaches, are routinely developed for lithium-ion cells. However, there is a need for standard electrochemical protocols to quantify changes resulting from these new material chemistries. Such protocols are being developed under this effort,

which allows us to benchmark various battery chemistries and evaluate the effect of material chemistry changes on cell performance and degradation characteristics. Furthermore, additional electrochemical characterization techniques are being developed and used to provide insights into cell performance mechanisms. The data from these electrochemical experiments are related to changes observed in post-test diagnostic studies of cell components, through phenomenological models being developed in this program. In this writeup, the information generated as part of this effort is presented in three sections as follows: (A) probabilistic modeling and benchmarking of coin cell electrochemistry; (B) investigating performance degradation resulting from cell cycling; and (C) electrochemical modeling.

## Approach

The objectives listed above are accomplished by using the following approaches:

- Develop standard electrochemical protocols to track, quantify, and characterize cell performance and performance degradation characteristics in a reproducible and time-efficient manner. These protocols will be disseminated to partnering institutions and individuals to allow comparison of data generated at multiple laboratories.
- Identify sources of performance degradation and provide appropriate feedback to team members. For example, experimenta data from electrochemical characterization techniques, such as AC impedance spectroscopy and galvanostatic intermittent titration, are used to develop electrochemical models that identify sources of cell performance degradation. This information is then used to develop materials and components that minimize cell performance degradation.

## Results

### A. Probabilistic Modeling and Benchmarking of Coin Cell Electrochemistry

The results from electrochemical testing on two large-sample-size baseline coin cell couples: $LiNi_{0.8}Co_{0.15}Al_{0.05}O_2$ (NCA) and $LiNi_{0.5}Co_{0.2}Mn_{0.3}O_2$ (NCM523) are presented. We highlight the variabilities present in electrochemical testing of full (coin) cells and use these uncertainties to set boundaries for defining improvements in performance.

### A.1. Protocol Details

The protocol implemented for the electrochemical testing is given in Figure IV- 98; the temporal current profile is shown in the top-left thumbnail of the figure. The voltage limits are between 3.0 and 4.4 V; the protocol duration is approximately 50 days; and, there are 5 “blocks” of cycles labeled sequentially in Figure IV- 98. A cycling block entails a hybrid pulse power characterization (HPPC) cycle followed by 20, C/3 “standard” cycles, which have a constant voltage charge hold or “trickle charge” at 4.4 V for 3 h. Each HPPC cycle is preceded by a diagnostic pre-HPPC, C/10 slow cycle. The rationale for the various test steps are as follows: (i) the HPPC cycles are designed to examine impedance of the cells as a function of state-of-charge or voltage; (ii) the standard cycles are meant to accelerate degradation of the cells; and (iii) the slow pre-HPPC cycles are diagnostic cycles designed to examine the shape of the voltage profile while trying to minimize impedance effects, i.e., examine evolution of the quasi-equilibrium voltage profile or differential capacity (dQ/dV) plots.

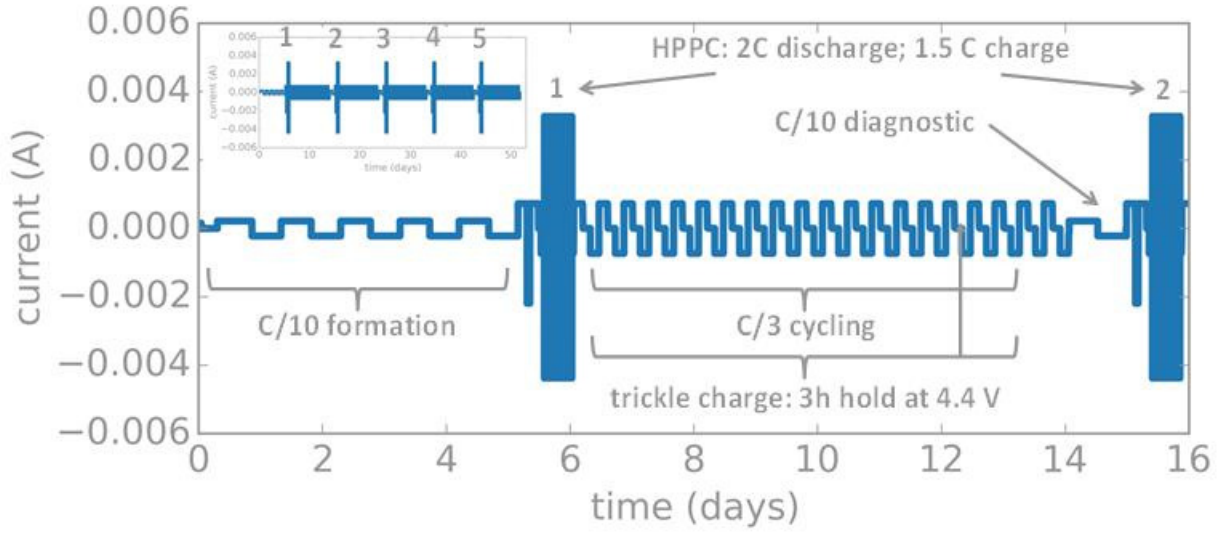


Figure IV- 98: Implemented protocol for electrochemical testing

### A.2. Protocol Outputs

#### A.2.A. Decay Trends

Our main test outputs are discharge capacity, discharge voltage, discharge energy and coulomb efficiency as a function of cycle number. Other parameters such as charge end-point slippage or the difference between charge and discharge voltage could also be chosen, however, since our focus is on cell-to-cell variability, we narrow down on parameters that are more common in the Li-ion literature. These parameters are plotted as a function of cycle number in Figure IV- 99.

In general, the chemistries (NCA and NCM-523) have performance "bands". These bands encompass all cells in the group and give a qualitative view for the performance of the ensemble. Alternatively, the data could be represented by taking the average and standard deviation of the cells for each cycle; however, this would hide information about the distribution of performances.

In Figure IV- 99a and Figure IV- 99c it can be seen that the decay rates for discharge capacity and discharge energy are similar, viz. energy loss is dominated by capacity fade since discharge voltage in Figure IV- 99b increases for both NCA and NCM-523. Initially (after the first HPPC cycle) the NCM523 energy decay band is in the range (we define an approximate range as [min value, max value]) of [650 Wh-kg$^{-1}$,740 Wh-kg$^{-1}$] and the NCA band is in the range of [650 W h kg$^{-1}$,725 Wh-kg$^{-1}$] and at the end of the protocol (ignoring bottom 2 outlier cells) the NCM523 band decays to [575 Wh-kg$^{-1}$,660 Wh-kg$^{-1}$] whereas the NCA band decays to approximately [640 Wh-kg$^{-1}$,660 Wh-kg$^{-1}$]. Thus, for both chemistries the bands decrease in width over the protocol and the width of the NCA band is smaller than that of the NCM523 band.

The coulombic efficiency band for NCA is higher and also tighter than that of the NCM523 band, though it should be noted that the cell-to-cell differences in coulombic efficiency are approaching the precision limits of the cycler, viz. the 4$^{th}$ digit in the coulombic efficiency value.

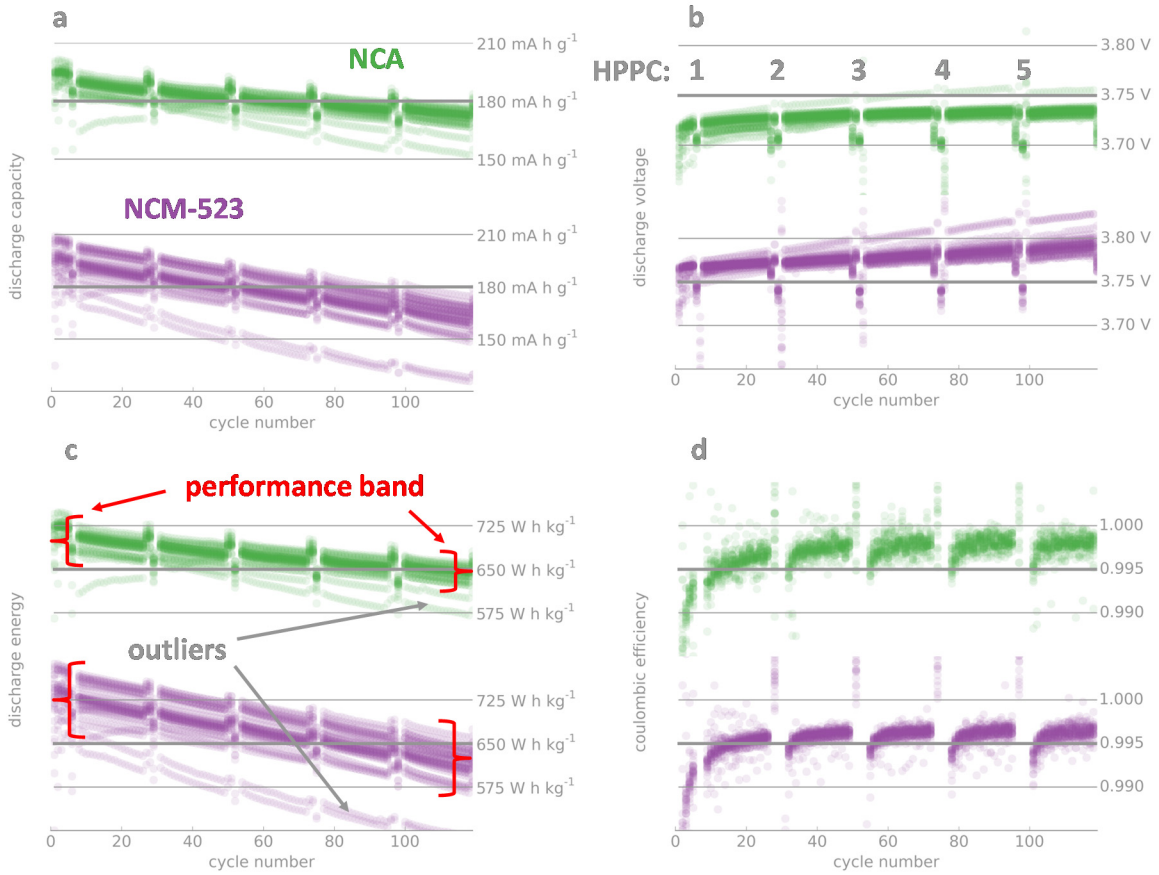


**Figure IV- 99: Discharge capacity (a), discharge voltage (b), discharge energy (c) and coulombic efficiency (d) for NCA (28 cells) and NCM523 (30 cells) full cells. A darker shade indicates a higher density of cells, i.e., in (c) there is a high density of cells near the top of the NCA band**

### A.2.B. Impedance Rise

Impedance values can be derived from the HPPC measurements and the outputs are shown in Figure IV- 100 for the discharge impedance. We show the change in the impedance-voltage relation from HPPC 1 to HPPC 5 for NCA (top) and NCM523 (bottom). The curves have a characteristic parabolic shape and, for simplicity, we will focus our discussion on the area of "minimum impedance", which is around 3.6 to 3.8 V or a state-of-charge of around 50%.

The initial minimum impedance of NCA is approximately 20 Ω-cm$^2$ and comparable to that of NCM523. However, the variability in the NCM523 data is larger than that of NCA; in accordance with Figure IV- 99. The minimum impedance of NCA rises to approximately 25 Ω-cm$^2$ and NCM523 rises to about 30 Ω-cm$^2$. Differences in variability are maintained from HPPC 1 to HPPC 5, viz., the variability for NCM-523 is still larger than that of NCA, at the end of aging cycles.

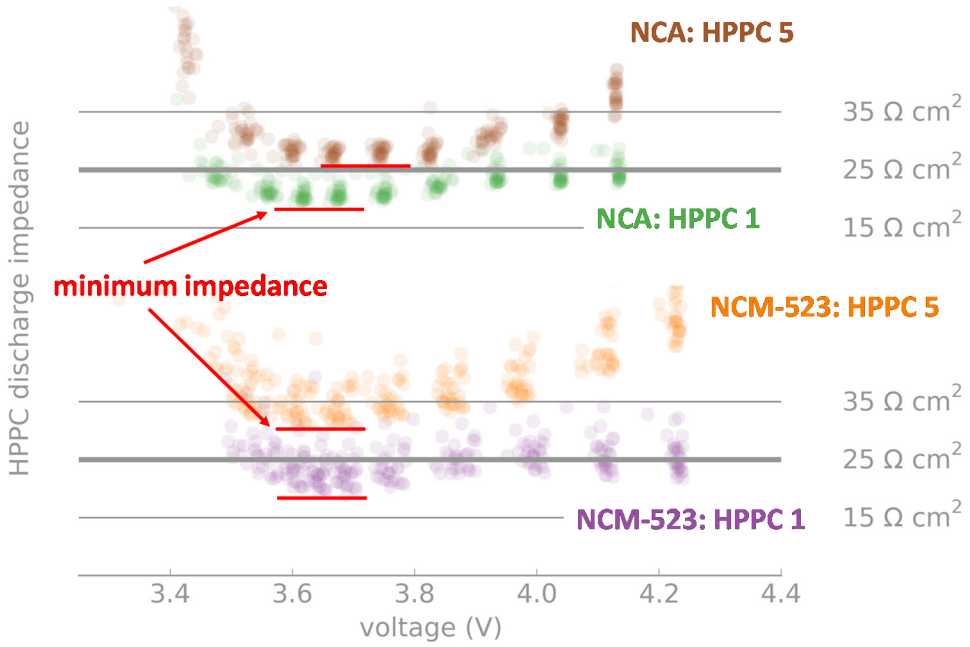


**Figure IV- 100: Initial and final impedance values derived from HPPC measurements for the two baseline chemistries**

### A.3. Defining Performance Boundaries

In Section 2, we highlighted a portion of the data output for our baseline study. Although there are many outputs to be analyzed in more detail, our goal in this section is to select some reference outputs and then define performance boundaries for these outputs using the baseline chemistries.

Figure IV- 101 shows performance ellipses derived from the baseline data. Although the data is not normally distributed, we used these ellipses as a semi-quantitative tool to determine performance boundaries for discharge energy (Figure IV- 101a) and impedance (Figure IV- 101b). We varied the standard deviation of the ellipse to include as many data points as possible without over-shooting the parametric region of interest into a zone that would be unrealistic.

The results mirror those presented in Figure IV- 99, viz. NCM523 has a larger cell-to-cell variability than NCA. The NCM523 performance boundary for discharge energy (Figure IV- 101a) is shifted (vertically and to the left) in comparison to NCA, thus there is a qualitative increase in initial discharge energy (vertical shift) but this benefit is partly offset by a steeper decay curve (left shift). The impedance performance boundary is shifted to the right thus the rise in HPPC minimum impedance from HPPC 1 to HPPC 5 of NCA is lower than that for NCM523.

From the perspective of materials benchmarking, such plots can be used as a diagnostic screening tool. For example, assume that NCM523 is modified with a cathode coating that is designed to improve impedance characteristics and cycle life while maintaining initial performance. This “new material” would ideally have a performance ellipse that does not overlap significantly (area overlap can be defined more explicitly) with the baseline NCM523 ellipse, viz., is shifted to the right in Figure IV- 101a as well as shifted to the left in Figure IV- 101b. Alternately, if the “new material” performance ellipse lies within the baseline performance ellipse then: (*i*) either more testing/development should be performed or (*ii*) the performance improvement claims can be disregarded.

Practically, the error ellipses for each “new material” can be developed using sample sizes smaller than baseline sample sizes. However an issue of higher priority for material screening via baseline comparisons is the testing time, viz. we need approximately 50 days of testing to make a valid comparison to the baseline. Accordingly, testing time needs to be reduced in order to accelerate material development.

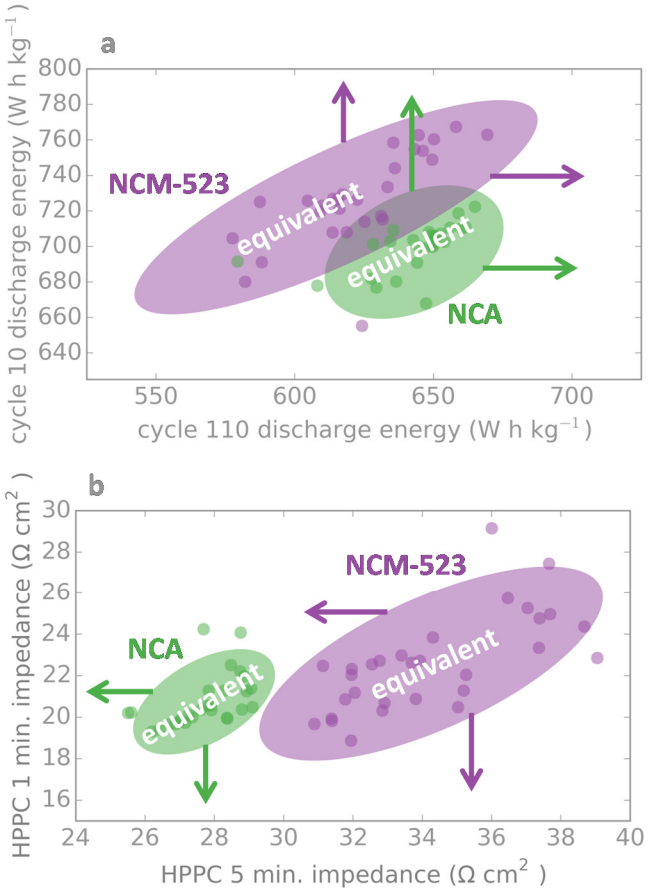


**Figure IV- 101: Performance ellipses for discharge energy (a) and HPPC impedance (b) for baseline chemistries NCA and NCM. Arrows indicate general directions for improvement, viz. a shift in the performance ellipse. The ellipses are based off a 1.85 standard deviation in (a) and 2.00 in (b)**

### A.4. Simplifying the Data: Low Precision Coulombic Efficiency as a Predictor for Energy Decay

With the goal of reducing testing time for materials evaluation we looked at the correlation matrix for 5 different outputs:

1. initial energy: cycle 1 discharge energy
2. energy retention: cycle 110 discharge energy / cycle 10 discharge energy
3. initial impedance: HPPC 1 minimum impedance
4. impedance rise: 1 – (HPPC 1 minimum impedance / HPPC 5 minimum impedance)
5. coulombic efficiency

Figure IV- 102 shows a correlation plot for energy retention and coulombic efficiency; the red line (estimated by hand-tuning) has a slope of 0.0251 and an intercept of 0.9737. Though the correlation is interesting and in line with other experiments from literature; the precision with which the test equipment can measure coulombic efficiency (~0.01% accuracy or 4$^{th}$ digit) is approaching the cell-to-cell variations within the tested cell chemistries. More specifically, we can be confident that there is a measurable difference between the coulombic efficiencies for NCA and NCM523 as respective populations; however, we are not as confident in discerning differences for individual cells when their coulombic efficiency values approach the precision threshold.

An on-going line of work involves a more detailed error analysis of coulombic efficiency measurements at the coin cell level. This endeavor would be valuable since the correlation and linear model in Figure IV- 102 could cut-down testing time from 50 to 16 days; allowing more rapid screening of materials and material modifications. We do stress again that these results are preliminary and need more stringent verification.

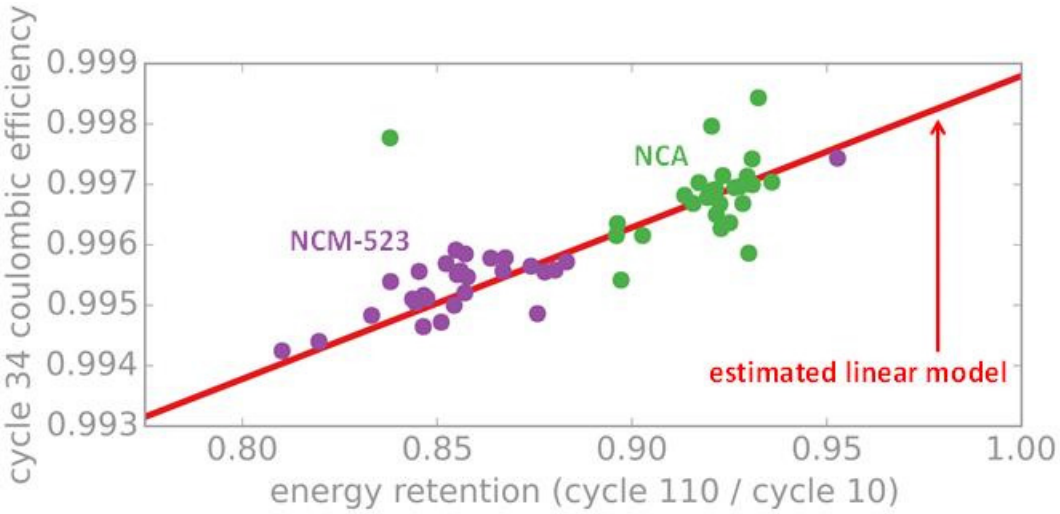


Figure IV- 102: Correlation plot for coulombic efficiency and energy retention

### A.5. Bootstrap Methodology for Evaluating Sample Sizes

We now examine the effect of sample size on determining regions of improved performance. Figure IV- 103 outlines the approach used and how it could govern the diagnostic detection of material improvements. Figure IV- 103a and Figure IV- 103b give the distributions of cycle 34 coulombic efficiency for the two chemistries: NCA is normally distributed and NCM-523 has a distribution that is skewed to lower coulombic efficiencies.

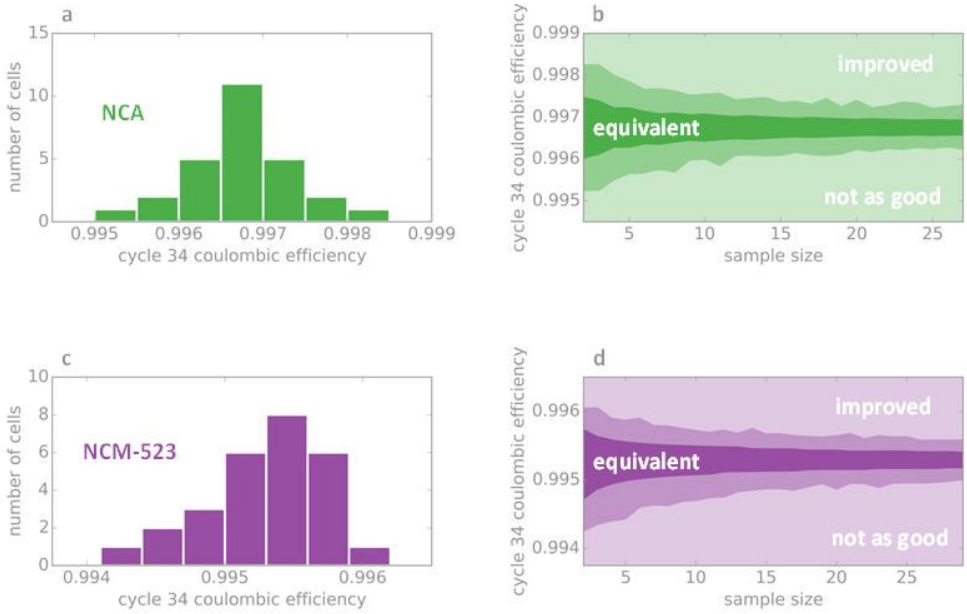


Figure IV- 103: Bootstrap analysis of coulombic efficiency

Figure IV- 103b and Figure IV- 103d give a representation of the boot-strapped distributions with regions highlighted as “equivalent”, “improved” and “not as good”. These notations are in reference to “new materials” that might be tested against the baseline. The plots indicate that for smaller sample sizes, proportionally larger improvements need to be shown. We propose a gated system: in gate 1 a “new material” of interest is initially tested in a 7 cell sample if the data lie in the improved region then the “new material” moves into gate 2 where it is tested in a 15 cell sample size, if the data lie in the improved region then the “new material” becomes the new baseline. Details still need to be explored and refined, however, the basic tenants of the process will ensure a systematic material development process.

### A.6. Summary

In section 1, we outlined a protocol to test full (coin) cells and in section 2, we highlighted and discussed some of the output data from the protocol for two baseline chemistries: NCA and NCM523. In section 3, we defined performance boundaries based on a probabilistic analysis of the inherent variability in cell data: the main conclusion was that large performance gains need to be shown in order to establish a "material improvement". A simple linear model for the relation between coulombic efficiency and energy retention was developed highlighting the predictive role of coulombic efficiency in accelerated ageing studies. Lastly in section 4 and section 5, we used coulombic efficiency to develop a gated system for tracking material improvements using probabilistic modeling techniques. Overall, we hope that the Li-ion community will pay closer attention to cell-to-cell variability when reporting claimed technological advances.

### B. Investigating Performance Degradation Resulting From Cell Cycling

We typically employ electrochemical and physicochemical techniques for our diagnostic studies. Our electrochemical measurements are conducted in cells that include coin cells, pouch cells, and reference electrode cells. Data from these experiments are used to identify cell components that contribute to performance degradation, mainly cell capacity fade and impedance rise.

### B.1. Capacity Fade in Coin Cells tested using the HEHV cycling protocol

In order to determine the source of capacity fade in NCM523//Graphite cells tested using the HEHV protocol we assembled coin cells (2032-type) with electrode samples harvested from aged-cells, lithium-metal counter electrode, fresh Celgard 2325 separator, and fresh Gen2 electrolyte. The cells containing the harvested positive electrodes were cycled between 3 and 4.5 V and the cells containing the harvested negative electrodes were cycled between 1.5 and 0.0 V; all cycling was conducted with a ~0.1C current at 30°C. The data from the harvested electrode cells were compared to data from cells assembled with pristine electrodes to determine the effect of aging on electrode capacity.

Voltage-capacity plots from cells containing the pristine and harvested positive electrodes are shown in Figure IV- 104a and Figure IV- 104b. Figure IV- 104a shows that capacity data from the electrodes are similar, indicating that there is no obvious "loss" of the oxide active material during the aging tests. Figure IV- 104b, which contains voltage-normalized capacity plots, shows that charge curves for the various electrodes are similar. The discharge curves are slightly lower for the harvested electrodes and reflect the higher impedance of these electrodes relative to the pristine samples. Figure IV- 104c and Figure IV- 104d contains voltage-capacity plots from pristine and harvested negative electrodes. Figure IV- 104c shows that capacity data from the electrodes are similar, indicating that there is no obvious loss of the graphite active material during cell aging. Figure IV- 104d, which contains voltage-normalized capacity plots, shows that the lithiation and delithiation curves are similar; the data indicate that the bulk graphite is not damaged during the hundred 3.0-4.4 V cycles.

The conclusions drawn from the above results are as follows:

- The capacity loss displayed by the cycled (aged) HEHV full cells results from $Li^+$ loss in "side reactions". Much of this $Li^+$ loss probably results from lithium trapping in the negative electrode SEI layer.
- Reducing $Li^+$ loss (and, thereby, capacity fade) can be achieved by improving stability of the graphite SEI layer. This improvement is typically achieved through the use of electrolyte additives that form passivation layers at the negative electrode. Another approach would be to create artificial SEI layers by coating the graphite particles or electrodes.

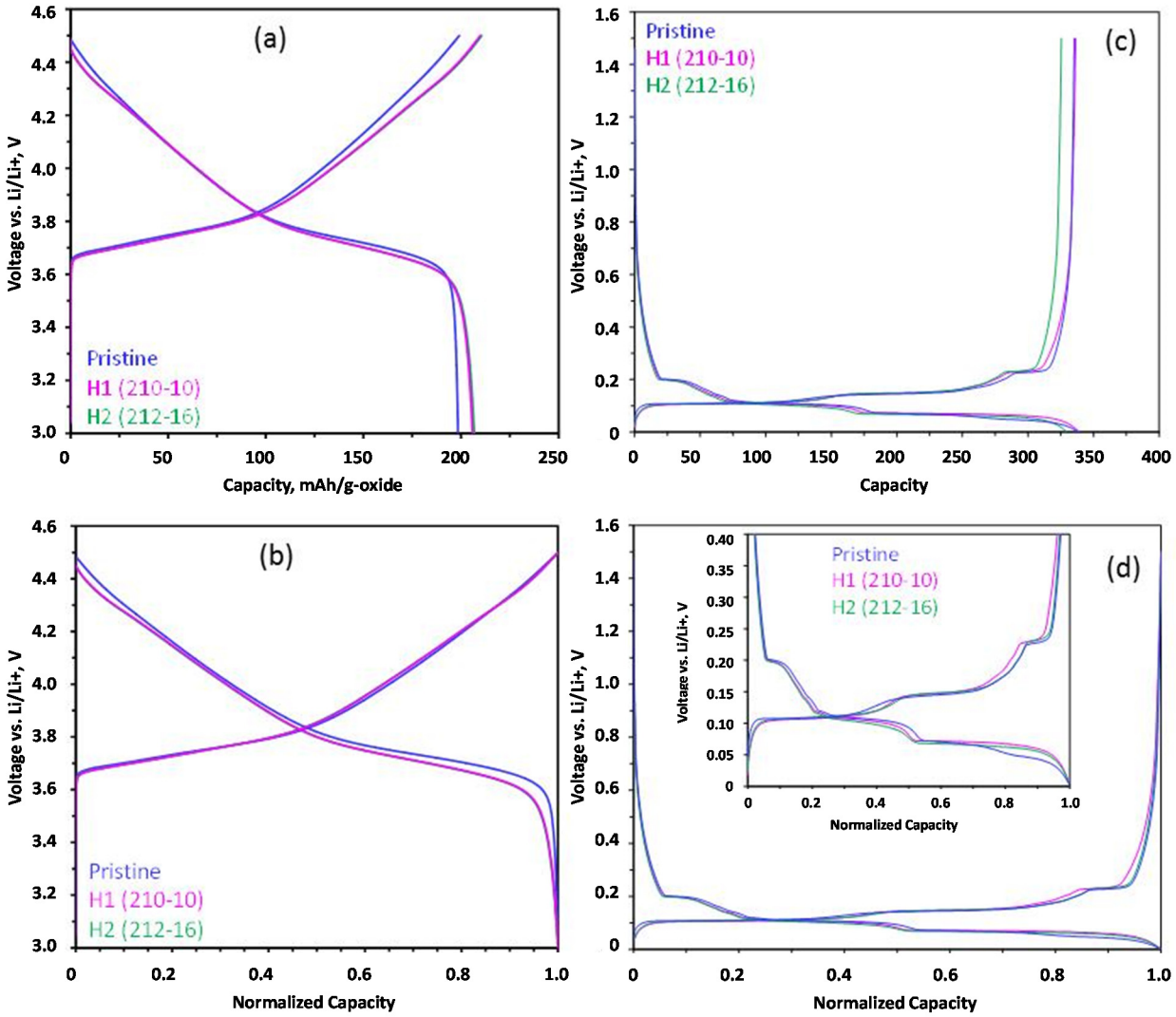


**Figure IV- 104: Voltage–capacity plots, and (b) voltage–normalized capacity plots for half-cells with pristine and harvested positive electrodes cycled between 3-4.5 V, at a ~C/10 rate and 30°C. (c) Voltage–capacity plots, and (d) voltage–normalized capacity plots for half-cells with pristine and harvested negative electrodes cycled between 1.5-0.0 V, at a ~C/10 rate and 30°C; the inset in (d) shows an expanded view of the data between 0.0 and 0.4 V. The captions H1 (210-10) and H2 (212-16) refer to coin cells that were the source of the harvested electrodes**

### B.2 Impedance Rise in Coin Cells tested using the HEHV cycling protocol

In order to determine the source of impedance rise in NCM523//Graphite and NCA//Graphite cells tested using the HEHV protocol, we first disassembled these cells after a 24 h hold at 3.7 V. Electrodes harvested from these cells were then used to prepare symmetric positive-electrode and symmetric negative-electrode (2032-type) coin cells that also contained fresh Celgard 2325 separator, and fresh Gen2 electrolyte. AC impedance data were obtained on these symmetric cells. These data were compared with initial (after formation cycling) data obtained on corresponding full cells, containing a Li-Sn reference electrode, held at 3.7 V.

Figure IV- 105 contains AC impedance data on positive and negative electrodes from the NCM523//Graphite and NCA//Graphite cells after initial/formation cycling and after ~100 aging cycles. In all cases, the impedance change at the positive electrode is significantly larger than the impedance change at the negative electrode. Furthermore, the impedance rise is mainly seen in the mid-frequency arc, which contains contributions from the positive electrode surface films and oxide structural changes at the electrode-electrolyte interface.

The conclusions drawn from the above results are as follows:

- Impedance increase of the NCA//Gr and NCM523//Gr cells arises mainly at the positive electrode. This impedance increase is mainly at the electrode-electrolyte interface and includes contributions from electrode surface films, and structural changes at the oxide surface.
- Previous experiments have shown that such impedance rise can be minimized by using electrolyte additives (such as LiDFOB) that modify the oxide-electrolyte interface and by using appropriate oxide particle or electrode coatings (such as alumina).

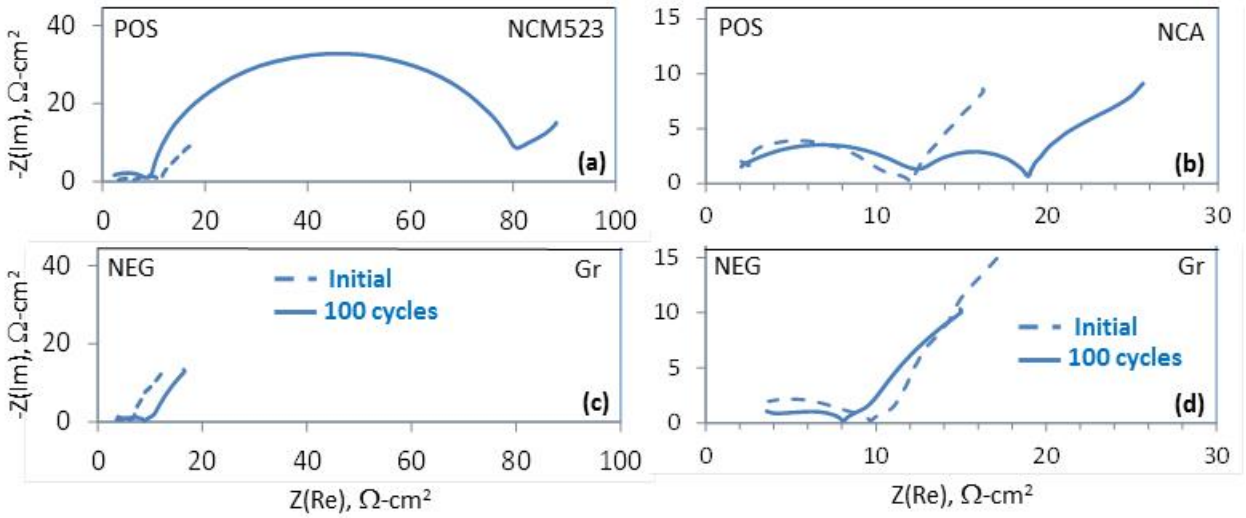


**Figure IV- 105: AC impedance data (30°C, 100 kHz - 5 mHz) from positive (POS) and negative (NEG) electrodes, after initial cycling and after 100 aging cycles. (a) and (c) are data from NCM523//Graphite cells, whereas (b) and (d) are data from NCA//Graphite cells**

### B.3 Electrochemical Testing in cells with Reference Electrodes

In order to determine contributions of the NCM523-based positive electrode and A12 graphite-based negative electrode to the full cell data, electrochemical measurements were conducted in cells with reference electrodes. Large format cells were assembled with 20.3 $cm^2$ area electrodes, two Celgard 2325 separators enveloping a Li-Sn reference electrode, a Li-metal reference electrode external to the electrode sandwich, and fresh Gen2 electrolyte. Cell cycling was based on the HEHV protocol, which includes formation cycles that are followed by aging cycles; pulse-power and AC impedance measurements are made periodically. The data discussed here and shown in Figure IV- 106 were obtained on cells cycled in the 3-4.4 V range.

Figure IV- 106a contains voltage-time plots obtained for the formation cycles, which includes the following in sequence: (a) 2h rest to allow electrode wetting; (b) 15 min tap charge to 1.5 V full cell voltage followed by a 4h rest; (c) Four ~C/10, 3-4.4 V, cycles. Figure IV- 106b is a close-up look at the first 20h. The data show that the full cell voltage is ~0 V during the initial 2h rest, indicating that the positive and negative electrode voltages are similar. During the 15 min tap charge to 1.5 V full cell voltage, the positive electrode shows a sharp initial voltage spike, which is related to a $Li_2CO_3$-based film on the oxide particles; the negative electrode voltage decreases as expected. However, during the 4h hold, the negative voltage rises, while the positive voltage decreases. The first C/10 cycle starts after the 4h rest; once again, the positive voltage shows a sharp rise to ~4.3 V, then decreases, then rises again. Again, this behavior of the positive is related to the $Li_2CO_3$ oxide surface film that induces a polarization (IR) resistance; the voltage starts to decrease after this surface film decomposes around ~4.3 V. In contrast to the positive, the negative electrode voltage decreases as expected during charge. The full cell voltage is the difference between the positive and negative electrode voltages; an initial spike is not observed in these data because the voltage decrease of the negative offsets the voltage increase of the positive electrode.

Figure IV- 106c is a close-up look at the 2nd cycle. The data shows that when the full cell is charged from 3 to 4.4 V, the positive electrode voltage increases from ~3.71 to ~4.48 V vs. $Li/Li^+$, whereas the negative electrode voltage decreases from ~0.71 to ~0.08 V vs. $Li/Li^+$. The positive and negative data resemble those obtained for these electrodes from half-cells, which confirms the proper functioning of the Li-metal reference electrode.

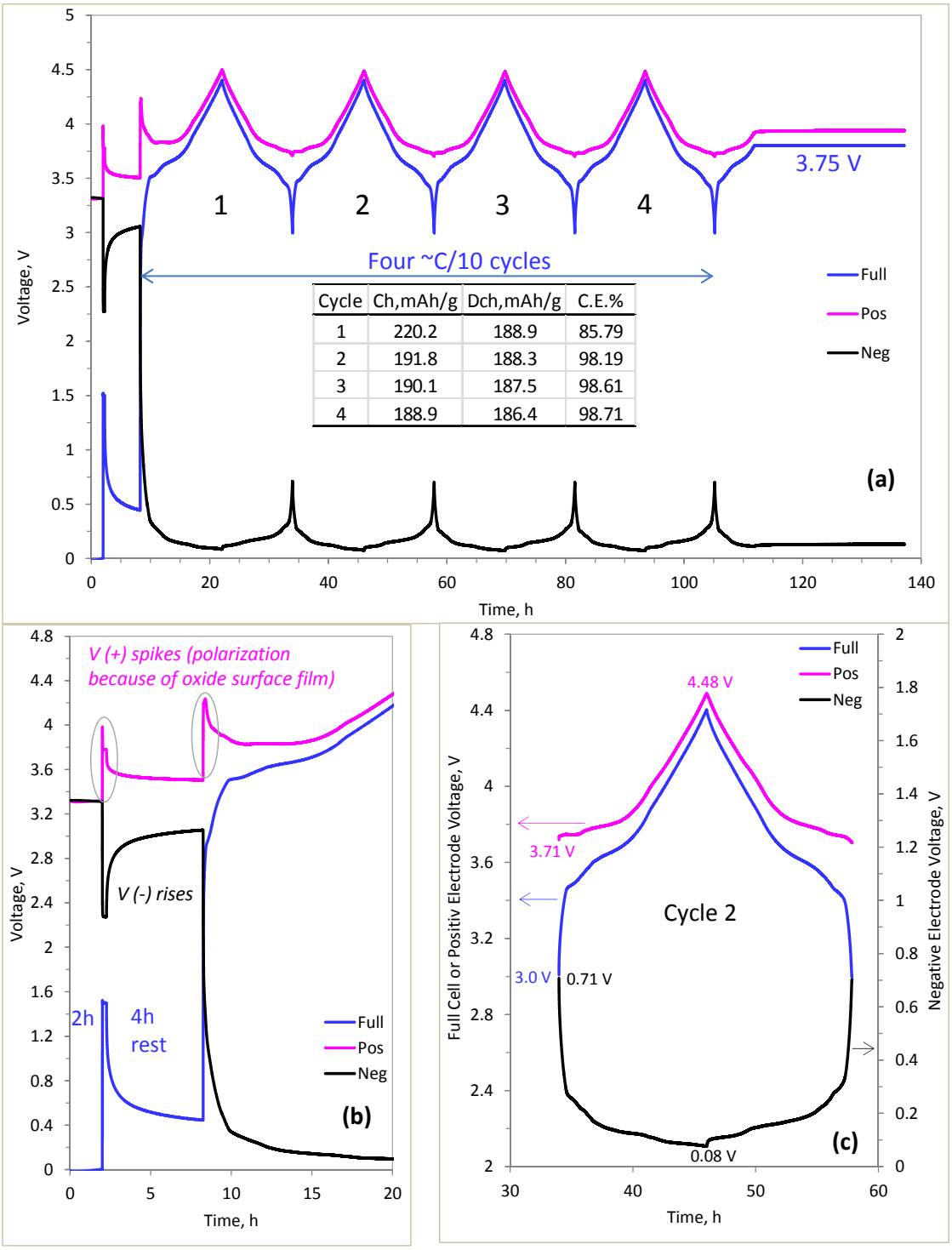


| Cycle | Ch,mAh/g | Dch,mAh/g | C.E.% |
|---|---|---|---|
| 1 | 220.2 | 188.9 | 85.79 |
| 2 | 191.8 | 188.3 | 98.19 |
| 3 | 190.1 | 187.5 | 98.61 |
| 4 | 188.9 | 186.4 | 98.71 |

**Figure IV- 106: Initial cycling (30°C) of an NCM523//Gr cell with a Li-metal reference electrode. (a) The cycling includes a 2h rest, a 15 min tap charge to 1.5 V full cell voltage followed by a 4h rest, and four ~C/10 cycles. (b) close-up of the first 20h, and (c) is a close-up of cycle 2**

Figure IV- 107 contains full cell, positive electrode, and negative electrode, area specific impedance (ASI) data from HPPC tests, conducted on a NCM523//Gr cell with a Li-Sn reference electrode, after formation cycling and after 100 aging-cycles (3-4.4 V) at 30 °C. The data are obtained after the cell is charged to 4.4 V, then gradually discharged to 3.0 V during which the cell is subjected to a current pulse profile that includes a 3C, 10-s discharge pulse, 40-s rest, then a 2.25C, 10-s charge pulse. The data in Figure IV- 107 shows that, after

formation cycling, the positive electrode impedance is larger than that of the negative electrode. In addition, after the 100, 3-4.4 V, aging cycles, the full cell impedance rise mainly results from an impedance rise at the positive electrode; the negative electrode contribution to impedance rise is small.

AC impedance data (not shown) were also obtained measured at a full cell value of 3.8 V for the (a) full cell, (b) positive electrode, and (c) negative electrode. The data were collected after formation cycling, and after the aging (3-4.4 V) cycles. The data showed that the initial cell impedance has a higher contribution from the positive than the negative electrode. Furthermore, the full cell impedance increase arises mainly at the positive electrode. These observations are consistent with those described above for the HPPC tests.

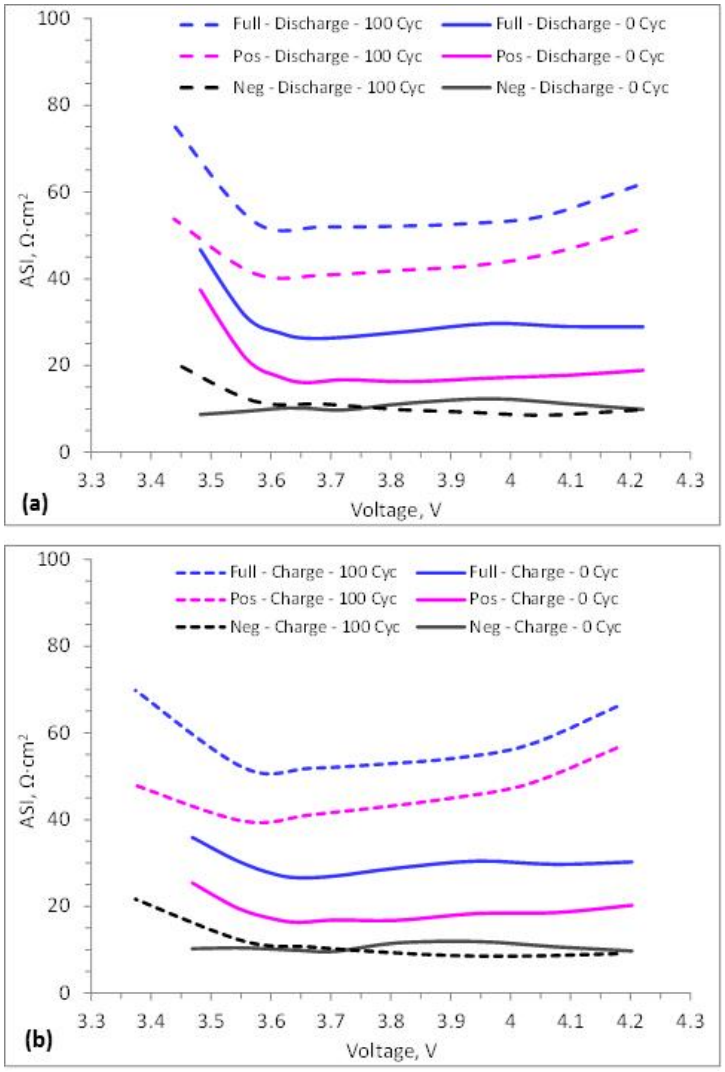


**Figure IV- 107: Full cell, positive electrode, and negative electrode, area specific impedance data (30°C) from HPPC tests, conducted on a NCM523//Gr cell with a Li-Sn reference electrode, after formation cycling and after 100 aging-cycles (3-4.4 V). The data are from (a) 3C, 10-s discharge pulses; (b) 2.25C, 10-s charge pulses**

The conclusions drawn from the above results are as follows:

- The (external) Li-metal reference electrode provides information on positive and negative electrode voltage profiles during full cell cycling. After formation, the positive electrode cycles between ~3.71 and ~4.48 V; the oxide is never fully lithiated during the discharge cycle. The negative electrode cycles between ~0.71 and ~0.08 V vs. $Li/Li^+$, and shows all the plateaus typically associated with lithium intercalation into graphite.
- Both HPPC and AC impedance measurements indicate that the full cell impedance has a higher contribution from the positive electrode. Furthermore, cell impedance increase arises mainly at the positive electrode. Passivation layers at the positive electrode should minimize impedance rise; these can be applied *exsitu* by techniques such as Atomic Layer Deposition (ALD) or *insitu* through the use of electrolyte additives that generate protective films at the positive electrode.

### C. Electrochemical Modeling

This modeling study is part of an integrated effort with the CAMP Facility (see section IV.B.1) to model cathodes for advanced lithium-ion battery technologies. The electrochemical modeling effort relies heavily on experimental analytical and electrochemical diagnostic and characterization studies across the HE-HV program. Experimental data presented in this section are part of that effort. The methodology for the electrochemical modeling effort is described in detail in the literature [1-9]. The model combines thermodynamic, kinetic, and interfacial effects with continuum based transport equations. The bulk transport model equations are given in Figure IV- 108. Volume-averaged transport equations account for the composite electrode geometry. Continuum based transport equations using concentrated solution theory describe the movement of salt in the electrolyte. The transport of ionic and electronic current throughout the cell is included, as is the diffusion of lithium in the solid-state active materials.

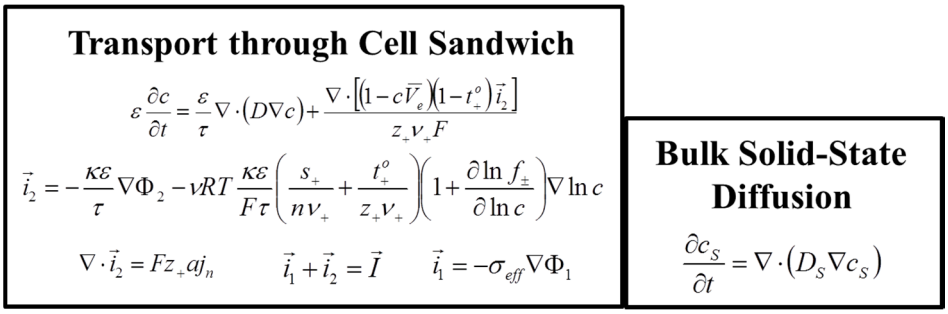


**Figure IV- 108: Intercalation electrochemical model equations, grouped according to electronic and ionic transport through cell sandwich and solid-state diffusion in active material**

### C.1 Impact of Oversized Anode in Coin Cell Testing

The above-described electrochemical model was developed for examining the impact of oversized anodes in coin cell testing of full lithium-ion cells. The methodology for the model was previously developed to examine reference electrodes in lithium-ion cells [2]. A NCA/graphite chemistry was adopted for this study because a complete parameter set for the electrochemical model was available. Similar results would be expected using a NCM523 cathode. A two-dimensional cylindrical geometry (i.e. R and Z) was used to account for the coin cell cathode/separator/anode sandwich, including a flooded electrolyte space outside the sandwich. Transport in the active material particles was followed by using a one-dimensional finite difference form of the bulk solid-state diffusion equation, given in Figure IV- 108. The lithium concentration at individual nodes of the active material particles was then carried as dependent variables in the numerical two-dimensional solver. The active material solid electrolyte interphase (SEI) is, at best, ill-defined and very complicated. The process of moving lithium ions across the SEI includes some combination of diffusion, migration, and reaction. While it is critically important to account for the potential effects associated with the SEI it is beyond the scope of this effort to include a detailed description of the SEI in the model. In the present study, a linear Butler-Volmer (BV) electrochemical reaction expression is used to account for the interfacial impedance.

Two types of coin cells were simulated, matched electrodes (14 mm cathode/16 mm separator/14 mm anode) and oversized anode (14 mm cathode/16 mm separator/15 mm anode). The two types of cells are cycled at a C/3 charge and discharge rate until the cycle-to-cycle differences are eliminated (i.e. steady-state). The radial distribution of the average and surface active material particle lithium concentration in both electrodes along the midpoint between the current collector and separator is given in Figure IV- 109 for both types of coin cells at the top of charge, (a) and (b), and the bottom of discharge, (c) and (d). In Figure IV- 109, the dotted lines identify the outer edge of the electrodes and zero is the center of the cell.

Typically in lithium-ion cells the SEI impedance is great enough to cause the current distribution between the current collector and separator to remain relatively uniform. Thus the lithium distribution represents an integrated current distribution across the face of the electrode. The lithium concentration for the matched electrode cell, Figure IV- 109(a) and (c) is relatively uniform when compared to the oversized anode cell, Figure IV- 109(b) and (d). Further, lithium concentration in the oversized anode tends to be more non uniform than the cathode. Also, the lithium concentration in the oversized part of the anode tends to lag behind the rest of the electrode (i.e. higher at bottom of discharge and lower at the top of charge). At the C/3 rate, the lithium concentration gradients are generally small. Thus the surface and average concentrations are approximately the same. The exception is the cathode in the oversized anode cell at the bottom of charge where the surface near the outer edge becomes loaded with lithium and the lithium diffusion coefficient drops off significantly.

Generally, the current distribution non-uniformity is approximately the same size as the anomaly. In the matched electrode cell the anomaly is the thickness of the cell (~0.1mm). While in the oversized anode cell the anomaly is the length that the anode extends past the cathode (0.5mm). Therefore, the non-uniform current distribution would be expected to be more dramatic in the oversized anode cell. From these simulations, one can start understanding the impact of electrode alignment. Ideally, the matched electrode cells should perform better. Of course, perfectly aligning the electrodes to within say less than 0.1 mm represents a huge challenge. The greater misaligned the electrodes, the more non-uniform the current distribution becomes, causing greater variation in the cell-to-cell performance. On the other hand, the oversized anode cells have essentially a buffer already built-in to deal with the misalignment.

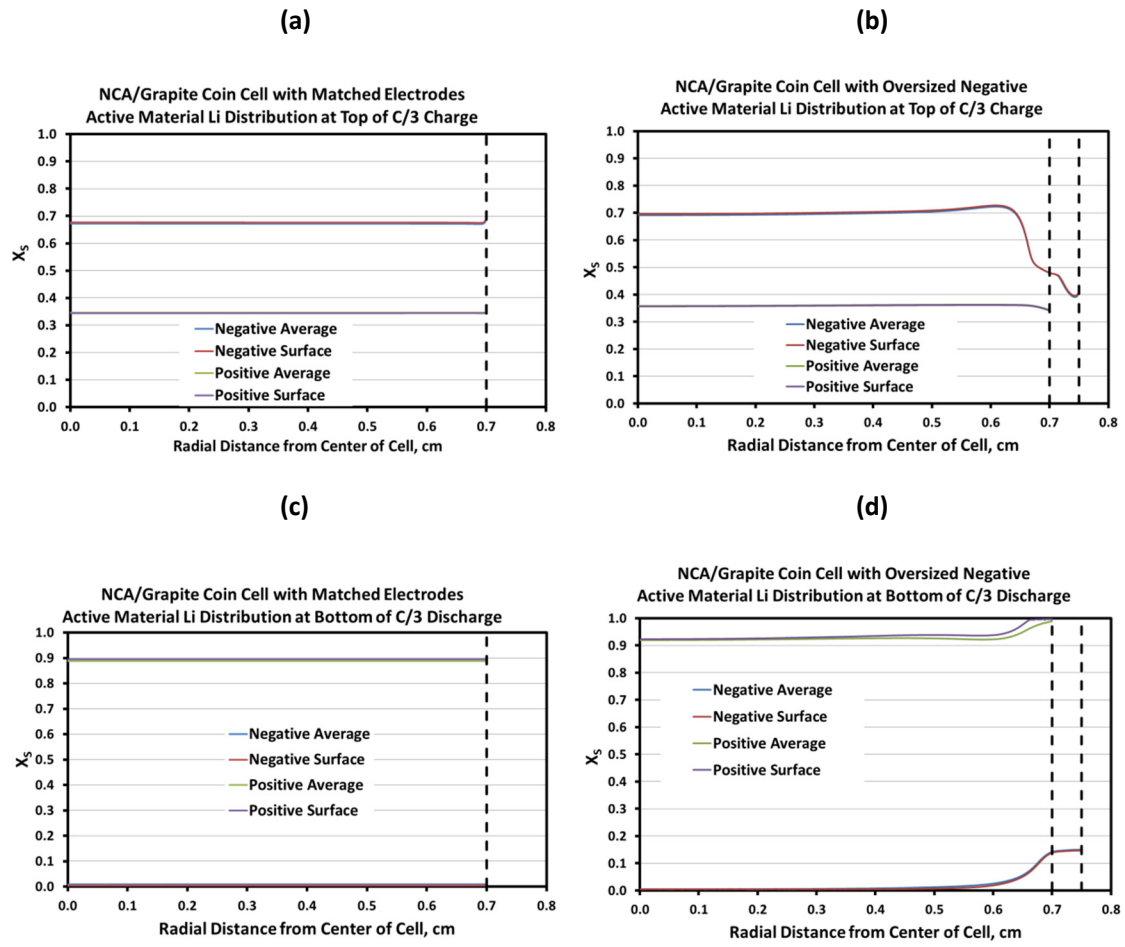


**Figure IV- 109: Average and surface active material particle lithium concentration (electrode midpoint) in coin cells with matched electrodes and oversized anode. (a) Matched electrodes at top of charge. (b) Oversized anode at top of charge. (c) Matched electrodes at bottom of discharge. (d) Oversized anode at bottom of discharge**

While the oversized anode coin cells have less sensitivity to misalignment, the simulations indicate they require several cycles to reach steady-state, as shown in Figure IV- 110. As may be expected, the anode tends to be the slower electrode to reach steady-state. After the first couple of cycles, the changes are small, but these small changes can impact the cell coulombic (i.e. current) efficiency by tenths of a percent. Alternatively, the matched electrode coin cell reaches steady-state after a couple of cycles. This sluggishness of the oversized anode to come to steady-state also comes into play when the testing protocols are changed. This can be seen in the cell cycling where the larger oversized anode coin cells have a slight drop in current efficiency following the HPPC discharge. The HPPC discharges for these tests require about 13 hours to complete. The impact on current efficiency of a C/15 discharge between C/3 cycles is shown in Figure IV- 111. Like the cycling results, the simulations indicate a drop in efficiency after the slow discharge.

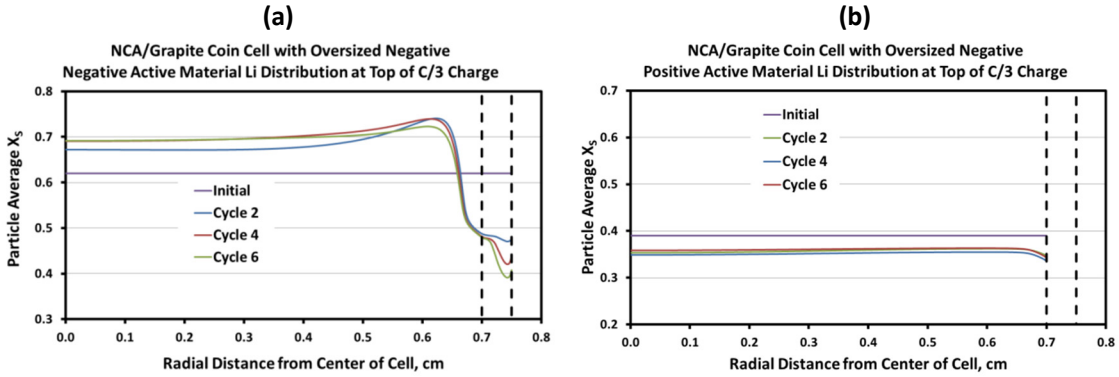


**Figure IV- 110: Average active material particle lithium concentration (electrode midpoint) in coin cells with oversized anode at top of a C/3 charge at the indicated cycle. (a) Anode. (b) Cathode.**

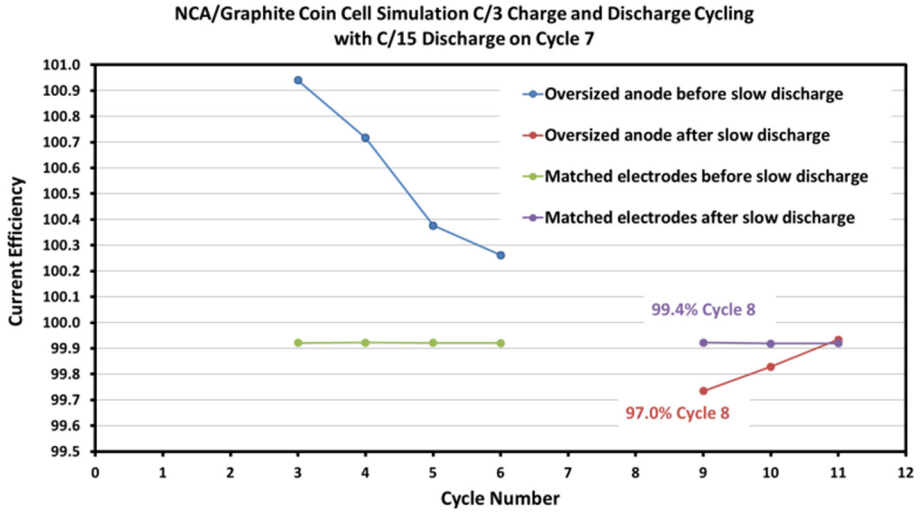


**Figure IV- 111: Current efficiency of oversized anode and matched electrode coin cells during C/3 cycling after a C/15 discharge**

The impact of the slow discharge on oversized anode coin cells can be seen in Figure IV- 112. The slow discharge allows the lithium in the excess anode to be more completely removed. Further, there is a significant change in the lithium distribution through most of the cell. As discussed above, the oversized anode coin cell then requires several cycles to again fully reach steady-state.

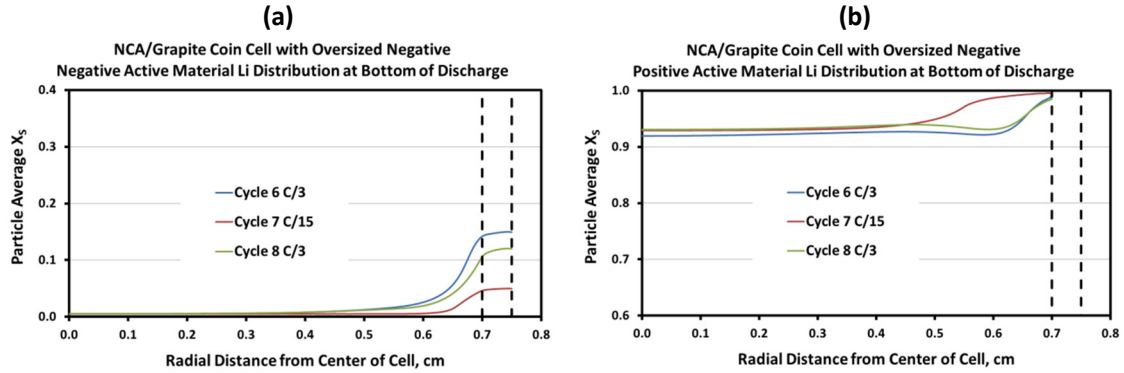


**Figure IV- 112: Average active material particle lithium concentration (electrode midpoint) in coin cells with oversized anode at bottom of discharge at the indicated cycle. (a) Anode. (b) Cathode**

### C.2. Change in the Thermodynamic Voltage Measurement resulting from an Electroactive Thin Surface Layer on a Cathode Active Material in a Half-Cell

Modifying the SEI by coating the cathode particles with a thin surface layer to improve its stability (and ultimately life) at high voltages is a significant part of the HE-HV effort. With a wide variety of materials and coating techniques, as well as subsequent annealing temperatures, the optimum coating and microstructure is not obvious. As a first step in examining the impact of the coating, an electrochemical model was developed to look at its effect on the thermodynamic voltage of the cathode material, as measured by its slow discharge in a half-cell configuration. The coating is initially assumed to be electroactive and completely covering of all electrochemically active surfaces of the base cathode material. While this case is effectively impossible to implement, it does represent the situation where the coating would potentially have the greatest impact on the half-cell thermodynamic voltage. As an aside, if the cathode material is completely covered by a true insulating layer (i.e. a layer that is not electroactive), then one would not have a functional half-cell.

For simplicity, it is assumed that the current distribution in the cathode is uniform and that potential effects from the lithium electrode, along with the transport in the electrolyte, can be accounted for with a resistive term. Further, the bulk active material and the surface layer are assumed to be dense electroactive lithium intercalation materials with their own individual properties. With these assumptions, the geometry reduces to one-dimensional diffusion in the active materials. The electrochemical reaction is assumed to occur on the electrolyte side of the layer and follow linear BV kinetics. A standard mass transfer expression with an electrochemical potential driving force is assumed to describe the lithium transport through the interface between the layer and the bulk active material (see below for bulk and surface layer materials *i* and *j*).

$$N_{ij} = k_{\mu ij}\left[\mu_{Li}(i) - \mu_{Li}(j)\right] = k_{\mu ij}F\left[U_j - U_i\right]$$

The electrochemical potential can easily be related to the open circuit voltage (OCV) of the material at the interface between materials. Finally, the bulk active material and surface layer are assumed to have the same volumetric capacity and lithium diffusion coefficients, but significantly different OCV curves. As a test case, the OCV curves, shown in Figure IV- 113, were assumed for the active material and surface layer. OCV curves of different slopes with a significant offset were assumed.

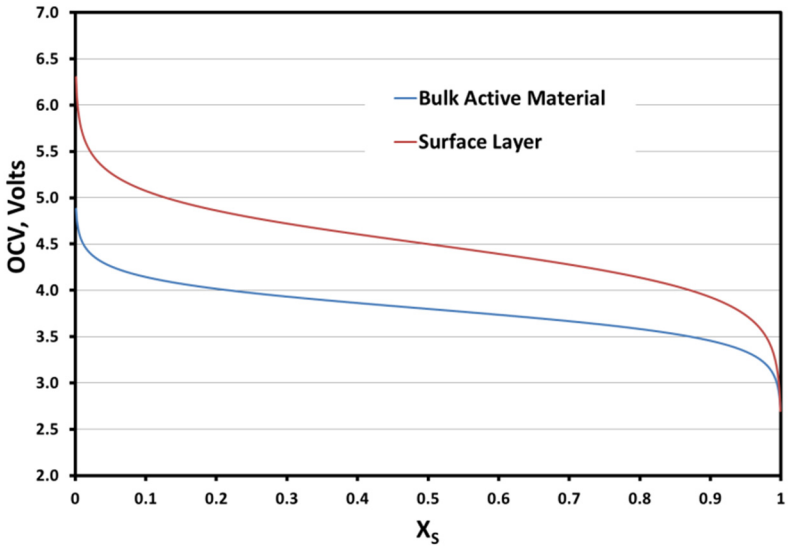


**Figure IV- 113: Assumed open circuit voltage curves for the bulk active material and surface layer as a function of the fraction of lithium in the material (i.e. lithium concentration over maximum lithium concentration)**

Key to this analysis is that the capacity of the bulk active material should be much greater than that of the surface layer. A factor of 100 is assumed. A relatively slow discharge rate (C/10) is used in the simulation to minimize the impact of lithium concentration gradients in the materials. A quick comparison of the material thermodynamic voltage curves in Figure IV- 113 with the discharge curve simulation, given in Figure IV- 114, suggests the cell follows the bulk active material OCV curve.

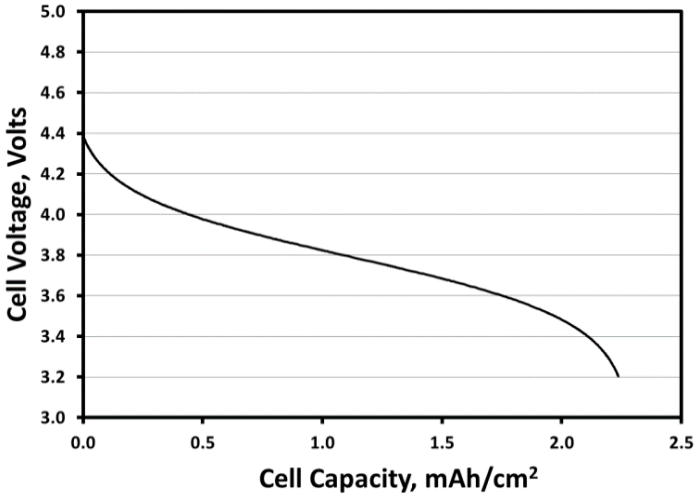


Figure IV- 114: Simulation of half-cell C/10 discharge curve

In actuality, the slow discharge simulation for the half-cell follows the thermodynamics of both the surface layer and the bulk materials, as shown in Figure IV- 115. If the materials are close to equilibrium, the bulk active material, having a significantly higher capacity, establishes the half-cell voltage by forcing the surface layer to follow the electrochemical potential of its lithium. Essentially, if the layer and the bulk material are not at equilibrium, then lithium will shift either in or out of the bulk material to establish equilibrium, with very little change in its lithium concentration. The net effect can be seen in Figure IV- 116 where the change in lithium concentration of the bulk material is effectively proportional to the cell capacity and that of the surface layer is nonlinear. As the discharge rate increases and the materials are farther from equilibrium the respective diffusion rates and interfacial transport come into play and can have a significant impact on the observed potential. Likewise, if the capacity of the surface layer approaches that of the bulk active material, then the cell potential would be a mixed potential of the two materials.

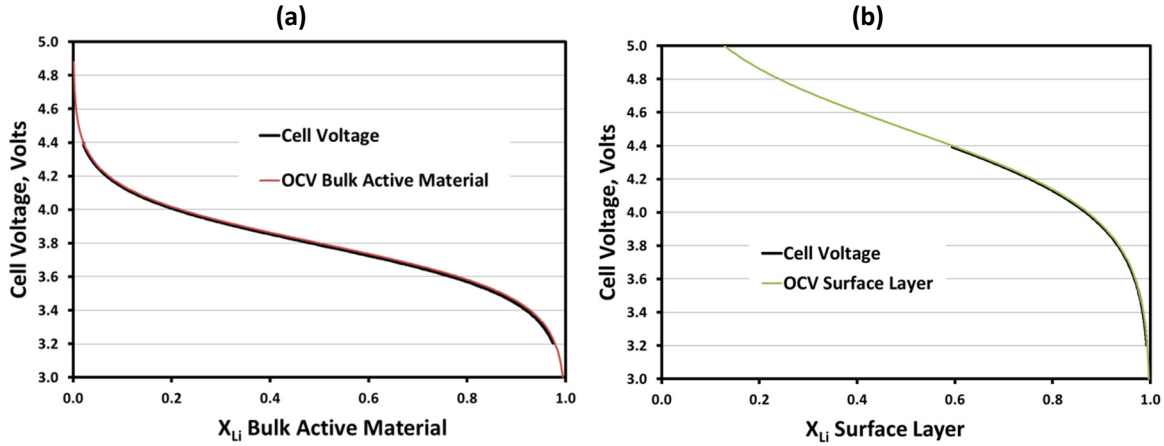


Figure IV- 115: Comparison of half-cell C/10 discharge simulation to the assumed open circuit voltage curves for the bulk active material (a) and surface layer (b) as a function of the fraction of lithium in the respective materials

### C.3 Reaction and Diffusion of Electrolyte Additives in Coin Cells: Impact of Excess Electrolyte

Similar to the surface layer studies, modifying the cathode SEI through the use of reactive additives in the electrolyte to improve its stability at high voltages and ultimately life is a significant part of the HE-HV effort. Accurately accessing the impact of electrolyte additives is not a straight-forward process and has been found to depend on the cell format (coin vs. pouch) used in the analysis. Electrolyte is added to the face of the electrodes during coin cell assembly and at the edges in pouch cells. In addition, the coin cells are often assembled with more excess electrolyte that resides in the space outside the cell sandwich, but within the can. As a first step, the impact of the excess electrolyte in the reaction and diffusion of additives was examined.

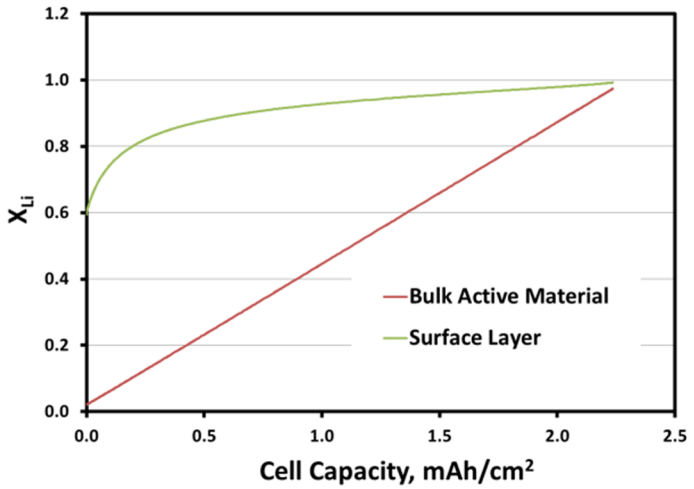


Figure IV- 116: Change in fraction of lithium in the bulk active material and surface layer as a function of discharge capacity during the half-cell C/10 discharge simulation

As a coin cell undergoes its first charge, solvents, salts, and/or additives react on the surfaces of both electrodes to form their SEI. Initially, this is expected to be relatively fast, but it slows as the SEI grows. If all the SEI forming additives in the electrolyte within the cell sandwich react before the SEI is fully formed, then the additives in the excess electrolyte outside the cell sandwich will diffuse into the cell and react. The time associated with this secondary process can be quite long and depends upon a number of unknowns (e.g. excess electrolyte access to edge of cell). However, a rough estimate can be obtained from the characteristic diffusion time (see the equation below) for the additive to diffuse to the center of the coin cell. Using a typical diffusion coefficient for liquids ($10^{-5}$ $cm^2/s$), one gets a time constant of more than a day.

$$t_{diffusion} = \frac{\left(r_{coin\,cell}\right)^2 \tau}{D}$$

Focusing initially on the electrolyte additives, the ultimate goal is to develop a model for their reaction and diffusion that can be integrated into the full electrochemical cell model. As can be seen in Figure IV- 117, a simple mass balance of the reacted additive surface concentration ($\Gamma_S$) on the electrode surfaces can be written. Here it is implicitly assumed that the reacted additive surface concentration reaches a maximum concentration. Also in Figure IV- 117, a standard diffusion equation for a dilute species in a liquid within a porous material is used to track the diffusion of the additive through the electrolyte. Since the cell is relatively thin when compared to its diameter, we simplify the problem by reducing the geometry to one-dimensional radial diffusion through the electrolyte in the electrode pours. Further, it is assumed that there is a continuous source of electrolyte additive just outside the cell sandwich. This should result in a best-case scenario for the additive to react within the cell sandwich.

**Electrolyte Additive Reaction-Diffusion**

$$\frac{\partial \varepsilon c}{\partial t} = \nabla \cdot \left( \frac{\varepsilon D}{\tau} \nabla c \right) - aR$$

$$\frac{\partial \Gamma_S}{\partial t} = R \qquad R = k_S \left( \frac{\Gamma_{S\max} - \Gamma_S}{\Gamma_{S\max}} \right) c$$

Figure IV- 117: Electrolyte additive reaction and diffusion model equations

In the model simulations, the speed at which the additive is reacted is dependent on the relative concentrations and reaction rate ($k_S$). In general, the reaction is believed to be a relatively fast process once a threshold electrode potential is reached. As an example, in this simulation, 5 minutes after the reaction has initiated the additive is exhausted, the SEI is about 80% of its maximum concentration, and diffusion of additive from outside the cell sandwich has begun. The reaction front progresses through the cell sandwich as the additive diffuses toward the center of the cell. An hour into the simulation, the reaction front is about halfway to the center of the cell. Also, the width of the reaction front is dependent on the interaction of the reaction rate and diffusion. The process only requires about 4 hours for the SEI additive reaction to be complete. For comparison, if after the additive is exhausted, the SEI is only about 40% of its maximum concentration, more additive has to diffuse in and the whole process will take about 14 hours.

### C.4 Electrochemical Impedance Spectroscopy (EIS) Initial Analysis of NCM523 Electrodes

EIS is a powerful electrochemical diagnostic tool used to examine the electrochemical performance of electrodes and cells. However, interpretation of results can be a challenge. To assist in the analysis an

electrochemical model, previously developed on another project, was utilized to examine EIS studies on NCM523 baseline electrodes [1, 3, and 4]. The model utilizes the framework presented in Figure IV- 108, but also includes phenomena associated with the complex SEI. These phenomena include the lithium ions diffusing and migrating through surface films formed by the interaction of the active material with the electrolyte and combined with the polymer binder and conductive carbon. The lithium ions then react electrochemically at the surface of the active material. Furthermore, the active material is assumed to have a thin surface layer, which has electronic and ionic properties that differ from those of the bulk material. A double-layer capacity is added in parallel with the BV kinetic reaction expression and a second capacitance is included in parallel with the surface film on the active material. Finally, a localized electronic resistance between the current-carrying carbon and the active material interface is included with its own separate capacitive effect. The transport and reaction equations for the SEI are given in Figure IV- 118.

**Electrode SEI Reaction/Transport**

$$\eta_f = \frac{i_n \delta_f}{\kappa_f} + \frac{RTs_+}{nF} \ln \frac{c_+|_{electrolyte}}{c_+|_{active\ material}} \qquad \frac{\partial c_+}{\partial t} = D_+ \left( \frac{\partial^2 c_+}{\partial y^2} \right)$$

$$\frac{\partial c_{Si}}{\partial t} = D_{Si} \left( \frac{\partial^2 c_{Si}}{\partial y^2} \right)$$

$$i_n = i_0 \left( \frac{c_+}{c_{+,ref}} \right)^{\alpha_A} \left( \frac{c_{Ti} - c_{Si}}{c_{Ti} - c_{Si,ref}} \right)^{\alpha_A} \left( \frac{c_{Si}}{c_{Si,ref}} \right)^{\alpha_C} \left\{ e^{\left[ \frac{\alpha_A F \eta_K}{RT} \right]} - e^{\left[ -\frac{\alpha_C F \eta_K}{RT} \right]} \right\}$$

$$\eta_R = \sigma_P z_+ F j_n$$

**Figure IV- 118: SEI reaction and transport electrochemical model equations**

An EIS study of the NCM523 baseline electrode using a micro-reference electrode cell fixture is given in Figure IV- 119. The NCM523 electrode impedance is compared to previously studied NCA and LMR-NMC electrodes [1, 3, and 8]. The impedance of all three oxide electrodes are known to depend on SOC, the results shown are of each electrode at or near its minimum in impedance, which occurred at electrode voltages between 3.8 and 3.95 V vs. lithium, depending on the active material. For all the electrodes the impedance is made up of at least two circular arcs (i.e. a high-frequency arc and a mid-frequency arc), associated with the interfacial phenomena, and a low frequency Warburg impedance tail, and associated with diffusion in the electrolyte and bulk active material. For all three electrodes the maximum in the high-frequency arc occurs on the order of 10 kHz and the maximum for the mid-frequency arc occurs between 10 and 100 Hz.

In general, the interfacial model parameters, given in Table IV- 14, can best be determined by fixing the active material and examining a wide variety of impedance studies including variations in SOC, temperature, electrolyte composition, and electrode formulation. It is expected that as the interface of the NCM523 material is modified, as part of the HE-HV effort, our confidence in the parameters should improve. For now, similarities between past electrode studies can be utilized to help fit the results. The relative time constant (i.e., fastest to slowest) of the individual interfacial phenomena used in fitting the EIS data are listed below, along with their associated parameters.

- Electronic resistance between carbon additive and active material if carbon additive has a significant capacitance ($\sigma_p$, $C_c$).
- Ion migration through surface film on active material (i.e. SEI resistance) ($\kappa_f$, $C_f$).
- Lithium ion diffusion through surface film on active material ($D_+$, $c_+$).
- Electrochemical reaction (i.e. Butler Volmer kinetics) ($i_o$, $C_d$).
- Lithium diffusion through active material surface layer ($D_{Si}$, $K_S$).

The NCM523 electrode performance is comparable to NCA and much better than the LMR-NMC. The LMR-NMC has fundamentally much poorer kinetics and diffusuion when compared to the other oxides, but the high electrochemical active area of the material (a) offsets some of these differences. The characteristic large high frequency circular arc on the NMC electrodes is associated with a high electronic contact resistance ($\sigma_p$). This work will help form the basis for comparison as the active material, surface film, and/or SEI are modified. The electrochemical modeling should provide valuable insight into the impact of electrode/electrolyte changes.

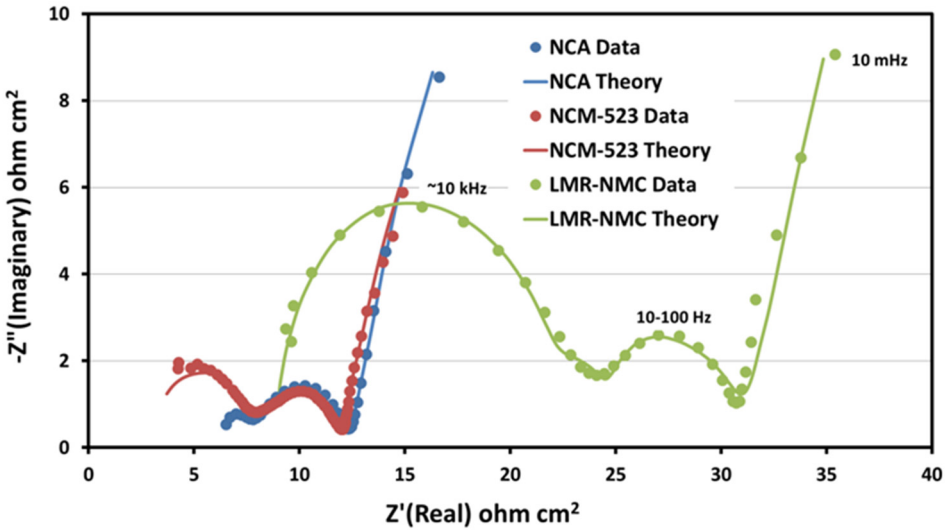


Figure IV- 119: Comparison of positive electrode EIS studies taken with a micro-reference electrode cell (100 kHz-10 mHz)

**Table IV- 14: Comparison of positive electrode interfacial and oxide active material parameters for electrochemical model**

| Positive Electrode | Active Material Surface Layer and Bulk | | | | SEI Film on Active Material | | | Electronic Contact Resistance | Kinetic and Capacitance | | | |
|---|---|---|---|---|---|---|---|---|---|---|---|---|
| | a | $D_{si}$ | $D_{sb}$ | $K_s$ | $D_+$ | $K_f$ | $C_+$ | $\sigma_P$ | $i_0$ | $C_c$ | $C_d$ | $C_f$ |
| | $cm^{-1}$ | $cm^2/s$ | | | $cm^2/s$ | $\Omega^{-1}cm^{-1}$ | M | $\Omega cm^2$ | $mA/cm^2$ | $\mu f/cm^2$ | | |
| NCA | 8900 | $5.5x10^{-11}$ | $4.0x10^{-11}$ | 5.0 | $3.0x10^{-9}$ | $1.0x10^{-7}$ | $7.0x10^{-3}$ | 0 | 0.49 | 0 | 45 | 0.3 |
| NCM-523 | 6797 | $8.0x10^{-12}$ | $3.0x10^{-10}$ | 1.5 | $5.0x10^{-9}$ | $1.3x10^{-7}$ | $8.0x10^{-3}$ | 70 | 1.60 | 0.045 | 60 | 0.3 |
| LMR-NMC | 48000 | $2.0x10^{-12}$ | $2.0x10^{-12}$ | 5.5 | $1.5x10^{-8}$ | $2.3x10^{-8}$ | $4.3x10^{-4}$ | 1800 | 0.045 | 0.009 | 20 | 0.09 |

## References


1. *Alternating Current Impedance Electrochemical Modeling of Lithium-Ion Positive Electrodes.* **D. Dees, E. Gunen, D. Abraham, A. Jansen, and J. Prakash.** 7, 2005, J. Electrochem. Soc., Vol. 152, pp. A1409-A1417.
2. *Theoretical Examination of Reference Electrodes for Lithium-Ion Cells.* **D.W. Dees, A.N. Jansen, D.P. Abraham.** 2007, J. Power Sources, Vol. 174, pp. 1001–1006.
3. Electrochemical Modeling of Lithium-Ion Positive Electrodes during Hybrid Pulse Power Characterization Tests. **D. Dees, E. Gunen, D. Abraham, A. Jansen, J. Prakash.** 8, 2008, Vol. 155, pp. A603-A613.
4. *Modeling the Impedance Versus Voltage Characteristics of LiNi0.8Co0.15Al0.05O2.* **D.P. Abraham, S. Kawauchi, and D.W. Dees.** 2008, Electrochim. Acta, Vol. 53, pp. 2121-2129.
5. Analysis of the Galvanostatic Intermittent Titration Technique (GITT) as Applied to a Lithium-Ion Porous Electrode. **D.W. Dees, S. Kawauchi, D.P. Abraham, J. Prakash.** 2009, J. Power Sources, Vol. 189, pp. 263–268.
6. *A Volume Averaged Approach to the Numerical Modeling of Phase-Transition Intercalation Electrodes Presented for LixC6.* **K.G. Gallagher, D.W. Dees, A.N. Jansen, D.P. Abraham, S.-H. Kang.** 12, 2012, J. Electrochem. Soc., Vol. 159, pp. A2029-A2037.
7. *Electrochemical Modeling the Impedance of a Lithium-Ion Positive Electrode Single Particle.* **D.W. Dees, K.G. Gallagher, D.P. Abraham, A.N. Jansen.** 3, 2013, J. Electrochem. Soc., Vol. 160, pp. A478-A486.
8. *Electrochemical Modeling and Performance of a Lithium and Manganese-Rich Layered Transition-Metal Oxide Positive Electrode.* **D.W. Dees, D.P. Abraham, W. Lu, K.G. Gallagher, M. Bettge, A.N. Jansen.** 4, 2015, J. Electrochem. Soc., Vol. 162, pp. A559-A572.

9. Examining the Electrochemical Impedance at Low States of Charge in Lithium- and Manganese-Rich Layered Transition-Metal Oxide Electrodes. **S.R. Gowda, D.W. Dees, A.N. Jansen, K.G. Gallagher.** 7, 2015, J. Electrochem. Soc., Vol. 162, pp. A1374-A1381.

### FY 2015 Publications/Presentations

1. "Enabling High-Energy/Voltage Lithium-Ion Cells for Transportation Applications: Electrochemistry", ES254_Burrell_2015_p, US DOE Vehicle Technologies Annual Merit Review, 2015.

# IV.D Next-Generation Li-ion Chemistries: "Improvements in Cell Chemistry, Composition, and Processing"

# IV.D.1. New High Energy Electrochemical Couple for Automotive Applications (ANL)

## Objectives

- The main objective of the project is to develop a new redox couple that meets and exceeds the DOE-targeted energy density of 200 Wh/kg and exhibits outstanding cycle and calendar life, low cost, and excellent abuse tolerance.

## Technical Barriers

- The primary technical barrier is the development of a safe and cost-effective battery with 40 mile range for a plug-in hybrid electric vehicle that meets or exceeds all DOE performance goals.

## Technical Targets

The technical target of this project is to develop a redox couple that provides specific energy in excess of 200 Wh/kg with cycle life of at least 500 cycles. This couple is to be based on (1) a high-voltage (~4.4 V) and high-capacity cathode composed of lithium manganese, cobalt, and nickel metal oxide (~230 mAh/g) with full concentration gradient across each particle (FCG) to stabilize the material at high voltage, and (2) a high-capacity and high-density composite anode composed of SiO-$Sn_xCo_yFe_{1-y}C_z$ with conductive binder to enhance cycle life. These active materials will be assembled in a high-energy prismatic cell (0.4 Ah) for independent testing and validation.

### Project Details

**Khalil Amine (PI)**
Argonne National Laboratory
9700 South Cass Avenue
Argonne, IL 60439-4837
Phone: 630-252-3838; Fax: 630-972-4451
E-mail: amine@anl.gov

Collaborators:
Huiming Wu, Argonne National Laboratory
Zonghai Chen, Argonne National Laboratory
Ali Abouimrane, Argonne National Laboratory
Jun Lu, Argonne National Laboratory
Yangie Cui, Argonne National Laboratory
Xiao Qing Yang, Brookhaven National Laboratory
Liu Gao, Lawrence Berkeley National Laboratory

Start Date: October, 2013
Projected End Date: September, 2015 (last report)

## Accomplishments

- Optimize the process of making FCG material and demonstrate capacity as high as 210 mAh/g with 2.7 g/cc tap density.
- Confirm thermal stability and safety of FCG material using soft and hard X-ray analysis in collaboration with BNL.
- Scale up FCG cathode to 1-kg level for electrode making using the Cell Analysis, Modeling, and Prototyping (CAMP) facility at ANL.
- Demonstrate that capacity, cycle life, and safety of the FCG (6:2:2) cathode outperform those of the NMC (6:2:2) baseline cathode.
- Improve the efficiency of the SiO-$Sn_{30}Co_{30}C_{40}$ anode to 81% by developing SiO-$Sn_{30}Co_{30}C_{40}$–MAG graphite composite and scale up the new composite to 1-kg level.
- Develop a suitable binder that works well with the new composite anode for Gen 1 cell fabrication.
- Continue to improve the performance of the conductive binder in collaboration with LBNL.

### Introduction

Lithium-ion batteries exhibit the highest power and energy density of any existing commercial battery system and offer many advantages for applications in the transportation sector. Among existing cathode chemistries

used in lithium batteries, $LiMn_2O_4$ spinel (LMO) and $LiFePO_4$ olivine (LFP) show considerable promise for high-power applications such as hybrid electric vehicles (HEVs), where power is more important than energy. However, these cathodes offer very limited capacity and thus are not suitable for plug-in hybrid vehicles (PHEVs) and all-electric vehicles (EVs). The layered oxide materials such as $LiNi_{0.8}Co_{0.1}Mn_{0.1}O_2$ or $LiNi_{0.8}Co_{0.15}Al_{0.05}O_2$ (NCA) and $Li_{1.1}[Ni_{1/3}Mn_{1/3}Co_{1/3}]_{0.9}O_2$ (NMC) offer higher capacity than LMO and LFP, but the capacity is not high enough to meet the PHEV (with 40-mile electric range) and full EV demands within a required volume and weight that does not compromise the trunk volume and vehicle performance. Therefore, cathodes possessing very high capacity (over 200 mAh/g), good cycle and calendar life, and outstanding safety are urgently needed for use in EVs and PHEVs-40, which require thousands of charge-depleting cycles and 15 years of calendar life.

Among the cathode materials that have the potential of providing either very high capacity or high voltage are the layered lithium mixed metal oxides such as Argonne's layered composite oxide $xLi_2MnO_3\bullet(1\text{-}x)LiMO_2$ (M=Ni, Co), and $LiNi_{1-x}Mn_yCo_zO_2$ for high energy, and $LiNi_{0.5}Mn_{1.5}O_4$ (4.8 V), $LiCo_{0.5}Mn_{1.5}O_4$ (5.1 V), $LiMnPO_4$ (4.1 V), and $LiCoPO_4$ (5.1 V) for high voltage.

The practical capacity of layered lithium mixed metal oxides, such as $LiNi_{0.8}Co_{0.1}Mn_{0.1}O_2$, NCA, and NMC, is only 50% of theoretical (275 mAh/g) under the operating potential window of 4.2 V~3 V. Operating at voltages higher than 4.3 V can lead to a significant increase in the specific capacity up to 220 mAh/g. However, at high potential, the cycle life of this material is very poor. This fast capacity decay with cycling is caused by the high interfacial reactivity of the fully charged electrode with the electrolyte, which leads to film growth at the surface of the cathode and an increase in the cell interfacial impedance with cycling. The high reactivity with the electrolyte is caused by the high concentration of unstable tetravalent Ni during high voltage charge, which reduces to stable divalent Ni and leads to $O_2$ release from the particle surface, oxidation of the electrolyte, and formation of a polymeric film at the surface of the cathode. Similar characteristics, mainly a capacity increase at high voltage accompanied by capacity fade during cycling, were also observed for NCA and NMC.

## Approach

Argonne National Laboratory (ANL) is working closely with the Brookhaven National Laboratory (BNL) and the Lawrence Berkeley National Laboratory (LBNL) to develop an advanced electrochemical couple. The cathode is a high-voltage, high-capacity, and dense material with FCG across each particle, and the anode is a high-capacity and high-density $SiO\text{-}Sn_xCo_yFe_{1-y}C_z$ composite that offers capacities higher than 600 mAh/g. This system will be investigated in cell tests using two electrolytes: a conventional electrolyte with additives that stabilize the interface of both the cathode and anode and a fluorinated electrolyte that will be supplied by industrial partners.

In the first year, a cathode of $LiNi_{0.6}Mn_{0.2}Co_{0.2}O_2$ with constant composition coupled with an anode of $SiO\text{-}Sn_xCo_yFe_{1-y}C_z$ composite was used as the baseline chemistry. The performance of the baseline chemistry was then compared to that of an FCG cathode with the same average composition, $LiNi_{0.6}Mn_{0.2}Co_{0.2}O_2$. The optimum chemistry based on an FCG cathode and carbon/$SiO\text{-}Sn_xCo_yFe_{1-y}C_z$ anode will be built and delivered to an independent laboratory for testing and validation.

## Results

### Optimization of full gradient

The second year of the project was focused on optimizing the synthesis conditions needed to obtain the FCG cathode material with high capacity, good cycle life at high voltage, high tap density that leads to high active material loading at the electrode level, and spherical morphology with sharp particle distribution. The focus was on an average composition $LiNi_{0.6}Mn_{0.2}Co_{0.2}O_2$ cathode (6:2:2) but with gradient concentration across the particle, as shown in Figure IV- 120. After a significant effort in optimizing the co-precipitation condition (including the speed of the precursor feed to the reactor, the stirring angle and condition, the pH of the solution, the chelating agent nature, and the co-precipitation agent concentration), we focused our attention on the calcination temperature, as it can impact the gradient concentration across the particle. Very high calcination temperature can lead to significant displacement of the metals within the particle, affecting the concentration gradient of Ni, Co, and Mn across the particle.

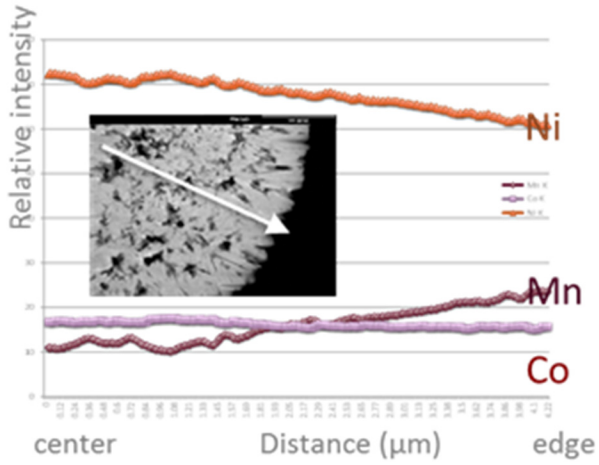


**Figure IV- 120: Electron probe micro-analysis showing a gradient composition across the particle of FCG $LiNi_{0.6}Mn_{0.2}Co_{0.2}O_2$**

(193 mAh/g) than the baseline cathode (174 mAh/g) when charged to 4.3 V at C/5. The cell based on FCG shows better cycle life at 4.3 V and C/3 rate compared to the baseline chemistry, in which the cathode has constant composition across the particle (Figure IV- 122b). This finding is due to the fact that the FCG (6:2:2) gradient has a lower concentration of charged $Ni^{4+}$, which is highly oxidizing at the outer layer of the particle. As a result, the reactivity of the electrolyte is reduced significantly at high voltage. The FCG material also shows better cycling performance at 55ºC, as shown in Figure IV- 123.

Figure IV- 121 shows the first charge and discharge capacity of different cells made with FCG (6:2:2) cathode calcined at different temperatures and the effect of the calcination condition on the rate capability. In this case, the material was pre-calcined at 500ºC at different times and further calcined at elevated temperatures (between 700ºC and 850ºC).

Figure IV- 122 shows the initial charge and discharge curve of the FCG (6:2:2) cathode and the baseline cathode. Both materials have similar average composition, $LiNi_{0.6}Mn_{0.2}Co_{0.2}O_2$. The electrolyte is 1.2 M $LiPF_6$ in ethylene carbonate/ethyl methyl carbonate (EC:EMC ratio = 3:7). The cells were charged to 4.3 V at the C/3 rate.

The FCG (6:2:2) cathode shows a higher capacity

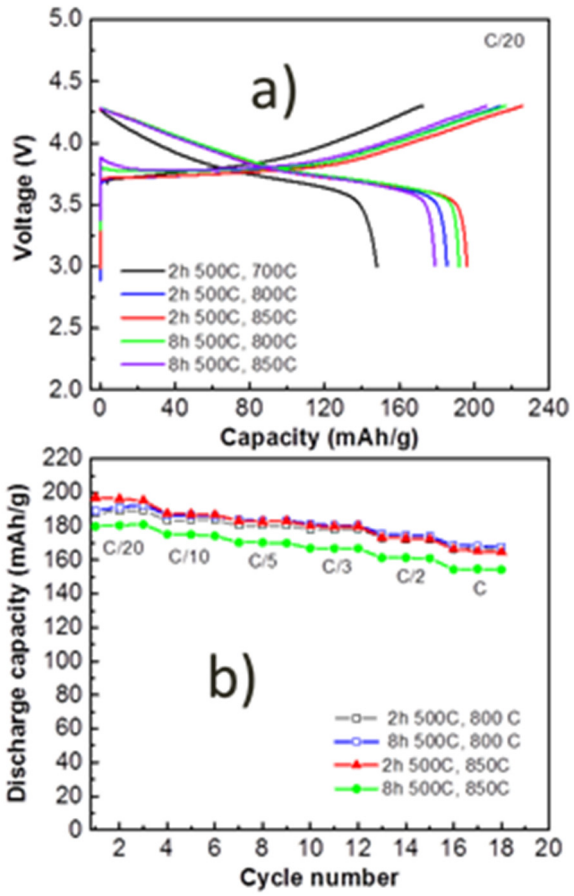


**Figure IV- 121: (a) Initial charge and discharge capacities with different calcination temperature and (b) capacity vs. rate at different calcination temperatures of FCG $LiNi_{0.6}Mn_{0.2}Co_{0.2}O_2$ cathode**

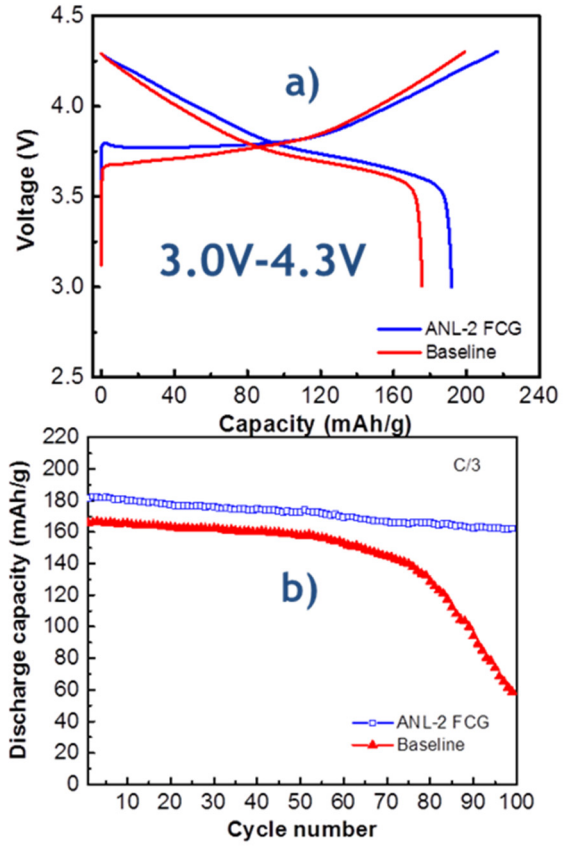


Figure IV- 122: (a) Initial charge and discharge capacities of FCG (6:2:2) cathode and baseline cathode and (b) capacity vs. cycle number of FCG and baseline cathode

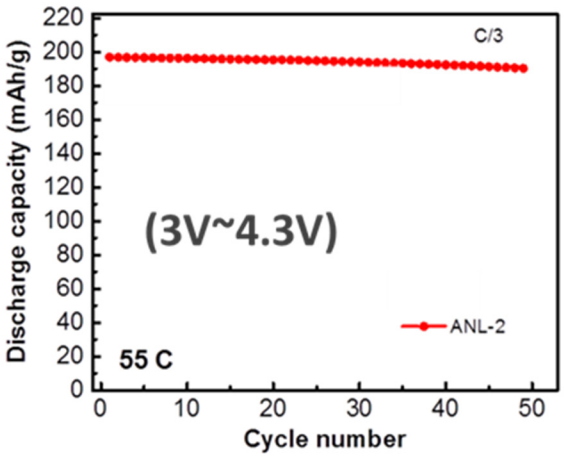


Figure IV- 123: Cycling performance of FCG cathode at 55°C

The structural stability of charged NMC (6:2:2) and FCG (6:2:2) materials was investigated using *in situ* time-resolved X-ray diffraction (TR-XRD) combined with mass spectroscopy (MS). Figure IV- 124 presents the TR-XRD patterns at the selected 2θ angle range and the corresponding profiles for the oxygen ($O_2$, m/z=32) gas release. During the course of the heating, the charged NMC (6:2:2) and FCG (6:2:2) materials show a similar route of structural changes from the initial layered structure to disordered spinel, followed by the final rock-salt structure. The coalescence of the $(108)_R$ and $(110)_R$ peaks and disappearance of $(003)_R$ peak in the layered structure indicate the onset of the formation of the disordered spinel phase. The evolution of the (220)s diffraction peak, which is prohibited by the rhombohedral symmetry, also confirms the formation of the disordered spinel phase. The main difference between the charged NMC (6:2:2) and FCG (6:2:2) material is the onset temperature of phase transitions from layered structure to disordered spinel structure. For the NMC (6:2:2), this onset temperature is as low as 150°C, and the phase transition is completed within the narrow temperature range of around 25°C (ca. 150 ~ 175°C), accompanying a sharp peak of oxygen release. In contrast, in the case of the charged FCG (6:2:2), this phase transition was pushed to higher temperature, at around 190°C, and completed over the wider temperature range of 40°C (ca. 190 ~ 230°C). The corresponding oxygen release for the FCG material also showed broader and milder features at higher temperature when compared with the NMC case. The onset temperature of the second phase transition from disordered to rock-salt structure for the FCG (6:2:2) material was also higher than that of the NMC (6:2:2) material. This clearly demonstrates that FCG could effectively suppress the oxygen release, push the onset of phase transition to higher temperatures, and spread the decomposition reaction to a wider temperature range, leading to the improved thermal stability.

### Anode Material Development

Silicon monoxide can provide a high capacity but suffers from poor cycle life. Also, Sn-Co-C has good cyclability and a high tap density, but its reversible capacity is not significantly better than that of commercial carbon anode. Our work will focus on a new anode material, based on the 50 wt.% SiO-50 wt.% $Sn_{30}Co_{30}C_{40}$ composite (molecular composition: $SiSn_{0.23}Co_{0.23}C_{0.3}O$), which is synthesized by a custom-made ultra-high energy ball milling (UHEM) method. The SiO-$Sn_xCo_yC_z$ composite has the potential to combine the advantageous properties of both SnCoC (long cycle life) and SiO (high capacity) and, thereby, improve the overall electrochemical performance.

Mechanical ball milling, which is known to produce nano-sized particles, is often used for improving electrochemical properties. The ball milling method is employed not only to reduce the particle size, but also to synthesize non-equilibrium alloys starting from blended elemental or pre-alloyed powders. Traditional ball mills employ stirred mills or vibration mills. However, these mills exhibit a limitation regarding product fineness: a size limit of 1 µm is often observed after several hours of grinding. This limitation is due to the particles being weakly confined in the breakage zone of these mills. Our custom-made milling machine works by a planetary mill method that creates a very high centrifugal field, confining the particles in the milling area and reducing the "dead zone" effect.

In the first year of this project, our focus was on scaling up the anode material to 1-kg level and using 90% of it as active material in the electrode. However, the irreversible loss during the initial cycling was extremely high (charge, 1600 mAh/g, and discharge, 900 mAh/g). As a result the energy density of the cell based on FCG and SiO-$Sn_xCo_yC_z$ composite becomes low since a large amount of lithium from the cathode was used to compensate for the large irreversible loss of the anode.

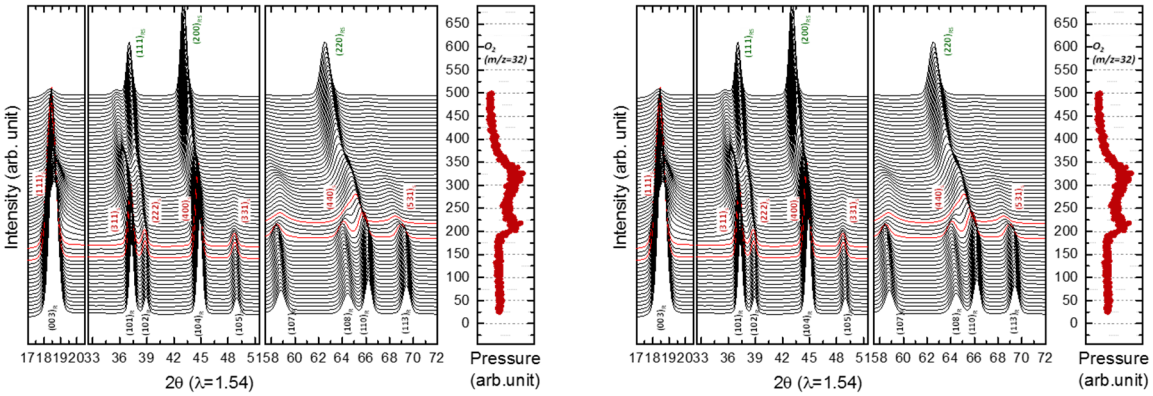


Figure IV- 124: TR-XRD/MS of FCG (6:2:2) and NMC (6:2:2) baseline

Soft X-ray absorption spectroscopy (XAS) enabled us to characterize elementally the surface and bulk properties of materials by detecting the partial electron yield (PEY) and fluorescence yield (FY) simultaneously. Normalized Ni L-edge spectra of NMC (6:2:2) and FCG (6:2:2) materials at different temperatures using the FY and PEY modes are shown in Figure IV- 125 and Figure IV- 126, respectively. Due to spin-orbit interaction of the core hole, the absorption spectra are split into two well-separated energy bands of the $L_3$ and $L_2$ edges. Changes in the energy position of the $L_3$ and $L_2$ edges indicate valence state changes during the heating process, since the energy position shifts about 1 eV per oxidation state change. The edge energy shift to lower energy indicates the reduction of Ni. In Figure IV- 125, at the charged state, both NMC (6:2:2) and FCG (6:2:2) have almost the same valence state of Ni as appeared at the Ni L-edge spectra measured at 25°C. The energy position of the Ni $L_3$ and $L_2$ spectrum for NMC (6:2:2) moves to lower energy levels at low temperature (150°C). In contrast, FCG (6:2:2) is more stable, and Ni is stable up to 250°C and gradually reduced, and the reaction is completed at 350°C. These results indicate that the FCG (6:2:2) is thermally more stable than normal NMC (6:2:2) at the highly charged state. The structural change at the near surface (PEY data in Figure IV- 126) also shows the same trend as the bulk structure, and the Ni reduction temperature coincides with the temperature of the phase transition and $O_2$ release in the TR-XRD/MS data, as shown in Figure IV- 124.

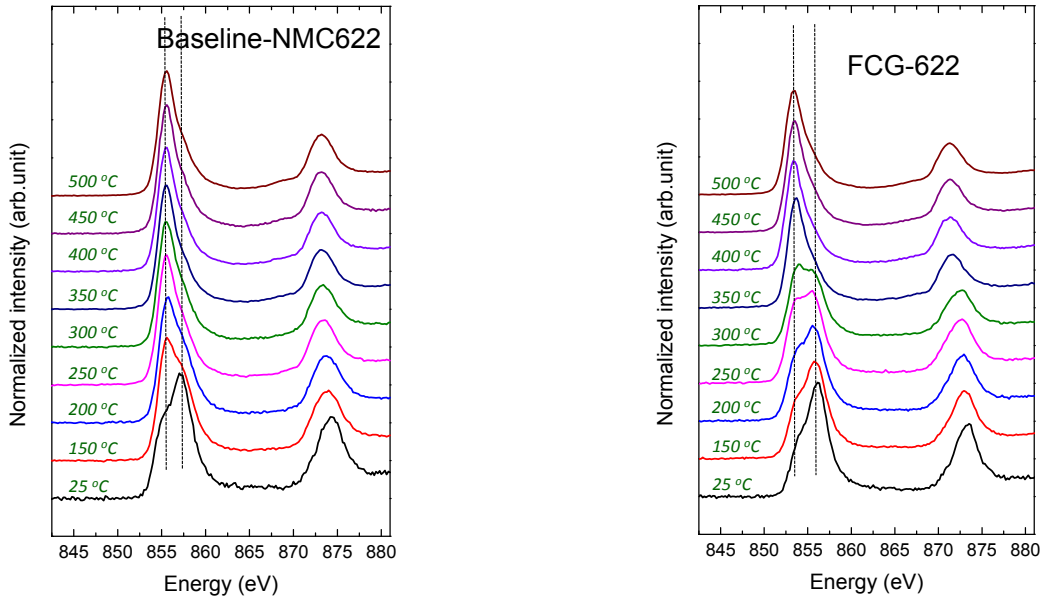


**Figure IV- 125: Ni L-edge soft XAS for baseline NMC (6:2:2) (left) and FCG (6:2:2) (right) using fluorescence detection (FY mode, bulk probing)**

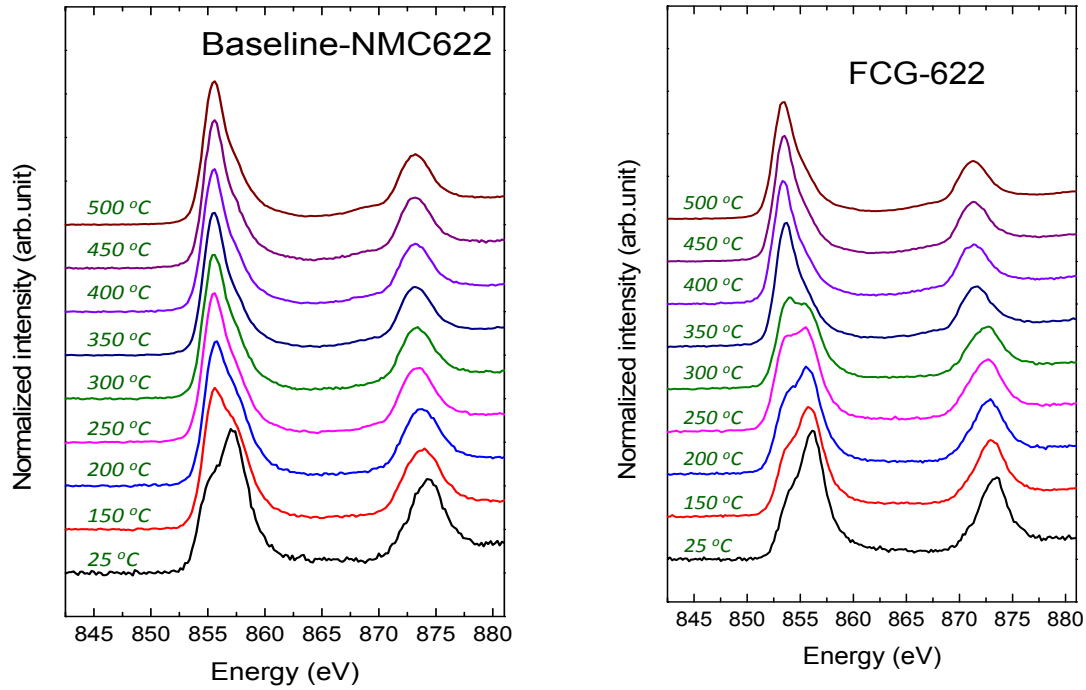


**Figure IV- 126: Ni L-edge soft XAS for baseline NMC (6:2:2) (left) and FCG (6:2:2) (right) using partial electron yield detection (PEY mode, surface probing)**

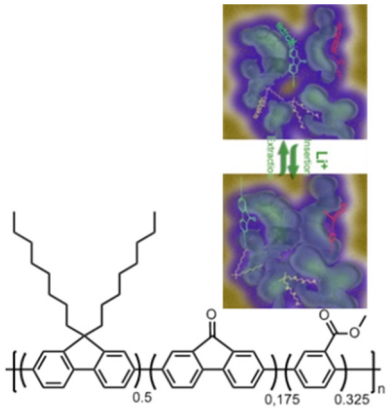


Figure IV- 127: Structure of conductive binder developed by LBNL

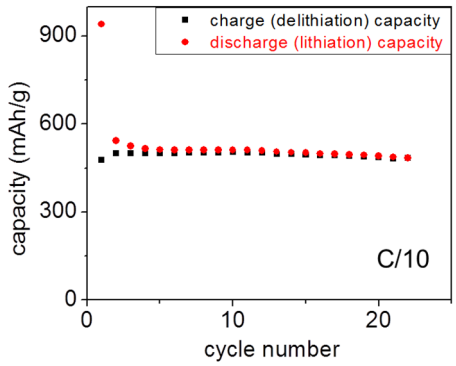


Figure IV- 128: Cycling performance of cell based on 5%PFM binder, 15% C-65 carbon additive, 60% SiO-$Sn_xCo_yC_z$, and 20% MAG anode using conductive binder (PFM)

In this fiscal year, the focus was on optimizing a blend of SiO-$Sn_xCo_yC_z$ composite with graphite to reduce the irreversible loss. In this case, both the graphite and SiO-$Sn_xCo_yC_z$ composite are active. Adding a large amount of graphite will provide the amble conductive network needed to prevent the SiO-$Sn_xCo_yC_z$ composite from particle isolation during the cycling process. The other focus was on selecting a binder that works well with this new anode. As proposed initially, we focused our effort on a conductive binder from LBNL (see Figure IV- 127). After extensive optimization by LBNL, the best performance was obtained using 5% PFM binder, 15% C-65 carbon additive, 60% SiO-$Sn_xCo_yC_z$, and 20% MAG graphite. The cell based on this configuration shows 500 mAh/g capacity and relatively good cycle life at the C/10 rate (Figure IV- 128). Unfortunately, the efficiency of the material is only 51%.

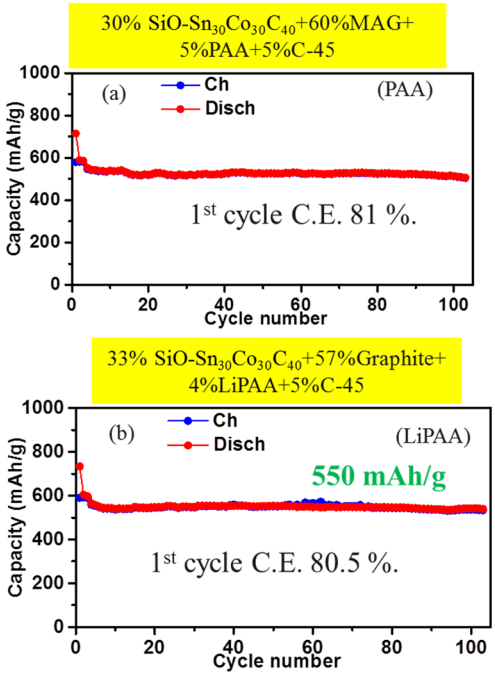


Figure IV- 129: Cycling performance of cells based on SiO-$Sn_xCo_yC_z$ and MAG anode using (a) 5% PAA binder and (b) 4% LiPAA binder

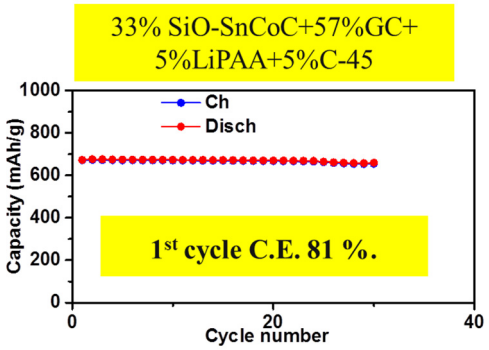


Figure IV- 130: Cycling performance of a cell based on SiO-$Sn_xCo_yC_z$ and MAG anode using 5% LiPAA binder

Since the cell performance using conductive binder in the anode was not satisfactory, we extensively investigated numerous other binders, such us polyimide binder (PI), polyacrylic binder (PAA), polyvinylidene fluoride (PVDF) binder mixed with PI, PVDF mixed with PAA, and lithiated polyacrylic binder (LiPAA). The cells with PAA and LiPAA show very good performance (Figure IV- 129): a capacity of 550 mAh/g and an efficiency of 81%, which are much better than those obtained with PVDF, PI, and the LBNL conductive binder that was originally selected. The best cell performance was obtained with 5% LiPAA: a capacity of 670 mAh/g and 81% efficiency. The cell with LiPAA binder showed no capacity loss after numerous cycles (Figure IV- 129 and Figure IV- 130).

The optimum composition of the composite anode was provided to the CAMP facility for making cells based on the FCG (6:2:2) cathode and SiO-$Sn_xCo_yC_z$/MAG graphite composite anode with LiPAA binder. However,

because the active material loading of the anodes made at the CAMP facility shows a different distribution within the same electrode, the decision was made to build a cell based on the FCG cathode and graphite anode as an intermediate cell build until the issue of electrode coating at the CAMP facility is addressed. These intermediate cells were built at the CAMP facility and were shipped to Idaho National Laboratory for testing. Table IV- 15 compares the expected usable energy density in Wh/kg and Wh/L, as well as the power density at minimum state of charge (SOC) in W/kg during a 10-s power pulse of cells based on the baseline cathode and FCG (6:2:2) cathode. These data were calculated from the BatPAC model based on two cell sizes: 20 Ah and 40 Ah. The predicted usable gravimetric energy densities of the FCG (6:2:2) based cell are 229 Wh/kg and 280 Wh/kg for the 20 Ah and 40 Ah cell, respectively. The volumetric energy densities are 541 Wh/L and 659 Wh/L for the 20 Ah and 40 Ah cells, respectively. Finally, the calculated power densities for the 20 Ah and 40 Ah cells are 1837 W/kg and 1120 W/kg, respectively. These BatPAC model results indicate that the FCG alone with the new high energy anode meets and exceeds the DOE energy performance requirements. These performance data are all higher those of the baseline cells.

**Table IV- 15: Battery performance based on baseline chemistry determined by BatPAC model**

| Deliverable | Device | Battery Performance (Cell Level) | | | |
|---|---|---|---|---|---|
| | | Usable Specific Energy (Wh/kg) | Energy Usable Density (Wh) | Power at SOCmin (W/kg, 10 sec) | Technology Info |
| Baseline | 20Ah Cell<br>40Ah Cell<br>BatPac Design | (~199)<br>(~237) | (~453)<br>(~548) | (~1591)<br>(~950) | SiO-SnCoC and NMC (6:2.2) |
| Gen1 | 20Ah Cell<br>40Ah Cell<br>BatPac Design | (~229)<br>(~280) | (~541)<br>(~659) | (~1837)<br>(~1120) | SiO-SnCoC MAG and FCG (6:2.2) |

### FY 2015 Publications/Presentations

1. Liu, B.; Abouimrane, A.; Balasubramanian, M.; Ren, Y.; Amine, K., Journal of Physical Chemistry C 2014, 118, 3960.

# IV.D.2 High Energy Novel Cathode / Alloy Automotive Cell (3M)

## Objectives

The program objectives are:

- Develop a >2 Ampere Hour (Ah) Cylindrical wound or stacked pouch cell with high energy density at low cost for automotive application.
- Integrate advanced chemistries including an advanced high-voltage cathode, high capacity alloy anode and advanced electrolyte materials as well as enabling technologies related to electrode preparation and cell build such as binder, condutive agent, and processing aids.

### Project Details

**John Tabacchi (NETL Program Manager)**
DE-EE0005449 Recipient: 3M Company

**Jagat Deep Singh (Program Manager)**
3M Center, Building 209-2C-26
St Paul, MN 55144
Phone: 651-575-1230; Fax: 651-736-7478
E-mail: jdsingh@mmm.com

Start Date: October 2011

Projected End Date: March 2015

## Technical Barriers

This project addresses the following technical barriers associated with the combination of high energy cathode and advanced alloy anode material:

- Low Cycle Life
- Low Rate Capability
- High irreversible capacity leading to low overall cell energy density
- Large volume expansion of alloy anode

## Technical Targets

The Technical targets for the projects are:

- Establish a baseline cell with similar energy density to USABC EV targets with commercial $LiMn_{1/3}Ni_{1/3}Co_{1/3}O_2$ (NMC 111) cathode and graphite anode.
- Provide an advanced cell with at least 40% (1.4 x base/L) increase in energy density compared to the baseline cell.
- Demonstrate as good or superior thermal stability, long-term cycling, and rate capability, of the advanced cell compared to baseline test cell.
- Demonstrate by calculation at least 25% lower cost per unit energy at the cell level for comparative integrated advanced materials cell to a baseline materials cell.

## Accomplishments

The key accomplishments in this project are:

- Down-selected high energy core shell cathode and Si alloy anode materials for 18650 performance optimization.
- Demonstrated material scale up to 100+ kg levels.
- Further optimized pilot process parameters to improve process robustness. Identified parameters to control process variability.
- Demonstrated >40% energy increase, with intermediate design (C/S||Si) in 18650 cells over baseline (NMC || Graphite).
- Sampled 18650 format cells to ANL for testing; 18 cells with baseline materials and 6 cells with intermediate materials.
- Post mortemed cycled 18650 to identify root cause for rapid capacity fade.
- Improved cycle life in 60% energy window.
- Identified voltage windows (60% energy) for better performance.
- Reduced 18650 formation time to a commercially viable time.

- Sampled the final deliverable cells, 18650 format cells with advanced chemistry, which showed the ~40% energy improvement compared to the baseline cells.
- Demonstrated~25% reduction in the cost per unit energy with the advanced chemistry compared to the baseline chemistry.

## Introduction

In order to design a lithium-ion cell with a step function increase in energy, it is necessary to start from scratch with new well-designed and matched active materials. First, the cathode needs to have a Cathode Energy Factor (CEF) beyond the traditional LCO and NMC materials. This invariably requires charging to higher cell voltage. Second, the cathode irreversible capacity has to "match" the irreversible capacity of the composite alloy anode. In fact, for cell balance and control of the lower cut of cell voltage, it is convenient if the irreversible capacity of the composite cathode is slightly larger than that of the anode. For the Active alloy, it is critical to have the proper morphology (amorphous active phase), the proper particle size (microns), and the proper activity leading to a volume expansion of 110 to 120% upon lithiation. Next, the composite electrode has to be formulated with graphite for highest density and best inter particle contact, while still providing the required volumetric energy when fully lithiated. Finally, the electrolyte and separator must be stable against the two active composite electrodes, across the complete cell voltage range, to eliminate any parasitic reactions.

## Approach

3M team has been leveraging its expertise in R&D of Lithium-ion Batteries to develop a high energy cell using synergistically matched anode and cathode electrodes. To achieve the goal, a three phase approach has been taken. The phases are -

- Phase 1 - Verify baseline materials performance, and select advanced cell material candidates for further evaluation and optimization.
- Phase II - Integration of individual optimized materials into full cells and optimization of EV test cell.
- Phase III - Final Optimization of integrated advanced materials in EV test cells, complete cell evaluation, fabrication of final cells and submission of final cells to National Labs.

## Results

The project was in Phase III with approximately 3.5 months (October 1$^{st}$, 2014 to January 16$^{th}$, 2015) remaining towards completion. Below is a summary of the work performed during this period.

### Anode Materials Development

The manufacturing of the alloy materials has been scaled up in the pilot plant for over a year. Optimizing and understanding the effect of process conditions have been the subject of ongoing efforts throughout this project. In 2014Q4 step changes were achieved in our understanding of the impact of process parameters and our ability to model the outcome of manufacturing run. As a consequence, the process is more robust and reliable and the alloy produced at the pilot scale is of greater quality and repeatability.

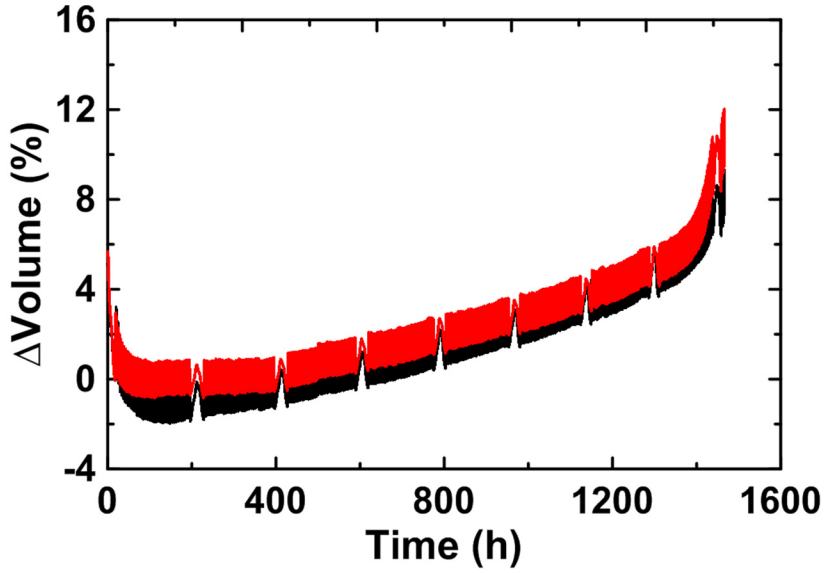


Figure IV- 131: In-situ volume change of CV7-containing pouch cells as a function of time. The slow cycle is can be seen every 50 cycles

In 2014Q3, machine made pouch cells containing 3M Si alloy (CV7) had been received. The negative electrodes in the cells contain 17% CV7 alloy. A more detailed description of these cells is found in the project quarterly reports. These cells were used in detailed *in situ* volume experiments, as volume change is one of the important characteristics and possible failure modes of cells containing any type of Si-based material. Volume measurements were performed by submerging the cells in silicone oil and measuring their weight during cycling. The volume change can then be calculated using the Archimedes principle as detailed in a previous report. Figure IV- 131 shows the *in situ* volume measured for a pouch cell cycling at C/2, with a C/20 cycle every 50 cycles. After approximately 400 cycles the cell goes through sudden failure and capacity loss. Interestingly, a massive increase in volume accompanies the sudden failure, which suggests the presence of gas generation. Also notable is the slow but steady increase in volume of the cells. Sudden failure in 18650s would also involve gassing though the failure mode would lead to triggering the pressure release present in the header of the can.

The *in situ* volume measurements were also used to study the impact the parameters for formation. Formation cycles are in part performed to wet and preform the SEI on the active materials. A designed experiment was performed to see the impact of the parameters listed in Table IV- 16.

**Table IV- 16: Parameters varied in the formation of pouch cells**

| Key | Temp (°C) | Current | Hold Length (h) | Voltage (V) |
|---|---|---|---|---|
| 1.1.1 | 70 | C/20 | 24 | 2 |
| 1.1.2 | 70 | C/20 | 24 | 1.5 |
| 1.1.3 | 70 | C/20 | 24 | 1 |
| 1.1.4 | 70 | C/20 | 24 | 0 |
| 1.1.5 | 70 | C/20 | 0 | n/a |
| 1.2.2 | 70 | C/10 | 24 | 1.5 |
| 1.2.3 | 70 | C/10 | 24 | 1 |
| 1.2.4 | 70 | C/10 | 24 | 0 |

Figure IV- 132 shows the results of the formation study. A voltage hold after assembly is clearly beneficial to overall gas formation. The differentiation between C/20 and C/10 is not strong, although C/10 appears somewhat better since it is faster, and similar results are obtained. Finally a voltage hold of near 1.0 V appears beneficial. These cells have been placed on cyclers for extended cycling. The cycling results and possible impact of formation on cycling will be reported in the next quarterly report.

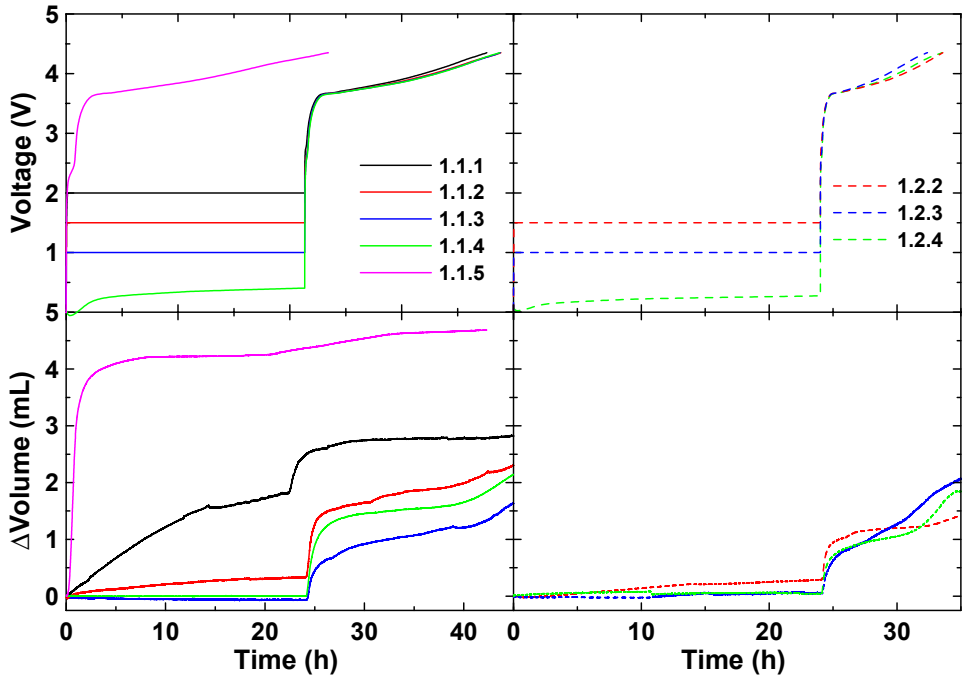


Figure IV- 132: Voltage and in-situ volume change during formation for cells listed in the adjacent table

The use of machine-made pouch cells enable this type of study as the 18650s hard cans and the variability obtained in our 18650s assembly would lead to a very low signal to noise ratio. In conclusion the work in 2014Q4 was focused on refining the manufacturing process, the study of volume changes in pouch cells during cycling and finally the exploration of formation parameters on gassing. These studies are performed with the end goal of improving the cycle-ability of alloy-containing Li-ion cells.

### Cathode Materials Development

The cathode team has looked into coating NMC based cathode particles for high voltages (>4.5V) applications. Promising results (Figure IV- 133) are seen but considering the remaining time in this project, the team plans to use core shell NMC based cathode (>4.5V) in the electrochemical couple.

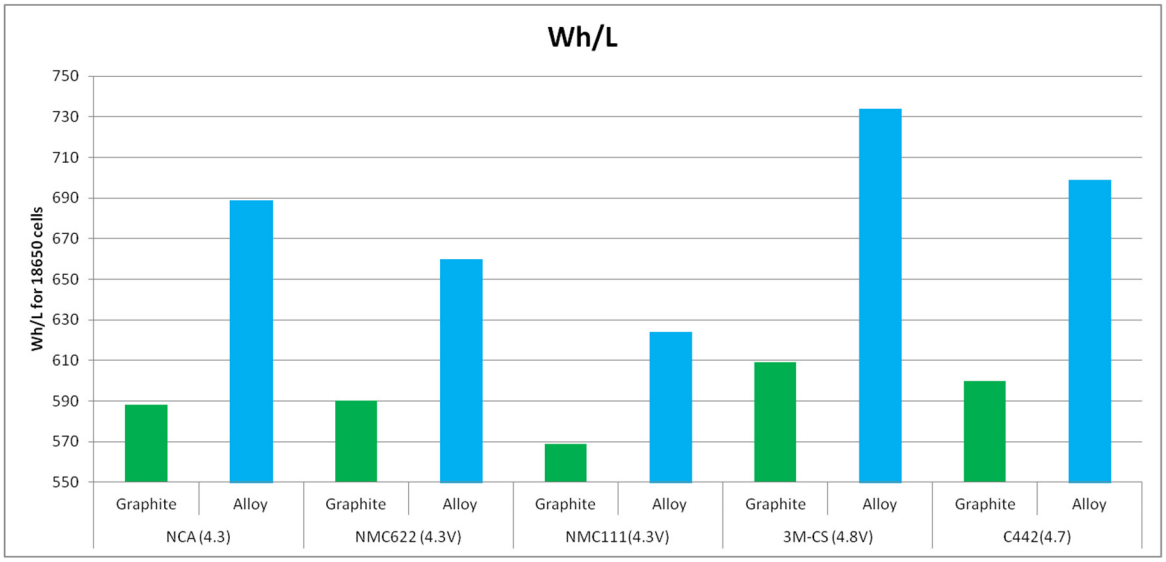


Figure IV- 133: BOL Wh/L with different coated NMC cathode

### Advanced Electrolyte Research

In Q4, the team focused on the preparation of electrolyte formulation to help enable the preparation of 18650 cell with advanced anode and cathode materials. These cells will be screened before shipment to ANL.

### Large Format (18650) Cell Evaluation

As the programs nears its end, the team focused on two key activities. The first activity focused on preparation of 18650 cells which would ultimately be shipped to Argonne National Laboratory. The second activity focused on down selecting the cycle life test protocol which shows the potential of the advanced chemistry and improvement over the intermediate cells. In the first activity number of anode and coating runs were made. Figure IV- 134 shows the cathode formulation. KS6 L was added to help enable the cathode to be calendared to a lower porosity. Kynar 761 PVDF was used. Table IV- 17 shows the Stage D of dispersion preparation process. In this stage the dispersion is diluted with solvent (NMP) to get to the desired viscosity.

Over 56 meters of this cathode coating were made. Figure IV- 136 shows the discharge capacity of the 18650 cells with the above mention cathode coating. Similar cells were started to assemble for the final deliverable to ANL.

**Coating Run 640C**

**Coating Request Information**

| | |
|---|---|
| Requestor | Singh |
| Request Date | 12/22/2014 |
| Ctg Type | Cathode |
| Project | DOE Anode |
| Type | Internal Data |
| Customer | |
| Format | 18650 |
| Foil | Al 15 micron |
| Reference # | Unique |

| | Description | Lot or NB Nbr | Ah/g | % Solids |
|---|---|---|---|---|
| Active Material 1 | C/S MHL | T2400 | | 95 |
| Active Material 2 | | | | |
| Binder | PVDF | | | 2.5 |
| Conductive | Super P | | | 1.25 |
| Misc | KS6L conduct dilutar | | | 1.25 |

| | | | |
|---|---|---|---|
| Est. Amt of Active (kg) | 5 | Design 1st Lithiation mAh/cm2 | 5.59 |
| Coating Patch Length (cm) | 75 | Total mg/cm2 (side 1) | 23.35 |
| | | Total mg/cm2 (side 2) | 23.35 |

Figure IV- 134: Advanced Cathode formulation for the roll to roll coating run

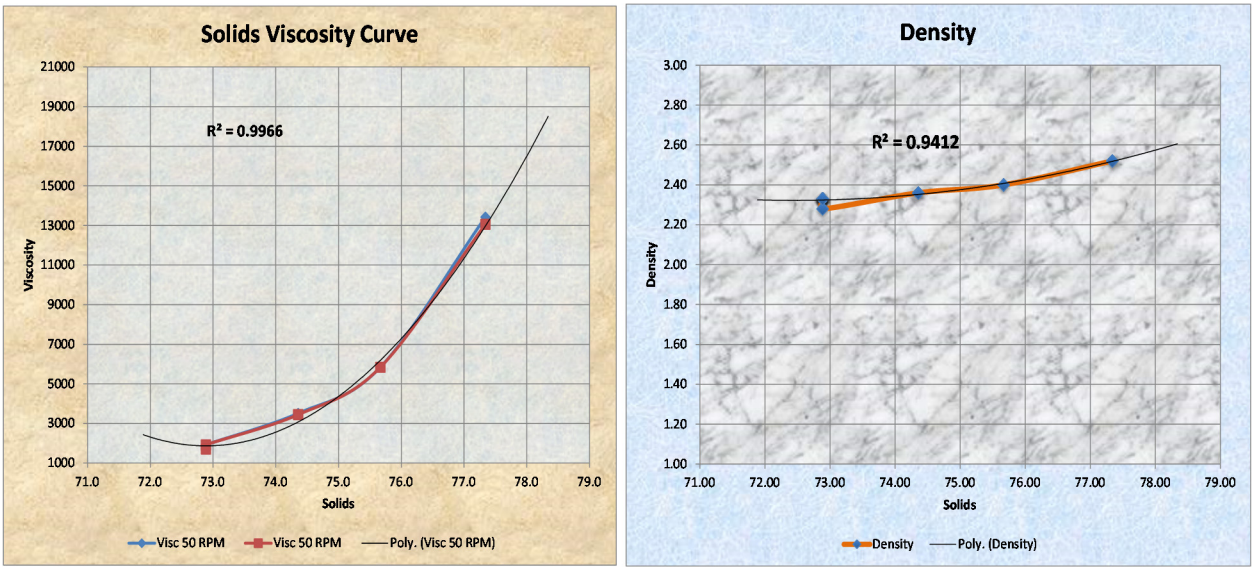


Figure IV- 135: Viscosity and density of the cathode dispersion within target specification

**Table IV- 17: Viscosity tuning of the prepared cathode dispersion**

| Viscosity (Stage D) | | | | | |
|---|---|---|---|---|---|
| **Time** | 10:15 AM | 10:30 AM | 11:00 AM | 11:15 AM | 12:10 AM |
| **Date** | 12/23/2014 | | | | |
| **Spindle#** | 5 | 5 | 5 | 5 | 5 |
| **Temperature °C** | 22.3 | 22.3 | 19.5 | 20.4 | 21.6 |
| **Total Extra Solvent (g)** | | 135 | 110 | 128 | 0 |
| **Calculated % Solids** | 77.34 | 75.67 | 74.36 | 72.89 | 72.89 |
| **Measured % Solids** | | | | | |
| **RPM** | **cps** | **cps** | **cps** | **cps** | **cps** |
| **5** | 25800 | 11200 | 6800 | 3520 | 3040 |
| **10** | 20300 | 8800 | 5320 | 2880 | 2440 |
| **20** | 16550 | 7200 | 4240 | 2340 | 2040 |
| **50** | 13420 | 5840 | 3512 | 1920 | 1712 |
| **100** | | 5360 | 3200 | 1740 | 1584 |
| **50** | 13060 | 5840 | 3448 | 1920 | 1704 |
| **20** | 15500 | 6950 | 4140 | 2320 | 1960 |
| **10** | 18500 | 8600 | 4960 | 2840 | 2360 |
| **5** | 23200 | 11200 | 6480 | 3840 | 2960 |
| **Comments** | | | | | After Vacuum |
| **Dispersion Analysis** | | | | | |
| **Hegman test (mil)** | | | | | |
| **% Solids** | 77.34 | 75.67 | 74.36 | 72.89 | 72.89 |
| **Wet Density (g/mL)** | 2.52 | 2.4 | 2.36 | 2.28 | 2.33 |

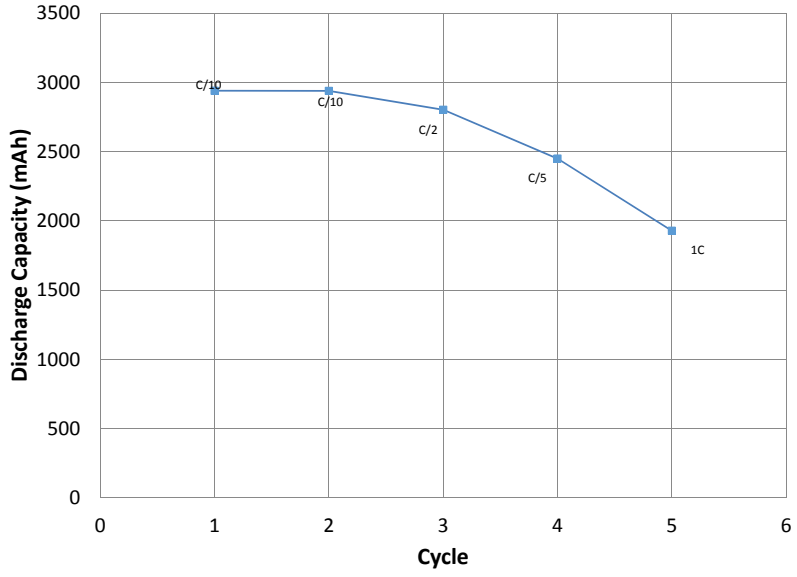


**Figure IV- 136: Rate test of the 18650 cell with advanced electrochemical couple**

In the 2nd activity, 18650 cells were tested for DST type testing. These cells did not demonstrate performance requirement. Since the cell was designed using high areal capacity (>4.0 mAh/cm2), it may have caused this fade. At this stage in the development of the advanced chemistry shallow cycling (60% energy window) seems to provide longer cycle life.

Table IV- 18 shows the performance of the 18650 cells which were shipped to ANL as the final deliverable cells.

**Table IV- 18: Capacity at different rate of 18650 cells shipped as final deliverable cells**

| Cell ID | Capacity | | | | |
|---|---|---|---|---|---|
| | C/10 rate | C/10 rate | C/5 rate | C/2 rate | 1C rate |
| 7907frt1a1 | 2941 | 2939 | 2803 | 2450 | 1929 |
| 7910frt1a1 | 2951 | 2933 | 2810 | 2527 | 2049 |
| 7911frt1a1 | 2922 | 2905 | 2769 | 2401 | 1969 |
| 7917frt1a1 | 2953 | 2934 | 2805 | 2454 | 1936 |
| 7918frt1a1 | 2997 | 2975 | 2838 | 2485 | 1960 |
| 7919frt1a1 | 2921 | 2927 | 2772 | 2254 | 1585 |
| 7920frt1a1 | 2927 | 2911 | 2776 | 2335 | 1744 |
| 7921frt1a1 | 2912 | 2913 | 2775 | 2279 | 1788 |
| 7922frt1a1 | 2939 | 2936 | 2839 | 2455 | 1896 |
| 7924frt1a1 | 2903 | 2906 | 2748 | 2247 | 1624 |
| 7927frt1a1 | 2985 | 2970 | 2831 | 2479 | 1945 |
| 7928frt1a1 | 2873 | 2899 | 2749 | 2231 | 1694 |
| 7929frt1a1 | 3000 | 2934 | 2835 | 2508 | 1780 |
| 7931frt1a1 | 2910 | 2901 | 2766 | 2404 | 1873 |
| 7937frt1a1 | 3038 | 2985 | 2860 | 2533 | 2052 |
| 7938frt1a1 | 2976 | 2964 | 2822 | 2309 | 1743 |
| 7940frt1a1 | 2969 | 2960 | 2825 | 2309 | 1742 |
| 7941frt1a1 | 2995 | 2969 | 2837 | 2305 | 1723 |
| 7950frt1a1 | 2976 | 2946 | 2809 | 2318 | 1759 |
| | | | | | |
| Average | 2943 | 2930 | 2796 | 2386 | 1860 |
| Standard Deviation | 48.8 | 34.3 | 37.3 | 94.3 | 154.3 |
| Max | 3038 | 2985 | 2860 | 2533 | 2188 |
| Min | 2817 | 2832 | 2709 | 2231 | 1585 |

## Conclusions and Future Directions

Final deliverable cells, i.e., 18650 cells, were shipped to the DOE designated facility which was Argonne National Laboraory (ANL). The cells are being tested at ANL. 3M will continue to be in contact with ANL for testing progress. 3M may also want to receive the cells after the testing is completed so that post mortem analysis can be performed to better understand the failure mechanism.

The learning from this project are extremely valuable and are being actively applied to the current DOE funded project (EE 0006448).

## FY 2015 Publications/Presentations

1. “Silicon Alloy Anode: Sudden Fade Challenge”, ES256_Singh_2015_p, US DOE Vehicle Technologies AMR, 2015.

# IV.D.3 High Energy Density Li-Ion Cells for EVs Based on Novel, High Voltage Cathode Material Systems (Farasis Energy, Inc.)

## Objectives

- Develop advanced electrode materials and cell components to enable stable high-voltage operation.
- Design and demonstrate a Li-ion cell using these materials that meets the PHEV40 performance targets.
- Design and demonstrate a Li-ion cell using these materials that meets the EV performance targets.

### Project Details

**Bruce Mixer (NETL Program Manager)**
DE-EE0006446 Recipient: Farasis Energy, Inc.

**Keith Kepler (Farasis Energy, Inc. – PI)**
21363 Cabot Blvd.
Hayward, CA 94545
Phone: 510-732-6600 x203
E-mail: kkepler@farasis.com

Subcontractors:
Argonne National Laboratory, Argonne, IL
Lawrence Berkeley National Laboratory, Berkeley, CA
OneD Materials, LLC, Palo Alto, CA

Partners:
DuPont

Start Date: October 2013

Projected End Date: December 2015

## Technical Barriers

- The major challenge to creating stable high energy cells with long cycle life is system integration. Although materials that can give high energy cells are known, stabilizing them towards long-term cycling in the presence of other novel cell components is a major challenge.

Barriers addressed:

- Low cathode specific energy.
- Electrolyte stability during high voltage operation.
- Capacity retention during deep discharge for Si-containing anodes.

## Technical Targets

- Develop a Ti-doped, high-voltage stabilized layered NCM cathode material with reversible capacities >230 mAh/g.
- Develop a layered-layered-spinel (LLS) composite cathode material capable of reversible capacities of >250 mAh/g at 1C rate.
- Develop an optimized composite positive electrode based on blending different positive electrode active materials.
- Develop a Si/C composite negative electrode with >1600 mAh/g reversible capacity.
- Develop electrolytes for these electrode systems that enable stable high-voltage cycling.
- Integrate materials into a PHEV40 cell designed to achieve 250 Wh/kg.
- Integrate materials into an EV cell designed to achieve > 400 Wh/kg.

## Accomplishments

- Improved capacity retention of NCM materials through both surface treatment and bulk-doping approaches.
- Realized stable reversible cycling of NCM positive electrode materials at greater than 210 mAh/g.
- Improved the rate capability of HE-NCM materials through novel synthesis approach, doubling the relative capacity at 1C over materials synthesized using standard methods.
- Manufactured cells that meet PHEV performance targets.
- Optimized electrolyte formulations to extend cycle life for high voltage, high energy systems.

## Introduction

Current Li-ion cell technology aimed at automotive applications provides an energy density of *ca.* 150 - 200 Wh/kg when used within a voltage range that has been defined to ensure sufficient cell life and safety. Increased energy density and power density are critical to lower costs and enable the widespread adoption of electric vehicles. In order to meet these goals, Farasis proposed a comprehensive effort to develop high voltage capable Li-ion technology designed around new positive electrode materials systems, with the potential to enable a PHEV40 cell with a >25% increase in energy density with a corresponding 2x increase in cycle life and a EV light duty cell with a 2x increase in energy density relative to comparable commercial Li-ion cells. The project builds on Farasis Energy's development and production expertise, leveraging our commercial, high performance Li-ion cell technology and incorporating advanced active materials.

The overall goal of this project is to develop and demonstrate a new class of high energy, high power Li-ion cells based on novel high voltage, high capacity active materials. In collaboration with our partners, multiple material classes are being developed simultaneously: On the positive electrode side, layered NCM materials are being developed and stabilized for high voltage operation using various coating technologies. Simultaneously, high capacity layered-layered-spinel composites are being explored using novel synthetic approaches based on ion-exchange reactions. High capacity negative electrode development is focused on silicon-carbon composites. Tying the cell together are electrolyte/separator systems optimized for high-voltage performance.

## Approach

The approach taken by Farasis to succeed in this project is to develop multiple materials in parallel, with periodic integration of materials in design of experiment studies to evaluate higher-order interactions between components. This approach relies on close collaboration with our partners, leveraging the strengths of each organization to accelerate development.

## Results

### Stabilization of NCM Materials

We have primarily focused on stabilizing NCM materials for high-voltage use through two approaches: surface treatments and bulk doping. Both approaches have proven successful, individually, at extending cycle life of NCM materials with upper cutoff voltages above 4.4 V (See Figure IV- 137). The general approach for bulk doping was developed by Dr. M. Doeff at Lawrence Berkeley Lab and a scaled-up synthesis was performed at Farasis. We are currently in the process of integrating these two stabilization technologies with the expectation that they will be complementary. The surface treatment approach is intended to minimize reactivity between the charged cathode and the electrolyte, while the bulk-doping strategy is thought to stabilize the crystalline structure against deleterious structural changes in the highly delithiated state.

### Improved conductivity of HE-NCM materials

Specific capacities in excess of 210 mAh/g are required to meet high-energy cell performance targets for EV applications. The most promising material class that can provide such high capacities are the lithium-excess manganese-rich HE-NCMs. While providing very high specific capacities, these materials are not suitable for implementation due to numerous problems including poor rate capability, large impedance increases, and a loss of material specific energy during cycling. We have made improvements in all of these areas through compositional and synthetic optimizations centering around an ion exchange step during material preparation. As illustrated in Figure IV- 138, the relative rate capability and overall cycling stability of HE-NCM materials have been significantly improved using this approach.

### High Capacity Anode Materials

High-capacity negative electrode active materials are being developed in conjunction with One D Materials. Their innovative approach is based on silicon nanowires grown directly on the surface of a graphite base stock to produce silicon/carbon composites with high reversible capacities. Extensive development around electrode formulation and use conditions has allowed implementation of negative electrode active materials with specific capacities of 600 – 900 mAh/g (depending on Si-content). This technology is currently being integrated in cells targeting EV performance goals.

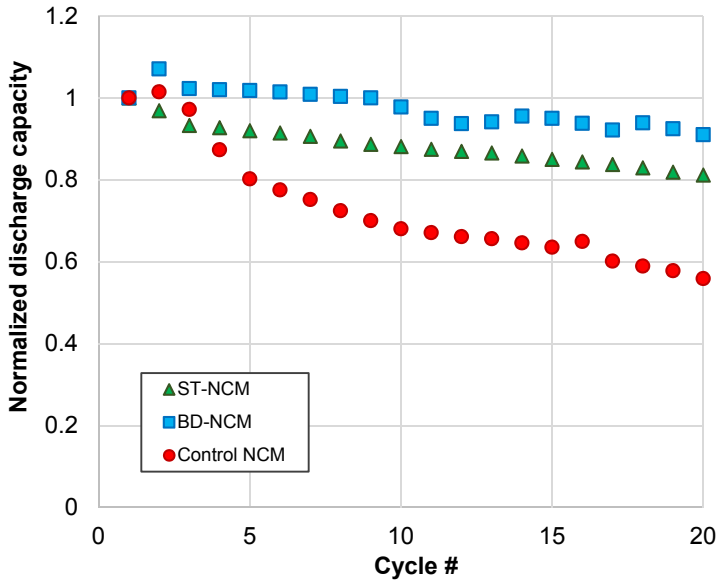


**Figure IV- 137: Comparison of NCM stabilization approaches. "ST" = Surface Treated NCM, "BD" = Bulk Doped NCM, "Control" = as-synthesized NCM. Cycling conditions: CCCV Charge: C/5 to 4.6 V, C/50 cutoff; Discharge: C/3 to 2.5 V; Li metal anode, $LiPF_6$ in EC/EMC electrolyte**

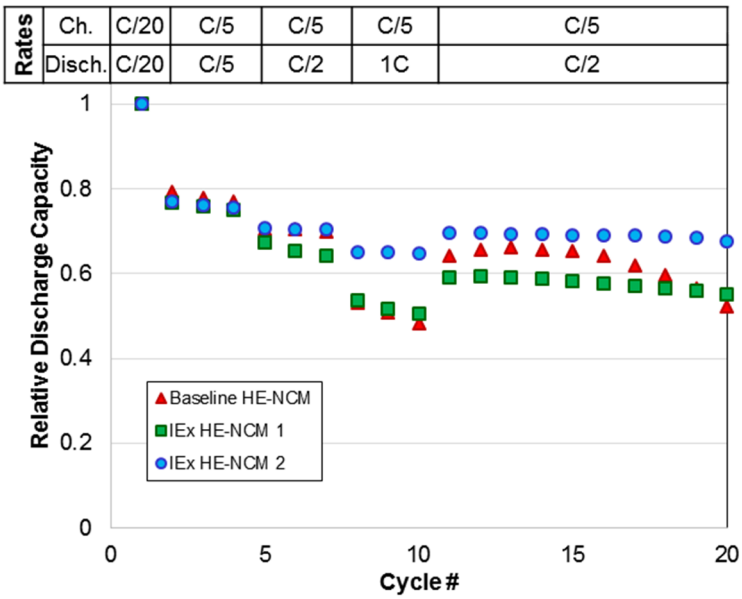


**Figure IV- 138: Comparison of rate capability of HE-NCM materials. Cycling conditions: Charge to 4.4 V at rate indicated in table; Discharge to 2 V at rate indicated in table; Li metal anode, $LiPF_6$ in EC/EMC electrolyte**

### High Voltage Electrolyte Development

Minimizing reactivity of electrolyte components with the strongly oxidizing positive electrode materials charged to high-voltage is the primary goal of electrolyte development in this project. Our approach is based around additive development and partial substitution of electrolyte components with fully or partially fluorinated compounds. By screening a large number of electrolytes in 18650 cells under accelerated testing conditions, we have identified formulations that dramatically extend cycle life (Figure IV- 139a).

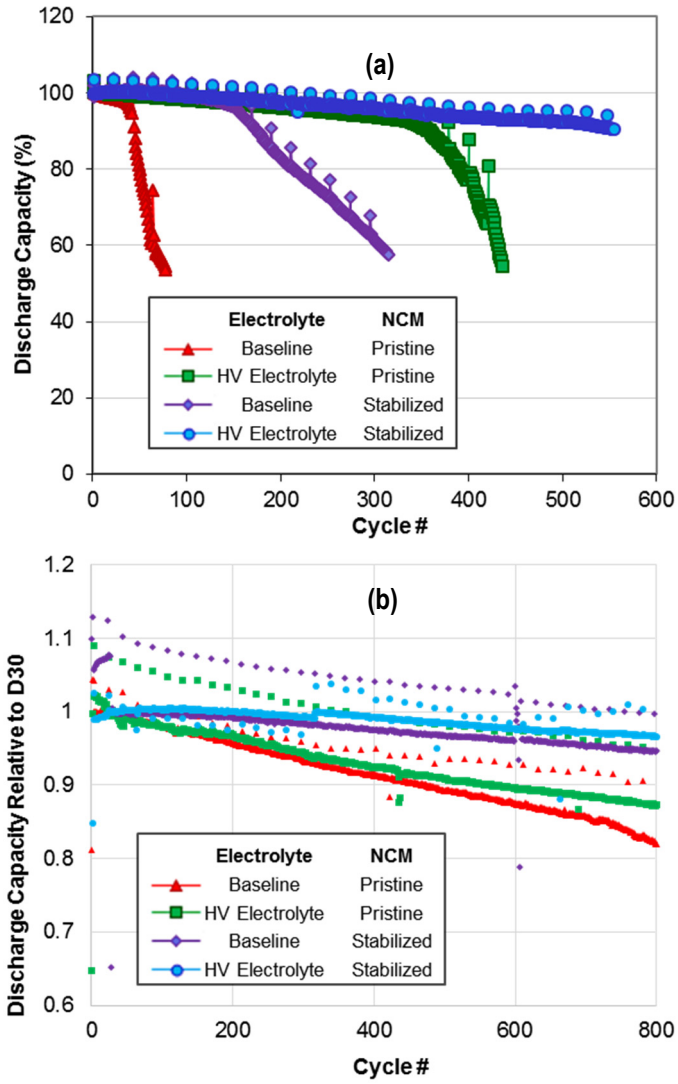


**Figure IV- 139: Stabilized NCM and HV stable electrolytes work together to improve cycle life. (a) Cycling conditions: CCCV Charge: C/2 to 4.4 V, C/20 cutoff; Discharge: C/2 to 3 V; C/20 cycle every 20 cycles; 2 Ah NCM//Graphite 18650 cells. (b) Cycling conditions: CC Charge: C/3 to 4.4 V; Discharge: C/3 to 3 V; C/20 cycle every 20 cycles; 1.4 Ah NCM//Graphite pouch cells**

## Conclusions and Future Directions

Farasis and its partners have succeeded in optimization and scale-up of cathode, anode, and electrolyte components for high-energy density Li-ion cells. These materials have been implemented in cell designs that meet PHEV40 performance goals. This success validates our approach to high energy cell development.

Final optimizations of cell designs that target EV performance goals and manufacture of prototype cells is currently underway.

## FY 2015 Publications/Presentations

1. "High Energy Density Li-Ion Cells for EV's Based on Novel, High Voltage Cathode Material Systems", ES213_Slater_2015_p, US DOE Vehicle Technologies AMR, 2015.

# IV.D.4 High Energy Lithium Batteries for PHEV Applications (Envia, LBNL, ORNL, GM)

## Objectives

- Understand the root-cause of cathodes' DC-R issues via spectroscopic, microscopic, and electrochemical analytical techniques.
- Mitigate HCMR™ cathodes' DC-R issues via four different surface coating strategies: (a) PE-CVD carbon coating (b) PVD of LiPON ionic coating, (c) ALD and solution-based coatings ($AlF_3$, $Al_2O_3$, TiN, etc.) and (d) conducting polymer-based coatings.
- Develop atomistic models for HCMR™ cathodes' DC-R rise, phase change, and voltage sag.
- Apply theoretical solutions from atomistic models to mitigate phase change, voltage sag, and DC-R issues for HCMR™ cathodes.
- Develop cell-level models to understand cell behaviors that contribute to DC-R issues.
- Develop suitable conducting polymeric binders for Si-anodes to enhance cycle life and meet the PHEV targets.

### Project Details

**Bruce Mixer (NETL Program Manager)**
DE-EE0006443 Recipient: Envia Systems Inc.

**Subramanian Venkatachalam (Envia Systems Inc. – PD/PI)**
7979 Gateway Boulevard, Suite 101
Newark, CA 94560
Phone: 510-962-3688; Fax: 510-790-7012
Email: mani@enviasystems.com

Subcontractor:
Lawerence Berkeley National Laboratory (LBNL), Berkeley, CA; Oak Ridge National Laboratory (ORNL), Oak Ridge, TN ; General Motors (GM), Warren, MI

Start Date: October 2013

Projected End Date: December 2015

## Technical Barriers

- Meeting PHEV power specifications at Beginning of Life (BOL).
- Meeting PHEV power and energy specifications throughout cycle-life.
- Loss of power with cycling.
- Cycle and calendar life.

## Technical Targets

- Develop high capacity HCMR™ cathodes, and Si-SiO-C based anodes and integrate them to build high capacity (0.25-40Ah) pouch-cells that exceed the ABR minimum target goals for PHEVs. Following is the list of cell targets for this program:

**Table IV- 19: Cell Specifications for ABR Target Goals**

| Characteristics | Unit | PHEV40 |
|---|---|---|
| Specific Discharge Pulse Power | W/kg | 800 |
| Discharge Pulse Power Density | W/L | 1600 |
| Specific Regen Pulse Power | W/kg | 430 |
| Regen Pulse Power density | W/L | 860 |
| Recharge Rate | NA | C/3 |
| Specific Energy | Wh/kg | 200 |
| Energy Density | Wh/L | 400 |
| Calendar Life | Years | 10+ |
| Cycle Life (at 30°C with C/3 Charge and 1C Discharge Rates) | Cycles | 5000 |
| Operating Temperature Rane | °C | -30 to +52 |

## Accomplishments

### Material and Cell Development

- Newly developed HCMR™-XE cathode material shows much improved usable energy (>88%) while maintaining high specific capacity. This material improves greatly on the performance of the previous HCRM$^{TM}$-XLE material.
- Large batch of HCMR$^{TM}$-XE (5~15 kg) was successfully synthesized using a 75 gal reactor. 5 kg of the resulting HCMR$^{TM}$-XE material was shipped to Envia's pilot cell fabrication facility to assemble 25 Ah cells.
- 25 Ah cells with 220 Wh/kg at 1C rate were fabricated with the HCMR™-XE//Si-SiO-C system. The cells qualified energy, power, and capacity requirements for the Beginning of Life (BoL) ABR program targets.

### Surface Coating Development

- $Al_2O_3$-coated HCMR™-XLE2 via ALD shows the least metal-ion dissolution among the various surface coated materials, highlighting the benefits of such a uniform nanocoating and its role on improving the calendar/cycle life of a given cathode.
- $Al_2O_3$-coated Si-SiO-C anode via ALD shows initial promise of improved cycle-life after being tested in coin-cells and pouch-cells.

### Analytical Techniques

- STEM analyses, XRD spectroscopy, and Raman spectroscopy studies suggest the presence of a single-phase structure rather than a two-phase structure in the bulk of the HCMR$^{TM}$ materials. For this class of Li-rich NCM materials, a single monoclinic *C2m* phase is suggested. The many geometrical variants of the monoclinic phase could be misinterpreted as a second *R-3m* phase in the cathode's bulk structure.
- Raman spectroscopy and synchrotron XANES studies show higher cycle-to-cycle reversibility for the HCRM$^{TM}$-XE material, while the HCRM$^{TM}$-XLE material shows large degradation within the first few cycles.

## Introduction

In order to reduce the demand of fossil-fuels as the main energy source for automotive vehicles, Plug-in Hybrid Electric Vehicles (PHEVs) that surpass the performance standards for commercially available automobiles are required. Successful development of such PHEVs depends on the development of batteries constructed with cathode and anode materials that provide high capacity, energy, power, and safety. The goal of this project is to develop these advanced cathode and anode materials to construct batteries that can enable the use of next-generation cost-efficient PHEVs.

With regards to cathode materials for PHEV applications, currently, some of the most attractive materials take on the chemical composition of $x\ Li_2MnO_3 \bullet (1\text{-}x)\ LiMO_2$, where $x$ represents the molecular fraction and $M$ represents any such elemental blend of Ni, Co, and Mn. This nomenclature system also reflects the hypothesized two-layered nature of this material, the $Li_2MnO_3$ Mn-rich layer responsible for the high capacity of the material and the transition-metal $LiMO_2$ layer responsible for the cycling stability. This class of materials, a.k.a. High Capacity Manganese Rich (HCMR$^{TM}$) cathodes are known to provide higher capacity, higher safety, and lower material cost than alternative cathode technologies. However, key issues with HCMR$^{TM}$ materials include high DC-resistance (DC-R), fading of voltage upon cycling, and poor durability, all of which are accentuated after several cycles. Altogether, increasing the content of Mn in the composition of the cathode results in higher capacity and higher safety at the cost of growing DC-R, and worsening voltage retention. For this reason, Envia Systems has developed a family of HCMR$^{TM}$ materials with ranging Mn-content in order to study and identify the optimal chemical composition for HCMR$^{TM}$ materials.

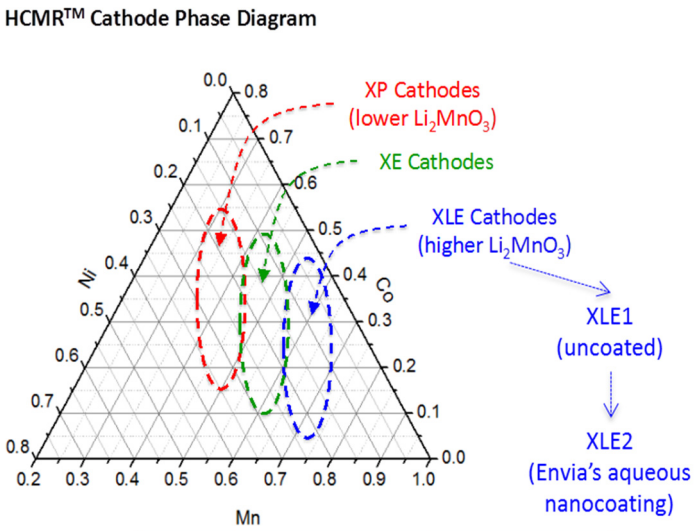


| HCMR™ Type | C/10 Capacity Range mAh/g (4.6-2.0V) | Status |
|---|---|---|
| XP | 200 ~ 220 | Commercialization |
| XE | 225 ~ 240 | R&D |
| XLE | 240 ~ 280 | R&D |

**Figure IV- 140: Ternary-phase diagram for Envia Systems' HCMR™ class of cathode materials**

Figure IV- 140 identifies Envia Systems' HCMR™ cathode material library in the terniary diagram as well as the listing basic electrochemical characteristis of such materials.

It is important to note that under this nomenclature, HCMR™-XLE1 refers to the cathode material as synthesized, while the XLE2 is the further processing of XLE1 material with an Al-halide nm-sized surface coating (nanocoating) deposited onto the material via an aqueous reaction. Usually, the nanocoated analog of the material, which shows improved cycle-life over the uncoated, is the baseline onto which further coatings such as LiPON, $Al_2O_3$, or TiN among others, are applied. The same nomenclature system applies to HCMR™- XP and XE materials.

At the beginning of this ABR program, the HCMR™-XLE class of materials (higher Mn content) were investigated in order to take advantage of the material's high capacity while preventing the growth of DC-R and loss of cycle ability. Preliminary studies showed that by adding a thin layer of conductive carbon on the surface of the of HCMR™-XLE2 particle, the resistance of the material as a function of SOC at the BoL was severely improved. For instance, the baseline HCMR™-XLE2 shows 75% usable energy, while the Carbon-coated analog showed and improved 82% usable energy. This was obtained by measuring the percentage of energy obtained at a resistance lower than 75 Ω/cm$^2$ (as measured by an HPPC test between 4.4-2.0V with 10 sec 1C pulse Ch/Dis pulses) from an HCMR™//Graphite cell. However, the HCMR™-XLE2 cathode showed a drastic increase in DC-R and drop in average voltage with each cycle, which could not be addressed by any type of surface modifications. A combination of electrochemical tests and analytical techniques, revealed that the HCMR™-XLE material's main degradation process took place in the bulk of the material by irreversible reactions which deteriorate the Mn-rich layer and poison the transition metal layer in addition to surface side-reactions.

Consequently, a second class of materials was introduced in Q5 of this program, the HCMR™-XE, which contains lower content of Mn and shows both higher usable energy (>88%) and energy retention with cycling than the HCMR™-XLE2 (75% usable energy BoL). Figure IV- 141 highlights the BoL DC-R improvement for the HCMR™-XE2 when compared the HCMR™-XLE2 analogs. Therefore, in this second year of the program, the development of HCMR™-XE2 cathode materials with surface coatings and the engineering of large capacity cells for cycle-life using this cathode have been the main focus.

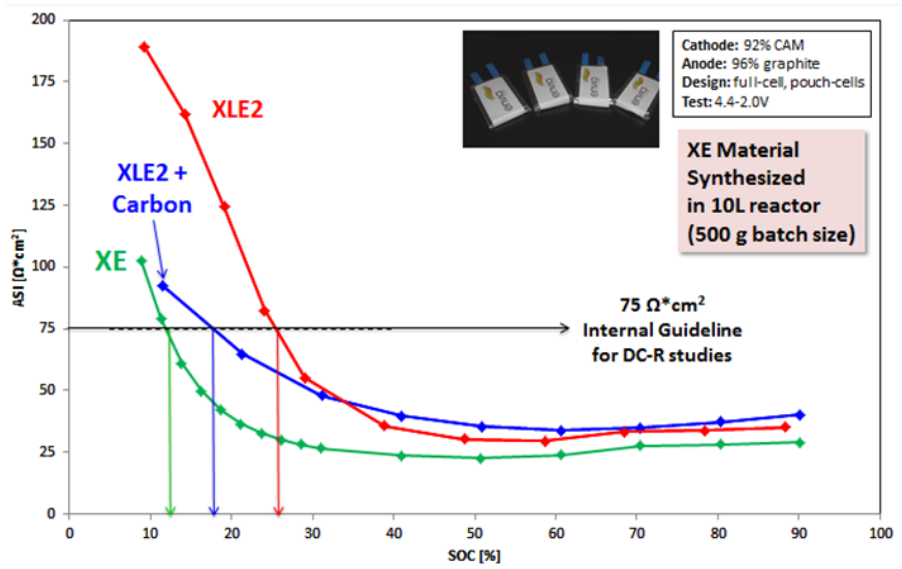


Figure IV- 141: DC-R profiles for HCMRTM-XE, HCMRTM-XLE and Carbon-coated HCMRTM-XLE materials in pouch-cell vs graphite anode

## Approach

**Material development**: Under this approach, cathode materials with varying compositions, and surface coatings were synthesized with the intention to minimize the (1) electronic, (2) ionic, and (3) charge-transfer contributions to DC-R. Figure IV- 142 summarizes the approach taken with respect to material development, and the collaboration with each partner institution.

**Analytical studies**: Utilize spectroscopic and microscopic techniques to identify the root-cause for material failure and areas of improvement. Such studies include:

i. **EIS:** provides information regarding the various modes that cause the increase in resistance, specifically determining whether the resistance is ionic or electronic in nature.
ii. **Raman spectroscopy:** helps observe the change in oxidation state of transition metals and the corresponding change in crystal structures especially when the cathode is approaching full discharge.
iii. **XAS:** provides in-depth knowledge regarding the change of transition metal oxidation state and chemical/structural origins for voltage fade.
iv. **STEM/HAADF:** the various forms of such spectroscopy can be used to identify the crystal structure in the bulk and the surface of the primary particle of the material, with focus on studying the hypothesized layered nature of the structure of the cathode.

**Silicon-based anode development**: The development of robust silicon-based electrodes with enhanced binders and surface coatings extends the cycle-life of large capacity cells.
**Modeling and large cell performance**: Cell-level modeling allows for engineering the optimal electrodes, cell size, and voltage window of operation to maximize usable energy and cycle-life.

## Results

The following is a summary of the highlights of the results achieved in the second year of this program.

### Material Development

#### LiPON coated HCMR$^{TM}$-XLE materials

As mentioned previously, preliminary studies show that adding a thin layer of conductive Carbon to the surface of HCMR$^{TM}$-XLE material shows a remarkable improvement on the material's usable energy at the BoL. While Carbon is known to be a good electronic conductor, part of the high resistance of the material at lower SOCs is attributed to poor ionic diffusion, which remains unaddressed unless an ionic conductor species is added to the material. With this goal in mind, LiPON (Lithium Phosphorus Oxynitride), an ionic conductor ceramic species developed by ORNL, was investigated for its potential to aid in the diffusion of Li-ions into and out from the cathode particles.

Nanometer-thick layers of LiPON were deposited by the team at ORNL using RF sputtering (Ref. 1) onto HCMR$^{TM}$-XLE2 cathode (XLE2 cathode analog contains a layer of Al halide processed via an aqueous reaction prior to the sputtering of the LiPON).

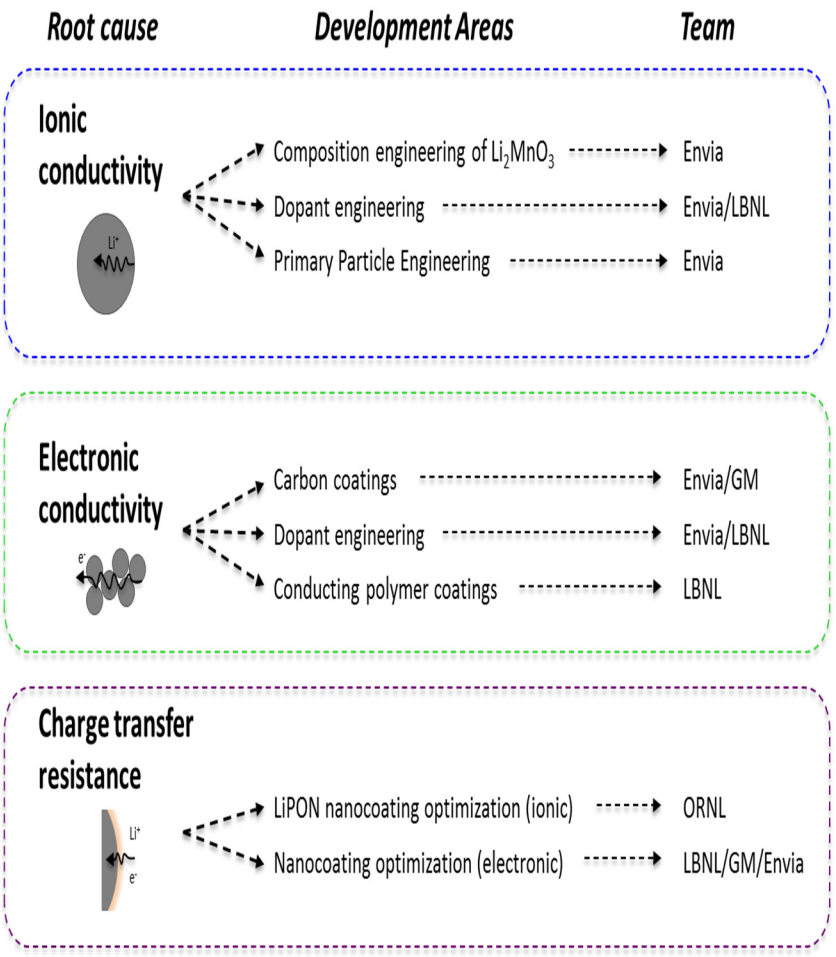


**Figure IV- 142: Overview for HCMR™ material development and surface modifications by addressing root causes for DC-R**

Electrochemical screening in half-cells of LiPON-coated HCMR™-XLE2 at various deposition times (1 through 12 hrs) shows no negative impact on capacity nor voltage even at fast rates. Given that a drop in capacity or voltage, especially at faster rates, is correlated with an increase in DC-R and high voltage fade, the promising half-cell results make LiPON an attractive candidate for the next stage of electrochemical testing in full-cells. Full-cells with graphite anode are utilized to test DC-R and loss of usable energy as a function of cycle life. The DC-R test involves measuring the resistance at different SOCs by applying a 10 second 1C discharge pulse every 10% SOC and computing the resulting Area Specific Impedence (ASI in $\Omega*cm^2$) during a C/3 discharge cycle. This test performed on the 1st cycle and after 25 and 125 1C cycles between 4.4-2.0V to observe the change of the DC-R profile in long-term cycling. In the case of LiPON coated

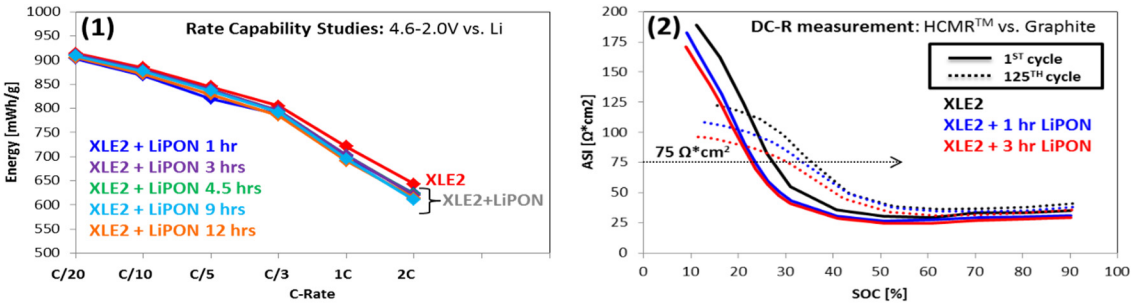


**Figure IV- 143: (1) Energy of HCMRTM-XLE2 coated materials at different discharge rates with varying LiPON sputtering deposition time measured in half-cells. (2) DC-R profiles of baseline, 1 hr, and 3 hr LiPON sputtering on HCMRTM-XLE2 cells vs graphite after 1 and 125 1C cycles between 4.4-2.0V**

HCMR™-XLE2 cells with 1 and 3 hr deposition times, LiPON increases usable energy by 2~5% in the initial cycle at the 75 Ω*cm$^2$ mark, but the loss of usable energy (or growth in DC-R) after 125 cycles remains unaddressed. Ultimately, the total available usable energy from coated and uncated HCMR™-XLE2 materials remains low after 125 cycles regardless of the LiPON coating. Figure IV- 143 shows the results from the electrochemical tests performed on LiPON coated materials.

Similar studies on HCMR™-XE2 cathode delivered similar results of no improvement on usable energy or clear indication of improved cycle-life.

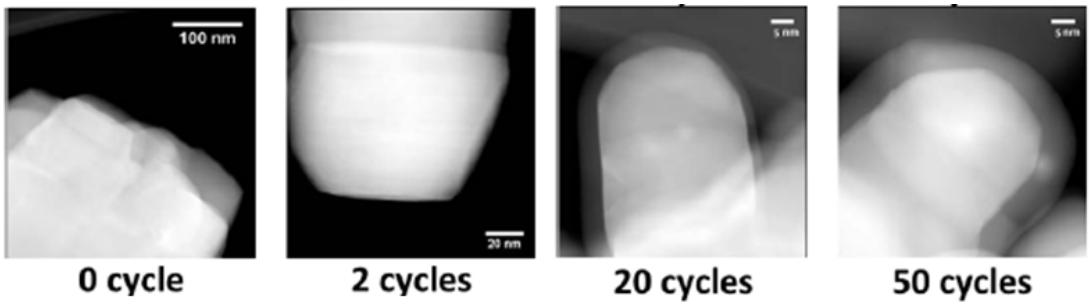


**Figure IV- 144: STEM images of baseline and $Al_2O_3$ coated HCMR™- materials via ALD evidencing a growth in ALD-coating thickness as a function of reaction cycle number**

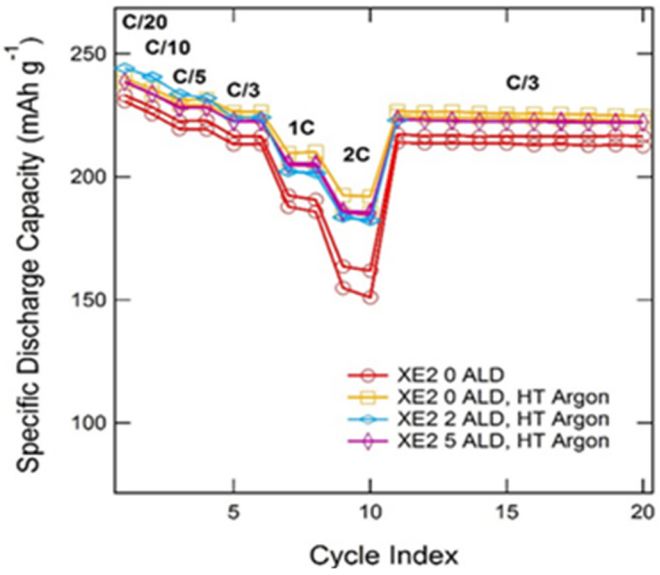


**Figure IV- 145: Rate capability of HCMR™-XE2 baseline, heat-treated (HT) under Argon, and HT with 2 and 5 reaction cycles of $Al_2O_3$ ALD coating**

### ALD coated HCMR™ materials

In addition to studies on LiPON coating ionic conductors, surface coatings that address the charge-transfer component to the DC-R growth and loss in usable energy with cycling were investigated. With this goal in mind, the team at GM, with its expertise and equipment to perform ALD coatings with different charge-tranfer aiding species, investigated the impact of $Al_2O_3$, $AlF_3$, AlN, ZnO, and TiN surface coatings with varying thicknesses on the performance of the HCMR™-XLE2 and XE2 materials. The ALD process provides uniform, conformal coating on the particles which protects against deleterious side reactions on the surface of the material by stabilizing the Solid-Electrolyte Interface (SEI) layer.

Additionally, the ALD coating technique allows for precise thickness control by limiting the number of reaction cycles during the coating process. Figure IV- 144 shows SEM images of $Al_2O_3$ coated HCMR™ materials via ALD, highlighting the control on coating thicknesses as a function of number of ALD cycles throughout the process.

On the first year of the ABR program, several ALD coatings on HCMR™-XLE materials concluded in results similar to the LiPON coating studies. Namely, while the ALD-coated materials showed similar energy than the uncoated analogs, the growth in DC-R remained unimproved. Therefore, on the second year of this program, with focus shifting from HCMR™-XLE to XE, an additional set of ALD studies, this time incorporating an annealing step after the ALD reaction, were performed. The heat treatment after the $Al_2O_3$ ALD processing involved heating the material at 300°C in 1 sccm of Ar flow for 12 hrs. The electrochemical screening of such materials in half-cells showed an improvement on rate capability as evidenced by higher 2C capacities when the material was annealed and ALD-coated. A summary of these results is shown in Figure IV- 145.

However, when tested in full-cells with graphite anode, these materials showed a 2~3% loss of BoL usable energy and no significant evidence of preventing DC-R growth after 25 cycles at 1C between 4.4-2.0V. Figure IV- 146 shows the DC-R profile on the 1st cycle and after 25 cycles for (i) the baseline HCMR™-XE2 cathode (ii) the heat treated cathode without ALD coating (HT-ALD 0c), (iii) the heat-treated material after 2 ALD reaction cycles (HT-ALD 2c), and (iv) heat-treated material after 5 ALD reaction cycles (HT-ALD 5c).

### Polymer coated HCMR™ materials

A third surface modification process was under investigation throughout the second year of this program: polymer coatings of Conducting Polymer #1 on HCMR™-XLE material. Polymer coatings can improve the conduction pathways and provide a breathable physical barrier between the electrode and the electrolyte. The polymer coating is achieved by precipitation of dissolved polymer particles suspended in the cathode material aqueous suspension upon solvent removal. Given that the Al halide coating part of the HCMR™ -XLE2 material is sensitive to water, for these studies the HCMR™-XLE1 analog was used as a baseline.

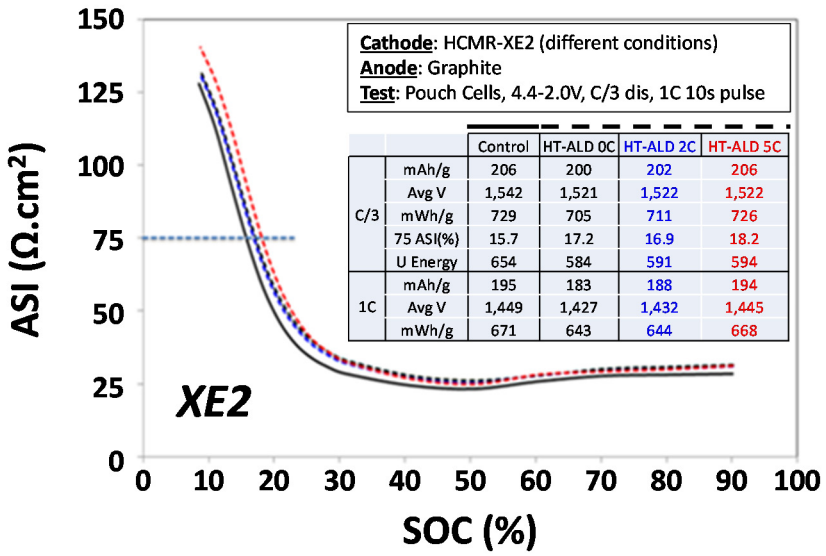


| | | Control | HT-ALD 0C | HT-ALD 2C | HT-ALD 5C |
|---|---|---|---|---|---|
| C/3 | mAh/g | 206 | 200 | 202 | 206 |
| | Avg V | 1,542 | 1,521 | 1,522 | 1,522 |
| | mWh/g | 729 | 705 | 711 | 726 |
| | 75 ASI(%) | 15.7 | 17.2 | 16.9 | 18.2 |
| | U Energy | 654 | 584 | 591 | 594 |
| 1C | mAh/g | 195 | 183 | 188 | 194 |
| | Avg V | 1,449 | 1,427 | 1,432 | 1,445 |
| | mWh/g | 671 | 643 | 644 | 668 |

Figure IV- 146: DC-R profile for HT-ALD coated HCMR™-XE2 materials on the 1st cycle and after 25 1C cycles

Unfortuantely, little success was achieved with the polymer coating technique. Half-cell screening of Conducting Polymer #1 coated samples showed poorer rate capability than the baseline material and in full-cell studies with anode graphite, the usable energy of the material decreases at a faster rate than the baseline. Figure IV- 147 shows the DC-R measurement profile of these materials on the 1st cycle and after 25 cycles.

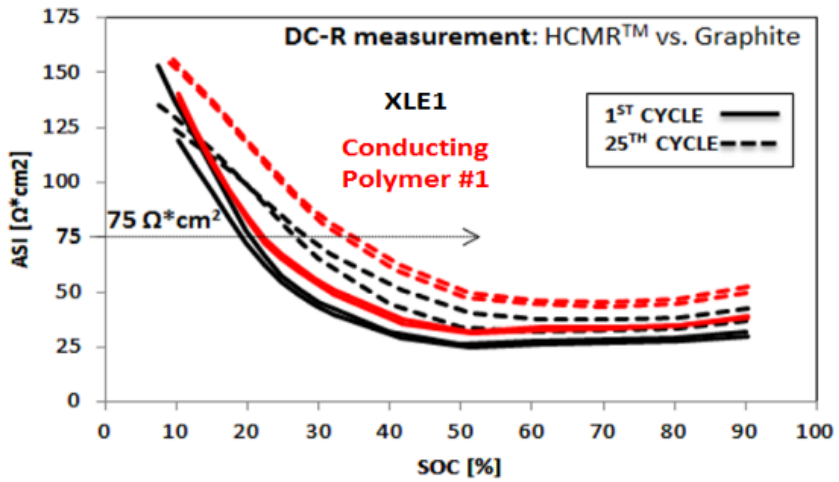


Figure IV- 147: DC-R profile for the HCMR™-XLE1 material coated with Conduction Polymer #1 on the 1st cycle and after 25 1C cycles between 4.4-2.0V

Given the poor performance of Conducting Coating #1 coatings on HCMR™-XLE1 cathode, this coating technique was not applied to the HCMR™-XE class of materials. Nevertheless, future optimization of this coating technique (outside the scope of this program) could result in improved cathode material electrochemical properties.

**Table IV- 20: PPM of Mn measured from metal dissolution studies on HCMR™//Graphite cells**

| | | Mn [ppm] | |
|---|---|---|---|
| | | Avg | |
| XLE1 | Control | 120 | 20 |
| | Conductive Polymer #1 | 106 | 1 |
| | Conductive Polymer #2 | 192 | 20 |
| XLE2 | Control | 101 | 21 |
| | 1 hr LiPON | 118 | 12 |
| | $Al_2O_3$ 2 cycles | 74 | 11 |
| | $Al_2O_3$ 2 cycles | 66 | 17 |
| | TiN 2 cycles | 113 | 26 |
| | TiN 5 cycles | 113 | 15 |

### Metal dissolution studies on surface modified HCMR™ materials

Altogether, the surface modification techniques so far attempted on a range of HCMR™ class of materials has yet to solve the DC-R growth issue after several cycles. These results suggest that the DC-R growth issue does not necessarily arise from deleterious surface reaction on the cathode's particle. Nevertheless, some of these coating techniques do show improved surface stability as measured by metal dissolution studies.

Metal dissolution studies consist of assembling a full cell with graphite anode, and, after the activation of the material at high voltages, storing the 4.5V charged cells at 60°C for 7 days. Afterwards, the cells are discharged, disassembled, and the graphite anode is processed in order to measure the metal ion content. A lower metal dissolution, indicates a higher level of protection against surface reactions between the cathode and the electrolyte. This surface stability of the cathode is correlated with benefits on calendar-life and long-term cycle ability. Table IV- 20 summarizes the metal dissolution studies as measured by ppm of Mn.

A highlight of these results is the improved metal dissolution measured from $Al_2O_3$-coated HCMR™-XLE2 cathodes after 2 and 5 reaction cycles of ALD. The drop from 101 ppm of Mn from the baseline to 66 and 74 ppm indicates that this type of ALD-$Al_2O_3$ coating offers benefits that are not observed by just focusing on DC-R and usable energy retention.

### Conclusions on material development (Go/No-Go)

Based on BoL DC-R, DC-R growth, usable energy, and metal dissolution studies, certain materials were selected for further development. The selection criteria was based on (1) >96% energy retention after 50 cycles when tested in half-cells and (2) >85% usable energy as measured by DC-R using the 75 Ω*cm$^2$ mark. The Go/No-Go analyses based on these criteria is shown in Table IV- 21. From the table it is observed that the HCMRTM-XE material in conjungction with Carbon-coating, has been selected for scale-up and further development.

**Table IV- 21: Go/No-Go of surface-coatings on HCMR™ materials**

| | | >96% Energy Retention | DC-R@ 75Ω*cm²<15% |
|---|---|---|---|
| SI # | Study | vs. Li | vs. Gr |
| 1 | Composition Engineering | Go | Go |
| 2 | Carbon Coating | Go | Go |
| 3 | LiPON Coating | Go | No Go |
| 4 | ALD-$Al_2O_3$ Coating | Go | No Go |
| 5 | Polymer Coating | No Go | No Go |

### Analytical Techniques

While the goal of the materials development approach to mitigate DC-R issues consists of experimentally testing cells with different cathode compositions and surface coatings, the second approach for this program involves in-depth analyses of the modes by which the HCMR™ cathodes degrade through cycling. A main goal of the LBNL team is to identify the underlying phenomena causing cell impedance and rise of DC-R of HCMR™ cathodes using three main types of analytical techniques: electrochemical, spectroscopic, and microscopic. A summary of important studies performed by the LBNL team aimed towards this objective, follows:

### Electrochemical studies on origins of DC-R of HCMR™ materials

Electrochemical studies have as goal translating the electrochemical performance of a cell into physical and chemical properties of the cathodes under investigation. Therefore, applying electrochemical techniques such as EIS on HCMR™-XE cathodes will reveal the material properties that cause HCMR™-XE's low resistance when compared to the HCMR™-XLE cathode. Here is a highlight of the results:

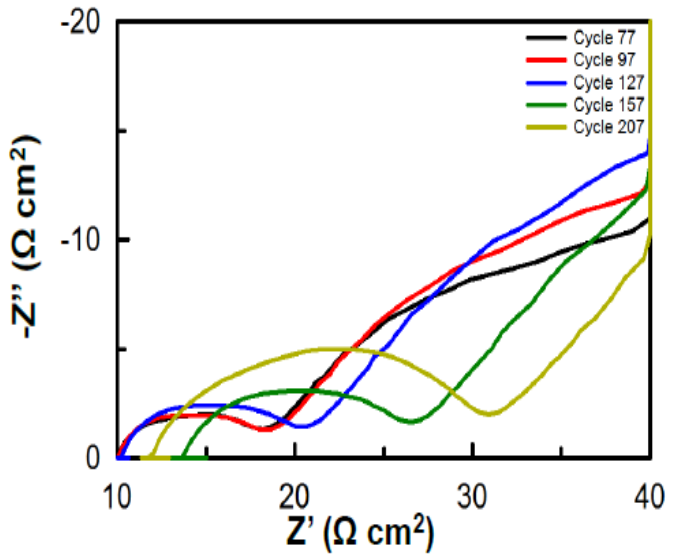


Figure IV- 148: EIS response of HCMR™-XE2 cathode as a function of cycle-life

- HPPC calculations show that HCMR™-XE's initial resistance is much lower than the HCMR™-XLE cathode.
- The marching rate of the HCMR™-XE material is minimal when compared to the HCMR™-XLE cathode. Marching rate is a measure of impedance rise and rate of electrode side reactions, consequently, a lower marching rate signals a more efficient cell performance.
- The EIS response of the HCMR™-XE2 cathode material shown in Figure IV- 148 shows the typical two semicircle behavior also observed in the HCMRTM-XLE2 material. The first semicircle is mainly associated with the surface film formation on the cathode as well as the contact resistance among the particles. The second semicircle is caused by the charge-transfer reactions in the cathode at each SOC. Impedance response at different SOC's (or voltages) with respect to cycling show an increase in the magnitude of the 1st semicircle, allegedly caused by formation of a thicker surface film as well as the loss of particle contact.
- The results from electrochemical analyses on HCMR™-XE and HCMR™-XLE cathodes show that DC-R is caused by surface film buildup at lower states of charge and by changes in cathode material diffusivity due to changes in the lattice parameter during a single cycle.

### Raman spectroscopy on HCMR™ materials

Post-mortem Raman spectroscopy analysis is an effective technique to understand the root cause of phase change and its impact on the DC-R of cathode materials. Specifically, Raman spectroscopy helps understand the possible structural changes on the surface and its effect on the transition metal oxidation states. Of interest, is the comparison between (1) HCMR™-XLE2 and HCMR™-XE2 materials and (2) between electrodes with limited cycling and prolonged cycling.

The Raman investigations for HCMR$^{TM}$-XLE2 cathode shown in Figure IV- 149 (1) show that after prolonged cycling, the main Ni signal in the delithiated state shifts from 540 cm$^{-1}$ ($Ni^{4+}$) to 630 cm$^{-1}$, thereby indicating the formation of a spinel-like structure early on during the cycle life of the material. Supporting analyses confirm that this shift occurs after the 1$^{st}$ delithiation of the cathode. In other words, an irreversible change with respect to Ni oxidation state occurs within the first 5 cycles and the degradation process increases with each cycle. Figure IV- 149 (2) shows the same study performed on 5 cycles and 50 cycles HCMR$^{TM}$-XE2 electrodes. Compared to the HCMR$^{TM}$-XLE2, the HCMR$^{TM}$-XE2 material shows an initial weak peak at 430 cm$^{-1}$ which disappears during cycling. With HCMR$^{TM}$-XE2, the Ni oxidation is reversible and remains in the 470 cm$^{-1}$ region during the fully delithiated state even after 50 cycles. These observations suggest that the HCMR$^{TM}$-XE2 material features much better reversibility than the higher Mn content analog, which further translates into lower transformation to spinel-like structure with the HCMR$^{TM}$-XE2.

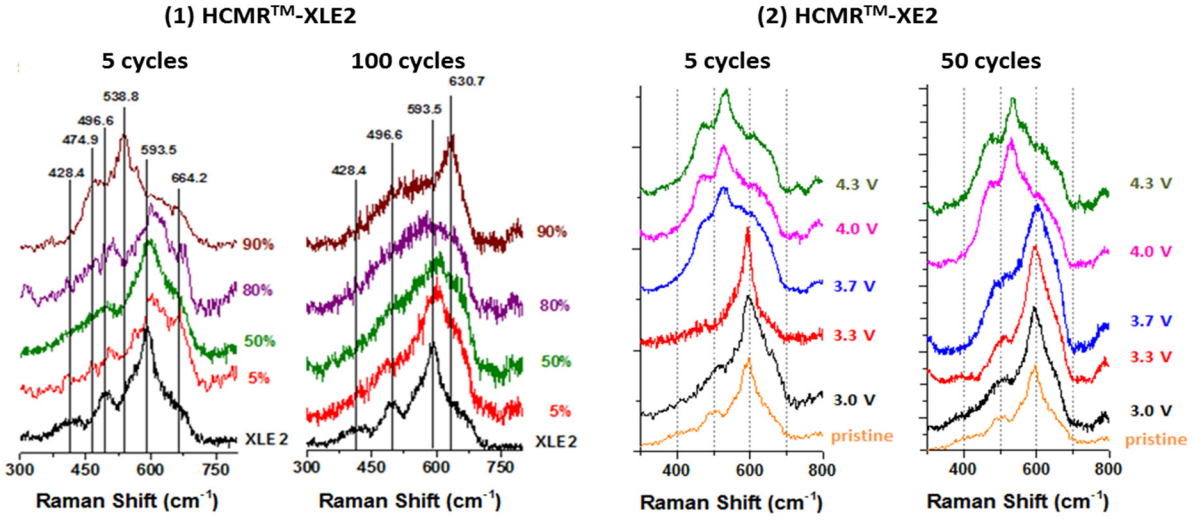


Figure IV- 149: Raman spectroscopy for (1) HCMR$^{TM}$-XLE2 cathode (5 and 100 cycles) and (2) HCMR$^{TM}$-XE2 cathode (5 and 50 cycles)

**XANES studies on HCMR$^{TM}$ materials**

To further confirm the structural transitions happening in HCMR$^{TM}$ materials, NE-XANES synchrotron analyses were performed. XANES is an attractive technique for it allows to compute the average oxidation number of Ni and other transition metals as a function of (1) applied voltage and (2) cycle number. The results from these analyses (Figure IV- 150) show that for both HCMR$^{TM}$ materials, there is a change in Ni oxidation number from 2+ to 4+ when charging the cell to 4.6V, yet the process by which this occurs and the behavior at each cycle is more stable for the HCMR$^{TM}$-XE2 material.

For the HCMR$^{TM}$-XLE2 cathode, during the 1$^{st}$ charge, the Ni oxidation state rapidly climbs from 2+ to >4+, reaching 4+ at around 3.5V. However, in the 2$^{nd}$ cycle, an irreversible change occurs in which the Ni oxidation number reaches 4+ only at ~4.5V. Subsequent cycles show a similar distribution as the 2$^{nd}$ cycle's profile, with the caveat that the maximum oxidation state of Ni at 4.6V drops slighltly with higher cycle number.

For the HCMR$^{TM}$-XE2 cathode, XANES reveals a different behavior than that of the HCMR$^{TM}$-XLE2 cathode. On the first charge, the HCMR$^{TM}$-XE2 Ni oxidation number starts climbing only at ~3.0V, whereas the HCMR$^{TM}$-XLE2 cathode the Ni oxidation number climbs starting at ~2.0V. For the HCMR$^{TM}$-XE2 cycle, there is little shift regarding oxidation number profile for Ni between the 1$^{st}$ and 50$^{th}$ cycles. Altogether, the HCMR$^{TM}$-XE2 cathode shows less irreversibility with respect to Ni oxidation number profile.

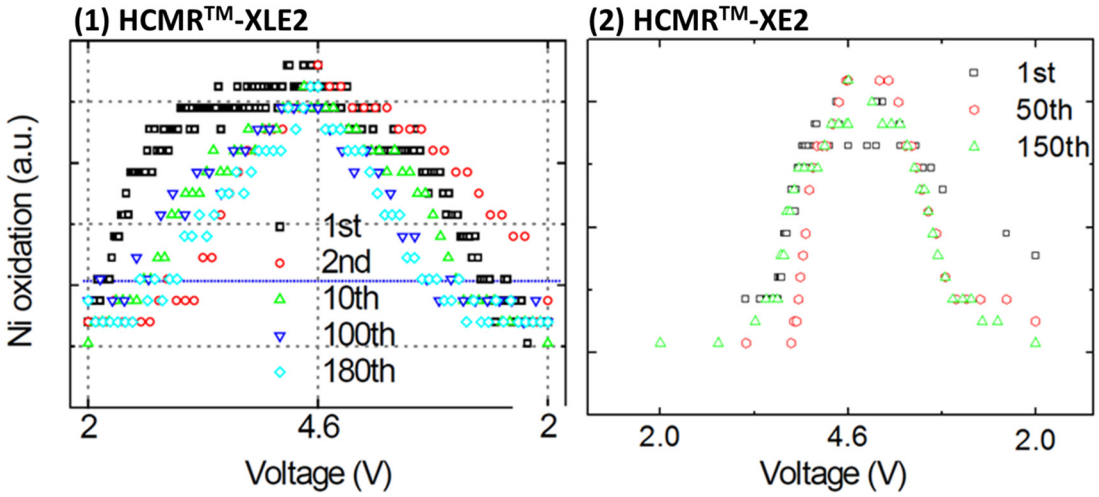


Figure IV- 150: Ni oxidation number distribution for (1) HCMR™-XLE2 cathode and (2) HCMR™-XE2 cathode

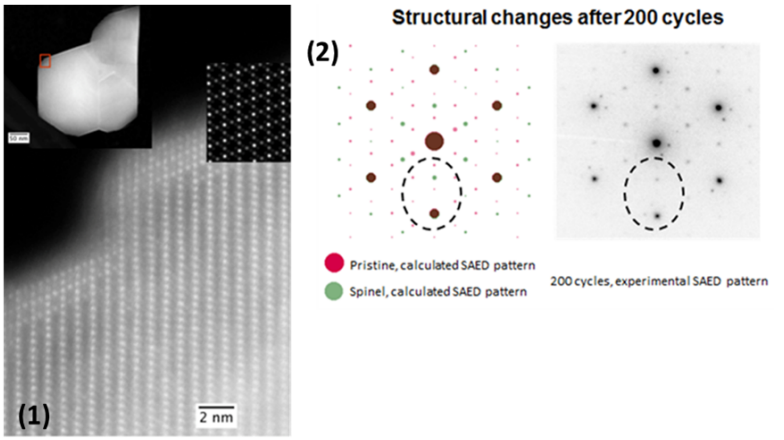


Figure IV- 151: (1) STEM image HCMRTM-XLE2 and (2) Electron Diffraction patterns of cycled HCMRTM-XLE2

**STEM studies on HCMR™ materials**

To understand the phase change at the atomic level of cathode materials, HR-STEM (HAADF) studies were performed at NCEM, LBNL on HCMR™-XLE2 cathodes. As reported earlier, HCMR™-XLE2 cathodes showed a predominantly single phase structure involving *C2m* monoclinic phase rather than composite nanodomains of *C2m* ($Li_2MnO_3$) and *R-3m* ($LiMO_2$) phases. The current STEM analysis studies multiple variants of monoclinic structure as shown in (Figure IV- 151). The following observations are made:

- Li- and Mn-rich transition metal oxides consist of randomly-sized monoclinic domains. The HAADF STEM image shows [100], [110] and [1-10] domains of the monoclinic phase stacked on (001) planes. This arrangement is observed throughout the primary particle, confirming that the bulk is made of a single phase (except for defects and surface layer).
- XEDS maps do not show any segregation of Mn. XEDS shows Ni and Co enrichment and O depletion at the surface
- 2-3 nm thick spinel phase observed on certain facets of primary particles

Another major challenge of HCMR™-XLE2 cathode material is the inherent phase change with respect to cycling. In order to understand the new phase that is formed with cycling, HCMR™-XLE2 material has been cycled for 200 times and the cathode material has been harvested and studied using STEM/HAADF.

- Preliminary (S)TEM studies of HCMR™-XLE2 material after 1 cycle shows negligible change of the spinel surface layer thickness.
- Electron diffraction and HRTEM studies after 200 cycles clearly show phase transformation of the bulk material. Preliminary analysis of the results show a possibility of layered to spinel structure transformation.

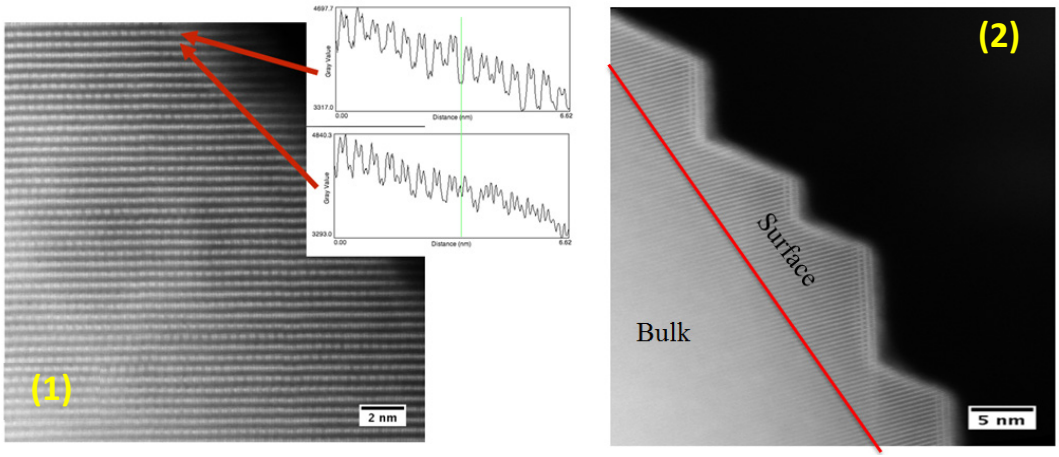


Figure IV- 152: STEM images of HCMR™-XP cathode (1) surface and (2) bulk structure

To better understand the degradation mechanism of HCMR™ materials, the STEM analysis on HCMR™-XP cathode (low Mn) was compared to that of the the HCMR™-XLE2 (high Mn) cathode. The main objective of this study is to see the influence of the compositional Li, Ni, Co and Mn content on the actual structure at the nanodomain level. The following main diffrences between both cathode compositions are observed (Figure IV-152).

**Bulk**

- HAADF STEM imaging shows domains similar to those observed in HCMR™-XLE2, but with much lower homogeneity within the domains.
- In particular, the column between the doublets seen in [100] monoclinic orientation that typically consists of both Li and TM show varied intensities even within the same row of columns. This is in contrast to that observed in HCMR™-XLE2 material where the periodicity is maintained within a domain.

**Surface**

- Surface spinel layer with orientation relationship similar to that observed in HCMR™-XLE2 material was observed. The thickness of this layer is approximately 2 nm.
- Although the thickness of the spinel layer is similar that observed in HCMR™-XLE2 material, it is possible that the total volume of spinel in the primary particle is different based on the difference in morphology or the total area of facets prone to spinel formation.

In addition to these studies, the cycled cathode HCMR™-XP material will be investigated to determine the effect of cycling on the phase stability. This will reveal the effect of composition on phase change with respect to cycling. Furthermore, to confirm the structural aspects of Li-rich NMC, stoichiometric NMC will be examined. This will baseline the presence of pure R-3m structure in the case of Li-NMC (111) since it has been confirmed that the HCMR™-XLE structure is pure monoclinic with multiple variants.

**Silicon-Based Anode Development**

One of the challenges to achieving the cycle life targets stated in this ABR program is the development of more robust silicon anodes. With this in mind, PFM binders have been developed at LBNL that benefit cycle life of silicon anodes. The PFM binder has shown impressive adhesion in tape peel tests but to this date it has not shown good performance when combined with SiOx-based anodes. The suspected cause for this performance is an interfacial effect between the PFM binder and the SiOx-based anode. For this reason a matrix approach was employed to test alternate electrolytes, active material loadings, laminate compositions, active materials and coatings with Envia's current binder. The experiments are summarized in Figure IV- 153. All lithium-containing half-cells were tested at C/10 cycling at 23°C.

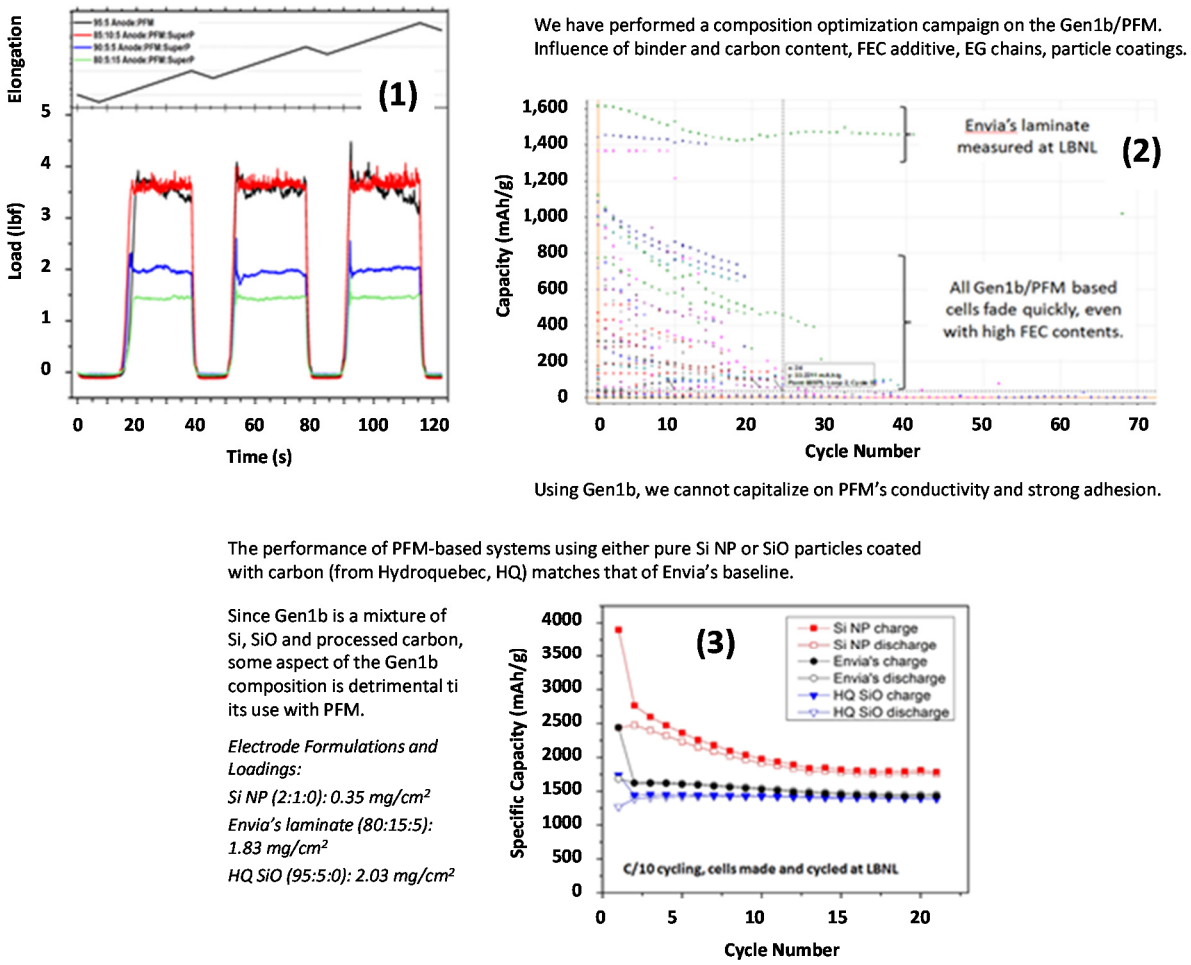


**Figure IV- 153: Conducting polymeric binder development (1) PFM binder showing high peel strength, (2) comparison of Eniva's binder with the PFM binder, (3) exploring the effect of binder on other forms of Si-anode**

The acquired data shows that only the following three conditions from the experimental matrix show stable capacities through cycling: (1) Envia's SiOx-based anode with its current binder, (2) hydroquebec carbon coated SiO with PFM binder (3) and Envia's SiOx-based anode with a CMC binder. PFM normally works well with other silicon based anodes but there is a unique compositional property of Envia's SiOx-based anode that prevents PFM from stable cycling. Interestingly, the constituents of SiOx-based anodes independently cycle with PFM therefore more work in ongoing to understanding this situation. For instance, electrochemical and spectroscopic tests have been performed on PFM on copper without the of SiOx-based anodes as a first step toward understanding where the problem might occur. The preliminary results show that the PFM deposited well onto copper and formed ~ 100 nm thickness when spin-coated. Furthermore, with electrochemical cycling the PFM shows very little activity at the potentials experienced by the anode. Additionally, PFM has very little redox activity which is good for electrochemistry but makes identifying the source of the poor capacity and cycling with of SiOx-based anodes more difficult.

Overall, our studies suggest the following

- PFM is an excellent binder for certain Si and SiO anode materials
- PFM shows excellent mechanical adhesion with Envia's SiOx-based anodes
- Yet, the interaction between PFM and SiOx-based anodes leads to rapid capacity fade
- PFM appears to be electrochemically stable in the reduction region on bare copper.

### Cell Sizing and Cycling Performance Modeling

In the case of the HCMR™ materials, the DC-R and the growth in DC-R has been directly related to the amount of lithium being removed from the cathode, which is directly proportional to the charging voltage. With this in mind, cell energy sizing was performed to identify the right voltage window of operation to

achieve the ABR project goals of 200 Wh/kg and 400 Wh/l. Figure IV- 154, shows the summary of the sizing analyses from where it can be observed that a charge voltage of 4.2V will achieve the targeted specific energy while very nearly achieving the energy density targets. Currently, cells will be assembled with the suggested design parameters shown in Table IV- 22 to validate these calculations. To further understand the root cause of DC-R, electrochemical modeling will be performed in using COMSOL.

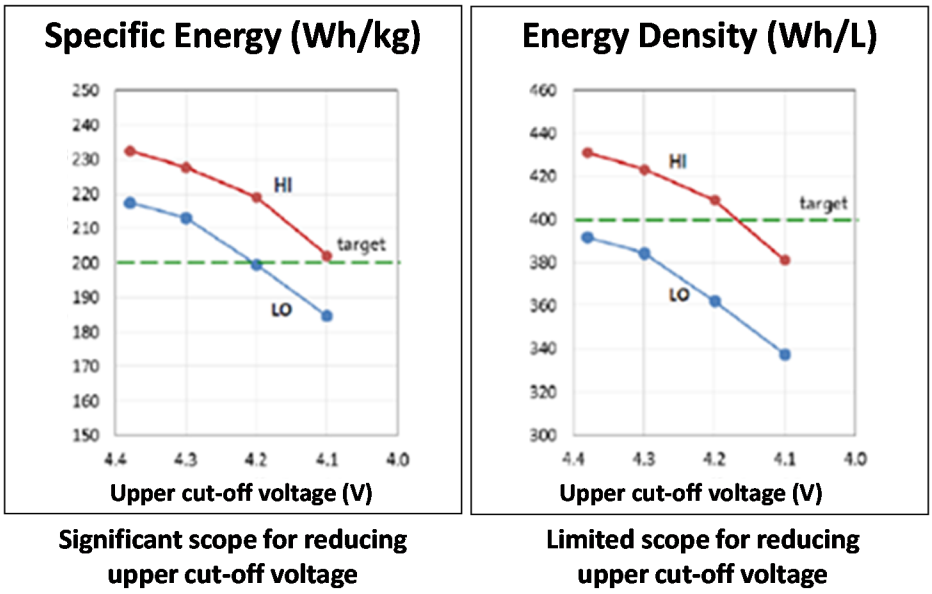


Figure IV- 154: Sizing calculations at different charging voltages targeting to meet the ABR project goals for both specific energy and energy density

**Large Format Cell Build #1 for Internal Testing and Validation of the PHEV40 Goals using HCMR™-XE2 Cathode and Si-SiO-C Anode – HPPC Studies and Gap Analysis**

After a continued effort on improving the DC-R characteristics of the HCMR™-XLE materials, Envia in collaboration with the ABR team have determined that surface modification of the cathode material has no major impact on DC-R. Rather, changes in the chemical composition of the HCMR™ materials show a large improvement on DC-R performance. Consequently, Envia developed a new Li-rich NMC with a different Li/Mn ratio: the HCMR™-XE. To evaluate the basic cell properties of HCMR™-XE across Si-SiO-C anode, 25 Ah cells were assembled targeting an energy density of 200 Wh/kg. The design for the Cell Build Iteration # 1 is shown in Table IV- 22. In comparison to the current cell build to baseline the newly developed XE material, an additional cell build with a different anode has been formulated and the design is shown in Table IV- 22.

**Table IV- 22: Two Iterations of Cell Designs Towards Planned Final Cell Build at the End of the Program**

| Design parameter | | Units | Design 1 | Design 2 |
|---|---|---|---|---|
| | | | 25 Ah | 25 Ah |
| **Cathode** | Active Material | N/A | HCMRTM-XE Blend | HCMRTM-XE Blend |
| | Total electrode area | $m^2$ | 0.5339 | 0.5339 |
| | Electrode Density | g/cc | >3 | >3 |
| **Anode** | Active Material | N/A | Si-$SiO_x$-C compatible | Si-$SiO_x$-C compatible |
| | Total electrode area | $m^2$ | 0.5746 | 0.5746 |
| | Electrode Density | g/cc | 1 | 1 |
| Cell weight | | g | 418 | 427 |
| Prelethiation | | N/A | SLMP™ | SLMP™ |
| Estimated capacity, 1C-Rate | | Ah | 25 | 25 |
| Energy density, 1C-Rate | | Wh/L | 400 | 423 |
| Specific Energy, 1C-Rate | | Wh/kg | 202 | 201 |

In order to meet all parameter metrics for the ABR program, Hybrid Pulse Power Characterization (HPPC) studies were performed and the corresponding GAP analysis is shown in Table 5. The typical 1C discharge curve exhibiting 200 Wh/kg is shown in Figure IV- 155 and the HPPC regen/discharge curves are shown in Figure IV- 156. As can be seen from Table IV- 23, all the project goals were met except for the cycle and calendar life, for which studies are ongoing. Currently, the cell has completed ~250 cycles at a C/3 charge, 1C discharge rate (Figure IV- 157).

**Table IV- 23: GAP Analysis of the HCMRTM-XE Baseline Cells From The HPPC Experiments**

| Characteristics | Unit | PHEV40 – ABR Targets | XE/Si-SiO Cells at RPT0 |
|---|---|---|---|
| Specific Discharge Pulse Power | W/kg | 800 | 1718 |
| Discharge Pulse Power Density | W/L | 1600 | 3693 |
| Specific Regen Pulse Power | W/kg | 430 | 2104 |
| Regen Pulse Power Density | W/L | 860 | 4523 |
| Specific Energy @1C | Wh/kg | 200 | 202 |
| Energy density @1C | Wh/L | 400 | 436 |
| Calendar Life | Years | 10+ | TBD |
| Cycle Life (C/3, ~1C) | Cycles | 5000 | TBD |
| Operating Temperature | °C | (-30 ~ +52) | 25°C |

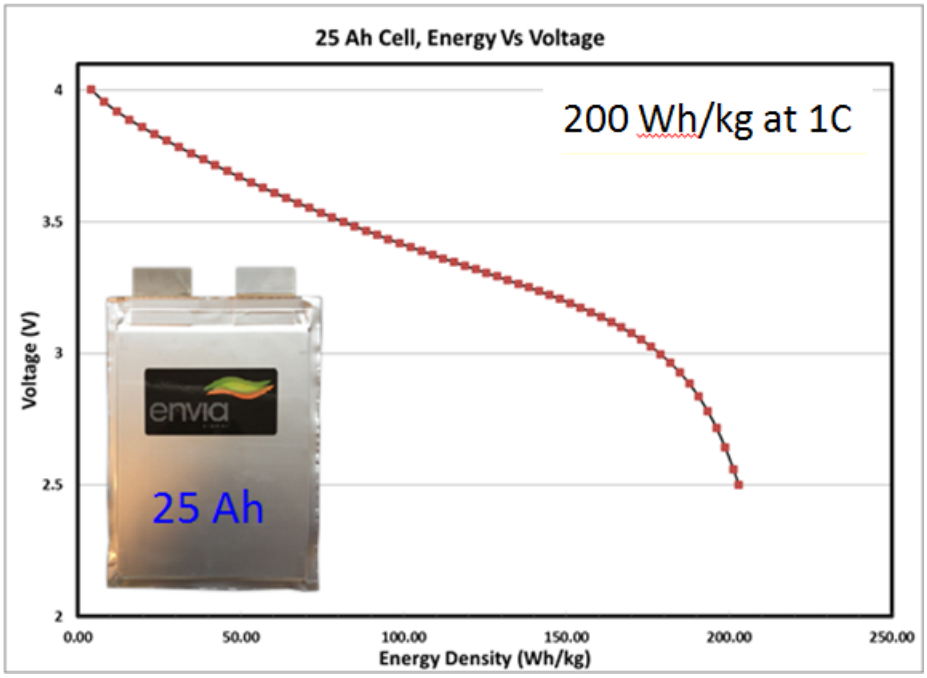


Figure IV- 155: Typical discharge curve for the HCMR™-XE based baseline cells vs. Si-SiO-C anode

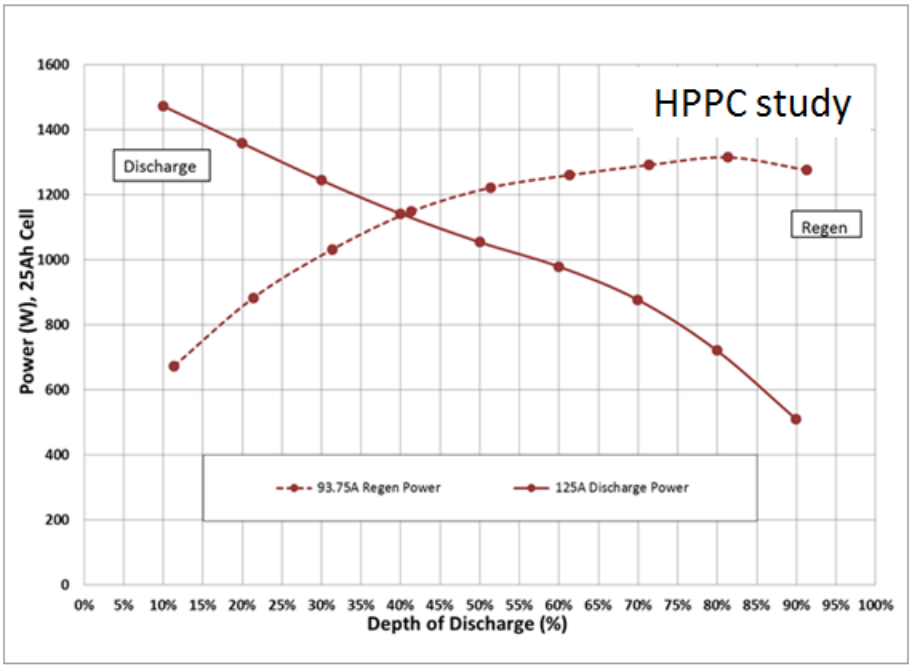


Figure IV- 156: HPPC studies for the HCMR™-XE based baseline cells vs. Si-SiO-C anode

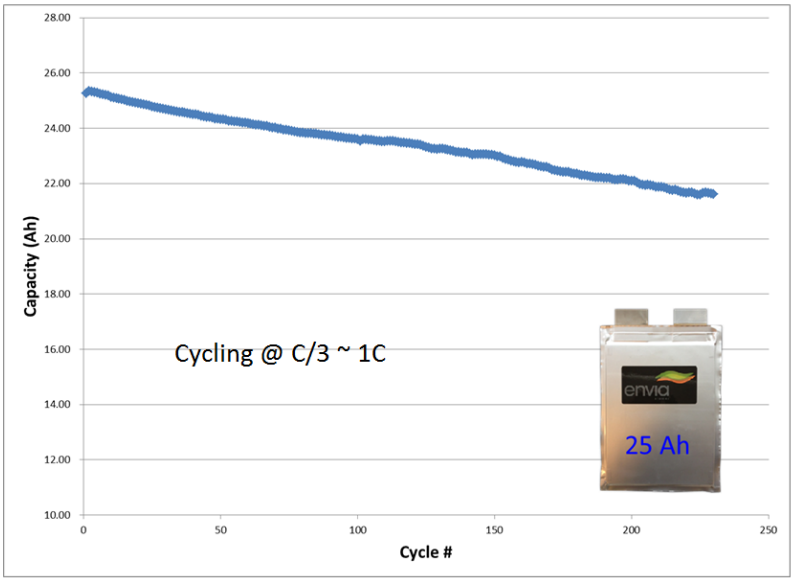


Figure IV- 157: Cycling performance for the HCMRTM-XE based baseline cells vs. Si-SiO-C anode

## Conclusions and Future Directions

One of the major findings from this project is that the DC-R affecting the usable energy of the Li-rich NMC cathode material is more dependent on the bulk composition rather than the suface modification. Envia has developed a composition from the HCMR™-XE family to meet the DC-R goals employing its conventional solution based metal fluoride nanocoating. Different surface modifications such as ionic conductors (via PVD), electronic conductors (via solid state process) and insulators/semi-conductors (via ALD) have been shown to have almost no impact on the DC-R characteristics of Li-rich NMC materials. Development of new polymeric binders for Envia's anode material did not provide favorable results. 25 Ah cells employing HCMR™ cathode and Si-based anode met all the ABR target metrics except the cycle life. Variety of cell engineering approaches

are on-going to find the optimal design towards achieving all the ABR project goals. This learning will be applied in the final cell build which due to be submitted to INL for testing and evaluation.

## References


1. Martha, et al, "Solid electrolyte coated high voltage layered-layered lithium-rich composite cathode: $Li_{1.2}Mn_{0.525}Ni_{0.175}Co_{0.1}O_2$", *J. Mater. Chem. A*, 2013, **1**, 5587-5595


## FY 2015 Publications/Presentations

1. "High Energy Lithium Batteries for PHEV Applications", ES211_venkatachala_2015_p, US DOE Vehicle Technologies Program Annual Merit Review, AMR, 2015.

# IV.D.5 High Energy, Long Cycle Life Lithium-Ion Batteries for EV Application (PSU)

## Objectives

Demonstrate a 2.5 Ah prismatic Li-ion battery cell capable of:

- an energy density of 330 Wh/kg (770 Wh/L) at C/3 rate.
- a power density of 1600 W/L while maintaining an energy density above the DOE PHEV goal of 200 Wh/kg.
- a long cycle life with 95% capacity retention in 500 cycles at C/3 and 1C rate at 80% depth of discharge (DOD).

### Project Details

**Dr. Christopher Johnson (NETL Program Manager)**
Recipient: Pennsylvania State University

**Donghai Wang (Project Manager)**
328 Reber Building
University Park, PA 16802
Phone: 814-863-1287; Fax: 814-863-4848
Email: dwang@psu.edu

Subcontractor: University of Texas at Austin
Subcontractor: EC Power
Collaborator: Lawrence Berkley National Laboratory
Collaborator: Argonne National Laboratory

Start Date: September 30, 2013
Projected End Date: September 30, 2015

## Technical Barriers

The development of the proposed Li-ion battery presents technical barriers for each of the system's components: anode, cathode, binder, and electrolyte. Although silicon-alloy anode materials have shown remarkable capacities above 2000 Ah/g, the silicon will undergo large volume change (~400%) upon lithiation/delithiation. In effect, other issues arise including unstable SEI, pulverization and aggregation of the Si particle, and low coulombic efficiency (less than 99.8%) compared with graphite (higher than 99.9%). Furthermore, layered oxide cathode materials will need to overcome a relatively low practical capacity (~170 mAh/g), along with other issues such as chemical and structural instability, transition metal dissolution, and transition metal redox potential changes. The technical barriers for the anode and cathode may partially be addressed with an appropriate binder/electrolyte; however the chemical composition of these components must be optimized to ensure compatibility.

## Technical Targets

- Anode:
- Continue optimization of Si-graphite anode and scale to 100g.
- Cathode:
- Surface-coated, Ni-rich layered oxide cathode with 220 mAh/g capacity, 95% capacity retention after 300 cycles at C/3.
- Electrolyte:
- Develop a suitable electrolyte and/or additive for silicon and Ni-rich high capacity electrodes.

## Accomplishments

- **Anode.** PSU Si materials have been scaled up to 100 g per batch. Si-based anodes with high flexibility and high areal capacity, ~3.5 mAh/cm$^2$, have been developed and tested with relatively stable performance. The influence of precycling and prelithiation on the cycling performance in full cells were investigated. The study on full cell degradation mechanism show that precycling and prelithiaiton which could improve the SEI layers of Si-based anode materials play key roles in full cell cycling performance.
- **Cathode.** $Li_2ZrO_3$ coated $LiNi_{0.7}Co_{0.15}Mn_{0.15}O_2$ cathodes have been prepared by sol-gel and precipitation methods.
- The post-treatment conditions on concentration-gradient samples have been further optimized to obtain improved electrochemical performance. Coin-type full cell with the concentration-gradient sample shows good cycling performance, with 73% capacity retention for 500 cycles with an areal

capacity of ~3.1 mAh/cm$^2$. Pouch-type full cell with the concentration-gradient sample shows a reasonable specific capacity and excellent cycle retention of 96% for 200 cycles.

- **Prelithiation.** Scalable SLMP coating is developed with simple solution processing method. A polymer solution systeme is developed for SLMP coating. Long-sustained, uniformly dispersed SLMP suspension has been achieved.
- The effect of SLMP is demonstrated through graphite/NMC and SiO/NMC full cell.
- **Electrolyte.** New electrolyte additive Triethyl phosphite (TEP) and Tris(2,2,2,-trifluoroethyl) phosphite (TTFP) were used as an additive for the Ni-rich cathode. New fluorinated electrolyte system were designed and investigated for the Ni-rich cathode. New batch Si anodes from PSU were tested in ANL.

## Introduction

With a relatively high energy density and long lifespan, Li-ion batteries have become the state-of-the-art technology for plug-in hybrid electric vehicle (PHEV) and electric vehicle (EV) applications. However, mainstream adoption of the current generation of PHEVs and EVs has been hindered by high-cost batteries, limited travelling distance, and restrained vehicle size. In effect, research in the field of battery chemistry and material science has focused on the development of complementary battery components that will significantly improve the practical performance of the Li-ion battery and optimize it for transportation applications. Within the last decade, these primary components - cathode, anode, binder, and polymer - have been enhanced through careful modification in chemical composition, although often independent of each other. In this effect, it is clear that realizing a Li-ion battery suitable for the rising demands in transportation applications can only be achieved when research on individual battery components are performed in conjunction.

## Approach

The development of a high energy/power Li-ion battery suitable for PHEV and EV applications can be accomplished through the expertise and experience of a multiple organization team with facilities and collaboration spanning Penn State University (PSU), University of Texas at Austin (UT-Austin), Lawrence Berkley National Laboratory (LBNL), Argonne National Laboratory (ANL), and the industrial partner EC Power (ECP). PSU and UT-Austin will use extensive knowledge in the state-of-the-art anode and cathode materials, respectively, to develop optimized and compatible electrodes in the Li-ion battery. Innovative polymer binders and electrolytes solutions will be developed by LBNL and ANL, respectively, based on their well-established expertise in this area. Finally, the culmination of these state-of-the-art battery components will be realized through the intelligent cell design and fabrication techniques of ECP.

## Results

**Anode.** In this quarter we have investigated the influence of prelithiation parameters on performance of our Si electrodes in full cells. New electrodes with a target capacity of 1000 mAh/g (based on total mass of the electrode) were developed using the low surface area PSU Si. Figure IV- 158 shows the cycling stability of these electrodes in half cell. An actual capacity of 600 mAh/g and a retention of 89% can be obtained after 140 cycles (Figure IV- 158a). The high mass loading gives a high areal capacity greater than 3 mAh/cm$^2$ (Figure IV- 158b). The 1$^{st}$ cycle coulombic efficiency is 66.9%. However, they exhibit high cycling coulombic efficiency of 99.7% after 19 cycles and maintain at that level afterward (Figure IV- 158c). In addition, they have good flexibility examined by deflection test. These electrodes were used as anodes and commercial NCM was used as cathode materials.

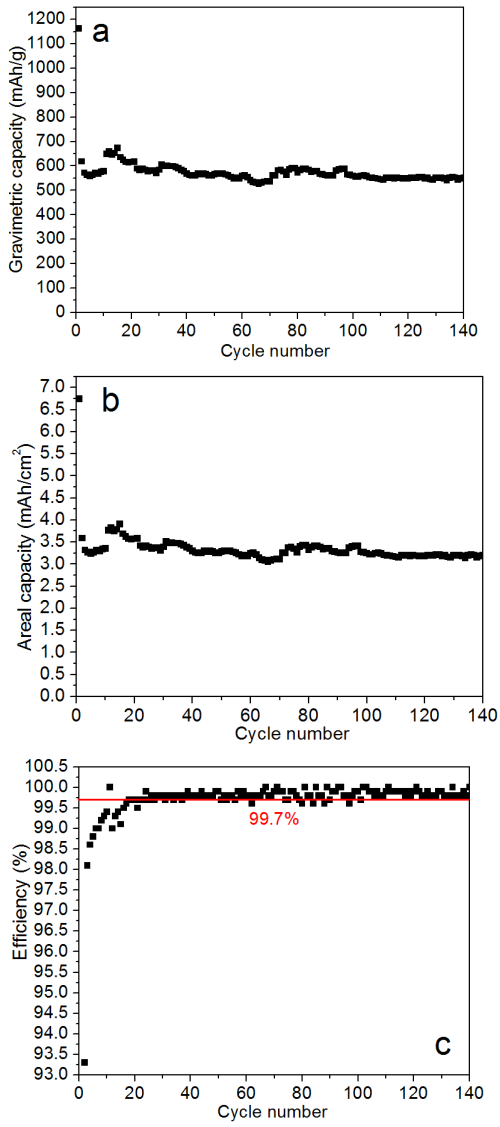


**Figure IV- 158: (a) and (b) Cycling performance, and (c) coulombic efficiency (from the 22nd cycle) of the PSU Si electrodes with 1000 mAh/g targeted capacity based on the whole electrode**

Figure IV- 159 shows the performance of a full cell constructed of the fresh Si anode coupled with the NCM cathode. The N/P ratio is around 1.2. The 1st cycle efficiency is 57.8%, lower than that in half cell, probably due to the presence of the cathode. Unlike the stable cycling performance of half cell, the full cell shows noticeable degradation along cycling. A capacity retention of 60.8% is obtained after 50 cycles (based on the 2nd charge capacity). This is associated with lower cycling efficiencies. In particular, the efficiencies of the first 20 cycles are much lower in comparison with half cells. It is believed that the difference in cycling stability and efficiency between half and full cells is caused by the unstable SEI layer of Si and the difference in amount of lithium source. While the lithium source can be practically unlimited in half cells, it is fixed by the cathode in full cells. With the continuous consumption of lithium due to unstable SEI layers of Si, less lithium can be used in full cells, leading to capacity fading.

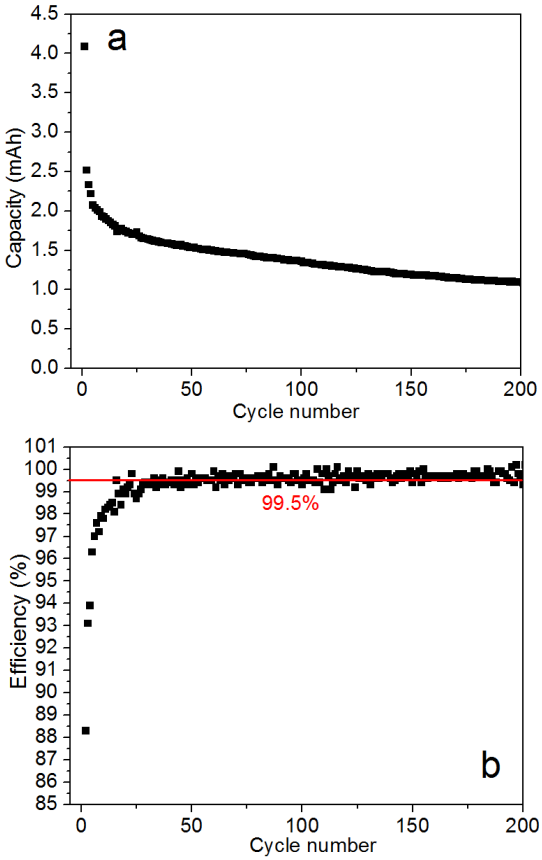


**Figure IV- 159: Cycling performance (a) and coulombic efficiency (b) of the full cell in coin cell format constructed of the fresh Si anode and NCM cathode**

To stabilize the SEI layers of Si, prelithiation has been carried out by cycling Si anodes in half cells. The precycled Si anodes (delithiated) were then coupled with fresh cathodes to form full cells. Different numbers of precycles have been done—5, 10 and 20. To provide more lithium source, an anode was lithiated to 0.2 V after 20 cycles and used for a full cell.

After 5 and 20 cycles in a half cell, the efficiency of the Si anode increased to 98.7% and 99.8%, respectively. Figure IV- 160 and Table IV- 24 show the performance of the full cells constructed of the Si anodes precycled for 5 times, 20 times and 20 times with prelithiation to 0.2 V (corresponding to 36.5%-39% lithiation). Data from Figure IV- 159 was also included to make the comparison clear. It is clear that the 1st cycle efficiency was improved with longer precycles. This is due to improved SEI layers of Si anodes precycled in half cells. In addition, the cycling stability and efficiency of resulting full cells were improved. It is worth noting that the performance was further improved by

prelithiation after precycles which provided more lithium source. The comparison made here is strong evidence that the failure mechanism of Si-based full cells is largely caused by unstable SEI layers of Si anodes which continuously consume lithium source limited by cathodes. The performance of full cells can be drastically improved by precycling/prelithiating Si anodes.

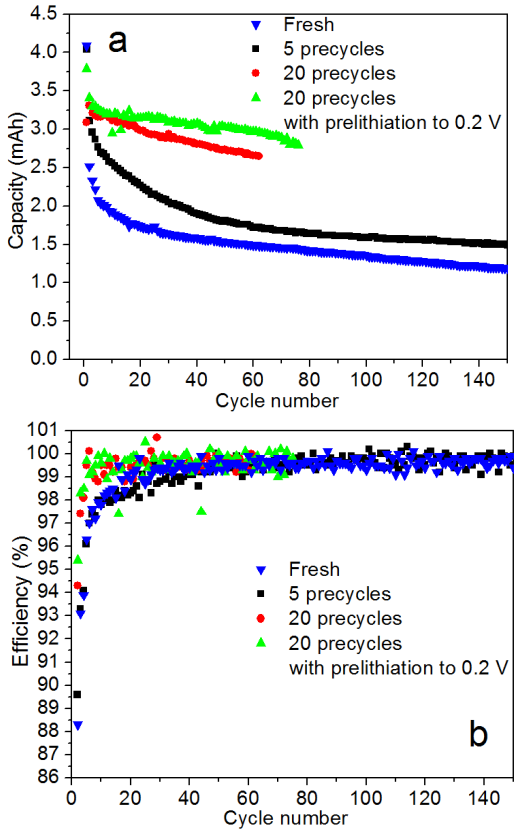


Figure IV- 160: Cycling performance (a) and coulombic efficiency (b) of full cells in coin cell format constructed of different precycled Si anodes and NCM cathodes

**Cathode.**

**1. Localization and visualization of the surface electrochemical degradation of $LiNi_{0.7}Co_{0.15}Mn_{0.15}O_2$**

To date, extensive work has been conducted for the visualization of the surface deterioration of high-voltage cathode materials in lithium-ion batteries. In upper Figure IV- 161, HAADF-STEM images reveal the local structure of the cycled NCM71515 ($LiNi_{0.7}Co_{0.15}Mn_{0.15}O_2$) primary particle surface (18–20 µm). A clear boundary is shown between the pristine layered $R\bar{3}m$ structure and the irreversibly formed rock-salt $Fm\bar{3}m$ phase during cycling, with distinctly differing thickness along different crystal orientations. It is expected that the rock-salt phase formation is promoted along the lithium diffusion pathway in the layered matrix of Ni-rich layered oxides. Of particular interest, the surface organic deposits due to electrode-electrolyte reactivity are largely nonexistent in the HAADF-STEM images due to their highly sensitive nature towards the high-energy electron-beam irradiation. Important also is a considerable difficulty in the elimination of ambient air-exposure-induced artifacts during sample preparation for high-resolution STEM. Consequently, illustrative TOF-SIMS high-resolution mappings were collected on the same sample as a function of etching depth, as seen in lower Figure IV- 162. In the figure, maps of the electrode along the *x*-*y* planes demonstrate that the surface of the particles (represented by the $NiO^-$ fragment), initially entirely covered by the degradation-induced chemical functional groups (represented by $F^-$), gradually emerges upon $Cs^+$ etching. Notably, corrosion pits on particles appear during sputtering. This implies that the attack of acidic species at the surface in all likelihood occurs in a highly localized manner, with the penetration sometimes reaching more than tenfold in depth of the average "thickness" of the corrosion products.

**Table IV- 24: Summary of performance of full cells with different precycled Si anodes**

| Cell | Fresh | 5 precycles* | 20 precycles | 20 precycles and prelithiated to 0.2v |
|---|---|---|---|---|
| 1st cycle efficiency | 57.8% | 74.1% | 84.9% | 80.6% |
| 2nd cycle charge capacity (mAh) | 2.517 | 3.11 | 3.31 | 3.41 |
| 50th cycle charge capacity (mAh) | 1.53 | 1.81 | 2.74 | 3.03 |
| Capacity retention at 50th cycle | 60.8% | 58.2% | 82.8% | 88.9% |
| Average efficiency (2nd to 50th cycle) | 98.49% | 98.22% | 99.33% | 99.50% |

Note: The voltage window for the full cell with the anode precycled for 5 times is 4.2 to 3 V while 4.2 to 2 V for the other cells.

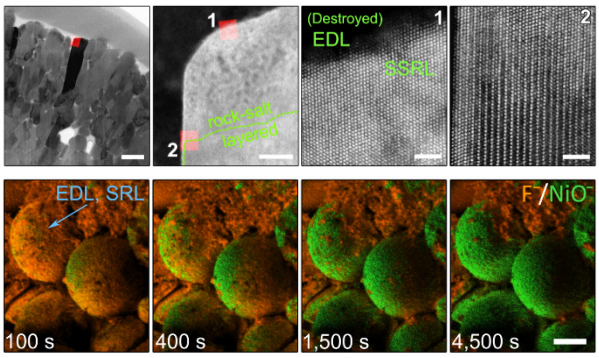


**Figure IV- 161: Visualization of the surface electrochemical degradation of NCM71515 electrodes (18–20 µm) after 100 cycles at room temperature. Upper: HAADF-STEM images showing the local structure at the primary particle surface; the scale bars are 400, 20, 2, and 2 nm from left to right; lower: TOF-SIMS mappings demonstrating the composite electrode surface with cathode secondary particles, additive carbon, and polymeric binder; the scale bar is 10 µm**

Figure IV- 162 illustrates the TOF-SIMS depth profiles of the 18–20 µm samples cycled for 100 times. In the upper figure Figure IV- 162, profiles of secondary ions of interest, such as $LiF_2^-$, are referenced to those obtained from the pristine electrode, while the normalized raw profiles are shown for a comparison in the lower portion. Evidently, the depth profiles reveal the complex multi-layer characteristics of the surface chemistry on Ni-rich layered oxide electrodes during high-voltage electrochemical operation, as proposed theoretically in literature. Importantly, we notice degradation products including: (i) LiF, represented by $LiF_2^-$, appearing mostly localized at the very surface of the electrode, the first layer, and also rich in the subsequent second layer; (ii) $MnF_2$, signified by $MnF_2^-$, showing the highest concentration in the second layer; and (iii) NiO, indicated here by the $NiO^-$ to $Ni^-$ ratio, emerging in the third layer. These three "layers" correspond to the various aspects of electrochemical degradation at the surface of Ni-rich layered oxide electrodes in the common EC-DEC/$LiPF_6$ solutions: (i) deposition of various solvent and salt decomposition products from the electrolyte, (ii) active mass dissolution aggravated by acidic species attack (*e.g.*, HF – generated in the presence of trace amount of electrolyte impurities such as $H_2O$), and (iii) intrinsic surface structural reconstruction from the layered to "rock-salt" phase due to destabilized Ni-ion migration towards neighboring Li layers in the highly delithiated state. As a consequence, we assign the three compounds in the upper Figure IV- 162 accordingly, as LiF is a well-known major salt decomposition product; $MnF_2$ arises through HF attack of Ni-rich layered oxides, during which LiF is also generated; NiO, on the other hand, is the main rock-salt phase. In this work, we refer to the aforementioned three "layers" as an electrolyte deposition layer (EDL), a surface reaction layer (SRL), and a surface structural reconstruction layer (SSRL), respectively, as shown in upper Figure IV- 162. Further, the raw profiles of $POF_2^-$ and $C_2P^-$(lower Figure IV-162), possible ionization products of $Li_xPO_yF_z$ (or $POF_3$) and $ROCO_2PF_4$, respectively, similarly exhibit peaks that line up with that of $LiF_2^-$ in EDL. This is anticipated since both of them are known surface deposits from the electrolyte breakdown. Detailed characterization and quantification of these three "layers" using TOF-SIMS, XPS, and HAADF-STEM will be presented in the next quarterly report.

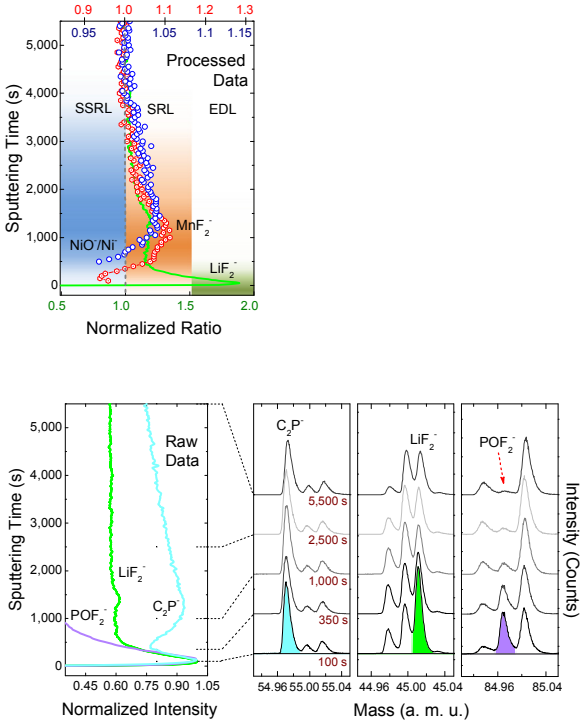


**Figure IV- 162: TOF-SIMS depth profiles of various chemical species from the surface of $LiNi_{0.7}Co_{0.15}Mn_{0.15}O_2$ composite electrodes (18–20 µm) after 100 cycles at room temperature. Upper: processed data referenced with the pristine electrode (not shown here); and lower: raw data (left) with the evolution of the corresponding secondary ion mass spectra as a function of sputtering time (right)**

## 2. Benefits of $Li_2ZrO_3$ coating on $LiNi_{0.7}Co_{0.15}Mn_{0.15}O_2$ particles

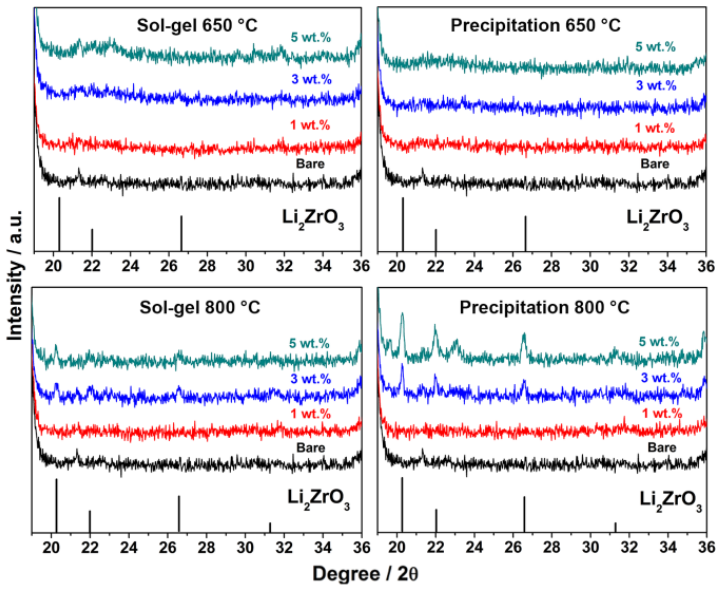


**Figure IV- 163: Powder X-ray diffraction patterns of $Li_2ZrO_3$-coated $LiNi_{0.7}Co_{0.15}Mn_{0.15}O_2$ samples prepared by sol-gel and precipitation methods**

To enhance the surface stability of the Ni-rich $LiNi_{0.7}Co_{0.15}Mn_{0.15}O_2$ cathode, $Li_2ZrO_3$ has been coated on the particles' surfaces as a protective agent by two methods: sol-gel and precipitation. Inspired by the thermodynamic mechanisms of solid-state diffusion of transition-metal ions at high temperatures, two sintering temperatures of 650°C and 800°C were chosen to investigate the possible bifunctional effects of doping and coating under different sintering conditions. As shown in (Figure IV- 163) both the samples prepared by sol-gel and precipitation methods sintered at 650°C present less crystallinity of the $Li_2ZrO_3$ phase compared to the counterparts sintered at 800°C, indicating amorphous structure formed at a lower temperature. In particular, the sample prepared by precipitation (800°C) shows the best crystallinity of the $Li_2ZrO_3$ phase, indicating an evident formation of protection layer on the surface of the secondary particles in addition to a partial $Zr^{4+}$ doping in the crystal lattice. In comparison, apparently the $Li_2ZrO_3$ phase formed at 650°C is less crystallized at the particles' surfaces but without strong doping effects into the lattice. Figure IV- 164 presents a comparative cross-sectional SEM-EDX mapping of the Zr element of all samples. Two observations are to be noted as important. First, the most uniform distribution of Zr at one secondary particle's surface was achieved by the precipitation method, followed by sintering at 650 °C. Second, the most uniform doping of $Zr^{4+}$ into the local lattice at one secondary particle was achieved by sol-gel method, followed by sintering at 800°C. Besides, the other two preparation conditions cause an aggregation of Zr to a certain extent at one secondary particle's surface. The reason for such variations in Zr distribution could be understood as follows: first, sol-gel leads to surface coating of $Li^+$ and $Zr^{4+}$ agents on primary particles while precipitation leads to the secondary particle's coating; second, 650 and 800°C sintering temperatures result in different levels of elemental diffusion across the particles. Figure IV- 165 shows the capacity retention during 100 cycles of all samples. Apparently, the $Li_2ZrO_3$-coated $LiNi_{0.7}Co_{0.15}Mn_{0.15}O_2$ cathodes prepared by precipitation and after sintering at 650°C provides the best cyclability compared to others, *i.e.*, 92.2, 92.8, and 97.7% capacity retention with respect to 1, 3, and 5 wt.% of coating agent. This observation agrees well with the conclusion from SEM-EDX mapping that the most uniform coating of Zr on one secondary particle could provide the most efficient protection from corrosive electrolyte. These experiments compare different coating methods and identified the most efficient one to improve the cyclability of the Ni-rich layered cathode. The coating agent $Li_2ZrO_3$ is not unique as it could be extended to others.

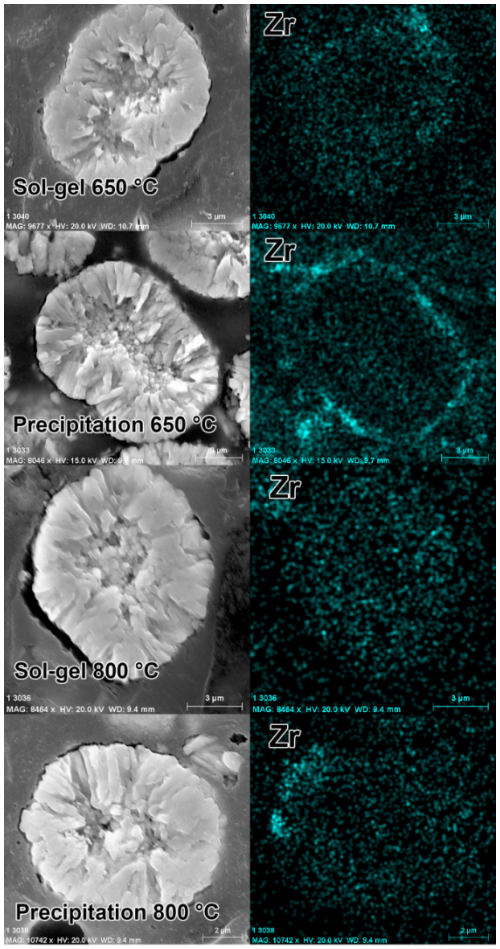


Figure IV- 164: Cross sectional SEM-EDX mapping of the Zr element in the $Li_2ZrO_3$-coated $LiNi_{0.7}Co_{0.15}Mn_{0.15}O_2$ samples prepared by sol-gel and precipitation methods

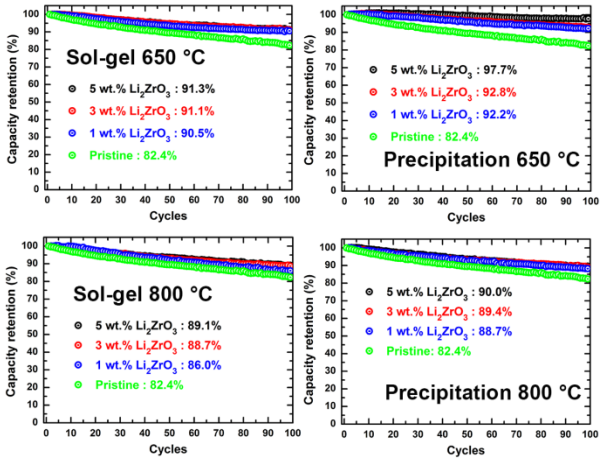


Figure IV- 165: Capacity retention of the $Li_2ZrO_3$-coated $LiNi_{0.7}Co_{0.15}Mn_{0.15}O_2$ cathodes prepared by sol-gel and precipitation methods. Cycling conditions: 3.0 – 4.5 V, C/3 rate, 25 °C

### 3. Double coating on the $LiNi_{0.7}Co_{0.15}Mn_{0.15}O_2$ cathode with Li-rich layered oxide and aluminum fluoride

Figure IV- 166 shows a scanning electron microscope (SEM) image of the 10 µm-sized bare sample, made up of 100 - 200 nm primary particles. After the double coating process, small nano-particles are formed at the surface of the secondary particles (Figure IV- 166b-d). The energy-dispersive X-ray spectroscopy (EDS) data in Figure IV- 166d indicate that the shell is composed of Mn-based Li-rich and $AlF_3$ particles. For a detailed structural analysis of the shell layer, high-resolution transmission electron microscopy (HR-TEM) and scanning transmission electron microscopy (STEM) images are shown in Figure IV- 167a-e. In Figure IV-164a, the thick coating layer, 100 - 150 nm thick, covers the pristine surface. Furthermore, Figure IV- 167b shows the clear interface between the core and shell, and the pattern obtained by fast Fourier transform (FFT) of the marked region in Figure IV- 164b matches that of the $Li_2MnO_3$ monoclinic phase (C2/m). The STEM image (Figure IV- 167c) and its filtered image (Figure IV- 167d) of the shell layer show a typical transition-metal arrangement of the $Li_{1.2}Ni_{0.2}Mn_{0.6}O_2$ phase (Figure IV- 167e), which include C2/m monoclinic phase and $R\bar{3}m$ layered phase. From these results, we can conclude that the bare material is covered by a thick $Li_{1.2}Ni_{0.2}Mn_{0.6}O_2$ surface layer with good surface coverage.

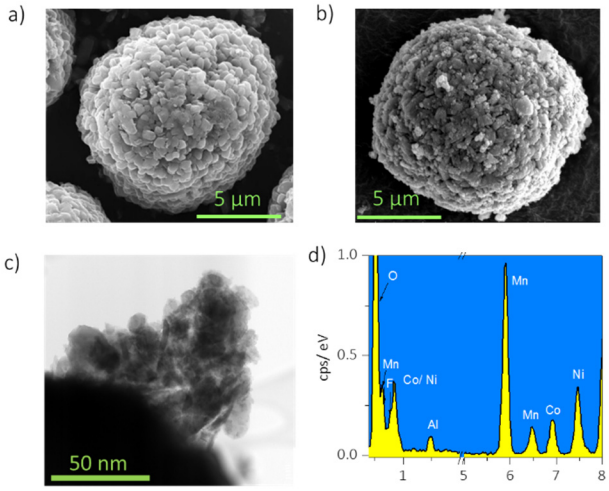


Figure IV- 166: Scanning electron microscopy (SEM) images of (a) the bare and (b) double-coated sample with lithium-rich layered oxide and $AlF_3$ (20LNM-ALF sample). (c) High-resolution transmission electron microscopy (HR-TEM) images and (d) the energy-dispersive X-ray spectroscopy (EDS) profile of the surface of the 20LNM-ALF sample

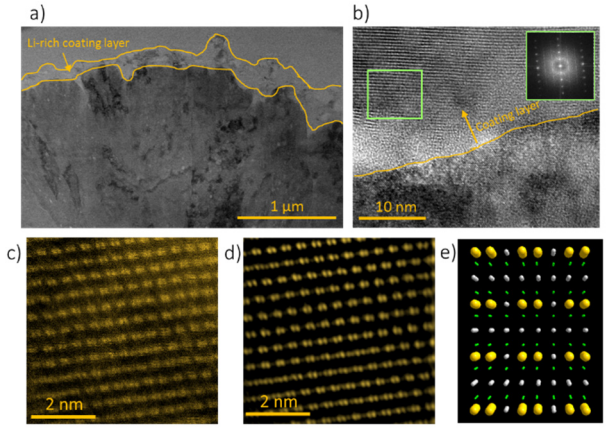


Figure IV- 167: High-resolution transmission electron micrograph of (a) the cross-sectional view and (b) the interface between core and shell of 20LNM-ALF. (Inset figure of (b) indicates a pattern of fast Fourier transform of the green square). (c) High angle annular dark field (HAADF) image and (d) the filtered image of the green square region in (b). (e) Simulated crystal structure of $Li_2MnO_3$ (C2/m) along rhombohedral [2 1 0] direction. (The balls with yellow, green, and grey respectively indicate transition metals, oxygen, and lithium ions)

### 4. Performance optimization of concentration-gradient materials

Figure IV- 168 shows the cycling performance at C/3 rate of two batches of concentration-gradient (CG) samples and a constant-concentration (CC) sample with the same transition-metal composition, $LiNi_{0.75}Co_{0.1}Mn_{0.15}O_2$. Both batch one (15 µm) and batch two (12 µm) samples are a concentration-gradient structure with a continuously decreasing Ni content from the interior to the surface and an increasing Mn content from the interior to the surface, which were developed employing a continuously stirred tank reactor. The concentration-gradient nickel-rich layered oxides with a high concentration of electrochemically inert $Mn^{4+}$ ions on the surface will exhibit improved cycling stability. Although the cell based on the CC sample retained 84% of the highest discharge value after 100 cycles, the modified batch one concentration-gradient ($1^{st}$-CG) and batch two CG ($2^{nd}$-CG) materials showed much higher capacity retentions of around 98% and 95%, respectively. The rapid capacity fade of the CC material was mainly caused by the direct exposure of a high content of the Ni ion to the non-aqueous electrolyte, resulting in a high reactivity of Ni ion with the electrolyte at high potentials, which led to the chemical decomposition of both the surface of the electrode and the electrolyte. In addition, the slightly higher capacity retention of $1^{st}$-CG sample may be due to its larger secondary particle size. However, the $2^{nd}$-CG sample with a secondary particle size of 12 µm shows higher capacity in the first 40 cycles.

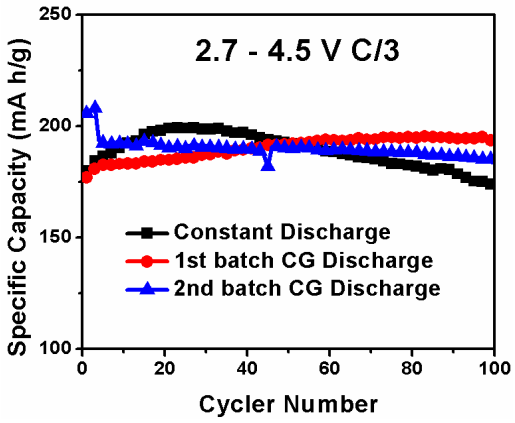


Figure IV- 168: Cycling performances of two concentration-gradient samples and constant-concentration sample with same transition-metal composition ($LiNi_{0.75}Co_{0.1}Mn_{0.15}O_2$)

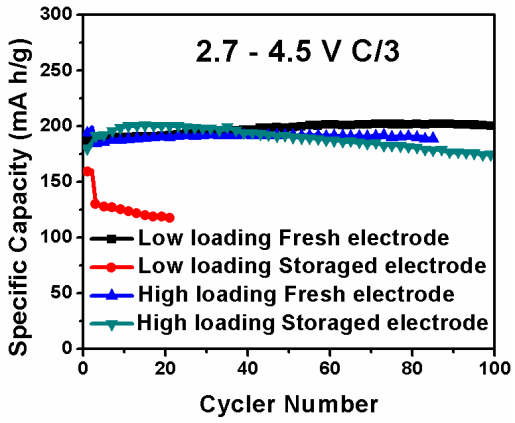


Figure IV- 169: Loading and storage effect (in air) on CG sample. Low-loading: 4 mg/cm$^2$; high-loading: 20 mg/cm$^2$; storage time: 6 months

As a high areal capacity of ~ 4 mAh/cm$^2$ is required for practical applications, we also evaluated the electrochemical performance of the 1$^{st}$-CG cathode material with thick electrode laminates with a loading of ~ 20 mg cm$^2$, as shown in Figure IV- 169. Compared to the low-loading electrode, the high-loading electrode shows slightly lower capacity and capacity retention after 100 cycles. However, the aged (6 months in air) low-loading electrode exhibits much decreased capacity and faster capacity fade. The low capacity and capacity retention may be due to the side reaction with water and $CO_2$, resulting in $Li_2O$ and $Li_2CO_3$ compounds on the surface, which has less effect on the high-loading electrode.

In order to further improve the capacity and cyclability of the concentration-gradient cathodes, a new batch of gradient material (3$^{rd}$–CG) was also obtained with optimized synthesis conditions. The SEM image of the precursors and EDS line scan profile are shown in Figure IV- 170(inset). Compared to the previous CG samples, the new CG material has a decreased Ni content of around 0.7 with an average composition of $LiNi_{0.7}Co_{0.15}Mn_{0.15}O_2$. In addition, the Ni content continuously decreases from the interior to the surface, and both Co and Mn contents increase from the interior to the surface. The electrochemical properties of the new CG sample at different lithiation conditions are shown in Figure IV- 170 (right side). Compared to the lower lithiation temperature of 750°C and a higher lithiation temperature of 800 °C, the medium lithiation temperature of 770°C shows higher capacity and superior capacity retention, indicating that a temperature of 770°C is the best lithiation condition for the new gradient samples. Since the capacity is still much lower than our project goal, further optimization will be carried out to improve its battery performance.

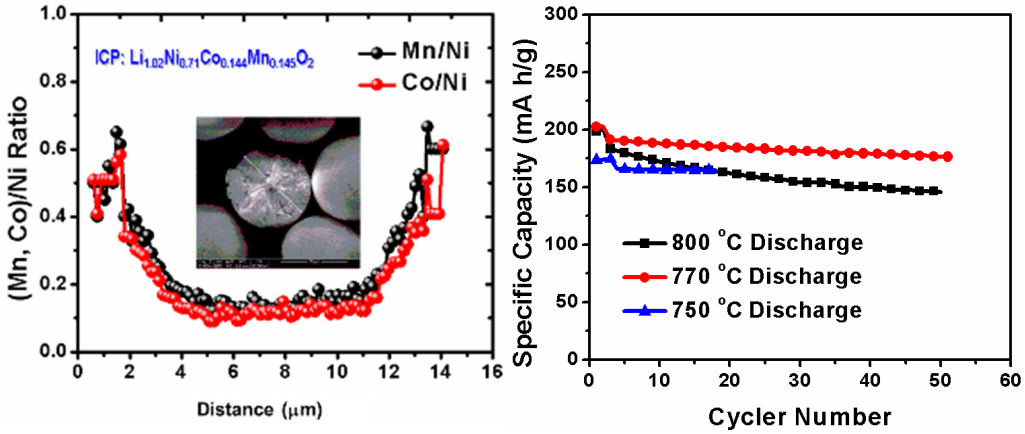


Figure IV- 170: SEM and EDS profiles of the newly prepared CG sample and electrochemical performance with different lithiation temperature

**5. Optimization of full cell**

To verify the real characteristic of the nickel-rich cathode materials, it is essential to measure the electrochemical performances in a full cell with a graphite anode. In the case of full cell fabrication, calculation of the negative and positive electrode energy density ratio (N/P ratio) is important. Figure IV- 171 shows the first and second charge discharge curves of the coin-type full cell with two different N/P ratios (0.95 and 1.05). All cells were charged to 4.4 V and discharged to 2.5 V with a constant current of C/10 rate for formation and C/3 rate for cycling. Comparing these two cells, we confirm that the optimized N/P ratio for the full cell is 1.05 which has higher areal capacity and coulombic efficiency at first cycle (73.2%) than that with a lower N/P ratio. We also measured the long-term cycling performances of these full cells during 250 cycles at C/3 rate which is shown in Figure IV- 172. As we expected, the optimized full cell shows excellent, stable cyclability during 250 cycles (94.1%). Meanwhile, the discharge capacities of another full cell (N/P ratio: 0.95) continuously increased during the initial 50 cycles and after that decreased rapidly. From these electrochemical results, we could conclude that optimization of the full cell fabrication is critical to achieve good performance.

After optimizing the N/P ratio and fabrication of the full cell, we also made the pouch-type full cell with our equipment. The electrode for the pouch-type full cell had 5 cm width and 8 cm length, which could have 35 times higher areal capacity than the electrode for the coin-type full cell. As shown in Figure IV- 173, the pouch-type full cell shows a reasonable specific capacity of 180 mAh/g at C/10 rate. The test condition for the pouch-type full cell was the same as that for the coin-type full cell. After the formation cycles, we measured the long-term cycling performances of our pouch-type full cell during 200 cycles at C/3 rate (Figure IV- 174). This cell showed excellent cycle retention of 96% for 200 cycles. We believe this remarkable cycle performance will continue for a greater number of cycles.

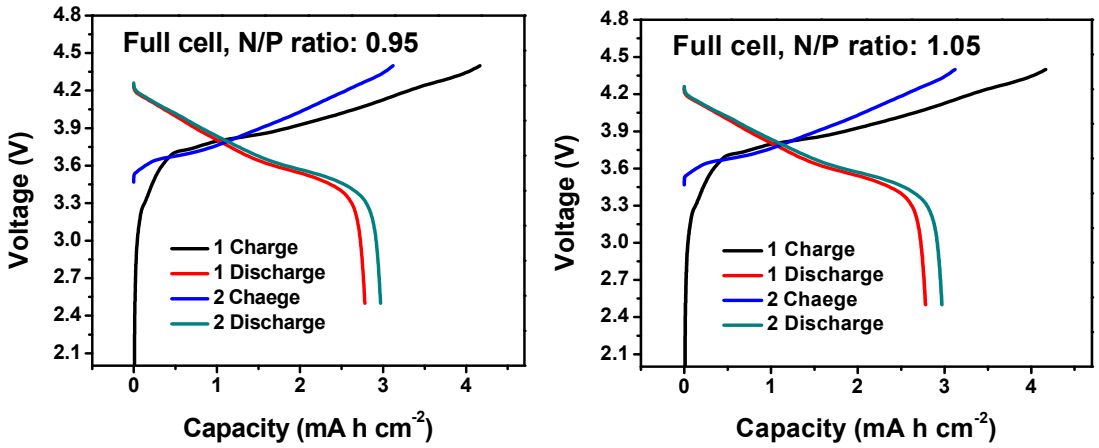


**Figure IV- 171: First two charge/discharge curves of the coin-type full cell with graphite anode with different negative and positive electrode energy density ratios of (a) 0.95 and (b) 1.05. All cells were charged to 4.4 V and then discharged to 2.5 V with a constant current of C/10 rate**

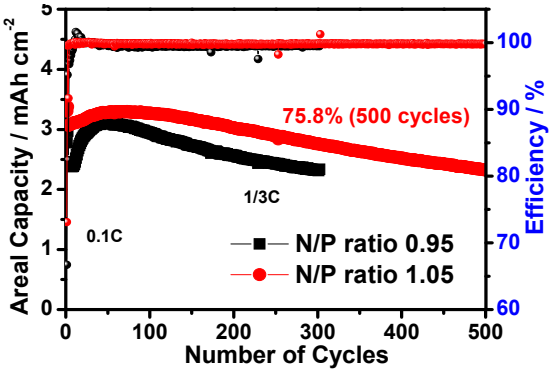


Figure IV- 172: Comparison of the long-term cycle performances of coin-type full cells with different N/P ratios. All cells were charged to 4.4 V and then discharged to 2.5 V with a constant current of C/3 rate

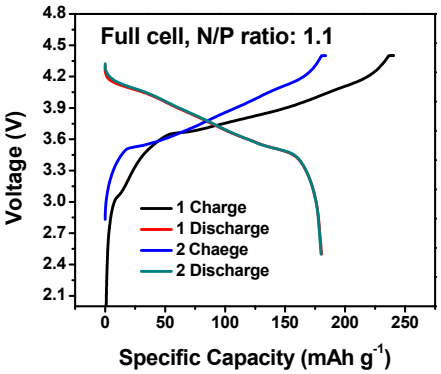


Figure IV- 173: First two charge/discharge curves of the pouch-type full cell with a graphite anode with negative and positive electrode energy density ratios of 1.1. The cell was charged to 4.4 V and then discharged to 2.5 V with a constant current of C/10 rate

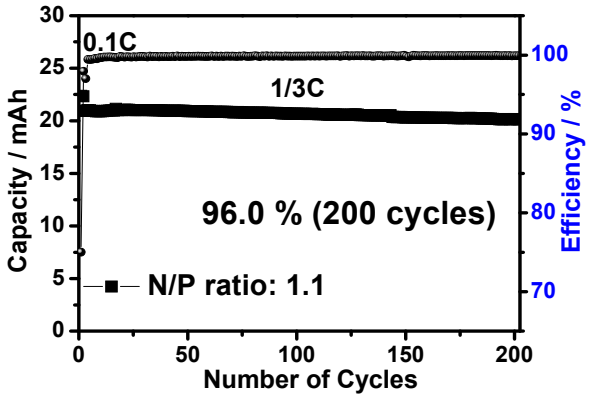


Figure IV- 174: Comparison of the long-term cycle performances of pouch-type full cells with N/P ratio of 1.1. Cell was charged to 4.4 V and then discharged to 2.5 V with a constant current of C/3 rate

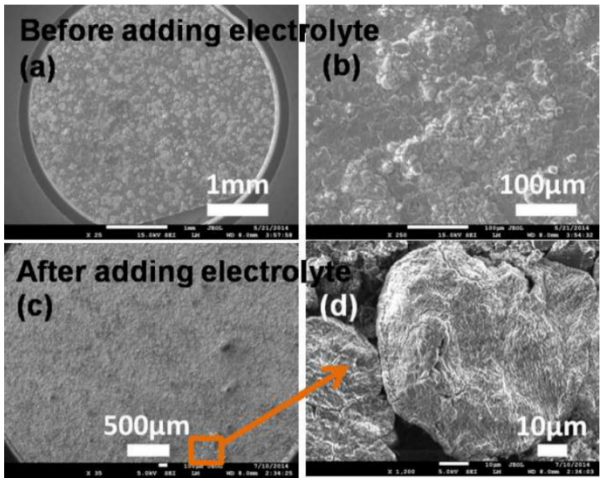


Figure IV- 175: The SEM morphology of (a), (b) SLMP coated anode surface after pressure activation and (c), (d) after immersing in electrolyte for 48 hours. The coating here uses 3% SBR solution

**Prelithiation**

The work in previous quarter established a polymer solution dispersion method to coat SLMP onto the anode electrode surface. To further optimize the coating condition for a uniform SLMP coating, as well as to disclose the mechanism for this prelithiation method, we did a detailed investigation of this coating method for SLMP prelithiation on a larger piece of anode electrode toward pouch cell application.

The SEM morphology of SLMP coated anode before and after adding electrolyte is studied in Figure IV- 175, and 3% concentration of SBR is used to demonstrate the effect of this polymer shell. By applying adequate pressure to the SLMP coated anode, most of the $Li_2CO_3$ coating of SLMP can be smashed, as shown in SEM images in Figure IV- 175 (a, b). After immersing the pressure activated, SLMP coated anode in the electrolyte for 48 hours, the prelithiated anode is observed via SEM again. All the smashed SLMP disappear from view in Figure IV- 175 (c). But when taking a closer look through high magnification SEM image, a few un-reacted SLMP particles can be found, as showed Figure IV- 175 (d). From the oblate morphology, we can suggest that these particles have been exposed to pressure, but the lithium is not directly electrically contacted with the electrode, they didn't react with the anode and electrolyte. Because SBR is well known for the high elasticity, the shell is not efficiently broken under pressure. This SBR shell on the SLMP surface prevents the electrical contact between lithium core, anode and electrolyte and lead to insufficient pressure SLMP activation.

There are two ways to eliminate the inefficient activation caused by the polymer binder shell. First, there is less chance to form a complete shell when the binder concentration is lower. But lower concentration may result into other issues, such as non-uniform SLMP dispersion; poor sustainability and poor attachment on the anode surface, etc. Second, polymer binder with less elasticity should be chosen as alternative for this application. The commercially available polystyrene (PS) is introduced. The transition temperature (Tg) is 95℃ for PS and -65℃ for SBR, which indicates that PS is more brittle and easier to break compared to SBR, which can largely help the pressure activation process. Additional, PS with high molecular weight was easily obtained, so a higher viscosity PS solution can be obtained than SBR when the concentration is the same.

SLMP slurries are made with the 1% PS, 1% SBR and 0.5% PS with 0.5% SBR solutions, respectively. The viscosity of the binder solutions with 1% PS, 1% SBR and 0.5% PS with 0.5% SBR is 4.83cP, 2.52 cP and 3.60 cP, respectively. This further gives evidence that PS with high molecular weight can lead to higher viscosity. Photo images of the SLMP suspension are taken after different time durations for 0 second, 30 seconds and 120 seconds, Figure IV- 176 (a, b and c). It showed that in all three solvents, SLMP are in uniform distribution for longer than 120 seconds. The phase separation of SLMP slurry begin to be observable after 5-6 minutes. Since this work is aimed at designing a slurry composition for continuous coating procedure performed right after the slurry is mixed, it indicates that this composition of this polymer binder can give us enough time to process the homogenously dispersed SLMP suspension with the continuous coating procedure.

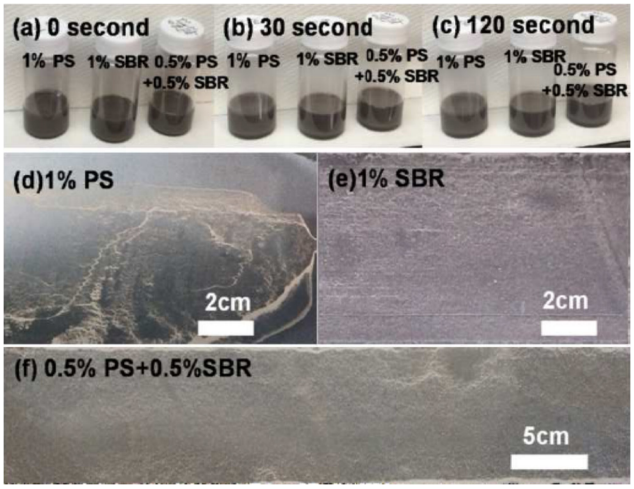


**Figure IV- 176: Photo images of SLMP suspension in 1% PS, 1%SBR and 0.5% PS with 0.5% SBR binder solution and rest for 0 second (a), 30 seconds (b) and 120 seconds (c). The photo images of SLMP loading on large piece of graphite anode surface with 1% PS (d), 1% SBR (e) and 0.5% PS with 0.5% SBR (f) binder solution**

Doctor blade method is performed for the coating with SLMP slurries in binder solution (1% PS, 1% SBR and 0.5% PS with 0.5% SBR in xylene). Photo images of SLMP coated graphite anodes with different binder solutions are used to exhibit their abilities in achieving uniform SLMP coating and good SLMP attachment. Although with three binder solutions, the sustainability of SLMP slurries is comparable and the appearances of SLMP coatings are similar before solvent evaporation. The SLMP coating with 1% PS binder solution exhibits poor attachment on the electrode surface. Most of SLMP particles tend to float to the edge instead of attaching on the anode surface after the solvent evaporates, Figure IV-176 (d). But with the 1% SBR and 0.5% PS with 0.5% SBR binder solutions, a uniform SLMP coating and good attachment of SLMP on the anode surface can be achieved after the solvent evaporates. The reason for this difference is that the transition temperature (Tg) is 95℃ for PS and -65℃ for SBR. The glass transition temperature is the temperature below which the polymers are in glass phase and the polymer structure is rigid. Therefore, at room temperature (25℃), the PS is in brittle glassy state, and can't act as soft glue; but the SBR is in soft, flexible rubbery state, and can act as good glue to fix SLMP on anode surface. The good attachment of SLMP with SBR binder benefits from the high flexibility of SBR chemical structure. In the case of 1% PS without SBR, the poor SLMP attachment is caused by the rigid PS structure.

The flexible SBR can help achieve a good SLMP attachment, while the rigid PS can help achieve much easier pressure activation. Therefore, with the overall consideration of achieving long sustained SLMP slurry, uniform SLMP coating, good SLMP adhesion and easy activation, the best composition of binders and solvent combination is 0.5% PS with 0.5% SBR binder in xylene solution for the processing method, and the superb coating effect is shown in Figure IV- 176 (f).

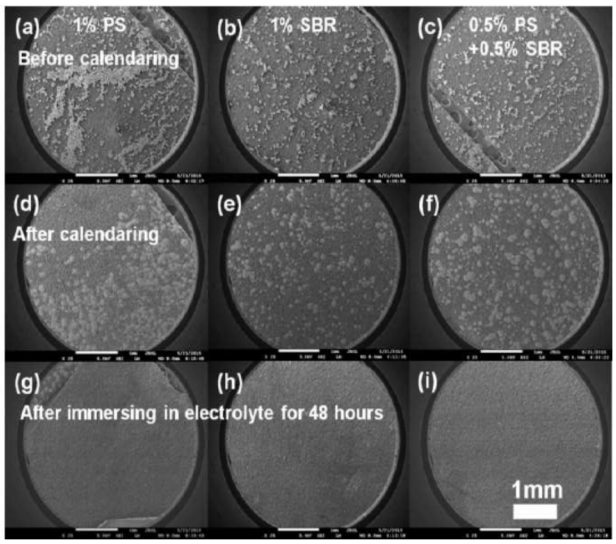


**Figure IV- 177: The SEM images of SLMP loading on graphite surface before, after calendaring and after immersing in electrolyte for 48 hours with 1% PS (a, d, g), 1% SBR (b, e, h) and 0.5% PS with 0.5% SBR (c, f, i) binder solution**

Three sets of binder solution (1% PS, 1% SBR and 0.5% PS with 0.5% SBR) are introduced to optimize the binder composition for easier pressure activation. The SEM images of SLMP loading on graphite surface before, after calendaring and after immersing in electrolyte for 48 hours with 1% PS, 1% SBR and 0.5% PS with 0.5% SBR binder solutions are shown in Figure IV- 177. Uniform SLMP coating is observed for SLMP coating with 1% SBR and 0.5% PS with 0.5% SBR binder solutions, Figure IV- 177 (b, c). The SLMP are smashed on the graphite surface after calendaring and the anodes have similar morphology with different binder solutions, Figure IV- 177 (d-f). After the calendared electrodes are immersed in the electrolyte for 48 hours, all the smashed SLMP particles disappear from SEM view. Almost none of the residual SLMP similar to Figure IV- 175(d) is observed under the high magnification SEM observation for SLMP coating with 1% PS solution and 0.5% PS with 0.5% SBR solution, Figure IV- 177 (g, i). This indicates that the optimized binder solutions, which partially or totally use PS as polymer binder, have positive effect in achieving high pressure activation efficiency.

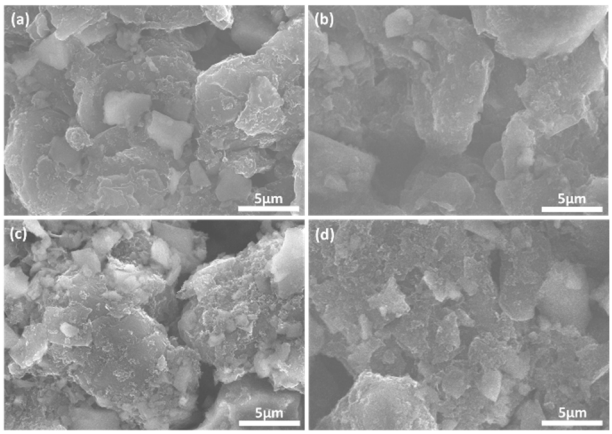


**Figure IV- 178: SEM characterization of pristine Si anode from PSU. (a) PSU_600_60. (b) PSU_600_80. (c) PSU_800_60 and (d) PSU_800_80**

Thus, the above study showed that SBR solution enables a uniform distribution of SLMP coating, PS helps the activation of SLMP afte electrolyte addition. 0.5% SBR and 0.5% PS co-solution is proved to be an ideal polymer solution system for the application of SLMP tow

**Electrolyte.** With the new batch of anodes from PSU, PSU_600_60, PSU_600_80, PSU_800_60 and PSU_800_80, we investigated the effect of 0.5% *N, N*-diethyltrimethylsilylamine as an additive in the baseline electrolyte ($LiPF_6$ in EC/EMC=3/7 in weight ratio with 10wt.% FEC) as the cosolvent. The cathode half cell using baseline electrolyte and baseline+0.5% additive were tested. The voltage window was set from 0.001V to 1.5V at room temperature. The first formation cycle was under the rate of 0.1C and the rest of cycling life was tested under 0.5C. SEM image of the pristine anode electrodes are shown in Figure IV- 178 and no obvious morphology difference was observed.

The cycling performance of PSU_600_60 and PSU_600_80 are shown in Figure IV- 179a, and the cycle life of PSU_800_60 and PSU_800_80 are shown in Figure IV- 179b. All of the electrodes showed similar capacity retention. The increasement of the capacity in the first 20 cycles should be caused by a SEI formation and the activation of the Si particle process. The Coloumbic efficiency of the four electrode cells is stable on 99.8% after the first 20 cycles. The Si-Graphite anode from ANL CAMP also shows a similar cycling data as we pervious reported.

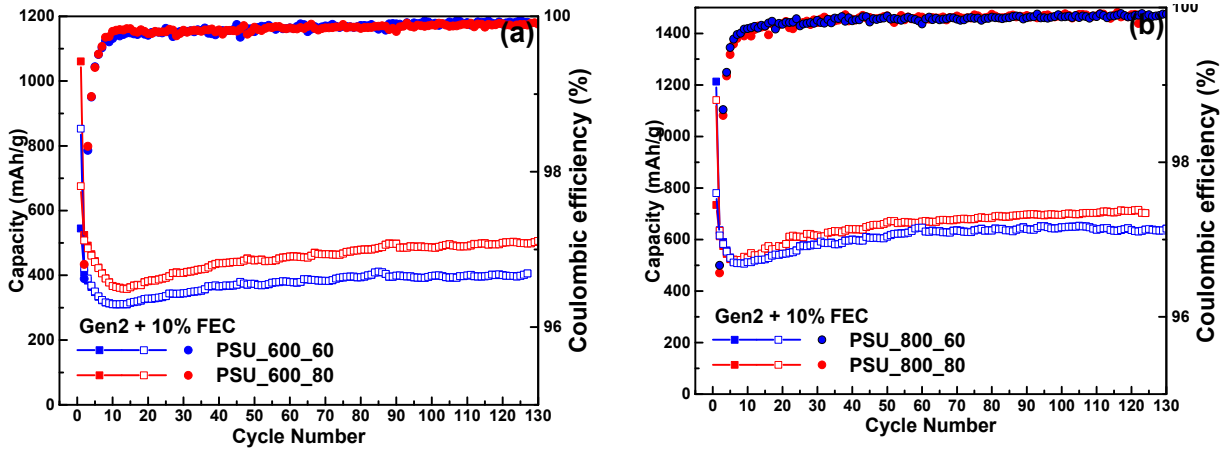


Figure IV- 179: Capacity retention and coulombic efficiency of PSU anode cathode /Li cells with baseline electrolyte (a) PSU_600_60 and PSU_600_80. (b) PSU_800_60 and PSU_800_80

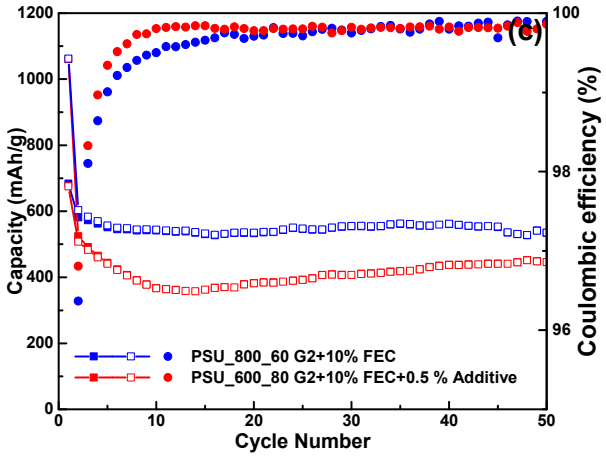


Figure IV- 180: Capacity retention and coulombic efficiency of PSU_600_80 cells with baseline electrolyte and additive

The cycling data of PSU_600_80/Li cells with 0.5% N,N-diethyltrimethylsilylamine as additive is improved over the baseline cell as shown in Figure IV- 180, indicating the more robust SEI formation by the new additive suppressing the parasitic reactions on the silicon particle surface.

For the cathode side, NCM523 from ANL CAMP was selected for the electrolyte addtive and cosolvent study.

Figure IV- 181a shows the first cycle's voltage profile of the NCM523 half cell at rate of 0.1C. With increasment of the cut off voltage from 4.2V to 4.6V, 20% more capacity is achieved. Figure IV- 181b, c and d showed the cycle life of the NCM523/Li half cell with different cut off voltages with a Gen 2 electrolyte. The half cells cannot be cycled for 60 cycles, which is caused by the Li dendrite. To avoid the impact of the Li metal, a NCM523/graphite full cell was used to investigate the effect of the electrolyte additive and cosolvent.

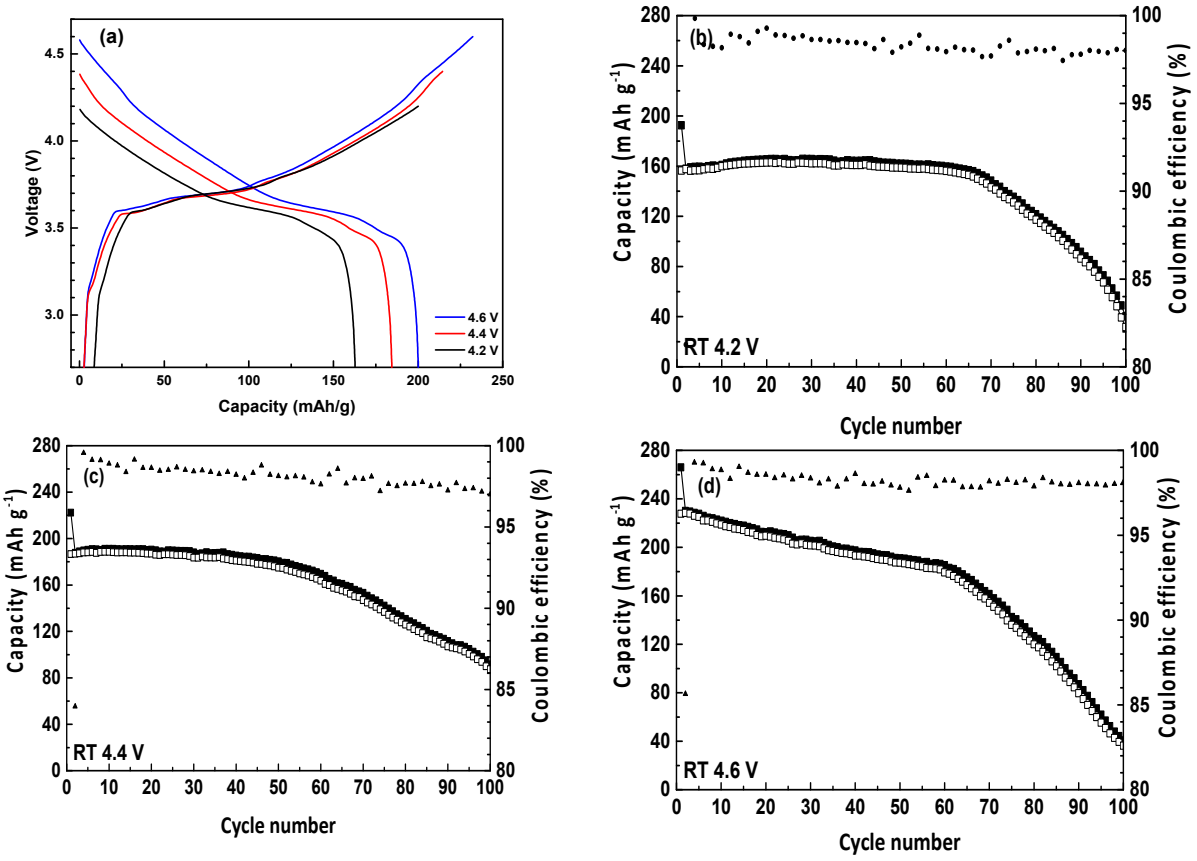


**Figure IV- 181: Electrochmeial performance for the $LiNi_{0.5}Mn_{0.3}Co_{0.2}O_2$/Li half cell. (a) Voltage profiles for the half cells in Gen 2 electrolyte in different cut off voltage (b) cycle life at 4.2V cut off voltage (c) cycle life at 4.4V cut off voltage (d) cycle life at 4.6V cut off voltage**

Figure IV- 182 gives the result of $LiNi_{0.5}Mn_{0.3}Co_{0.2}O_2$/graphite cells were cycled in Gen 2 electrolyte with different cut off voltage. The initial capacity with a 4.6V cut off voltage is 10% higher than that of 4.5 V. However, the capacity retention is poor.

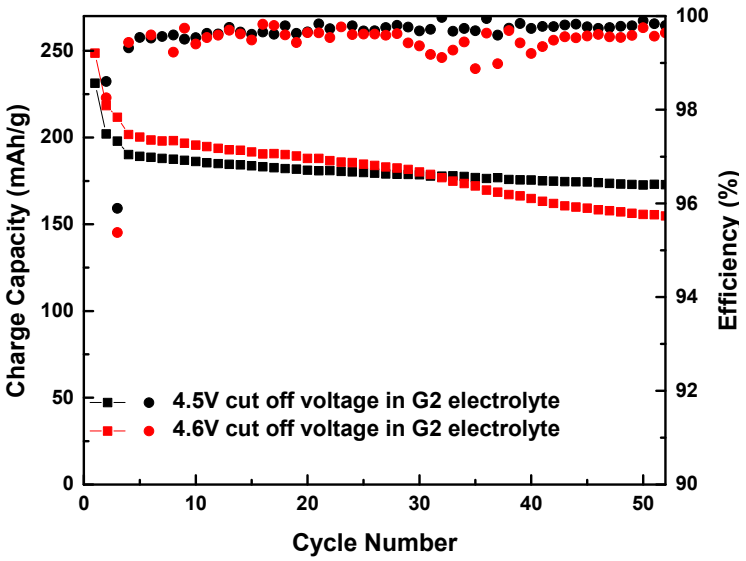


**Figure IV- 182: Cycling performance of $LiNi_{0.5}Mn_{0.3}Co_{0.2}O_2$/Graphite cell in different cut off voltages**

To enable the improved performance of the NCM523/Graphite cell under high cut off voltage, we have designed and synthesized a number of electrolyte additives for 4.6 V application. Among those additives, trisethlyl phosphite (TEP) and tris(2,2,2,-trifluoroethyl)phosphite (TTFP) showed attractive properities on the full cells. The chemical structures of the additives are depicted in Figure IV- 183.

Figure IV- 184 compares the cycling ability of NCM523/graphite cells at 4.6 V with and without 1% TEP or TTFP additive at C/3. The cell cycled in the baseline electrolyte suffers a fast capacity fading with 84.9% initial Coulombic efficiency. With 1% TEP, the cell shows improved cycling performance. The initial charge and discharge capacities are 250 and 204 mAh/g, respectively, leading to an initial Coulombic efficiency of 81.9%. The cell with TEP as the additive suffers a poor Coulombic efficiency, which is maintained close to 98.5% over 50 cycles. However, with 1% TTFP, the cell shows significantly improved cycling performance. The first cycle charge and discharge capacities are 260 and 222mAh/g with 85.5% initial Coulombic efficiency. The capacity retention is 88% after 50 cycles. Also, Coulombic efficiency is maintained close to 99.7%. Both capacity retention and Coulombic efficiency from the cell with 1% TTFP suggests that the electrolyte decomposition was suppressed and a protective SEI film was formed bdue to the preferential oxidation of TTFP on the cathode surface.

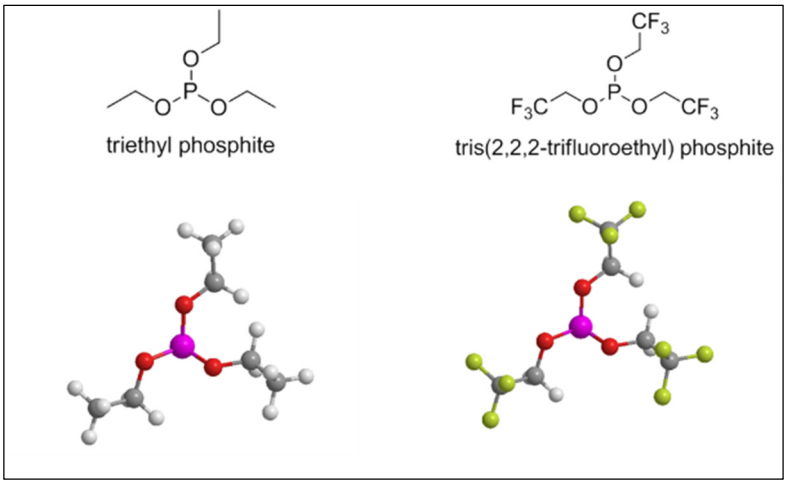


Figure IV- 183: Molecular structures of trisethlyl phosphite (TEP) and tris(2,2,2,-trifluoroethyl)phosphite (TTFP)

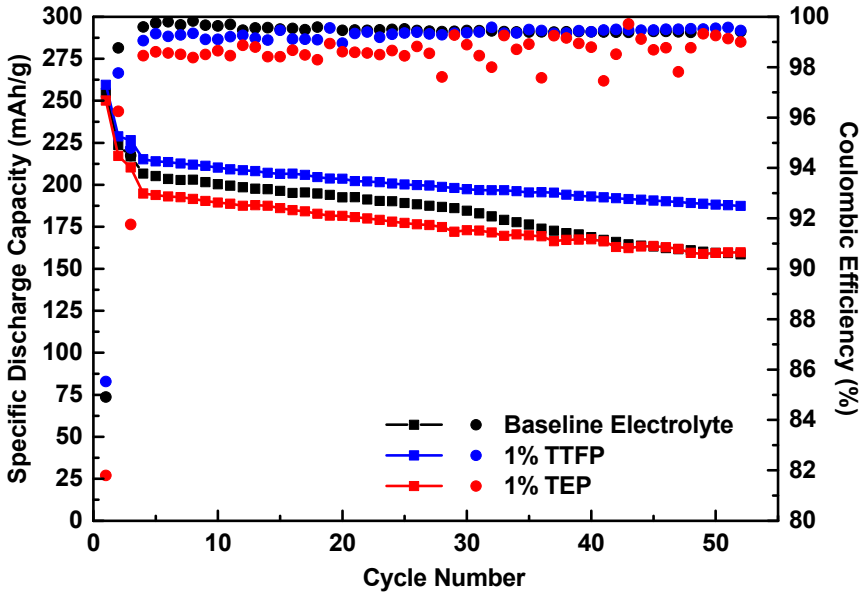


Figure IV- 184: Cycling performance of the NCM523/Graphite cells with TEP and TTFP as additives

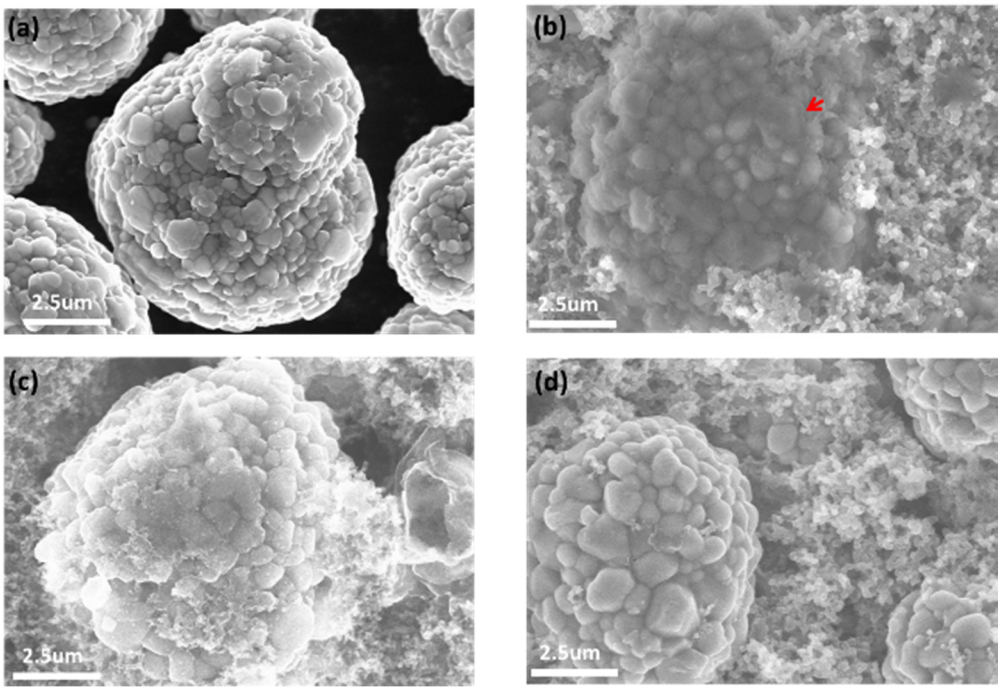


**Figure IV- 185: SEM images of (a) pristine electrode, (b) cycled with baseline electrolyte, (c) 1% TEP containing and (d) 1% TTPF containing**

The harvested NCM523 electrodes from the full cells were characterized by SEM after the cycling test. Figure IV- 185a shows the morphology of the pristine cathode material. Figure IV- 185b, c and d show the morphology of the harvested electrodes. As seen in Figure IV- 185b the surface of cycled cathode in the baseline electrolyte is covered with thick deposits, which suggests that electrolyte decomposition proceeds dramatically and the passivation couldn't be formed. Electrodes cycled with additive TTFP showed a different surface morphology as shown in Figure IV- 185c and Figure IV- 185d as compared with the pristine cathode indicating the existence of the passivation layer on the particle surface.

Four new fluorinated linear carbonate-based electrolytes were also studied for NCM523/Graphite cell with high cut off voltage. Their structures are shown in Figure IV- 186.

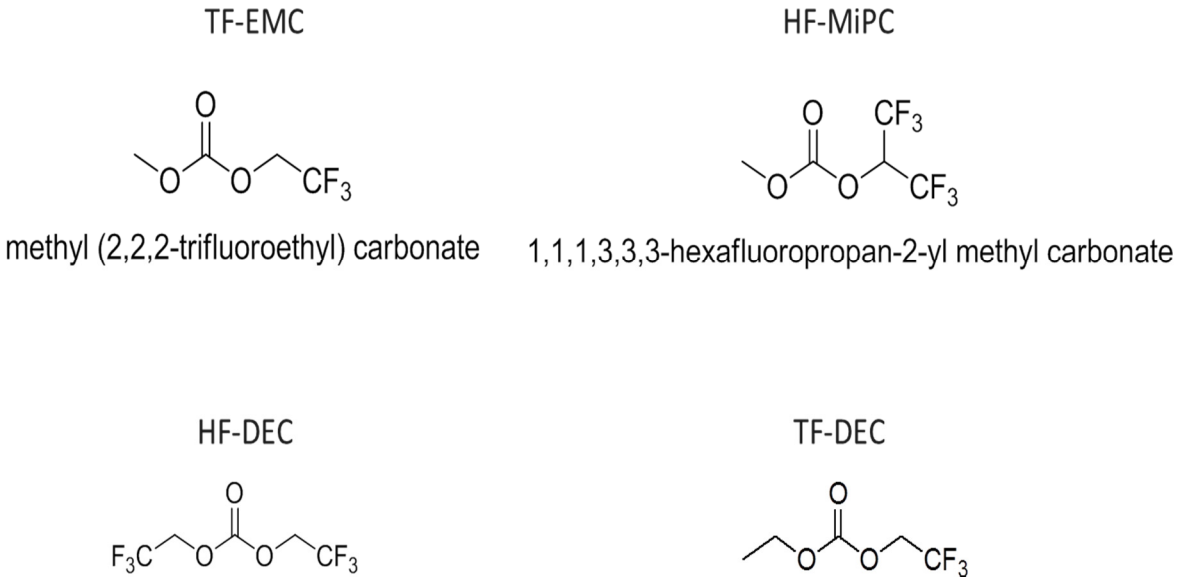


**Figure IV- 186: Molecular structures of fluorinated linear carbonate solvents**

Figure IV- 187a and b showed the voltage profiles of the cells with Gen 2 electrolyte or 1.0 M $LiPF_6$ FEC/HF-DEC 1/1 in volume ratio with 1% LiDFOB. The voltage difference between charge and discharge profiles reflects the polarization of the cycled cell. For the cell cycled in the baseline electrolyte, the polarization increasing with cycling. In the same time, a less polarization change was observed from the cell with fluorinated electrolyte, indicating an improved interfacial stability between electrode and electrolyte.

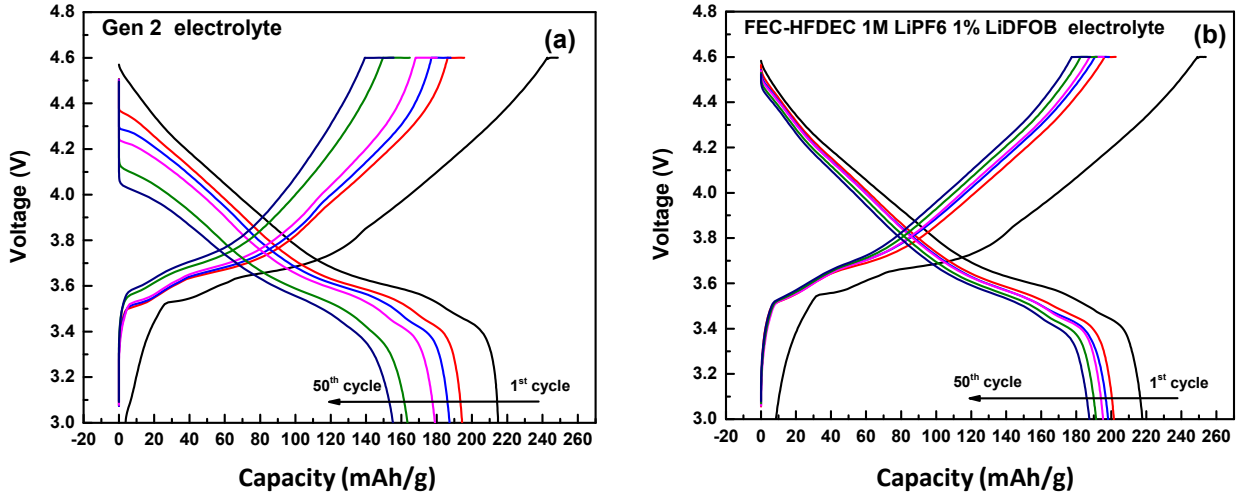


**Figure IV- 187: Voltage profiles for NCM523/graphite cells in (a) baseline electrolyte and (b) 1.0 M $LiPF_6$ in FEC/HF-DEC in 1/1 volume ratio with 1% LiDFOB**

## Opportunities for Training and Professional Development

More than 8 graduate students have been trained to gain knowledge and skills on materials development by working on the project with advisors and postdoc researchers.

6 postdoc researchers have attended professional conference to present their study.

## Conclusions and Future Directions

**Anode.** PSU Si materials have been scaled up to 100 g per batch. Si-based anodes with high flexibility and high areal capacity, ~3.5 mAh/$cm^2$, have been developed. The highly flexible Si-based electrodes developed by the PSU team are capable of achieving high areal capacities over the course of 100 cycles. Precycling and prelithiation have been found to play significant roles in determining cycling stability of full cells.

Future directions include optimizing the composition and structure of electrodes to maximize cycling stability and energy density, and to further investigate the degradation mechanism of full cells.

**Cathode.** TOF-SIMS and HAADF-STEM have been used to characterize the surface electrochemical degradation of Ni-rich $LiNi_{0.7}Co_{0.15}Mn_{0.15}O_2$ cathode materials upon battery operation. Various degradation products originating from (i) electrolyte oxidative breakdown, (ii) corrosion reaction of the active mass, and (iii) surface structural reconstruction have been localized and visualized. Two different surface modification methods have been applied on the baseline $LiNi_{0.7}Co_{0.15}Mn_{0.15}O_2$ cathode material, which show improved battery performance. Post-treatment conditions on concentration-gradient materials have been further optimized to improve the capacity and cycling performance. Coin-type full cells fabricated with a concentration-gradient sample and graphite show good cycling performance with a capacity of around 3.12 mAh $cm^{-2}$. Pouch-type full cells were fabricated with optimized concentration-gradient cathode and graphite anode. The full cell shows a reasonable specific capacity of 180 mAh/g and excellent cycle performance during 200 cycles.

Future directions include developing an in-depth understanding of the degradation mechanism of layered lithium Ni-rich transition-metal oxides with surface diagnostic tools (ToF-SIMS, XPS) and TEM (or STEM), optimizing the preparation conditions of Ni-rich materials by adjusting the co-precipitation process, amount of Li in the firing process, and sintering temperature to reduce the side reactions of the cathode surface with electrolyte and maximize the electrochemical performance and coating the baseline and concentration-gradient samples with other agents like $Li_2MnO_3$, $Li_2ZrO_3$, and $AlF_3$ to improve the electrochemical performance.

**Prelithiation.** A detailed morphology study using SEM indicates 0.5% PS and 0.5% SBR co-solution is an ideal polymer solution system to enable a uniform SLMP coating on anode electrode laminate, while helping the following SLMP activation by the electrolyte. Together with the work in previous quarter, this polymer solution-enabled SLMP coating is demonstrated to be effective for both graphite and SiO electrode laminate. We are now applying this method onto the Si/C composite developed at Penn State toward a prelithiation in the pouch cell configuration.

**Electrolyte.** Electrolyte additive with Si-N skeleton forms a less resistant SEI on the surface of silicon anode (from PSU) as evidenced by the evolution of the impedance at various lithiation/de-lithiation stages and the cycling data.

New fluorinated additive was investigated to stabilize the interphase of the NCM523/electrolyte.

New fluorinated linear cosolvents were designed and synthesized for a high cut off voltage NCM523-Graphite system.

## Publications

### Journal papers:


1. A. Manthiram, J. C. Knight, S.-T. Myung, S.-M. Oh, and Y.-K. Sun, "Nickel-rich and Lithium-rich Layered Oxide Cathodes: Progress and Perspectives," *Advanced Energy Materials* (in press).
2. Meinan He, Libo Hu, Zheng Xue, Chi-Cheung Su, Paul Redfern, Larry A. Curtiss, Bryant Polzin, Arthur von Cresce, Kang Xu, Zhengcheng Zhang*. Fluorinated Electrolytes for 5-V Li-ion Chemistry: Probing Voltage Stability of Electrolytes with Electrochemical Floating Test. J. Electrochem. Soc., (2015), 162(9), A1725-A1729.
3. Xiaodong Yan, Zhihui Wang, Min He, Zhaohui Hou, Ting Xia, Gao Liu, and Xiaobo Chen. TiO2 nanomaterials as anode materials for lithium-ion rechargeable batteries. Energy Technology, **2015**, 3, 801-814.
4. Hui Zhao, Zhe Jia(**co-first author**), Wen Yuan, Heyi Hu, Yanbao Fu, Gregory Baker, and Gao Liu. Fumed silica based single-ion nanocomposite electrolyte for lithium batteries. ACS Applied Materials & Interfaces, **2015**, 7, 19335-19341.
5. Kehua Dai, Zhihui Wang(**co-first author**), Guo Ai, Hui Zhao, Wen Yuan, Xiangyun Song, Vincent Battaglia, Chengdong Sun, Kai Wu, and Gao Liu. The transformation of graphite electrode materials in lithium ion batteries after cycling. J. Power Sources, **2015**, 298, 349-354.
6. Hui Zhao, Fadi Asfour(**co-first author**), Yanbao Fu, Zhe Jia,Wen Yuan, Ying Bai, Min Ling, Heyi Hu, Gregory Baker, and Gao Liu. Plasticized polymer composite single-ion conductors for lithium batteries.ACS Applied Materials & Interfaces, **2015**, 7, 19494-19499.
7. Ying Bai, Xingzhen Zhou, Zhe Jia, Chuan Wu, Liwei Yang, Mizi Chen, Hui Zhao, Feng Wu, and Gao Liu. Understanding the combined effects of microcrystal growth and band gap reduction fo Fe(1-x)TixF3 nanocomposites as cathode materials for lithium-ion batteries. Nano Energy, **2015**, 17, 140-151.
8. Zhe Jia, Hui Zhao, Ying Bai, Ting Zhang, Amanda Siemens, Andrew Minor, and Gao Liu. Solvent processed conductive polymer with single-walled carbon nanotube composites. Journal of Materials Research, **2015**, Accepted.


### Presentations:


1. A. Manthiram, "Structural and Electronic Stabilities of Oxide Cathodes for Lithium-ion Batteries," *5th Polish Forum on Smart Energy Conversion and Storage,* Bialka Tatrzanska, Poland, September 22 – 25, 2015.
2. N, N-Diethyltrimethylsilylamine (DETMSA) As Electrolyte Additive for Si Based High Energy Lithium-Ion Batteries. Meinan He, Libo Hu, Yan Wang, Kang Xu and Zhengcheng Zhang. 227th ECS meeting, Chicago, May 24-28.
3. Side-Chain Conducting and Phase-Separated Polymeric Binders for High-Performance Silicon Anodes in Lithium-Ion Batteries. Oral presentation, Presenter (Zhe Jia). Electrochemical Society 228th meeting, 2015 Fall, Phoenix (Oct. 11th to 15th, 2015).

4. Functional Conductive Polymer Binders for High-Performance Silicon-Based Anodes in Lithium-Ion Batteries, invited oral presentation, presenter (Zhe Jia). Electrochemical Society 228th meeting, 2015 Fall, Phoenix (Oct. 11th to 15th, 2015).
5. Functional Conductive Polymer Binders Enabled High Stability Cycling of Alloy Anodes (Gao Liu, invited oral presentation). 66th Annual Meeting of the International Society of Electrochemistry, 2015, Taipei (Oct. 4th to 9th, 2015).

### Participants & Other Collaborating Organizations

Name: Donghai Wang (Penn State)
Project Role: Principal investigator
Nearest person month worked: 1
Contribution to Project: Dr. Wang has managed the project as a whole and worked on the development of Si-based anodes.

Name: Arumugam Manthiram (UT Austin)
Project Role: Co-principal investigator
Nearest person month worked: 1
Contribution to Project: Dr. Manthiram has managed and worked on the development of cathodes.

Name: Rong Kou (EC Power)
Project Role: Co-principal investigator
Nearest person month worked: 6
Contribution to Project: Dr. Kou has managed and worked on cell design and fabrication.

Name: Gao Liu (LBNL)
Project Role: Key Collaborator
Nearest person month worked: 3
Contribution to Project: Dr. Liu has managed and worked on the development of polymer binders for Si-based anodes.

Name: Zhengcheng Zhang (ANL)
Project Role: Key Collaborator
Nearest person month worked: 3
Contribution to Project: Dr. Zhang has managed and worked on the development of electrolytes for Si-based anodes and nickel-rich layered cathodes.

### Changes/Problems

No unforeseen challenges or changes to plan-of-action.

### Budgetary Information

No cost extenstion has been approved to extend the project by May 31 2016.

# IV.D.6 High Energy High Power Battery Exceeding PHEV40 Requirements (TIAX LLC)

## Objectives

TIAX is working to develop a lithium-ion battery system that meets the PHEV40 performance and life goals by implementing CAM-7™ based cathode with a Si-based anode chemistry.

## Technical Barriers

The major technical challenge faced by Li-ion batteries is simultaneously meeting energy, power, and life targets for PHEV batteries over a wide temperature range.

## Technical Targets

- Demonstrate >200Wh/kg and >400Wh/L energy and >800W/kg and >1600W/L pulse power targets.
- Demonstrate cycle and calendar life.

### Project Details

**Dr. Christopher Johnson (NETL Program Manager)**
DE-EE0006452 Recipient: TIAX, LLC

**Dr. Jane Rempel (PI)**
35 Hartwell Avenue
Lexington, MA 02421
Phone: 781-879-1238; Fax: 781-879-1202
Email: rempel.jane@tiaxllc.com

Subcontractor:
none

Start Date: October 2013

Projected End Date: March 2016

## Accomplishments

- Identified CAM-7 dopant compositions and synthetic modifications that result in improved material performance for PHEV applications.
- Developed a higher capacity CAM-7 cathode with good cycle life, delivering >220mAh/g at C/20 and >200mAh/g at 1C.
- Evaluated many Si-based anode materials from leading materials suppliers worldwide and down selected two materials for larger cell assembly.
- Demonstrated improved cycle life of silicon-based anodes by blending or by forming a composite with carbons, modifications of the electrolyte and binder.
- Showed that by implementing pre-lithiation and using cells with high anode:cathode ratio, we can improve full cell capacity retention while fully utilizing the cathode.
- Demonstrated excellent cycle life with a blended anode formulation that did not require pre-lithiation or anode over-sizing.
- Identified electrode designs and inactive components that maximize cell specific energy and power.
- Improved 18650 cell hardware and inactive components to maximize specific power and energy.
- Designed, assembled and tested baseline 18650 CAM-7/Graphite Li-ion cells demonstrating excellent cycle life with >80% capacity retention after 2500 cycles between 2.7-4.1V (90% DOD) and after 2000 cycles between 2.7-4.2V (full DOD) at RT and little capacity loss or impedance rise during storage. Baseline cells were also delivered to Argonne National Laboratory for independent verification of performance.
- Designed, assembled, and tested Gen 1 CAM-7/Si 18650 cells utilizing Si/carbon composite, showing that these cells can deliver 800W/kg power and ~200Wh/kg usable energy target.
- Implemented higher capacity CAM-7 cathode with graphite in 18650 cells demonstrating superior specific power and energy relative to baseline cells.

## Introduction

State-of-the-art PHEV battery systems are currently limited to only 50-80Wh/kg and 100-150Wh/L (Dave Howell, Presentation at the 30th International Battery Seminar & Exhibit, March 2013). Even if the specific energy and energy density for the cells in these battery systems are approximately twice the battery-level

values, these cells cannot meet the PHEV40 200Wh/kg specific energy target. These limitations are due to the cells' utilization of low energy density LMO-based cathodes, or blends of LMO with higher capacity but lower power NCM cathode material. The energy density of PHEV cells is also limited by the graphite anodes they employ. In addition, power delivery capability of the current cell designs is limited by the inactive components employed, thus resulting in cells with a large contribution from inactive components to the final cell weight, volume, and cost. In order to improve cell specific energy and power, a system-level approach is needed that combines novel high energy cathode and anode active materials in optimized electrode and cell designs to simultaneously achieve high energy, power and life of the DOE's PHEV40 targets.

## Approach

Our overall approach is to combine cathodes based on TIAX's high-energy and high-power cathode material, CAM-7, with silicon-based anode in electrode designs optimized for PHEV40 application in cells using high-performance inactive components to meet the energy and power targets:

- **CAM-7$^{TM}$ high energy, high power cathode material**: CAM-7 is a family of stabilized high-nickel-content cathode materials developed and patented by TIAX that combines both high-energy and high-power capabilities. The CAM-7 version employed in baseline cells delivers over 210mAh/g at C/20 and 150mAh/g at 50C, with excellent cycle and calendar life. During this project, additional modifications to the material composition of CAM-7 resulted in a further increase in its discharge capacity (detailed later in this section). With over a decade of research and development effort and direct sampling evaluations by major battery companies, CAM-7 is now in transition to commercial production, currently being scaled-up from ~ 30kg/week in a lab-scale facility to ~ 50 ton-per-year in our powder production plant located in Rowley, Massachusetts.
- **Blended Si/Carbon anode:** we are working with multiple leading silicon anode materials developers on implementing their anodes in blended electrodes formulated specifically for high energy and power delivery capability. We are selecting inactive components, electrolytes, and electrode formulations that are capable of meeting the energy and power targets while maintaining long life.
- **System approach to cell design:** TIAX has developed methodologies for high throughput testing of materials, electrode components, and electrode designs that are predictive of performance in scaled-up cells. Combining electrochemical data with engineering cell design models, we can rapidly assess the impact that design factors can have towards enabling high cell energy while delivering PHEV-scaled power levels, before implementing these changes in 18650 cells. Using these methods, we are optimizing electrode designs and integrating high performance inactive components and cell hardware to maximize cell power and energy delivery capability.

## Results

### Baseline CAM-7/Graphite 18650 Cell Performance

Baseline 18650 cells containing CAM-7-based cathode and graphite-based anode were fabricated at TIAX in 2014 and delivered to Argonne National Laboratory for evaluation. Several cells were retained at TIAX for performance, cycle and calendar life testing. Baseline cells were designed using low active material loading (~2mAh/cm²) and high porosity electrodes targeting high power applications. These 18650 cells delivered 6.7Wh at C/5 rate corresponding to 167Wh/kg (235Wh/kg at the electrode stack level, excluding 18650 cell hardware), while providing 800W/kg 10s pulse power at 10% SOC.

Cycle life and calendar life testing of the baseline cells at TIAX is ongoing with >2500 cycles at RT and >400 days of storage recorded to date. Capacity retention during 2.7-4.1V (90% SOC swing) and 2.7-4.2V (full DOD) cycling are shown in Figure IV- 188 and Figure IV- 189, respectively. Capacity retention and impedance growth during 4.1V storage at 45ºC are shown in Figure IV- 190.

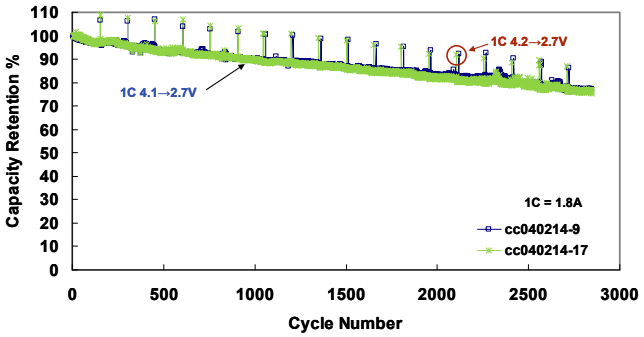


Figure IV- 188: Room temperature cycling of baseline CAM-7/Graphite 18650 cells between 2.7 and 4.1V. C/2 charge - 1C discharge; 1C discharge from 4.2V every 150 cycles. Note that cycling between 2.7 and 4.1V corresponds to 90% SOC swing. Cells fabricated at TIAX

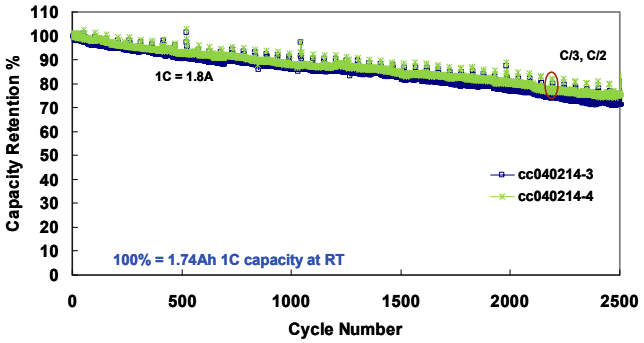


Figure IV- 189: Room temperature cycling of baseline CAM-7/Graphite 18650 cells over the full DOD range. C/2 charge - 1C discharge, 4.2 to 2.7V; C/3 and C/2 discharge every 50 cycles. Cells fabricated at TIAX

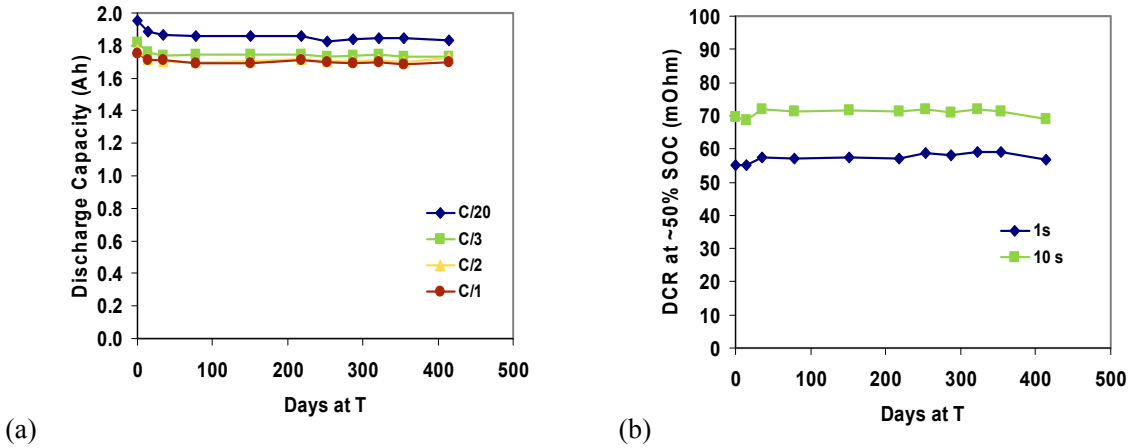


(a) (b)

Figure IV- 190: 45ºC storage of baseline CAM-7/Graphite 18650 cells at 4.1V. (a) Intermittent C/20, C/3, C/2, and 1C discharge between 4.2 to 2.7V and (b) 1C 10s HPPC rate characterization at RT

### Cathode Material Optimization

While CAM-7 cathode material used for baseline cell production has excellent properties for use in PHEV applications, additional improvements are possible. Specifically, in this program we focused on identifying synthetic modifications and dopant compositions that can further reduce impedance growth during high temperature operation in an under-the-hood environment. In order to facilitate rapid materials screening, we developed an accelerated high temperature electrochemical testing protocol that allows high-fidelity characterization of impedance growth within a week of testing, significantly shortening materials development efforts. As a proxy for impedance growth, we monitor time spent at constant voltage during charge – higher impedance results in longer time spent at constant voltage. Using this accelerated testing procedure, we mapped out the impact that different bulk and surface dopants in the CAM-7 structure have on cycle life (Figure IV- 191a). We also identified synthetic additives that reduce impedance growth, without significant change in cathode capacity (Figure IV- 191b).

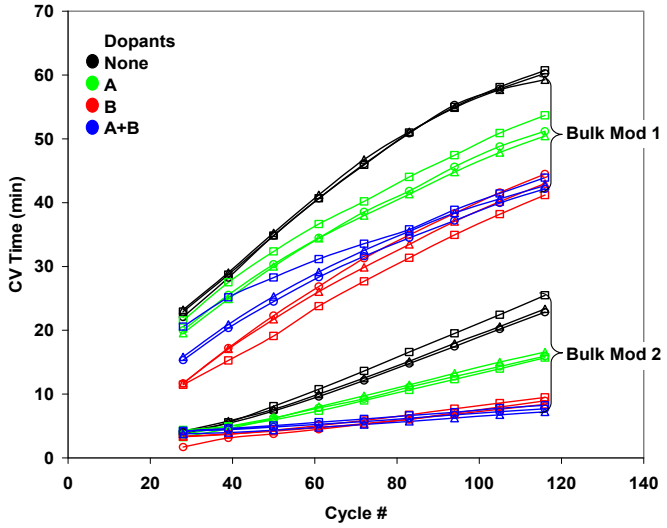


(a)

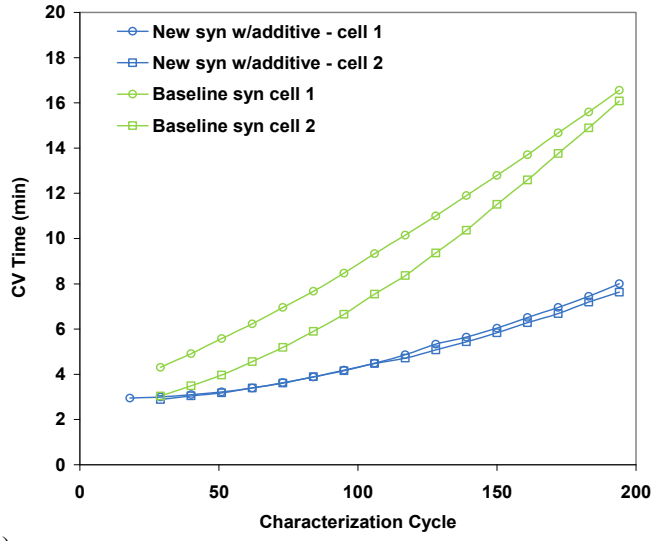


(b)

**Figure IV- 191: Impact of (a) dopants and (b) synthesis modification on high temperature impedance rise. Accelerated cycle life testing at 45ºC using high rate charge and discharge cycles with intermittent 1C/1C characterization cycles at 45ºC between 4.2V and 2.7V. CAM-7/Graphite coin cells with ~2mAh/cm² loading. CV charge time used as an impedance characterization metric**

Combining the doping strategy with synthetic modifications, we have developed a higher capacity CAM-7 cathode material that exhibits good cycle life in initial coin cell testing, while delivering >220mAh/g at C/20 and >200mAh/g at 1C (Figure IV- 192).

| Half Cells vs. Li metal | Discharge Capacity (mAh/g) | | | |
|---|---|---|---|---|
| | C/20 | C/10 | C/5 | 1C |
| Baseline CAM-7 | 212 | 205 | 199 | 185 |
| Higher Capacity CAM-7 | 224 | 218 | 212 | 201 |

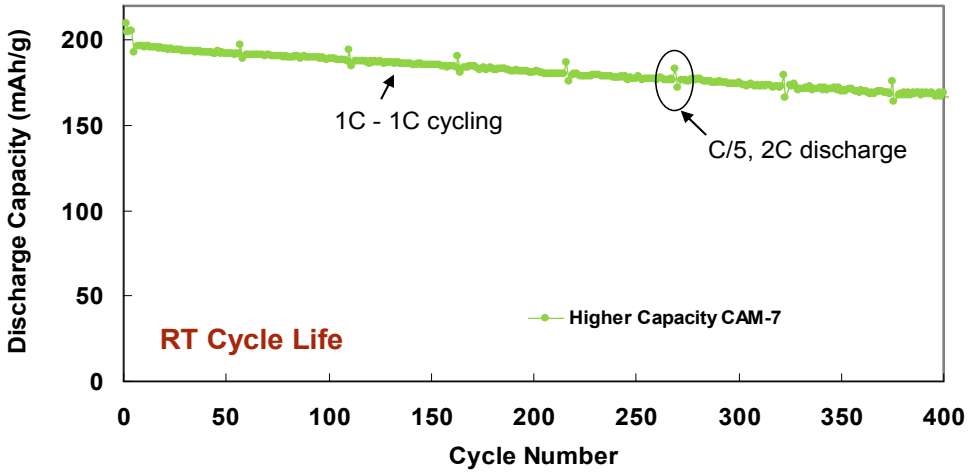


Figure IV- 192: Table above shows the discharge capacity of the baseline and higher capacity CAM-7 cathode materials measured in half cells with Li metal anode (3.0-4.3V). The bottom figure shows cycle life of the higher capacity CAM-7 at room temperature with graphite anode (2.7-4.2V, 1C/1C)

### Anode Material Selection

During the program, we have continuously sourced many state-of-the-art silicon anode materials from leading materials suppliers worldwide. Specifically, we focused on materials that are available in the multi-kg quantities essential for 18650 cell production. All anode materials were evaluated for capacity, first cycle efficiency, cycle life and cycle-to-cycle columbic efficiency vs. Li-metal in coin cells (see Table IV- 25 and Figure IV- 193).

**Table IV- 25: Range of Si-based anode materials evaluated in the program**

| Representative Materials* | Description | Capacity (mAh/g) | 1st Cycle Efficiency | Cycle Life | Columbic Efficiency |
|---|---|---|---|---|---|
| Company A-1 | Si/Carbon composite | 500 | 82% | Good | OK |
| Company A-2 | Si/Carbon composite | 600 | 84% | Good | OK |
| Company A-3 | Si/Carbon composite | 1650 | 86% | OK | OK |
| Company A-4 | Si/Carbon composite | 1850 | 86% | OK | OK |
| Company B-1 | Micron-scale Si | 3800 | 90% | Fast initial fade, then OK | Good |
| Company B-2 | Micron-scale Si | 3400 | 89% | Fast initial fade, then OK | Good |
| Company B-3 | SiOx | 1400 | 71% | Good | Good |
| Company C-1 | Nano-Si | 3100 | 88% | Good | Poor |

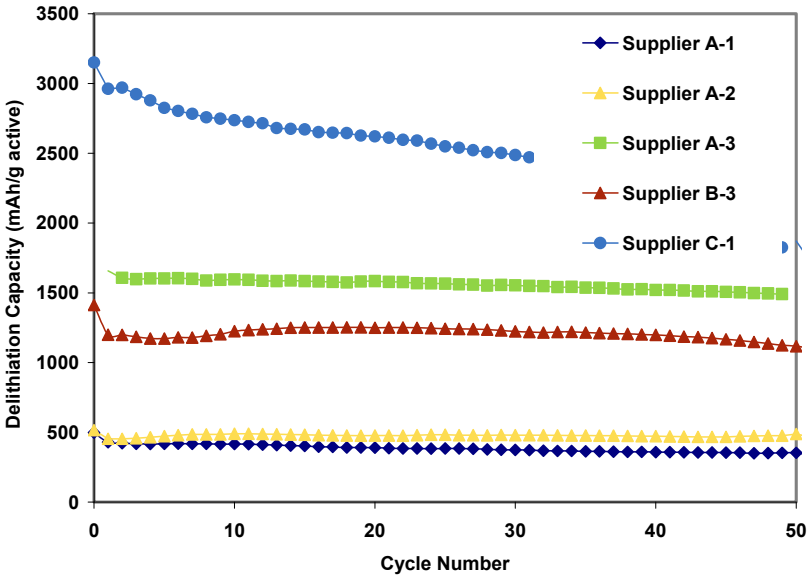


(a)

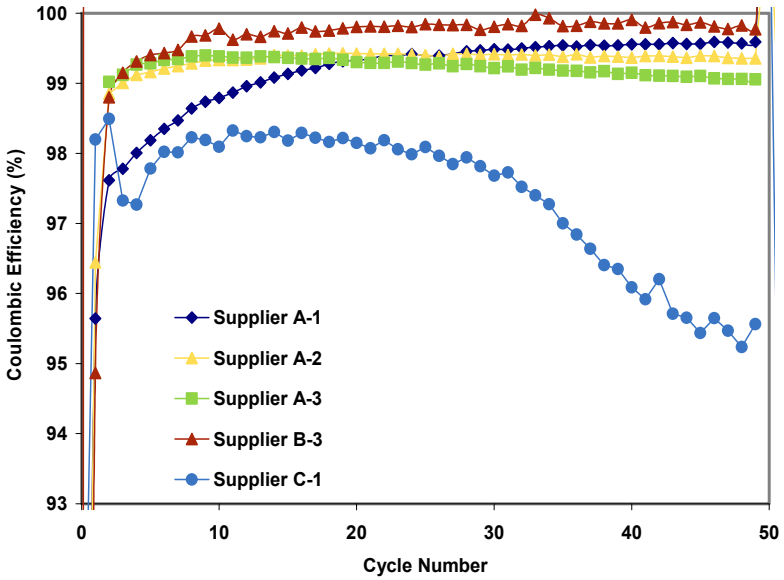


(b)

**Figure IV- 193: Capacity retention and coulombic efficiencies of Si-based anodes evaluated in coin cells with Li metal counter electrode. Materials tested with 75% active (except C-1 with 60%) content electrodes**

We explored different strategies to improve capacity retention and coulombic efficiency, which are both critical to ensure adequate cycle life when Si-based anodes are paired with any cathode. Specifically, we have tested the impact of reducing the SOC range over which Si is cycled, modifying electrolyte formulation, changing binder, and blending Si-based anodes with graphite. A representative example of the cycle life and coulombic efficiency that can be achieved by blending Si-based anode with graphite in small quantities is shown in Figure IV- 194.

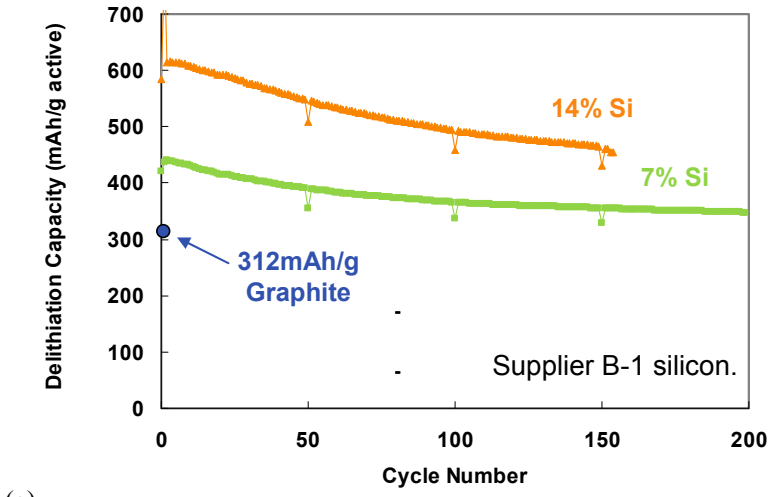


(a)

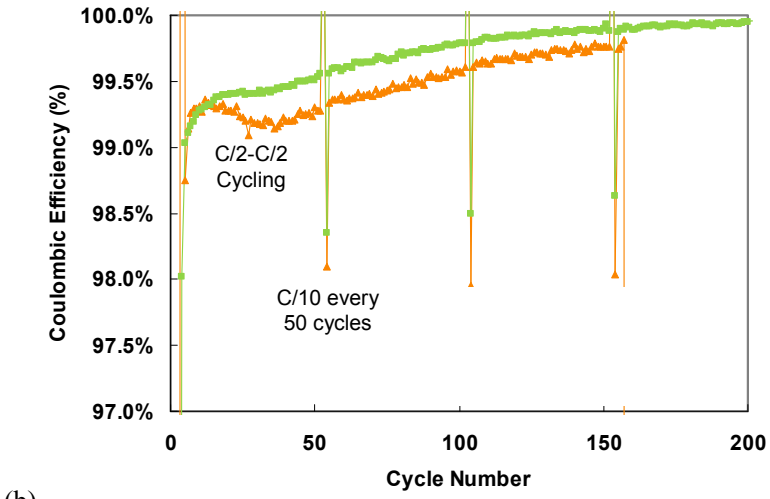


(b)

**Figure IV- 194: Representative example for capacity retention and coulombic efficiencies of blended Si-based anodes with graphite evaluated in coin cells with Li metal counter electrode**

### CAM-7/Si Full Cell Evaluation

Most promising Si-based anodes and their blends with graphite were tested in coin cells with CAM-7 cathode. Initial capacity, rate capability during continuous discharge and during pulse power were evaluated along with cycle life. We also explored different strategies to improve cycle life of silicon-carbon based anodes in full cells. Specifically, we have demonstrated improved cycle life with reduced voltage window cycling, but at the expense of gravimetric cathode capacity. We also showed improved cycle life with increased anode:cathode ratio, again at the expense of gravimetric capacity. Moreover, we showed that by implementing pre-lithiation and using cells with high anode:cathode ratios, we can improve full cell capacity retention while fully utilizing the cathode gravimetric capacity (Figure IV- 195).

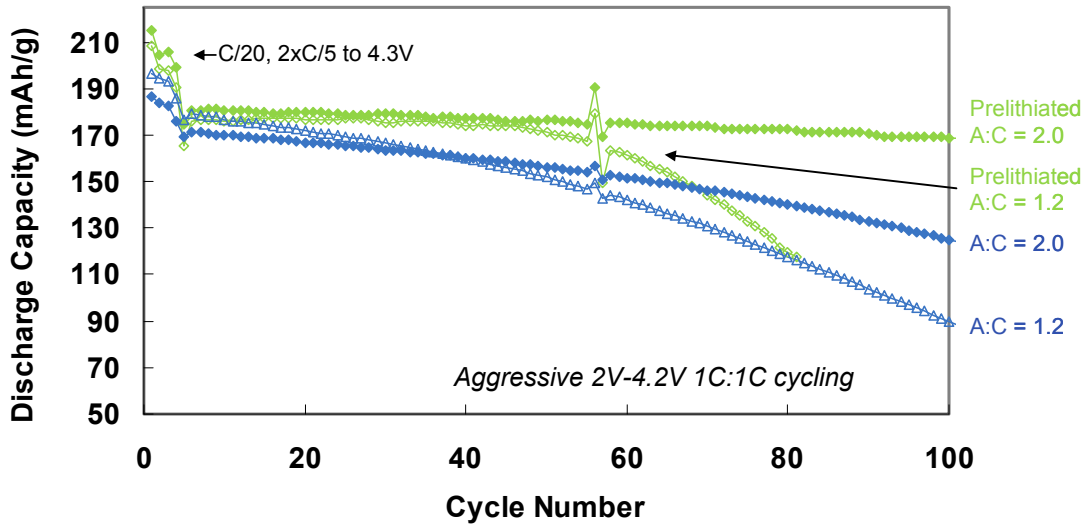


Figure IV- 195: Impact of pre-lithiation and anode over-sizing on full cell cycling of silicon/carbon composite anode paired with CAM-7 cathode in coin cells. Discharge capacity normalized by cathode active material weight

We also developed a blended electrode formulation with graphite and Si-containing anode, with excellent coulombic efficiency, that demonstrated stable capacity retention during full cell cycling with CAM-7-based cathode with an A:C ratio of ~1 and no pre-lithiation (Figure IV- 196)

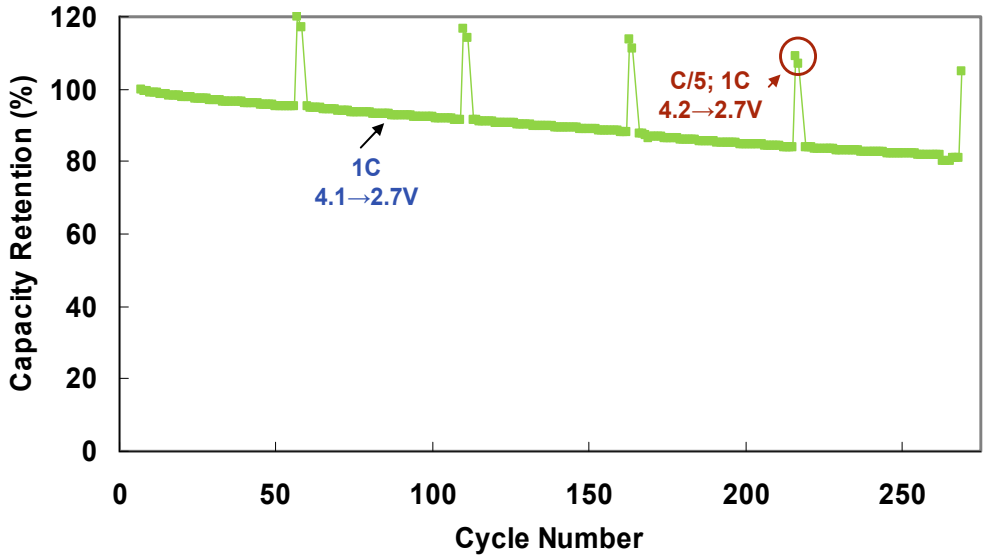


Figure IV- 196: Cycle life of CAM-7-based cathode paired with a blended Graphite/Si-containing anode evaluated in coin cells. (A:C ~ 1 and no pre-lithiation)

**Electrode and Cell Engineering**

Scoping experiments were carried out to optimize electrode energy and power capability for CAM-7/Graphite full cells. Specifically, CAM-7-based cathodes were paired with graphite-based anodes using various loadings, formulations, electrode porosities, separators and electrolyte salt concentrations. Full cells were tested in coin cells using a scaled version of the protocol used for baseline 18650 cells tested by ANL. An 18650 engineering model was used to calculate cell weight and determine projected cell-level specific energy and power. Representative examples for projected W/kg as a function of degree-of-discharge in Wh/kg from 4.2V are shown Figure IV- 197. We found that by reducing electrode porosity and increasing loading, the available energy can be increased without loss in power capability within the parameter range investigated. Switching

the separator to a higher permeability separator, cell power and energy can be improved. Using these scoping experiments, we have narrowed down cathode electrode designs that will allow us to meet the PHEV performance targets even with graphite anodes.

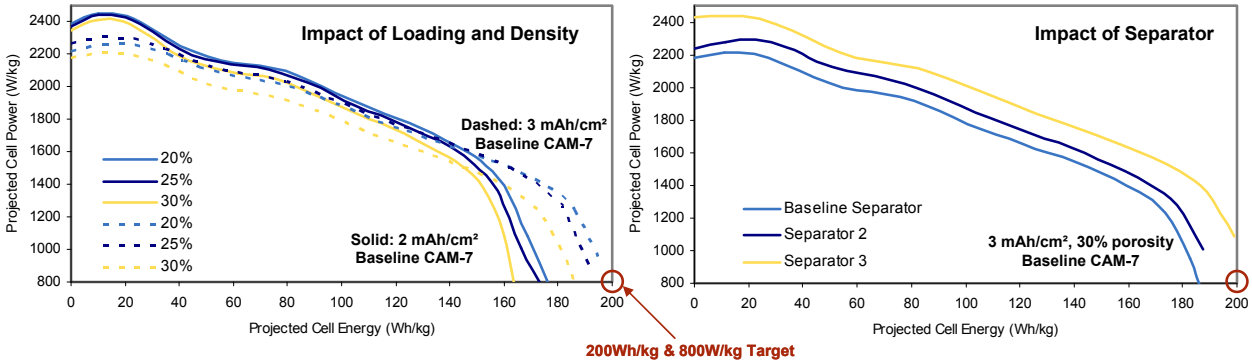


**Figure IV- 197: Impact of electrode design on projected 18650 cell power and energy. Power based on HPPC measurements in coin cells using graphite anodes (ASI vs. SOC for 10s 3C pulse). Energy based on 1C discharge from 4.2V. Cell engineering model used to scale coin cell measurements to 18650 cells**

We have also tested different design changes needed to improve gravimetric energy and power capability of 18650 cells. Specifically, we have fabricated 18650 cells using multiple electrode tabs both on the anode and the cathode electrodes in order to reduce cell resistance. We have also tested thinner higher permeability separators in 18650 cells. In addition, by incorporating modified cell hardware we were able to demonstrate reduced cell resistance during pulse power testing of the baseline 18650 cells (Figure IV- 198).

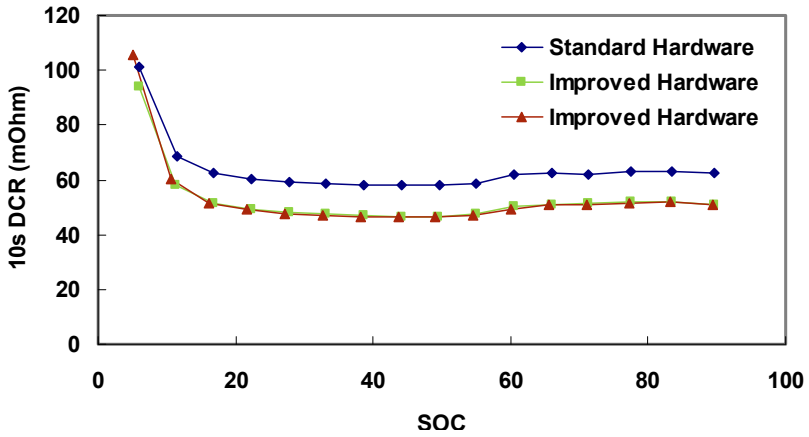


**Figure IV- 198: Impact of 18650 hardware modifications on cell power capability. Baseline 18650 cell design with CAM-7 cathode and graphite anode with ~2mAh/cm² active material loading. HPPC power testing done using 5A 10s Discharge**

### 18650 Cell Design and Testing

First generation CAM-7/Si 18650 cells were fabricated and tested, demonstrating higher capacity and energy density than the baseline cells. Comparison of the HPPC resistance and projected power shows that the Gen 1 CAM-7/Si cells can provide comparable power while providing higher energy density than the baseline 18650 cells, coming close to meeting the 200Wh/kg and 800W/kg energy and power targets (Figure IV- 199). Cycle life of these cells will need to be improved to meet life targets, however.

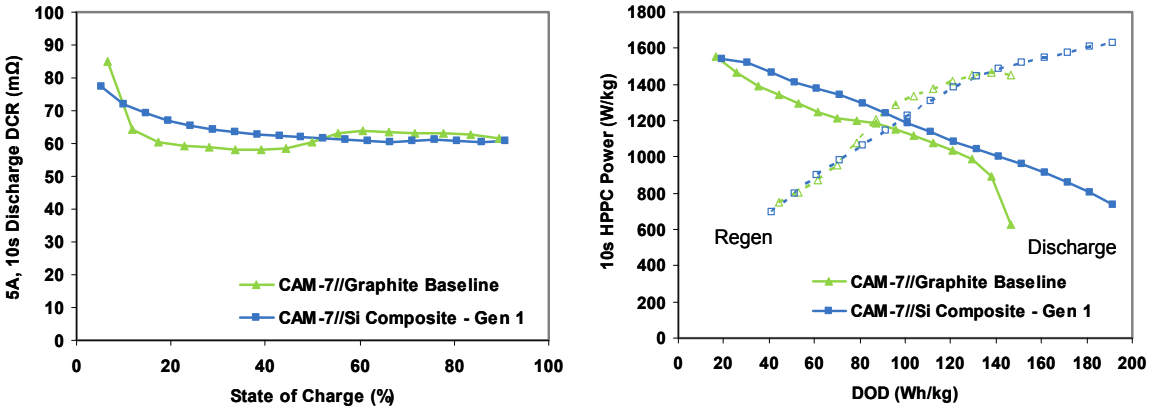


Figure IV- 199: HPPC testing shows that the Gen 1 CAM-7/Si cells can provide comparable power while providing higher energy density than the baseline 18650 cells. Si: 5A 10s Discharge, 3.75A 10s Charge. Vmin = 2.0V, Vmax = 4.3V for HPPC power calculation. Graphite: 5A 10s Discharge, 3.6A 10s Charge. Vmin = 2.6V, Vmax = 4.3V for HPPC power calculation

We have also assembled and tested 18650 cells with higher capacity CAM-7 cathode paired with graphite-based anode using an equivalent cell design to Baseline CAM-7/Graphite cells (equal electrode length and ~2mAh/cm² active material loading). Both specific energy and power were higher with improved CAM-7 cathode material with comparable capacity retention (Figure IV- 200).

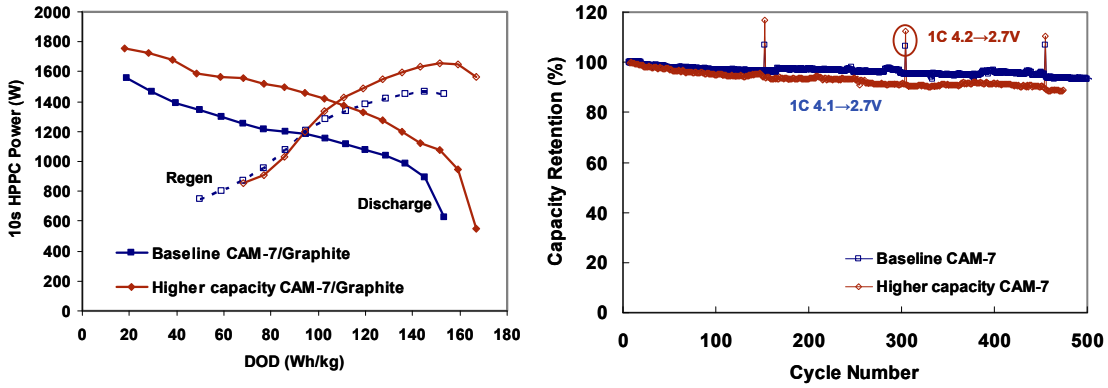


Figure IV- 200: Comparison of cell power capability and 2.7-4.1V C/2 - 1C room temperature cycle life for baseline and improved CAM-7/Graphite cells with equivalent design (equal electrode length with ~2mAh/cm² active material loading). HPPC power testing done using 5A 10s Discharge, 3.6A 10s Charge. Vmin = 2.6V, Vmax = 4.3V for HPPC power calculation

## Conclusions and Future Directions

In this program, we have developed improved cathode material compositions that translate to improved cell-level energy and power capability. We have down-selected a CAM-7 composition for assembly of program demonstration cells. We have also tested many Si-based anodes and developed blended electrode formulations capable of meeting energy and power targets while maintaining long life. We have evaluated different strategies for improving cycle life of Si-based anode materials including blending, binder and electrolyte selection, electrode engineering and anode pre-lithiation. We have also identified electrode designs and cell design changes that will allow us to increase 18650 cell specific energy and power. Our focus going forward will be on finalizing anode material selection and blended electrode formulation and implementing the optimized materials and electrode designs in the program demonstration 18650 cells. In addition, we will continue cycle life testing of the baseline CAM-7/Graphite cells that already show excellent capacity retention after >3000 cycles.

## FY 2015 Publications/Presentations

1. "Materials Development for High Energy High Power Battery Exceeding PHEV40 Requirements", DOE VTP Merit Review, 2015.
2. "High Energy High Power Battery Exceeding PHEV40 Requirements", DOE VTP Merit Review, 2015.
3. A portion of the work from this project was presented at the 32nd International Battery Seminar & Exhibit, Ft. Lauderdale, FL, March 2015.
4. A portion of the work from this project was presented at AABC 2015 in Detroit, MI, June 2015 (poster).

# IV.E Process Development and Manufacturing R&D at National Laboratories

# IV.E.1 Process Development and Scale up of Advanced Active Battery Materials (ANL)

## Objectives

- The program is a key missing link between discovery of advanced active battery materials, market evaluation of these materials and high-volume manufacturing. We evaluate and select the synthesis route and develop a customized process for the advanced active battery materials which were recently developed by various R&D groups. After the optimization of synthesis process and material composition, several kilogram material is scaled up and supplied to support further basic research and industrial validation in large format cells. We also provide a systematic engineering research with reproducibility, development of cost-effective process and evaluation of emerging manufacturing technologies.


### Project Details

**Gregory K. Krumdick**
Argonne National Laboratory
9700 South Cass Avenue
Argonne, IL 60439-4837
Phone: 630-252-3952
E-mail: gkrumdick@anl.gov

Collaborators:
Youngho Shin, Argonne National Laboratory
Ozgenur K. Feridun, Argonne National Laboratory
Anthony Burrell, Argonne National Laboratory
Michael Thackeray, Argonne National Laboratory
Andrew Jansen, Argonne National Laboratory
Bryant Polzin, Argonne National Laboratory
Jason Croy, Argonne National Laboratory
Steve Trask, Argonne National Laboratory
Dean Miller, Argonne National Laboratory
Brandon Long, BASF
Jordi Cabana, UIC



Start Date: October 2010
Projected End Date: September 2016


## Technical Barriers

- Newly invented advanced active materials have been synthesized in gram quantity at bench-scale without quality control and reproducibility which are not yet available commercially. Development and optimization of a tailored synthesis process is the key issue to produce sufficient quantities of these materials with high quality.
- Barriers addressed:
- Manufacturing cost reduction with advanced processing method.
- Material quality control and process reproducibility.
- Selection of synthesis route and process and its optimization for maximum performance.

## Technical Targets

- Develop customized synthesis processes for newly invented advanced active battery materials.
- Scale up multi-kilogram material under rigorous quality control.
- Provide a systematic material engineering research with reproducibility.
- Evaluate emerging manufacturing technologies and their application.

## Accomplishments

- Layered layered material ($Li_{1.067}Ni_{0.61}Mn_{0.33}Co_{0.06}O_y$) has been prepared via carbonate and hydroxide synthesis routes. Carbonate synthesis route was selected for scale-up research and synthesis condition was optimized by design of experiments (ANOVA).
- Kilogram production of layered layered material was completed using 20L continuous stirred tank reactor (CSTR).

- Layered layered spinel material ($Li_{1.14}Ni_{0.28}Mn_{0.53}Co_{0.19}O_y$) has been improved by adjusting the content of its spinel phase via hydroxide synthesis route. We proved that the existence of 5% spinel phase greatly stabilize material structure, increase rate performance and minimize capacity loss.
- To evaluate an emerging manufacturing technology, a Taylor Vortex Reactor (TVR) was installed.
- 40L batch, 20L CSTR and 1L TVR systems were compared as co-precipitation processes using the optimized synthesis condition of layered layered material. TVR generated very promising particle showing dense spherical morphology.
- 1L wet surface coating system was developed and aluminum fluoride coating was applied on high energy LMR-NMC material ($Li_{1.2}Ni_{0.13}Mn_{0.54}Co_{0.13}O_2$) to mitigate its capacity loss during cycling. We showed that 4 wt.% $AlF_3$-coated LMR-NMC material shows only 1% capacity drop after 30 cycles.
- Bench-scale Full Concentration-Gradient (FCG) material was analyzed as a next scale-up candidate and preliminary synthesis work was started.

## Introduction

Newly invented advanced active battery materials are generally synthesized on the gram scale without quality control and reproducibility, and lack commercial availability. These chemistries need to be tested and validated in large format prototype cells before going to high-volume manufacturing which needs a fair amount of material. Moreover, kilogram scale stocks of these materials are necessary as baseline materials for in-depth characterizations and further applications such as surface coating. Therefore, material scale-up with high quality is critical for both industrial validation and further basic research. However, from an engineering perspective, newly invented advanced active material needs to be synthesized and scaled via its own tailored synthesis process and optimization to maximize its performance and is challenging. The systematic material engineering and customized scaled process that we develop, will resolve the scale-up constraints of these materials and bridge the gap between basic material research and commercialization.

## Approach

**Innovative Approach:** Kilogram material production with high quality will be accomplished by developing a customized synthesis process and systematic material engineering. We will use well-defined flow chart to achieve the maximum quality of target material (See Figure IV- 201).

1. Define target material to be scaled by evaluating bench-scale samples from R&D groups.
2. Conduct preliminary evaluation of conventional synthesis processes (batch, CSTR) together with emerging technologies (TVR).
3. Select a customized synthesis process.
4. Evaluate and select synthesis route.
5. Optimize synthesis process by Design of Experiments (ANOVA).
6. Produce 100g intermediate product for material evaluation and reproducibility check.
7. Obtain kilogram production, characterization, delivery and feedback from collaborators.

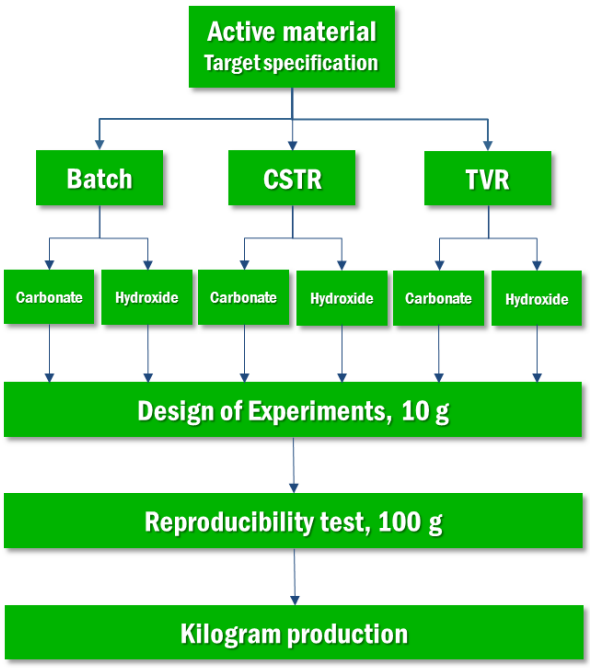


Figure IV- 201: Flow chart of material scale-up

## Results

We have achieved the following progress:

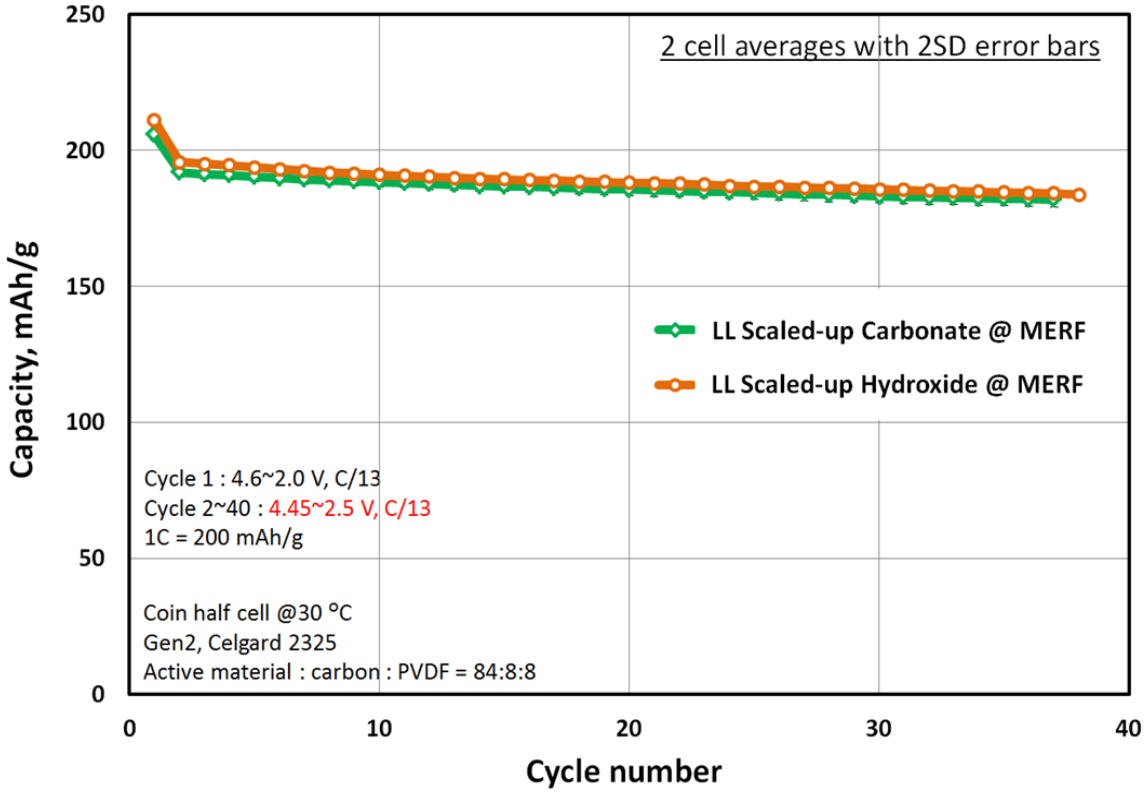


Figure IV- 202: Coin cell result of preliminary synthesized layered layered material

**Synthesis process optimization and kilogram production of layered layered material**

Layered layered material was initially synthesized as another candidate material of scale-up research to support basic R&D groups for surface coating application. After preliminary discussions, this composition was determined to be scaled to kilogram quantity for HE/HV program at Argonne National Laboratory. For the preliminary prepared materials, both carbonate and hydroxide synthesis route show similar electrochemical performance when cycled between 2.5 and .45 V at C/13 (See Figure IV- 202). However, carbonate synthesis route was chosen to be further optimized because it generated more spherical, uniform and denser particle which are essential factors for a uniform surface coating application.

We selected CSTR (continuous stirred tank reactor) system as a co-precipitation process and set up a statistical design of experiments (Response Surface Modeling) to evaluate process stability and effect of key operation variables. Reaction temperature and the ratio of $NH_4OH$ to transition metals (TM) were key variables and a total of thirteen-12h continuous operations were carried out (See Figure IV- 203).

| RunOrder | TEMP | $NH_4OH$/TM |
|---|---|---|
| 1 | 40.0 | 0.10 |
| 2 | 40.0 | 0.10 |
| 3 | 32.9 | 0.16 |
| 4 | 40.0 | 0.10 |
| 5 | 32.9 | 0.04 |
| 6 | 30.0 | 0.10 |
| 7 | 47.1 | 0.04 |
| 8 | 40.0 | 0.02 |
| 9 | 47.1 | 0.16 |
| 10 | 40.0 | 0.10 |
| 11 | 40.0 | 0.18 |
| 12 | 50.0 | 0.10 |
| 13 | 40.0 | 0.10 |

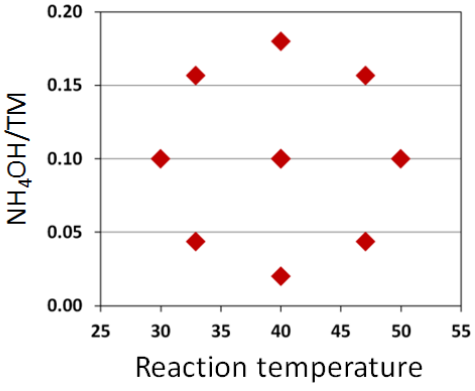


Figure IV- 203: Statistical design of experiments (DoE)

Figure IV- 204 shows main effect plot of process variables. Reaction temperature is not a significant variable for carbonate synthesis route but the ratio of $NH_4OH$ to transition metals affects the density of synthesized materials. R-Sq(adj) value of 90.65% indicates that this regression model accurately fits the

experimental data and ANOVA shows that $NH_4$/TM, $NH_4$/TM*$NH_4$/TM and Temp*$NH_4$/TM terms are statistically significant (See Figure IV- 205).

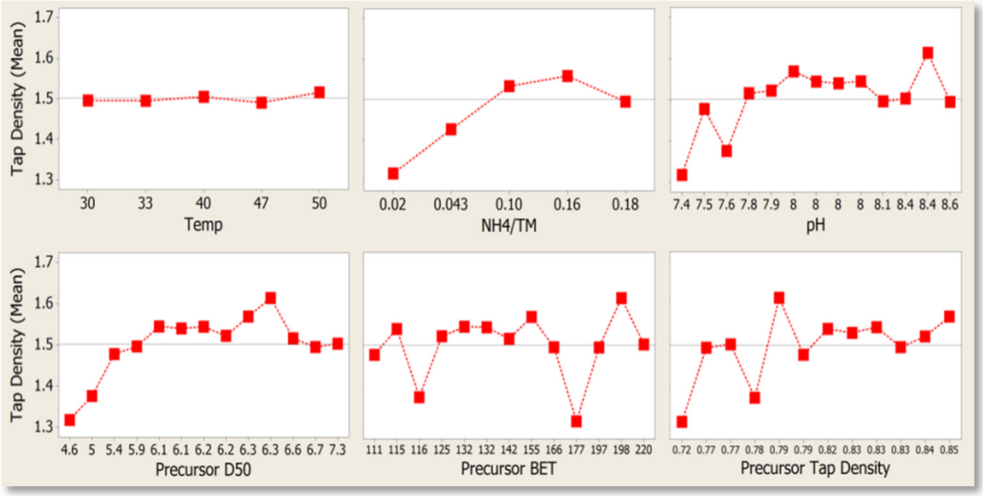


Figure IV- 204: Main effects plot of process variables

**Response Surface Regression: Tap Density vs. Temp, NH4/TM**

R-Sq = 94.55% R-Sq(pred) = 69.78% R-Sq(adj) = 90.65%

**Analysis of variance for tap density**

| Source | F | P |
|---|---|---|
| Regression | 24.28 | 0.000 |
| Linear | 28.97 | 0.000 |
| Temp | 0.08 | 0.783 |
| NH4/TM | 57.87 | 0.000 |
| Square | 21.75 | 0.001 |
| Temp*Temp | 1.19 | 0.311 |
| NH4/TM*NH4/TM | 43.45 | 0.000 |
| Interaction | 19.93 | 0.003 |
| Temp*NH4/TM | 19.93 | 0.003 |
| Residual Error | | |
| Lack-of-Fit | 3.38 | 0.135 |

**Contour plot of cathode tap density**

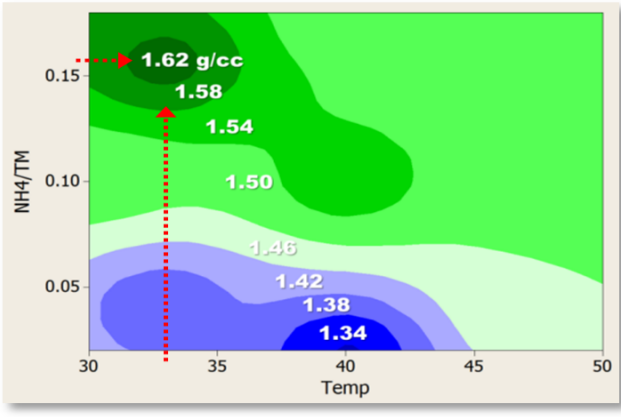


Figure IV- 205: ANOVA and response surface regression

We determined the optimized reaction temperature (33°C) and $NH_4OH$/TM ratio (0.16) based on the contour plot of cathode tap density and then kilogram production of layered layered material was accomplished. Scaled product was delivered to basic R&D groups and CAMP facility for material evaluation and characterization (See Figure IV- 206).

Argonne NATIONAL LABORATORY
The Materials Engineering Research Facility (MERF), 370, ES, 9700 South Cass Avenue, Argonne, IL 60439
Gregory K. Krumdick(630-252-3952, gkrumdick@anl.gov), Youngho Shin(630-252-4861, yshin@anl.gov)

| Outgoing Inspection Data Sheet | Sender | Receiver | Manager |
|---|---|---|---|
| | Youngho Shin | Stephen E. Trask | |
| | | | |

| Target Cathode Composition | Prepared by | Lot Number | Weight | Delivery date |
|---|---|---|---|---|
| $Li_{1.03}Ni_{0.61}Mn_{0.33}Co_{0.06}O_y$ | Youngho Shin<br>Ozge F. Feridun | ES20150514 | 50 g | 7/1/2015 |

| Analysis | | Results | Target | Judgement | Note | Method |
|---|---|---|---|---|---|---|
| Particle Size Distribution | D10 (㎛) | 5.2 | | | | Particle Size Analyzer |
| | D50 (㎛) | 9.9 | | | | |
| | D90 (㎛) | 18.8 | | | | |
| Specific Surface Area (㎡/g) | | 0.83 | | | | BET |
| Tap Density (g/cc) | | 1.93 | | | | Tap Density Meter |
| Element mol % | Li / (Ni+Mn+Co) | 1.03 | | | | ICP-MASS |
| | Ni / (Ni+Mn+Co) | 0.61 | | | | |
| | Mn / (Ni+Mn+Co) | 0.33 | | | | |
| | Co / (Ni+Mn+Co) | 0.06 | | | | |
| For Use | | Lithium Ion Secondary Battery | | | | |

SEM

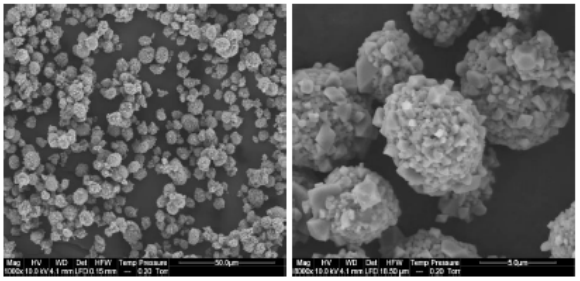

Remark

This material and data is confidential non-public that may not be communicated in any way without the consent of provider.

We recommend re-analysis of Li content for better accuracy.

Coin Cell Test : Initial charge (mAh/g) @15 mA/g : 230.2 Initial discharge (mAh/g) @15 mA/g : 200.1

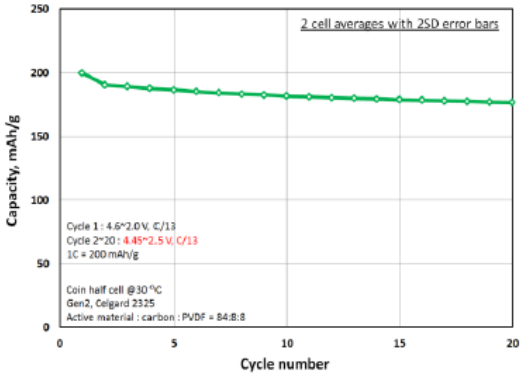


ANL-ES-001(11/29/2011) Argonne National Laboratory Energy Systems Division

**Figure IV- 206: Outgoing inspection data sheet of scaled layered layered material**

**Structure stabilization of layered layered spinel material by adjusting spinel content**

Layered layered spinel material was selected as a candidate material of scale-up research to support basic R&D of Michael Thackeray's research group at Argonne National Laboratory.This material was requested for composition stability studies and surface coating research. As shown in Figure IV- 207, preliminary synthesis of layered layered spinel materials by both carbonate and hydroxide synthesis routes shows stable discharge performance which were cycled between 2.5 and 4.45 V at C/13. On the basis of these results, carbonate process shows better capacity and hydroxide process shows better cycling stability. These two preliminary synthesized materials were delivered to basic R&D groups to evaluate and compare the electrochemical performances and to support their initial surface coating studies.

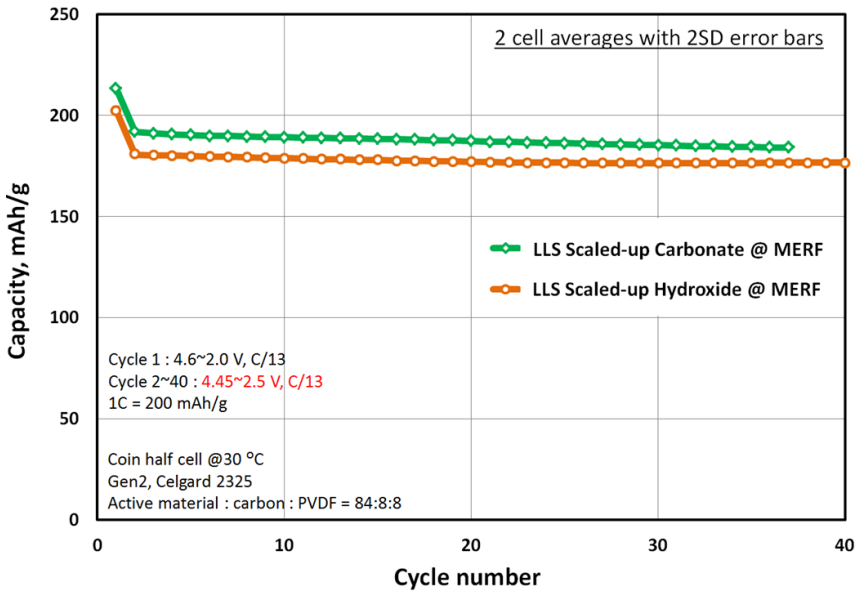


Figure IV- 207: Coin cell result of preliminary synthesized layered layered spinel material

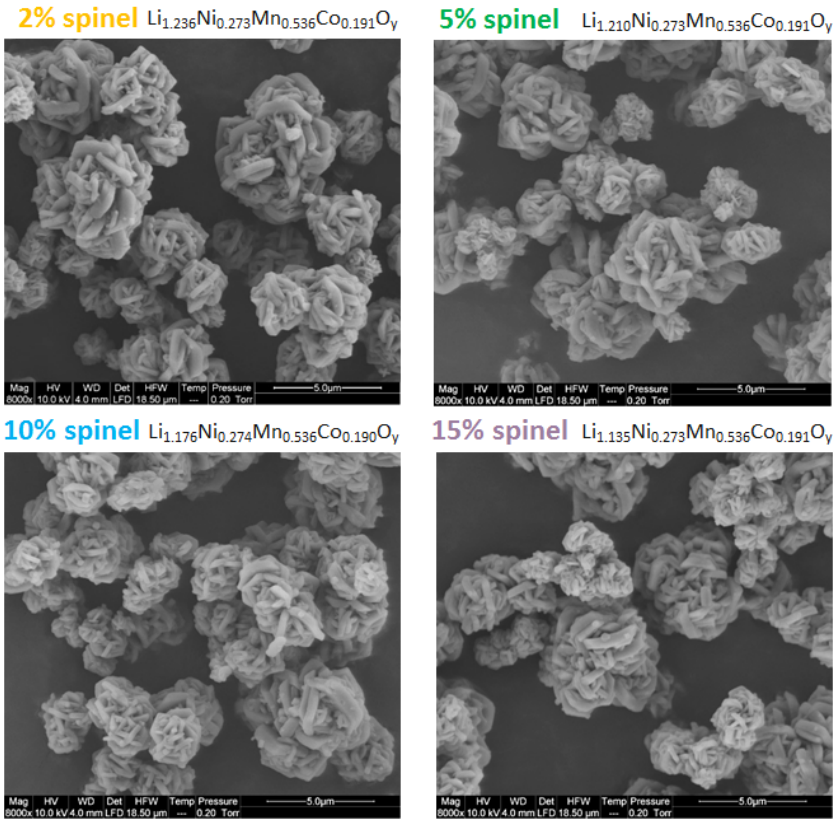


Figure IV- 208: SEM images of layered layered spinel materials with different spinel content

To get improved structure stability of this composition, we decided to find optimal spinel phase ratio based on hydroxide process and successfully synthesized 2%, 5%, 10% and 15% spinel phase contents in this composition by collaboration with Michael Thackeray's research group (See Figure IV- 208). All prepared layered layered spinel materials show similar morphology and particle size ($D_{10}$ = 2.5$\mu$m, $D_{50}$ = 4.3$\mu$m, $D_{90}$ = 7.3$\mu$m) in spite of the spinel amount change.

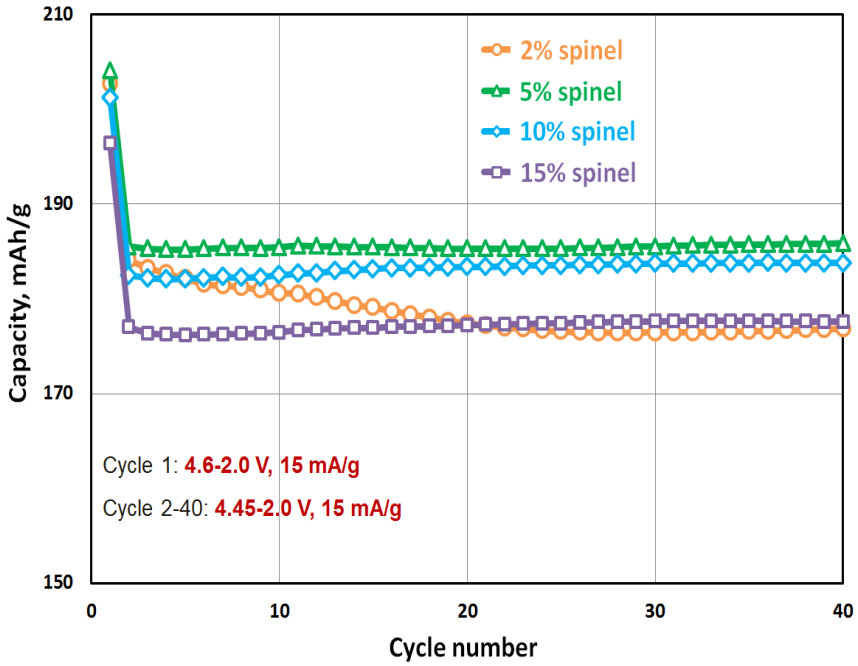


Figure IV- 209: C/13 cycling result of layered layered spinel materials

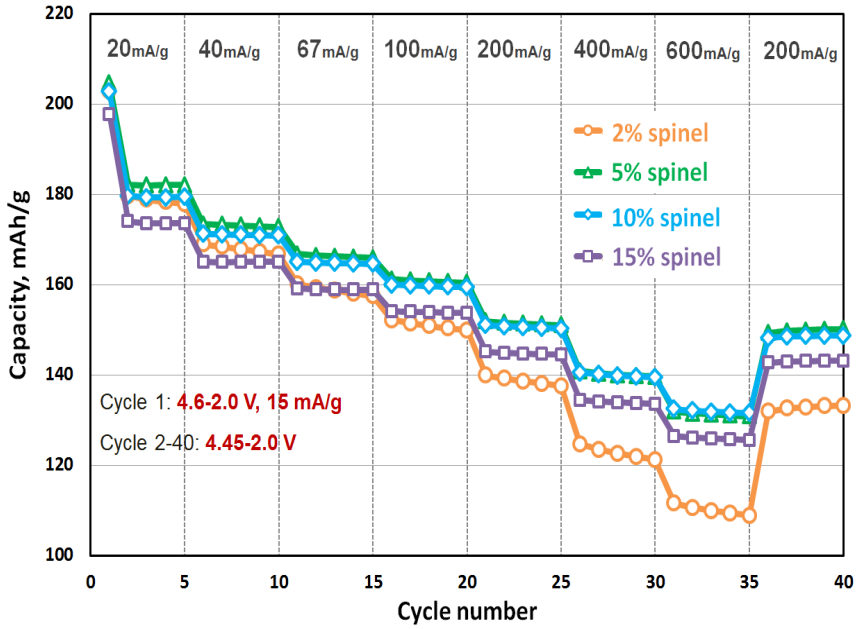


Figure IV- 210: Rate performance of layered layered spinel materials

Figure IV- 208 shows very encouraging results. When it is cycled between 2.0 and 4.45 V at 15 mA/g, 2% spinel content still shows some capacity loss. However, 5%, 10% and 15% spinel contents do not show any capacity loss during 40 cycles which indicates that the capacity loss can be minimized to a level that does not exist if we carefully control the amount of spinel phase and its synthesis. It is also found that when the spinel ratio in the structure is higher than 10% (in this case, at 15%), the capacity is relatively lower compared to lower spinel ratios, as is shown in Figure IV- 209. Interestingly, the capacity of 5% spinel content is higher than less spinel content which should be examined closely in collaboration with basic research groups.

Rate performance of layered layered spinel materials has also very compelling results. As shown in Figure IV- 210, more than 5% spinel content shows much improved rate performance at high C-rate compared to 2% spinel content. Higher spinel content shows better rate performance which clearly indicates that spinel phase increases the lithium ion transfer significantly. 5% spinel material was delivered to basic research group for electrochemical test and material characterization. We have made considerable improvement in the cycle and rate performance of layered layered spinel material by adjusting the amount of spinel phase and our achievement has given strong impulse and power to the basic material composition research.

**Co-precipitation process comparison between traditional (batch, CSTR) and emerging (TVR) technologies**

Figure IV- 211: Taylor vortex reactor system

We set up Taylor vortex reactor system to evaluate one of emerging synthesis technologies for material preparation (See Figure IV- 211). This TVR provides high mass transfer and homogeneous micro-mixing inside the reactor by generating Taylor vortices (acting as unitary CSTR cells) which shortens the reaction time and removes dead-zones. Accordingly, dense particles with uniform spherical morphology and sharp particle size distribution can be obtained.

To evaluate co-precipitation processes, we made comparison of conventional 40L batch, advanced 20L CSTR and 1L TVR using the optimized synthesis condition (reaction temperature = 33°C, $NH_4OH$/TM ratio = 0.16) of layered layered material. Table IV- 26 shows the comparison result of 3 co-precipitation processes. ICP-MS analysis confirmed that the target composition of layered layered material was successfully achieved by all processes. The average particle sizes of synthesized material vary from 11$\mu$m to 15$\mu$m. The cross-sectional image (FIB-SEM) of the particle of batch process (not fully optimized) shows a porous internal structure surrounded by a dense outside layer. However, in case of TVR, densely packed grains without internal porosity was obtained at its first trial. We proved that TVR has high potential to generate dense spherical particles with uniform size.

**Table IV- 26: Process comparison between batch, CSTR and TVR**

| Process | Conventional 40L Batch | Advanced 20L CSTR | 1L TVR (Taylor Vortex Reactor) |
|---|---|---|---|
| Synthesis condition | Precursors were obtained after 24hr operation at reaction temp. = 33°C and $NH_4OH$/TM = 0.16 | | |
| Calcined material FIB-SEM | 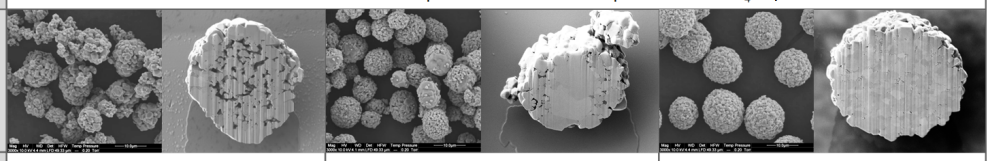 | | |
| ICP-MS analysis | $Li_{1.067}Ni_{0.61}Mn_{0.33}Co_{0.06}O_y$ | $Li_{1.065}Ni_{0.61}Mn_{0.33}Co_{0.06}O_y$ | $Li_{1.073}Ni_{0.60}Mn_{0.34}Co_{0.06}O_y$ |
| $D_{10}/D_{50}/D_{90}$ [µm] | 3.9 / 13.0 / 19.9 | 6.4 / 11.2 / 19.7 | 8.9 / 15.1 / 25.9 |
| BET [$m^2/g$] | 0.71 | 0.53 | 0.46 |
| Tap density [g/cc] | **1.73** | **2.06** | **2.04** |
| *Press density [g/cc] | **2.92** | **2.95** | **2.88** |
| Initial disch. gravi. capacity [mAh/g] | **200.0** | **203.4** | **198.0** |
| **Initial disch. vol. capacity [mAh/cc] | **584.0** | **600.0** | **570.2** |

* Press density was measured at 2.5 t/$cm^2$ ** Calculated based on press density

Figure IV- 212 shows the voltage profiles of synthesized layered layered material by batch, CSTR and TVR processes between 2.0 and 4.6 V at C/13 and cyclability was checked at the voltage window of 2.5 and 4.45 V at C/13 (See Figure IV- 213).

There is no significant difference in electrochemical performance of 3 materials but this layered layered composition shows some capacity loss during cycling.

**Surface coating process development and $AlF_3$-coating on high energy LMR-NMC material**

We developed 1L and 4L wet coating systems to maximize material performance to assist HE/HV program at Argonne National Laboratory by carrying out systematic surface modification research, and process development and scale up. We already have several surface coating capability such as pilot scale mechanofusion dry coater (500 g/batch) and pilot scale spray drying coater (200 ~ 500 g/hour) and showed surface coating improves electrochemical performance and cycle life of active material. In FY15, as an initial surface coating evaluation using an installed 1L wet coating system, we carried out aluminum fluoride surface coating on the high energy LMR-NCM material which was scaled at FY14 in collaboration with JPL/NASA. As a wet surface coating procedure, we charge cathode powder into reactor with DI water, feed aluminum nitrate and ammonium fluoride solutions into reactor separately, keep reaction at 70ºC with stirring, dry filtered slurry product after reaction completion and apply heat treatment in $N_2$ condition.

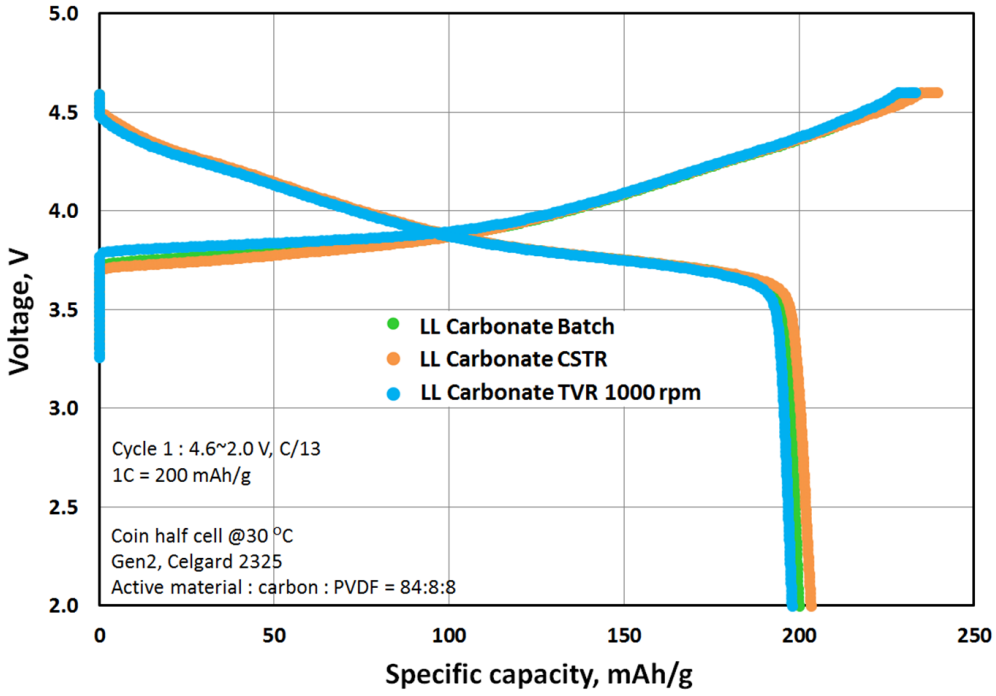


Figure IV- 212: Voltage profiles of layered latered materials produced by 3 processes

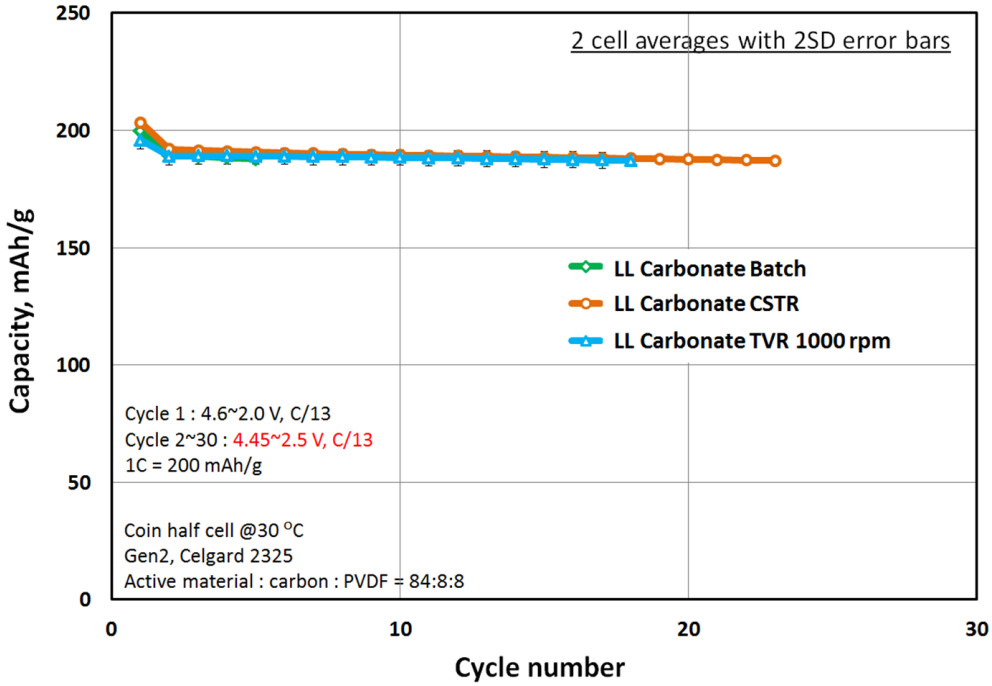


Figure IV- 213: Cyclability of layered latered materials produced by 3 processes

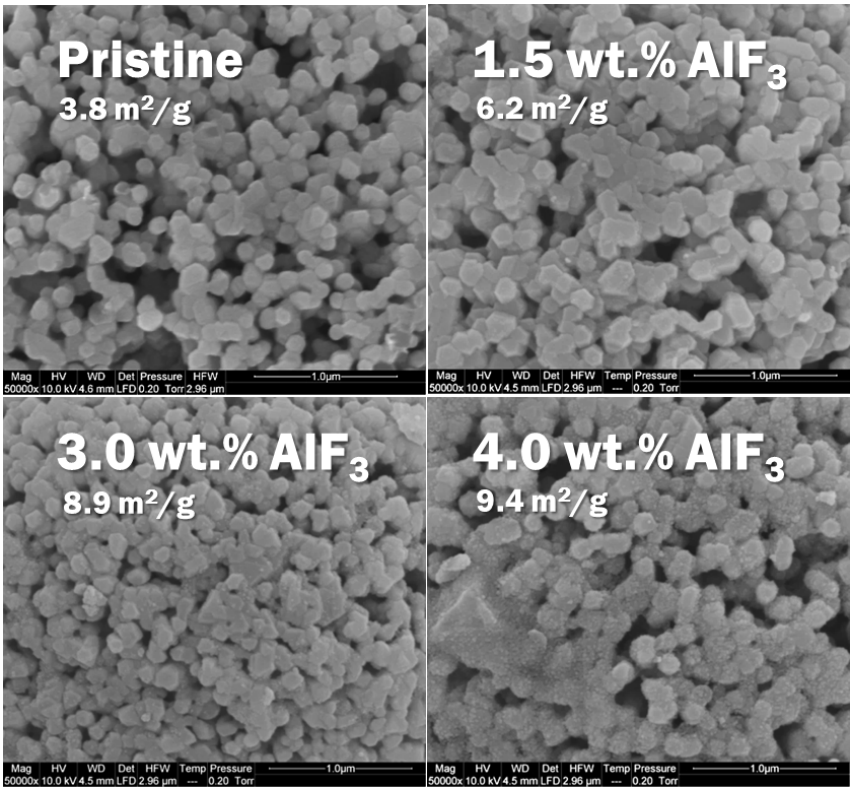


Figure IV- 214: SEM images of pristine and $AlF_3$-coated materials

Figure IV- 214 shows the morphology of the pristine material along with the $AlF_3$-coated of the same, at different coating ratios. As it is seen, all materials regardless of coating amounts have the similar bulk morphologies: comprised of nano grains at 100 -150 nm scale. It is found that when the coating amount is increased, the surface area increases accordingly; although this increase is not linear and the appearance of surface tends to be blur when the coating ratio reaches to 3.0 wt.% and above. It should be also noted that the coating doesn't create a full coverage (3D continuous film) on the surface, instead the $AlF_3$ on the pristine material is in the form of nano-islands attached to the grains of the host, creating approximately 2.5 times larger surface area than that of the host material itself, e.g; 4.0 wt.% $AlF_3$ coating.

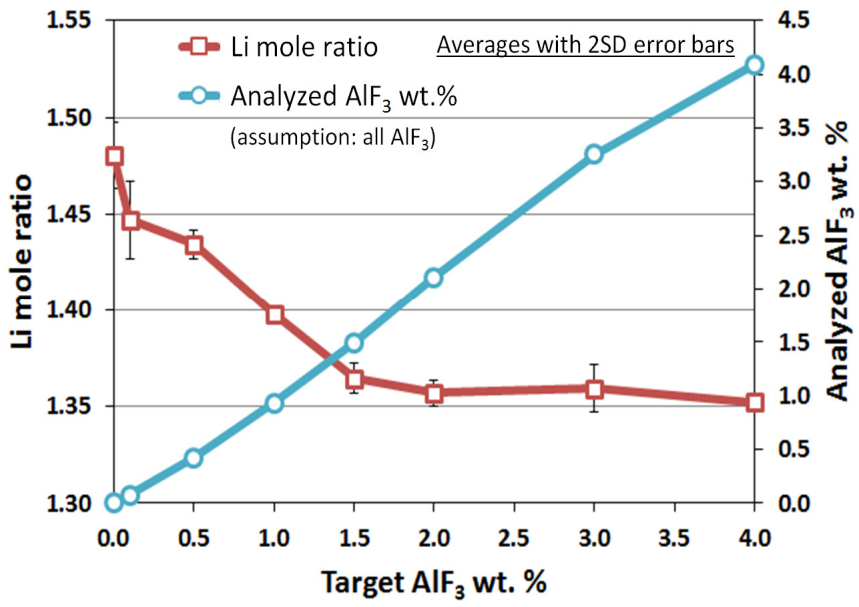


Figure IV- 215: ICP-MS analysis of $AlF_3$-coated materials

As a first trial to verify the coating material, ICP-MS analysis of the pristine and $AlF_3$-coated materials was carried out (See Figure IV- 215). The calculated amount of $AlF_3$ based on feed chemical stoichiometry (X-axis of Figure IV- 215) and the analyzed $AlF_3$ content of coated materials (right Y-axis of Figure IV- 215) were compared and matched one another, which is an indirect evidence of $AlF_3$ surface coating. Further investigation of these coated materials is being planned and carried out by collaboration.

Wet coating generates more uniform and compact surface coverage compared to mechanical dry coating. However, lithium dissolution during coating process and its effect on electrochemical performance should be evaluated. We analyzed the lithium content of each $AlF_3$-coated materials and found that lithium dissolution increases to a certain point (1.5 wt.% $AlF_3$ coating) when $AlF_3$ coating amount increases but Ni, Mn and Co mole ratio remains the same in the pristine material.

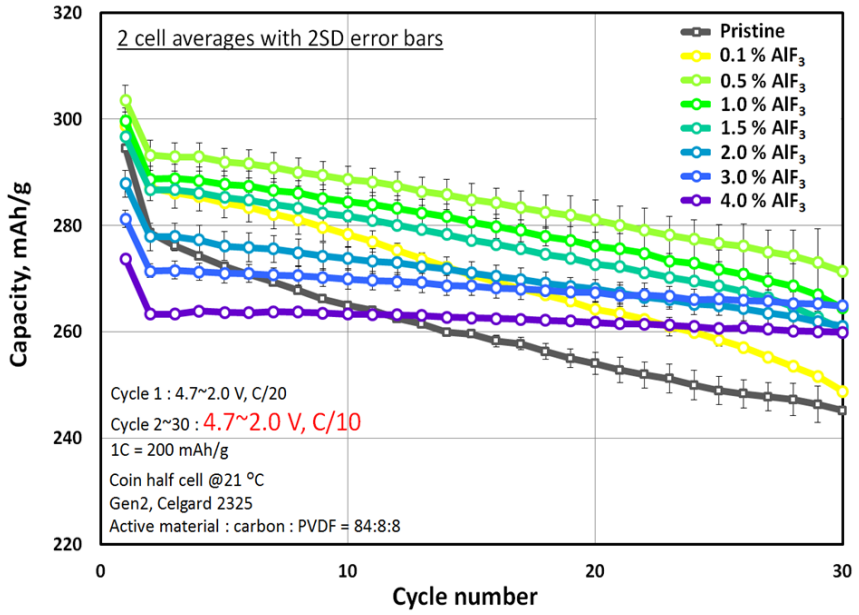


Figure IV- 216: Cycle performance of $AlF_3$-coated materials

The electrochemical performance of pristine and $AlF_3$-coated material was tested and compared (See Figure IV- 216 and Figure IV- 217).

The pristine material shows 12% capacity drop after 30 cycles. On the other hand, 4 wt.% $AlF_3$-coated material shows only 1% capacity drop after 30 cycles. This is quite an impressive example indicating that the cycle life of active material can be considerably extended by surface modification even though the increased $AlF_3$ amount decreases the initial discharge capacity as a tradeoff.

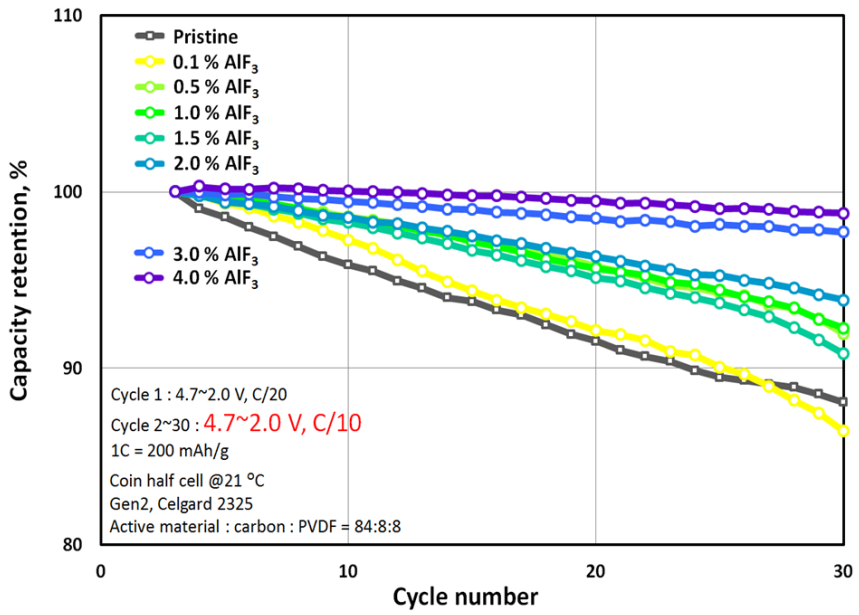


Figure IV- 217: Capacity retention of $AlF_3$-coated materials

Using this surface coating, we have achieved considerable improvement in the cycle performance of high energy LMR-NCM material. The developed wet surface coating process will be scaled and used to evaluate the effect of various coating materials on other scaled active materials.

**Characterization of bench-scale Full Concentration-Gradient (FCG) material as a next scale-up candidate**

Nickel-rich cathode material has high reversible capacity of around 200 mAh/g and is being tested as a practical candidate for electric vehicle applications. However, this material shows poor thermal stability and cycle life especially at elevated temperatures and that should be improved. As an alternative, FCG cathode material (Khalil Amine, DOE project ID:ES208) was chosen and is being studied to enable long cycle life and excellent abuse tolerance for 40 miles PHEV and EVs.

Each particle of FCG material is composed of a core part that is Ni-rich with higher capacity and an outer layer that is Mn-rich with better thermal stability. From the center to the surface of the particle, there is a gradient profile of the transition metals: Ni concentration decreases gradually while Mn and Co concentrations increase as the surface is approached.

**Composition analysis by ICP-MS: $LiNi_{0.76}Co_{0.12}Mn_{0.12}O_2$**

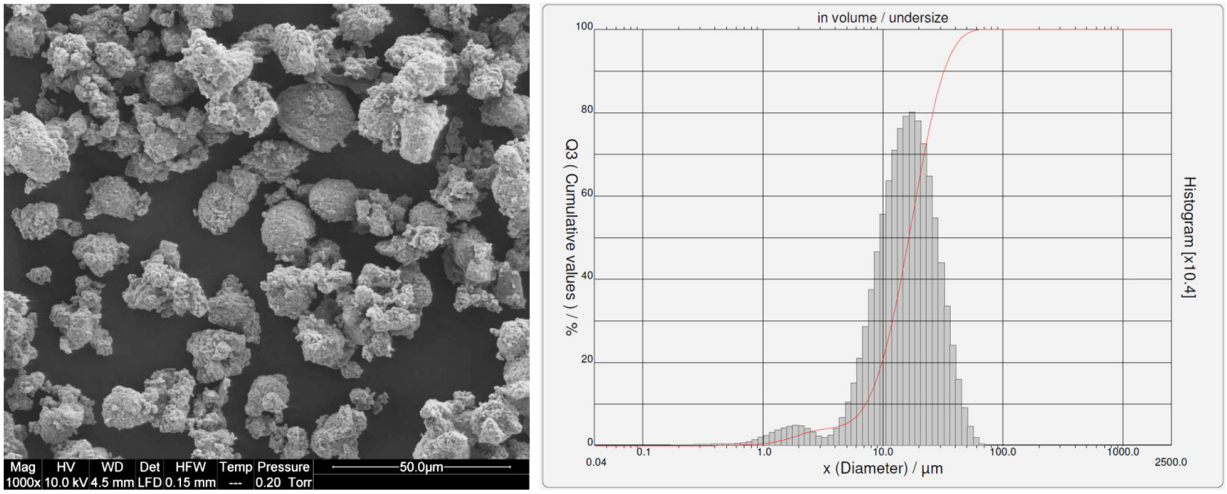


Figure IV- 218: ICP-MS, SEM and particle size analysis results of bench-scale FCG material

Figure IV- 218 shows the analysis result of bench-scale FCG material synthesized by Khalil Amine's research group at Argonne National Laboratory. The average composition of bench-scale FCG (lot # 011915) is $LiNi_{0.76}Co_{0.12}Mn_{0.12}O_2$ which is close to NCM811. Through the morphological examination, the particles tend to form in irregular shapes with wide particle size distribution ($D_{10}$ = 7.2$\mu$m, $D_{50}$ = 16.5$\mu$m, $D_{90}$ =32.3$\mu$m), although a small portion is found to be spherical.

We will develop a customized synthesis process, specifically focusing on spherical morphology, for this FCG material which has NCM811 composition as core part, NCM424 as out layer and NCM622 as average

composition. After our systematic material engineering, we will prove that scaled FCG shows the best of core and out layer compositions and has better electrochemical performance than commercial NCM material. The scaled FCG material will be delivered to basic R&D groups for in-depth characterization, further research and pouch cell evaluation.

### FY 2015 Publications/Presentations


1. "Process Development and Scale up of Advanced Active Battery Materials", ES167_Krumdick_2015_p, US DOE Vehicle Technologies AMR, 2015.
2. G. Krumdick, Y.H. Shin and O. Kahvecioglu Feridun, "Method for Continuous Production of Concentration-Gradient Size-selected Particles", (Invention ANL-IN-14-045, 2014), US Patent filing pending, 2014.
3. Y.H. Shin, O. Kahvecioglu Feridun and G. Krumdick, "Modified Taylor Vortex Reactor", (Invention ANL-IN-15-082, 2015), US Patent filing pending, 2015.
4. Y. Shin, O. K. Feridun, G. Krumdick, (2014). Scale up and optimization for $Li_{1.2}Mn_{0.54}Ni_{0.13}Co_{0.13}O_2$ cathode materials, Material Science and Technology (MS&T 2014), Oct 12-16, 2014, Pittsburgh, PA, USA, Oral Presentation.
5. Y. Shin, O. K. Feridun, G. Krumdick, (2015). Effect of $AlF_3$ Surface Coating on High Energy LMR-NMC Material, 227$^{th}$ Electrochemical Society Meeting, May 24-28, 2015, Chicago, IL, USA, Oral Presentation.
6. O. K. Feridun, Y. Shin, G. Krumdick, (2015). $Li_{1.14}Mn_{0.53}Ni_{0.28}Co_{0.19}O_y$ layered-spinel material prepared using Taylor vortex reactor, 227th Electrochemical Society Meeting, May 24-28, 2015, Chicago, IL, USA, Oral Presentation.
7. O. K. Feridun, Y. Shin, G. Krumdick, (2015). Continuous production of a layered-layered cathode material using a Taylor vortex reactor, June 15-19, 2015, Detroit, MI, USA, Poster Presentation
8. M. M. Thackeray, B. Long, J. R. Croy, E. Lee, J. S. Park, Y. Shin, G. Krumdick, O. K. Feridun, J. Wen, D. Miller, (2015). Addressing the Instability of High Capacity Lithium Battery Cathodes, ECS Conference, July 26-31, 2015, Glasgow, Scotland, Invited Oral Presentation.

# IV.E.2 Process R&D and Scale up of Critical Battery Materials (ANL)

## Objectives

- The objective of this task is to conduct process engineering research for scale-up of new advanced materials for Li-ion batteries. New, innovative materials are being constantly invented to improve safety, energy density, cycle, and calendar life of lithium-ion batteries for HEV and PHEV applications. Up to this point, these materials have only been synthesized in small batches. Scaling up the original route used by discovery scientists involves modification of the bench-scale chemistry and process R&D to allow for the semi-continuous production of materials, development of an engineering flow diagram, and design of a mini-scale system layout, construction of the experimental system and validation of the optimized process. The experimental system will be assembled and the materials will be manufactured in quantities sufficient for full scale industrial evaluation. The materials produced by the program will be analyzed to confirm chemical identity and purity. Analytical methods will be developed for quality control purpose. The electrochemical performance of the materials will be validated to confirm that the properties match the original materials.

### Project Details

**Gregory K Krumdick (ANL Program Manager)**
Argonne National Laboratory
9700 South Cass Avenue
Argonne, IL, 60439-4837
Phone: 630-252-3952; Fax: 630-252-1342
Email: gkrumdick@anl.gov

Collaborators:
Krzysztof Pupek, Argonne National Laboratory
Trevor Dzwiniel, Argonne National Laboratory
Andrew Jansen, Argonne National Laboratory
Bryant Polzin, Argonne National Laboratory
Daniel Abraham, Argonne National Laboratory
John Zhang, Argonne National Laboratory
Gao Liu, Lawrence Berkeley National Laboratory
Chris Orendorff, Sandia National Laboratory
Xiao-Guang Sun, Oak Ridge National Laboratory
Bob Powell, General Motors
Ion Halalay, General Motors
Jerry Martin, Boulderionics
Andrew Risco, Boulderionics

Start Date: October 2010
Projected End Date: September 2016

Start Date: June 2010
Projected End Date: September 2016

## Technical Barriers

- Advanced battery materials are primarily synthesized in small batches by discovery scientists who produce gram quantities of substances. High quality, uniform materials in sufficient quantity cannot be generated using bench-scale procedures. A suitable process R&D and scale-up facility is required to manufacture quantities of new materials that allow for prototyping and thorough evaluation which is required prior to scaling to the next level.

  Barriers addressed:

- Suitability: Bench scale processes are labor intensive, time-consuming, and unsuited for manufacturing.
- Quality: Bench scale products are often un-optimized, not validated, and of inconsistent purity and yield.

## Technical Targets

- Scale-up 3-5 new materials.
- Distribute synthesized materials to industry and R&D community.
- Investigate impurity profile effect on performance for selected electrolyte materials.

## Accomplishments

- Scale-up work has been completed on the following materials:
  - SNL-PFPBO (electrolyte salt/ additive)
  - F-DEC (fluorinated electrolyte solvent)
  - F-EMC (fluorinated electrolyte solvent)
  - GM Mn-Ion Trap (Separator Modifier)
  - LBNL PFM Binder – Si nanoparticle formulation studies.
- Completed study of trace impurities analysis and electrochemical performance of various sampls of LiFSI with collaboration with Boulder Ionics
- Work on the following materials is ongoing:
  - ORNL- Li-BMFMB
  - LBNL 3rd generation binder for Si based anode
  - TFPC (fluorinated electrolyte solvent)
- We are in the process of establishing capabilities and protocols for electrochemical study to develop materials specification (minimum required purity and impurity profile).

### Introduction

Researchers in the battery materials programs across the DOE complex refer to scale up as synthesis of battery materials in gram quantities, and with time consuming, multiple small-scale runs. There is a need to develop scale-up processes for battery materials (primarily lithium-ion based batteries) to the kilogram and tens-of-kilograms quantities at DOE labs. This allows for full scale evaluation, supports further research, and assists the transition of these technologies to industry. Currently, there is no such capability or program across the DOE complex that would accelerate the transition of new materials and technologies from discovery stage to high-volume manufacturing.

### Approach

A formal approach for process R&D and scale-up of advanced battery materials has been defined. This approach starts with the initial discovery of a new material and an initial electrochemical evaluation. This determines if the material is to be added to the inventory database, ranked and prioritized. At this point, the scale-up process begins with the feasibility study, followed by proof of concept testing, first stage scale-up and final second scale scale-up. Go/No Go decisions are located after feasibility determination and electrochemical validation testing.

For each material scaled, we will develop a scalable manufacturing process, analytical methods and quality control procedures. We will also prepare a “technology transfer package” which will include:

- Summary of the original process used by discovery researchers to synthesize the material.
- Summary of the scalable (revised) process suitable for large scale manufacturing.
- Detailed procedure of the revised process for material synthesis.
- Analytical data/Certificate of Analysis for the material (chemical identity and purity).
- The material impurity profile.
- Electrochemical performance test data.
- Preliminary estimates of production cost.
- SDS for the material.
- Material specifications.

We also make kilogram quantities of the material available for industrial evaluation and to the research community. Samples are fully characterized chemically and electrochemically and are available free of charge.

### Results

We have achieved the following progress:

**Scale-Up of SNL-PFPBO LiF complex**

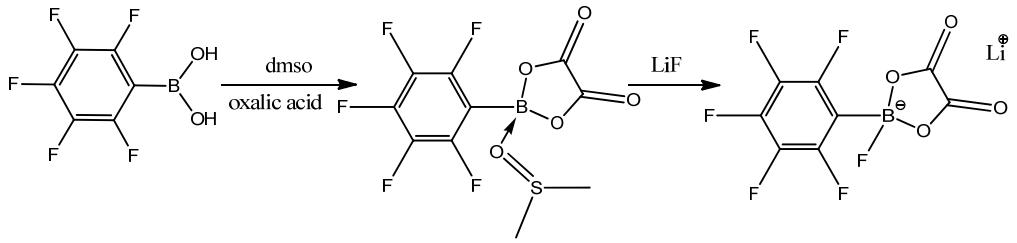


Figure IV- 219: Synthesis of PFPBO-LiF complex

The lithium fluoride complex of PFPBO, originally developed as an anion binding agent (ABA), was modified by Chris Orendorff at Sandia National Lab (SNL). (See Figure IV- 219.)This material shows good performance and improved safety features in calorimeter studies compared to $LiPF_6$ electrolytes. MERF researchers scaled the material to a single 1715g batch and developed several improvements to the synthesis, resulting in a higher throughput and lowered waste generation. Samples of the material were sent to SNL for evaluation as well as to 24M and Argonne's Post Test Facility. Argonne's CAMP provided set of electrodes (NMC 523, $LiCoO_2$, Toda NCA, NEI $LiMn_{1.5}Ni_{0.5}O_4$, HE5050, all paired with CP graphite) to SNL and to MERF as well as testing protocols (life cycling, rate study, HPPC). Details and procedure for testing the material in parallel at SNL, CAMP, and MERF are pending development.

**Scale-Up of F-DEC**

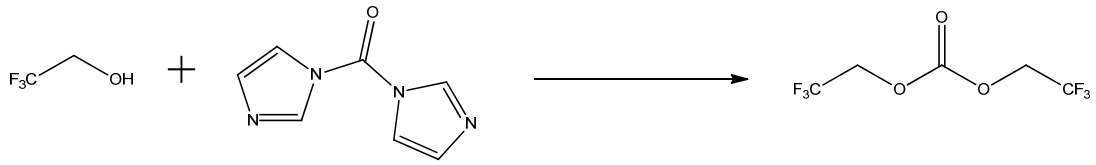

Figure IV- 220: Improved Synthesis of F-DEC

The compound F-DEC (bis-2,2,2-trifluoroethyl)carbonate) (see Figure IV- 220) has been used by several groups looking for an alternative to Gen2 electrolytes for both high voltage applications and applications for safer batteries. MERF researchers developed a conceptually new method to synthesize this compound and have scaled the material to a kilogram level. A wide variety of additional solvents were investigated, but since the neat reaction worked well and showed only moderate exothermicity, the added complication of the fractional distillation eliminated the solvents from further consideration for the kilo scale.

**Scale-Up of F-EMC**

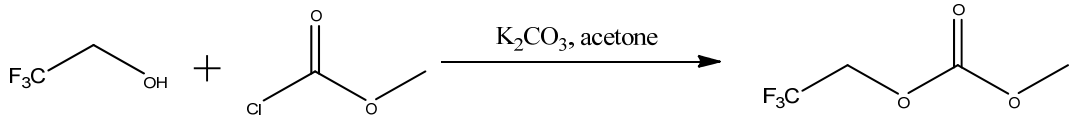


Figure IV- 221: Improved Synthesis of F-EMC

The compound F-EMC (methyl (2,2,2-trifluoro-ethyl)carbonate) has been used by several groups looking for an alternative to Gen2 electrolytes for both high voltage applications and applications for safer batteries (see Figure IV- 221). MERF researchers developed an improved method to synthesize this compound and have scaled the material to a kilogram level. The batch-to-batch reproducibility of the process (yield and purity) was shown to be excellent on a kilo scale.

### GM Mn-Ion Trap

A new economical process for derivation of base chloromethyl polymer with aza-15-crown-5 was developed, forming the new polymer poly(aza-15-c-5-VB-co-DVB), with an overall process simplification achieved by reduction of dialysis and freeze-drying steps as well as a substantial (50%) reduction in the required amount of aza-15-crown-5. (See Figure IV-122.) New cross-linking product specifications were developed, particularly ≥95% conversion from chloromethyl to aza-15-crown-5 and spherical particles of 10-30 nm size. MERF prepared several samples with a cross-linking ratio of 3% to 40% for analysis. (See Figure IV- 223, Figure IV- 224.) A previously unknown correlation between % cross-linking and substitution ratios was identified. This had an immediate effect on product performance, where the amorphous low percentage cross-linked polymers were unable to be formulated to a blended polymer. Although higher cross-linking gave good polymer morphology, the higher amount unreacted chloride led to poor performance in the cell tests. Currently, GM is developing a new method to remove residual chloride in the higher crosslinked polymers.

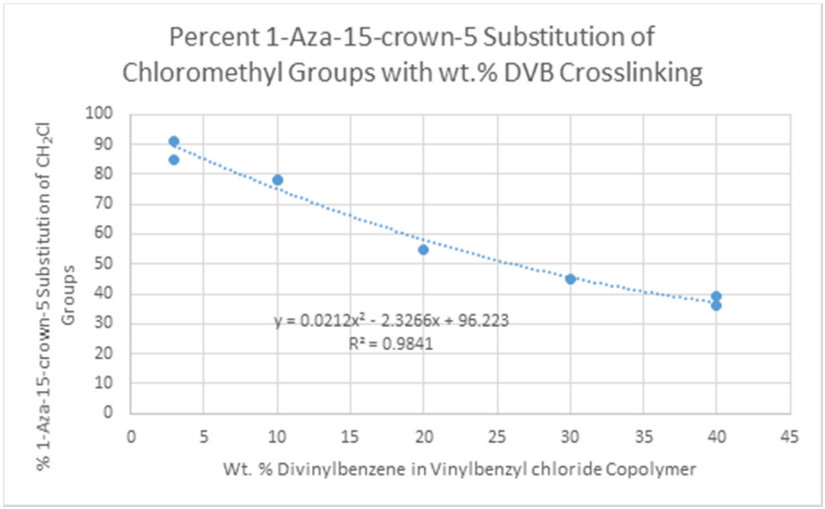


Figure IV- 222: Crosslinking vs. % residual Chloride

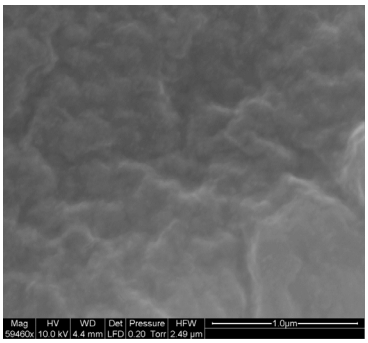

Figure IV- 223: 3% crosslinked

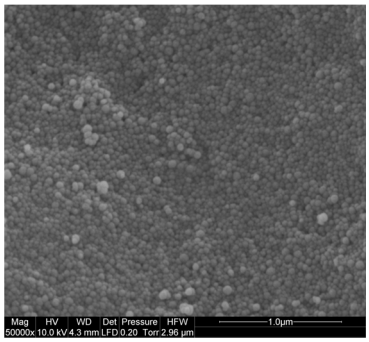

Figure IV- 224: 24% crosslinked

### Si-PFM/PEFM for Si-Graphite Electrode

Initial evaluation at Argonne's CAMP facility suggested that the binder formulation could be optimized for improved performance. MERF effected changes to the binder morphology in the formulation with Nanoamor's 50 nm silicon, and established two separate binder formulations using both wet-coating and dry-coating methods. In the wet-coating method, the PFM was dissolved in THF (1/100 w/v), and the silicon nanoparticles were added (Si/PFM 9/1 w/w) to the solution. The solvent was removed under vacuum and dried at 30°C. This material was ball milled to yield a multimodal PSD. (See Figure IV- 225.)

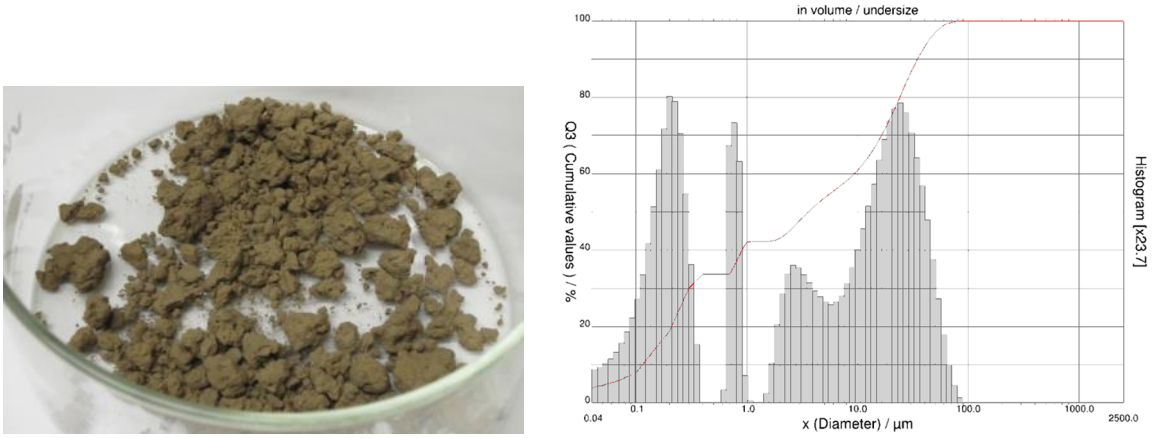


**Figure IV- 225: 50 nm silicon coated with 10% w/w PFM (before milling); PSA of wet-blended Si-PFM/Nano-Si after milling**

In the dry coating method, a high dilution PFM solution (1/350 w/v) in THF was added to excess methanol to precipitate a fine powder. This powder was allowed to settle, the organic solvents removed as much as possible, and then were replaced with water. This final suspension was freeze-dried (see Figure IV- 226, Figure IV- 227). This fine powder of uniform PFM particles was dry blended 1:9 with Nanoamor Si giving a bimodal PSD. Samples of this material were forwarded to CAMP.

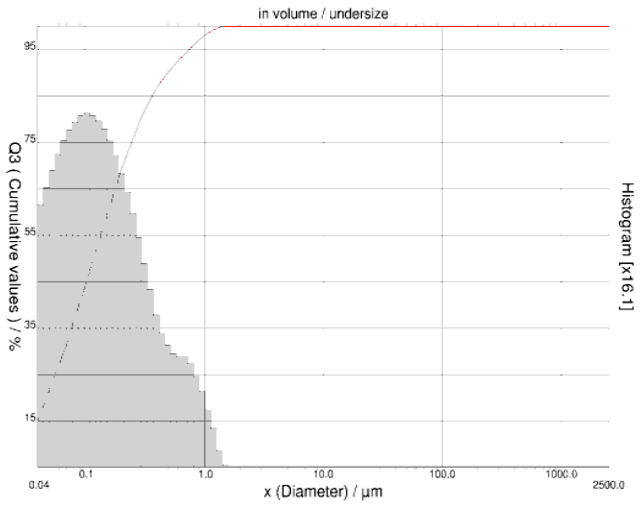


**Figure IV- 226: PSA of Si-PFM/Nano-Si**

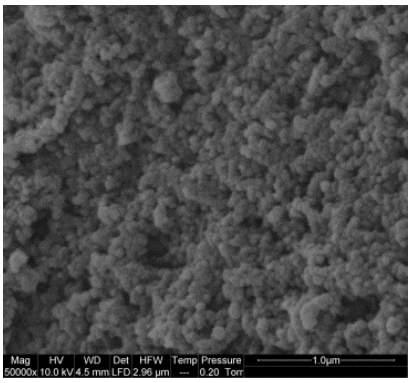


**Figure IV- 227: Freeze-dried PFM powder**

CAMP results showed a slight benefit using the LBNL binder on nano-silicon tested in half cells using (NanoAmor 50-70 nSi), 1.2M $LiPF_6$ in EC:EMC (3:7 wt.%) + 10wt.% FEC. Voltage limits were set to 0.05 to 1.5V. The half cells were cycled through formation (C/10 x 10 cycles), then a rate study of C/5 x 5 cycles, C/2 x 5 cycles and 1C x 5 cycles. A cycle life test of C/5 x 100 cycles finished the evaluation. (See Figure IV-228.)

These data suggested that the LBNL material be evaluated as a "surface modifier" for nano Si. Three samples (20 g each) of modified nano Si was produced by MERF and forwarded to CAMP.

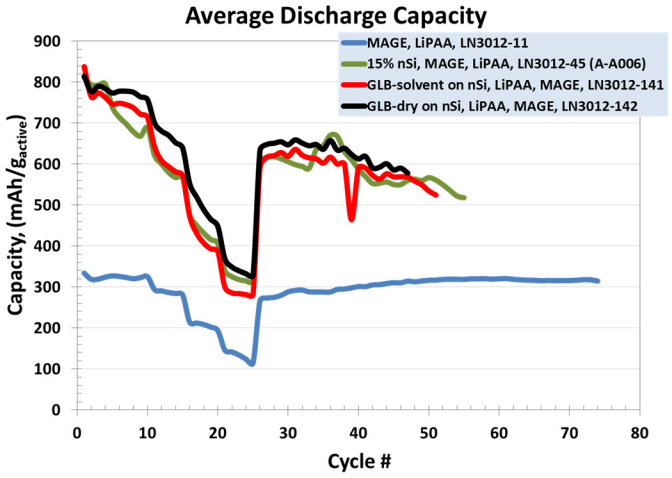


Figure IV- 228: Cell performance of LBNL binder vs. non-treated Si

Sample 1: Si nanoparticles were wet-coated with 1.5% PFM, dried, and milled.

Sample 2: the Si nanoparticles were wet-coated with 1.5% PEFM, dried, and milled.

Sample 3: the Si nanoparticles were processed the same way as above but without any polymer (reference sample).

These materials are all pending electrochemical evaluation.

### LiFSI trace impurities and electrochemical performance of the material

There is growing interest in lithium bis(fluorosulfonyl)imide (LiFSI) as an alternative to $LiPF_6$ and as an additive to electrolytes used in lithium-ion cells. LiFSI has attracted attention because it is reported to have higher ionic conductivity, better high temperature stability, and enhanced stability toward hydrolysis, Also, LiFSI additive to electrolytes can bring benefits of improved storage properties and reduced gas evolution in the cells.

Different levels of different electrochemically active impurities could affect the performance of LiFSI as an electrolyte salt for Li-ion batteries, generating inconsistent and conflicting interpretations of the experimental data.

Argonne in collaboration with Boulder conducted comparative study of several commercial samples of LiFSI to assess effect of impurity profile on electrochemical performance of the materials. Additionaly, we investigated the effects of added impurities on self-discharge current, cycle life and calendar life of the cells.

Ion chromatography (IC) was used for chemical analyses of trace impurities in the samples. We found that purity and impurity profile of commercial samples of LiFSI vary significantly both from vendor to vendor and from lot to lot. Table IV- 27 summarizes IC analyses (ppm), K-F moisture titration results and pH of 1 M aqueous solution for various samples of LiFSI. The values for impurities were measured in water solution of LiFSI and in formulated electrolyte after filtration through 0.2 µm filter (* no standard available, values are estimated).

**Table IV- 27: Summary IC analyses, K-F moisture titration results and pH of 1 M aqueous solution for various samples of LiFSI**

| | Vendor A Lot #1 | Vendor A Lot #2 | Vendor B | Vendor C | Vendor D | Vendor E |
|---|---|---|---|---|---|---|
| Fluoride | 38/11 | 66/21 | 59/35 | 69/54 | 40/13 | 42/50 |
| Sulfamate | 250/123 | 162/183 | 281/298 | 280/310 | 9/46 | 821/864 |
| Chloride | 5/3 | 2/2 | 8/4 | 3/2 | 10/5 | 35/29 |
| Sulfate | 64/14 | 440/34 | 324/40 | 212/91 | 24/27 | 6,358/1,049 |
| Unkn. 1* | ND | ND | 49,700/12,100 | 26,700/10,000 | ND | ND |
| Unkn. 2* | ND | 590/660 | ND | ND | ND | 5,600/3,580 |
| Moisture (ppm) | 6 | 7 | 7 | 7 | 17 | 4 |
| pH (1 M in water) | 4.71 | 4.50 | 4.17 | 4.16 | 5.68 | 3.52 |

### Self-Discharge Current

To assess the effect of impurity profile on self-discharge current the cells were charged from 3.5 to 5.0 V in 0.1V steps and held for 5 hr at each step. Self-discharge current is defined as a current observed by the end of

each 5 hr period. All experiments were carried out at 30°C in Al Clad CR2032 NCM523//Graphite full cells using a Celgard 2325 separator. The electrolytes were formulated to contain 1.2 M LiFSI in EC/EMC 3/7 by weight. (See Figure IV- 229, Table IV- 28)

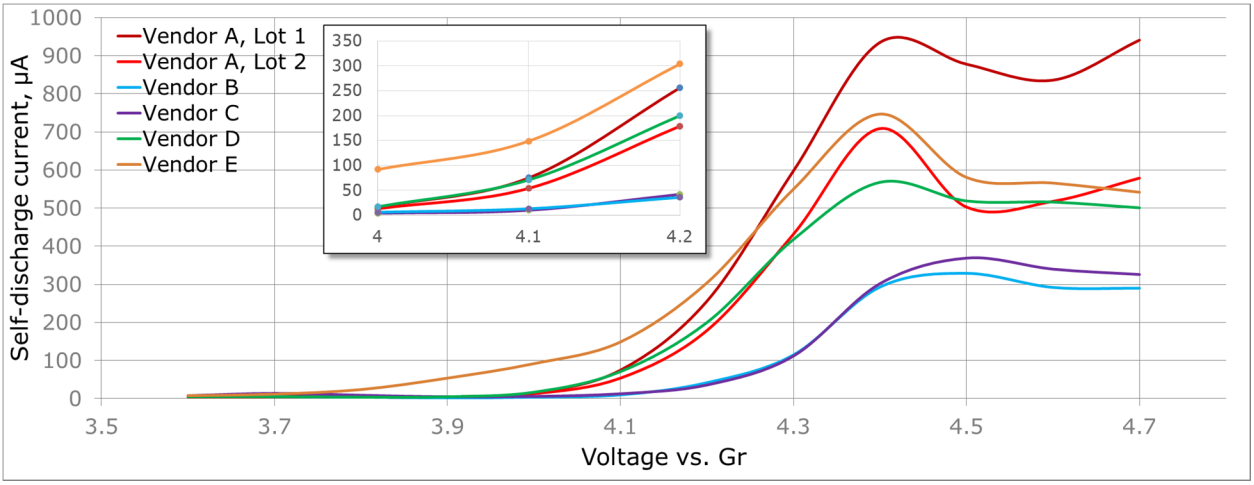


Figure IV- 229: Self-Discharge Current

**Table IV- 28: Self Discharge Current Results**

| Self-discharge Current (µA) at 4.1V | | | | | |
|---|---|---|---|---|---|
| Vendor A Lot #1 | Vendor A Lot #2 | Vendor B | Vendor C | Vendor D | Vendor E |
| 75 | 54 | 10 | 13 | 71 | 149 |

Self-discharge current shows some dependence on sample investigated. It was noticeably lower at 4.1V for electrolytes formulated from samples B and C. Samples from the two vendors both contain substantial amount of unknown impurity absent in any other samples. We believe that the impurities partially passivate metals thus lovering the self-discharge current associated with corrosion.

To evaluate impact of a particular impurity, we spiked commercial sample of LiFSI (Vendor A, Lot # 1) with warious additives. All samples were prepared from stock solution of 1.2 M LiFSI in EC/EMC 3/7 by weight. The mixtures were filtered through 0.2 µm PTFE filter and analyzed by IC prior use. Table IV- 29 lists formulated samples and procedures for their preparation.

**Table IV- 29: Formulated samples and procedures for preparation**

| | |
|---|---|
| Sample A1-1 | Added 500 ppm water and aged 24 h at 50°C |
| Sample A1-2 | Added excess of lithium chloride and aged 24 at room temperature |
| Sample A1-3 | Added excess of sulfamic acid and aged 24 at room temperature |
| Sample A1-4 | Added 500 ppm of sulfamoyl fluoride and aged 24 h at room temperature |
| Sample A1-5 | Added 250 ppm of lithium chloride and aged 24 h at 50°C |
| Sample A1-6 | Added excess of lithium fluoride and aged 24 at room temperature |

Table IV- 30 lists ion chromatograpy analyses for electrolyte formulated from original Vendor A, Lot #1 LiFSI and samples A1-1 to A1-6.

**Table IV- 30: Ion chromatograpy analyses for electrolyte**

| | Vendor A Lot #1 | A1-1 | A1-2 | A1-3 | A1-4 | A1-5 | A1-6 |
|---|---|---|---|---|---|---|---|
| Fluoride | 11 | 19.9 | 13.7 | 10.7 | 118.6 | 9.9 | 14.5 |
| Sulfamate | 123 | 57.9 | 25.0 | 204.7 | 498.8 | 34.1 | 28.4 |
| Chloride | 3 | 3.4 | 929.0 | 4.0 | 4.5 | 267.1 | 21.5 |
| Sulfate | 14 | 27.0 | 5.5 | 6.3 | 10.4 | 3.9 | 5.8 |

We found that treatment of the electrolyte with lithium chloride has a detrimental effect on self-discharge current (Table IV- 31, Sample A1-2 and A1-5) and the current increased with concentration of chlorine ion as measured by IC. Due to extremaly low solubility of lithium flouride in the electrolyte, the effect of the salt can not be observed.

**Table IV- 31: Effect of the treatment of electrolyte with lithium chloride on self-discharge current**

| | Vendor A Lot #1 | A1-1 | A1-2 | A1-3 | A1-4 | A1-5 | A1-6 |
|---|---|---|---|---|---|---|---|
| Voltage (V) | Self-Discharge Current (uA) | | | | | | |
| 3.6 | 6 | 19 | 210 | 7 | 18 | 18 | 11 |
| 3.7 | 12 | 25 | 338 | 9 | 33 | 25 | 20 |
| 3.8 | 7 | 34 | 426 | 7 | 26 | 30 | 17 |
| 3.9 | 5 | 43 | 601 | 8 | 32 | 39 | 12 |
| 4.0 | 16 | 70 | 858 | 28 | 55 | 72 | 14 |
| 4.1 | 75 | 136 | 1107 | 111 | 116 | 164 | 60 |
| 4.2 | 256 | 265 | 1427 | 364 | 235 | 379 | 218 |

### Cycle Life Aging

The electrolytes were formulated to contain 1.2 M LiFSI in EC/EMC 3/7 by weight from each vendor. The cells were cycled between 3.0 and 4.1 V at C/2 rate for 100. All experiments were carried out at 30°C in Al clad CR2032 NCM523//Graphite full cells using a Celgard 2325 separator. (See Figure IV- 230.)

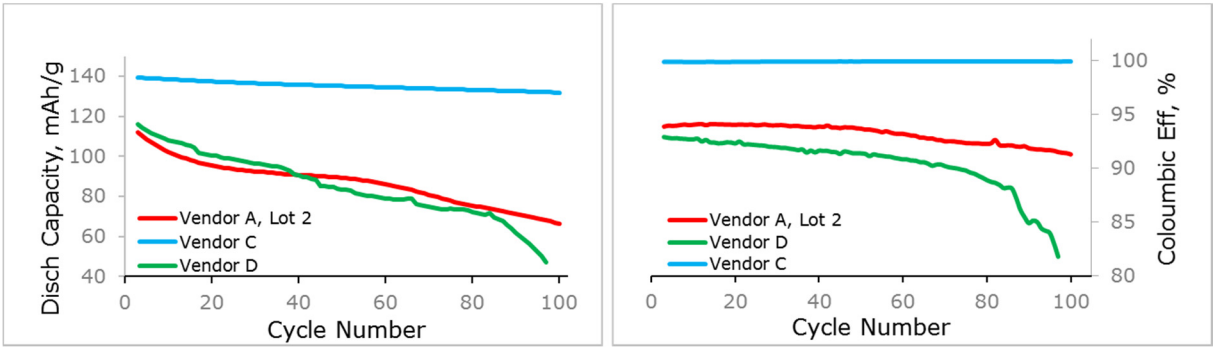


**Figure IV- 230: Cycling behavior of LiFSI from different commercial vendors**

Samples from vendor B and C (only C is shown here) performed significantly better on cycle life aging tests. Capacity fade for sample C was 5.3% after 100 cycles versus 40.7% for sample A, lot #2 and 59.3% for sample D, respectively. Columbic Efficiency for sample C was very high, near steady around 99.9% across 100 cycles. Columbic Efficiency for samples A, lot #2 and D were rapidly degraded (93.9/91.3% and 92.9/84.2% from 3rd to 100th cycle respectively, for sample A, lot #2 and D). The superior performance of the electrolyte prepared from vendor B and C samples corelates with lower self-discharge current.

**Table IV- 32: Effect of added impurity on cell degradation**

| | Electrolyte Formulation | | | | | |
|---|---|---|---|---|---|---|
| | A1-1 | A1-2 | A1-3 | A1-4 | A1-5 | A1-6 |
| Ch, CF% | 53.4 | n/a | 91.4 | 93.0 | n/a | 70.2 |
| DCh, CF% | 54.5 | n/a | 92.2 | 93.1 | n/a | 71.3 |
| CoulEff% | 94.0 | n/a | 84.7 | 94.5 | n/a | 91.5 |

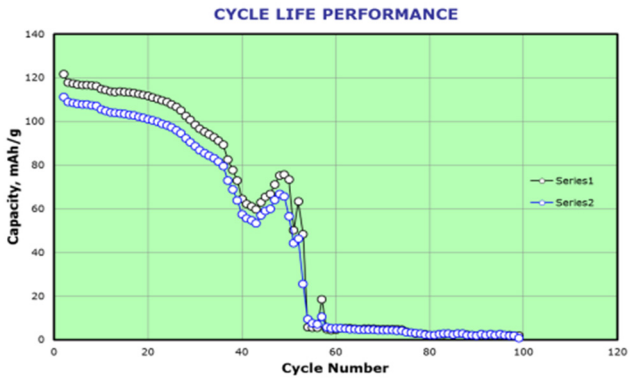


Figure IV- 231: Rapid capacity fade in cells formulated with electrolyte A1-5

As expected, added impurities caused the cells to degraded quicker. Table V lists capacity fade (%) for charge cycle, capacity fade (%) for discharge cycle, and coulombic efficiency (%) after 100 cycles. Cells made using formulation A1-2 (high chlorine content, see Table IV- 32) did not cycled at all. Cells A1-5 with moderate amount of chlorind broke down rapidly withing the first 50 cycles (Figure IV- 231).

### Calendar Life Aging

The calendar life aging investigation utilized that same electrolyte formulations and experimental setting as the cycle life aging study. The cells were charged and held at 4.1 V for 100 h at 30°C while the current was observed.

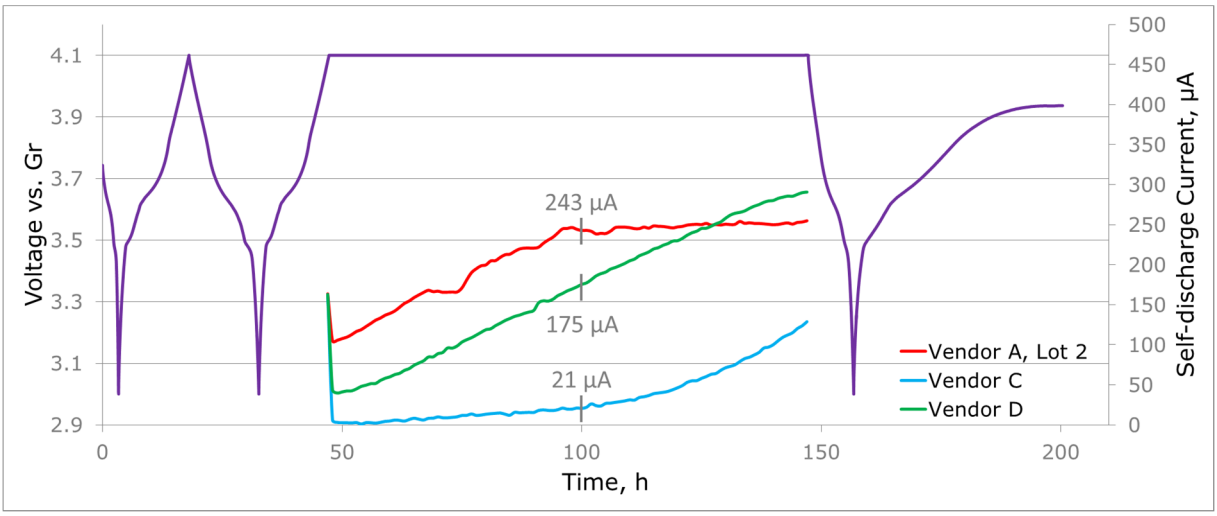


Figure IV- 232: Self-discharge current in calendar life aging experiments

Although samples from vendor B and C performed slightly better on the calendar life aging test the experiment revealed substantial self-discharge current at 4.1 V for all six LiFSI samples (Figure IV- 232).

### Coin cells vs. pouch cells

We noted, while studing LiFSI impurity profile impact on cycling behavior, that some cells in triplicate batches were erratic. The phenomenon was observed in all samples except samples from vendors B and C.

The probable cause was imperfect Al clad in coin cell casing that allows exposure of the stainless steel backing to the electrolyte and corrosion causing high self-discharge current. Samples from both vendor B and C contain large amount of unidentified impurity that may acts as a stainless steel corrosion inhibitor (Figure IV- 233).

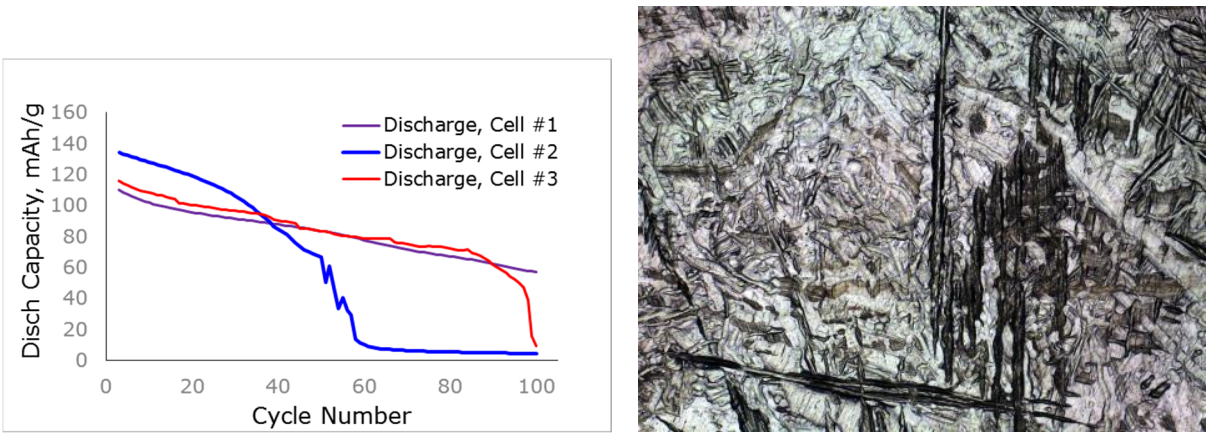


Figure IV- 233: An example of an erratic triplicate cells and photomicrograph of imperfections in Al-clad coin cell casing

Since Al clad coin cells may not be the best format to study LiFSI based electrolytes a set of cycling life aging experiments were run using pouch cell.

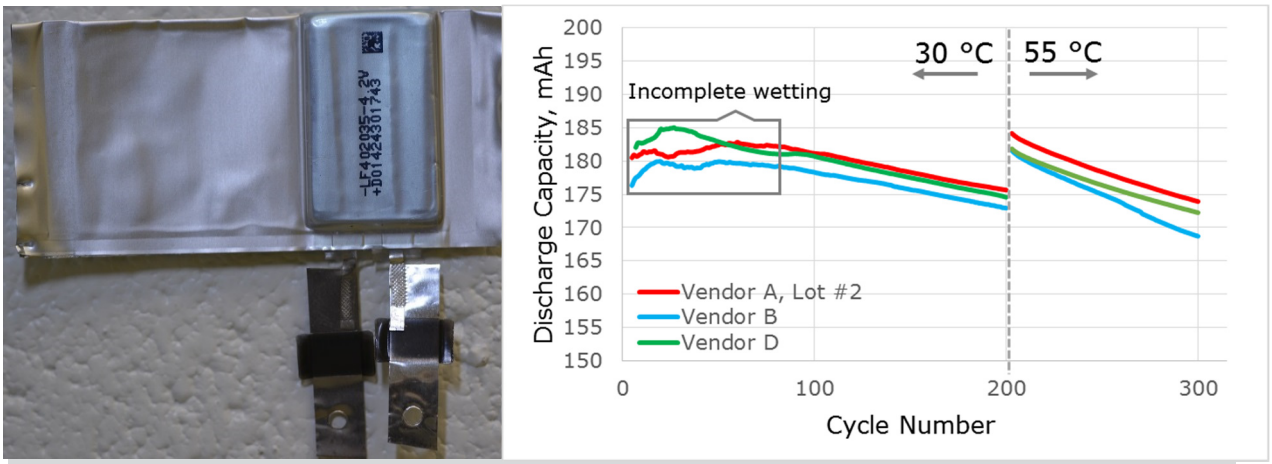


Figure IV- 234: Cycling behavior of electrolytes prepared from selected LiFSI samples in NCA//Gr pouch cells

Machine-made (Li-Fun) 200 mAh NCA//Gr pouch cells were cycled between 3.0 and 4.1 V at 1C rate in triplicate using electrolyte formulated from selected LiFSI samples.
The experiment revealed that electrolytes formulated from different LiFSI samples all perform similarly in pouch cells test (average from triplicate trials are plotted). Unlike coin cell trials, no erratic behavior was observed in pouch cell experiments (Figure IV- 234).

### LBNL 3rd generation binder for Si based anode

MERF is preparing a small sample of the 3rd generation LBNL binder, a co-polymer of pyren-1-ylmethyl methacrylate and 2-(2-(2-methoxyethoxy)ethoxy)ethyl methacrylate, in a 10 to 4 ratio. (See Figure IV- 235.) The material will be forwarded to Argonne's CSE for electrode manufacturing and performance evaluation.

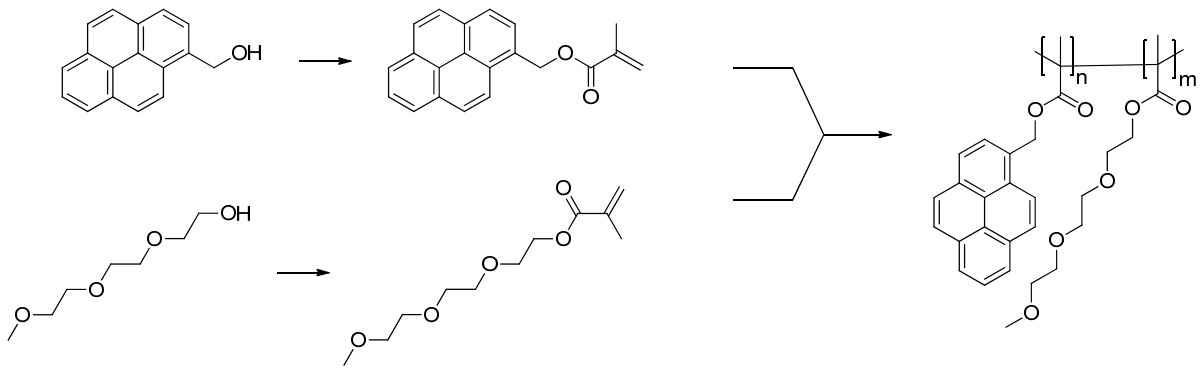


Figure IV- 235: Synthesis of 3rd Generation Si-Binder

## Conclusions and Future Directions

The scale-up work was completed and technology transfer packages for SNL-PFPBO, F-DEC and F-EMC were created. Process R&D on conductive binders for Si electrode (LBNL-PFM and LBNL-PEFM) was completed. The materials were electrochemically evaluated in collaboration with Argonne's CAMP facility.

- 3-5 electrolyte materials are targeted for scale-up in FY15. Materials from Army Lab Research, the University of Kentucky and Argonne National Laboratory are all under evaluation.
- 1 purity/impurity study are to be conducted per year
- Emerging manufacturing technologies such as flow reactors or reactive distillations to lower manufacturing costs are to be evaluated.

In addition, a detailed trace impurity analysis and electrochemical study of Li-FSI was conducted in collaboration with Boulderionics. The objective of this project was to develop battery grade specification for the materials by correlating impurities level and profile with electrochemical performance.

The objective of the project is to develop specifications for the materials by correlating impurity levels and profiles with electrochemical performance. We will acquire samples of the material and conduct a comparative electrochemical performance study and trace impurity analysis to establish minimum purity (specification) required for acceptable performance.

Standardized protocols for validation of electrochemical performance for various classes of materials (electrolyte solvents, additives, redox shuttles) are being developed.

One hundred six samples, totaling 11,200 g of battery grade materials have been provided to industry and scientific community for evaluation and to support further research (20 samples, 1,560 g in FY15 alone).

## FY 2015 Publications/Presentations

1. "Process R&D and Scale up of Critical Battery Materials", ES168_Pupek_2015_P, US DOE Vehicle Technologies AMR, 2015.
2. Process for producing redox shuttles. Pupek, Krzysztof; Dzwiniel, Trevor; Krumdick, Gregory US 8,921,611 December 30, 2014.
3. Method for producing redox shuttles. Pupek, Krzysztof; Dzwiniel, Trevor; Krumdick, Gregory US 8,969,625 March 3, 2015.
4. ANL-IN-15-007 "Advanced Wetting Process for Battery Cell Production" Gregory Krumdick, Ana Kiricova, Trevor Dzwiniel, filing in progress.
5. ANL-IN-15-015 "Process for the Production of High Voltage Electrolyte Solvents for Li-ion Batteries" Trevor Dzwiniel, Krzysztof Pupek, and Gregory Krumdick, filing in progress.
6. ANL-IN-15-018 "Fluorinated Electrolyte Solvent" Trevor Dzwiniel, Krzysztof Pupek, and Gregory Krumdick, filing in progress.
7. ANL-IN-15-059 "Supramolecular Binder For Li-Ion Battery Si Anode" Krzysztof Pupek, Trevor L. Dzwiniel, Gregory K. Krumdick, filing in progress.
8. Scale-up of High Voltage Redox Shuttles. Dzwiniel, Trevor; Pupek, Krzysztof; Krumdick, Gregory Materials Science & Technology 2014 Pittsburgh, PA, October 15, 2014.

9. "Exploring Cycling Behavior of LiFSI-Bearing Electrolytes in Li1.03(Ni0.5Mn0.3Co0.2)0.97O2//Graphite cells" Krzysztof Pupek, T.L. Dzwiniel, G.K. Krumdick, M. Klett, D.P. Abraham, Spring ECS − 2015 Meeting, Chicago IL, May 26, 2015.
10. "Effect of Impurity Profile on Cycling Behavior of LiFSI Electrolytes" Krzysztof Pupek, Daniel Abraham, Trevor Dzwiniel, Gregory Krumdick. Advanced Automotive Battery Conference, Detroit, MI, June 15, 2015.

# IV.E.3 Electrode Coating Defect Analysis and Processing NDE for High-Energy Lithium-Ion Batteries (ORNL)

## Objectives

The goal of this project is to reduce the amount of scrap electrode by at least 75% and the associated amount ***assembled into finished cells***.

- Reduce lithium-ion battery system cost by implementing in-line NDE and electrode QC.
- Quantification of effects of different defect types on rate performance and cell lifetime.
- Identify manufacturing defects and their relation to cell failure.
- Implement materials characterization to investigate the cell failure mechanism(s).
- Collaborate with battery makers for QC technology development.
- Use electrode thermal excitation and associated IR emissivity to determine in-line porosity (ORNL/NREL).
- Use active IR thermography to determine electrode thickness or areal weight uniformity across and down the web (ORNL/NREL).
- Leverage NREL FCTO funds on fuel cell component in-line NDE with ORNL VTO funds on battery electrode in-line NDE.

### Project Details

**Peter Faguy (EERE-VTO-ABR Program Manager)**

**David Wood III (Oak Ridge National Laboratory)**
One Bethel Valley Road
P.O. Box 2008, MS 6083
Oak Ridge, TN 37831
Phone : 865-574-1157; Fax: 865-241 4034
E-mail: wooddl@ornl.gov

Subcontractor:
National Renewable Energy Laboratory

Start Date: October 1, 2014

Projected End Date: September 30, 2016

## Technical Barriers

- Material processing cost and electrode quality control.
- Cell calendar life and performance.

## Technical Targets

- Implementation of critical QC methods to reduce scrap rate by ***creating feedback loops*** (by 2020, reduce EV battery cost to $125/kWh).
- Quantification of various defect effects on cycle life (to achieve 750-1000 deep-discharge cycles for EVs by 2020).

## Accomplishments

- Developed methods to generate different electrode coating defects such as pinholes, blisters, large agglomerates, divots, and metal particle contaminants for evaluation in full coin-cell test matrix
- Obtained comprehensive, statistically representative full coin-cell data on different types of electrode coating defects to determine which types of defects cause cell failures or substandard performance (rate performance *and* capacity fade)
- Investigated and correlated IR thermography electrode QC data with full coin-cell statistical data.
- Obtained microstructural information for understanding cell failure mechanism(s) associated with electrode defects
- ***Porosity*** proof-of-concept experiments were completed at progressively more realistic conditions: Stationary, steady state
  - Stationary, transient temperature decay
  - Line speed = 0.5 ft/min, pseudo-steady-state
  - Samples investigated: 1) thinner, high-porosity NMC 532; 2) thicker, low-porosity NMC 532; 3) thinner low-porosity CP A12; 4) thicker high-porosity CP A12

- Mathematical modeling results: Comparison of modeling results with experimental measurements
  - Hypothetical samples (why anode responses were the same)
  - Effect of porosity on the temperature profile
  - Effect of thickness on the temperature profile

## Introduction

Due to high scrap rates of 10% or more associated with lithium secondary cell production, new methods of quality control (QC), which have been successful in other industries, must be implemented. Often flaws in the electrodes are not detected until the formation cycling when the entire series of manufacturing steps has been completed (significantly increasing the value added), and the associated percentage of defective cells drives the cost of lithium secondary cells to an unacceptable level. If electrode flaws and contaminants could be detected in-line near the particular processing steps that generate them, then the electrode material could be marked as unusable and the processing equipment could be adjusted to eliminate the defects more quickly. ORNL is considering in-line analysis methods such as laser thickness sensing of the electrode wet thickness measurement for improved homogeneity across and down the roll, IR imaging for detection of electrode thickness inhomogeneity and coating defects such as pinholes and blisters, and systematic investigation of the performance effect of different contaminants (metal particles) and defects (agglomerates and divots) in full coin cell format. These in-line methods have been effectively utilized in other industries such as photovoltaic, flexible electronics, and semiconductor manufacturing, but the equipment and measurement methods must still be tailored for lithium secondary cell production. In previous annual reports (FY12-14), we demonstrated i) successful implementation of the laser caliper technology to monitor the wet electrode thickness during slot-die coating, ii) implementation of IR thermography for detecting the flaws in the dried electrode coming out from the slot-die coater, and iii) effect of these defects on the electrochemical performances (rate capability tests, and capacity fade). In this report, our goal is to present the comparison of the cell degradation rate with the nature of defects, and microstructural investigation to understand the degradation mechanisms. Porosity of the cathode/anode is an important property that plays a major role in the lithium-ion transport process and alters the capacity at high discharge rates. If the porosity of the electrodes is monitored at the desired value during the coating process and is known prior to cell assembly, cell capacity at high discharge rates (power density) can be increased through optimized lithium-ion mass-transport through the thickness of the electrodes. Through a successful collaboration with NREL, a low-cost method for in-line porosity measurement is being developed that will realize this measurement technique.

## Approach

For correlating electrode coating defects with electrochemistry, our approach was to intentionally create different type of defects in the baseline NMC 532 during coating and electrochemically test the electrodes with those defects to obtain a comprehensive understanding between the defect nature and electrochemistry. In order to further this understanding, cells were disassembled after electrochemical testing for microstructural analysis (SEM and EDS mapping).

For in-line porosity measurements, white light or thermal excitation of the electrode coatings was utilized to generate an IR emissivity signature from electrode coatings. Subsequently, IR emissivity was measured and correlated to a coating temperature profile for input into a mathematical model based on electrode physical properties (IR absorbance, heat capacity, thermal conductivity, bulk density, etc.); or experimentally obtained calibration curves could be used. Comparison between modeled and measured heat loss down the web was completed to generate electrode porosity and/or thickness profiles.

## Results

### A. Defect, electrochemistry, and microstructure correlations

#### Cycle life test from different defective electrodes

Discharge capacity fading tests for the defective NMC 532 electrodes were performed for 200 cycles at two different conditions: 2C and 5C discharging (the charge rate was 0.2 C in both cases), and the results were compared to data from testing the baseline electrode. Electrodes with the five different types of defects were

chosen for analysis. Gravimetric discharge capacity during the 200 cycles is plotted for the baseline and defective electrodes in Figure IV- 236. Gravimetric capacity and total cell capacity before and after the 200 cycles is shown in Figure IV- 237a-b, and capacity retentions after 200 cycles (at both 2C and 5C discharge rates) are shown in Figure IV- 237c.

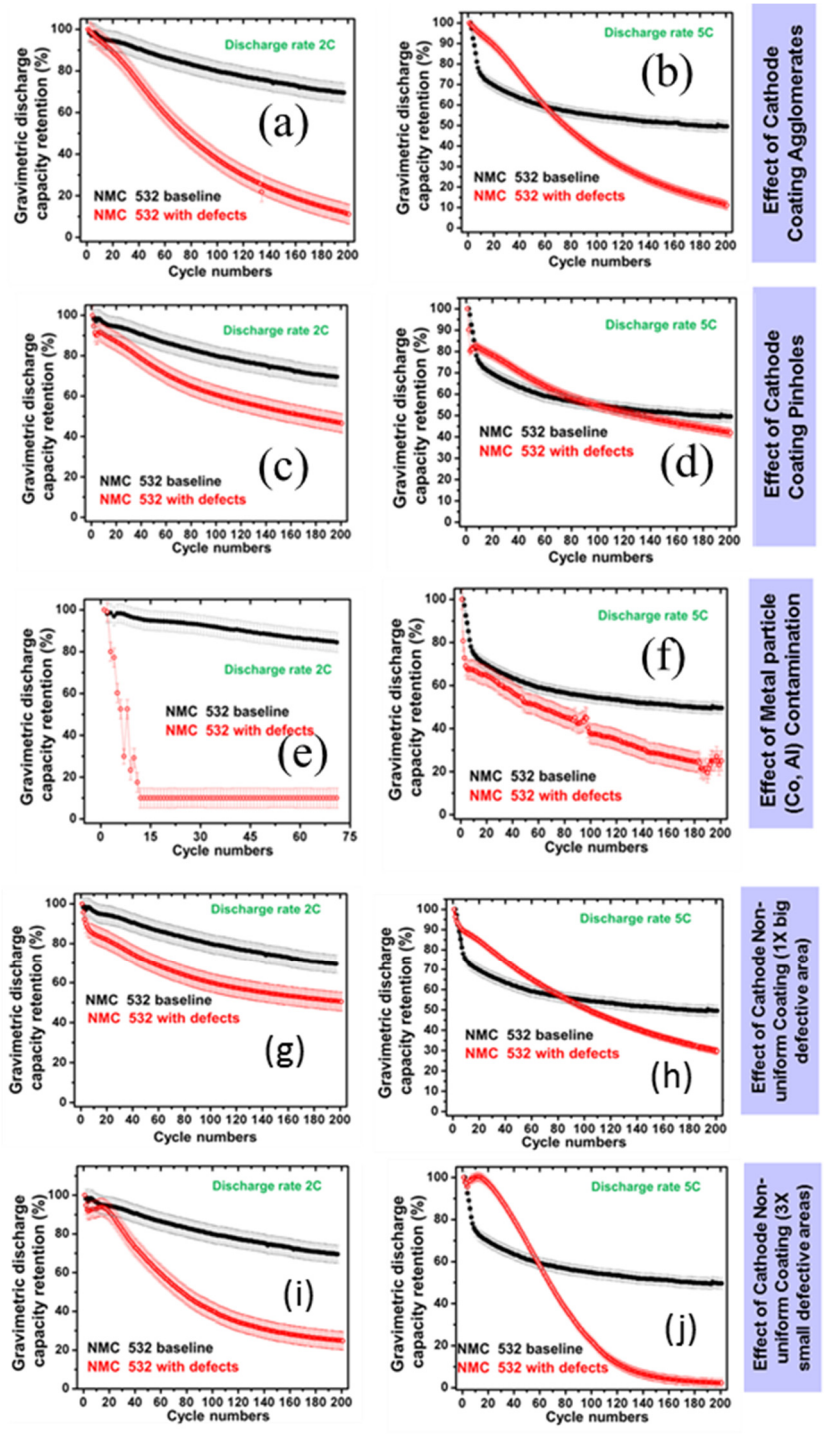


Figure IV- 236: Comparison between gravimetric capacity-fading results for the baseline and defective NMC 532 electrodes at 2C and 5C current rates (triplicate full coin cells)

### a) Electrode agglomerates

#### Greater capacity degradation

Figure IV- 236a and Figure IV- 236b show the capacity fade results from full coin cells for baseline electrodes and those having large agglomerates. Corresponding gravimetric and full-capacity values before and after 200 cycles at 2C, and 5C discharge rates is shown in Figure IV- 237a-b. Approximately 70% of the total cell and gravimetric capacity was retained after 200 cycles at 2C for the baseline electrode, whereas for the electrode containing agglomerates, 12% of discharge capacity was retained after 200 cycles. At the 5C rate, the baseline electrode showed ~50% discharge capacity retention after 200 cycles. In contrast, discharge capacity retention of ~14% was observed for the electrodes with large agglomerates. These observations show that large coating agglomerates must be avoided through optimized dispersion chemistry, thorough mixing protocols, and excellent coating deposition.

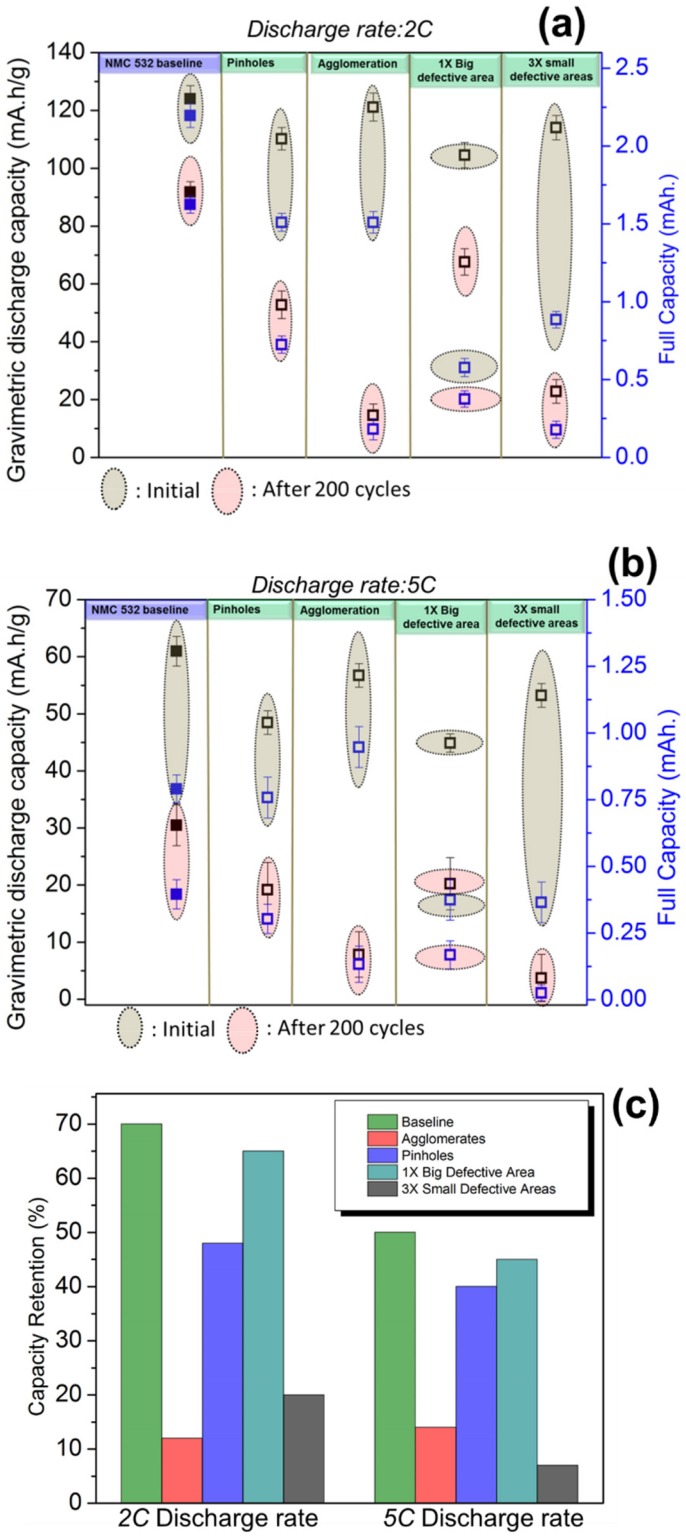


**Figure IV- 237: Gravimetric and total cell capacity before and after 200 charge-discharge cycles at 2C (a) and 5C (b) discharge rates. Capacity retention values after 200 cycles for the baseline and defective electrodes at the 2C discharge rate and at the 5C discharged rate (c)**

**b) Electrode pinholes**

**Less severe capacity degradation**

Figure IV- 236c and Figure IV- 236d show the capacity-fading results for electrodes having pinholes compared to the baseline electrodes (corresponding gravimetric and total cell capacity before and after 200 cycles is shown in Figure IV- 237a-b). With pinholes present in the cathode coatings, capacity fading was significant; however, it was much less severe than the fading caused by the large agglomerates. The capacity retention was 47% and 40% after 200 charge-discharge cycles at the 2C and 5C rates, respectively. Total cell capacity retention was also higher for electrodes having pinholes than it was for the electrodes having agglomerates.

**c) Metal particle contaminants**

**Unstable cell performance at high discharge rate**

Figure IV- 236e and Figure IV- 236f show capacity-fade testing results for cathodes with Co metal particle contaminants compared to the baseline electrodes (corresponding gravimetric and total cell capacity before and after 200 cycles is shown in Figure IV- 237a-b). The results obtained show no measureable capacity for the defective electrodes after about 10 cycles when operated at 2C; beyond this point, complete failure was observed. Figure IV- 236f shows the capacity-fade testing results for the 5C discharge rate, and it is seen that the cells made it through 200 cycles unlike the 2C discharge case. However, the capacity fade was still much more severe for the cathode coatings with the Co particle contamination than the baseline NMC 532 electrodes.

**d) Non-uniform electrode coating with 1X 6-mm defect and 3X 2-mm defects**

**Severe capacity degradation for electrodes having the 3X defects**

Figure IV- 236g and Figure IV- 236h show a comparison of the capacity-fading results for the baseline cathodes to those having a 6-mm-wide missing coating strip (denoted ad “1X defect”) at 2C and 5C discharge rates, respectively. Figure IV- 236i and Figure IV- 236j show the same comparison for a cathode having three parallel 2-mm-wide missing coating strips (denoted as “3X defects”). Figure IV- 237a-b shows the comparison of gravimetric and total cell capacities before and after 200 cycles for the 1X defect and 3X defect cases at 2C and 5C discharge rates. Our analysis revealed that the capacity degradation rate was considerably higher for the electrodes having a greater interfacial length (i.e., the 3X defects case) than for electrodes having the smaller interfacial length (i.e., the 1X defect case). At 5C, the gravimetric discharge capacity retention was only 7% after 200 cycles for the 3X defects case, whereas 45% total cell capacity retention was observed for the 1X defect case.

5C capacity fade rates for the different defects are summarized as follows: non-defective baseline < 1X defect (non-uniform coating) < pinholes < large agglomerates < 3X defects (non-uniform coating) < Co powder metal contamination (see Figure IV- 237c). In the next section, a microstructural investigation is discussed that was conducted to understand the poor 3X-defects electrochemical performance.

**Understanding the defect electrochemistry-microstructure correlation:**

In Figure IV- 238, SEM micrographs and corresponding X-ray elemental mapping results are shown for the baseline NMC 532 cathode (Figure IV- 238a) and for an electrode with large agglomerates (Figure IV- 238b). The SEM micrographs and the elemental mapping from the baseline electrode show a uniform distribution of the inactive components and spherical active particles. The images of the agglomerated electrodes clearly show evidence of phase-rich regions for both active and inactive (carbon-rich) material. Particle disintegration was also observed near the agglomerated region.

Cross-sectional SEM images of baseline electrodes and electrodes having missing 2-mm or 6-mm coating strips (“3X defects” and “1X defect”, respectively) were investigated to gain insights into the observed poor electrochemical performance (see Figure IV- 239). The SEM images reveal that the coating is uniform across the baseline electrodes (Figure IV- 239a–c); however, for the electrodes with non-uniform coatings, the interface between the coated and uncoated regions does not show a 90-degree angle between the coated and uncoated regions. Rather, it shows a lip and a gradual slope decreasing from the coated to the uncoated region. The interface has less active material and poor or no adhesion to the Al current collector (Figure IV- 239d-g). The loss of contact between the Al current collector and the cathode coating also significantly increases cell impedance and could lead to complete electrode delamination (at least in local areas) resulting in

underutilization of active material. Consequently, cell capacity fade would be more severe as was observed in Figure IV- 236g-j. The 3X defects coating has significantly higher interfacial length than the 1X defect coating, and that difference might account for the observed greater capacity degradation for the 3X defects case.

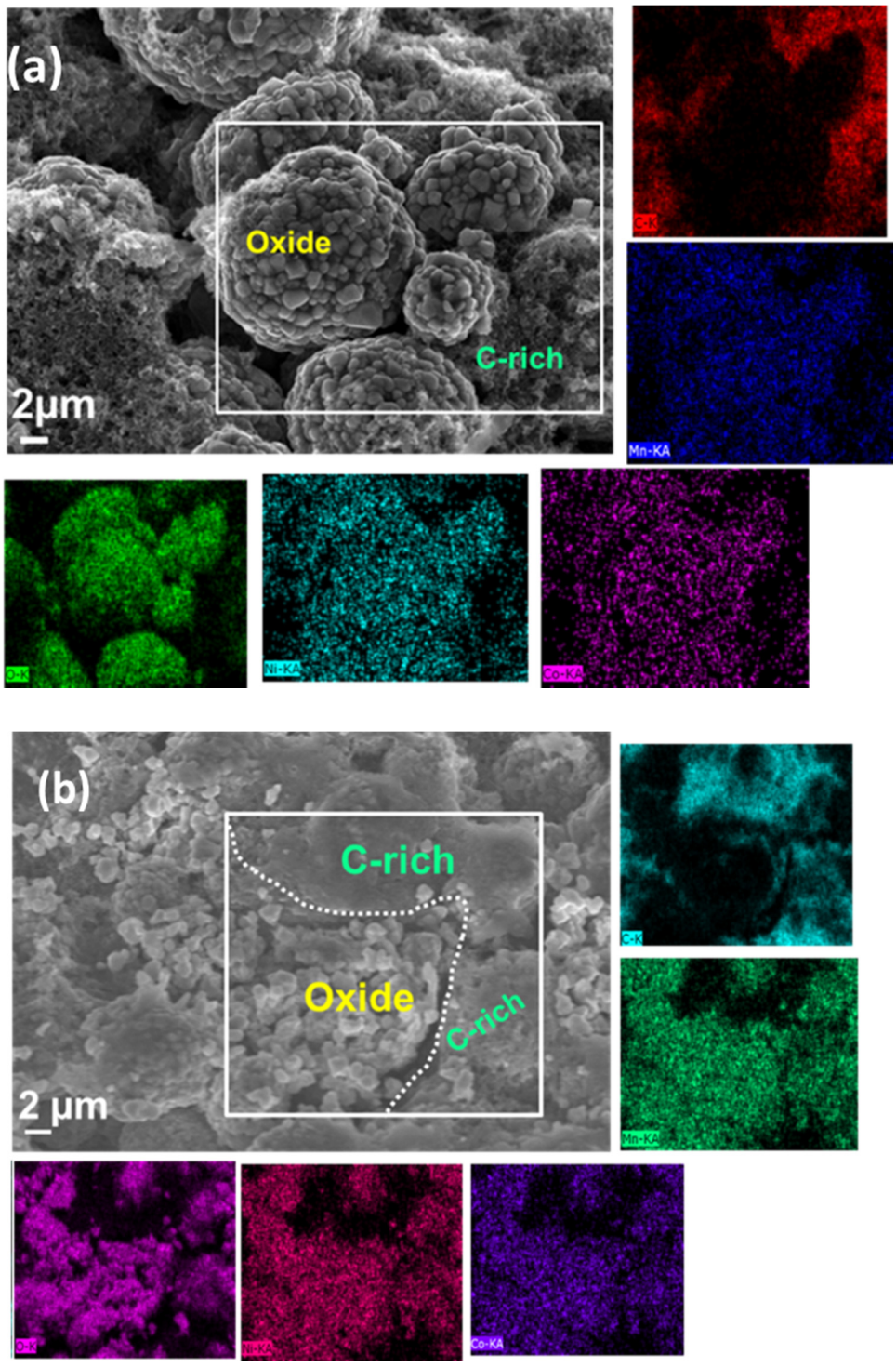


**Figure IV- 238: Scanning electron micrographs and elemental EDS maps (Mn, Ni, Co, C, O) from (a) the baseline NMC 532 electrode and (b) a defective electrode with large agglomerates**

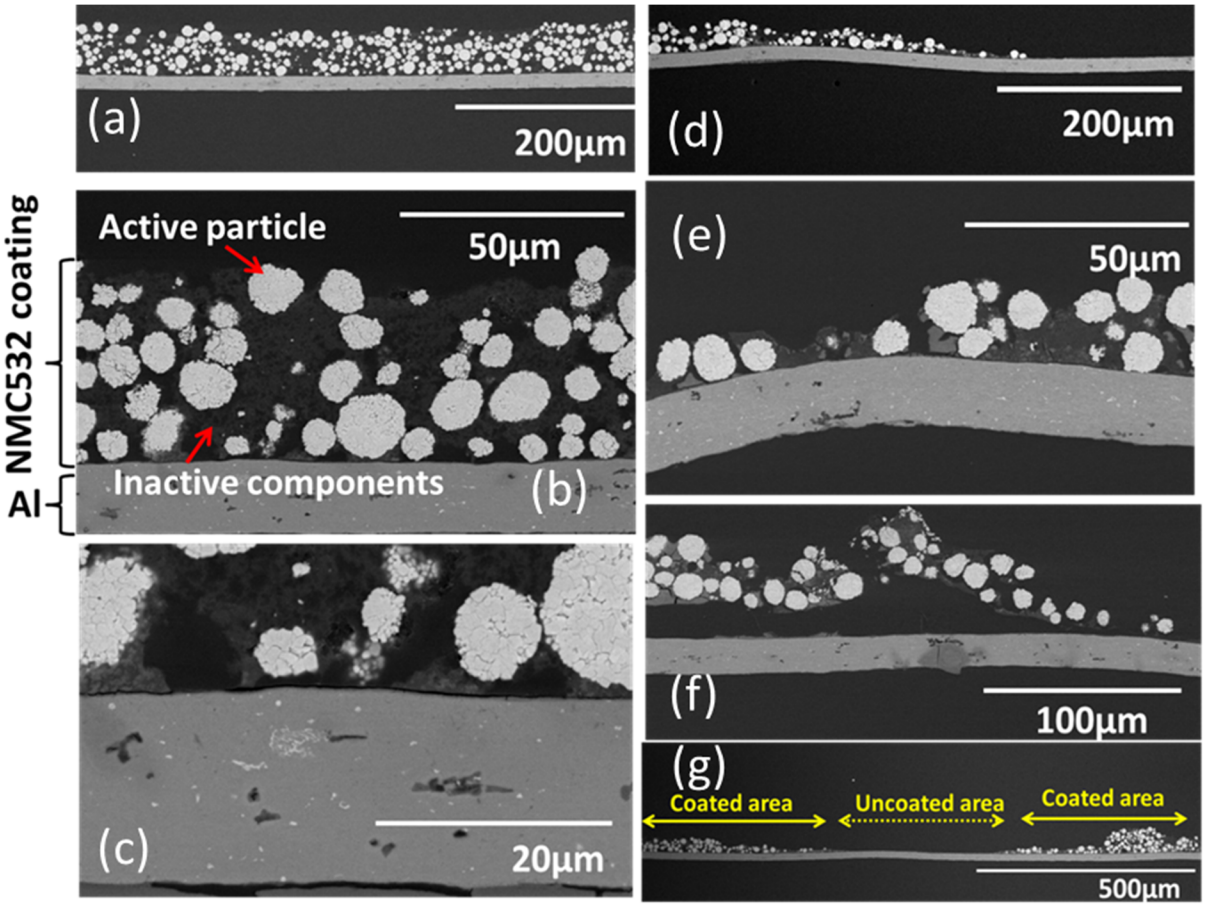


**Figure IV- 239: (a–c) Cross-sectional SEM images of the baseline NMC 532 electrodes, (d–g) cross-sectional SEM images from an electrode having missing coating strips (i.e. "1X defect" or "3X defects")**

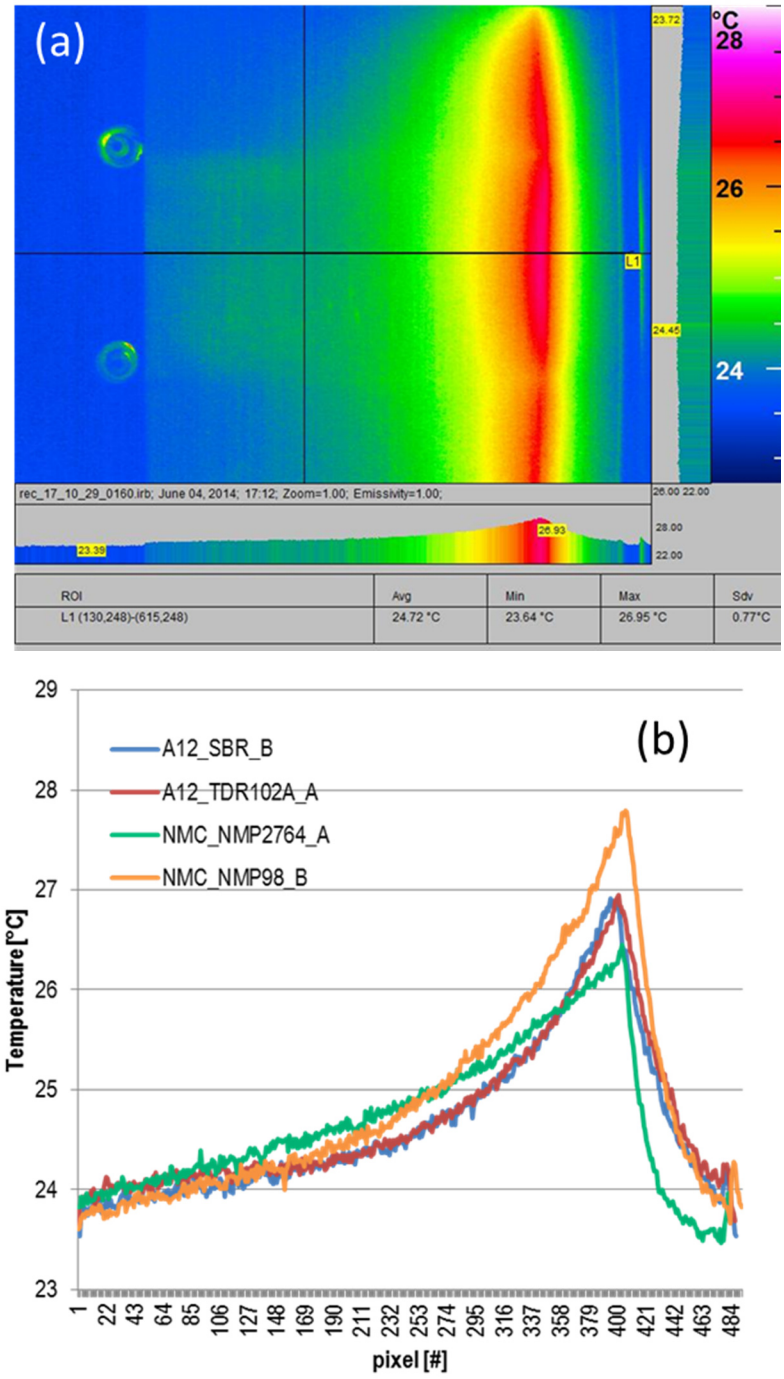


Figure IV- 240: (a) Temperature distribution of A12_SBR anode; (b) Temperature profiles along line L1 for two anodes, and two cathodes

### A. In-line porosity measurements and validation of experimental results with modeling (ORNL/NREL)

The temperature distribution (from IR excitation) of A12 graphite electrodes and temperature profiles along the line L1 for two A12 anodes, and two NMC cathodes at steady state (line speed = 0.5 ft/min) are shown in Figure IV- 240a-b, respectively. These results showed that the cathodes responded differently from each other due to different electrode architectures, and temperature profiles of the anodes were identical despite the different porosities. This difference in the thermal response of the cathodes was attributed to variation in electrode areal loading, porosity or thickness. Anode behavior was most likely due to a smaller difference in

areal loading as well as the high thermal conductivity of graphite. System sensitivity would have to be improved to be able to measure such differences in the anode.

Macroscale modeling was done by considering physical properties such as specific heat capacity, bulk electrode density, material absolute densities, and thermal conductivity. The method has been adopted from Eshelby ("The Determination of the Elastic Field of an Ellipsoidal Inclusion and Related Problems.") and Stránský et al. ("Mori-Tanaka Based Estimates of Effective Thermal Conductivity of Various Engineering Materials"). The $T_{max}$ results from modeling and experiments for the cathode and anode are shown in Figure IV- 241, and good agreement was found. The difference between the cathode $T_{max}$ values was about two times greater for the experimental results than that from the modeling results. For the two anodes, the same temperature profiles were obtained with the model despite the fact that the samples had different thickness and porosity (again, this is primarily attributed to the high graphite thermal conductivity). Similar behavior was observed for the experimental data.

Modeling was also performed by altering the porosity of the anode, and the results are presented in Figure IV-242. It is seen that greater porosity caused an increase in $T_{max}$; however, an increase in thickness reduced $T_{max}$. These two effects are of opposite sign and similar magnitude and, therefore, cancel each other, resulting in the same temperature distribution for the two anode samples. A correlation between $T_{max}$ and the electrode porosity range is shown in Figure IV- 243. The model shows that for the two considered cases $T_{max}$ changes approximately linearly over entire range of porosities.

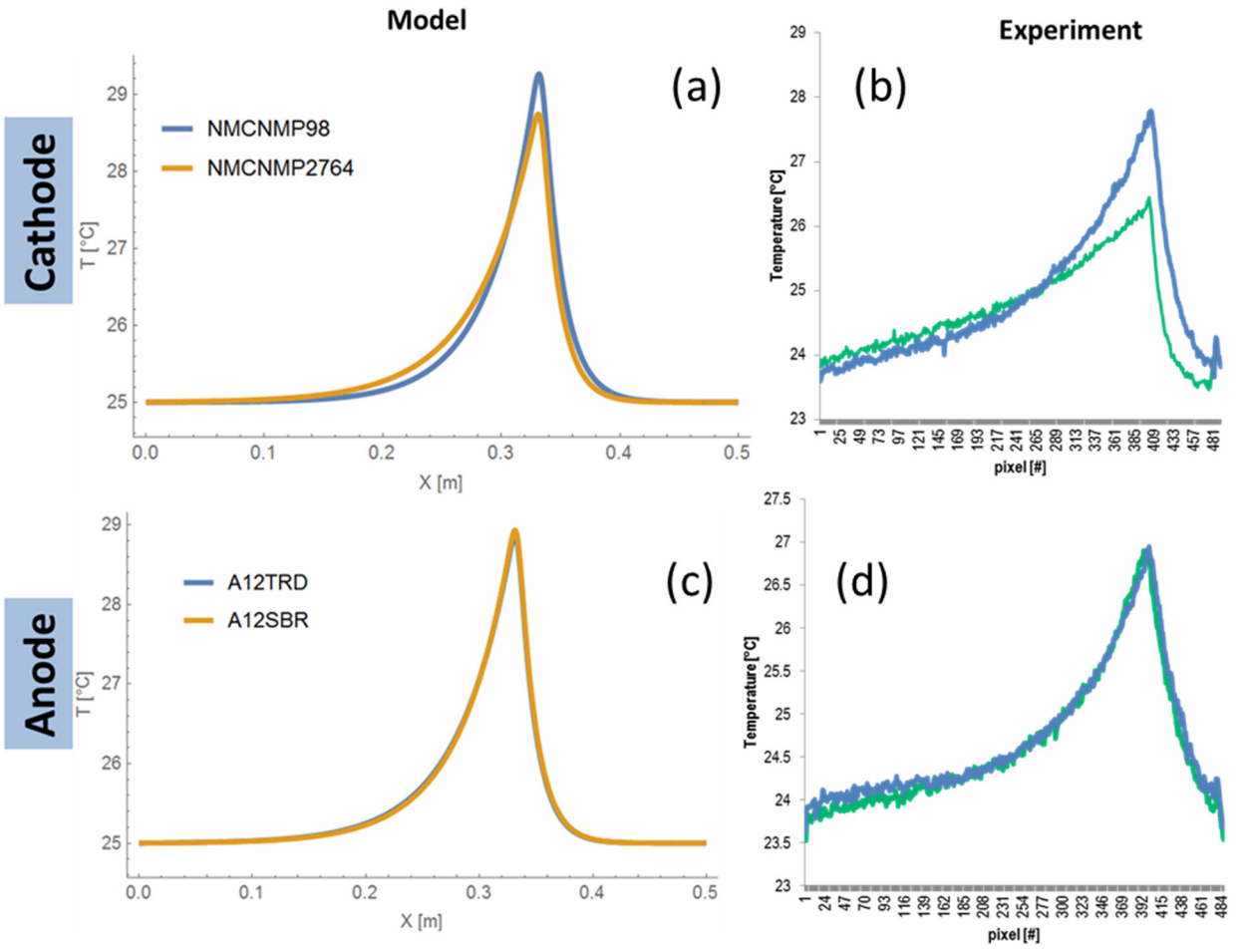


**Figure IV- 241: Standing wave comparison with experiment for NMC cathodes (a: model, b: experiment); standing wave comparison with experiment anode (c: model, d: experiment)**

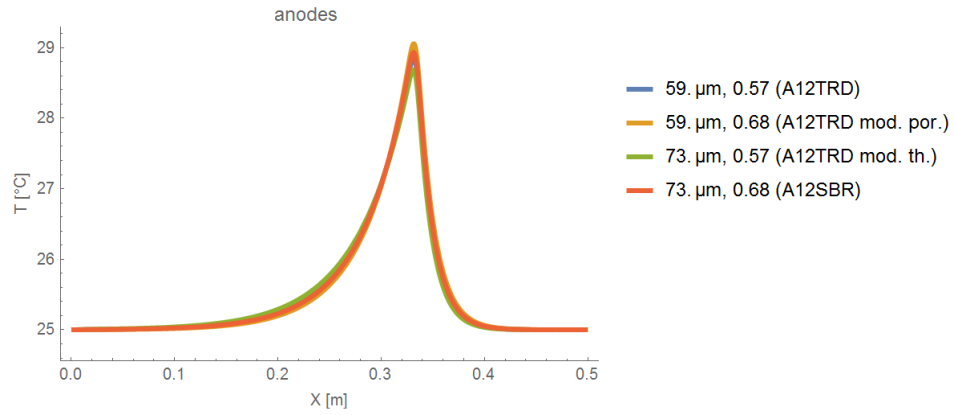


**Figure IV- 242: Modeling results of hypothetical anodes (offsetting properties)**

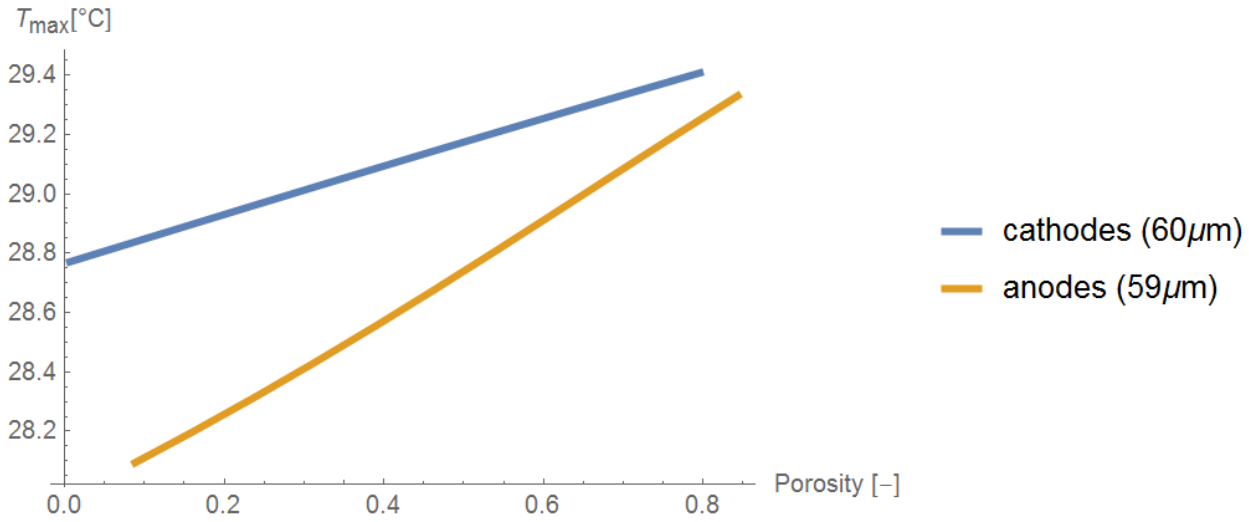


**Figure IV- 243: Correlation of Tmax to electrode porosity range**

## FY 2015 Publications/Presentations

1. D. Mohanty, J. Li, R. Born, C.L. Maxey, R.B. Dinwiddie, C. Daniel and D.L. Wood, "Reducing the Scrap Rate in Lithium-Ion Battery Manufacturing by Implementing In-Line Non-Destructive Electrode Evaluation Techniques," 3rd International Conference and Exhibition on Materials Science & Engineering, San Antonio, Texas, October 6-8, 2014. (**Invited)**
2. D. Mohanty, J. Li, S. Nagpure, D.L. Wood, III, and C. Daniel, "Correlating Electrode Defects with Electrochemical Performance of Lithium-Ion Batteries," 2015 MRS Spring Meeting & Exhibit, San Francisco.
3. D. Mohanty, J. Li, C. Daniel, D. L. Wood, "Effect of Electrode Defects on Electrochemical Performance of a Lithium Ion Battery; From Non-Destructive Evaluation to Microstructural Investigation"; *Journal of Power Sources*, In Review, 2015.

# IV.E.4 Thick Low-Cost, High-Power Lithium-Ion Electrodes via Aqueous Processing (ORNL)

## Objectives

- The main objective of this project is to transform lithium-ion battery (LIB) electrode manufacturing by the elimination of processing with costly, toxic organic solvents while simultaneously doubling energy density. To this end, we proposed to 1) replace NMP processing with a water-based cathode $LiNi_{0.5}Mn_{0.3}Co_{0.2}O_2$ (NMC 532) and natural graphite anode; 2) evaluate different commercially available waterborne binders and water-dispersible conductive carbon additives for increased power density; 3) investigate effect of doubling electrode thicknesses (i.e. develop a thick, high-power cathode architecture); 4) eliminate expensive solvent recovery steps, reduce capital equipment cost, and eliminate expensive inactive components; 5) enhance wetting and adhesion of the electrode coating on current collectors; and 6) optimize power density by controlling particle-size distribution, electrode porosity, pore-size distribution, and porosity gradient in the electrodes.

**Project Details**

**Jianlin Li, Claus Daniel, Debasish Mohanty, and David Wood (Oak Ridge National Laboratory)**
One Bethel Valley Road,
P.O. Box 2008, MS-6479
Oak Ridge, TN 37831
Phone: 865-946-1561
Email: lij4@ornl.gov

Start Date: October 1, 2014
Projected End Date: September 30, 2018

## Technical Barriers

- By 2020, further reduce EV battery-pack cost towards the ultimate USABC target of $125/kWh.
- Advance lithium-ion HEV/PHEV battery systems with low-cost electrode architectures.
- Achieve ultimate USABC energy density targets of 350 Wh/kg and 750 Wh/L without compromising power density.

## Technical Targets

- Reduce battery pack cost by 20-25%.
- Preserve long-term performance: 10 years and 1000 cycles at 80% DOD of EVs and 5000 deep charge cycles for PHEVs.
- Reduce battery cost to $300/kWh in short term for PHEV40s.

## Accomplishments

- Cost reduction analysis on aqueous processed electrode with 2× electrode thickness (100 to 200 micron calendered cathode thickness).
- Repeatability and durability of 1.5-Ah pouch cells with ABR baseline electrodes (ConocoPhillips A12 anode / TODA America NMC 532 cathode).
- All-aqueous NMC 532 and CP A12 graphite scale-up and assembly of 1.6-Ah pouch cells.
- Evaluation of the effect of surface properties of current collector on electrode performance.
- Improvement in pouch cell cyclability via calendering of electrodes.
- Scale-up and fabrication of NMC 532 and $LiFePO_4$ cathodes via aqueous processing with industrial partner electrode formulations.
- Initiation of systematic electrolyte volume and SEI-property study with ANL to determine effect on battery performance and calendar life.

## Introduction

Improvement in certain areas is still required for widespread transportation applications of LIBs (in EVs and PHEVs) such as reducing battery cost and increasing battery energy density. The major portion of the LIB cost results from active materials and electrode processing. Conventional LIB electrodes are manufactured through organic solvent processing, but switching the solvent to water introduces significant economic and environmental advantages. In addition, increasing electrode thickness reduces the amount of inactive materials, such as current collectors and separators, resulting in simultaneous cost reduction and energy density improvement. We proposed to manufacture thick electrodes via aqueous processing and novel electrode architecture for significantly lower cost and higher energy ***and*** power density.

## Approach

The objectives outlined above were accomplished by:

1. Completing a preliminary cost reduction analysis in thick electrode manufacturing via aqueous processing.
2. Developing chemistry-specific aqueous formulation designs by standardized dispersant selection and rheological optimization methods: Tailored Aqueous Colloids for Lithium-Ion Electrodes (TACLE)→J. Li, et al., U.S. Patent No. 8,956,6888 (UT-Battelle, LLC).
3. Implementing surface charge measurement, rheology characterization, agglomerate size optimization, order of constituent addition, and mixing protocol optimization.
4. Introducing novel binder development beneficial to electrode conductivity and power density.
5. Optimizing coating parameters for TACLE→viscosity control, current-collector surface energy optimization, and tailoring of drying protocol.
6. Investigating dual slot-die coating and optimizing calendering of electrode architectures (pore structure gradients for better liquid-phase Li+ transport) for high energy and power electrodes.
7. Collaborating closely with the ABR efforts of ANL and SNL, cell manufacturers, active material suppliers, and inactive material suppliers.
8. Scaling TACLE methodology with key industry partners and working with key waterborne binder suppliers such as Ashland, Solvay Specialty Polymers, JSR Micro, and SABIC.
9. Studying systematically the effects of electrolyte volume on battery performance, formation protocol on SEI properties, and battery performance with ANL.

## Results

### LIB aqueous electrode processing patent issued

Our patent entitled, "Aqueous Processing of Composite Lithium-ion Electrode Material" was filed on October 12$^{th}$, 2012 and issued on February 17$^{th}$, 2015 with U.S. Patent No. 8,956,688.

### Estimation on cost reduction from thick electrode via aqueous processing

We have demonstrated a detailed processing cost breakdown for LIB electrodes focusing on 1) elimination of toxic, costly NMP dispersion chemistry; 2) doubling the electrode thickness to raise energy density; and 3) reducing the wetting and formation steps at the end of cell assembly. The estimation is based on low volume (<1000 battery packs) production of 52-Ah automotive "power cells". When switching from NMP based processing to aqueous processing plus doubling the electrode thickness, it enables $111/kWh-usable of the total pack cost (based on 70% depth of discharge limit, corresponding to 22% cost reduction (See Figure IV-244.) Based on the initial assumptions and calculations, the major part of the cost reduction comes from a lower electrode processing cost (specifically electrode primary drying and solvent recovery), where NMP is eliminated and no solvent recovery is required, and less of current collectors and separator due to the doubling of electrode thickness. Other reasons for cost reduction include less electrolyte needed due to lower total pore volume in the battery from fewer separators. This work was published in the *Journal of Power* Sources, **275**, 234-242 (2015). It is being followed up with an in-depth joint study between B&W MEGTEC, ORNL, and ANL and will consider real-world coating lines and solvent recovery equipment to improve the cost reduction estimates in switching from NMP to water, and then added to the ANL BatPAC model.

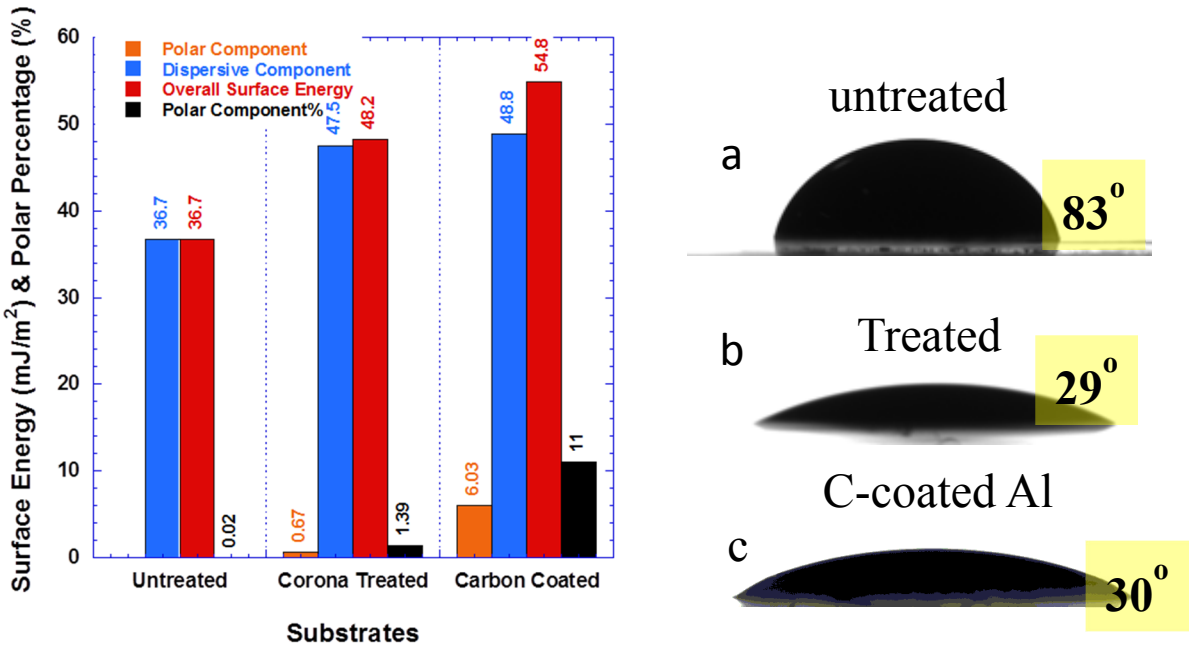


Figure IV- 244: Surface energy of various substrates and contact angles of NMC532 slurry on various substrates

**Slurry wetting on different Al foil surfaces and improvement in adhesion and cell rate performance**

The wetting of aqueous NMC 532 slurry on untreated Al foil is poor with a contact angle of 83° (Figure IV-244), due to its low surface energy. One strategy to improve the wetting is to raise the surface energy of the Al foil, by corona treatment or carbon coating of the Al surface. Substantially increased surface energy results in better wetting as evidenced by the much smaller contact angles (Figure IV- 244). Impedance and rate performance of the NMC 532 cathodes on the various Al foils were characterized (Figure IV- 245). The cathode on C-coated Al showed the smallest semicircle and that on untreated Al the largest, indicating lower interfacial impedance for the NMC 532 cathodes on corona-treated and C-coated Al foils. Consequently, the rate performance was much better, especially at high C-rates. It should be noted that these electrodes were not calendered and the rate performance could be further improved via appropriate porosity control.

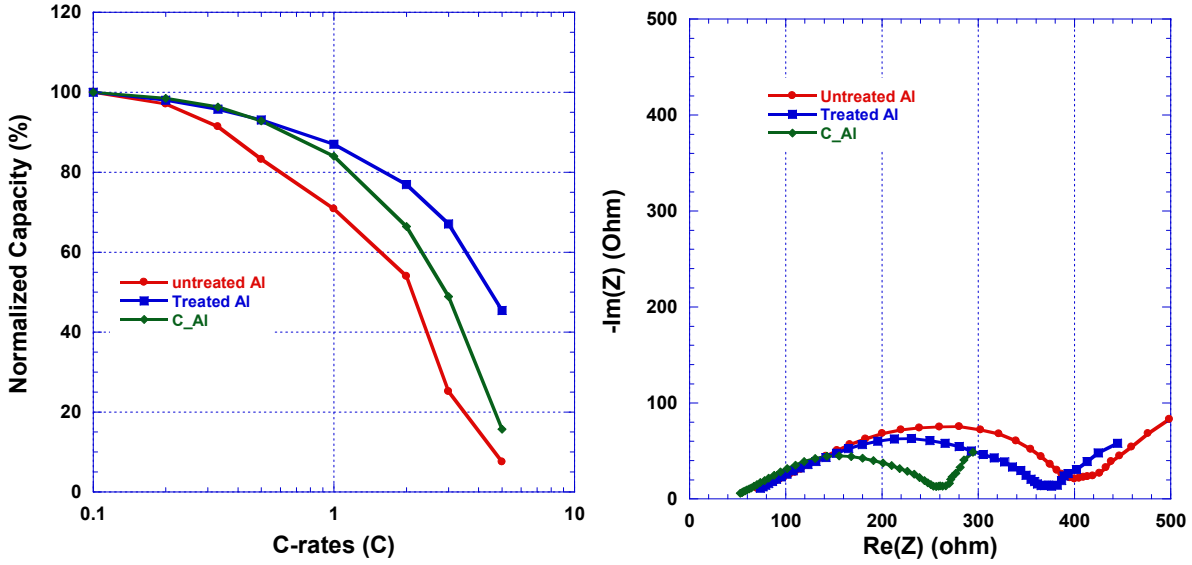


Figure IV- 245: NMC532 cathode on C-coated and corona treated Al foils demonstrate better rate performance (left) and lower interfacial impedance (right)

**Table IV- 33: Electrode parameters for pouch cells**

| Processing | Electrode | Areal Loading (mg/cm$^2$) | Porosity (%) |
|---|---|---|---|
| PVDF/NMP | NMC532 | 25.2 | 36.8 |
| PVDF/NMP | A12 | 16.4 | 32.5 |
| Aqueous | NMC532 | 26.5 | 35.6 |
| Aqueous | A12 | 14.8 | 34.2 |

**Excellent reproducibility and performance of full-scale pouch cells via NMP/PVDF and aqueous processing**

Large-format pouch cells (1.6 Ah) were assembled with NMC 532 and CP A12 electrodes processed via conventional PVDF/NMP processing (baseline) and aqueous processing (All aqu), and the electrode parameters are listed in Table IV- 33.

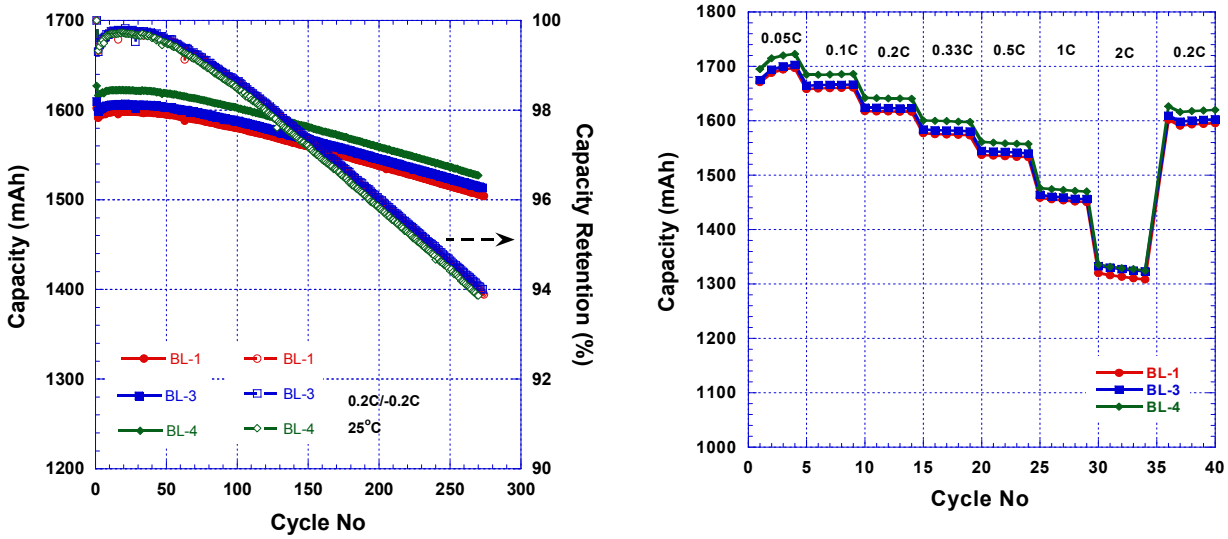


Figure IV- 246: Rate performance (left) and cyclability (right) of baseline (conventional PVDF/NMP) pouch cells

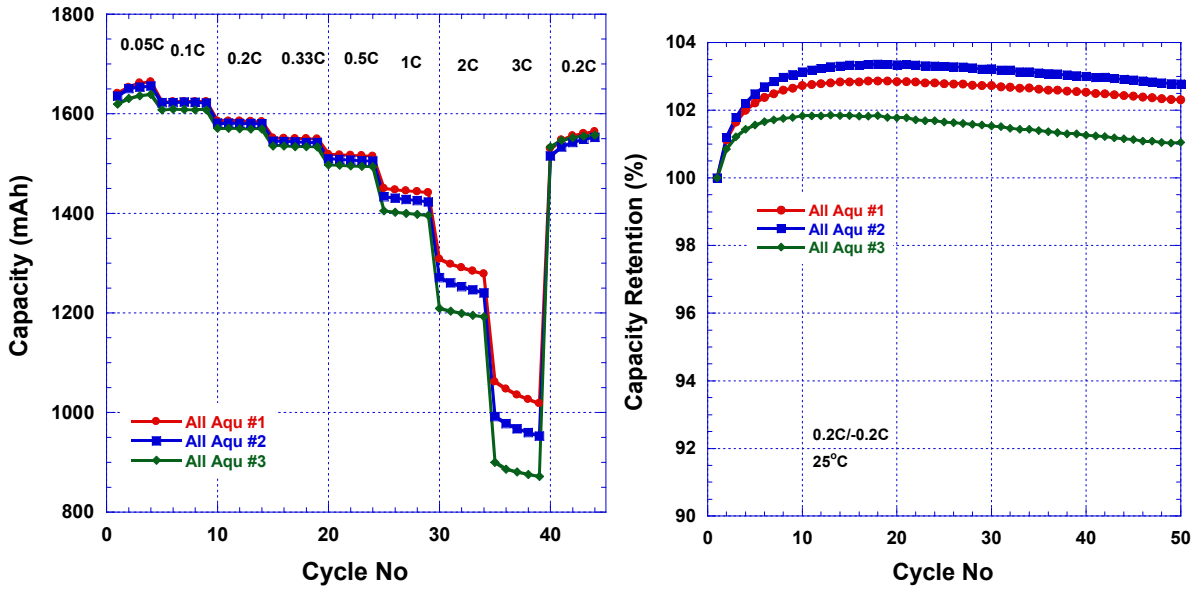


Figure IV- 247: Rate performance (left) and capacity retention (right) of pouch cells with all-aqueous processed electrodes

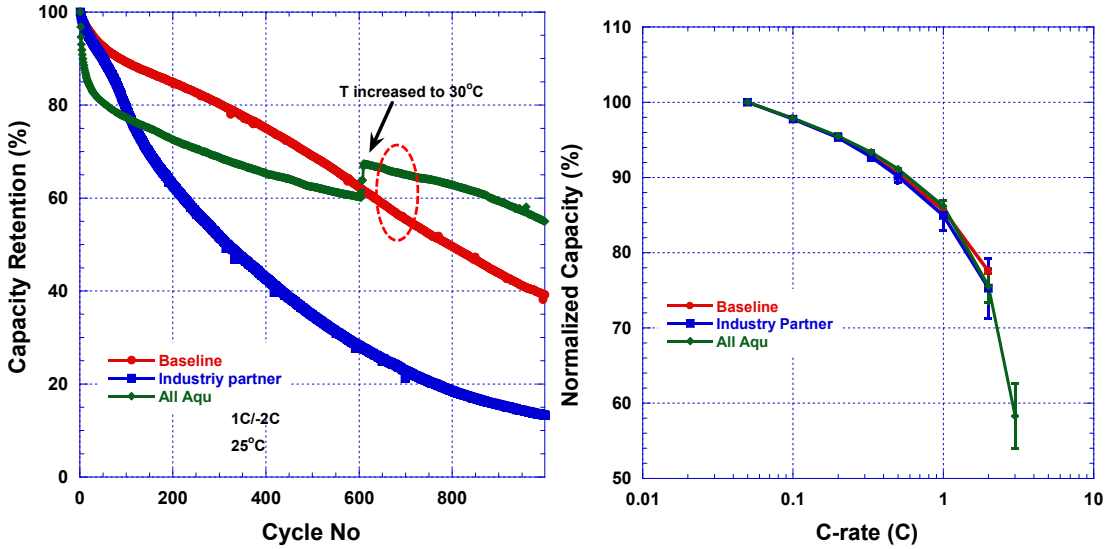


**Figure IV- 248: Comparison of pouch cell performance with ORNL baseline electrodes, ORNL all-aqueous processed electrodes, and aqueous processed cathodes with industry formulation; capacity retention under accelerated degradation (left); rate capability (right)**

Excellent cell reproducibility was observed for pouch cells with both NMP/PVDF and all-aqueous processing as shown in Figure IV- 246 and Figure IV- 247. These cells were cycled at 25°C between 2.5 and 4.2 V. More than 94% capacity retention was retained for the baseline cells after 250 cycles. At this linear capacity fade rate, it is estimated that these baseline cells would have had 78-79% capacity retention after 1000 deep discharge cycles at (0.2C/-0.2C). The pouch cells with all aqueous processed electrodes exhibited a gradual capacity increase in the first several cycles, which could be attributed to the dissolved lithium during slurry mixing relithiated into the NMC 532. Excellent capacity retention was observed from these cells: ~102% of the capacity in the 1st cycle after 50 0.2C/-0.2C cycles. Figure IV- 248 shows the comparison in performance of 1.5-1.7 Ah pouch cells with baseline PVDF/NMP electrodes, ORNL all-aqueous processed electrodes, and cells with PVDF/NMP anodes and aqueous-formulated cathodes from a prominent industry partner. The electrode parameters achieved with the industrial formulations were similar to the aqueous processed electrodes listed in Table IV- 33. All three types of pouch cells demonstrate identical rate performance (Figure IV- 248). When cycled at 1C/-2C, however, both the ORNL all-aqueous electrode and industrial formulated aqueous cathode pouch cell showed rapid capacity fading within the first 100-150 cycles. While the pouch cell with the industrially formulated cathode continued to fade at a high rate, capacity fade for the ORNL pouch cells with all-aqueous processed electrodes slowed, and the retention even surpassed the PVDF/NMP baseline cell capacity within the 600-700 cycle range (~60% retention level). It should be noted that the environmental chamber containing the all-aqueous processed cells was increased from 25°C to 30°C for other purposes. However, the capacity retention for the all-aqueous-processed cells was much higher than the baseline cells after 1000 cycles even after subtracting the capacity improvement from the temperature effect. Therefore, this difference verifies that the electrodes made via aqueous processing demonstrate better ***long-term*** cyclability than the baseline PVDF/NMP electrodes, even though the sharp initial decline in capacity was observed for the former cells (Figure IV- 248).

### Electrode cyclability improved by calendering

The effect of porosity on electrode cyclability was investigated in full pouch cells with electrode porosities of 33-37% (calendered) and 53-55% (non-calendered). Both electrodes had identical areal weight and went through the same formation cycles. As shown in Figure IV- 249, the cells with calendered electrodes demonstrated much higher capacity retention even though they were discharged at 2C, compared to 1C for the cells with uncalendered electrodes. This finding verified the significance that calendering plays in improving electrode cyclability through better electrode adhesion to the current collector and agglomerate adhesion (i.e., improved contact resistance at the particle and bulk electrode level).

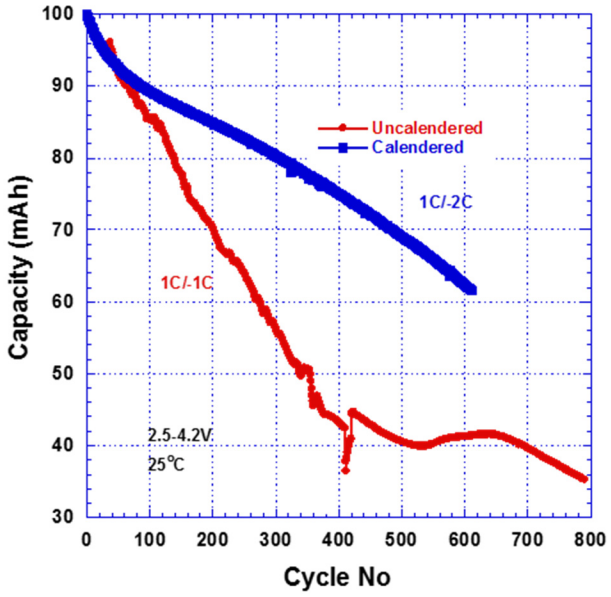


Figure IV- 249: Comparison between calendered and non-calendered pouch cells cycled at high-rate accelerated testing conditions

### Collaboration with ANL Post-Test Characterization Facility

ORNL Battery Manufacturing Facility (BMF) researchers also collaborated with ANL on characterizing the SEI layers formed after both PVDF/NMP and aqueous electrode processing. Two other processing variables were investigated, including formation protocol (specific formation conditions for each protocol are listed in Table IV-34) and adsorbed moisture level on the electrodes.

Three of the eight possible conditions were investigated in our preliminary work, and sample conditions are listed in Table IV- 35. Single-unit-cell pouches were assembled at ORNL and went through wetting and formation before being sent to ANL for post-test characterization. The cells were disassembled in an Ar-filled glove box, the electrodes were washed with dimethyl carbonate (DMC), and never exposed to air during subsequent chemical and materials characterization. The surface morphology and composition was characterized by SEM/TEM and XPS, respectively. F and O XPS data is shown in Figure IV- 250 and Figure IV- 251, and different amounts of organic and inorganic F and O were found for both anode and cathode surfaces for different formation and secondary drying protocol. Testing and characterization is still underway, and more results are to be present next year that will include similar evaluation after 0 (formation protocol only), 1, 100, and 1000 0.33C/-0.33 cycles.

Table IV- 34: Formation cycle procedures

| Formation Protocol |
|---|
| • Tap charge to 2.5 V for 5 min<br>• Rest at 45°C for 24 hours<br>• 3 shallow cycles between 2.5-3.3 V at 0.1C/-0.1C<br>• 2 full-range cycles between 2.5-4.2 V at 0.1C/-0.1C<br>• Rest at room temperature for 48 hour<br>• Tap charge to 2.5 V for 5 min<br>• 4 full-range cycles between 2.5-4.2 V at 0.05C/-0.05C at room temperature |

Table IV- 35: Sample conditions

| | A1 | A2 | A3 | C1 | C2 | C3 |
|---|---|---|---|---|---|---|
| Processing | NMP | NMP | Aqueous | NMP | NMP | Aqueous |
| Dry/wet* | Dry | Dry | Wet | Dry | Dry | Wet |
| Formation protocol | ORNL1 | ORNL2 | ORNL1 | ORNL1 | ORNL2 | ORNL1 |

*Dry—the electrodes were dried under vacuum at 90°C overnight before cell assembly; Wet—the electrodes were saturated with ambient humidity (~15-20°C dew point) before cell assembly.

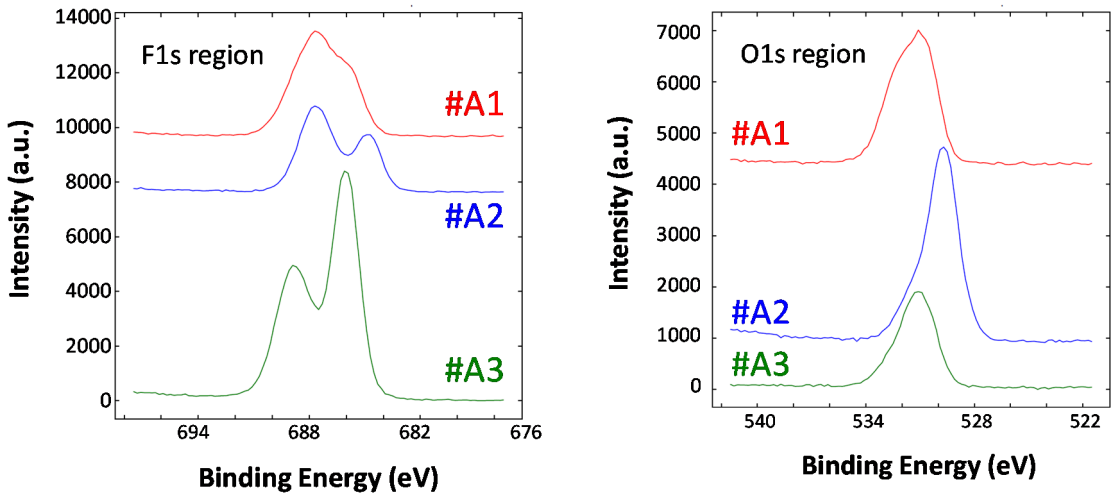


Figure IV- 250: F 1s and O 1s signals from XPS of ConocoPhillips natural graphite anode washed by DMC

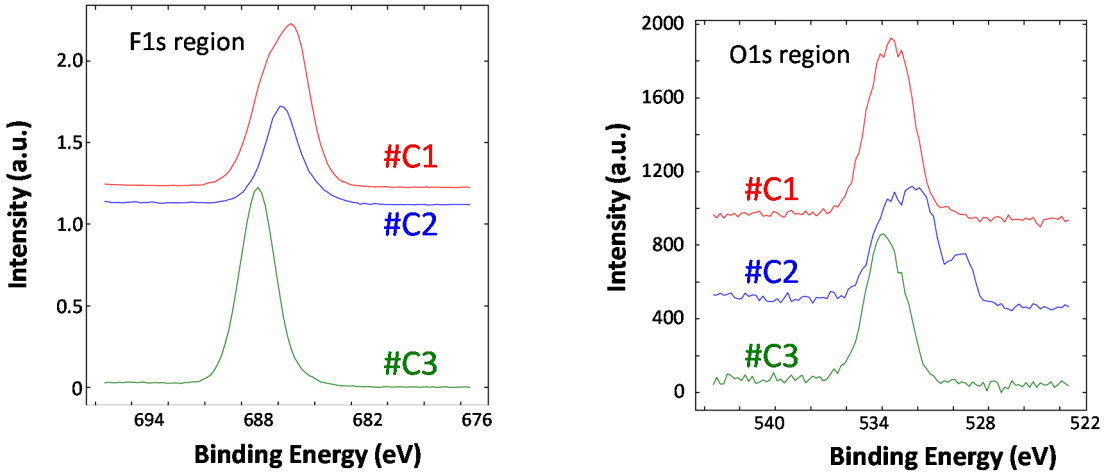


Figure IV- 251: F 1s and O 1s signals from XPS of NMC 532 cathode washed by DMC

## FY 2015 Publications, Patents, and Presentations

1. J. Li, D. L. Wood, C. Daniel, and B.L. Armstrong, "Aqueous Processing of Composite Lithium-ion Electrode Material," U.S. Patent No. 8,956,688 (UT-Battelle, LLC), February 17, 2015.
2. J. Li, C. Daniel, and D.L. Wood, "Aqueous Processing and Performance of $LiNi_{0.5}Mn_{0.3}Co_{0.2}O_2$ Cathodes," *Journal of the Electrochemical Society,* In Preparation, 2015.
3. J. Li, C. Daniel, D. L. Wood, et al., "Processing and Performance of $LiNi_{0.5}Mn_{0.3}Co_{0.2}O_2$ Cathode on Various Current Collectors", *Journal of Power Sources*, In Preparation, 2015.
4. D. L. Wood, J. Li, and C. Daniel, "Prospects for Reducing the Cost of Lithium-ion Electrode Processing and Pouch Cell Formation Steps," *Journal of Power Sources*, **275**, 234-242 (2015).
5. J. Li, D. Mohanty, B. Brown, C. Daniel, and D.L. Wood, "Fabrication and Performance of $LiNi_{0.5}Mn_{0.3}Co_{0.2}O_2$ cathodes through aqueous processing with various binders," Advanced Automotive Battery Conference (AABC) 2014, LLIBTA Symposium Track A, Atlanta, GA, February 3-7, 2014.
6. D.L. Wood, J. Li, C. Daniel, and B. L. Armstrong, "Aqueous Colloidal Chemistry for Low-Cost, Green Manufacturing of Lithium-Ion Battery Electrodes," MS&T' 14, Pittsburgh, PA, October 12-15, 2014 **(Invited)**.
7. D. Wood, "Hydrogen and Electrochemical Energy Storage at Oak Ridge National Laboratory: Enabling Widespread Fuel Cell and Battery Electric Vehicle Commercialization," SAE 2014 New Energy Vehicle Forum, Shanghai, China, September 24-25, 2014. **(Invited)**

8. J. Li, D. L. Wood, and C. Daniel, “Enabling Manufacturing Composite Cathodes through Aqueous Processing for Lithium-Ion Batteries,” 3rd International Conference and Exhibition on Materials Science & Engineering, San Antonio, TX, October 6-8, 2014.
9. J. Li, C. Daniel, and D. L. Wood, “Effect of Interface Between Current Collector and $LiNi_{0.5}Mn_{0.3}Co_{0.2}O_2$ Composite Cathodes on the Electrode Performance,”, 227th ECS meeting, Chicago, IL, May 24-28, 2015.
10. J. Li, Claus Daniel, and D. L. Wood, “Coating of $LiNi_{0.5}Mn_{0.3}Co_{0.2}O_2$ cathode on various substrates via slot-die coating and their performance”, European Coating Symposium 2015, Eindhoven, Netherlands, September 9-11, 2015.

# IV.E.5 Development of Industrially Viable Electrode Coatings (NREL)

## Objectives

- The objective of this work is the development of a system for deposition of thin protective electrode coatings using a novel "in-line" atomic layer deposition reactor design that can be integrated into manufacturing to address needs for improvement in rate capability, cycle life, and abuse tolerance in a cost effective manner.

### Project Details

**Peter Faguy – DOE Program Manager**
DOE Agreement Number 27007
Recipient: National Renewable Energy Laboratory

**Robert Tenent (NREL - PI)**
16253 Denver West Parkway
Phone: 303-384-6775
Email: robert.tenent@nrel.gov

Subcontractor:
University of Colorado at Boulder

Start Date: October 2014

Projected End Date: September 2016

## Technical Barriers

- Limited calendar and cycle life
- Abuse tolerance
- High cost

## Technical Targets

- Design and construction of prototype in-line ALD coater for deposition on porous substrates

## Accomplishments

- NREL and CU-Boulder demonstrated the ability to coat ALD alumina on flexible substrates using an in-line rotary reactor system at effective line speeds of approximately 300 ft/min.
- Developed a model system for assessing the ability to coat porous materials using the in-line rotary reactor.
- Performed initial coating of battery electrode materials and is currently assessing coating performance at both NREL and ANL.
- Initiated new partnerships with Argonne National Laboratory (ANL), Oak Ridge National Laboratory (ORNL) and Lawrence Berkeley National Laboratory (LBNL) in support of the High Energy/ High Voltage project to provide ALD coatings as required.

### Introduction

In previous work, NREL, in partnership with the University of Colorado, has shown that extremely thin, conformal coatings deposited with the Atomic Layer Deposition (ALD) technique are capable of dramatically improving the cycleability of lithium-ion cells. Current technology for performing ALD is not amenable to high throughput manufacturing methods and thus represents a high-priced bottleneck in the implementation of ultrathin electrode coatings at commercial scale.This project seeks to convert the common ALD processing format into a new reactor geometry compatible with battery electrode manufacturing.

In earlier work, NREL and CU-Boulder successfully completed design and construction of a new in-line ALD reactor. This work focused on modification of previous reactor designs to build a system capable of ALD-type coating processes in an in-line format under acceptable battery manufacturing conditions and demonstrating successful coating of aluminum oxide on flexible form factors using the in-line reactor system. The emphasis is on understanding the impact of coating on porous substrates including battery electrode materials.

## Approach

ALD coating methods are conducted by sequential and separate exposure of a sample substrate surface to gas phase precursors that react to form a film. Deposition is typically performed in a closed reactor system at mild vacuum as shown in Figure IV- 252. Precursor exposure steps are conducted in a single chamber and separated *in time*. In a typical exposure "cycle" a sample is exposed to one precursor and the chamber is then purged with inert gas prior to exposure to the second precursor that completes the coating reaction. The "cycle" ends with another extensive inert gas purging step before the process can be started again. Film growth takes place by repeating this cycling precursor exposure process multiple times. The sequential and separate exposures are keys to achieving the excellent conformal film deposition on highly textured substrates for which the ALD technique is known.

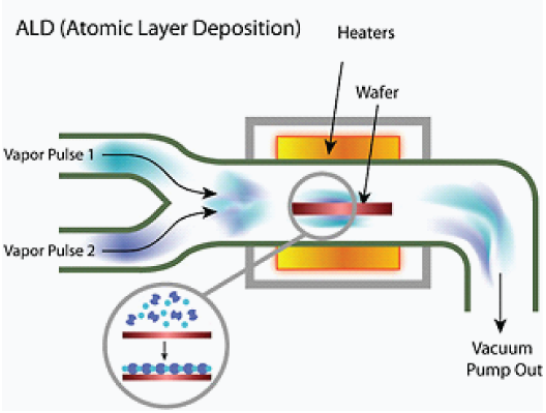


Figure IV- 252: Standard "static" ALD chamber reactor

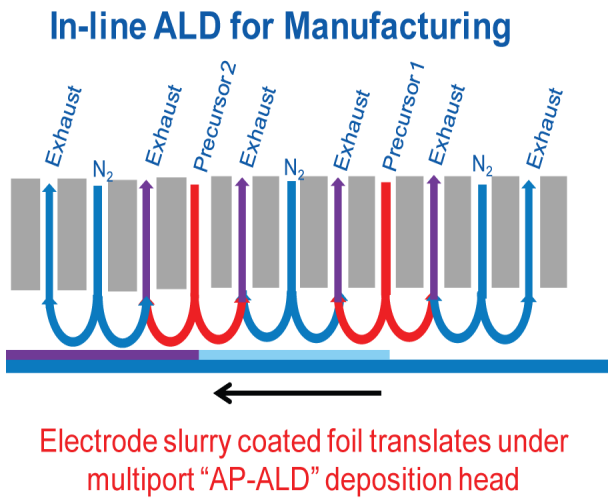


Figure IV- 253: Conceptual example of a spatial "in-line" ALD reactor

As an alternative to the temporal separation of precursor exposure in the same reaction chamber, our work proposes a ***spatial*** separation of precursor exposure steps that is more consistent with "in-line" processing techniques. Figure IV- 253 shows a simplified conceptual schematic of our proposed apparatus. Our "spatial" ALD approach employs a multichannel gas manifold deposition "head" that performs sequential exposure of precursor materials as an electrode foil translates beneath it. It is important to note that similarly designed deposition heads are currently employed by glass manufacturers for production of a variety of coated glass products using high-volume, in-line atmospheric pressure chemical vapor deposition (AP-CVD). Our approach leverages this existing knowledge base as well as our ALD expertise in order to enable in-line ALD coating that will allow the transfer of our previously demonstrated ALD-based performance improvements to larger format devices.

## Results

### Demonstration of ALD Alumina Deposition on Flexible Substrates using Rotary In-Line ALD

A simple schematic of our in-line ALD reactor system is shown in Figure IV- 254. We refer to the reactor as a "drum-in-drum" design system which consists of a rotating inner drum on which substrates are mounted and is set inside a fixed outer drum that contains all gas sources as well as purge and exhaust lines. The inner drum rotates the web radially while maintaining sufficient tension on the line to ensure accurate gas head to substrate spacing.

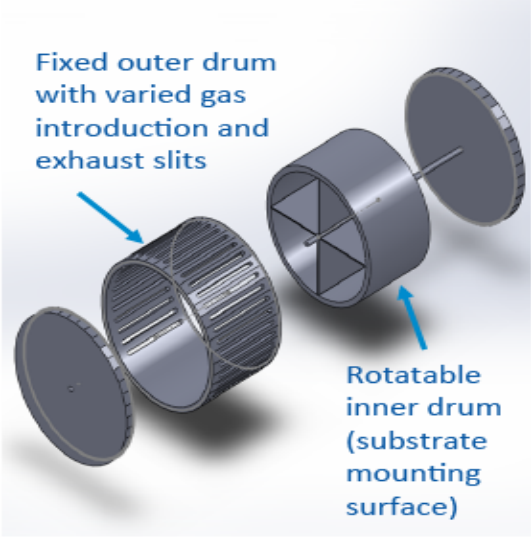


Figure IV- 254: Computer rendering of "drum-in-drum" reactor format

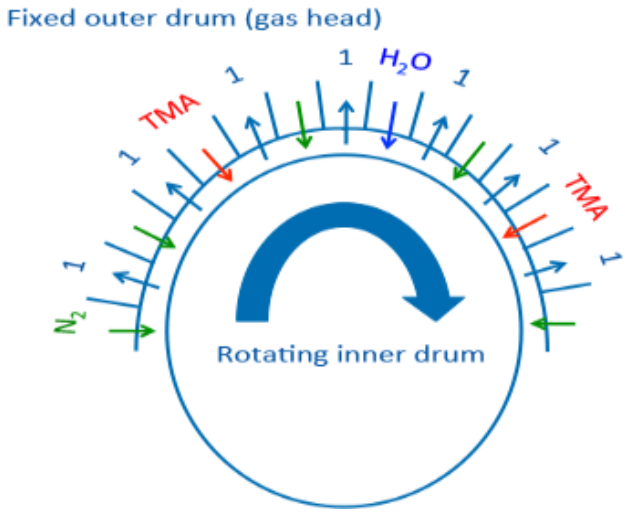


Figure IV- 255: Example schematic of "drum-in-drum" design showing configuration of gas introduction and exhaust channels

In order to maximize reactor flexibility and enable extensive deposition condition optimization work, we have adopted what we term a "digital modular" system design. Figure IV- 255 shows a more detailed schematic of the drum-in-drum reactor design and demonstrates the digital modular design. To implement the "digital modular" design, the fixed outer drum of the reactor is faceted and has slots drilled every 2.5 cm. Precursor introduction as well as reactant exhaust occurs through the attachment of specific "modules" to these slots. Precursor dosing and vacuum exhaust modules have been fabricated that are able to fit to any of the slots in the external drum. This design will allow the modules to be moved interchangeably on the external drum to allow the maximum amount of variability in dosing and vacuum modules spacing. This enables extensive experimentation across a broad range of deposition conditions in order to optimize performance.

Initial depositions of aluminum oxide were conducted on flexible plastic films (PET) with an existing metal coating. These experiments were used to demonstrate the ability to perform a controlled ALD deposition process within the rotary reactor system. Metal-coated samples were employed to eliminate penetration of the flexible plastic model sample with the precursor reactors and ensure that accurate film growth measurements were obtained. Our initial reactor configuration was set to allow one cycle of the ALD deposition process to be conducted per rotation of the sample. Figure IV- 256 shows photographs of a metal coated PET film prior to being loaded into the reactor (A) and immediately after deposition of ~ 650 nm of alumina (B). The color change of the sample is indicative of film growth and does show some degree of non-uniformity on the edges of the sample surface which appear as blue/gray lines. Figure IV- 257 shows film thickness across the sample surface as measured using spectroscopic ellipsometry. This data shows that the edges of the samples are showing slightly higher thickness (~ 670nm) as compared to the center portion. This may be caused by some mixing of reactants near the edges of the sample reactor zone, however, the overall thickness does not vary across the sample any more than 3% which represents excellent uniformity for initial characterization.

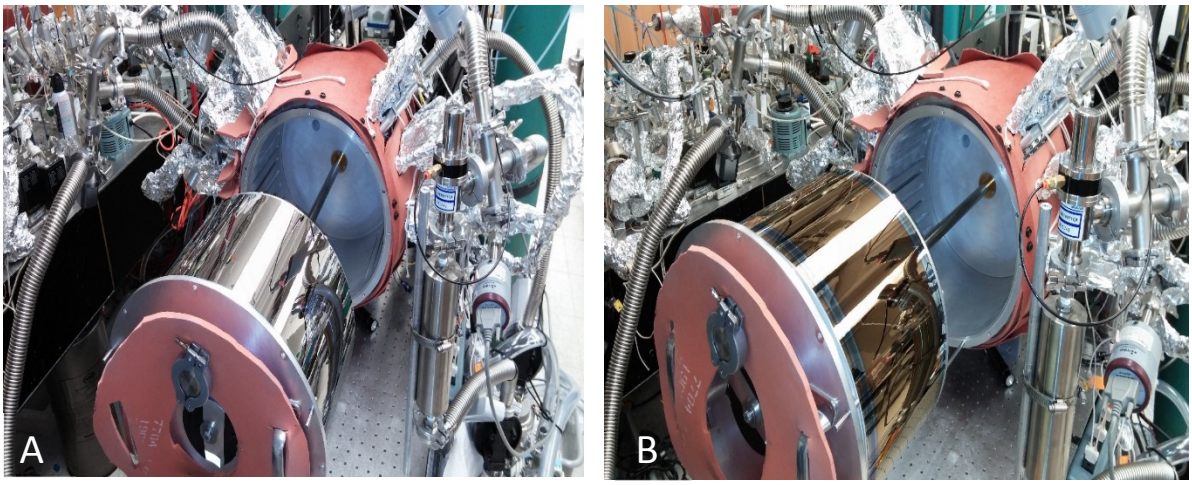


Figure IV- 256: Photographs of a flexible metal coated plastic film before loading (A) into the rotary reactor and (B) after deposition of ~ 650 nm of alumina

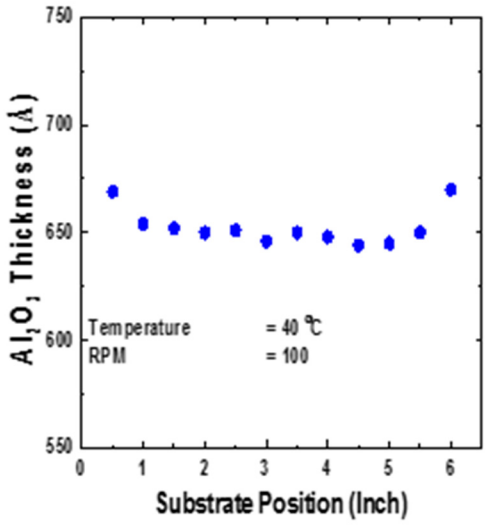


Figure IV- 257: Thickness measurement for alumina coatings deposited across metal coated plastic sample

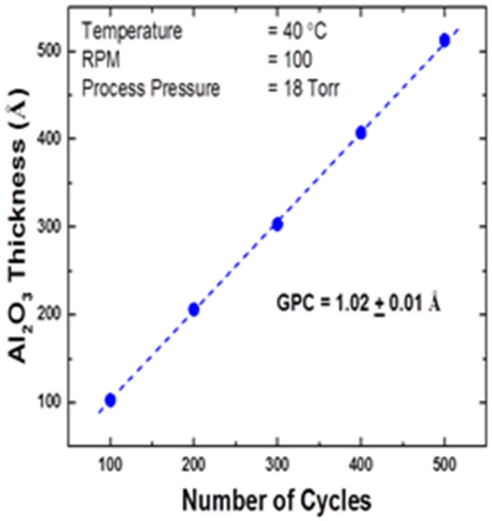


Figure IV- 258: Plot of measured alumina film thickness as a function of number of ALD cycles, which is equivalent to the number of reactor rotations

Figure IV- 258 shows data for film thickness growth as a function of number of rotation cycles for the aluminum oxide growth chemistry conducted with the in-line ALD reactor design using optimized deposition conditions. Note that the film thickness increases linearly as is expected for the ALD sequential reaction cycle conducted under a well-controlled condition. The growth rate per rotation cycle (GPC) was determined from the slope of this line to be ~1.02 Angstroms per cycle. This growth rate is consistent with that observed for well controlled ALD alumina deposition using standard reactors. The linear growth rate as a function of cycle and consistency with standard reactor deposition rates indicates that under the selected conditions we appear to be achieving a well-controlled ALD deposition process using the in-line reactor design.

Further experiments were conducted to assess the ability to obtain a well controlled ALD process as a function of rotation rate and "effective" line speed. The "effective" line speed is simply calculated based on the rotation rate and the circumference of the inner reactor drum and gives an estimate of what practical manufacturing conditions may be feasible with our reactor design. It is crucial that the ALD chemistry be conducted not only on an in-line format, but also at relevant manufacturing process line speeds in order for it to be adopted by industrial partners. Figure IV- 259 shows the measured ALD growth rate (GPC, in Angstroms/cycle) as a function of the rotation rate of the internal reactor cylinder. Note that up to a rotation rate of ~100 RPM the measured growth rate remains constant at just over 1 Angstrom per cycle, however as rotation speed increases GPC begins to decrease. This is likely due to a combination of the limited "residence" time of the reactants near the sample surface and limitations of the reaction kinetics at our current processing temperatures (40° C). In more recent experiments, the impact of reactant residence time was explored by reconfiguring the spacing between reactant introduction and exhaust zones which increased deposition rate further and is currently under continued study.

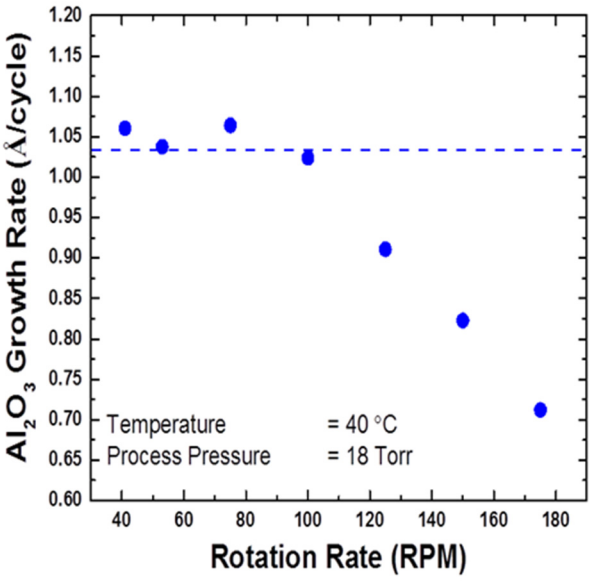


Figure IV- 259: Measured ALD growth rate for alumina as a function of reactor rotation rate

It is important to note that while we are pushing the ability of the reactor to enable controlled deposition at higher rotation rates, the 100 RPM limit with the current configuration translates to an effective line speed of ~ 300 ft/min which is roughly twice the current rate of state of the art lithium-ion battery electrode manufacturing lines.

### Determination of the Ability to Coat Porous Substrates

While earlier results indicated the ability to obtain a controlled ALD deposition at effective line speeds nearly twice that of current manufacturing, this work was conducted with flat substrates and are not representative of battery electrodes. We have further developed a model system to assess the ability to perform quality and well controlled ALD alumina deposition on porous samples in order to optimize conditions for eventual battery electrode coatings. Figure IV- 260 shows a simple schematic of anodic aluminum oxide (AAO) materials which we have chosen as our model porous substrate. These samples consist of a highly uniform distribution of well controlled pore structures over large sample areas with pore sizes in the nanometer size regime. This sample format allows detailed experimentation for performing ALD alumina deposition on a wide variety of pore sizes and at a variety of rotation rates.

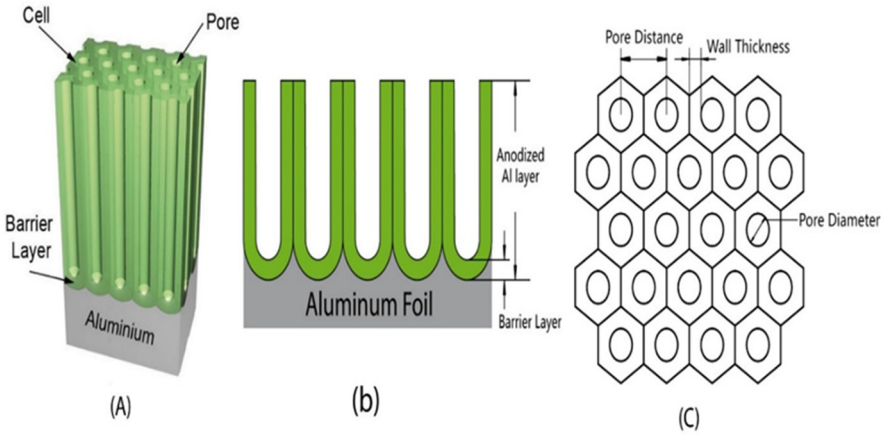


Figure IV- 260: Schematic of anodic aluminum oxide samples

In order to characterize the ability to perform ALD processing on the anodic alumina samples, a new ALD process was developed to allow deposition of Zinc oxide to enable characterization of the coating on the AAO sample which would not be possible with the deposition of ALD aluminum oxide on the already existing aluminum oxide (AAO) material. Significant efforts were placed on development of a well controlled ALD ZnO chemistry, although data is not shown here.

Analysis of the ability to coat the highly porous AAO samples was conducted by a combination of electron microscopy and energy dispersive x-ray spectroscopy(EDX). Figure IV- 261 shows an example of data collected using this technique as well as an example schematic of the AAO sample showing areas in which measurements were made. The plot in Figure IV- 261 shows the Zn signal measured by EDX as moving across the AAO structure from the surface that was in closest proximity to the ALD reactant gasses in the in-line system to the bottom of the pore structure. This gives an assessment of the amount of ZnO deposited near the top of the pore structure as compared to the bottom. A uniform coating of ZnO across the entire structure would give roughly the same signal for Zn moving across the pore length

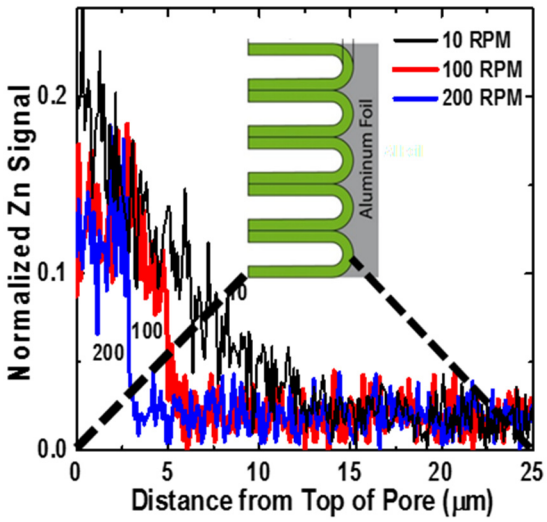


Figure IV- 261: Plot of normalized Zn concentration EDX signal across porous AAO sample structure

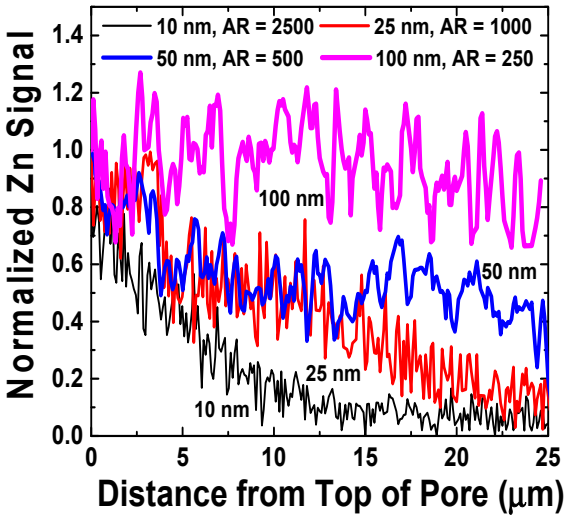


Figure IV- 262: Plot of normalized Zn concentration EDX signal across AAO samples with varied porosity

while a non-uniform deposition would show distinct differences between Zn signal as a function of distance from top of the pore. The data in Figure IV- 261 clearly shows the impact of rotation rate on the Zn concentration profile across the pore structure for an average pore diameter of 10 nm. The data clearly shows non-uniformity with a high Zn concentration near the top of the structure indicating the inability of the ZnO precursors to penetrate into the film under these conditions and also indicates the ability to detect changes in Zn concentration profiles under varied conditions.

Note that at 10 RPM, the Zn concentration clearly reaches further into the pores than at the 100 RPM or 200 RPM rotation rates. NREL and CU-Boulder are in the process of conducting extensive studies to optimize in-line ALD deposition on porous substrates. Figure IV- 262 shows an example data set for deposition on a series of different pore size samples at a 100 RPM rotation rate. This data shows that at 100 RPM, it appears to be feasible to obtain a uniform Zn concentration profile for a 100 nm pore structure with decreasing uniformity as pore diameter decreases. Experiments to further understand the limitations of coating of porous samples are on-going with further optimization.

In parallel with the continued optimization of coating of porous materials, NREL, CU-Boulder and Argonne National Laboratory are now collaborating to begin assessment of in-line ALD coatings on standardized battery electrodes through the ABR program with samples currently under test.

## Conclusions and Future Directions

In FY15, the NREL/CU team successfully demonstrated the ability to deposit alumina using a new in-line ALD reactor under well controlled conditions at an effective line speed of ~300 ft/min. In addition, experiments were initiated to determine optimium conditions for coating of porous materials through controlled experiments using standard porous substrate models. Further work is beginning to assess the impact of early coating processes on battery electrode performance through a partnership between NREL and ANL.

Moving into FY16, the NREL team has been tasked with a new role of serving as an ALD coating resourse for the ABR program as a whole. Work in FY16 will focus on the development of standardized ALD coating processes using both status and in-line spatial ALD in order to provide partners will well characterized materials for further studies. NREL will be partnering with ANL both through the CAMP effort as well as with the High Energy / High Voltage research teams to provide coated materials. Further work will focus on also providing support to additional commercial partners with the longer term goal of achieving integration of the in-line ALD process within manufacturing processes.

## FY 2015 Publications/Presentations

1. “Development of Industrially Viable Electrode Coatings”, ES159_Tenent_2015_p, US DOE Vehicle Technologies AMR, 2015
2. “Spatial Atomic Layer Deposition on Flexible Porous Substrates: ZnO in Anodic Aluminum Oxide Membranes and Al2O3 in Li Ion Battery Electrodes” K. Sharma et al. J. Vac. Sci. Technol. A 33, 01A132 (2015)

# IV.F Process Development and Manufacturing R&D with U.S. Industry

# IV.F.1 Low Cost, Structurally Advanced Novel Electrode and Cell Manufacturing (24M Technologies)

## Objectives

- 24M will demonstrate that its novel electrode and cell design and manufacturing approach can be scaled to mass production of lithium-ion systems for automotive applications. Activities in Phase 1 include increasing the energy density of 24M's electrodes and demonstrating production quality processes. Phase 2 focuses on increasing the total size and energy of the system and demonstrating high volume manufacturing methods.


**Project Details**

**Tien Duong (DOE-VT)**
DE-EE0006830 Recipient: 24M Technologies

**Taison Tan (24M Technologies - PI)**
130 Brookline St.
Cambridge, MA 02139
Phone: 617-553-1012
Email: ttan@24-m.com


Start Date: October 2014

Projected End Date: September 2016

## Technical Barriers

- Increase energy density of semisolid suspensions while maintaining processability for manufacturing.
- Demonstration of high volume manufacturing capability with a novel electrode and cell manufacturing technology.
- Maintain manufacturing quality and tolerance for large electrode designs.

## Technical Targets

- Increase cathode semisolid volume loading to greater than 50 volume %.
- Increase anode semisolid volume loading to greater than 50 volume %.
- Deliver 10 cells to Argonne National Laboratory with capacity greater than 4Ah for evaluation at the end of the first year.
- Demonstrate manufacturing tolerances of ±5% for electrode weight and thickness.
- Achieve greater than 95% electrode yield in manufacturing.
- Achieve greater than 75% cell yield for first year cell deliverables.
- Increase electrode footprint while maintaining quality metrics.
- Deliver 10 cells to Argonne National Laboratory with capacities 35Ah or greater for evaluation at the end of the program.

## Accomplishments

- Both cathode and anode volume loadings have been increased to greater than 50 volume %.
- Greater than 90% electrode yield achieved with weight and thickness tolerances less than ±5% for both cathode and anode electrodes for cells delivered to ANL.
- 89% and 90% cell yield based on capacity and impedance tolerances of ±5% and ±10%, respectively.
- 10 cells (4.5Ah) were delivered to ANL for testing in October 2015.
- Cathode and anode electrodes successfully formed with areas larger than 250cm$^2$.

### Introduction

24M Technologies, Inc. has developed a novel/non-conventional electrode and cell manufacturing technology that utilizes proven and emerging lithium-ion (or other) chemistries, and results in automotive-capable batteries with a smaller ratio of inactive to active material than any previous lithium-ion battery.

## Approach

24M's approach to lithium-ion manufacturing utilizes a novel electrode and cell design that requires fewer unit operations for higher process yield and removes the need for entire electrode factories with cell fabrication in one-fifth the time of conventional lithium-ion. The manufacturing approach achieves low cost without giant factories ($1/5^{th}$ of conventional lithium-ion manufacturing space), in which production can be scaled with "copy exact" module plants. This creates the opportunity for locating production near customers for lower cost. The semisolid electrodes developed by 24M require no drying and no organic solvents.

## Results

We have achieved the following progress:

### Cathode and anode semisolid loadings greater than 50 volume %

Cells manufactured with cathode and anode semisolid suspensions of greater than 50v% loading are currently on test. The cells have reached more than 100 cycles. New formulations are under evaluation to further increase the loadings for both anode and cathode semisolid suspensions. Various active material morphologies are under investigation.

### Delivery of 10 cells to Argonne National Laboratory for testing

10 cells have been shipped to ANL for testing. A duplicate set of 10 cells is currently on test at 24M. The cells will be tested to characterize their capacity, calendar life, and cycle life.

### Demonstrate manufacturing tolerances of ±5% for electrode weight and thickness

Figure IV- 263 and Figure IV- 264 show the electrode quality for the cells fabricated for the Phase 1 deliverable. Greater than 90% of the electrodes met the weight and thickness tolerance targets.

### Achieved and electrode footprint greater than 250cm$^2$

The electrodes made for the Phase 1 deliverable had an electrode footprint of approximately 80cm$^2$. 24M has now increased the electrode footprint to greater than 250 cm$^2$. These electrodes will be used for the end of Phase 2 deliverable for cells with a capacity of 35Ah or greater. 24M work continues with the larger footprint electrodes in order to gain metrics such as weight and thickness for all electrodes. This capability will be similar to what has already been achieved on the Gen1 prototype line that can automatically record the weight and thickness of every electrode fabricated. Vision systems are also in place to monitor for defects.

## Conclusions and Future Directions

24M has successfully achieved the Phase 1 Go/No-Go milestone of delivering 10 cells to Argonne National Laboratory for evaluation. The Gen1 prototype line is currently functional with metrics for weight and thickness obtained automatically for both cathodes and anodes. Vision system equipment is also in place for the detection of any defects.

The process of further increasing the electrode footprint will continue in the second phase of the program with a final goal of delivering 10 cells with capacities of 35Ah or greater. Manufacturing processes will be further evaluated and optimized in order to maintain the quality of the electrodes from the 80cm2 footprint to the >250cm$^2$ footprint. More metrics recording equipment will be implemented by 24M in order to ensure the quality and the electrodes and cells produced.

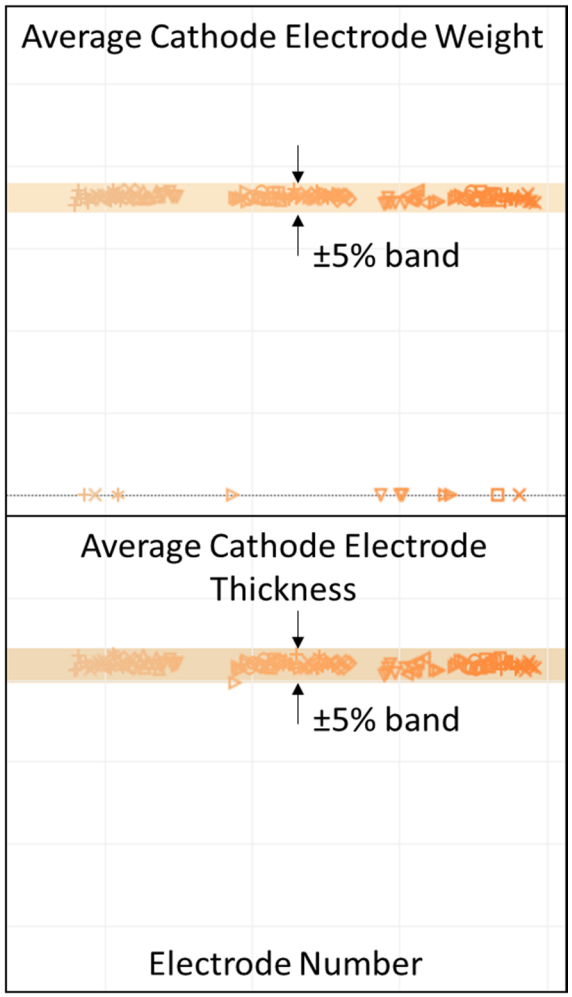


Figure IV- 263: Plot of cathode average weights and thicknesses for cells used for Phase 1 deliverable

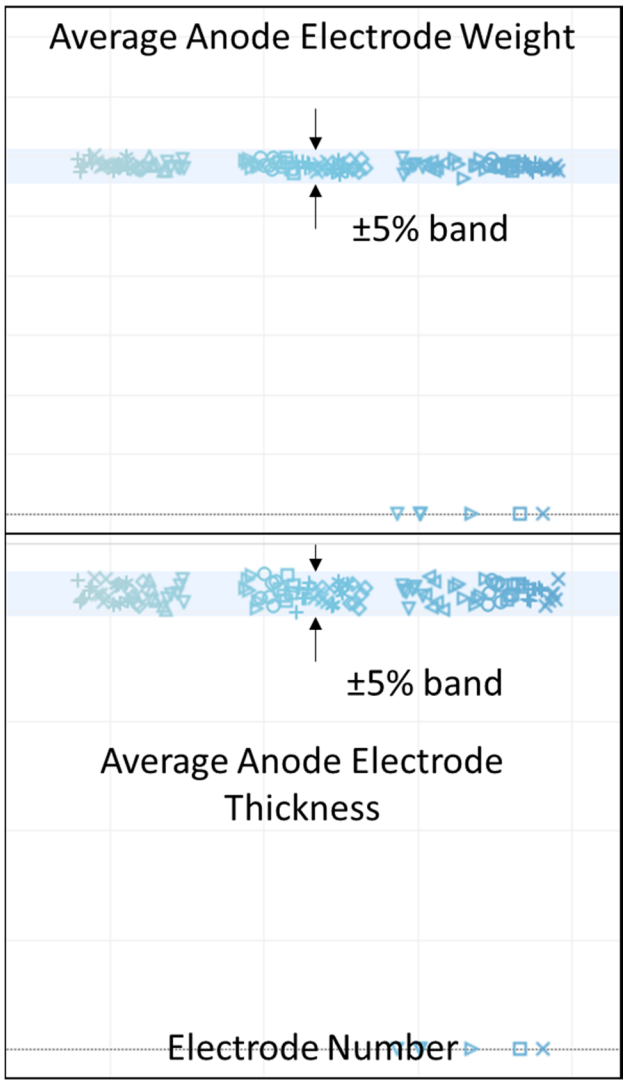


Figure IV- 264: Plot of anode average weights and thicknesses for cells used for Phase 1 deliverable

### FY 2015 Publications/Presentations

1. "Low Cost, Structurally Advanced Novel Electrode and Cell Manufacturing", ES245_Tan_2015_p, US DOE Vehicle Technologies AMR, 2015.

# IV.F.2 Advanced Drying Process for Low Cost Manufacturing of Electrodes (Lambda Technologies)

## Objectives

- We propose to develop a prototype of the Advanced Drying Process (ADP) of high loading electrodes for lithium-ion batteries. The ADP prototype is anticipated to rapidly dry (5x faster) the casted aqueous slurry, resulting in a 30-50% reduction in the operating cost and hence the overall cost of lithium-ion batteries.
- The electrodes will be evaluated for physical and electrochemical properties, while the fabricated cell will be tested for capacity, energy and rate capability. Cycle life testing will be performed to evaluate that the cells are capable of meeting the power density targets and are equivalent to the baseline process.

### Project Details

**Bruce Mixer (NETL Program Manager)**
DE-EE0006869 Recipient: Lambda Technologies

**Iftikhar Ahmad (Lambda Technologies, PI)**
860 Aviation Parkway, Suite 900
Morrisville, NC 27560
Phone: 919-462-1919; Fax: 919-462-1929
Email: iahmad@microcure.com

Subcontractor:
Navitas Systems
4880 Venture Drive
Ann Arbor, MI

Start Date: October 1, 2014

Projected End Date: April 1, 2016

## Technical Barriers

- In order for EVs to achieve mass adoption in U.S and global production, the key problems of high cost and energy density must be addressed.

Barriers addressed:

- Cost: Rapid drying should reduce operating cost.
- Energy Density: Capability to rapidly dry higher loading electrodes is expected to increase active material and energy density.

## Technical Targets

- To reduce electrode drying time by a factor of 2 – 5 with ADP.
- To demonstrate a cycle life of >1000 (80% DOD) of the ADP electrodes in 2Ah Li ion cells with EV battery relevant conditions.

## Accomplishments

- Static rapid ADP drying of aqueous anode slurry (5x faster) and NMP based cathode slurry (2x faster) was performed which provided information for the chamber size for continuous electrode coating.
- Solvent content analyses, dry/wet adhesion tests, binder distribution ratio and half cell testing for electrochemical performance, all show identical data when compared to the standard method.
- One of the major components of the ADP Prototype was the microwave choke which could accommodate a 150 mm wide web without leaking microwaves. The choke was designed and tested to conform to the international safety standards.
- The rest of the ADP Prototype components were designed to allow necessary resident time for the slurry coated foil in the process chamber, as well as other features for easy integration of the equipment at Navitas pilot coating line.
- The designs were released to the vendors for fabrication of these components.
- As the fabricated components were received they were inspected, tested for functionality/fit and assembled on the ADP Prototype.
- The entire ADP Prototype system assembly was completed and powered up electrically to check functionality. After the system testing was completed VFM power was delivered to check for any microwave leakage especially at the wide choke openings.

- A temporary web handling setup with variable speed control was acquired and installed. A doctor blade and pump to deliver slurry were mounted on the system to allow casting the slurry on the continuously moving foil.
- Premixed anode slurry from Navitas was received before the scheduled Go/No-Go demonstration. The binder was mixed right before the slurry was casted on the moving copper foil. The high loading aqueous anode slurry was dried in the ADP Prototype in one minute with the foil moving at 0.5m/min.
- On successful completion of the Go/No-Go demo, the temporary web handling setup, the doctor blade and pump were uninstalled and the ADP system was packed and shipped to Navitas.
- Lambda personnel visited Navitas for installation of the ADP Prototype and training for appropriate use of the innovative ADP tool. Drying tests of aqueous anode and NMP cathode slurries casted on moving foil were performed.
- Optimization of processing parameter on the rapid drying ADP tool for various slurries is in progress at Navitas.
- Material and electrochemical characterization will be performed at Navitas, which includes binder distribution, adhesion test, solvent content, SLP formation, rate capability, DCR and life cycling.

## Introduction

In high volume production of electrodes for lithium-ion batteries, the drying process is a high cost unit operation. In conventional processing the electrodes are slurry-casted onto metal foils and dried using surface heating methods under highly controlled conditions in very long furnaces. The furnace length (which can reach up to 40 meters) is dictated by the limited rate at which water or NMP can be removed from the slurry without binder migration, particle segregation, orange peels defects or pore blocking skin formation. The long furnaces cause both high capital equipment and operating costs.

## Approach

**Innovative Approach:** The objectives outlined above are accomplished by employing penetrating Variable Frequency Microwave (VFM) which interacts with the polar molecules of the solvent deep in the thickness of the slurry to drive them out. This Advanced Drying Process (ADP) includes hot air flow on the surface of slurry which collects the vapors and carries them out to the system exhaust thereby resulting in efficient drying of the slurry. The major technology innovations undertaken to accomplish the objectives of this effort include:

1. Perform static specimen drying of anode and cathode slurries to estimate the resident time required in the ADP equipment when the slurry is casted on continuously moving metal foil. Based on the casting speed for each slurry type the resident time in the ADP and the chamber size was determined. The electrodes were tested for physical and electrochemical properties. Cells were evaluated for capacity, energy and rate capability. Cycle life testing was performed to evaluate that the cells were capable of meeting the power density targets and were comparable to the baseline process.
2. Since a continuous foil width of 150 mm needed to pass through the ADP chamber, microwave chokes had to be designed, fabricated and tested to allow 150 mm wide foil to pass through without any microwave leakage hazard to the personnel working in the area.
3. The ADP prototype system was designed to fit into the existing coating line at Navitas. Various designed components were released to vendors for fabrication.
4. As the fabricated parts were received, the ADP prototype system was assembled and tested. VFM power was delivered to check for any microwave leakage especially at the wide choke openings.
5. A temporary web handling setup with variable speed control was acquired and installed. A doctor blade and pump to deliver slurry were mounted on the system to allow casting the slurry on the continuously moving foil.
6. Navitas personnel visited Lambda Technologies to perform the continuous casting of electrode and drying of the slurry.
7. On successful completion of the Go/No-Go demo, and after NETL approval, the ADP system was packed and shipped to Navitas.
8. Lambda personnel visited Navitas to install the ADP prototype and test system functionality. Drying tests of slurries casted on moving foil were performed.
9. The processing parameters for drying each slurry is to be optimized.

10. The analytic testing on electrode and cells will be repeated again for the specimens obtained from the continuous casting and drying process.

## Results

The progress made on the design and fabrication of the ADP prototype and the analytic results will be presented below. Although the analytic work as well as the design and fabrication of the prototype were performed in parallel, the design, build, shipment and install of the ADP will be presented first. Then the summary of the analytic work will follow, to allow for the continuity in each aspect of the project.

### Design, fabrication of components and assembly of the ADP Prototype Equipment

Based on the static sample slurry drying, the casting speed, the space available and integration requirements on the pilot coating line at Navitas in Ann Arbor, the chamber and the rest of the equipment were designed and sent out for fabrication from various vendors. As the fabricated components were received, they were tested individually and assembled.

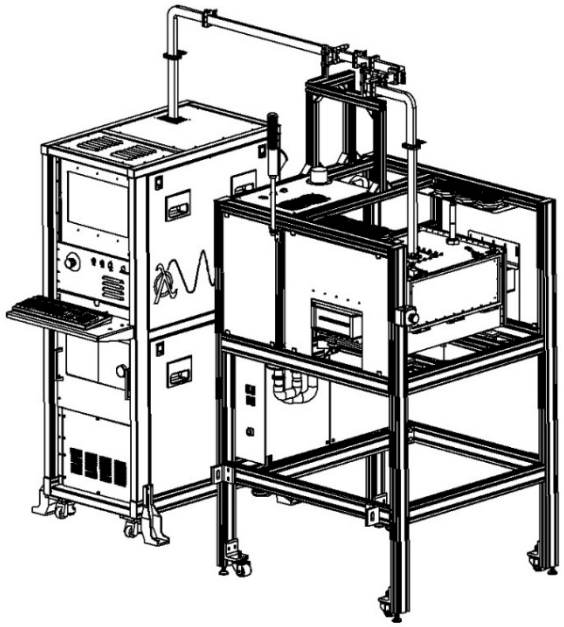

Figure IV- 265: ADP Prototype configured for installation at Navitas

The most critical components were the scaled-up wider microwave chokes capable of allowing 150 mm wide metal foil to pass through without any appreciable microwave leakage that could be a hazard to the personnel working in the area. It was made sure that the leakage from the equipment was within the International Electrotechnical Commission (IEC) emission standard of 5 $mW/cm^2$ at 5 cm. At the operator distance, the leakage was essentially nonexistent when operated as per intended use.

While additional details were presented in earlier quarterly reports, the various stages of design, fabrication and assembly of the ADP Prototype are outlined above. It shows the final overall designed equipment in Figure IV- 265. Figure IV- 266 shows a digital image of the equipment set up in our laboratory ready for the Go/No-Go demonstration run. The power module can be placed wherever convenient (shown on right).

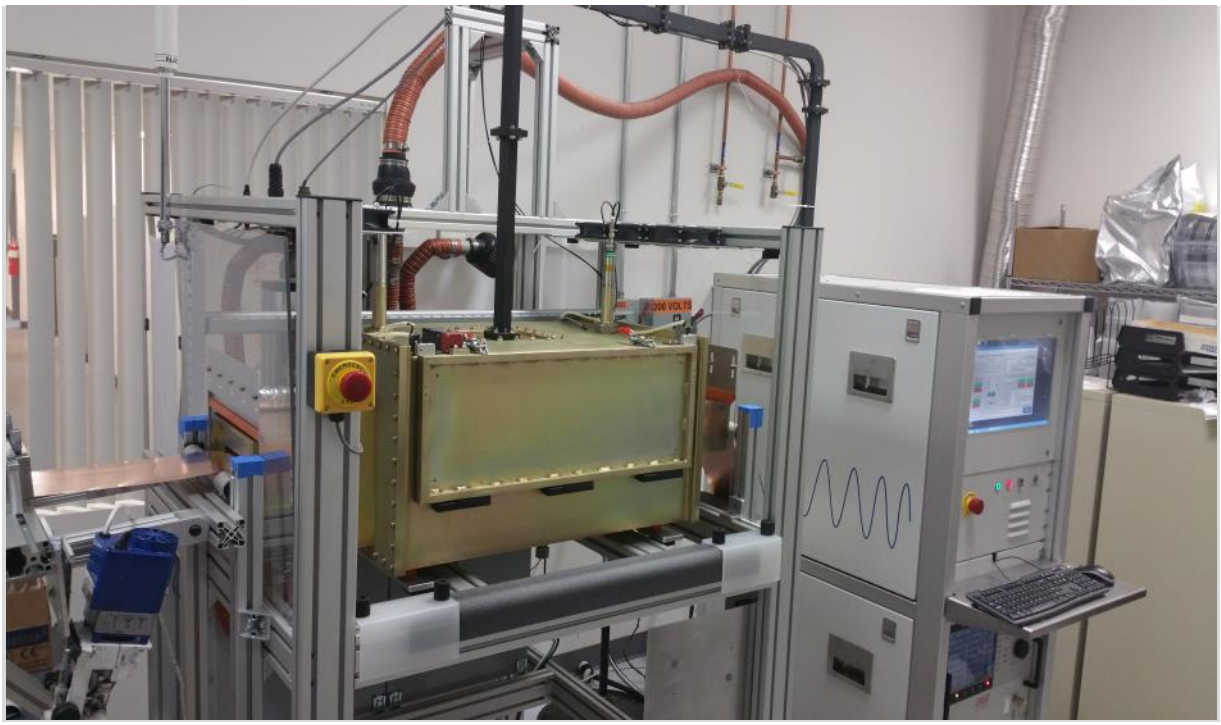

Figure IV- 266: Digital Image of Process Module placed on the left and Power Module configured on the right at Lambda

Figure IV- 267 shows the Process Module (within red ellipse) designed to be integrated into the pilot coating line at Navitas in Ann Arbor, MI.

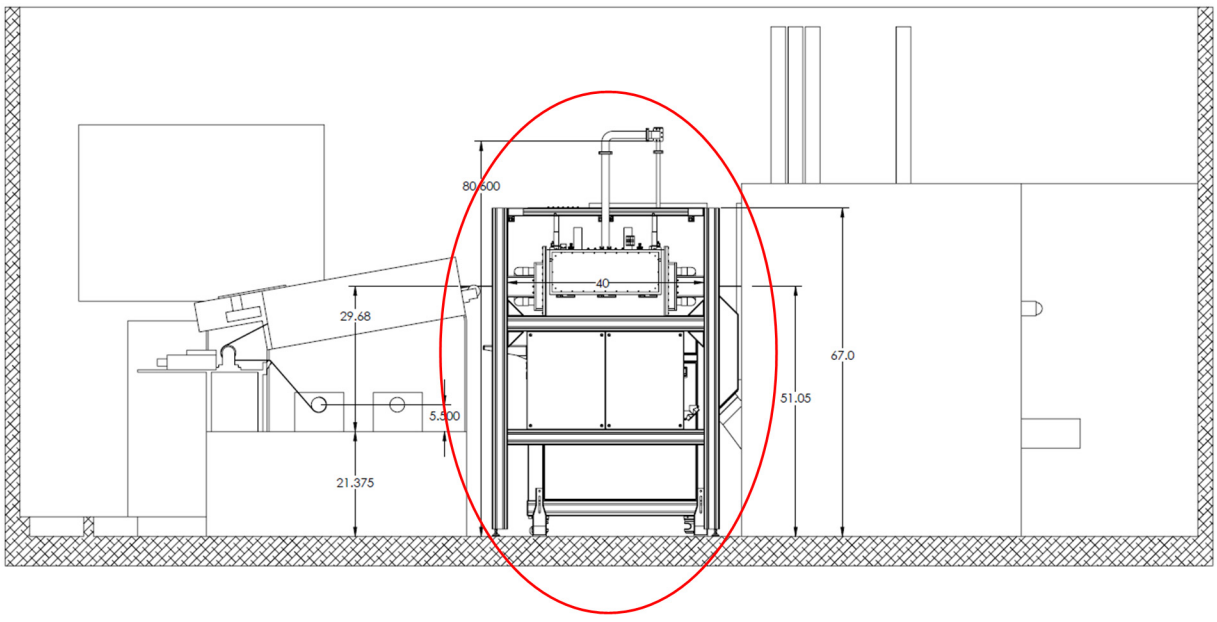


Figure IV- 267: Schematic of the Process Module to be integrated in the pilot coating line. The Power Module will be actually placed behind the Process Module for this particular set up

After the successful (Go/No-Go) demonstration of the ADP Prototype operation and identical analytic results for samples dried with the newly assembled tool, the equipment was packed and shipped to Navitas facilities where it was integrated and installed on their pilot coating line. Figure IV- 268 shows the digital image of the installed ADP Prototype equipment. Figure IV- 268 (a) shows a clear view of the Process Module, while Figure IV- 268 (b) shows the Power Module placed behind the Process Module. VFM power is transmitted and delivered by the waveguide on the top connecting the two modules.


**Figure IV- 268: (a) Digital image of the ADP Prototype installed at Navitas. The Process Module is in front while the Power Module is placed behind the Process Module, shown below it. (b) Digital image of the Power Module placed behind the Process Module delivering VFM power through the waveguide connecting both modules**

### Electrodes and cell characterization data from static ADP dried samples

#### Solvent Content Analysis

Solvent content analyses was performed on aqueous anodes dried by standard as well as (static) ADP method. Initial solvent content for samples received at Navitas was ~2000 ppm, which is lower than the target value of 5000 ppm. Solvent content was further reduced to < 800 ppm after vacuum oven drying (standard step before cell fabrication) for both samples (Standard and ADP), as shown in Figure IV- 269.

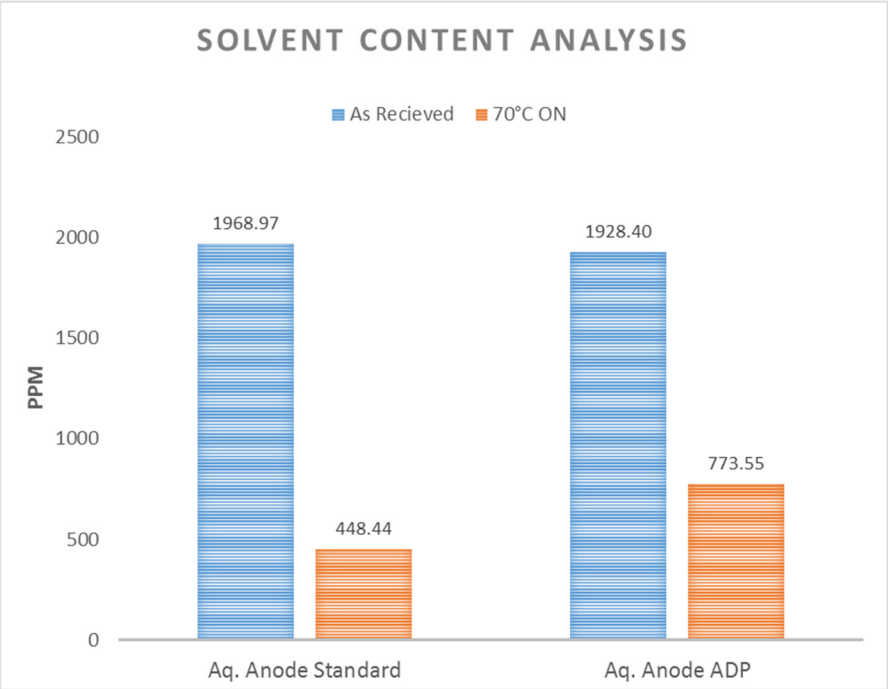


**Figure IV- 269: Solvent content (moisture) analysis for anode electrodes (water based binder) dried using standard and ADP samples**

### Adhesion and binder distribution

All samples (both aqueous and NMP cathode) passed Navitas' dry and wet adhesion tests. Both sets of electrodes show good cohesion properties during dry test. The binder distribution ratio (the amount of binder on electrode surface over amount of binder near foil substrate) observed values were below the target of 1.3 (common for standard dried electrodes) as shown in Table IV- 36.

**Table IV- 36: Adhesion (combined dry and wet) and binder distribution results for anode (water based binder) and cathode (NMP based binder) electrodes**

| Electrode | Drying Method | Solvent | Drying Time (min) | Adhesion | Binder Distribution Ratio |
|---|---|---|---|---|---|
| Anode Water | Standard | Water | 7.0 | Pass | 1.08 |
| | ADP | Water | 1.5 | Pass | 1.06 |
| Cathode NMP | Standard | NMP | 7.0 | Pass | 1.03 |
| | ADP | NMP | 3.5 | Pass | 1.04 |

### Electrochemical characterization

The hand casted (doctor blade) anode and cathode electrodes prepared at Lambda were used to fabricate half coin and full single layer pouch (SLP) cells. The electrodes were dried using both standard and ADP methods. Electrochemical characterization includes formation, rate capability and cycle life (only performed on SLPs). Electrode loadings were ~3.5 mAh/cm$^2$ (10.5 mg/cm$^2$) and ~3.0 mAh/cm$^2$ (18.5 mg/cm$^2$) for anode and cathode respectively. As noted in Table IV- 37 and Table IV- 38 the drying times were improved when the ADP was used (2X for NMP based and 5X for water based electrodes).

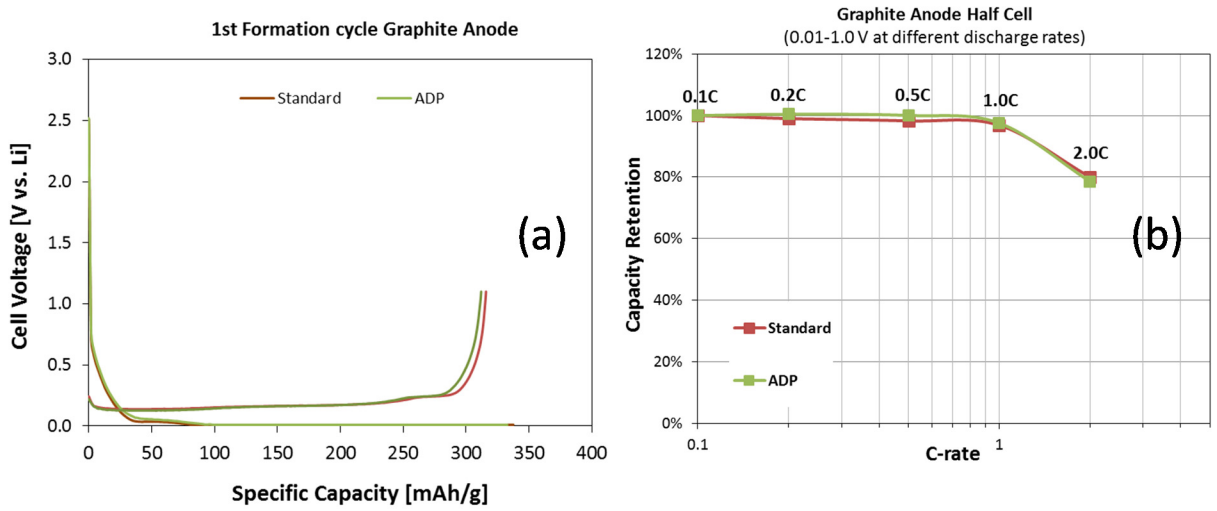


Figure IV- 270: Electrochemical performance results for anode electrodes dried using standard and ADP methods. (a) First formation cycle (0.01-1.0V @ 0.1C) (b) rate capability (lithiated at 0.1C and delithiated at 0.1, 0.2, 0.5, 1.0 and 2.0C currents)

**Table IV- 37: Anode properties and electrochemical characteristics for anodes dried using standard and ADP methods**

| Electrode | Drying Method | Drying Time (min) | Loading | | Reversible Capacity (mAh/g) | ICL ( %) |
|---|---|---|---|---|---|---|
| | | | (mg/cm$^2$) | (mAh/cm$^2$) | | |
| Anode Water | Standard | 7.0 | 10.4 | 3.4 | 325.6 | 7 |
| | ADP | 1.5 | 10.7 | 3.5 | 322.9 | 7 |

### Half Cell Testing

Graphite anodes (with water-based binder) and NCM cathodes (with NMP-based binder) were used in half cells experiments. These small cells were used for initial capacity check (formation) and quick rate performance control before fabricating large size cells.

Figure IV- 270 and Table IV- 37 above summarized the results for half cell anodes, while Figure IV- 271 and Table IV- 38 below present results for half cell cathodes. As expected formation voltage profiles for both anodes and cathode were similar whether the electrodes were dried with ADP or Standard drying methods.

In addition, numerical values such as specific capacities and initial capacity loss (ICL) were the same (within error). Similarly, rate capability results followed identical trends as the current rate is increased from 0.1C to 2C.

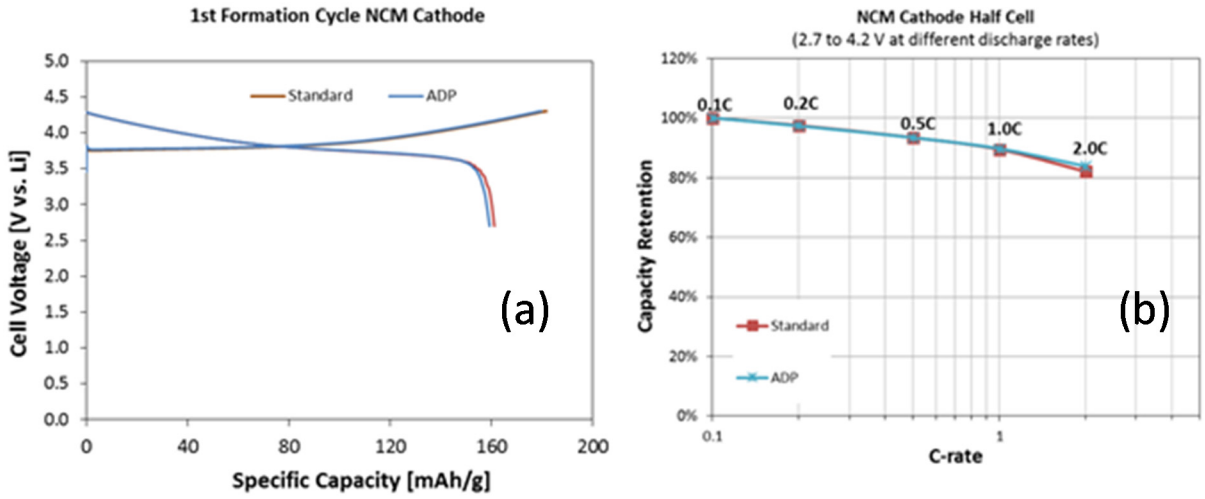


Figure IV- 271: Electrochemical performance results for cathode electrodes dried using standard and ADP approaches. (a) First formation cycle (3.0-4.2V @ 0.1C) (b) rate capability (lithiated at 0.1C and delithiated at 0.1, 0.2, 0.5, 1.0 and 2.0C currents)

**Table IV- 38: Cathode properties and electrochemical characteristics for anodes dried using standard and ADP processes**

| Electrode | Drying Method | Drying Time (min) | Loading | | Reversible Capacity (mAh/g) | ICL ( %) |
|---|---|---|---|---|---|---|
| | | | (mg/cm$^2$) | (mAh/cm$^2$) | | |
| Cathode NMP | Standard | 7.0 | 18.2 | 2.9 | 161.3 | 12 |
| | ADP | 3.5 | 18.9 | 3.0 | 159.4 | 11 |

### Full Cell (SLP) Testing

Three sets of SLPs were assembled at Navitas and are described below. The Navitas anodes and cathodes were fabricated with graphite and NCM respectively and both used NMP based binder; these electrodes were dried with conventional methods. The Lambda anodes (water-based binder) and cathodes (NMP-based binder) were dried using ADP (hot air plus VFM). The cell sets were Navitas baseline, Lambda anode – Navitas cathode, and Lambda cathode – Navitas Anode.

### Formation

Figure IV- 272 present formation voltage vs. capacity profiles for both Lambda-cathode and Lambda-anode cells and Table IV- 39 summarizes numerical values for all three set of cells.

Voltage profiles as well as quantitative values were similar for all three sets of cells. The average specific capacity for all cells was ~167 mAh/g (3.0 mAh/cm$^2$) with an ICL ~ 13%. These results are consistent with data obtained with half coin cells and confirm the feasibility of using ADP as drying method for standard size lithium-ion batteries.

Rate capability for both cathode and anode dried with ADP show equal performance compared to Navitas baseline. After formation some of the cells were charged at C/10 and then discharged at different currents (0.1-2.0C) to study their responses. Figure IV- 273 shows discharge capacity retention vs. C-rate for all three sets.

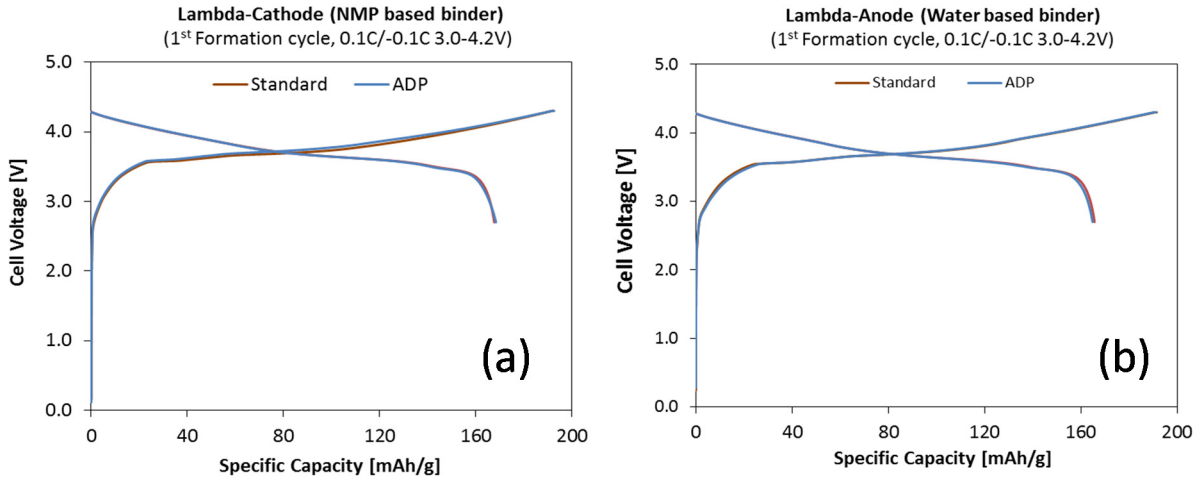


**Figure IV- 272: Formation voltage vs. specific capacity plots for (a) Lambda-cathode (with Navitas anode) and (b) Lambda-anode (with Navitas cathode) against Navitas' baseline. Cycles were run from 3.0 to 4.2V at C/10 current**

### Table IV- 39: Formation characteristics for pouch cells fabricated with Lambda anode and cathodes matched with Navitas electrodes

| Electrode | Drying Method | Loading (mAh/cm$^2$) | Reversible Capacity (mAh/g) | ICL (%) |
|---|---|---|---|---|
| Lambda-Cathode & Navitas-Anode | ADP | 3.0 | 168.3 | 13 |
| Navitas-Cathode & Lambda-Aq. Anode | ADP | 2.9 | 165.8 | 14 |
| Navitas Baseline | Standard | 3.0 | 166.7 | 13 |

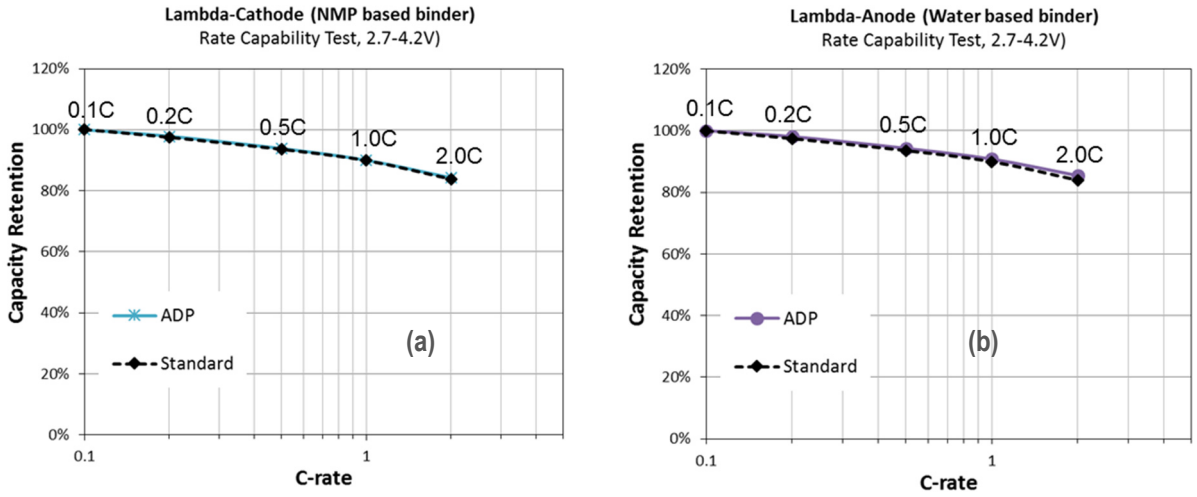


**Figure IV- 273: Rate capability results for (a) Lambda-cathode (with Navitas anode) and (b) Lambda-anode (with Navitas cathode) against Navitas baseline. All cell were charged at C/10 and then discharge at 0.1, 0.2, 0.5, 1.0 and 2.0C currents between 2.7 and 4.2 V**

### Cycle Life Testing

Cycle life data for single layer pouch (SLP) cell (3.0 mAh/cm$^2$, @ C/2,100% DoD) made with electrodes dried under static ADP is shown in Figure IV- 274. After 500 cycles SLPs show similar behavior regardless of the drying method employed.

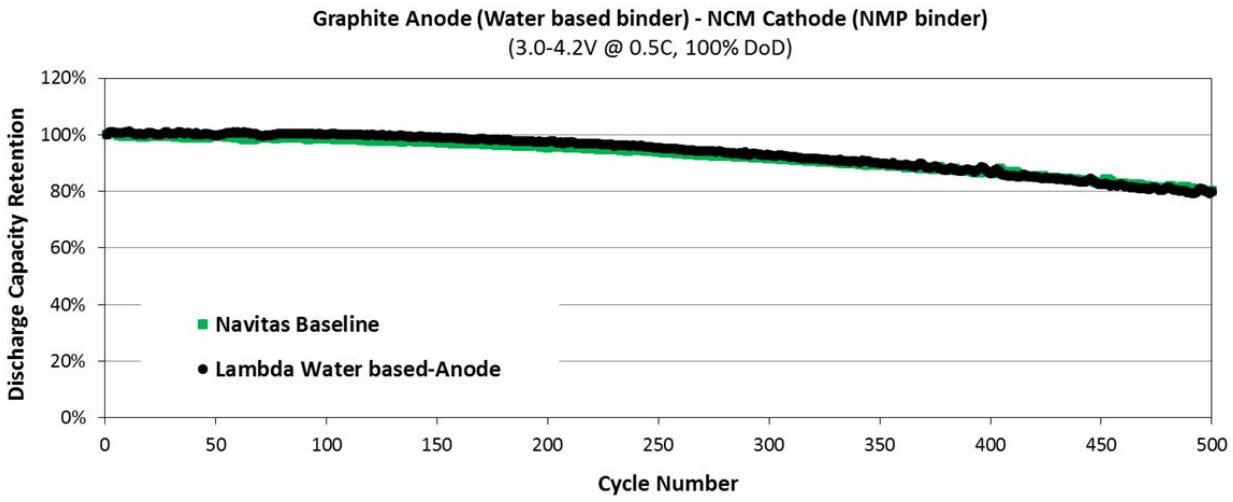


**Figure IV- 274: Cycle life testing for single layer pouch cells for Navitas cathode (NMP based binder) matched with ADP dried anode (water based binder) compared to Navitas baseline cell. The baseline cells were dried with conventional drying methods**

### Electrodes and cell characterization data from continuously casted ADP dried samples

For the Go/No-Go demonstration some aqueous anode slurry was prepared at Navitas and shipped overnight to Lambda Technologies, where the binder was freshly mixed into the slurry. The slurry was then continuously casted on copper foil and dried in the newly assembled ADP prototype. The analytic data on the continuous ADP drying is compared below to the static drying performed earlier.

### Adhesion Testing

Calendared electrodes were soaked in standard electrolyte for 2 h at 80°C then cooled to room temperature. Both samples show similar adhesion when applying the cross hatch technique. The score given was 3 for both (similar scores have been given to Navitas standard anodes). Figure IV- 275 shows digital imagines of the electrodes after wet adhesion, (a) continuous and (b) static ADP drying.

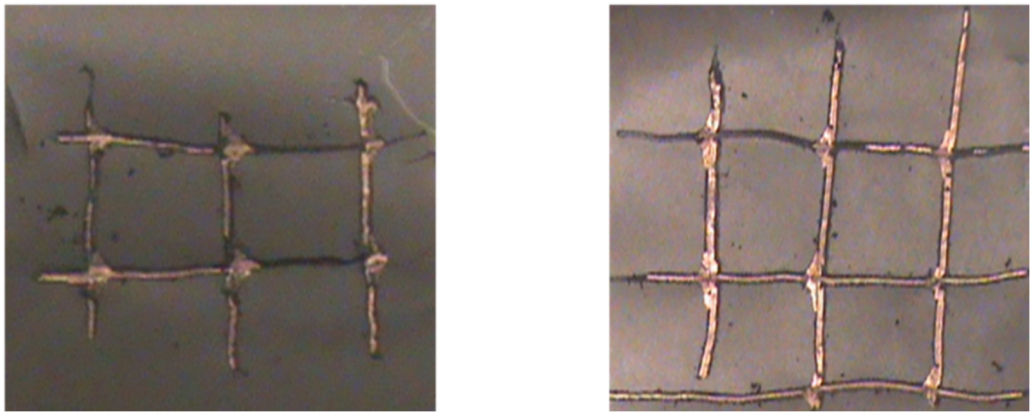

(a) (b)

**Figure IV- 275: Digital images showing result from wet adhesion test for aqueous anode dried using ADP under (a) continuous (0.5m/min) and (b) static drying**

### Solvent Content Analysis

Moisture analysis was performed on the as received samples to quantify the amount of solvent (water) left after the anode slurry dried. Initial solvent content (as received) was ~2000 ppm (target <5000 ppm) for both samples, dried under static and moving (0.5m/min) drying conditions as shown in Figure IV- 276 below. With further drying (i.e. vacuum oven) the moisture content can be reduced to < 800 ppm.

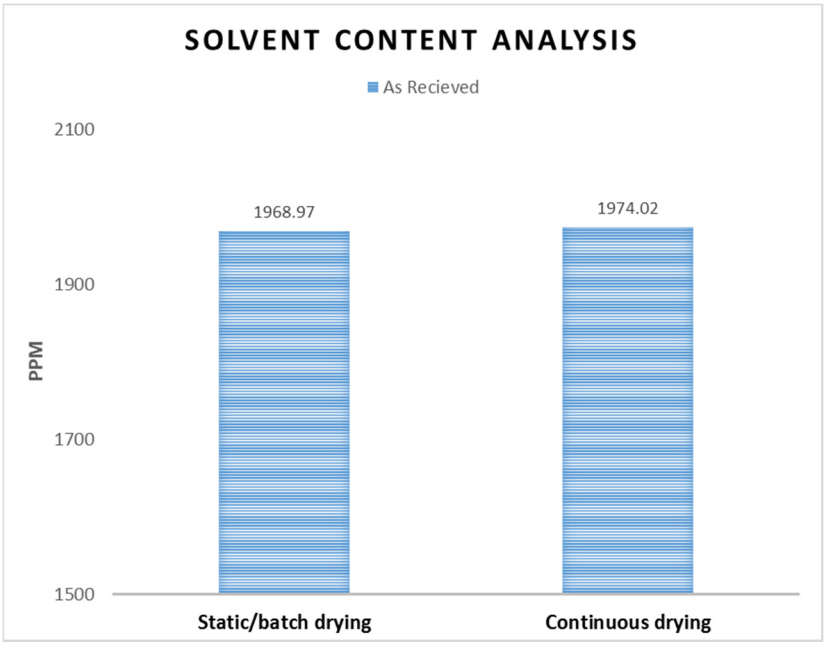


**Figure IV- 276: Moisture analysis shows the solvent content after static and continuous ADP drying. For both cases the values are lower than the target (< 5000 ppm)**

### Half Cell Testing: Anode

Similar to the experiments performed for static drying, half coin cells were used to characterize the electrochemical properties of the ADP continuous dried electrode. The anode formation half-cell testing data comparison is shown below in Figure IV- 277 (a) and Table IV- 40. Rate capability results are presented in Figure IV- 277 (b). Specific capacities and initial capacity loss (ICL) are similar for both sets of cells. In addition these values are comparable to the ones obtained for half-cell made with graphite electrodes fabricated using Navitas coating/drying pilot scale system.

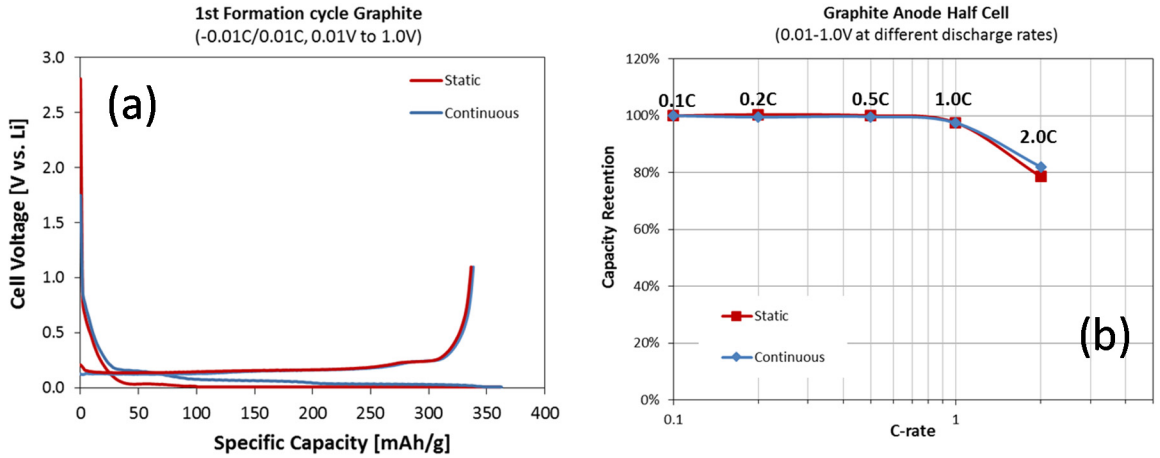


**Figure IV- 277: Half-cell electrochemical performance results for anode electrodes dried under static and continuous ADP (a) first formation cycle at C/20 0.01V to 1.0V and (b) rate capability lithiated at C/10 and delithiated at 0.1, 0.2, 0.5, 1.0 and 2.0C**

**Table IV- 40: Comparison of anode performance by static and continuous ADP drying**

| Electrode | ADP Drying Conditions | Loading | | Reversible Capacity (mAh/g) | ICL ( %) |
|---|---|---|---|---|---|
| | | (mg/cm$^2$) | (mAh/cm$^2$) | | |
| Anode Water | Static | 10.1 | 3.7 | 343.2 | 7 |
| | Continuous | 10.2 | 3.8 | 345.1 | 7 |

Figure IV- 274 above shows cycle life results for SLP with electrodes dried under static ADP. Since the continuous ADP drying results presented in Figure IV- 275, Figure IV- 276 and Figure IV- 277are equivalent to the static dried cells, it is expected that the continuous ADP dried electrodes will behave identically in cycle life experiments.

### Conclusions and Future Directions

Drying electrode slurries is a high cost operation for lithium-ion batteries. ADP (hot air plus VFM) can rapidly dry electrode slurries on metal substrates. It is expected that using ADP drying process will reduce the cost of lithium-ion manufacturing.

With the ADP system VFM penetrates into the slurry and targets the polar solvent molecules deep in the electrode and drives the solvent out. With the penetrating nature of microwaves more advantages are expected when drying thick electrodes. The hot air flow will then exhaust the solvent vapors out of the ADP chamber.

Early this year the ability of the ADP to efficiently dry anode (with water-based binder) and cathode (with NMP-binder) coatings in shorter periods of time under static conditions was demonstrated as compared to conventional methods. Standard analytic techniques were carried out at Navitas to test adhesion, solvent content and binder distribution of these films. Additionally half coin cell were fabricated to test electrochemical properties. Both, the material and electrochemical characterization have shown that the faster drying process using ADP did not change the overall properties of the dried electrodes. Additionally, single layer pouch cells were fabricated for long term cycling experiments. Life studies were carried out for 500 cycles at 1.0C (100% DoD) showing ~80% capacity retention for both standard and ADP dried electrodes.

For the Go/No-Go demonstration, the entire ADP prototype system was assembled and ran with a temporary web handling setup as a semi-automatic coating system. This setup allowed for the ADP to be tested under continuous coating conditions. At high loading (~10 mg/cm$^2$ ) the anode slurry was dried in the ADP in one minute with the foil moving at 0.5m/min. The dried electrodes were shipped to Navitas for further testing. Physical and electrochemical properties were characterized at Navitas showing similar results to the standard and to the static ADP-dried electrodes tested earlier.

The equivalent results demonstrate the feasibility of using the ADP system in a continuous manner. The ADP Prototype was then shipped to Navitas for integration into the Navitas prototype coating line. Lambda personnel visited Navitas to install the ADP Prototype and provide training.

Navitas will continue testing the ADP system to optimize drying conditions/parameters to effectively and efficiently dry electrodes. Navitas will qualify the ADP electrodes for EV battery relevant performance in small scale cells, such as half coin cells and single-layer pouch cells. Navitas will produce pilot scale ADP electrode coatings (>50m) to build large format Li ion cells (>2Ah) after the qualification. Ten prismatic pouch cells (>2Ah) will be assembled and tested for EV battery application in Navitas.

### FY 2015 Publications/Presentations/Patents

1. “Advanced Drying Process for Low Cost Manufacturing of Electrodes”, ES246_Ahmad_2015_p, US DOE Vehicle Technologies AMR, 2015.
2. “Apparatus and Method for Drying Battery Electrodes”, Ahmad et al, Provisional Application, September 2015.

# IV.F.3 Dramatically Improve the Safety Performance of Li Ion Battery Separators and Reduce the Manufacturing Cost using Ultraviolet Curing and High Precision Coating Technologies (Miltec UV International)

## Objectives

- To further develop and demonstrate the use of Ultraviolet (UV) curing technology to reduce the cost of manufacturing Lithium-ion battery ceramic coated separators by more than 50% while improving the porosity of the ceramic coating and retaining or improving the safety attributes.
- Previously identified UV curable binders and associated curing technology will be shown to reduce the time required to cure separator ceramic coatings from tens of minutes to less than one second. This can result in increases in process speeds and significantly reduced capital cost, operating cost, energy consumption.
- Investigate the use of patterns applied with high speed coating technology to improve the safety performance of ceramic coated separators as well as to reduce the cost of separators in a Lithium-ion battery.
- Investigate the feasibility of manufacturing thinner (6-10 µm) base separators.

### Project Details

**John Tabacchi (NETL Program Manager)**
DE-EE0006868 Recipient: Miltec UV International

**Gary Voelker, PD**
**Dr. John Arnold, PI**
146 Log Canoe Circle
Stevensville, MD 21666
Phone:410-604-2900; Fax: 410-604-2906
Email: gvoelker@miltec.com, jarnold@miltec.com

Subcontractors:
Argonne National Laboratory
Celgard LLC

Start Date: October 2014

Projected End Date: November 2016

## Technical Barriers

- The identification of specific UV curable binder chemistries that provide adequate adhesion, inertness, and other parameters that result in ceramic coatings that meet the porosity, shrinkage and other performance goals.
- Demonstration of high speed coating techniques on polyethylene (PE), polypropylene (PP), and trilayer base separators.
- Demonstration of thin base separators that retain acceptable strength and porosity.

## Technical Targets

The performance goals for a ceramic coated separator using UV curable binder are:

- 16 µm Trilayer, PP, and PE Base Separator Material
- 4 µm Aluminum Oxide coating (0.5-1.0 µm particle size) thickness
- <10% increase of Gurley # for ceramic coated over base uncoated separator
- Shrinkage MD < 5% at 1 hr, 150ºC
- Shrinkage TD < 3% at 1 hr, 150ºC
- 6-10 µm reduced thickness base separator

## Accomplishments

- Miltec UV continues to make significant progress using a laboratory scale flexographic printing unit modified to accommodate the coating and UV curing of ceramic coated separators with and without printed patterns at thicknesses of 2-6 microns.
- Ceramic-coated separators on a base trilayer, PP, and PE have been made with <10% increase in air permeability measured with a Gurley meter. The <10% increase in air permeability meets the overall

project goal. Recent test results on C210 trilayer, PP and PE base material has resulted in shrinkage <3% at 150C for 1 hour which also meets the project goal. .

- We also demonstrated the feasibility of cell shutdown with a ceramic coating on a single layer PP base separator.
- By treating membranes using an unconventional technology, wet process (solvent based) PE products were confirmed to have significant improved high temperature and battery cycling performance at <10µm separator thickness. The technology did not work well for PE and PP membranes made by a dry process.

## Introduction

The overall objective of this cost shared contract is to develop safer coatings and better processes for ceramic coated separators. It is the intent of this project that the development of this technology will lead to safer vehicle batteries and faster market incorporation and acceptance of hybrid and electric vehicles.

We are developing and demonstrating the use of Ultraviolet (UV) curing technology to reduce lithium-ion battery manufacturing costs. In this project, we apply and cure ceramic-coated separators with an environmentally clean UV process. The performance of these coatings must meet current industry standards and be ready to meet tomorrow's standards as well.

Cost reduction will largely come from simplification, line reduction, and improved throughput. Thin separator film is fragile. It is difficult to handle this material on a web. Separator film tends to kink, crinkle, shred and tear. Market and technical forces push this film to be thinner and more fragile every year—thickness reduction with a clean process even a subobjective of this project.

For a given speed, a UV process can exponentially reduce the length of the line. Reducing the length of the line, reduces web handling. This increases throughput, which will be critical to high speed and volume manufacturing needed as the automotive industry adopts more and more lithium-ion cells.

In addition to a UV process, we are developing this around a flexographic process. The flexographic process has many advantages 1) higher viscosity than gravure (therefore, less drying), 2) ability to print and change patterns at a fraction of the cost, 3) less downtime. Less downtime comes from the fact that a gravure cylinder cannot be removed while the line is running. Aluminum oxide is abrasive and will wear and clog a gravure plate as well as a flexo plate. The difference is the flexo plate can be removed while the press runs—using 2 flexo stations—cheaper than one gravure station. Therefore, if equipped with the correct accumulators the flexo press never needs to stop.

The ability to print patterns is another innovation of this project. By printing patterns we should be able to maximize ionic flow through the separator while still providing the protection of a ceramic layer and still reinforcing the separator against thermal shrinkage.

## Approach

This project employs an iterative process of technology evaluation, implementation, testing, and resulting optimization. Multiple samples of ceramic-coated separators are prepared using a combination of various UV curable binder chemistries and printing patterns. The coated separators are evaluated by Celgard, LLC and ANL and selected samples will be made into cells and tested for performance. In addition, multiple analytical tests will be conducted to determine characteristics such as: porosity, tear strength, thermal transfer, puncture strength, thermal shrinkage, and permeability. ANL conducts the electrochemical and physical tests on the cells as well as the analytical tests. Celgard supplies candidate separator materials, including thinner separators (<10 µm) and conduct tests on the coated samples provided by Miltec UV. At the end of this iterative development, printing patterns and optimum UV chemistries and base separator materials will be coated using commercial scale printers, and printed ceramic coated separators will be prepared for extensive evaluation by Celgard.

## Results

Miltec has achieved the following progress:

**Achieved both the shrinkage goal of <5% MD at 150C and the goal of not increasing the Gurley number >10% above the base with a ceramic coating**

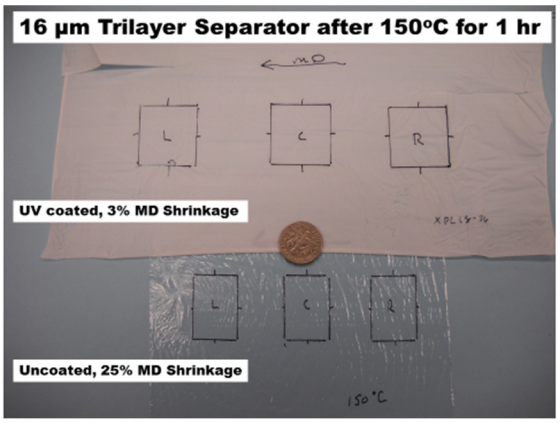


Figure IV- 278: 4 µm thick UV ceramic Coating reduced shrinkage

As shown in Figure IV- 278, the UV ceramic coating on a trilayer base separator controls the shrinkage to 3% MD (and 0.9% TD). In addition the high pressure Gurley increased from 19 sec to 21 sec, which meets the Gurley specification as well.

As shown in Figure IV- 279, the UV ceramic coating on a PP base separator controls the shrinkage to 3% MD (and 0.9% TD). In addition the high pressure Gurley increased from 19 sec to 21 sec, which meets the Gurley specification as well.

As shown in Figure IV- 280, the UV ceramic coating on a PE base separator controls the shrinkage to 3% MD (and 0.9% TD). In addition the high pressure Gurley increased from 19 sec to 21 sec, which meets the Gurley specification as well.

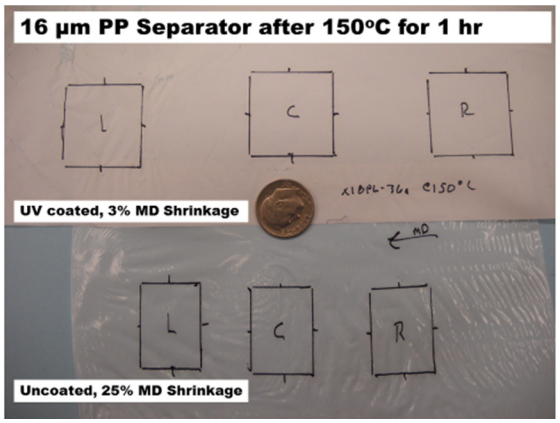


Figure IV- 279: 4 µm thick UV ceramic Coating reduced shrinkage

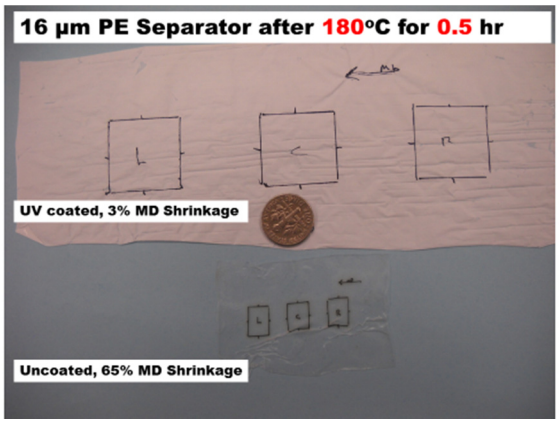


Figure IV- 280: 4 µm thick UV ceramic Coating reduced shrinkage

**Made significant progress in reducing Gurley numbers for ceramic coated separators using UV curable binder**

Table IV- 41 show the progress on reducing the Gurley values for the single side UV ceramic coating. The first work was all performed on the trilayer separator and the values were high 60-300. During the year we significantly reduced the Gurley's as shown for the continuous coatings (non- patterned) shown in Table IV- 41.

**Table IV- 41: High Pressure Gurley Values Have Dropped**

| | Uncoated | First UV Coating | Current UV Coating |
|---|---|---|---|
| **16 µm Trilayer** | 19 | 60-300 | 21 |
| **16 µm PP** | 12 | 21 | 17-21 |
| **9 µm PE** | 5 | 23 | 15-18 |
| **16 µm PE** | 12 | 27 | 18-21 |

One of the concerns with ceramic coated seperators is their ability to handle high voltage. While this is not an immediate concern for vehicles, electronic devices push the limits of the technology. Eventually these improvements will find their way into vehicle manufacturing as well. UV coatings get their chemical resistance through crosslinking. Solvent coatings get their resistance by using higher molecular weight resins. In most applications, the UV coatings have superior chemical and oxidative resistance. We tested NMC half cells and higher and higher voltages with

ceramic coatings made with UV and acyrlic coatings. The results show both had similar resistance in capacity retention. (See Figure IV- 281.) At higher voltages the NMC cathodes were falling apart.

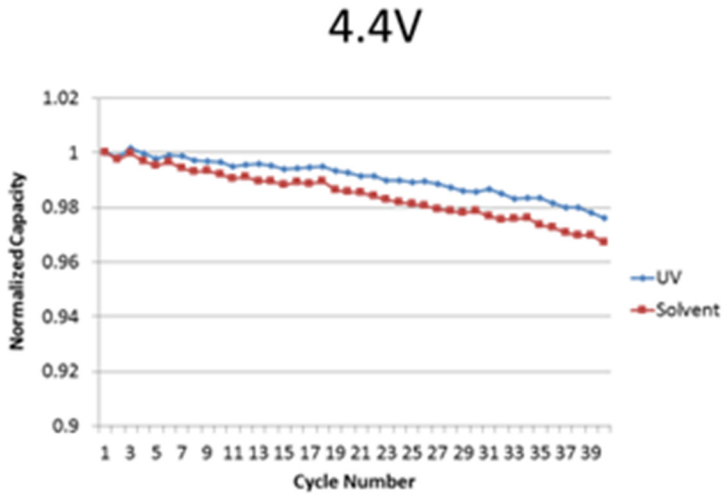


Figure IV- 281: Results for NMC half cells and higher voltages with ceramic coatings made with UV and acyrlic coatings

**Demonstrated the ability of ceramic coated separators using UV curable binder to operate at higher voltages up to 4.8V and demonstrated a shutdown capability with a single layer PP separator.**

Since the NMC cathodes were showing unstable behavior at 4.4 V, ANL tested UV ceramic coated trilayer separators in a more stable cell. This was a LiMN1.5Ni0.5O4-LTO cell. As shown the capacity of this 4.8 V cell was very stable over 50 cycles. No deleterious effects were observed. This suggests UV ceramic coated separators can be used in high voltage-high density batteries of the future. (See Figure IV- 282, Table IV- 42.)

In another development to create safer batteries, we developed a UV ceramic coating that offers a shut down feature similar to the thermal shut down feature of a trilayer seperator. In this case we apply the coating on a simple PE or PP seperator. With this UV coating, the pores in the PE or PP will close below the meltpoint of the seperator film to shut down ion flow and prevent thermal runnaway. In addition, the UV coating offers additional features including: reduced shrinkage with temperature, ceramic insulation between the anode and cathode, an ion path with increased tortuosity over the uncoated seperator.

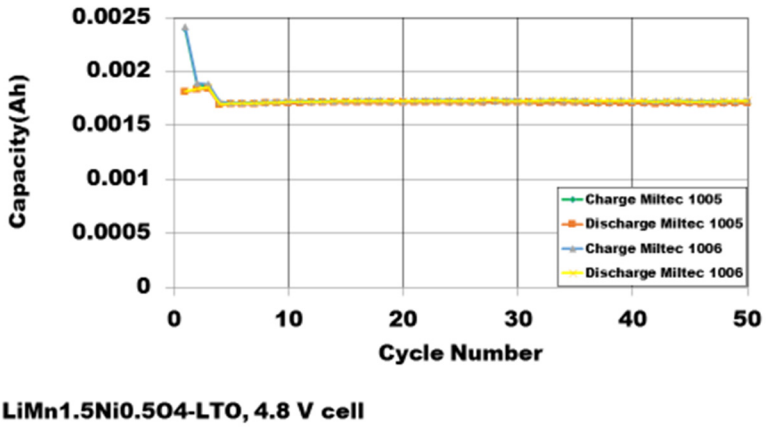


Figure IV- 282: UV Ceramic Coatings Cycling In 4.8 V Cell

Table IV- 42: UV ceramic coating details

| Properties | UV Coated PP Separator | Uncoated PP Separator |
|---|---|---|
| Gurley at 25°C | 400 | 325 |
| Gurley after 100°C | 550 | 300 |
| Gurley after 150°C | ∞ | 825 |
| Shrinkage @ 100°C | <5% | <5% |
| Shrinkage @ 150°C | 20% | 25% |
| Thickness | 3 µm +16 µm | 16 µm |

## Conclusions and Future Directions

The Miltec UV team has made very good progress in demonstrating the use of UV curing and printing technology to apply a ceramic coating on PE, PP and trilayer (PP/PE/PP) separator stocks and for these coatings achieve performance goals of shrinkage, adherence, porosity, and safety performance. During the second and final year of this effort we will proceed to demonstrate the performance as well as cost saving attributes of this technology on a commercial scale printing system. In addition, new types of resin with higher mechanical strength and new treatment techniques will be considered to make new thinner (<10μm) dry base separator.

## FY 2015 Publications/Presentations

1. "Improve the Safety Performance of Li-ion Battery Separators and Reduce the Manufacturing Cost using Ultraviolet Curing and High Precision Coating Technologies", ES243_Arnold_2015, US DOE Vehicle Technologies AMR, 2015.

# IV.F.4 A Commercially Scalable Process for Silicon Anode Prelithiation (Amprius)

## Objectives

- A manufacturing process for prelithiation – the insertion of extra lithium before cell assembly – is a prerequisite for the commercialization of silicon anodes that enable cost competitive, high energy, and long life lithium-ion PEV batteries. Amprius proposes to develop and demonstrate a cost-effective and commercially scalable manufacturing process for silicon anode prelithiation.

### Project Details

**Bruce Mixer (NETL Program Manager)**
DE- EE0006856 Recipient: Amprius, Inc.

**Ionel Stefan (Amprius, Inc. – PI)**
225 Humbolt Court
Sunnyvale, CA 94089
Phone: 800-425-8803; Fax: 866-685-7420
Email: ionel@amprius.com

Start Date: October 2014

Projected End Date: March 2016

## Technical Barriers

- Numerous prelithiation methods enable the insertion of lithium into silicon, but are not commercially scalable because of cost and process integration challenges with existing battery manufacturing workflows. Amprius' project will be successful when the company is able develop a prelithiation method that is cost-effective and has minimal impact on existing battery assembly processes.

  Barriers addressed:

- **Cost:** Impact of prelithiation on the cost of production silicon anodes.
- **Process Integration:** Impact on cell build processes, including changes to industrial setups for battery manufacturing.

## Technical Targets

- **Cost:** Develop a prelithiation process that will add no more than 10% to the cost of producing silicon nanowires.
- **Process Integration:** Develop a prelithiation method that has minimal impact on cell build processes and requires only limited changes to industrial setup (dry zones, automatic tools, etc.).

## Accomplishments

- Analyzed the cost and scalability of numerous prelithiation methods (six electrochemical methods, five chemical methods and three physical methods).
- Identified five prelithiation methods (three electrochemical, one chemical and one physical) with limited impact on cost and cell build processes. Found that the most of the methods evaluated are not scalable because of their high cost and/or significant impact on existing cell production processes.
- Evaluated the technical feasibility of electrochemical (involving "in cell" and roll-to roll bath type prelithiation), chemical (involving organometallic compounds) and physical (involving the decomposition of lithium salts) methods with limited impact on cost and cell build processes.
- Selected one electrochemical (involving "in cell" prelithiation) for further evaluation. Found that the scalable electrochemical (involving roll-to roll bath type prelithiation), chemical (involving organometallic compounds) and physical (involving the decomposition of lithium salts) methods either require a dry environment for the entire assembly process and raise safety issues in handling or irreparably damage the integrity of Amprius' silicon nanowire anodes.
- Tested the impact of an electrochemical method on cell capacity and cycle life.

## Introduction

Silicon offers nearly 10 times the theoretical energy of graphite. But silicon – particularly in the nano-dimensions developed by Amprius and others – has higher first cycle loss than does graphite, limiting or negating silicon's energy advantage and accentuating silicon's cycle life challenge. Silicon therefore requires significantly more lithium than does graphite for three reasons.

First, silicon consumes a higher percentage of lithium during solid-electrolyte interphase (SEI) formation (10-25%) than graphite (5%). Second, silicon traps a higher percentage of lithium during discharge (5-10%) than graphite (1-2%); the high anode voltage necessary to fully extract lithium from silicon is not practicable (because it would result in an impractically low cell voltage cutoff). Third, nanostructures amplify the material's challenges; nanostructured silicon has more surface area than micron-sized graphite, further increasing silicon's need for lithium. (See Figure IV- 283.)

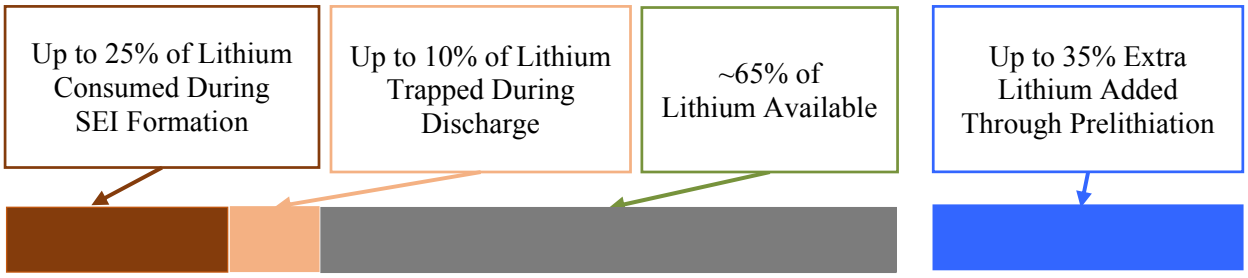


**Figure IV- 283: Silicon anodes consume and trap significant amoutns of lithium, reducing first cycle efficiency and cell-level energy. Current lab-scale prelithiation methods add extra lithium and address first cycle loss – but are not scalable**

## Approach

**Innovative Approach:** Numerous prelithiation methods enable the insertion of lithium into silicon, but are not commercially scalable because of cost and process integration challenges with existing battery manufacturing workflows. Novel prelithiation protocols, tools, and equipment must therefore be developed and integrated into battery assembly processes before silicon anodes can be commercialized. Amprius tackled prelithiation's challenges head-on by evaluating cost and manufacturability as *a priori* concerns. For example, before testing specific materials (e.g. lithium salts that are less expensive than Li metals), Amprius initially researched their price and evaluated their impact on cell assembly processes.

Amprius then evaluated the technical and commercial feasibility of several prelithiation processes, including:

1. Electrochemical insertion of lithium from liquid electrolytes,
2. Physical lithiation by direct contact with lithium metal or other Li-containing materials, and
3. Chemical lithiation with lithium containing reactants.

Amprius tested candidate processes on silicon nanowire anodes, which are particularly well-suited for research because (a) they are made of pure silicon and (b) do not use any binders or conductive additives. As a result, nanowires enable Amprius to directly study the effects of new prelithiation regimes on silicon anodes, without needing to isolate and/or control for secondary reactions (during formation) with the binders, conductive carbons, and other additives that are common in silicon-carbon composite anodes.

## Results

We have achieved the following progress:

### Analyzed the cost and scalability of numerous prelithiation methods

Amprius considered the development status, advantages and disadvantages of numerous prelithiation methods. Amprius evaluated the methods by considering their cost, operational complexity, and impact on subsequent cell build process steps. Table IV- 43 details the results of Amprius' analysis on 10 of the methods evaluated.

**Table IV- 43: Silicon anodes consume and trap significant amounts of lithium, reducing first cycle efficiency and cell-level energy. Current lab-scale prelithiation methods add extra lithium and address first cycle loss – but are no scalable**

| Method | Status | Pros | Cons |
|---|---|---|---|
| Bath type R2R with Li-foil or inert electrodes | Some patents in the 90's | • similar to plating baths<br>• inexpensive machines and materials<br>• in advanced development stage | • relatively slow (hours)<br>• requires rinsing<br>• roll has to be sealed or protected by a layer<br>• dry air exposure limited to hour(s) |
| Bath type jelly roll with Li-foil or inert electrodes | Not studied | • allows assembly process in normal conditions up to pouch installation | • very slow (tens of hours)<br>• Possible non-uniform prelithiation and dendrite formation |
| In cell prelithiation with auxiliary electrode | Patents and articles exist | • allows assembly process in normal conditions up to pouch sealing<br>• Auxiliary electrode can be removed at degassing step | • adds an assembly process step that requires lithium handling and is not automated<br>• slow and potentially non-uniform |
| In cell prelithiation with dissolved salt lithium source | Not studied | • allows assembly process in normal conditions up to pouch sealing<br>• does not change the process flow<br>• can be done in electrolyte filling type machine, already dry/inert | • relatively slow (hours)<br>• high concentration, high lithium content salt (>10%) required<br>• requires electroactive anions but stable toward cathode chemistry |
| Excess lithium phase (ex. Li2O) in cathode | Published articles in the 90's | • does not change the process flow<br>• relatively inexpensive | • can affect the cathode structure stability and cycle life<br>• not available mixed commercially<br>• dilutes the cathode energy density |
| Direct contact with lithium foil, ex-situ | Wet and dried contact studied at Amprius | • likely possible to be scaled up to R2R<br>• relatively fast (<1h) | • Highly sensitive to anode surface shape and chemistry<br>• Requires inert environment and protection after prelithiation |
| Direct contact with lithium foil, in-situ | Not studied | • Possible with protected foil? | • Requires very thin Li foils, expensive, difficult to handle<br>• High risk of incomplete use of Li |
| Lithium powders (SLMP) | Commercial | • Available, used in research by many groups for composites | • Expensive<br>• Requires calendaring |
| Unstable Li salt coating | Not studied | • No protection needed<br>• No change in process flow | • May not find a compatible salt |
| Evaporation or sputtering | Commercial tools available | • Possible to be integrated with the process flow in anode fabrication | • Very high and difficult maintenance<br>• Inert (dry not enough) atmosphere required<br>• Slow and expensive<br>• Requires protective film or dry room for cell assembly |

**Identified five prelithiation methods with limited impact on cost and cell build processes**

Amprius made a best effort to source quotes from high-volume manufacturers of materials, machines or subassembly parts. These quotes enabled Amprius to consider which prelithiation methods are likely to have the least disruptive operational impact and/or would be most easy to integrate into existing cell assembly processes. Amprius' analysis suggests that (1) methods that use (a) lithium salts or (b) lithium metal and/or are applied (2) in cell are most likely to be cost-effective.

Based on cost and process impact, Amprius selected five methods (three electrochemical, one chemical and one physical) for feasibility evaluation:

1. Electrochemical – In cell electrochemical lithium plating from concentrated lithium salt solutions; this method requires only a small change to the existing electrolyte injection step
2. Electrochemical – Roll-to roll bath type prelithiation with downstream dry room or dry air enclosure of the machines; this method can use industrial foil plating setups.
3. Chemical – Roll-to roll bath type prelithiation by exposure to lithiation reagents; relatively simple setup in protected/inert environment.
4. Physical – Lithium salt application and in cell decomposition; this method requires no changes to downstream process flow

**Evaluated the technical feasibility of the five methods with limited cost and proces impact**

Amprius found that the chemical method (involving the use of lithium organo-metallic compounds) and the physical method (involving the decomposition of lithium salt) irreparably damaged the integrity of Amprius' silicon nanowire anodes and/or negatively affected the cycle life of the cells. The roll-to-roll method produced good cycling and capacity results, but required a dry environment for the entire assembly process and raised safety issues in handling and electrode processing.

Amprius determined that the electrochemical method (involving "in cell" prelithiation) successfully prelithiated Amprius' anodes in single and multi-layer configurations that allow for a large excess of electrolyte. In formed pouch cups with limited electrolyte, the method had limited charge capacity improvement. Amprius therefore focused on increasing the prelithiation charge by increasing the amount of salt available.

**Tested the impact of two electrochemical methods on cell capacity and cycle life**

Amprius tested the "in cell" prelithiation method in (1) single layer cells, (2) jelly roll wound cells and (3) stacked multilayer cells in formed pouch cups. The (1) single layer cells and the (2) wound cells were housed in oversized pouch bags which allowed for high electrolyte volume relative to anode surface area. (The prelithiation reaction proceeds at higher voltages during the cell charging process, before lithium is extracted from the cathode. This behavior is not a pre-requisite for the method, which can also proceed in parallel with cell charging as well). See Figure IV- 284 for the comparative charge and discharge capacities of "in cell" prelithiated cells and cells that did not undergo any prelithiation. The prelithiation electrolyte formulations increased cell capacity by about 3%.

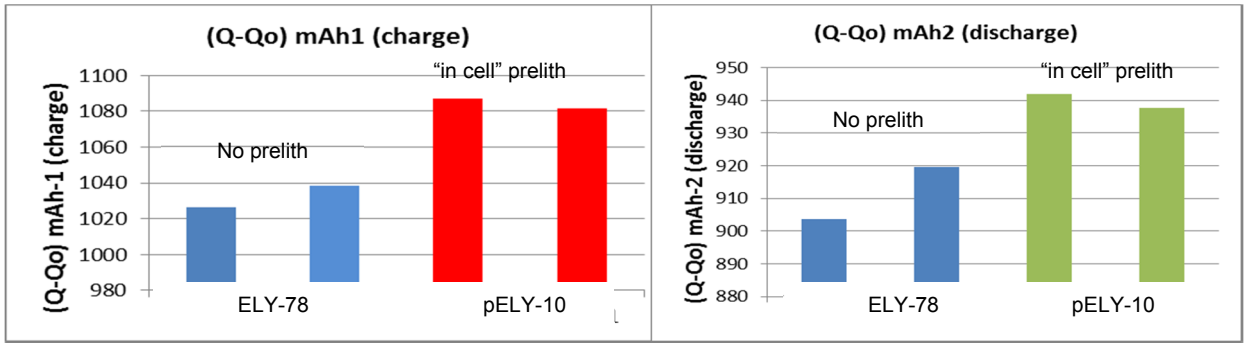


**Figure IV- 284: Prelithiation formulations increase capacity by about 3%**

However, when "in cell" prelithiation is applied to stacked multilayer cells in formed pouch cups, the available electrolyte volume is limited (by the pouch cups). As a result, the "in cell" prelithiated cells in Amprius' test did not reach the cell capacity achieved by similar cells assembled with anodes prelithiated by an "ex situ" electrochemical method using lithium foil. (See Figure IV- 285.)

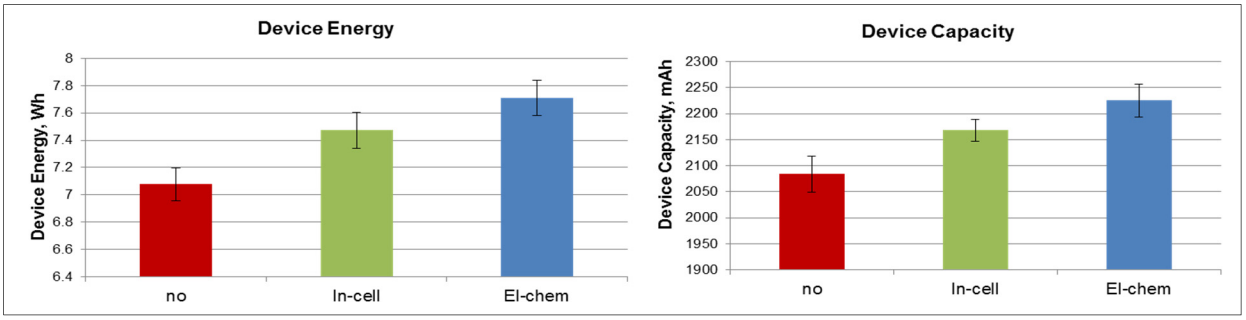


**Figure IV- 285: "In cell" prelithiation increased cell capacity, but by less than "ex situ" prelithiation increased cell capacity**

"In cell" prelithiation did not, however, appear to reduce cell cycle life. The cycle life of cells assembled with similar components but different prelithiation methods – no prelithiation, "in cell" prelithiation and electrochemical prelithiation in fixtures – seems to be relatively similar.

Importantly, Amprius concluded that although the "in cell" prelithiation method is feasible if only limited prelithiation is required, it is not applicable to all cases – because of its high electrolyte volume requirements (which are not possible in formed pouch cups) – for the higher amounts of prelithiation that silicon nanowire anodes require.

To address the electrolyte volume limitation, Amprius is evaluating options for increasing the amount of lithium salt available. Experiments are ongoing at the time of this Annual Progress Report.

## Conclusions and Future Directions

Amprius will continue to explore the technical feasibility of "in cell" and other prelithiation methods. After identifying a method with (1) limited cost and process integration impacts and (2) no adverse consequences on cycle life or capacity (vis-à-vis Amprius' existing lab-scale prelithiation process), Amprius will select one method for further evaluation and ultimately pilot scale up. Amprius will then design and test a pilot installation. Finally, Amprius will develop a commercialization plan for the prelithiation process and deliver 10 cells (prelithiated using the process selected) to DOE for testing.

## FY 2015 Publications/Presentations

1. "A Commercially Scalable Process for Silicon Anode Prelithiation", ES250_Stefan_2015, US DOE Vehicle Technologies AMR, 2015.

# IV.F.5 A Disruptive Concept for a Whole Family of New Battery Systems (Parthian Energy)

## Objectives

- We propose to develop a new platform geometry for batteries to enable high capacity electrode materials, such as silicon with a target cycle-life of >1000, and an eventual goal of achieving a cell level energy of 450 Wh/kg and 1000 Wh/L at the end of the program. Conventional parallel plate platform has not allowed high capacity electrodes. Our novel geometry, called Scell, allows the inclusion of lithium metal depot inside the cell for pre-lithiation and Li-ion loss compensations. In addition, our novel cell geometry significantly reduces the amount of inactive materials, both at cell and system levels. Such a platform could be used to create a battery for an EV capable of driving 400 miles on a single charge and showing a path to achieving a system level cost target of <200 $/kWh.

### Project Details

**Bruce Mixer (NETL Project Manager)**
DE-EE0006851 Recipient: Parthian Energy, LLC

**Farshid Roumi (Principal Investigator)**
1200 E. California Blvd. MC 131-24
Pasadena, CA 91125
Phone: 1-626-755-7776
Email: froumi@parthiannrg.com

Start Date: January 2015

Projected End Date: January 2017

## Technical Barriers

- In order for EVs to achieve mass adoption and make a significant dent in U.S and global $CO_2$ production, the key problems of driving range per charge & cost per kWh must be addressed.

  Barriers addressed:
- Performance: Low Wh/kg & Wh/L.
- Life: Poor deep discharge cycles.
- Cost: High $/kWh.

## Technical Targets

- Developing scalable manufacturing methods for the new cell-pack geometry.
- Cell Targets: 450 Wh/kg, 1000 Wh/L, >1000 cycles at end of the project.

## Accomplishments

- Identified and developing three new fabricating methods to make the anode.
- Identified and developing two new fabricating methods to make the cathode.
- Identified and developing two new fabricating methods to make the separator/conformal solid electrolyte.
- Identified and developing three novel fabricating methods for the Sell.
- Identified and developing a novel method to assemble, package and test the Scells 20x faster than our original method, compatible with and as fast as conventional coin cell making-testing, and also compatible with commercial 18650 and pouch cell making.

### Introduction

This work introduces a novel concept of chemistry-agnostic, scalable geometry for electrochemical cells, including batteries and flow batteries. The novel architectural design may be the natural design for high energy electrode materials in mid-large scale energy storage systems, such as in transportation applications. The outcome can be an efficient multifunctional system for high energy electrochemical cells that may overcome the challenges with high energy lithium-ion battery materials, such as air cathode, and silicon anode. Such high

performance and low cost systems are required to enable electric vehicles to compete with conventional combustion engine vehicles. (See Figure IV- 286, Figure IV- 287.)

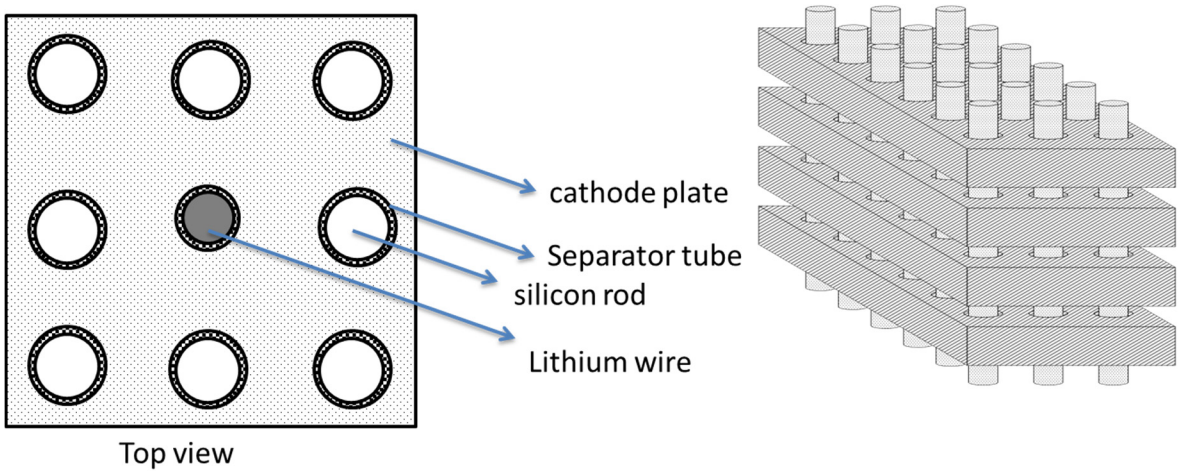


**Figure IV- 286: Scell concept: The perpendicular anode-cathode structure of S-cell with silicon anode (slow discharge, fast charging) and lithium anode (fast discharge, slow charging). The geometry enables in-situ lithiation of non-lithiated cathode and anode materials. Each of the two anode materials has a separate electrical tab. The cathode is perforated plates of commercial cathode electrodes. Note that each of the rods can consist a bundle of micro or nano sized features, such as nano or micro rods**

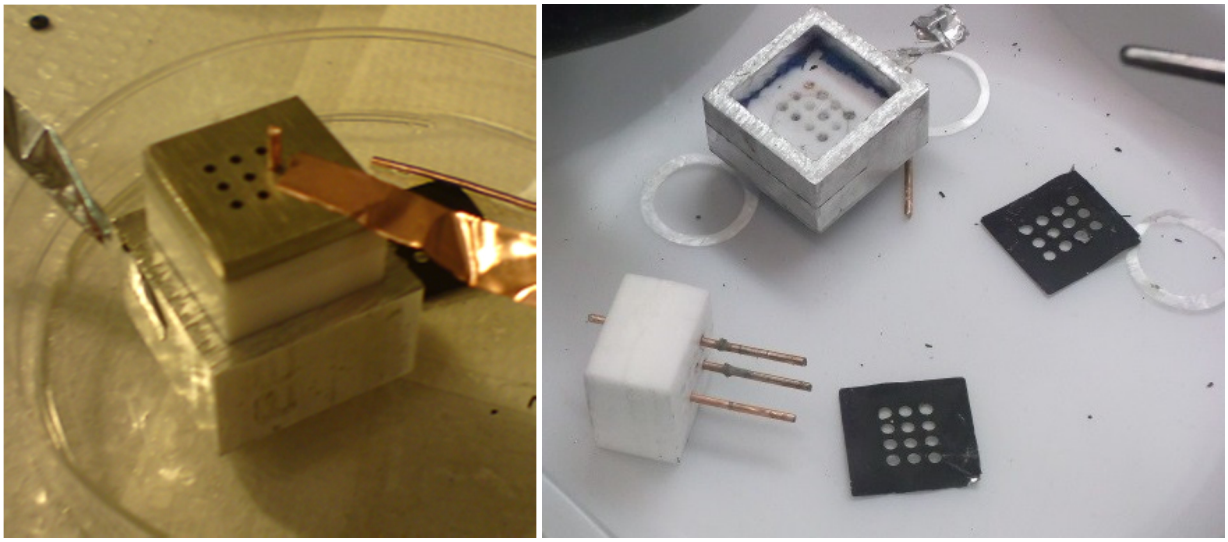

**Figure IV- 287: Early prototypes of Scell, before the start of the project. Perforated cathode plates (commercial LiCoO2 films, two-sides) and copper anode rods (lithium deposited on copper rods from the cathode)**

## Approach

**Innovative Approach:** The objectives outlined above will be accomplished by designing a new scalable cell geometry, Scell™, which overcomes the limitations of the conventional parallel-plates geometry, shown in Figure IV- 288. The Scell™ geometry, for the first time, allows using more that only two electrodes in the cell, and thus makes it possible to fabricate cells with tunable properties. As an example, it is now possible to include lithium depot in the cell to compensate for lithium-ion loss and for pre-lithiation of electrodes. Our focus is thus on the fabrication methods and we will use conventional active materials, such as carbon, silicon, $LiCoO_2$, NMC and $LiFePO_4$.

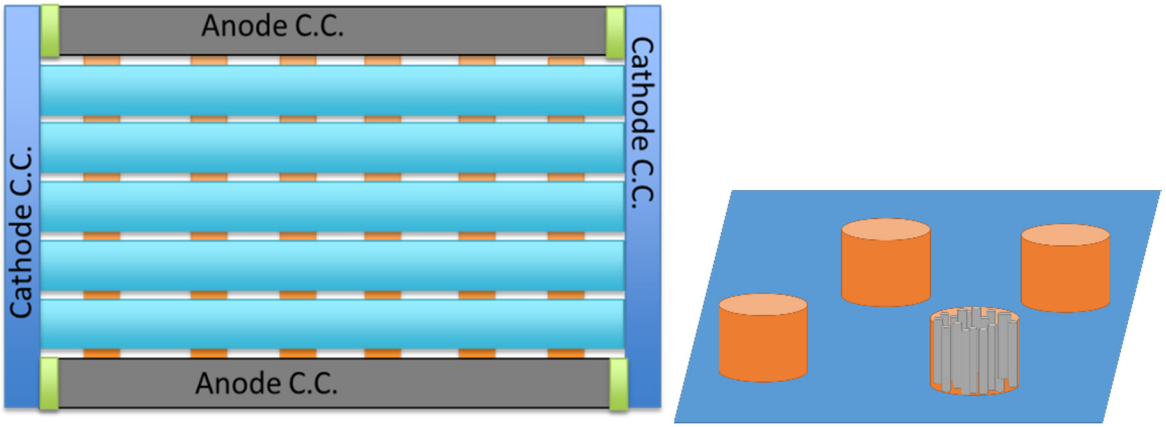


**Figure IV- 288: Proposed Scell may deliver 125 Wh (10.2, 10.2, 1.2 cm) (300 gr). 100 units of this S-cell may power a mid-size PEV to run for 50 miles (Total system: 20 L, 40 kg). Assumption: NCA, 640 mAh/cm3 and Silicon-Carbon 1000 mAh/cm3. Each of the rods consists of a bundle of micro or nano rods with silicon particles on them (deposition methods) or between them (slurry injecting methods). This micro-nano structure accommodates the large shape changes of silicon lithiation-delithiation; it also results in short charges paths for higher rate capabilities. In this project we have focused on rods with 0.5 mm diameter and 0.5 mm height. The distance between the rods depends on the ratio of the anode to cathode capacity and thus on the voltage-capacity range of silicon-carbon anode**

The major technology innovations to be undertaken to accomplish the objectives of this effort:

1. Develop two distinct methods for fabrication of Scell technology: Cathode starting and Anode starting. In cathode starting fabrication method, perforated cathode plates and silicon-carbon anode slurry are used. In anode starting fabrication method, grown silicon-carbon pillars and cathode slurry are used.
2. Develop two distinct methods for fabrication of the conformal separator/solid electrolyte. One around the anode rods and one around the cathode holes.
3. Achieve anode performance of 1000 mAh/g in the "rod" format, for both fabrication methods.
4. Achieve increased endurance of cycle-life to >1000, equivalent to 0.9998 average columbic efficiency.
5. Achieve cell energy density of 450 Wh/kg and volumetric density of 1000 Wh/L, at least for the Anode starting fabrication method.
6. Achieve cost reduction resulting in <$100/kWh (cell level), at least for the Cathode starting fabrication method. Currently we expect this cost to be comparable to conventional cells, ~$200/kWh. We expect that the increase in the cell efficiency drops the cost to half, by the end of the project.

## Results

### Feasibility of the Scell geometry

We have been continuously working on developing scalable fabrication methods. The following list summarizes the various anode types and architectures that were investigated in this report. The slurry composition for the In-house anodes consisted of 75% Si, 15% PVDF binder, and 10% carbon black with NMP as the solvent. (See Figure IV- 289, Figure IV- 290.)

- *Commercial Si30 SC*: Active material consisted of Si 95%. The capacity of anode is ~1200mAh/g. Coating Thickness is 20 microns.
- *In-house T4-Micro*: In house rod type coated with micro-silicon slurry.
- *In-house Thick Rod-Micro*: In house single thick copper wire coated with micro-silicon slurry
- *In-house Coin Cell-Micro*: In house 2D coating with slurry made out of micro-silicon slurry. Coating Thickness is 15 microns.

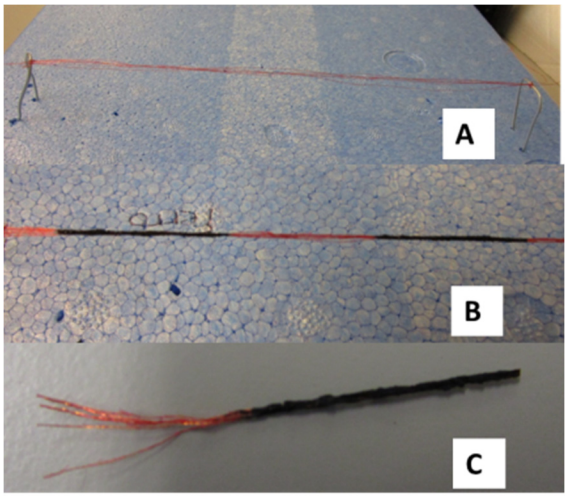


Figure IV- 289: Fabrication process for Si rod T4. A: Stretched Cu wire substrate. B: Stretched Cu wire substrate coated with some sections coated with Si slurry. C: Final cut Si T-4 rod. Six strands of thin Cu wire were stretched on a fixture and coated with Si slurry in 2.5 cm long sections. The strands of Cu wire were allowed to dry overnight. When dried, the Cu strands were cut to appropriate length

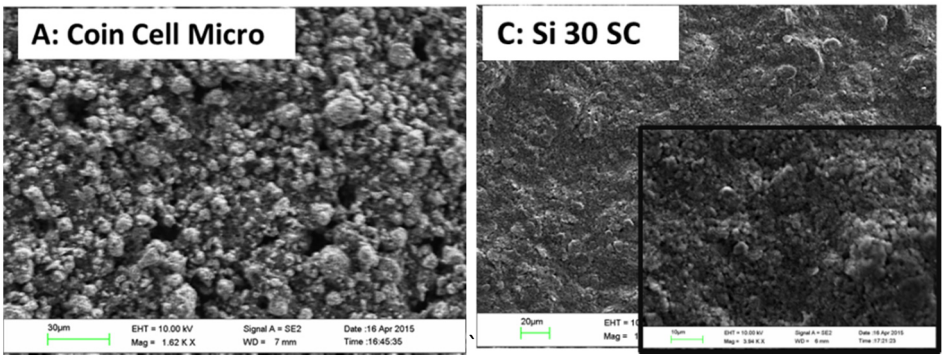


Figure IV- 290: SEM image of two types of silicon powder tested

**Electrochemical measurements**

The electrochemical behavior of the micro-silicon and commercial silicon anodes were examined using CR2032 coin type cells for 2D anodes, and costume-made vial cells for Scell (rod) anodes. All the electrochemical measurements were carried out in half-cells with Li acting as the counter electrode. Electrolyte was a solution of 1 M $LiPF_6$ in fluoroethylene carbonate and dimethyl carbonate (FEC:DMC = 1:4, v/v). The cells cycling performance were measured by galvanostatic discharge-charge method in the voltage range of 1.5V to 0.05V, at 30 mA/g_si on an Arbin battery testing system. Following the constant current lithiation (discharge) step, the anodes were further lithiated at constant voltage (0.05 V) with current of 15 mA/g_si. Repetitive cyclic voltammetry was performed using Bio-Logic potentiostat (SP-150). Potential range for the first cycle was open circuit voltage (OCV) to 0.05 V, and 2 V to 0.05 V for the following cycles at a scan rate of 1 $mVs^{-1}$. The recorded electrical current values for the cyclic voltammetry were normalized for the mass of active material in the anode.

Electrochemical impedance spectroscopy measurements were carried out over a frequency range from 100 kHz to 100 mHz with an AC signal of 5 mV in amplitude as the perturbation. Impedance values in the Nyquist plots were normalized for the anode approximate surface area (full cylinder). The Nyquist plots were fitted to an appropriate equivalent circuit model using Zview software, and the circuit element values were obtained. (See Figure IV- 291, Figure IV- 292.)

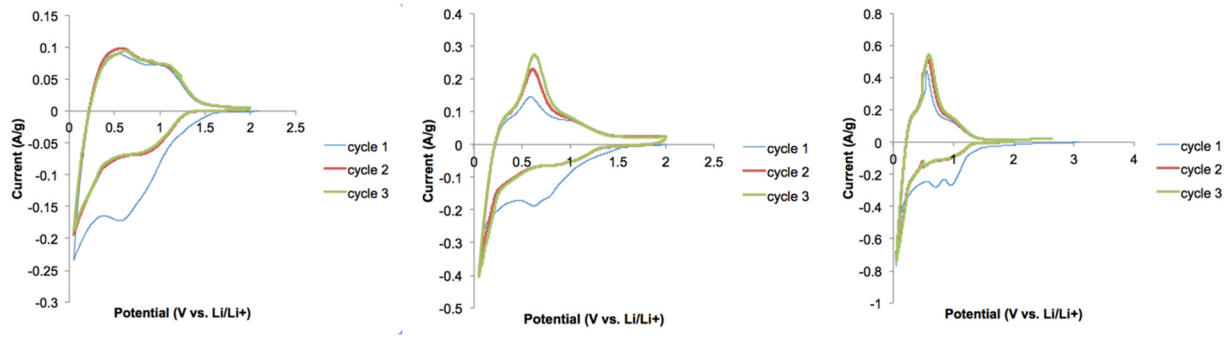


**Figure IV- 291: Left: T4-micro-silicon rod, center: Micro-silicon anode in coin cell structure. Right: Thick Rod-Micro-silicon anode**

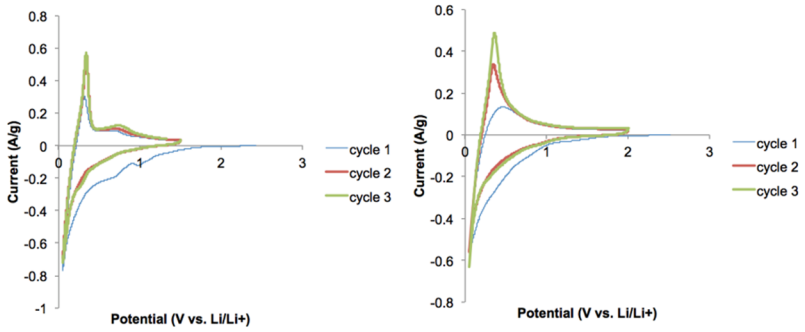


**Figure IV- 292: Left: Si30-SC-rod. Right: Si30-SC-coin cell**

In order to further investigate the anodes performances, electrochemical impedance spectroscopy (EIS) measurements were conducted in both Scell and coin cell architectures. The DC potential for EIS measurements was OCV, and the experiments were carried after three consecutive cyclic voltammetry were recorded on each anode. Each impedance measurement was carried out three times to confirm the stability of the cells. The EIS curves were fitted by an equivalent circuit, below, where $R_{el}$ is the bulk resistance of the cell, which was attributed to the electric conductivity of electrolyte, separator, electrodes and connections. $R_{int}$ and $C_{int}$ is the resistance and capacitance of interphase electronic path between the active material and the current collector, which corresponded to the first semicircle at high frequencies, J. Guo et al. / Electrochimica Acta 56 (2011) 3981–3987. $R_{ct}$ and $C_{ct}$ are the charge transfer impedance on electrode-electrolyte interface and double-layer capacitance, which corresponded to the second semicircle at medium frequencies. (See Figure IV- 293.)

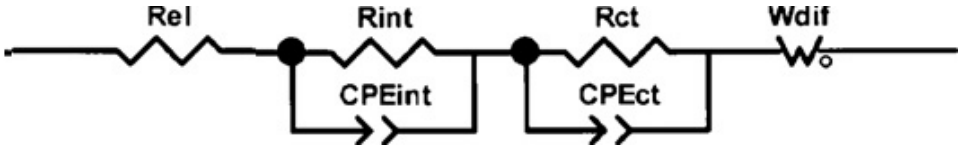


**Figure IV- 293: Equivalent electrical circuit**

All capacitors were replaced with constant phase elements to factor in the porous nature of anode surfaces. W which was indicated by a sloping line at low frequencies, was the Warburg impedance related to the diffusion effect of $Li^+$ transfer in the electrode bulk and the diffusion of salt in the electrolyte. (See Table IV- 44.)

**Table IV- 44: Summarized modeling results for the Nyquist plots**

| Cell name | $R_{el}$ Ω | $R_{int}$ Ω | $CPE_{int}$ $\mu\Omega^{-1} s^{n1}$ | $n_1$ | $R_{ct}$ Ω | $CPE_{ct}$ $\mu\Omega^{-1} s^{n2}$ | $n_2$ |
|---|---|---|---|---|---|---|---|
| Rod-T4-Micro-Si | 8.4 | 113 | 64 | 0.6 | 73 | 423 | 0.8 |
| Coin Cell-Micro-Si | 1 | 5.9 | 32 | 0.5 | 21 | 19 | 1 |
| Thick Rod-Micro-Si | 8.8 | 15 | 6 | 0.8 | 40 | 21 | 0.6 |
| Coin Cell-Si30SC | 4.1 | 3.9 | 18 | 0.7 | 29.4 | 43 | 0.9 |
| Rod-Si30SC | 5.3 | 4 | 3 | 0.7 | 15.6 | 15 | 0.7 |

### Electronic Connectivity between Particles and Current collector

The EIS data and the CV graphs indicate that it is essential to ensure sufficient ionic and electronic conductivity in the anode structure, and the maximum distance between any silicon particle and any part of the current collector or its extension should be limited to less than a few tens of micrometers, if the amount of conductive filler is kept at 10%. Finally the graphs suggest that it not necessary to apply pressure on the anode for the purpose of sufficient electronic conductivity. However, from CV graphs at very low rate, it is not possible to judge the effect of the pressure on the SEI formation that can limit the cycle life and rate. Our experiments further showed that at mid-high rates the cycle life rapidly drops, suggesting that we need to focus on "large shape change of silicon particles during cycling" as the base of our fabrication methods. Nano-silicon particles, rods and coating, either in slurry or grown on a substrate, such as carbon based substrates, are then possible directions. At the same time, the EIS data also suggests that our equivalent circuit model might be too simplistic and may require a more complex model.

### Fabrication methods

Based on the results from the above EIS and CV data we identified 3 different fabrication methods that appear to be the most promising:

1) Anode-starting based on silicon coating on carbon nano-micro-machining or vertically aligned carbon nanotubes templates. Nano-micro-machining and semi-conductor processing.
2) Anode-starting based on silicon coating on continuous carbon micro-fibers. Reel-to-reel processing.
3) Cathode-starting based on silicon-carbon slurry injection into cathode holes.

In all above methods, commercially available cathode and micro-nano carbon template, carbon fiber and Si-C powder are used, and the focus is on the fabrication of the Scell with desired performance.

In addition, conformal coating of separator or solid electrolyte between the anode rods and perforated cathode plates is a major important technical task. In this regard, we have identified 2 most promising fabrication methods for conformal coating on the perforated cathode plates or on the anode rods:

1) Template based coating
2) Electrostatic based coating

In temple based coating, we use a template mask that combined with the rod electrode pattern (or the cathode perforation), leaves only a conformal gap between the anode rods (or cathode apertures) and the mask, such that the polymer separator in solvent or solid electrolyte gel can be injected in the conformal gap. (See Figure IV- 294.)

Figure IV- 294: Template mask for separator-solid electrolyte coating

## Conclusions and Future Directions

We are developing a potentially disruptive platform, Scell, for the next generation of advanced batteries that may result in significant lower cost, while achieving higher energy and cycle life. However, the high risk high reward nature of this innovation means that there are challenges at different levels. Scell is chemistry and geometry agnostic, so our focus has been on developing promising scalable manufacturing techniques.

We studied numerous different fabrication methods and have identified and down selected a couple of most promising methods. The next step is performing detailed experimental analyses on the fabrication methods in the next 6-9 months. In this regard we have started several new collaborations and have filed 3 patent applications.

Regarding the speed of cell assembly and testing, we have been able to develop a novel method that can speed up the Scell assembly and testing by 20x and comparable to the speed of conventional parallel plate platform.

Further, our calculations based on the selected fabrication methods suggest that reaching 450 Wh/kg and 1000 Wh/L at the cell level is possible.

We are determining the optimal fabrication method, including the viscosity of the Si-C slurry and the gel electrolyte, so that we are able to achieve high energy density in the cells with good C-rate performance and cycling performance. In order to be able to directly compare the performance of Scell with conventional parallel plate and also to manage the number of unknown scientific parameters in the project, we use commercial powder chemistries.

We believe that the proposed technical approach **is** viable.

# IV.F.6 Low Cost, High Capacity Non-Intercalation Chemistry Automotive Cells (Sila Nanotechnologies)

## Objectives

- The objective of this project is to research, develop, and demonstrate (RD&D) ultra-high capacity alloy-type Si anodes and conversion-type mixed metal fluoride (MFx) cathodes within milli-ampere hour (mAh)+ Lithium-ion (Li-ion) cells, capable of achieving the following performance characteristics by the end of the project.


### Project Details

**Peter Faguy (Program Manager)**
DE-0006862 Recipient:
Sila Nanotechnologies, Inc.

**Alex Jacobs (Sila Nano – PD/PI)**
2450 Mariner Square Loop
Alameda, CA 94501
Phone: 408-475-7452
Email: alex@silanano.com

Subcontractor:
Georgia Institute of Technology



Start Date: October 2014
Projected End Date: September 2016


## Technical Barriers

- In order to achieve global adoption of electric vehicles (EVs) and make a significant impact on the reduction in $CO_2$ emission, the key problems of driving range per charge & cost per kWh must be addressed.

  Barriers addressed:

- Performance: Low Wh/kg & Wh/L.
- Life: Poor cycle stability for high capacity (e.g., MFx) cathodes.
- Cost: High $/kWh.

## Technical Targets

- Cathode Targets: > 80% of theoretical capacity; and >65 cycles (Year 1) and > 100 cycles (Year 2).
- Cell Targets: 580 Wh/kg, 1200 Wh/L, 2400W/L, 1160 W/kg, 200 cycles at end of the project.

## Accomplishments

**Table IV- 45: Performance characteristics sought**

| Parameter | Metric |
|---|---|
| Energy Density | ≥1,200 Watt Hour per Liter (Wh/L) |
| Specific Energy | ≥580 Watt Hour per kilogram Wh/kg |
| Discharge Power Density | ≥2,400 Watt per Liter (W/L) |
| Specific Power | ≥1,160 Watt per kilogram (W/kg) |
| Degradation | ≤20% over 200 Cycles |
| Cost Reduction | ~3x |

- We have exceeded our GO/NO GO Milestone 1 for the Budget Period #1 and demonstrated over 80% of theoretical cathode capacity in half cells on the first cycle. (See Table IV- 45.)
- We have significantly exceeded our GO/NO GO Milestone 2 for the Budget Period #1 and demonstrated over 65% half cell theoretical capacity with a stability of 65 cycles. In fact, we demonstrated over 500 cycles at ~ 80% of theoretical capacity.
- We have gained insights on the ability to successfully build a protective surface layer on the cathode *in situ*.
- We have demonstrated dendrite-free Li plating during our experiments on cathode half-cells.

### Introduction

Development of higher energy density electrodes for Li-ion batteries is highly needed in order to greatly enhance cell energy storage characteristics. As discussed in the Feasibility section of the work proposal, Sila has already demonstrated successful development of high energy density anodes. Complementary novel high

energy density cathodes are needed to enhance the energy characteristics of the entire cell. Such cathodes also need to be both safer and cheaper than state of the art. However, the majority of commercial and exploratory high energy density cathodes (such as lithium cobalt oxide (LCO), lithium nickel cobalt manganese oxide (NCM), lithium nickel cobalt aluminum oxide (NCA), etc.) contain either Ni or Co or both, which are toxic and rare elements. They are additionally relatively expensive, and thus Ni and Co-based cathodes face difficulties in meeting the demand to lower the cost of Li-ion technology. Finally, these oxygen-containing, high energy density, high voltage cathodes possess significant safety risks (thermal runaway) when used in cells. We propose development and utilization of mixed metal fluoride - based cathodes based on some of the inexpensive, abundant and mass-produced metals. The proposed conversion cathode technology requires only one metal atom to store 2-3 Li atoms (in contrast with the conventional intercalation-type chemistry, where one metal atom stores only ½-1 of Li atom, on average). Because of its drop-in replacement nature for existing production processes, the proposed technology will offer a smooth path to lower cost automotive cells. In addition, the absence of oxygen in the cathode will minimize Li-ion cell safety hazards. Therefore, the proposed project is well aligned with DOE goals: higher battery energy and power density, reduction in cell cost, and enhancement in safety, all of which promote the adoption of EVs.

## Approach

**Innovative Approach:** The proposed cathode technology features: (1) micron-scale particles will allow "drop-in" replacement of conventional cathode powders (such as NCM and NCA); (2) ultra-high capacity (~400 mAh/g); (3) a composite structure to achieve low volume changes and mechanical stability during cycling; (4) compatibility with liquid or solid electrolytes and (5) protection of metal fluorides from undesirable interactions with the electrolyte in order for them to achieve long-term cycle stability. Microstructure optimization of such composite particles focuses on achieving low electrical and ionic resistance within the individual particles, which, in combination with slurry/coating optimization, will allow us to achieve low polarization and low voltage hysteresis at high rates.

Sila recently developed and demonstrated a low-cost Si-based composite anode technology offering a unique combination of high volumetric and gravimetric capacity, high rate, low volume changes on the particle level (comparable to that of graphite) and the resulting stable solid electrolyte interphase (SEI) in carbonate-based electrolyte solvents. In the course of the project, the conversion-type nanocomposite cathodes being developed will be matched with Si-based nanocomposite anodes to achieve ultra-high specific energy and ultra-high energy density in full cells. Electrolyte composition and slurry processing will be pre-optimized to achieve good cycle stability in matched full cells.

## Results

### *In situ* Formation of the Protective Layer on the Cathode Surface

In this study we investigated if electrolyte reduction taking place at the potential above that of the initial conversion reaction (above ~ 1.5 V) may induce formation of the surface layer, which would effectively resist undesirable reactions between liquid electrolyte and discharged cathode components and ideally be impermeable to small metal ions. We were also interested to see if formation of such a protective layer may impact the first cycle hysteresis. Some of such electrolytes, including ether-based, performed particularly well for this task.

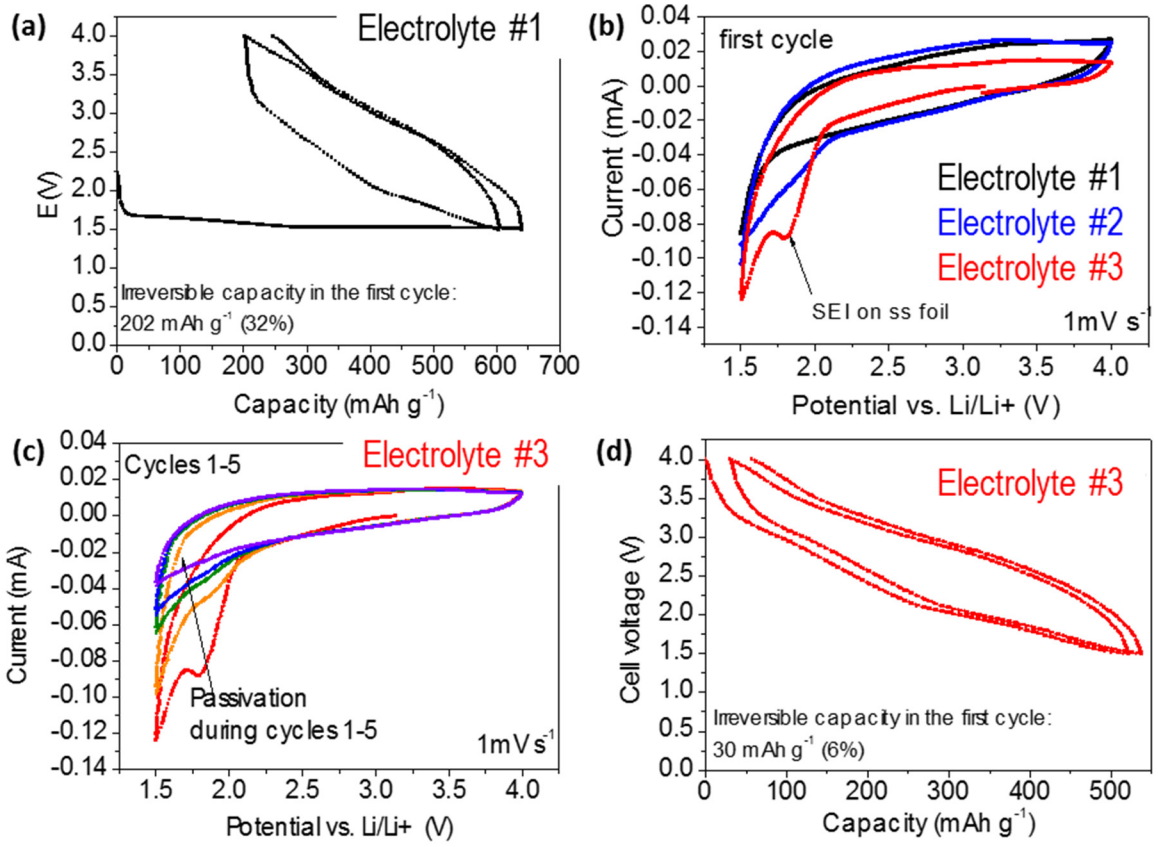


**Figure IV- 295: (a,d) The charge and discharge profiles of the nanocomposite MFx –based Li half cells in three electrolytes in the initial 2 cycles; (b) The first cycle cyclic voltammetry diagrams of the nanocomposite FeF2/C – Li cells; (c) The 5 cycles cyclic voltammetry diagrams of the nanocomposite half cells in electrolyte #3**

Figure IV- 295a shows the room temperature discharge curve of the cathode, revealing high capacity utilization and a significant over-potential in the first discharge. Figure IV- 296b shows cyclic voltammetry of a bare stainless steel (ss) foil vs. a Li counter electrode cell in three exemplary electrolytes. Interestingly, for electrolyte # 3 we observe a noticeable increase in the intensity of the reduction peak at ~1.8 V vs. $Li/Li^+$. The area under the anodic current curve is becoming significantly larger than that of the cathodic curve with coulombic efficiency (CE) reducing from 98% (electrolyte #1) to 87% (electrolyte #2) and 56% (electrolyte #3), respectively. These results indicate irreversible electrolyte reductions with the likely formation of the solid electrolyte interphase (SEI) on the surface. Furthermore, because the reduction potential for the electrolytes is within the cycling window for the cathode (see Figure IV- 295a, d) the passivation layer formation is also expected to occur at the cathode surface. Our initial experiments revealed that both the overpotential for the first discharge and the first cycle irreversible capacity loss could be reduced dramatically in selected electrolytes (Figure IV- 295d). Since the electrodes in these experiments are identical and since the electrolyte #3 exhibits lower bulk ionic conductivity, we concluded that the reduced first cycle overpotential in the electrolyte #3 likely originates from surface phenomena, such as lower electrolyte/electrode interfacial energy and reduced charge transfer resistance. These may, in turn, be linked to the formation of the favorable electrode passivation layer.

### Cycle Life Enhancement for 400+ mAh/g Cathode

Figure IV- 296 shows results of the charge-discharge tests conducted at a moderately high (for this system) current density of 140 mA $g^{-1}$. Electrolyte #3 exhibited noticeably improved performance compared to electrolyte #1 and 2. This improvement correlates with noticeably increased reduction of this electrolyte at potentials below 2.1 V vs. $Li/Li^+$ (Figure IV- 295b).

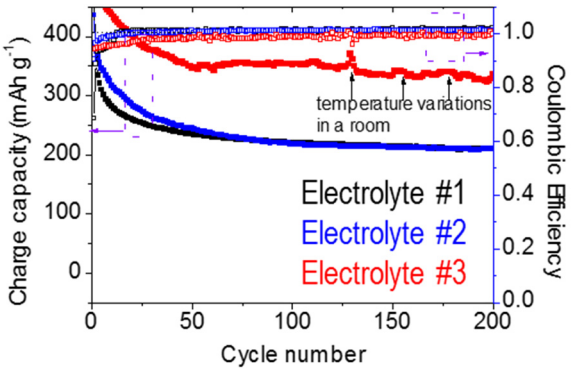


Figure IV- 296: Charge capacities and coulombic efficiencies of nanocomposite MFx cathode half cells in different electrolytes

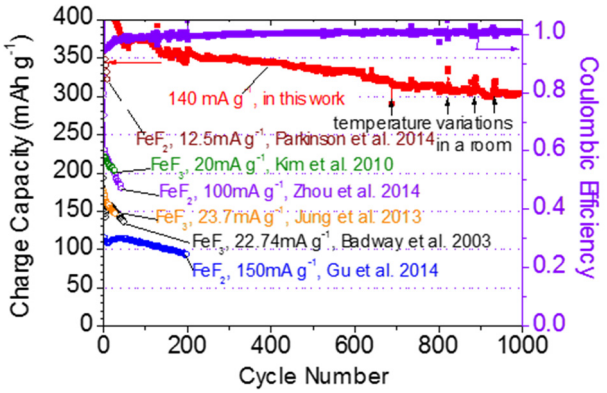


Figure IV- 297: Charge capacity and coulombic efficiency of nanocomposite nanocomposite MFx cathode half cells in electrolyte #3 for 1000 cycles. Previously reported performances of similar materials are compared

Since many applications of high energy cells require cycle stability in the range from 200 to 1000 cycles, we conducted the long-term cycle stability test of the most promising cell (Figure IV- 297). The achieved combination of the outstanding (for metal fluorides) stability and high capacity utilization at high current density is unprecedented. As we see, even some of the best prior-art studies of similar chemistry demonstrated 2-3 times lower capacity in spite of the lower current densities used (Figure IV- 297). We explain this significant improvement by (i) excellent mechanical stability of the MFx nanocomposite, (ii) better protection from undesirable reactions with electrolyte (including metal and LiF dissolution) and (iii) resistance of MFx to segregation due to the nanocomposite microstructure.

**Hysteresis Reduction for 400+ mAh/g Cathode**

In contrast to our initial expectations, the cell with lower conductivity electrolyte (electrolyte #3) that induced formation of a passivating layer (Figure IV- 295b and Figure IV- 295c) exhibited smaller hysteresis (the difference of discharge and charge voltages) than the cell with higher conductivity electrolyte (electrolyte #1) that exhibited significantly reduced passivation (compare Figure IV- 298a and Figure IV- 298b).

The half cells with electrolyte #3 retain capacity well. After the initial capacity fading, the cell stabilizes (compare the charge discharge profile at the 50$^{th}$ and 100$^{th}$ cycle, Figure IV- 298b). The average charge and discharge voltages (calculated by dividing the integral of the area beneath the voltage curve with the total capacity) of the electrolyte #3 cell remain constant with cycling (Figure IV- 299). More importantly, the average overpotential in this cell is 0.1-0.2V smaller than that in electrolyte #1 and #2 cells. Considering the higher ionic resistance of electrolyte #3, the smaller charge transfer resistance of this cell may explain the observed phenomenon. The ~0.5 V hysteresis observed in the best cell at 140 mA g$^{-1}$ is certainly larger than what typically observed in intercalation-type materials at similar current densities (0.05-0.2 V), but noticeably smaller than what was achieved in prior art studies of metal fluorides at room temperature and comparable (or even lower) currents (0.6-1.5 V). As a result, the average discharge voltage of all our cells (2.2-2.4 V) is significantly higher than what was reported in the prior art studies. We explain the favorable performance of our material by (i) high electrical conductivity of the MFx nanocomposites as well as fast transport of both (ii) electrons and (iii) ions to the electrochemical reaction sites. In addition, the resistance of MFx, M and LiF to segregation due to their confinement in the composite as well as significantly reduced M dissolution likely contribute to the small value of the hysteresis.

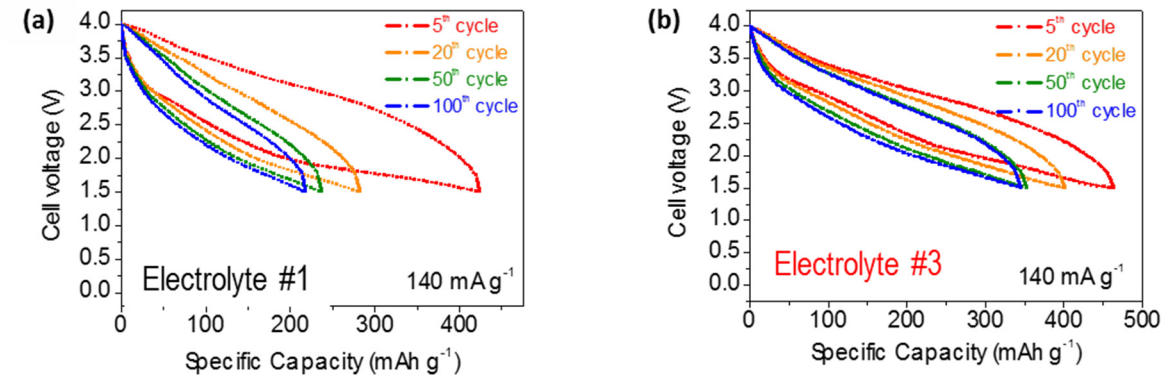


**Figure IV- 298: Charge-discharge profiles of nanocomposite MFx cathode half cells in electrolytes # 1 and #3 during 5th, 20th, 50th, and 100th cycles**

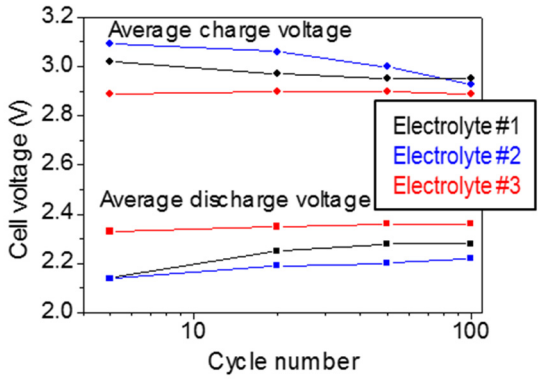


**Figure IV- 299: Average charge and discharge voltages of nanocomposite MFx cathode half cells in electrolytes # 1, #2 and #3 during the first 100 cycles**

### Composition of the *in situ* Formed Protective Surface Layer on the Cathode

To examine the chemical nature of the protective surface coatings formed, we performed X-ray photoelectron spectroscopy (XPS) characterization of the cycled nanocomposite cathodes (Figure IV- 300). The major peak of the $C_{1s}$ spectra (Figure IV- 300a) at 285eV is attributed to C-C bonds from carbon additives, and $-CH_2-CH_2-$ bonds from a polymerized electrolyte solvent. At higher electrolyte concentration, the C-F peak attributed to PVdF binder at 290.5eV is diminished, which is due to the much thicker layer of the reduced electrolyte. The peak at 286.4eV corresponding to C-O-C bonds from polymerized solvent is particularly intensive in electrolyte #3, as expected from more vigorous electrolyte polymerization at the cathode surface. We also observe a C=O peak at higher electrolyte concentrations, which may originate from the breakdown of the backbone chain of solvent monomers. The O1s spectra (Figure IV- 300b) confirmed the appearance of C=O peak in electrolyte #3. The major peak at 532.4eV is assigned to O-C bonds in electrolyte solvent and O=S in electrolyte salt and its reduction products. The F1s spectra shows dampening of the LiF peak at 685eV and rise of the F-S peak at 687.8eV (Figure IV- 300c). In this process, a large fraction of the LiF detected could be contributed to the lithiation of MFx. The reduced LiF/F-S ratio for electrolyte #3 indicates thicker surface layer blocking the signal from the cathode core. Finally, with the increase in the electrolyte concentration, peaks representing $FSI^-$ (170.1eV and 171.4eV) and its decomposition products (167.1 eV) are increasing in $S_{2p}$ spectra (Figure IV- 298d), as shall be expected for thicker surface layer.

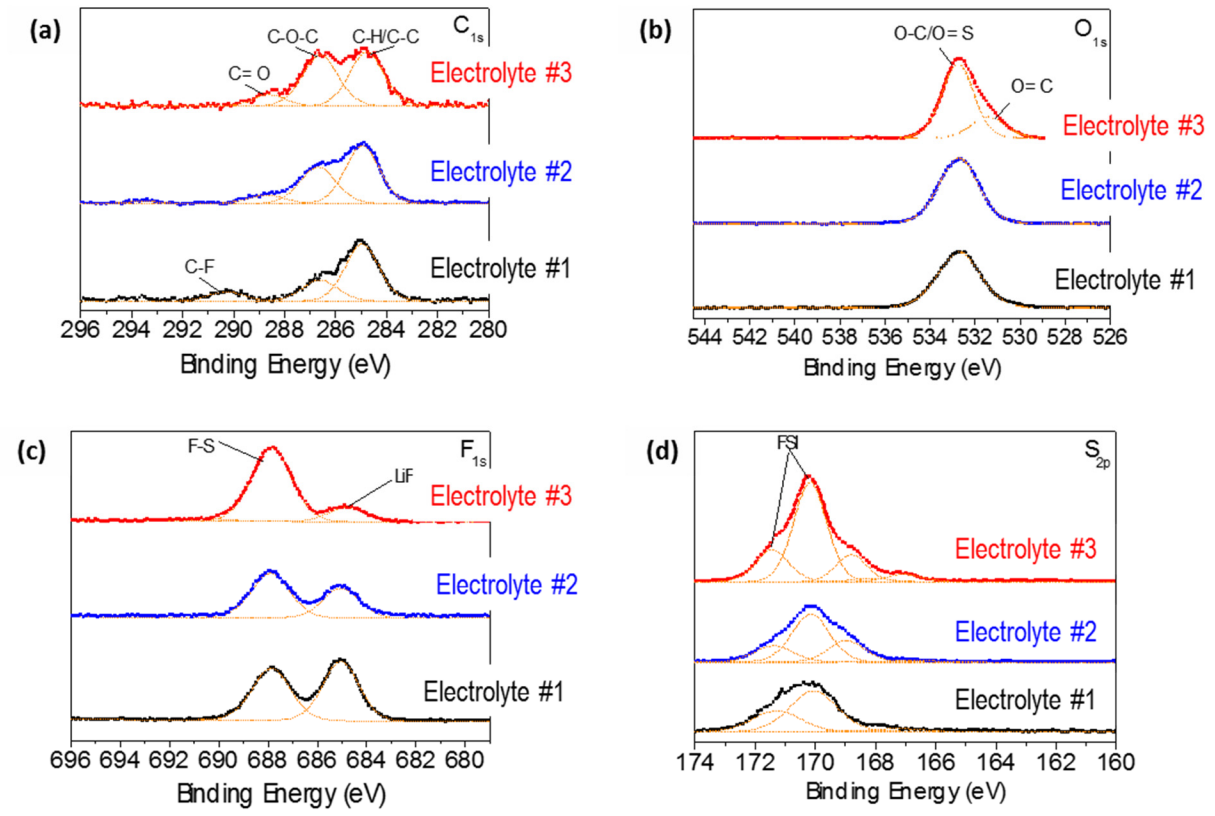


**Figure IV- 300: High resolution XPS spectra of MFx nanocomposite cathode cycled in different electrolytes: (a) $C_{1s}$; (b) $O_{1s}$; (c) $F_{1s}$; (d) $S_{2p}$**

### Composition of the In-situ Formed Protective Surface Layer on the Cathode

Other promising results were obtained when studying the surface morphology of Li foil cycled in the described cells. Long-term plating and striping of Li onto/from the Li foil is known to induce severe surface roughening and dendrite growth, which presents cell safety hazard_ENREF_43. This is one of the key reasons why bare Li foils are not used in commercial cells. In contrast, the surfaces of Li foils cycled in our cells are remarkably smooth (compare Figure IV- 301a with Figure IV- 301b-d), particularly the one cycled in the electrolyte #3 (Figure IV- 301d). A number of explanations are possible. Enhancement in Li anode stability during cycling in symmetric Li-Li cells may be related to the decomposition of electrolyte salt on the surface of both electrodes, which induces formation of decomposition products and a more stable Li electrodeposition due to increased Li surface energy. The electrolyte composition itself may similarly prevent Li dendrite growth and smooth out the Li surface due to expectedly high energy of the interface between the Li and the electrolyte. Furthermore, elastic modulus and hardness of the Li SEI could be sufficiently high to provide additional resistance to the growth of dendrites. The high ionic transport through such passivating layers on both the anode and the cathode surfaces, as evidenced by low polarization during cycling of a symmetric Li-Li cells (not shown) as well as by low polarization of our half cells (Figure IV- 296d), shall similarly lead to large improvements in the stability of Li electrodeposition.

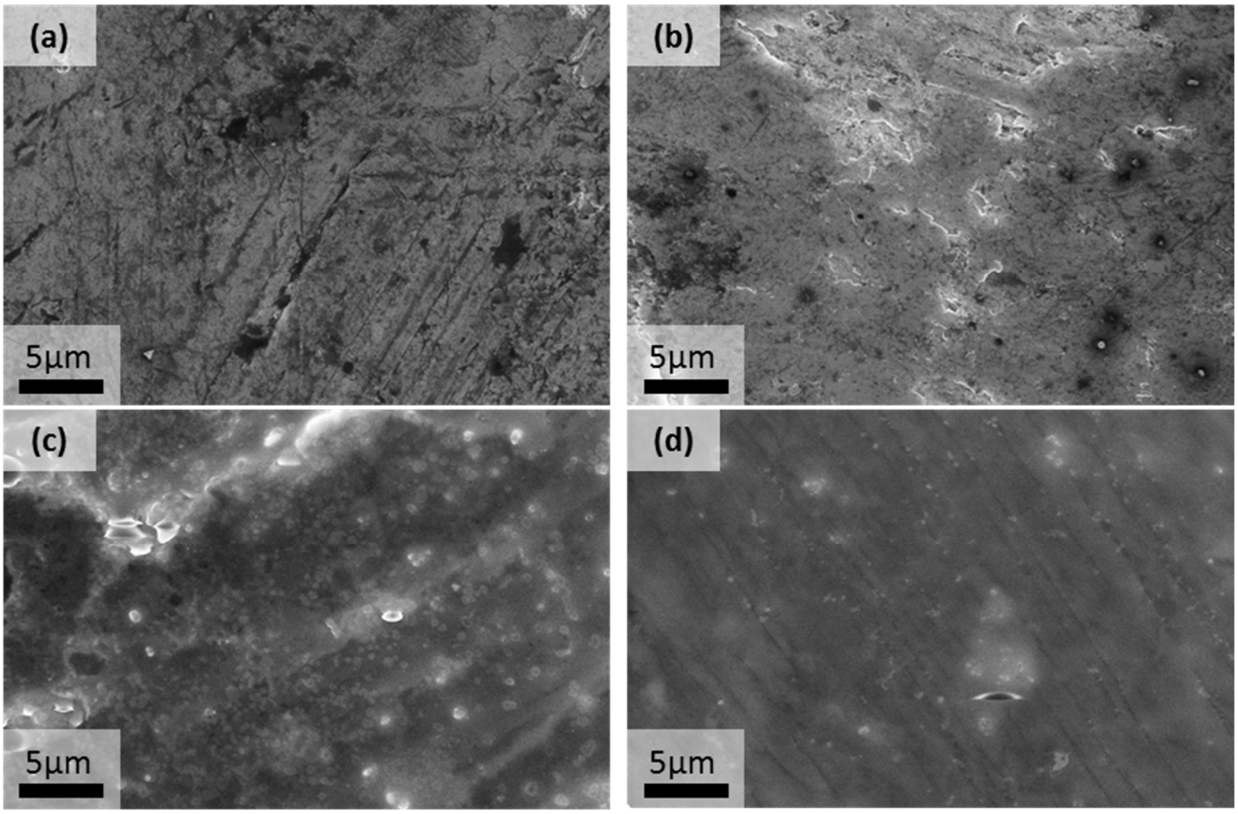


Figure IV- 301: (a-d) SEM of original Li foil (a) and Li foil cycled in electrolytes (b) #1, (c) #2 and (d) #3

## Summary

In summary, *in-situ* formation of the conformal Li-ion permeable solid coatings of the reduced electrolyte around metal fluoride–based nanocomposite cathode particles was found to be a successful strategy to protect the cathode from dissolution and to achieve exceptionally long-term stability of the rechargeable MFx-Li cells. By fine-tuning the nanocomposite microstructure, by utilizing electrolyte that greatly minimizes Li dendrite and Li impedance growth and additionally produces redox active species that aid charge transfer in the cathode. We have further demonstrated near-theoretical capacity and remarkable (for this chemistry) rate performance characteristics. The success of this study further emphasizes the great potential of the rechargeable Li-ion batteries with conversion-based cathodes.

## FY 2015 Publications/Presentations

1. "Low Cost, High Capacity Non-Intercalation Chemistry Automotive Cells", US DOE Vehicle Technologies AMR, 2015.